

**A Three-Dimensional
Momentum Space Formulation
for The NN System
and The Nd Break-Up Process**

Dissertation zur Erlangung
des Grades eines Doktors der Naturwissenschaften
in der Fakultät für Physik und Astronomie
der Ruhr-Universität Bochum

von
Imam Fachruddin
aus Jakarta

Bochum 2003

Die Forschungsarbeiten zur Dissertation wurden am Institut für theoretische Physik II der Ruhr-Universität Bochum durchgeführt.

Referent : Prof. Dr. W. Glöckle (Ruhr-Universität Bochum)

Koreferentin : Prof. Dr. Ch. Elster (Ohio University)

Ort und Tag der Disputation : Bochum, 21. Juli 2003

to my parents, my family, my brothers and sisters

ZUSAMMENFASSUNG UND AUSBLICK

Wir haben ein Verfahren zur Berechnung von Wenignukleonsystemen im Impulsraum entwickelt, ohne eine Partialwellenzerlegung (PW Zerlegung) anzuwenden. Wir nennen dies das dreidimensionale (3D) Verfahren. Wir begannen mit dem Nukleon-Nukleon (NN) System und fuhren mit dem Dreinukleonstreuprozeß (3N Streuprozeß) fort. Dies war speziell der Nd Aufbruchsprozeß in erster Ordnung in der NN T-Matrix. Das 3D Verfahren war als eine vielversprechende Alternative zu der erfolgreichen PW Zerlegung beabsichtigt, da es sich bei höheren Energien besser als ein auf Partialwellen basierendes Verfahren eignen sollte. Hier fassen wir zusammen, sowohl wie wir das 3D Verfahren für das NN System und den Nd Aufbruchsprozeß entwickelten als auch die Durchführung und die Ergebnisse des 3D Verfahrens. Die Berechnungen in dieser Arbeit wurden basierend auf den NN Potentialen AV18 [20] und Bonn-B [21] durchgeführt. Schließlich geben wir einen Ausblick auf weitere Untersuchungen und auch Entwicklungen des 3D Verfahrens.

NN Streuprozeß

Um das 3D Verfahren zu entwickeln, war es notwendig, mit dem NN Streuprozeß zu beginnen, weil die NN T-Matrix der Input zur Berechnungen von komplexeren Wenignukleonsystemen ist. Der erste Schritt war es, 3D Basiszustände des NN Systems zu definieren. Wir definierten Impuls-Helizität-Basiszustände, welche antisymmetrisch unter Austausch zwischen den beiden Nukleonen im Impuls-, Spin- und Isospinraum sind. Wie der Name sagt, wurden die Impuls-Helizität-Basiszustände aus Impulsvektorzuständen und Helizitätszuständen zum gesamten NN Spin konstruiert. Es wurden nicht die individuellen Spins der beiden Nukleonen sondern der NN Gesamtspin genommen. Dies ermöglichte es, eine kleinere Zahl von zu lösenden Lippmann-Schwinger-Gleichungen (LSG'en) zu erhalten. Die Symmetrieeigenschaften der T-Matrix- und der NN Potentialmatrixelemente in den Impuls-Helizität-Basiszuständen lassen die Reduzierung

der Zahl der LSG'en für die NN T-Matrix von 10 auf 5 für jeden NN Gesamtisospinzustand zu. Alle diese LSG'en im 3D Verfahren sind Integralgleichungen in zwei Variablen. Diese sind der Betrag des Relativimpulses zwischen den beiden Nukleonen und der Streuwinkel.

Das NN Potential wird durch eine Gruppe von sechs unabhängigen Operatoren, Ω , ausgedrückt. Wir definierten die Ω Operatoren geeignet für die Impuls-Helizität-Basiszustände, sodaß eine sehr einfache Ausarbeitung der NN Potentialmatrixelemente ermöglicht wird. Wir leiteten eine Relation zwischen der Gruppe der Ω Operatoren und der Gruppe der sechs Operatoren, die als die Wolfenstein Operatoren [26] bekannt sind, ab. Diese Gruppe von Operatoren wird über Invarianzen, eine Symmetriebedingung und die Hermitizität des NN Potentials [41] eingeschränkt. Wir möchten darauf hinweisen, daß ein beliebiges in Operatorform gegebenes NN Potential im 3D Verfahren angewandt werden kann. Repräsentative Potentiale sind die AV18 und Bonn-B Wechselwirkungen, die in dieser Arbeit angewandt wurden.

Um Observablen zu berechnen und sie mit NN Daten zu vergleichen, verknüpften wir die T-Matrixelemente in den Impuls-Helizität-Basiszuständen mit denen in einer physikalischen Darstellung. Die physikalische Darstellung benützt die Spins und Isospins der individuellen Nukleonen, wobei die Spins bezüglich einer beliebigen aber festen z-Achse quantisiert sind. Deshalb ist die physikalische Darstellung eng mit den experimentellen Spineinstellungen eines NN Streuprozeßes verbunden. Wir entwickelten auch die T-Matrixelemente in den Impuls-Helizität-Basiszuständen in Partialwellen und verglichen die NN Streuphasen aus den 3D Berechnungen mit den normalen PW Berechnungen. Die Übereinstimmungen mit den PW Berechnungen sowohl für NN Streuphasen als auch für NN Observablen sind perfekt. Die Vergleiche in den NN Observablen zeigten, daß viele Partialwellen besonders bei den höheren Energien in den PW Berechnungen gebraucht werden, um Konvergenz der PW Berechnungen in bezug auf die 3D Berechnungen zu erhalten. Zum Beispiel, bei $E_{lab} = 300$ MeV muß man in der PW Berechnung für den np differentiellen Wirkungsquerschnitt mindestens $j_{max} = 16$ nehmen, welches 98 LSG'en entspricht. Wir verglichen auch unsere 3D Berechnungen sowohl mit Observablen, die auf den Streuphasen basieren, welche in einer Partialwellenanalyse (PWA) bestimmen wurden, als auch direkt mit NN Daten bei Laborenergien, die höher als 300 MeV waren. Später, wenn wir den Nd Aufbruchprozeß bei verschiedenen Energien berechneten, brauchten wir die NN T-Matrix auch für solche höhere Energien. Da das 3D Verfahren für alle Energien in gleicher Weise anzuwenden ist, waren die Vergleiche beabsichtigt, um die Anwendungen der zwei NN Potentiale AV18 und Bonn-B im 3D Verfahren bei höheren Energien zu testen. Obwohl diese zwei parametrisierten NN Potentiale nur an NN Daten bei Energien, die niedriger als 350

MeV sind, angepaßt wurden, zeigten die Vergleiche mit den Ergebnissen der PWA und NN Daten trotzdem recht gute Übereinstimmungen.

Das Deuteron

Konventionell wird das Deuteron immer über gekoppelte Gleichungen für die Drehimpulse $l = 0$ und $l = 2$ berechnet. Es war interessant, zu untersuchen, ob wir die Impuls-Helizität-Basiszustände für eine Lösung des NN Bindungszustandes benutzen können. Für diesen Zweck projizierten wir den Deuteronzustand und die Eigenwertgleichung auf die Impuls-Helizität-Basiszustände. Somit definierten wir Deuteronwellenfunktionskomponenten, die dreidimensional in den Impuls-Helizität-Basiszuständen sind. Wir definierten auch Deuteronwahrscheinlichkeitsdichten in den Impuls-Helizität-Basiszuständen. Die abgeleiteten Deuterongleichungen in den Impuls-Helizität-Basiszuständen resultierten als zwei gekoppelte Integralgleichungen in zwei Variablen, dem Betrag des Relativimpulses zwischen den beiden Nukleonen und einem Winkel, der sich auf eine beliebige z-Richtung bezieht. Wir verknüpften die Deuteronwellenfunktionskomponenten in den Impuls-Helizität-Basiszuständen mit denen der PW Basiszustände. Diese Verbindung ermöglicht es, die auf Partialwellen projizierten Deuteronwellenfunktionskomponenten in S- und D-Wellen aus den Deuteronwellenfunktionskomponenten in den Impuls-Helizität-Basiszuständen zu berechnen. Die Vergleiche mit den PW Berechnungen in den S- und D-Wellen des Deuterons zeigten gute Übereinstimmungen.

Als nächstes formulierten wir wieder die Deuterongleichung und die Deuteronwellenfunktionskomponenten durch die Impuls-Helizität-Basiszustände auf eine andere Weise. Zunächst beließen wir den Deuteronzustand in Partialwellen, und leiteten dann eine Operatorform der Deuteronwellenfunktion im Impulsraum ab. Vermöge der Impuls-Helizität-Basiszustände führte die Deuteronwellenfunktion in Operatorform zu den Deuteronwellenfunktionskomponenten in den Impuls-Helizität-Basiszuständen, welche jetzt aber analytisches Winkelverhalten hatten. Dieses analytische Winkelverhalten bestätigte das numerisch gefundene in der ersten Formulierung. Das analytische Winkelverhalten ließ es nun zu, die Deuterongleichung in nur einer Variablen, nämlich dem Betrag des Relativimpulses zwischen den beiden Nukleonen, abzuleiten. Wir lösten diese Gleichung und erhielten die gleichen Ergebnisse wie die bei der ersten Formulierung. Auch hier stellten wir eine Verbindung mit der normalen PW Zerlegung her und bekamen gute Übereinstimmungen in den auf Partialwellen projizierten Deuteronwellenfunktionskomponenten in S- und D-Wellen. Zuletzt untersuchten wir in dreidimensionaler Weise über die Deuteronwellenfunktion in Operatorform die Wahrscheinlichkeitsdichte mehrerer

Spinkonfigurationen der zwei Nukleonen im Deuteron für ein insgesamt polarisiertes Deuteron.

Der Nd Aufbruchsprozeß

Schließlich kamen wir bei dem 3N System an und wir erweiterten das 3D Verfahren auf den Nd Aufbruchsprozeß. Wir interessieren uns für höhere Energien und entschieden uns, nur den führenden Term der vollen Nd Aufbruchsamplitude zu nehmen. Somit wollten wir sehen, ob der führende Term allein den Nd Aufbruchsprozeß bei den betrachteten höheren Energien über $\simeq 200$ MeV Laborenergie des Nukleons ausreichend beschreiben konnte. Wir wandten das Faddeev Schema an, um den Nd Aufbruchsprozeß zu behandeln. Der Einfachheit halber beließen wir den Deuteronzustand in Partialwellen. Das war ein natürlicher Schritt, da die Deuteronwellenfunktion nur zwei Partialwellenkomponenten in S- und D-Wellen hat. Wir begannen damit, den führenden Term der vollen Nd Aufbruchsamplitude in den 3N Basiszuständen, welche in einer physikalischen Darstellung waren, auszuarbeiten. Wie beim NN Streuprozeß geht man in der physikalischen Darstellung von Spins und Isospins der individuellen Nukleonen aus, die entlang einer beliebigen aber festen z -Achse quantisiert sind. Die Kinematik der drei Nukleonen wurde von zwei Jacobi Impulsen so beschrieben, daß das 3N System als ein System betrachtet wurde, das aus einem Nukleon und einem 2N Subsystem besteht. Symmetrieeigenschaften unter Austausch der drei Nukleonen wurden durch Permutationoperatoren im führenden Term der vollen Nd Aufbruchsamplitude eingeführt. Als Folge bekamen wir einen Ausdruck des führenden Termes in den NN T-Matrixelementen in der physikalischen Darstellung. Durch die vorher abgeleitete physikalische Darstellung der NN T-Matrixelemente war es einfach, den führenden Term der vollen Nd Aufbruchsamplitude in den NN T-Matrixelementen in den Impuls-Helizität-Basiszuständen zu erhalten. In dem resultierenden Ausdruck zeigten die 2N Anfangsrelativimpulse als Argumente der NN T-Matrixelemente in den Impuls-Helizität-Basiszuständen in beliebige Richtungen. Um die NN LSG'en für die NN T-Matrix zu lösen, wählen wir notwendigerweise eine feste z -Richtung als die Richtung der NN Anfangsrelativimpulse. Deshalb drehten wir als einen letzten Schritt die NN T-Matrixelemente in den Impuls-Helizität-Basiszuständen, die sich im führenden Term der vollen Nd Aufbruchsamplitude befinden, sodaß die 2N Anfangsrelativimpulse in eine feste z -Richtung zeigten. Diese Drehung führte zu einem komplizierten zusätzlichen Phasenfaktor.

Mittel dieses führenden Termes der vollen Nd Aufbruchsamplitude in den Impuls-Helizität-Basiszuständen berechneten wir Observablen. Da man bei höheren Energien mit

relativistischen Effekten rechnen mußte, nahmen wir einen weiteren Schritt vor, nämlich relativistische Kinematik in der Formulierung miteinzuschließen. Wir leiteten jedoch nicht den führenden Term mit zusätzlichen relativistischen Strukturen ab, sondern machten nur einen ersten aber wichtigen Schritt, nämlich die nichtrelativistischen Jacobi Impulse und Energieargumente des nichtrelativistischen führenden Termes durch die relativistischen Größen zu ersetzen. Als Folge änderte sich der führende Term. Zuletzt leiteten wir den Wirkungsquerschnitt entsprechend der üblichen relativistischen Streutheorie ab. Daher änderte sich der Phasenraumfaktor des Wirkungsquerschnittes verglichen mit dem der nichtrelativistischen Streutheorie.

Wir wandten die Formulierung des Nd Aufbruchsprozesses in einem 3D Verfahren auf die Proton-Neutron Ladungsaustauschreaktion im inklusiven pd Aufbruchsprozeß an. In diesem Prozeß wird ein Proton auf ein Deuteron geschossen, das dann aufbricht, und am Ende wird das Neutron detektiert, während die zwei Protonen nicht gemessen werden. Wir berechneten den spingemittelten differentiellen Wirkungsquerschnitt (kurz den Wirkungsquerschnitt) und mehrere Spinsobservablen: die Polarisierung des Neutrons, die Analysierstärke des Protons und die Polarisierungstransferkoeffizienten. Wir diskutierten drei Aspekte unserer Berechnungen. Erstens verglichen wir unsere Berechnungen mit den PW Berechnungen bei Laborenergien des Protons bis 197 MeV. Es wurde gezeigt, daß unsere Berechnungen mit den PW Berechnungen bis $E_{lab} = 100$ MeV noch übereinstimmten. Es gab jedoch schon eine Diskrepanz von ungefähr 1.7% in der Spitze des Wirkungsquerschnittes bei 100 MeV, wobei die PW Berechnungen 2N Zustände von 2N Gesamtdrehimpulsen $j \leq 7$ und 3N Zustände von 3N Gesamtdrehimpulsen $J \leq 31/2$ berücksichtigten. Mit dieser großen Zahl von Drehimpulszuständen in den PW Berechnungen erreicht man tatsächlich schon die Grenzen der heutzutage möglichen PW Berechnungen. Bei $E_{lab} = 197$ MeV stimmten unsere Berechnungen nicht mit den PW Berechnungen basierend auf $j \leq 7$ und $J \leq 31/2$ überein, weil die PW Berechnungen nicht ausreichend konvergierten, wie in einem Konvergenztest gezeigt wurde. Der Test zeigte auch, daß 2N Gesamtdrehimpulszustände für die PW Berechnungen für die Konvergenz wichtiger sind als 3N Gesamtdrehimpulszustände. Für die gleiche Zahl von Gesamtdrehimpulszuständen nehmen die Diskrepanzen zwischen unseren Berechnungen und den PW Berechnungen bei wachsender Energie schnell zu. Wir kamen zum Schluß, daß PW Berechnungen bei $E_{lab} > 100$ MeV nicht sicher benutzt werden können, um den Nd Aufbruchsprozeß gut zu beschreiben.

Zweitens wollten wir zeigen, wie wichtig Mehrfachstreueffekte sind. Dazu verglichen wir bei $E_{lab} = 197$ MeV unsere Berechnungen mit den vollen Faddeev PW Berechnungen, in welchen nicht nur der führende Term sondern auch die Mehrfach-

streuterme der vollen pd Aufbruchsamplitude eingeschlossen wurden. Die Vergleiche zeigten, daß Mehrfachstreueffekte bei dieser Energie tatsächlich eintreten und meistens in dem Wirkungsquerschnitt und der Analysierstärke zu sehen sind. Für diese beiden Observablen führte der Einschluß der Mehrfachstreuterme in den Berechnungen zu Ergebnissen, die näher bei den Daten liegen. Wir kamen zum Schluß, daß Mehrfachstreuterme der vollen Nd Aufbruchsamplitude bei $E_{lab} = 197$ MeV in den Berechnungen beachtet werden müssen.

Bei Energien, die höher als 197 MeV sind, hatten wir keine vollen Faddeev PW Berechnungen zur Verfügung, mit denen man vergleichen konnte. Deshalb verglichen wir direkt mit den Daten bei $E_{lab} = 346$ und 495 MeV. Bei diesen Energien konnten wir nur vermuten, daß Mehrfachstreuterme vielleicht auch benötigt sind, da Diskrepanzen mit den Daten zu sehen waren.

Schließlich betrachteten wir den Effekt relativistischer Kinematik in unseren Berechnungen. Dazu verglichen wir unsere 3D Berechnungen in nichtrelativistischer und relativistischer Kinematik miteinander, und dies bei Energien von 197, 346 und 495 MeV, wo auch experimentelle Daten vorliegen. Bei diesen Energien sahen wir relativistische Effekte vor allem in den Wirkungsquerschnitten und den Analysierstärken. Für diese beiden Observablen führte die relativistische Kinematik zu besseren Ergebnissen bezüglich der Daten. Die Effekte wurden größer, wenn die Energie stieg, welches man von relativistischen Effekten erwartet. Aus den Vergleichen zu den Daten führten die beobachteten relativistischen Effekte zusammen mit den vorher gesehenen Mehrfachstreueffekten zu der Vermutung, daß in dem Energiebereich von $\simeq 200$ –500 MeV beides notwendig ist, Mehrfachstreuterme und relativistische Korrekturen, um den pd Aufbruchprozeß besser zu beschreiben. Um herauszufinden, bei welcher Energie relativistische Effekte bereits wichtig werden, verglichen wir unsere 3D Berechnungen in nichtrelativistischer und relativistischer Kinematik bei 16 and 65 MeV. Wir fanden, daß relativistische Effekte schon bei $E_{lab} = 65$ MeV anfangen, deutlich sichtbar zu werden.

Zum Schluß wollen wir unsere Arbeit in einem Abschnitt zusammenfassen. Wir entwickelten ein 3D Verfahren für den NN Streuprozeß, das Deuteron und den Nd Aufbruchprozeß. Das 3D Verfahren erwies sich als eine gute Alternative zu der PW Zerlegung und erscheint bei höheren Energien unausweichlich. Im Gegensatz zu der PW Zerlegung erfordert das 3D Verfahren viel weniger algebraische Arbeit. Bei niedrigen Energien, wo die PW Berechnungen noch zuverlässig sind, zeigen die 3D Berechnungen perfekte Übereinstimmungen mit den PW Berechnungen.

Ausblick

Von der Stelle an, wo wir unsere Arbeit beendeten, gibt es noch viele Untersuchungen über Wenignukleonsysteme, die im 3D Verfahren durchzuführen sind. Im Fall des NN Systems ist es interessant, neueste und in Zukunft erscheinende NN Potentiale, wie z.B. das auf der chiralen Störungstheorie basierende NN Potential [60], im 3D Verfahren umzusetzen. Auf Wenignukleonbindungssysteme mit Nukleonenzahlen größer als 2 sollte das 3D Verfahren in jedem Fall angewandt werden, da das Triton [61, 62, 63], das α -Teilchen [64, 65] und andere noch komplexere Wenignukleonbindungssysteme sehr viele Drehimpulszustände enthalten. Bei dem 3N Streuprozeß lösten wir noch nicht die volle Faddeev Gleichung, welches aber, wie wir zeigten, erforderlich ist. Wir berücksichtigten auch noch nicht 3N Kräfte. Im Hinblick auf Relativität betrachteten wir bis jetzt nur relativistische Kinematik. Wir berücksichtigten noch nicht die Lorentztransformation der NN T-Matrix [58] und die Wignerrotationen [59]. Diese werden interessante und herausfordernde Untersuchungen sein. Besonders bei Berücksichtigung dynamischer Merkmale von Relativität wird das 3D Verfahren sich als sehr lohnend erweisen. Aus unserer Sicht wird der nächste Schritt sein, die Mehrfachstreuterme der vollen Nd Aufbruchsamplitude und 3N Kräfte zu berücksichtigen, und zunächst nur relativistische Kinematik anzuwenden. Dies wird ein Gebiet höherer Energien zugänglich machen, welches bis jetzt noch nicht gründlich untersucht wurde.

Contents

ZUSAMMENFASSUNG UND AUSBLICK	v
1 INTRODUCTION	1
2 SCATTERING OF TWO NUCLEONS	5
2.1 Kinematics of the Two-Nucleon System in Laboratory and Center of Mass Reference Frames	5
2.2 Scattering Matrix and Lippmann-Schwinger Equation	7
2.3 Cross Section and Spin Observables	8
3 THREE-DIMENSIONAL FORMULATION FOR NUCLEON-NUCLEON SCATTERING	17
3.1 Momentum-Helicity Basis States	18
3.2 General Structure of the Potential Operator and the Potential Matrix Ele- ment	23
3.3 Lippmann-Schwinger Equation	28
3.4 Connection to the Physical T-Matrix Representation	31
3.5 Connection to the Standard Partial Wave Representation	34
4 APPLICATION TO NN SCATTERING	43
4.1 The NN Potentials	43
4.1.1 One-Boson-Exchange Potential	44
4.1.2 Phenomenological Potential	46
4.2 Results and Discussions	48
4.2.1 Phase Shifts	49
4.2.2 T-Matrix	49
4.2.3 Observables	60
5 THREE-DIMENSIONAL FORMULATION FOR THE DEUTERON	71
5.1 Formulation I	73

5.1.1	Deuteron Wave Function in the Momentum-Helicity Basis	73
5.1.2	Two-Dimensional Deuteron Eigenvalue Equation	76
5.1.3	Deuteron Partial Wave Projected Wave Function	77
5.1.4	Explicit Solution of the Two-Dimensional Deuteron Eigenvalue Equation	79
5.2	Formulation II	80
5.2.1	Deuteron Wave Function in Operator Form	80
5.2.2	Analytic Angular Behavior of the Deuteron Wave Function	88
5.2.3	One-Dimensional Deuteron Eigenvalue Equation	90
5.2.4	Connection to the Standard Partial Wave Representation	92
5.3	Probability Densities for Different Spin Configurations	94
6	THREE-DIMENSIONAL FORMULATION FOR THE NUCLEON-DEUTERON BREAK-UP PROCESS	105
6.1	Review on the Nucleon-Deuteron Break-Up Process	106
6.1.1	Kinematics of the Three-Nucleon System in Laboratory and Center of Mass Reference Frames	106
6.1.2	Break-up Amplitude and the Faddeev's Equation	108
6.1.3	Cross Section and Spin Observables	109
6.2	Three-Dimensional Nucleon-Deuteron Break-Up Amplitude	112
6.3	Relativistic Kinematics	118
6.3.1	Maximum of Magnitude of Nucleon's Outgoing Momentum	118
6.3.2	Jacobi Momenta	120
6.3.3	S-Matrix and Cross Section	125
7	APPLICATION TO THE PROTON-NEUTRON CHARGE EXCHANGE REACTION	131
7.1	Comparison with Partial-Wave Calculations	132
7.2	Contributions from the Rescattering Terms	159
7.3	Effects of Relativity	177
8	SUMMARY AND OUTLOOK	223
	APPENDICES	229
	A THE ROTATION MATRIX	231
	B THE Ω OPERATORS	233

C	THE BONN ONE-BOSON-EXCHANGE POTENTIAL	237
D	THE ARGONNE AV18 POTENTIAL	243
E	NUMERICAL REALIZATION FOR NN SCATTERING	247
	E.1 Integration	247
	E.2 Principal Value Singularity	250
	E.3 Solving the Lippmann-Schwinger Equation for the T-Matrix	250
F	TWO SUCCESSIVE ROTATIONS	253
	F.1 Two Successive Rotations in Momentum Space	254
	F.2 Two Successive Rotations in Spin Space	257
G	NUMERICAL REALIZATION FOR THE PROTON-NEUTRON CHARGE EXCHANGE REACTION	261
	G.1 Momentum Addition	262
	G.2 Integration	263
	G.3 Interpolation	263
	G.4 Momenta and Energy Ranges for the Interpolation	267
	Bibliography	273
	Acknowledgement	277
	Lebenslauf	279

Chapter 1

INTRODUCTION

The goal of this work is the development of a practical and accurate scheme for few-body calculations, which does not rely on the traditionally preferred method of angular momentum decomposition.

The vast information about the nuclear (or strong) interaction has been and still is obtained with collision experiments. Because of the short range of the nuclear interaction and thus the small distances involved, collision experiments testing the short-range part of the strong force should be carried out at higher energies. Experimental efforts at the Kernfysikalische Versneller Institute (KVI) in the Netherlands, the Research Center for Nuclear Physics (RCNP) in Japan, the Cooler Synchrotron (COSY) in Germany, the Indiana University Cyclotron Facility (IUCF) in the United States, and other laboratories concentrate on probing the nuclear force in a three-nucleon (3N) context to find out if the strong force acts only between two nucleons at a time or if there is a significant contribution of a force acting directly between three nucleons.

Theory and calculations of three nucleon systems have a long history. After the first formulation of a basic scheme by Faddeev [1] and a reformulation in terms of triads of Lippmann-Schwinger equations [2], the first applications were carried out by Amado [3], calculating low energy neutron-deuteron (nd) scattering in a simple model based on rank 1 Yamaguchi S-wave nucleon-nucleon (NN) potentials [4]. This was followed up by allowing for higher rank NN potentials, which however did not yet include the full complexity of NN forces. The restriction to finite rank NN forces leads to a simplification, namely that the amplitude in the Faddeev equations depended only on one continuous variable. This was of course highly desirable at that time due to the limited computer resources. For a list of references on those early investigations see Ref. [5].

With the advent of more realistic NN forces, like e.g. the Paris [6], Nijmegen [7], Bonn [8] and Argonne [9] potentials, which were local or non-local in nature and therefore quite

different from finite rank forces, the challenge was to employ them directly, which then leads to a dependence on two continuous variables in the amplitudes of the 3N Faddeev equations. Pioneering calculations along that line were carried out by the Utrecht group [10]. All these investigations were concerned with low energies including the 3N bound states. Here it was most natural to take advantage of conserved quantities in the 3N system, e.g. the conservation of the total angular momentum, and set up the calculations in a basis, where the basis states are eigenstates of the total angular momentum. Especially at low energies, only a few angular momenta (often only s-waves) are expected to contribute to observables due to the angular momentum barrier.

During the last two decades calculations of nd scattering based on momentum space Faddeev equations experienced enormous improvement and refinement. It is fair to state that below 200 MeV projectile energy the momentum space Faddeev equations for 3N scattering now can be solved with very high accuracy for the most modern two and three nucleon forces. A summary of these achievements is given in Ref. [5].

During the same two decades experimental facilities with higher beam energy were built, and older facilities were either upgraded or seized to exist, with a few exceptions. This is a natural trend if one wants to probe the strong interaction at shorter distances. However, this trend to ever higher beam energies has a fatal consequence for the traditional 3N scattering calculations carried out in a partial wave (PW) truncated basis. Working in an angular momentum basis means that continuous angle variables are replaced by discrete orbital angular momentum quantum numbers. This reduces the number of continuous variables, which have to be discretized in a numerical treatment. For low projectile energies this procedure appears physically justified due to arguments related to the centrifugal barrier. Now going to high energies the algebraic and algorithmic work carried out in a PW decomposition can be quite involved when solving Faddeev equations. The most crucial fact however is, that if one wants to consider 3N scattering at a few hundred MeV projectile energy, the number of partial waves needed to achieve numerical convergence proliferates, and limitations with respect to computational feasibility and accuracy are being reached. At this point, the method of PW decomposition loses its physical transparency, and using angular variables directly becomes more appealing. It appears therefore natural to abandon PW representations completely and work directly with vector variables. As an aside, this is common practice in bound state calculations based on variational [11] and Green's Function Monte Carlo (GFMC) methods [12], which are carried out in coordinate space.

A momentum space approach along this vein was pioneered for a system of three bosons in Refs. [13, 14], where the momentum space Faddeev equations were solved for

the bound as well as the scattering state.

The aim of this work is more ambitious. We want to employ realistic NN interactions in our calculations. This means we have to incorporate spin degrees of freedom into a formulation of the Faddeev equations. Since the first step to any Faddeev calculation is the solution of the Lippmann-Schwinger (LS) equation for the two-nucleon T-matrix, this will have to be our first focal point.

Although there are already suggestions in the literature how to solve the two-body LS equations for realistic NN potentials without PW decomposition [15, 16, 17] we prefer to develop our own scheme which will be consistent with our later use of the NN T-matrix in 3N scattering calculation. We choose an approach based on the total helicity of the NN system as spin variable. From our point of view this is the preferred starting point to later progress to the 3N system. In this work we will not solve the full Faddeev equations for three nucleons, but rather consider the first term in the multiple scattering series built up by the Faddeev equations, and concentrate on break-up observables. Of particular interest are the spin-transfer coefficients in the (p,n) charge exchange reaction on the deuteron, which recently has been measured at IUCF [18] and RCNP [19]. Since these measurements are carried out at ‘intermediate energies’, i.e. 197 MeV and 346 MeV, the first assumption is that it may be sufficient to consider only the first order term. However, since the projectile energies are already high, we will also consider relativistic kinematic effects.

The thesis is organized as follows. Chapter 2 is written only to provide a short review of NN scattering. There some definitions and quantities are introduced, which are used in the next chapters.

In Chapter 3 we begin to develop the formulation for NN scattering based on vector momenta and helicity eigenstates, in the following called momentum-helicity basis states and the formulation is shortly called the 3D formulation. These basis states are defined with all necessary symmetry properties for fermion states. We then define six invariant operators characterizing any Galilei invariant NN potential, which is invariant under parity, time-reversal and rotations. For our application we consider two different NN potentials, the Argonne V18 (AV18) potential [20] as representative of the most modern NN potentials describing the NN data below 350 MeV with a χ^2/datum of ≈ 1 , and the Bonn-B potential [21] as representative for a meson exchange potential. For our work it is crucial that the potentials can be given either in direct operator form (AV18) or as Feynman diagrams (Bonn-B). Other modern potentials, which are fitted by parameters that depend on partial waves, are not suited for our formulation.

In Chapter 4 we show results from our calculations for NN scattering and discuss

the NN potentials in some detail. We compare some NN phase shifts obtained from the 3D calculations to those obtained from traditional PW calculations. We also show the behavior of the T-matrix elements and compare NN scattering observables to data and to the results of the PW calculations.

In Chapter 5 we formulate a 3D approach for the deuteron using momentum-helicity basis states. We derive two formulations. The first is based on a 3D ansatz, while the second one is a mixture of 3D and PW techniques. For both formulations we introduce a set of 3D deuteron wave function components and derive the deuteron eigenvalue equation. In the second formulation we derive the deuteron wave function in operator form. Projected onto the momentum-helicity basis states this lead to the 3D deuteron wave function components with analytic angular behavior. We perform calculations for both formulations and connect the numerical results to standard PW calculations. Finally, using the deuteron wave function in operator form, we investigate some spin configurations of the two nucleons inside the deuteron.

In Chapter 6 we formulate the nucleon-deuteron (Nd) break-up process in a 3D, non-relativistic Faddeev scheme. We derive the leading term of the full Nd break-up amplitude in the momentum-helicity basis. The leading term is given in terms of the T-matrix elements. Then we include relativistic kinematics in the formulation and derive the cross section according to relativistic scattering theory. The application of relativistic kinematics affects not only the phase space factor of the cross section but also the leading term of the full Nd break-up amplitude.

In Chapter 7 we show results from our 3D calculations for the (p,n) charge exchange reaction in the inclusive proton-deuteron (pd) break-up process. In this process a proton is directed towards a deuteron, which then breaks up, and finally the neutron is detected, while the two protons are not detected. We show the spin averaged differential cross section and some spin observables, which are the neutron polarization, the proton analyzing power and the polarization transfer coefficients. We begin with comparisons to the PW calculations at various energies below 200 MeV and test the convergence of the PW calculations for energies up to $\simeq 200$ MeV. Next we compare at $\simeq 200$ MeV to the full Faddeev PW calculations, which include also the rescattering terms of the Nd break-up amplitude, and check the importance of rescattering terms at energies $\simeq 200$ MeV. Unfortunately for energies higher than 200 MeV there is no full Faddeev PW calculation to compare with. Therefore, we compare our results up to $\simeq 500$ MeV directly to the data. Last but not least we compare between our 3D calculations with and without relativistic kinematics, and find that as expected the importance of the relativistic kinematics increases with increasing energy. Finally we summarize in Chapter 8.

Chapter 2

SCATTERING OF TWO NUCLEONS

This chapter is not meant as a thorough presentation of scattering theory for two nucleons or even more general for two particles since that is already given at many places such as quantum mechanics textbooks and those specializing in scattering processes, for example Ref. [22]. In fact, compact presentations of two nucleon (2N) scattering can be found in Refs. [23, 24, 25]. Hence, the presentation here will be even more compact and this chapter is meant for practical purpose and to give a short summary of necessary formulas. In addition, definitions of some terminologies and quantities used in the next chapters can be found here.

2.1 Kinematics of the Two-Nucleon System in Laboratory and Center of Mass Reference Frames

A proton and a neutron are commonly called nucleon. Though the proton mass $m_p = 938.272$ MeV differs from the neutron mass $m_n = 939.56533$ MeV, this difference is relatively small ($\sim 0.14\%$). Therefore, the 'nucleon mass' m may be given by the average of m_p and m_n .

Let \mathbf{k}_i and \mathbf{k}'_i be the nucleon's momentum in the laboratory reference frame (laboratory frame) in initial and final state, respectively, where $i = 1, 2$ indicates the i^{th} nucleon. The corresponding nonrelativistic energies are denoted by E_i and E'_i , respectively. Assuming nucleon 1 is the projectile and nucleon 2 is the target ($\mathbf{k}_2 = 0$), the momentum situation can be displayed by Fig. 2.1, where θ_{lab} is the scattering angle in the laboratory frame. The figure also shows quantities belonging to the center of mass reference frame (c.m. frame),

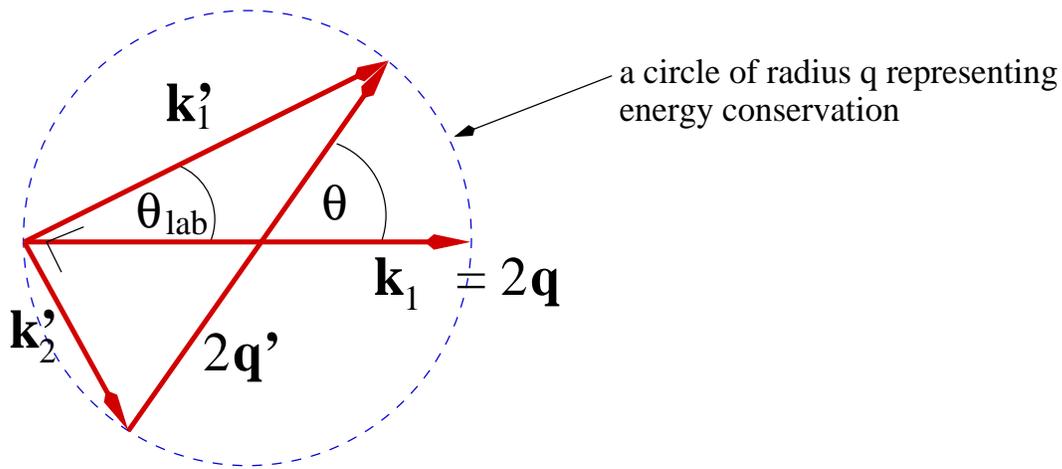


Figure 2.1: The initial and final momenta, both in laboratory and c.m. frames, in a 2N scattering process, where nucleon 1 acts as the projectile and nucleon 2 as the target ($\mathbf{k}_2 = 0$). The circle of radius q represents the energy conservation.

i.e. the scattering angle θ and the relative momentum between the two nucleons in initial and final states, $\mathbf{q} = \frac{1}{2}\mathbf{k}_1$ and $\mathbf{q}' = \frac{1}{2}(\mathbf{k}'_1 - \mathbf{k}'_2)$, respectively. It is clear that $\theta = 2\theta_{lab}$.

The total energy in the laboratory frame (E_{lab}) and that in the c.m. frame (E_{cm}) are

$$E_{lab} = E_1 = E'_1 + E'_2 \quad (2.1)$$

$$E_{lab} = \frac{k_1^2}{2m} = \frac{k_1'^2}{2m} + \frac{k_2'^2}{2m} \quad (2.2)$$

$$E_{cm} = \frac{q^2}{2\mu} = \frac{q'^2}{m} = \frac{q'^2}{m}, \quad (2.3)$$

where $\mu = \frac{1}{2}m$ is the reduced mass of the 2N system. E_{cm} together with the energy of motion of the center of mass of the two nucleons sum up to E_{lab} and consequently we can get the relation between E_{lab} and E_{cm}

$$\begin{aligned} E_{lab} &= \frac{(\mathbf{k}'_1 + \mathbf{k}'_2)^2}{4m} + E_{cm} \\ &= \frac{k_1^2}{4m} + E_{cm} \\ &= \frac{1}{2}E_{lab} + E_{cm} \\ &= 2E_{cm}, \end{aligned} \quad (2.4)$$

which can also be directly seen from the fact that $\mathbf{k}_1 = 2\mathbf{q}$. Note that this relation between E_{lab} and E_{cm} is correct if one of the two nucleons is initially (or finally) at rest.

2.2 Scattering Matrix and Lippmann-Schwinger Equation

The essential information of a nucleon-nucleon (NN) scattering process is contained in the scattering matrix. There are T-matrix, S-matrix, M-matrix and these matrices are related to each other as

$$S = 1 - 2\pi i \delta(E' - E) T \quad (2.5)$$

$$M = -\mu(2\pi)^2 T. \quad (2.6)$$

The delta function in the expression for the S-matrix indicates that the S-matrix is an on-the-energy-shell (on-shell) quantity whereas the other two scattering matrices are not affected by this restriction and therefore have off-shell as well as on-shell properties. We solve for the T-matrix in our NN scattering calculations and later use it as input for our 3N calculations, where the T-matrix appears as an off-shell quantity.

The T-matrix obeys the equation

$$T = V + V G_0 T, \quad (2.7)$$

which is the Lippmann-Schwinger Equation (LSE) for the T-matrix. V is the matrix operator of the NN potential, $G_0(z) = (z - H_0)^{-1}$ is the free propagator with H_0 being the free Hamiltonian and z a complex number. The scattering wave is spreading out from the scattering center, and for an outgoing wave the corresponding free propagator is $G_0^+(E) \equiv \lim_{\epsilon \rightarrow 0} G_0(E + i\epsilon)$, where E is the energy at which the scattering occurs and the limit can be understood as to bring z close to the physical spectrum of H_0 .

The T-matrix element is defined as

$$T(\mathbf{q}', \alpha'; \mathbf{q}, \alpha) \equiv \langle \mathbf{q}', \alpha' | T | \mathbf{q}, \alpha \rangle, \quad (2.8)$$

with α, α' being the discrete quantum numbers considered, like spin and isospin, and $|\mathbf{q}, \alpha\rangle, |\mathbf{q}', \alpha'\rangle$ representing the initial, final state of the 2N system, respectively. A similar definition applies also to the NN potential matrix element

$$V(\mathbf{q}', \alpha'; \mathbf{q}, \alpha) \equiv \langle \mathbf{q}', \alpha' | V | \mathbf{q}, \alpha \rangle. \quad (2.9)$$

With the 2N states $|\mathbf{q}, \alpha\rangle$ being complete

$$\sum_{\alpha} \int d\mathbf{q} |\mathbf{q}, \alpha\rangle \langle \mathbf{q}, \alpha| = 1, \quad (2.10)$$

it is straightforward that the LSE for the T-matrix element, which is the main equation in the calculations, is given by

$$T(\mathbf{q}', \alpha'; \mathbf{q}, \alpha) = V(\mathbf{q}', \alpha'; \mathbf{q}, \alpha) + \sum_{\alpha''} \int d\mathbf{q}'' V(\mathbf{q}', \alpha'; \mathbf{q}'', \alpha'') G_0^+(E_q) T(\mathbf{q}'', \alpha''; \mathbf{q}, \alpha), \quad (2.11)$$

with

$$G_0^+(E_q) = \lim_{\epsilon \rightarrow 0} \frac{1}{E_q + i\epsilon - E_{q''}} \quad E_q \equiv \frac{q^2}{m} \quad E_{q''} \equiv \frac{q''^2}{m}. \quad (2.12)$$

2.3 Cross Section and Spin Observables

Here we specify the quantum number α in the 2N state $|\mathbf{q}, \alpha\rangle$ as the magnetic spin quantum numbers of both nucleons

$$|\mathbf{q}, \alpha\rangle = |\mathbf{q}, m_{s1} m_{s2}\rangle, \quad (2.13)$$

with $m_{si} = \pm\frac{1}{2}$ ($i = 1, 2$). Thus, there are four spin states which constitute a complete basis, in which any spin state of the two nucleons can be given. A general pure state $|\mathbf{q}, n\rangle$ can be written as

$$|\mathbf{q}, n\rangle = \sum_{m_{s1}, m_{s2} = -\frac{1}{2}}^{\frac{1}{2}} a^{(n)}(m_{s1}, m_{s2}) |\mathbf{q}, m_{s1} m_{s2}\rangle. \quad (2.14)$$

With regard to spin the state $|\mathbf{q}, n\rangle$ is a vector of four components and the T-matrix element given in Eq. (2.8) is a 4 x 4 matrix. The general spin operator for such a state is also a 4 x 4 matrix and may be chosen as a product of two 2 x 2 matrices

$$\sigma_\mu^{(1)} \sigma_\nu^{(2)} \equiv \sigma_\mu^{(1)} \otimes \sigma_\nu^{(2)}, \quad (\mu, \nu = 0, 1, 2, 3), \quad (2.15)$$

with σ_0 and σ_i ($i = 1, 2, 3$) being a matrix of one and the Pauli matrices, respectively:

$$\sigma_0 = \begin{pmatrix} 1 & 0 \\ 0 & 1 \end{pmatrix}, \quad \sigma_1 = \begin{pmatrix} 0 & 1 \\ 1 & 0 \end{pmatrix}, \quad \sigma_2 = \begin{pmatrix} 0 & -i \\ i & 0 \end{pmatrix}, \quad \sigma_3 = \begin{pmatrix} 1 & 0 \\ 0 & -1 \end{pmatrix}, \quad (2.16)$$

and the upper indices 1, 2 denoting the nucleon on the state of which the σ_μ operator works.

In experiments we deal not only with two nucleons but many more in the beam and the target. Therefore, the state is a mixed state of pure 2N states as given in of Eq. (2.14), and the expectation value of an observable $\langle O \rangle$ is calculated by mean of a density matrix ρ

$$\rho \equiv \sum_n |n\rangle p_n \langle n|, \quad (2.17)$$

where p_n is the normalized probability of the n^{th} pure spin state according to Eq. (2.14)

$$|n\rangle \equiv \sum_{m_{s1}, m_{s2} = -\frac{1}{2}}^{\frac{1}{2}} a^{(n)}(m_{s1}, m_{s2}) |m_{s1} m_{s2}\rangle. \quad (2.18)$$

For instance, in the final state:

$$\langle O \rangle = \frac{\text{Tr} \{ \rho_f O \}}{\text{Tr} \{ \rho_f \}}, \quad (2.19)$$

with

$$\begin{aligned} \rho_f &= \text{final density matrix} \\ &= M \rho_i M^\dagger \\ \rho_i &= \text{initial density matrix.} \end{aligned} \quad (2.20)$$

Using Eq. (2.19) one derives the expression for the expectation value of a general spin observable $\langle \sigma_\mu^{(1)} \sigma_\nu^{(2)} \rangle_f$ in the final state in relation to the values $\langle \sigma_\alpha^{(1)} \sigma_\beta^{(2)} \rangle_i$ in the initial state

$$I \langle \sigma_\mu^{(1)} \sigma_\nu^{(2)} \rangle_f = \frac{1}{4} \sum_{\alpha, \beta} \langle \sigma_\alpha^{(1)} \sigma_\beta^{(2)} \rangle_i \text{Tr} \{ M \sigma_\alpha^{(1)} \sigma_\beta^{(2)} M^\dagger \sigma_\mu^{(1)} \sigma_\nu^{(2)} \}, \quad (2.21)$$

where I is the differential cross section summed over all possible final spin states

$$I = \sum_j \frac{d\sigma_j}{d\Omega} = \frac{\text{Tr} \{ \rho_f \}}{\text{Tr} \{ \rho_i \}} = \frac{1}{4} \sum_{\alpha, \beta} \langle \sigma_\alpha^{(1)} \sigma_\beta^{(2)} \rangle_i \text{Tr} \{ M \sigma_\alpha^{(1)} \sigma_\beta^{(2)} M^\dagger \} \quad (2.22)$$

(in the last equality Eq. (2.21) is applied again).

The simplest case is if the beam and target are unpolarized and no spin measurements in the final state are made. In this case one measures the spin averaged differential cross section

$$I_0 = \frac{1}{4} \text{Tr} \{ M M^\dagger \}. \quad (2.23)$$

The spin projections on a certain axis must be specified and therefore unit vectors are needed. Since there are two reference frames - laboratory and c.m. frames - two sets of unit vectors are defined, one set for each frame. But as can be checked in Ref. [25] for the 2N system the two sets are the same:

$$\text{unit vectors for the initial state} : \begin{cases} \text{c.m. frame} & : \hat{\mathbf{q}}, \hat{\mathbf{N}}, \hat{\mathbf{N}} \times \hat{\mathbf{q}} \\ \text{laboratory frame} & : \hat{\mathbf{l}}, \hat{\mathbf{n}}, \hat{\mathbf{s}} \end{cases} \quad (2.24)$$

$$\text{unit vectors for the final state} : \begin{cases} \text{c.m. frame} & : \hat{\mathbf{P}}, \hat{\mathbf{N}}, \hat{\mathbf{K}} \\ \text{laboratory frame} & : \hat{\mathbf{l}}', \hat{\mathbf{n}}', \hat{\mathbf{s}}' \end{cases} \quad (2.25)$$

with

$$\hat{\mathbf{n}} = \hat{\mathbf{n}}' \equiv \frac{\hat{\mathbf{k}}_1 \times \hat{\mathbf{k}}_1'}{|\hat{\mathbf{k}}_1 \times \hat{\mathbf{k}}_1'|} = \hat{\mathbf{N}} \equiv \frac{\mathbf{q} \times \mathbf{q}'}{|\mathbf{q} \times \mathbf{q}'|} \quad (2.26)$$

$$\hat{\mathbf{l}} \equiv \hat{\mathbf{k}}_1 = \hat{\mathbf{q}} \quad (2.27)$$

$$\hat{\mathbf{s}} \equiv \hat{\mathbf{n}} \times \hat{\mathbf{l}} = \hat{\mathbf{N}} \times \hat{\mathbf{q}} \quad (2.28)$$

$$\hat{\mathbf{l}}' \equiv \hat{\mathbf{k}}_1' = \hat{\mathbf{P}} \equiv \frac{\mathbf{q} + \mathbf{q}'}{|\mathbf{q} + \mathbf{q}'|} \quad (2.29)$$

$$\hat{\mathbf{s}}' \equiv \hat{\mathbf{n}}' \times \hat{\mathbf{l}}' = \hat{\mathbf{K}} \equiv \frac{\mathbf{q}' - \mathbf{q}}{|\mathbf{q}' - \mathbf{q}|}. \quad (2.30)$$

In connection with a Cartesian coordinate system the beam's momentum \mathbf{k}_1 is set typically to point along the positive z-axis and the scattered nucleon's momentum \mathbf{k}_1' is in the xz-plane. Thus, the scattering takes places in the xz-plane and the unit vectors are

$$\hat{\mathbf{l}} = \begin{pmatrix} 0 \\ 0 \\ 1 \end{pmatrix}, \quad \hat{\mathbf{s}} = \begin{pmatrix} 1 \\ 0 \\ 0 \end{pmatrix}, \quad \hat{\mathbf{n}} = \hat{\mathbf{n}}' = \begin{pmatrix} 0 \\ 1 \\ 0 \end{pmatrix}, \quad (2.31)$$

$$\hat{\mathbf{l}}' = \begin{pmatrix} \sin \theta_{lab} \\ 0 \\ \cos \theta_{lab} \end{pmatrix}, \quad \hat{\mathbf{s}}' = \begin{pmatrix} \cos \theta_{lab} \\ 0 \\ -\sin \theta_{lab} \end{pmatrix}.$$

According to Eq. (2.21) there seems to be $16 \times 16 = 256$ possible initial-to-final spin transitions in a NN scattering process. Rotational, parity, time-reversal and isospin invariances (the last one together with parity invariance lead to spin invariance), however, forbid many transitions and moreover cause some permitted transitions to be related to each other. Under these invariances the scattering matrix M can be expressed in terms of a few parameters called Wolfenstein parameters [26, 23] (a, c, m, g, h), which depend on the magnitudes q' of final and q of initial relative momenta as well as the angle between the two momenta \mathbf{q}' and \mathbf{q}

$$\begin{aligned} M &= a + c(\boldsymbol{\sigma}^{(1)} + \boldsymbol{\sigma}^{(2)}) \cdot \hat{\mathbf{N}} + m(\boldsymbol{\sigma}^{(1)} \cdot \hat{\mathbf{N}})(\boldsymbol{\sigma}^{(2)} \cdot \hat{\mathbf{N}}) \\ &\quad + (g + h)(\boldsymbol{\sigma}^{(1)} \cdot \hat{\mathbf{P}})(\boldsymbol{\sigma}^{(2)} \cdot \hat{\mathbf{P}}) + (g - h)(\boldsymbol{\sigma}^{(1)} \cdot \hat{\mathbf{K}})(\boldsymbol{\sigma}^{(2)} \cdot \hat{\mathbf{K}}) \end{aligned} \quad (2.32)$$

$$a = \frac{1}{4} Tr \{ M \} \quad (2.33)$$

$$c = \frac{1}{8} Tr \{ M \sigma_y^{(1)} + M \sigma_y^{(2)} \} \quad (2.34)$$

$$m = \frac{1}{4} Tr \{ M \sigma_y^{(1)} \sigma_y^{(2)} \} \quad (2.35)$$

$$g = \frac{1}{8} \text{Tr} \{ M \sigma_x^{(1)} \sigma_x^{(2)} + M \sigma_z^{(1)} \sigma_z^{(2)} \} \quad (2.36)$$

$$h = \frac{1}{8} \text{Tr} \{ [-M \sigma_x^{(1)} \sigma_x^{(2)} + M \sigma_z^{(1)} \sigma_z^{(2)}] \cos \theta + [M \sigma_x^{(1)} \sigma_z^{(2)} + M \sigma_z^{(1)} \sigma_x^{(2)}] \sin \theta \} \quad (2.37)$$

Note that these expressions for the Wolfenstein parameters are for the chosen xz-scattering frame, see Eq. (2.31). The NN scattering observables can be calculated using M directly or the Wolfenstein parameters.

Finally, we close this chapter by showing briefly seven typical types of experiments and the corresponding spin observables. Comprehensive descriptions of these experiments can be found in Ref. [23]. The experiments are denoted by the reactions as

1. $N2(N1, N1)N2$
2. $N2(N1, \vec{N}1)N2$
3. $N2(\vec{N}1, N1)N2$
4. $N2(\vec{N}1, \vec{N}1)N2$
5. $N2(\vec{N}1, N1)\vec{N}2$
6. $N2(N1, \vec{N}1)\vec{N}2$
7. $\vec{N}2(\vec{N}1, N1)N2$,

where $N1$ and $N2$ stand for nucleon 1 (the projectile) and nucleon 2 (the target), respectively, the little arrows over $N1$ or $N2$ mean that the corresponding nucleon is polarized or that the polarization of that nucleon is measured. Let us take for example the fifth experiment: $N2(\vec{N}1, N1)\vec{N}2$. This reaction means that a polarized projectile ($\vec{N}1$) is directed to an unpolarized target ($N2$) and finally the polarization of the recoil nucleon ($\vec{N}2$) is measured. The polarization of the scattered nucleon ($N1$) is not measured. Note that processes 4 and 5 are only distinguishable for a np system.

In the first experiment the beam and target are unpolarized and no spin measurement on the outgoing nucleons are made. One measures only the spin averaged cross section

$$\begin{aligned} I_0 &= \frac{1}{4} \text{Tr} \{ M M^\dagger \} \\ &= |a|^2 + |m|^2 + 2|c|^2 + 2|g|^2 + 2|h|^2. \end{aligned} \quad (2.38)$$

In the second experiment the beam and target are unpolarized. The polarization of the scattered nucleon is of interest and therefore after the process one measures the spin direction of this nucleon. According to the general formula for spin observables (Eq. (2.21)) the polarization $\mathbf{P}_0 = \langle \boldsymbol{\sigma}^{(1)} \rangle = \langle \boldsymbol{\sigma}^{(1)} \sigma_0^{(2)} \rangle$ of the scattered nucleon is

$$\begin{aligned} \mathbf{P}_0 &= \frac{1}{4I_0} \text{Tr} \{ M M^\dagger \boldsymbol{\sigma}^{(1)} \} \\ &= \hat{\mathbf{n}} \frac{1}{4I_0} \text{Tr} \{ M M^\dagger \sigma_n^{(1)} \} \\ &= \hat{\mathbf{n}} \frac{2 \text{Re} \{ (a + m)c^* \}}{I_0}, \end{aligned} \quad (2.39)$$

where I_0 is the spin averaged cross section given in Eq. (2.38). Parity invariance affects the process such that the polarization must be normal to the scattering plane.

The third experiment is to measure the asymmetry A_{LR} defined as

$$A_{LR} \equiv \frac{I_L - I_R}{I_L + I_R}, \quad (2.40)$$

where $I_L = I(\theta, \phi)$ and $I_R = I(\theta, \phi + \pi)$ are the left-scattering and right-scattering cross sections, respectively. A polarized beam is directed to an unpolarized target. Due to parity invariance a contribution to the cross section arises only if the polarization is normal to the scattering plane. The cross section is

$$\begin{aligned} I &= \frac{1}{4} \sum_{\alpha=0}^3 \langle \sigma_{\alpha}^{(1)} \rangle_i Tr \{ M \sigma_{\alpha}^{(1)} M^{\dagger} \} \\ &= I_0 + \frac{1}{4} \mathbf{P}_i \cdot \hat{\mathbf{n}} Tr \{ M(\boldsymbol{\sigma}^{(1)} \cdot \hat{\mathbf{n}}) M^{\dagger} \} \end{aligned} \quad (2.41)$$

and the left- and right-scattering cross sections are

$$I_L = I_0 + \frac{1}{4} \mathbf{P}_i \cdot \hat{\mathbf{n}} Tr \{ M(\boldsymbol{\sigma}^{(1)} \cdot \hat{\mathbf{n}}) M^{\dagger} \} \quad (2.42)$$

$$I_R = I_0 - \frac{1}{4} \mathbf{P}_i \cdot \hat{\mathbf{n}} Tr \{ M(\boldsymbol{\sigma}^{(1)} \cdot \hat{\mathbf{n}}) M^{\dagger} \}. \quad (2.43)$$

Therefore,

$$\begin{aligned} A_{LR} &= \frac{\mathbf{P}_i \cdot \hat{\mathbf{n}} Tr \{ M(\boldsymbol{\sigma}^{(1)} \cdot \hat{\mathbf{n}}) M^{\dagger} \}}{4I_0} \\ &= \mathbf{P}_i \cdot \hat{\mathbf{n}} A_n, \end{aligned} \quad (2.44)$$

with

$$\begin{aligned} A_n &= \frac{1}{4I_0} Tr \{ M(\boldsymbol{\sigma}^{(1)} \cdot \hat{\mathbf{n}}) M^{\dagger} \} \\ &= \frac{2Re\{(a+m)c^*\}}{I_0} \\ &= P_0. \end{aligned} \quad (2.45)$$

This quantity A_n called analyzing power is often denoted by A_y , since $\hat{\mathbf{n}} = \hat{y}$ for the typical scattering frame given in Eq. (2.31).

In experiment 4 one starts with a polarized beam and an unpolarized target and finally measures the polarization of the scattered nucleon, $\mathbf{P}_f = \langle \boldsymbol{\sigma}^{(1)} \rangle$

$$\begin{aligned} I\mathbf{P}_f &= \frac{1}{4} \sum_{\alpha=0}^3 \langle \sigma_{\alpha}^{(1)} \rangle_i Tr \{ M \sigma_{\alpha}^{(1)} M^{\dagger} \boldsymbol{\sigma}^{(1)} \} \\ &= I_0 \mathbf{P}_0 + \frac{1}{4} \mathbf{P}_i \cdot Tr \{ M \boldsymbol{\sigma}^{(1)} M^{\dagger} \boldsymbol{\sigma}^{(1)} \} \\ &= I_0 \left\{ \hat{\mathbf{n}} [P_0 + D(\mathbf{P}_i \cdot \hat{\mathbf{n}})] + \hat{\mathbf{l}}' [A'(\mathbf{P}_i \cdot \hat{\mathbf{l}}) + R'(\mathbf{P}_i \cdot \hat{\mathbf{s}})] \right. \\ &\quad \left. + \hat{\mathbf{s}}' [A(\mathbf{P}_i \cdot \hat{\mathbf{l}}) + R(\mathbf{P}_i \cdot \hat{\mathbf{s}})] \right\}. \end{aligned} \quad (2.46)$$

Here we meet other spin observables, summarized in the depolarization tensor D_{ij} , which is defined as

$$I_0 D_{ij} \equiv \frac{1}{4} \text{Tr} \left\{ M(\boldsymbol{\sigma}^{(1)} \cdot \hat{\mathbf{j}}) M^\dagger(\boldsymbol{\sigma}^{(1)} \cdot \hat{\mathbf{i}}) \right\}, \quad (2.47)$$

and the observables D, R, R', A, A' appearing in the polarization \vec{P}_f are

$$\begin{aligned} I_0 D \equiv I_0 D_{nn} &= \frac{1}{4} \text{Tr} \left\{ M(\boldsymbol{\sigma}^{(1)} \cdot \hat{\mathbf{n}}) M^\dagger(\boldsymbol{\sigma}^{(1)} \cdot \hat{\mathbf{n}}) \right\} \\ &= |a|^2 + |m|^2 + 2|c|^2 - 2|g|^2 - 2|h|^2 \end{aligned} \quad (2.48)$$

$$\begin{aligned} I_0 R \equiv I_0 D_{s's} &= \frac{1}{4} \text{Tr} \left\{ M(\boldsymbol{\sigma}^{(1)} \cdot \hat{\mathbf{s}}) M^\dagger(\boldsymbol{\sigma}^{(1)} \cdot \hat{\mathbf{s}}') \right\} \\ &= (|a|^2 - |m|^2 - 4\text{Re}\{gh^*\}) \cos \frac{\theta}{2} - 2\text{Im}\{(a-m)^*c\} \sin \frac{\theta}{2} \end{aligned} \quad (2.49)$$

$$\begin{aligned} I_0 R' \equiv I_0 D_{l's} &= \frac{1}{4} \text{Tr} \left\{ M(\boldsymbol{\sigma}^{(1)} \cdot \hat{\mathbf{s}}) M^\dagger(\boldsymbol{\sigma}^{(1)} \cdot \hat{\mathbf{l}}') \right\} \\ &= (|a|^2 - |m|^2 + 4\text{Re}\{gh^*\}) \sin \frac{\theta}{2} + 2\text{Im}\{(a-m)^*c\} \cos \frac{\theta}{2} \end{aligned} \quad (2.50)$$

$$\begin{aligned} I_0 A \equiv I_0 D_{s'l} &= \frac{1}{4} \text{Tr} \left\{ M(\boldsymbol{\sigma}^{(1)} \cdot \hat{\mathbf{l}}) M^\dagger(\boldsymbol{\sigma}^{(1)} \cdot \hat{\mathbf{s}}') \right\} \\ &= -(|a|^2 - |m|^2 - 4\text{Re}\{gh^*\}) \sin \frac{\theta}{2} - 2\text{Im}\{(a-m)^*c\} \cos \frac{\theta}{2} \end{aligned} \quad (2.51)$$

$$\begin{aligned} I_0 A' \equiv I_0 D_{l'l} &= \frac{1}{4} \text{Tr} \left\{ M(\boldsymbol{\sigma}^{(1)} \cdot \hat{\mathbf{l}}) M^\dagger(\boldsymbol{\sigma}^{(1)} \cdot \hat{\mathbf{l}}') \right\} \\ &= (|a|^2 - |m|^2 + 4\text{Re}\{gh^*\}) \cos \frac{\theta}{2} - 2\text{Im}\{(a-m)^*c\} \sin \frac{\theta}{2}. \end{aligned} \quad (2.52)$$

Experiment 5 is similar to experiment 4 and can be distinguished only in a np system. One starts with a polarized beam and an unpolarized target but finally one measures the polarization of the recoil nucleon $\mathbf{P}_f = \langle \boldsymbol{\sigma}^{(2)} \rangle$

$$\begin{aligned} I\mathbf{P}_f &= \frac{1}{4} \sum_{\alpha=0}^3 \langle \sigma_\alpha^{(1)} \rangle_i \text{Tr} \left\{ M \sigma_\alpha^{(1)} M^\dagger \boldsymbol{\sigma}^{(2)} \right\} \\ &= I_0 \mathbf{P}_0 + \frac{1}{4} \mathbf{P}_i \cdot \text{Tr} \left\{ M \boldsymbol{\sigma}^{(1)} M^\dagger \boldsymbol{\sigma}^{(2)} \right\} \\ &= I_0 \left\{ \hat{\mathbf{n}} [P_0 + D_t(\mathbf{P}_i \cdot \hat{\mathbf{n}})] + \hat{\mathbf{l}}' [A_t(\mathbf{P}_i \cdot \hat{\mathbf{l}}) + R_t(\mathbf{P}_i \cdot \hat{\mathbf{s}})] \right. \\ &\quad \left. + \hat{\mathbf{s}}' [A'_t(\mathbf{P}_i \cdot \hat{\mathbf{l}}) + R'_t(\mathbf{P}_i \cdot \hat{\mathbf{s}})] \right\} \end{aligned} \quad (2.53)$$

$$P_0 = \frac{1}{4I_0} \text{Tr} \left\{ M M^\dagger(\boldsymbol{\sigma}^{(2)} \cdot \hat{\mathbf{n}}) \right\} = \frac{2\text{Re}\{(a+m)c^*\}}{I_0}. \quad (2.54)$$

Here we have again new spin observables, summarized in the polarization-transfer tensor K_{ij} , which is defined as

$$I_0 K_{ij} \equiv \frac{1}{4} \text{Tr} \left\{ M(\boldsymbol{\sigma}^{(1)} \cdot \hat{\mathbf{j}}) M^\dagger(\boldsymbol{\sigma}^{(2)} \cdot \hat{\mathbf{i}}) \right\}, \quad (2.55)$$

and the observables $D_t, R_t, R'_t, A_t, A'_t$ appearing in the polarization \mathbf{P}_f are

$$\begin{aligned} I_0 D_t \equiv I_0 K_{nn} &= \frac{1}{4} Tr \left\{ M(\boldsymbol{\sigma}^{(1)} \cdot \hat{\mathbf{n}}) M^\dagger(\boldsymbol{\sigma}^{(2)} \cdot \hat{\mathbf{n}}) \right\} \\ &= 2(Re\{am^*\} + |c|^2 + |g|^2 - |h|^2) \end{aligned} \quad (2.56)$$

$$\begin{aligned} I_0 R_t \equiv I_0 K_{l's} &= \frac{1}{4} Tr \left\{ M(\boldsymbol{\sigma}^{(1)} \cdot \hat{\mathbf{s}}) M^\dagger(\boldsymbol{\sigma}^{(2)} \cdot \hat{\mathbf{l}}') \right\} \\ &= 2Re\{(a+m)g^* + (a-m)h^*\} \sin \frac{\theta}{2} + 4Im\{cg^*\} \cos \frac{\theta}{2} \end{aligned} \quad (2.57)$$

$$\begin{aligned} I_0 R'_t \equiv I_0 K_{s'l} &= \frac{1}{4} Tr \left\{ M(\boldsymbol{\sigma}^{(1)} \cdot \hat{\mathbf{s}}) M^\dagger(\boldsymbol{\sigma}^{(2)} \cdot \hat{\mathbf{s}}') \right\} \\ &= 2Re\{(a+m)g^* - (a-m)h^*\} \cos \frac{\theta}{2} - 4Im\{cg^*\} \sin \frac{\theta}{2} \end{aligned} \quad (2.58)$$

$$\begin{aligned} I_0 A_t \equiv -I_0 K_{ll} &= -\frac{1}{4} Tr \left\{ M(\boldsymbol{\sigma}^{(1)} \cdot \hat{\mathbf{l}}) M^\dagger(\boldsymbol{\sigma}^{(2)} \cdot \hat{\mathbf{l}}') \right\} \\ &= -2Re\{(a+m)g^* + (a-m)h^*\} \cos \frac{\theta}{2} + 4Im\{cg^*\} \sin \frac{\theta}{2} \end{aligned} \quad (2.59)$$

$$\begin{aligned} I_0 A'_t \equiv -I_0 K_{s'l} &= -\frac{1}{4} Tr \left\{ M(\boldsymbol{\sigma}^{(1)} \cdot \hat{\mathbf{l}}) M^\dagger(\boldsymbol{\sigma}^{(2)} \cdot \hat{\mathbf{s}}') \right\} \\ &= 2Re\{(a+m)g^* - (a-m)h^*\} \sin \frac{\theta}{2} + 4Im\{cg^*\} \cos \frac{\theta}{2}. \end{aligned} \quad (2.60)$$

Note the minus sign in the definitions for A_t and A'_t . These are the definitions given in Center for Nuclear Studies Data Analysis Center (CNS DAC, <http://gwdac.phys.gwu.edu/>). We take these definitions since later we compare with experimental data from this site. In Ref. [23] the definitions for A_t and A'_t have the opposite sign. In case of identical particles these expressions are the same as the ones given in Eqs. (2.48)-(2.52) if one replaces θ by $\pi - \theta$ (see for instance [23]).

In experiment 6 the beam and target are unpolarized. In the final state the spins of the two outgoing nucleons are simultaneously measured

$$\begin{aligned} I \langle \boldsymbol{\sigma}^{(1)} \boldsymbol{\sigma}^{(2)} \rangle_f &= \frac{1}{4} Tr \left\{ MM^\dagger \boldsymbol{\sigma}^{(1)} \boldsymbol{\sigma}^{(2)} \right\} \\ &= I_0 \left(C_{NN} \hat{\mathbf{N}} \hat{\mathbf{N}} + C_{PP} \hat{\mathbf{P}} \hat{\mathbf{P}} + C_{KK} \hat{\mathbf{K}} \hat{\mathbf{K}} + C_{KP} (\hat{\mathbf{P}} \hat{\mathbf{K}} + \hat{\mathbf{K}} \hat{\mathbf{P}}) \right). \end{aligned} \quad (2.61)$$

C_{ij} is called the spin correlation parameter and is defined as

$$I_0 C_{ij} \equiv \frac{1}{4} Tr \left\{ MM^\dagger (\boldsymbol{\sigma}^{(1)} \cdot \hat{\mathbf{i}}) (\boldsymbol{\sigma}^{(2)} \cdot \hat{\mathbf{j}}) \right\}. \quad (2.62)$$

Accordingly, $C_{NN}, C_{PP}, C_{KK}, C_{KP}$ are

$$I_0 C_{NN} = \frac{1}{4} Tr \left\{ MM^\dagger (\boldsymbol{\sigma}^{(1)} \cdot \hat{\mathbf{N}}) (\boldsymbol{\sigma}^{(2)} \cdot \hat{\mathbf{N}}) \right\} = 2(Re\{am^*\} + |c|^2 - |g|^2 + |h|^2) \quad (2.63)$$

$$I_0 C_{PP} = \frac{1}{4} Tr \left\{ MM^\dagger (\boldsymbol{\sigma}^{(1)} \cdot \hat{\mathbf{P}}) (\boldsymbol{\sigma}^{(2)} \cdot \hat{\mathbf{P}}) \right\} = 2Re\{(a-m)g^* + (a+m)h^*\} \quad (2.64)$$

$$I_0 C_{KK} = \frac{1}{4} Tr \left\{ MM^\dagger (\boldsymbol{\sigma}^{(1)} \cdot \hat{\mathbf{K}}) (\boldsymbol{\sigma}^{(2)} \cdot \hat{\mathbf{K}}) \right\} = 2Re\{(a-m)g^* - (a+m)h^*\} \quad (2.65)$$

$$I_0 C_{KP} = \frac{1}{4} Tr \left\{ MM^\dagger (\boldsymbol{\sigma}^{(1)} \cdot \hat{\mathbf{K}}) (\boldsymbol{\sigma}^{(2)} \cdot \hat{\mathbf{P}}) \right\} = -4Im\{ch^*\}. \quad (2.66)$$

It can be shown that $C_{PK} = C_{KP}$.

In the last experiment both the beam and target are polarized and no spin measurements are made in the final state. One measures the cross section

$$\begin{aligned} I &= \frac{1}{4} \sum_{\alpha, \beta} \langle \sigma_{\alpha}^{(1)} \sigma_{\beta}^{(2)} \rangle_i Tr \{ M \sigma_{\alpha}^{(1)} \sigma_{\beta}^{(2)} M^{\dagger} \} \\ &= I_0 (1 + 2P_{iy}A_y + P_{ixx}A_{xx} + P_{iyy}A_{yy} + P_{izz}A_{zz} - 2P_{ixz}A_{zx}). \end{aligned} \quad (2.67)$$

The indices are for the scattering frame given in Eq. (2.31). $P_{iy} = \langle \sigma_y^{(1)} \rangle_i = \langle \sigma_y^{(2)} \rangle_i$ and $P_{ikl} = \langle \sigma_k^{(1)} \sigma_l^{(2)} \rangle_i$ are the polarization and tensor polarization in initial state, respectively. A_y is the already shown analyzing power. The other observables are the spin correlation parameters A_{ij} 's, which are also called tensor analyzing powers defined as

$$A_{ij} \equiv \frac{1}{4I_0} Tr \{ M(\boldsymbol{\sigma}^{(1)} \cdot \hat{\mathbf{i}})(\boldsymbol{\sigma}^{(2)} \cdot \hat{\mathbf{j}})M^{\dagger} \}. \quad (2.68)$$

Accordingly, $A_{xx}, A_{yy}, A_{zz}, A_{zx}$ are

$$\begin{aligned} I_0 A_{xx} \equiv I_0 A_{ss} &= \frac{1}{4} Tr \{ M(\boldsymbol{\sigma}^{(1)} \cdot \hat{\mathbf{s}})(\boldsymbol{\sigma}^{(2)} \cdot \hat{\mathbf{s}})M^{\dagger} \} \\ &= 2Re\{(a-m)g^* - (a+m)h^* \cos \theta\} + 4Im\{ch^*\} \sin \theta \end{aligned} \quad (2.69)$$

$$\begin{aligned} I_0 A_{yy} \equiv I_0 A_{nn} &= \frac{1}{4} Tr \{ M(\boldsymbol{\sigma}^{(1)} \cdot \hat{\mathbf{n}})(\boldsymbol{\sigma}^{(2)} \cdot \hat{\mathbf{n}})M^{\dagger} \} \\ &= 2(Re\{am^*\} + |c|^2 - |g|^2 + |h|^2) = I_0 C_{NN} \end{aligned} \quad (2.70)$$

$$\begin{aligned} I_0 A_{zz} \equiv I_0 A_{ll} &= \frac{1}{4} Tr \{ M(\boldsymbol{\sigma}^{(1)} \cdot \hat{\mathbf{l}})(\boldsymbol{\sigma}^{(2)} \cdot \hat{\mathbf{l}})M^{\dagger} \} \\ &= 2Re\{(a-m)g^* + (a+m)h^* \cos \theta\} - 4Im\{ch^*\} \sin \theta \end{aligned} \quad (2.71)$$

$$\begin{aligned} I_0 A_{zx} \equiv -I_0 A_{ls} &= -\frac{1}{4} Tr \{ M(\boldsymbol{\sigma}^{(1)} \cdot \hat{\mathbf{l}})(\boldsymbol{\sigma}^{(2)} \cdot \hat{\mathbf{s}})M^{\dagger} \} \\ &= -2Re\{(a+m)h^*\} \sin \theta - 4Im\{ch^*\} \cos \theta \end{aligned} \quad (2.72)$$

It can be shown that $A_{zx} = A_{xz}$. Again, note the minus sign in the definition for A_{zx} , which is taken from CNS DAC. In Ref. [23] the definition for A_{zx} has the opposite sign.

Chapter 3

THREE-DIMENSIONAL FORMULATION FOR NUCLEON-NUCLEON SCATTERING

In the standard partial wave decomposition for NN scattering (see for instance Chapter 2 of Ref. [25]) a set of the Lippmann-Schwinger equations (LSE's) for the T-matrix is solved for each total angular momentum j of the two nucleons and one calculates up to j_{max} , where the calculation converges, which means that the contribution from $j = j_{max} + 1$ to the value of the investigated observable is relatively small or negligible. If both isospins exist (np scattering) the set for each $j > 0$ consists of six one-dimensional LSE's: two sets of two coupled equations plus two uncoupled ones. For $j = 0$ there are only two uncoupled LSE's. The largest number of LSE's is then $6j_{max} + 2$, which applies to np scattering. For example, with $j_{max} = 2$ there are 14 LSE's in np scattering. For pp scattering the number of LSE's is roughly half of that for a np system with the same j_{max} . The higher the energy involved in the process the larger j_{max} and the more LSE's are to be solved. For instance, at 300 MeV nucleon laboratory energy one needs up to $j_{max} = 16$ in order to describe the np differential cross section sufficiently well [27].

In this chapter we formulate the technique to treat NN scattering without partial wave decomposition. The goal is to have a small set of the LSE's for the T-matrix, so that in contrast to the standard partial wave calculations just described one solves only a fixed small number of the LSE's regardless of the energy involved in the process. We begin the formulation with the definition of the basis state followed by discussions on its properties and end up with the set of the LSE's. In order to calculate NN scattering observables, we

connect the T-matrix obtained from this set of the LSE's to the "physical" T-matrix more appropriate for calculating observables. This "physical" T-matrix is given as function of relative momentum and individual spin (quantized in the z-axis) and isospin quantum numbers of the two nucleons. We also connect this formulation to the standard partial wave representation.

We do not use a spin representation with a fixed quantization axis, for example the z-axis. Instead, the total spin of the two nucleons is given in its helicity representation, where the quantization axis points in the direction of their relative momentum. One practical advantage of working with helicity states is that these states are the eigenstates of the helicity operator appearing in the NN potentials given in momentum space. NN potentials of one-boson-exchange type are constructed directly in terms of helicity operators, but in this case referring to the individual nucleons [28, 29]. Another advantage of using helicities is related to a relativistic scheme. Going to high energies one may encounter relativistic effects. If the formulation is extended to a relativistic scheme then using the helicity representation is less complicated than using the spin representation with a fixed quantization axis [30].

3.1 Momentum-Helicity Basis States

For our purpose we define basis states called the momentum-helicity basis states - a name, which is simply taken from the components of which they are constructed. To represent a system of two nucleons the basis states must have some properties, i.e. they have to be antisymmetric and have a definite parity. Here we present step by step the construction of the basis states so that they have these properties. We follow with a discussion on their other properties.

We consider the helicity representation of the total spin $\mathbf{S} = \mathbf{S}_1 + \mathbf{S}_2$ rather than that of individual spins \mathbf{S}_1 and \mathbf{S}_2 of the two nucleons. This has the advantages, that instead of four we deal only with two spin states, i.e. the singlet ($S = 0$) and the triplet ($S = 1$) states. Also, the total spin S is conserved (to a high degree of accuracy). Another advantage is that if it is necessary to apply the formulation to systems of not spin-half particles the modification is minor.

The total spin state $|\hat{\mathbf{z}}S\Lambda\rangle$ of a two nucleon system with quantization axis along the z-axis, and Λ being the total-spin projection on this axis, has the form

$$|\hat{\mathbf{z}}S\Lambda\rangle = \sum_{m_1 m_2} C\left(\frac{1}{2}\frac{1}{2}S; m_1 m_2 \Lambda\right) \left| \hat{\mathbf{z}}\frac{1}{2}m_1 \right\rangle \left| \hat{\mathbf{z}}\frac{1}{2}m_2 \right\rangle, \quad (3.1)$$

where $C\left(\frac{1}{2}\frac{1}{2}S; m_1 m_2 \Lambda\right)$ is the Clebsch-Gordan coefficient, $\left| \hat{\mathbf{z}}\frac{1}{2}m_i \right\rangle$ ($i = 1, 2$) is the spin

state of the individual nucleon quantized along the z-axis and m_i being its spin projection on this axis. The helicity representation $|\hat{\mathbf{q}}S\Lambda\rangle$ results from rotating the state $|\hat{\mathbf{z}}S\Lambda\rangle$ into the direction of \mathbf{q} , which is the relative momentum of the two nucleons

$$|\hat{\mathbf{q}}S\Lambda\rangle = R(\hat{\mathbf{q}}) |\hat{\mathbf{z}}S\Lambda\rangle. \quad (3.2)$$

Note that the spin projection Λ on the quantization axis is unchanged. Here $R(\hat{\mathbf{q}})$ is the rotation operator (see Refs. [31, 32] for detailed descriptions of this operator)

$$R(\hat{\mathbf{q}}) = R(\phi\theta 0) = e^{-iS_z\phi} e^{-iS_y\theta}, \quad (3.3)$$

where S_z, S_y are the z- and y-components of the total spin operator \mathbf{S} , respectively, and (θ, ϕ) determines the direction of \mathbf{q} . We would like to emphasize that different from Ref. [30], which performs a rotation through three Euler angles $(\alpha, \beta, \gamma) = (\phi, \theta, -\phi)$, we perform a rotation through the angles $(\alpha, \beta, \gamma) = (\phi, \theta, 0)$, since the third rotation through the angle $\gamma = -\phi$ is unnecessary and therefore γ is set to be zero.

As the state $|\hat{\mathbf{z}}S\Lambda\rangle$ is the eigenstate of the z component $\mathbf{S} \cdot \hat{\mathbf{z}}$ of the spin operator, the state $|\hat{\mathbf{q}}S\Lambda\rangle$ is the eigenstate of the helicity operator $\mathbf{S} \cdot \hat{\mathbf{q}}$

$$\mathbf{S} \cdot \hat{\mathbf{q}} |\hat{\mathbf{q}}S\Lambda\rangle = \Lambda |\hat{\mathbf{q}}S\Lambda\rangle. \quad (3.4)$$

This can be shown as follows using the relation $\mathbf{S} \cdot \hat{\mathbf{q}} = R(\hat{\mathbf{q}})\mathbf{S} \cdot \hat{\mathbf{z}}R^{-1}(\hat{\mathbf{q}})$:

$$\begin{aligned} \mathbf{S} \cdot \hat{\mathbf{q}} |\hat{\mathbf{q}}S\Lambda\rangle &= R(\hat{\mathbf{q}})\mathbf{S} \cdot \hat{\mathbf{z}}R^{-1}(\hat{\mathbf{q}})R(\hat{\mathbf{q}}) |\hat{\mathbf{z}}S\Lambda\rangle \\ &= R(\hat{\mathbf{q}})\mathbf{S} \cdot \hat{\mathbf{z}} |\hat{\mathbf{z}}S\Lambda\rangle \\ &= \Lambda R(\hat{\mathbf{q}}) |\hat{\mathbf{z}}S\Lambda\rangle \\ &= \Lambda |\hat{\mathbf{q}}S\Lambda\rangle. \end{aligned} \quad (3.5)$$

The orthogonality and the completeness relations for this state $|\hat{\mathbf{q}}S\Lambda\rangle$ are similar to the ones for the state $|\hat{\mathbf{z}}S\Lambda\rangle$:

$$\langle \hat{\mathbf{q}}S'\Lambda' | \hat{\mathbf{q}}S\Lambda \rangle = \delta_{S'S} \delta_{\Lambda'\Lambda} \quad (3.6)$$

$$\sum_{S\Lambda} |\hat{\mathbf{q}}S\Lambda\rangle \langle \hat{\mathbf{q}}S\Lambda| = 1, \quad (3.7)$$

which can be verified as follows:

$$\begin{aligned} \langle \hat{\mathbf{q}}S'\Lambda' | \hat{\mathbf{q}}S\Lambda \rangle &= \langle \hat{\mathbf{z}}S'\Lambda' | R^{-1}(\hat{\mathbf{q}})R(\hat{\mathbf{q}}) |\hat{\mathbf{z}}S\Lambda\rangle \\ &= \langle \hat{\mathbf{z}}S'\Lambda' | \hat{\mathbf{z}}S\Lambda \rangle \\ &= \delta_{S'S} \delta_{\Lambda'\Lambda}, \end{aligned} \quad (3.8)$$

$$\begin{aligned}
\langle \hat{\mathbf{q}}S'\Lambda' | \hat{\mathbf{q}}S\Lambda \rangle &= \sum_{S''\Lambda''} \langle \hat{\mathbf{q}}S'\Lambda' | \hat{\mathbf{q}}S''\Lambda'' \rangle \langle \hat{\mathbf{q}}S''\Lambda'' | \hat{\mathbf{q}}S\Lambda \rangle \\
&= \sum_{S''\Lambda''} \delta_{S'S''} \delta_{\Lambda'\Lambda''} \delta_{S''S} \delta_{\Lambda'\Lambda} \\
&= \delta_{S'S} \delta_{\Lambda'\Lambda}.
\end{aligned} \tag{3.9}$$

We begin to construct the momentum-helicity basis state, starting with a direct product of the momentum vector state $|\mathbf{q}\rangle$ and the helicity state $|\hat{\mathbf{q}}S\Lambda\rangle$

$$|\mathbf{q}; \hat{\mathbf{q}}S\Lambda\rangle \equiv |\mathbf{q}\rangle |\hat{\mathbf{q}}S\Lambda\rangle. \tag{3.10}$$

This is justified, since we work in a nonrelativistic scheme. In this scheme the momentum vector state and the helicity state are independent of each other, whereas in a relativistic scheme the two states are related (see for example Ref. [30]).

This starting state $|\mathbf{q}; \hat{\mathbf{q}}S\Lambda\rangle$ has no definite parity. It is not eigenstate of the parity operator P , which acts on the momentum vector state

$$P |\mathbf{q}; \hat{\mathbf{q}}S\Lambda\rangle = |-\mathbf{q}; \hat{\mathbf{q}}S\Lambda\rangle. \tag{3.11}$$

We define from this state a different state $|\mathbf{q}; \hat{\mathbf{q}}S\Lambda\rangle_\pi$, which is parity eigenstate as

$$|\mathbf{q}; \hat{\mathbf{q}}S\Lambda\rangle_\pi \equiv \frac{1}{\sqrt{2}}(1 + \eta_\pi P) |\mathbf{q}; \hat{\mathbf{q}}S\Lambda\rangle. \tag{3.12}$$

Here $\eta_\pi = \pm 1$ are the parity eigenvalues as can be checked by applying P on this state

$$\begin{aligned}
P |\mathbf{q}; \hat{\mathbf{q}}S\Lambda\rangle_\pi &= \frac{1}{\sqrt{2}}(P + \eta_\pi) |\mathbf{q}; \hat{\mathbf{q}}S\Lambda\rangle \\
&= \eta_\pi \frac{1}{\sqrt{2}}(\eta_\pi P + 1) |\mathbf{q}; \hat{\mathbf{q}}S\Lambda\rangle \\
&= \eta_\pi |\mathbf{q}; \hat{\mathbf{q}}S\Lambda\rangle_\pi.
\end{aligned} \tag{3.13}$$

The antisymmetric property is introduced by taking into account isospin and using the permutation operator P_{12} , which exchanges the two nucleons' labels, meaning that the permutation takes place in all space: momentum, spin and isospin. In momentum space P_{12} acts as P in Eq. (3.11) whereas in spin and isospin space the actions of P_{12} are

$$P_{12} |\hat{\mathbf{q}}S\Lambda\rangle = (-)^{1+S} |\hat{\mathbf{q}}S\Lambda\rangle \tag{3.14}$$

$$P_{12} |t\rangle = (-)^{1+t} |t\rangle. \tag{3.15}$$

Here $|t\rangle \equiv |tm_t\rangle$ is the total isospin state of the two nucleons, where the total isospin t equals 0 for singlet and 1 for triplet isospin states and m_t is the isospin projection along its quantization axis, which tells also the total electric charge of the system. We suppress

m_t for simplicity, since electric charge is conserved. Now we define the momentum-helicity basis state $|\mathbf{q}; \hat{\mathbf{q}}S\Lambda; t\rangle^{\pi a}$ as

$$\begin{aligned} |\mathbf{q}; \hat{\mathbf{q}}S\Lambda; t\rangle^{\pi a} &\equiv \frac{1}{\sqrt{2}}(1 - P_{12}) |\mathbf{q}; \hat{\mathbf{q}}S\Lambda\rangle_{\pi} |t\rangle \\ &= \frac{1}{\sqrt{2}} \left(1 - \eta_{\pi}(-)^{S+t}\right) |\mathbf{q}; \hat{\mathbf{q}}S\Lambda\rangle_{\pi} |t\rangle, \end{aligned} \quad (3.16)$$

and the antisymmetricity of this state is obvious

$$\begin{aligned} P_{12} |\mathbf{q}; \hat{\mathbf{q}}S\Lambda; t\rangle^{\pi a} &= \frac{1}{\sqrt{2}}(P_{12} - 1) |\mathbf{q}; \hat{\mathbf{q}}S\Lambda\rangle_{\pi} |t\rangle \\ &= -|\mathbf{q}; \hat{\mathbf{q}}S\Lambda; t\rangle^{\pi a}. \end{aligned} \quad (3.17)$$

The factor in Eq. (3.16) tells that parity, spin and isospin must meet the condition $\eta_{\pi}(-)^{S+t} = -1$.

We evaluate now the normalization of the state given in Eq. (3.16). For this purpose we need the relation between $|\hat{\mathbf{q}}S\Lambda\rangle$ and $|\hat{-\mathbf{q}}S\Lambda\rangle$. This relation can be derived using the definition in Eq. (3.2) for $|\hat{-\mathbf{q}}S\Lambda\rangle$ and the Wigner D-function (see Refs. [31, 32] for detailed description of the Wigner D-function)

$$\begin{aligned} D_{\Lambda'\Lambda}^S(\hat{\mathbf{q}}) = D_{\Lambda'\Lambda}^S(\phi\theta) &\equiv \langle \hat{\mathbf{z}}S\Lambda' | R(\hat{\mathbf{q}}) | \hat{\mathbf{z}}S\Lambda \rangle \\ &= \langle \hat{\mathbf{z}}S\Lambda' | e^{-iS_z\phi} e^{-iS_y\theta} | \hat{\mathbf{z}}S\Lambda \rangle \\ &= e^{-i\Lambda'\phi} \langle \hat{\mathbf{z}}S\Lambda' | e^{-iS_y\theta} | \hat{\mathbf{z}}S\Lambda \rangle \\ &\equiv e^{-i\Lambda'\phi} d_{\Lambda'\Lambda}^S(\theta), \end{aligned} \quad (3.18)$$

together with the following relation for the d-matrices $d_{\Lambda'\Lambda}^S(\theta)$ (see Appendix A for the derivation)

$$d_{\Lambda'\Lambda}^S(\pi - \theta) = (-)^{S+\Lambda'} d_{\Lambda',-\Lambda}^S(\theta). \quad (3.19)$$

We obtain

$$\begin{aligned} |\hat{-\mathbf{q}}S\Lambda\rangle &= R(-\hat{\mathbf{q}}) |\hat{\mathbf{z}}S\Lambda\rangle \\ &= \sum_{\Lambda'} |\hat{\mathbf{z}}S\Lambda'\rangle \langle \hat{\mathbf{z}}S\Lambda' | R(-\hat{\mathbf{q}}) | \hat{\mathbf{z}}S\Lambda \rangle \\ &= \sum_{\Lambda'} D_{\Lambda'\Lambda}^S(-\hat{\mathbf{q}}) |\hat{\mathbf{z}}S\Lambda'\rangle \\ &= \sum_{\Lambda'} e^{-i(\phi+\pi)\Lambda'} d_{\Lambda'\Lambda}^S(\pi - \theta) |\hat{\mathbf{z}}S\Lambda'\rangle \\ &= \sum_{\Lambda'} e^{-i(\phi+\pi)\Lambda'} (-)^{S+\Lambda'} d_{\Lambda',-\Lambda}^S(\theta) |\hat{\mathbf{z}}S\Lambda'\rangle \\ &= (-)^S \sum_{\Lambda'} D_{\Lambda',-\Lambda}^S(\hat{\mathbf{q}}) |\hat{\mathbf{z}}S\Lambda'\rangle \\ &= (-)^S |\hat{\mathbf{q}}S - \Lambda\rangle. \end{aligned} \quad (3.20)$$

Now the normalization of the states given in Eq. (3.16) can be worked out as follows:

$$\begin{aligned} \pi'^a \langle \mathbf{q}' ; \hat{\mathbf{q}}' S' \Lambda' ; t' | \mathbf{q} ; \hat{\mathbf{q}} S \Lambda ; t \rangle^{\pi a} &= \frac{1}{2} \left(1 - \eta_{\pi'}(-)^{S'+t'} \right) \left(1 - \eta_{\pi}(-)^{S+t} \right) \delta_{t't} \\ &\times {}_{\pi'} \langle \mathbf{q}' ; \hat{\mathbf{q}}' S' \Lambda' | \mathbf{q} ; \hat{\mathbf{q}} S \Lambda \rangle_{\pi}, \end{aligned} \quad (3.21)$$

with

$$\begin{aligned} {}_{\pi'} \langle \mathbf{q}' ; \hat{\mathbf{q}}' S' \Lambda' | \mathbf{q} ; \hat{\mathbf{q}} S \Lambda \rangle_{\pi} &= \frac{1}{2} \langle \mathbf{q}' ; \hat{\mathbf{q}}' S' \Lambda' | (1 + \eta_{\pi'} P)(1 + \eta_{\pi} P) | \mathbf{q} ; \hat{\mathbf{q}} S \Lambda \rangle \\ &= \frac{1}{2} \langle \mathbf{q}' ; \hat{\mathbf{q}}' S' \Lambda' | (1 + \eta_{\pi'} P) (| \mathbf{q} ; \hat{\mathbf{q}} S \Lambda \rangle + \eta_{\pi} | -\mathbf{q} ; \hat{\mathbf{q}} S \Lambda \rangle) \\ &= \frac{1}{2} \langle \mathbf{q}' ; \hat{\mathbf{q}}' S' \Lambda' | (| \mathbf{q} ; \hat{\mathbf{q}} S \Lambda \rangle + \eta_{\pi} | -\mathbf{q} ; \hat{\mathbf{q}} S \Lambda \rangle \\ &\quad + \eta_{\pi'} | -\mathbf{q} ; \hat{\mathbf{q}} S \Lambda \rangle + \eta_{\pi'} \eta_{\pi} | \mathbf{q} ; \hat{\mathbf{q}} S \Lambda \rangle) \\ &= \frac{1}{2} \left\{ (1 + \eta_{\pi'} \eta_{\pi}) \delta(\mathbf{q}' - \mathbf{q}) \delta_{S'S} \delta_{\Lambda'\Lambda} \right. \\ &\quad \left. + (\eta_{\pi'} + \eta_{\pi}) \delta(\mathbf{q}' + \mathbf{q}) \langle \hat{\mathbf{q}}' S' \Lambda' | -\hat{\mathbf{q}} S \Lambda \rangle \right\} \\ &= \frac{1}{2} \left\{ (1 + \eta_{\pi'} \eta_{\pi}) \delta(\mathbf{q}' - \mathbf{q}) \delta_{S'S} \delta_{\Lambda'\Lambda} \right. \\ &\quad \left. + (\eta_{\pi'} + \eta_{\pi}) \delta(\mathbf{q}' + \mathbf{q}) (-)^S \delta_{S'S} \delta_{\Lambda', -\Lambda} \right\} \\ &= \delta_{\eta_{\pi'} \eta_{\pi}} \delta_{S'S} \left\{ \delta(\mathbf{q}' - \mathbf{q}) \delta_{\Lambda'\Lambda} + \eta_{\pi} (-)^S \delta(\mathbf{q}' + \mathbf{q}) \delta_{\Lambda', -\Lambda} \right\}. \end{aligned} \quad (3.22)$$

Thus the normalization is

$$\begin{aligned} \pi'^a \langle \mathbf{q}' ; \hat{\mathbf{q}}' S' \Lambda' ; t' | \mathbf{q} ; \hat{\mathbf{q}} S \Lambda ; t \rangle^{\pi a} &= \left(1 - \eta_{\pi}(-)^{S+t} \right) \delta_{t't} \delta_{\eta_{\pi'} \eta_{\pi}} \delta_{S'S} \\ &\times \left\{ \delta(\mathbf{q}' - \mathbf{q}) \delta_{\Lambda'\Lambda} + \eta_{\pi} (-)^S \delta(\mathbf{q}' + \mathbf{q}) \delta_{\Lambda', -\Lambda} \right\}. \end{aligned} \quad (3.23)$$

Next we verify the completeness relation of the state defined in Eq. (3.16). Starting with

$$\sum_{S \Lambda \pi t} \int d\mathbf{q} | \mathbf{q} ; \hat{\mathbf{q}} S \Lambda ; t \rangle^{\pi a} \rho^{\pi a} \langle \mathbf{q} ; \hat{\mathbf{q}} S \Lambda ; t | = 1, \quad (3.24)$$

with ρ being a factor not yet defined and using the normalization given in Eq. (3.23) the completeness relation is verified as follows:

$$\begin{aligned} \pi'^a \langle \mathbf{q}' ; \hat{\mathbf{q}}' S' \Lambda' ; t' | \mathbf{q}'' ; \hat{\mathbf{q}}'' S'' \Lambda'' ; t'' \rangle^{\pi'' a} &= \pi'^a \langle \mathbf{q}' ; \hat{\mathbf{q}}' S' \Lambda' ; t' | \sum_{S \Lambda \pi t} \int d\mathbf{q} | \mathbf{q} ; \hat{\mathbf{q}} S \Lambda ; t \rangle^{\pi a} \rho^{\pi a} \langle \mathbf{q} ; \hat{\mathbf{q}} S \Lambda ; t | \mathbf{q}'' ; \hat{\mathbf{q}}'' S'' \Lambda'' ; t'' \rangle^{\pi'' a} \\ &= \sum_{S \Lambda \pi t} \rho \int d\mathbf{q} \left(1 - \eta_{\pi}(-)^{S+t} \right) \delta_{t't} \delta_{\eta_{\pi'} \eta_{\pi}} \delta_{S'S} \left(1 - \eta_{\pi}(-)^{S+t} \right) \delta_{t't''} \delta_{\eta_{\pi} \eta_{\pi''}} \delta_{S S''} \\ &\quad \times \left\{ \delta(\mathbf{q}' - \mathbf{q}) \delta_{\Lambda'\Lambda} + \eta_{\pi} (-)^S \delta(\mathbf{q}' + \mathbf{q}) \delta_{\Lambda', -\Lambda} \right\} \\ &\quad \times \left\{ \delta(\mathbf{q} - \mathbf{q}'') \delta_{\Lambda \Lambda''} + \eta_{\pi} (-)^S \delta(\mathbf{q} + \mathbf{q}'') \delta_{\Lambda, -\Lambda''} \right\} \\ &= \rho \left(1 - \eta_{\pi'}(-)^{S'+t'} \right)^2 \delta_{t't''} \delta_{\eta_{\pi'} \eta_{\pi''}} \delta_{S' S''} \end{aligned}$$

$$\begin{aligned}
& \times \left\{ \delta(\mathbf{q}' - \mathbf{q}'')\delta_{\Lambda'\Lambda''} + \eta_{\pi'}(-)^{S'}\delta(\mathbf{q}' + \mathbf{q}'')\delta_{\Lambda',-\Lambda''} \right. \\
& \left. + \delta(\mathbf{q}' - \mathbf{q}'')\delta_{\Lambda'\Lambda''} + \eta_{\pi'}(-)^{S'}\delta(\mathbf{q}' + \mathbf{q}'')\delta_{\Lambda',-\Lambda''} \right\} \\
& = 4\rho \left(1 - \eta_{\pi'}(-)^{S'+t'}\right) \delta_{t't''}\delta_{\eta_{\pi'}\eta_{\pi''}}\delta_{S'S''} \\
& \quad \times \left\{ \delta(\mathbf{q}' - \mathbf{q}'')\delta_{\Lambda'\Lambda''} + \eta_{\pi'}(-)^{S'}\delta(\mathbf{q}' + \mathbf{q}'')\delta_{\Lambda',-\Lambda''} \right\} \\
& = 4\rho^{\pi^a} \langle \mathbf{q}'; \hat{\mathbf{q}}'S'\Lambda'; t' | \mathbf{q}''; \hat{\mathbf{q}}''S''\Lambda''; t'' \rangle^{\pi^a}. \tag{3.25}
\end{aligned}$$

In the last equality we used again Eq. (3.23) and thus determine $\rho = \frac{1}{4}$. Consequently the completeness relation reads

$$\sum_{S\Lambda\pi t} \int d\mathbf{q} |\mathbf{q}; \hat{\mathbf{q}}S\Lambda; t\rangle^{\pi^a} \frac{1}{4} \pi^a \langle \mathbf{q}; \hat{\mathbf{q}}S\Lambda; t | = 1. \tag{3.26}$$

3.2 General Structure of the Potential Operator and the Potential Matrix Element

As shown in Eq. (2.11) the NN potential is the input for the NN scattering calculations. Therefore, before we continue to find the set of the LSE's in the momentum-helicity basis derived in the previous section we figure out first the general structure of the potential operator, which fits well to this momentum-helicity basis and investigate the potential matrix element in this basis.

The NN potential is invariant under the operation of rotation, parity and time-reversal. These invariance properties exclude many terms among all possible terms assumed as components of a NN potential (see Ref. [25] for more educative discussions). There are six terms left [26] in which the most general structure of a NN potential can be given, as

$$V(\mathbf{q}', \mathbf{q}) \equiv \langle \mathbf{q}' | V | \mathbf{q} \rangle = \sum_{i=1}^6 v_i(q', q, \gamma) \mathbf{W}_i. \tag{3.27}$$

Here $v_i(q', q, \gamma)$ are scalar (spin independent) functions, which depend on the magnitudes of \mathbf{q}' , \mathbf{q} , and the angle between the two, $\gamma \equiv \hat{\mathbf{q}}' \cdot \hat{\mathbf{q}}$, and \mathbf{W}_i ($i = 1$ to 6) are operators to the spin states of the two nucleons such that

$$\begin{aligned}
V_{m'_{s1}m'_{s2}m_{s1}m_{s2}}(\mathbf{q}', \mathbf{q}) & \equiv \langle \mathbf{q}'m'_{s1}m'_{s2} | V | \mathbf{q}m_{s1}m_{s2} \rangle \\
& = \langle m'_{s1}m'_{s2} | \langle \mathbf{q}' | V | \mathbf{q} \rangle | m_{s1}m_{s2} \rangle \\
& = \sum_{i=1}^6 v_i(q', q, \gamma) \langle m'_{s1}m'_{s2} | \mathbf{W}_i | m_{s1}m_{s2} \rangle. \tag{3.28}
\end{aligned}$$

The \mathbf{W}_i 's are constructed as combinations of projected-spin operators along some axes,

given in terms of momentum combinations with the exception of \mathbf{W}_1 , which is unity:

$$\begin{aligned} \mathbf{W}_1 &= 1 & \mathbf{W}_2 &= (\boldsymbol{\sigma}_1 + \boldsymbol{\sigma}_2) \cdot \hat{\mathbf{N}} \\ \mathbf{W}_3 &= \boldsymbol{\sigma}_1 \cdot \hat{\mathbf{N}} \boldsymbol{\sigma}_2 \cdot \hat{\mathbf{N}} & \mathbf{W}_4 &= \boldsymbol{\sigma}_1 \cdot \hat{\mathbf{P}} \boldsymbol{\sigma}_2 \cdot \hat{\mathbf{P}} \\ \mathbf{W}_5 &= \boldsymbol{\sigma}_1 \cdot \hat{\mathbf{K}} \boldsymbol{\sigma}_2 \cdot \hat{\mathbf{K}} & \mathbf{W}_6 &= \boldsymbol{\sigma}_1 \cdot \hat{\mathbf{P}} \boldsymbol{\sigma}_2 \cdot \hat{\mathbf{K}} + \boldsymbol{\sigma}_1 \cdot \hat{\mathbf{K}} \boldsymbol{\sigma}_2 \cdot \hat{\mathbf{P}} \end{aligned} \quad (3.29)$$

Remember that these are the same operators appearing in the expression for the M-matrix given in Eq. (2.32). (In that equation (2.32) and the whole Chapter 2 we attached to the Pauli matrix $\boldsymbol{\sigma}$ the nucleon labels 1,2 as superscript for clarity.)

In terms of \mathbf{W}_i 's a NN potential is expressed in the individual spin operators $\mathbf{S}_i = \frac{1}{2}\boldsymbol{\sigma}_i$ ($i = 1,2$) of the two nucleons instead of in the total spin operator $\mathbf{S} = \frac{1}{2}(\boldsymbol{\sigma}_1 + \boldsymbol{\sigma}_2)$. The latter one is more appropriate to the momentum-helicity basis state given in Eq. (3.16), since though algebraically possible, it is not practical to carry out matrix elements of the potential given in Eq. (3.27) in the momentum-helicity basis. Therefore, it is necessary to define a set of six operators constructed from the helicity operators $\mathbf{S} \cdot \hat{\mathbf{q}}$ of which the momentum-helicity basis state is eigenstate. Such operators have been defined in Ref. [17]. Here we construct similar operators denoted by Ω_i :

$$\begin{aligned} \Omega_1 &= 1 & \Omega_2 &= \mathbf{S}^2 & \Omega_3 &= \mathbf{S} \cdot \hat{\mathbf{q}}' \mathbf{S} \cdot \hat{\mathbf{q}}' \\ \Omega_4 &= \mathbf{S} \cdot \hat{\mathbf{q}}' \mathbf{S} \cdot \hat{\mathbf{q}} & \Omega_5 &= (\mathbf{S} \cdot \hat{\mathbf{q}}')^2 (\mathbf{S} \cdot \hat{\mathbf{q}})^2 & \Omega_6 &= \mathbf{S} \cdot \hat{\mathbf{q}} \mathbf{S} \cdot \hat{\mathbf{q}} \end{aligned} \quad (3.30)$$

In order to maintain the invariance properties of the potential the Ω_i operators must be linearly independent and have to be connected to the \mathbf{W}_i 's. The connection of the Ω_i to the \mathbf{W}_i operators is given as

$$\mathbf{W}_i = \sum_j A_{ij} \Omega_j, \quad (3.31)$$

where the transformation matrix $A = \{A_{ij}\}$ depends on q , q' and γ (see Appendix B). Expressed in the Ω_i operators the general form of a NN potential is

$$V(\mathbf{q}', \mathbf{q}) = \sum_{i,j=1}^6 v_i(q', q, \gamma) A_{ij} \Omega_j. \quad (3.32)$$

Taking also into account the spin states of the two nucleons, which are now represented as helicity states given in Eq. (3.2), and using Eq. (3.10) we have

$$\begin{aligned} V_{\Lambda'\Lambda}^S(\mathbf{q}', \mathbf{q}) &\equiv \langle \mathbf{q}'; \hat{\mathbf{q}}' S \Lambda' | V | \mathbf{q}; \hat{\mathbf{q}} S \Lambda \rangle \\ &= \langle \hat{\mathbf{q}}' S \Lambda' | \langle \mathbf{q}' | V | \mathbf{q} \rangle | \hat{\mathbf{q}} S \Lambda \rangle \\ &= \sum_{i,j=1}^6 v_i(q', q, \gamma) A_{ij} \langle \hat{\mathbf{q}}' S \Lambda' | \Omega_j | \hat{\mathbf{q}} S \Lambda \rangle. \end{aligned} \quad (3.33)$$

The matrix elements $\langle \hat{\mathbf{q}}' S \Lambda' | \Omega_j | \hat{\mathbf{q}} S \Lambda \rangle$ are easier to evaluate, as it is intended by defining the Ω_i operators, . These are

$$\langle \hat{\mathbf{q}}' S \Lambda' | \Omega_1 | \hat{\mathbf{q}} S \Lambda \rangle = \langle \hat{\mathbf{q}}' S \Lambda' | \hat{\mathbf{q}} S \Lambda \rangle \quad (3.34)$$

$$\begin{aligned} \langle \hat{\mathbf{q}}' S \Lambda' | \Omega_2 | \hat{\mathbf{q}} S \Lambda \rangle &= \langle \hat{\mathbf{q}}' S \Lambda' | \mathbf{S}^2 | \hat{\mathbf{q}} S \Lambda \rangle \\ &= S(S+1) \langle \hat{\mathbf{q}}' S \Lambda' | \hat{\mathbf{q}} S \Lambda \rangle \end{aligned} \quad (3.35)$$

$$\begin{aligned} \langle \hat{\mathbf{q}}' S \Lambda' | \Omega_3 | \hat{\mathbf{q}} S \Lambda \rangle &= \langle \hat{\mathbf{q}}' S \Lambda' | \mathbf{S} \cdot \hat{\mathbf{q}}' \mathbf{S} \cdot \hat{\mathbf{q}} | \hat{\mathbf{q}} S \Lambda \rangle \\ &= \langle (\mathbf{S} \cdot \hat{\mathbf{q}}')^2 \hat{\mathbf{q}}' S \Lambda' | \hat{\mathbf{q}} S \Lambda \rangle \\ &= \Lambda'^2 \langle \hat{\mathbf{q}}' S \Lambda' | \hat{\mathbf{q}} S \Lambda \rangle \end{aligned} \quad (3.36)$$

$$\begin{aligned} \langle \hat{\mathbf{q}}' S \Lambda' | \Omega_4 | \hat{\mathbf{q}} S \Lambda \rangle &= \langle \hat{\mathbf{q}}' S \Lambda' | \mathbf{S} \cdot \hat{\mathbf{q}}' \mathbf{S} \cdot \hat{\mathbf{q}} | \hat{\mathbf{q}} S \Lambda \rangle \\ &= \langle (\mathbf{S} \cdot \hat{\mathbf{q}}') \hat{\mathbf{q}}' S \Lambda' | \mathbf{S} \cdot \hat{\mathbf{q}} | \hat{\mathbf{q}} S \Lambda \rangle \\ &= \Lambda' \Lambda \langle \hat{\mathbf{q}}' S \Lambda' | \hat{\mathbf{q}} S \Lambda \rangle \end{aligned} \quad (3.37)$$

$$\begin{aligned} \langle \hat{\mathbf{q}}' S \Lambda' | \Omega_5 | \hat{\mathbf{q}} S \Lambda \rangle &= \langle \hat{\mathbf{q}}' S \Lambda' | (\mathbf{S} \cdot \hat{\mathbf{q}}')^2 (\mathbf{S} \cdot \hat{\mathbf{q}})^2 | \hat{\mathbf{q}} S \Lambda \rangle \\ &= \langle (\mathbf{S} \cdot \hat{\mathbf{q}}')^2 \hat{\mathbf{q}}' S \Lambda' | (\mathbf{S} \cdot \hat{\mathbf{q}})^2 | \hat{\mathbf{q}} S \Lambda \rangle \\ &= \Lambda'^2 \Lambda^2 \langle \hat{\mathbf{q}}' S \Lambda' | \hat{\mathbf{q}} S \Lambda \rangle \end{aligned} \quad (3.38)$$

$$\begin{aligned} \langle \hat{\mathbf{q}}' S \Lambda' | \Omega_6 | \hat{\mathbf{q}} S \Lambda \rangle &= \langle \hat{\mathbf{q}}' S \Lambda' | \mathbf{S} \cdot \hat{\mathbf{q}}' \mathbf{S} \cdot \hat{\mathbf{q}} | \hat{\mathbf{q}} S \Lambda \rangle \\ &= \Lambda^2 \langle \hat{\mathbf{q}}' S \Lambda' | \hat{\mathbf{q}} S \Lambda \rangle \end{aligned} \quad (3.39)$$

All resulting expressions are simply the overlap of the helicity states defined in Eq. (3.2) multiplied with a factor, which is just a number. Using Eq. (3.18) and that $d_{m'm}^j(\theta)$ being a real number this overlap $\langle \hat{\mathbf{q}}' S \Lambda' | \hat{\mathbf{q}} S \Lambda \rangle$ is

$$\begin{aligned} \langle \hat{\mathbf{q}}' S \Lambda' | \hat{\mathbf{q}} S \Lambda \rangle &= \sum_M \langle \hat{\mathbf{q}}' S \Lambda' | \hat{\mathbf{z}} S M \rangle \langle \hat{\mathbf{z}} S M | \hat{\mathbf{q}} S \Lambda \rangle \\ &= \sum_M D_{M\Lambda'}^{S*}(\phi'\theta'0) D_{M\Lambda}^S(\phi\theta0) \\ &= \sum_{M=-S}^S e^{iM(\phi'-\phi)} d_{M\Lambda'}^S(\theta') d_{M\Lambda}^S(\theta). \end{aligned} \quad (3.40)$$

For \mathbf{q} points in z -direction $d_{M\Lambda}^S(0) = \delta_{M\Lambda}$ and this overlap becomes simple

$$\langle \hat{\mathbf{q}}' S \Lambda' | \hat{\mathbf{z}} S \Lambda \rangle = e^{i\Lambda\phi'} d_{\Lambda\Lambda'}^S(\theta'). \quad (3.41)$$

We evaluate now the matrix elements of the potential V in the momentum-helicity basis firstly without applying the general structure of the potential given in Eq. (3.32). We assume that parity, spin and thus isospin are conserved (which is valid to a high degree of accuracy) and restrict ourselves to evaluate only

$$V_{\Lambda'\Lambda}^{\pi S t}(\mathbf{q}', \mathbf{q}) \equiv \pi^a \langle \mathbf{q}'; \hat{\mathbf{q}}' S \Lambda'; t | V | \mathbf{q}; \hat{\mathbf{q}} S \Lambda; t \rangle^{\pi a}. \quad (3.42)$$

Using Eq. (3.16) and the parity invariance of V we obtain for these matrix elements

$$\begin{aligned}
V_{\Lambda'\Lambda}^{\pi St}(\mathbf{q}', \mathbf{q}) &= \frac{1}{2} \left(1 - \eta_{\pi}(-)^{S+t}\right)^2 \langle t | {}_{\pi} \langle \mathbf{q}' ; \hat{\mathbf{q}}' S \Lambda' | V | \mathbf{q} ; \hat{\mathbf{q}} S \Lambda \rangle_{\pi} | t \rangle \\
&= \frac{1}{\sqrt{2}} \left(1 - \eta_{\pi}(-)^{S+t}\right) \langle t | (\langle \mathbf{q}' ; \hat{\mathbf{q}}' S \Lambda' | + \eta_{\pi} \langle -\mathbf{q}' ; \hat{\mathbf{q}}' S \Lambda' |) V | \mathbf{q} ; \hat{\mathbf{q}} S \Lambda \rangle_{\pi} | t \rangle \\
&= \frac{1}{\sqrt{2}} \left(1 - \eta_{\pi}(-)^{S+t}\right) \langle t | (\langle \mathbf{q}' ; \hat{\mathbf{q}}' S \Lambda' | V | \mathbf{q} ; \hat{\mathbf{q}} S \Lambda \rangle_{\pi} \\
&\quad + \eta_{\pi} \langle -\mathbf{q}' ; \hat{\mathbf{q}}' S \Lambda' | V | \mathbf{q} ; \hat{\mathbf{q}} S \Lambda \rangle_{\pi}) | t \rangle \\
&= \frac{1}{\sqrt{2}} \left(1 - \eta_{\pi}(-)^{S+t}\right) \langle t | (\langle \mathbf{q}' ; \hat{\mathbf{q}}' S \Lambda' | V | \mathbf{q} ; \hat{\mathbf{q}} S \Lambda \rangle_{\pi} \\
&\quad + \eta_{\pi} \langle -\mathbf{q}' ; \hat{\mathbf{q}}' S \Lambda' | P^{-1} V P | \mathbf{q} ; \hat{\mathbf{q}} S \Lambda \rangle_{\pi}) | t \rangle \\
&= \sqrt{2} \left(1 - \eta_{\pi}(-)^{S+t}\right) \langle t | \langle \hat{\mathbf{q}}' S \Lambda' | \langle \mathbf{q}' | V | \mathbf{q} \rangle_{\pi} | \hat{\mathbf{q}} S \Lambda \rangle | t \rangle, \tag{3.43}
\end{aligned}$$

where

$$|\mathbf{q}\rangle_{\pi} \equiv \frac{1}{\sqrt{2}} (|\mathbf{q}\rangle + \eta_{\pi} |-\mathbf{q}\rangle). \tag{3.44}$$

Similarly we could also have gotten

$$V_{\Lambda'\Lambda}^{\pi St}(\mathbf{q}', \mathbf{q}) = \sqrt{2} \left(1 - \eta_{\pi}(-)^{S+t}\right) \langle t | \langle \hat{\mathbf{q}}' S \Lambda' | {}_{\pi} \langle \mathbf{q}' | V | \mathbf{q} \rangle | \hat{\mathbf{q}} S \Lambda \rangle | t \rangle. \tag{3.45}$$

Using Eq. (3.43) together with Eqs. (3.20) and (3.44) we can connect $V_{-\Lambda'\Lambda}^{\pi St}(\mathbf{q}', \mathbf{q})$ to $V_{\Lambda'\Lambda}^{\pi St}(-\mathbf{q}', \mathbf{q})$ as

$$\begin{aligned}
V_{-\Lambda'\Lambda}^{\pi St}(\mathbf{q}', \mathbf{q}) &= \sqrt{2} \left(1 - \eta_{\pi}(-)^{S+t}\right) \langle t | \langle \hat{\mathbf{q}}' S - \Lambda' | \langle \mathbf{q}' | V | \mathbf{q} \rangle_{\pi} | \hat{\mathbf{q}} S \Lambda \rangle | t \rangle \\
&= \sqrt{2} \left(1 - \eta_{\pi}(-)^{S+t}\right) \langle t | (-)^S \langle -\hat{\mathbf{q}}' S \Lambda' | \langle \mathbf{q}' | V | \mathbf{q} \rangle_{\pi} | \hat{\mathbf{q}} S \Lambda \rangle | t \rangle \\
&= \sqrt{2} \left(1 - \eta_{\pi}(-)^{S+t}\right) \langle t | (-)^S \langle -\hat{\mathbf{q}}' S \Lambda' | \langle \mathbf{q}' | P^{-1} V P | \mathbf{q} \rangle_{\pi} | \hat{\mathbf{q}} S \Lambda \rangle | t \rangle \\
&= \sqrt{2} \left(1 - \eta_{\pi}(-)^{S+t}\right) \eta_{\pi}(-)^S \langle t | \langle -\hat{\mathbf{q}}' S \Lambda' | \langle -\mathbf{q}' | V | \mathbf{q} \rangle_{\pi} | \hat{\mathbf{q}} S \Lambda \rangle | t \rangle \\
&= \eta_{\pi}(-)^S V_{\Lambda'\Lambda}^{\pi St}(-\mathbf{q}', \mathbf{q}). \tag{3.46}
\end{aligned}$$

In the same way we find

$$V_{\Lambda',-\Lambda}^{\pi St}(\mathbf{q}', \mathbf{q}) = \eta_{\pi}(-)^S V_{\Lambda'\Lambda}^{\pi St}(\mathbf{q}', -\mathbf{q}) \tag{3.47}$$

$$V_{-\Lambda',-\Lambda}^{\pi St}(\mathbf{q}', \mathbf{q}) = V_{\Lambda'\Lambda}^{\pi St}(-\mathbf{q}', -\mathbf{q}). \tag{3.48}$$

Equations (3.46), (3.47) and (3.48) are denoted as the symmetry relations of the potential matrix element in the momentum-helicity basis.

Inserting now the general structure of the potential given in Eq. (3.32) into Eq. (3.43) we obtain

$$\begin{aligned}
V_{\Lambda'\Lambda}^{\pi St}(\mathbf{q}', \mathbf{q}) &= \left(1 - \eta_{\pi}(-)^{S+t}\right) \langle t | \{ \langle \hat{\mathbf{q}}' S \Lambda' | \langle \mathbf{q}' | V | \mathbf{q} \rangle | \hat{\mathbf{q}} S \Lambda \rangle \\
&\quad + \eta_{\pi} \langle \hat{\mathbf{q}}' S \Lambda' | \langle \mathbf{q}' | V | -\mathbf{q} \rangle | \hat{\mathbf{q}} S \Lambda \rangle \} | t \rangle
\end{aligned}$$

$$\begin{aligned}
&= \left(1 - \eta_\pi(-)^{S+t}\right) \langle t | \{ \langle \hat{\mathbf{q}}' S \Lambda' | \langle \mathbf{q}' | V | \mathbf{q} \rangle | \hat{\mathbf{q}} S \Lambda \rangle \\
&\quad + \eta_\pi(-)^S \langle \hat{\mathbf{q}}' S \Lambda' | \langle \mathbf{q}' | V | -\mathbf{q} \rangle | -\hat{\mathbf{q}} S - \Lambda \rangle \} | t \rangle \\
&= \left(1 - \eta_\pi(-)^{S+t}\right) \sum_{i,j=1}^6 A_{ij} \left\{ v_i(q', q, \gamma) \langle \hat{\mathbf{q}}' S \Lambda' | \Omega_j | \hat{\mathbf{q}} S \Lambda \rangle \right. \\
&\quad \left. + \eta_\pi(-)^S v_i(q', q, -\gamma) \langle \hat{\mathbf{q}}' S \Lambda' | \Omega_j | -\hat{\mathbf{q}} S - \Lambda \rangle \right\}. \quad (3.49)
\end{aligned}$$

As an example, we work out in the following the Ω_4 term of the potential matrix element denoted as $V_{\Lambda'\Lambda}^{\pi St}(\mathbf{q}', \mathbf{q})|_{\Omega_4}$:

$$\begin{aligned}
V_{\Lambda'\Lambda}^{\pi St}(\mathbf{q}', \mathbf{q})|_{\Omega_4} &= \left(1 - \eta_\pi(-)^{S+t}\right) \sum_{i=1}^6 A_{i4} \left\{ v_i(q', q, \gamma) \langle \hat{\mathbf{q}}' S \Lambda' | \Omega_4 | \hat{\mathbf{q}} S \Lambda \rangle \right. \\
&\quad \left. + \eta_\pi(-)^S v_i(q', q, -\gamma) \langle \hat{\mathbf{q}}' S \Lambda' | \Omega_4 | -\hat{\mathbf{q}} S - \Lambda \rangle \right\} \\
&= \left(1 - \eta_\pi(-)^{S+t}\right) \sum_{i=1}^6 A_{i4} \left\{ v_i(q', q, \gamma) \langle \hat{\mathbf{q}}' S \Lambda' | \mathbf{S} \cdot \hat{\mathbf{q}}' \mathbf{S} \cdot \hat{\mathbf{q}} | \hat{\mathbf{q}} S \Lambda \rangle \right. \\
&\quad \left. + \eta_\pi(-)^S v_i(q', q, -\gamma) \langle \hat{\mathbf{q}}' S \Lambda' | \mathbf{S} \cdot \hat{\mathbf{q}}' \mathbf{S} \cdot (-\hat{\mathbf{q}}) | -\hat{\mathbf{q}} S - \Lambda \rangle \right\} \\
&= \left(1 - \eta_\pi(-)^{S+t}\right) \sum_{i=1}^6 A_{i4} \left\{ \Lambda' \Lambda v_i(q', q, \gamma) \langle \hat{\mathbf{q}}' S \Lambda' | \hat{\mathbf{q}} S \Lambda \rangle \right. \\
&\quad \left. - \Lambda' \Lambda \eta_\pi(-)^S v_i(q', q, -\gamma) \langle \hat{\mathbf{q}}' S \Lambda' | -\hat{\mathbf{q}} S - \Lambda \rangle \right\} \\
&= \left(1 - \eta_\pi(-)^{S+t}\right) \Lambda' \Lambda \sum_{i=1}^6 A_{i4} \{ v_i(q', q, \gamma) - \eta_\pi v_i(q', q, -\gamma) \} \langle \hat{\mathbf{q}}' S \Lambda' | \hat{\mathbf{q}} S \Lambda \rangle \\
&= \left(1 - \eta_\pi(-)^{S+t}\right) \Lambda' \Lambda \sum_{i=1}^6 A_{i4} \{ v_i(q', q, \gamma) - \eta_\pi v_i(q', q, -\gamma) \} \\
&\quad \times \sum_{M=-S}^S e^{iM(\phi' - \phi)} d_{M\Lambda'}^S(\theta') d_{M\Lambda}^S(\theta). \quad (3.50)
\end{aligned}$$

In the derivation we used Eqs. (3.37), (3.20) and (3.40).

We would like to exhibit the angular behavior of the potential matrix elements given in Eq. (3.49). The scalar functions $v_i(q', q, \gamma)$ as well as A_{ij} depend on γ , where

$$\gamma = \hat{\mathbf{q}}' \cdot \hat{\mathbf{q}} = \cos \theta' \cos \theta + \sin \theta' \sin \theta \cos(\phi' - \phi). \quad (3.51)$$

Therefore, their azimuthal dependence is determined by $\cos(\phi' - \phi)$. The matrix elements $\langle \hat{\mathbf{q}}' S \Lambda' | \Omega_j | \hat{\mathbf{q}} S \Lambda \rangle$ depend on the azimuthal angles ϕ' and ϕ as shown in Eq. (3.40). Thus the azimuthal dependence of the potential matrix elements can be described as

$$V_{\Lambda'\Lambda}^{\pi St}(\mathbf{q}', \mathbf{q}) \equiv V_{\Lambda'\Lambda}^{\pi St} \left\{ e^{iM(\phi' - \phi)}, \cos(\phi' - \phi) \right\}. \quad (3.52)$$

For the special case $\hat{\mathbf{q}} = \hat{\mathbf{z}}$ the azimuthal dependence is only in the matrix elements $\langle \hat{\mathbf{q}}' S \Lambda' | \Omega_j | \hat{\mathbf{q}} S \Lambda \rangle$ as given in Eq. (3.41). Hence, the potential matrix elements reduce to

the simpler form

$$V_{\Lambda'\Lambda}^{\pi St}(\mathbf{q}', q\hat{\mathbf{z}}) = e^{i\Lambda\phi'} V_{\Lambda'\Lambda}^{\pi St}(q', q, \theta'). \quad (3.53)$$

3.3 Lippmann-Schwinger Equation

In this section we formulate the LSE for the T-matrix in momentum-helicity basis. Similar to the potential matrix element given in Eq. (3.42) the T-matrix element in momentum-helicity basis is defined as

$$T_{\Lambda'\Lambda}^{\pi St}(\mathbf{q}', \mathbf{q}) \equiv \pi^a \langle \mathbf{q}'; \hat{\mathbf{q}}' S \Lambda'; t | T | \mathbf{q}; \hat{\mathbf{q}} S \Lambda; t \rangle^{\pi a}. \quad (3.54)$$

It is obvious that the symmetry relations given in Eqs. (3.46)-(3.48) for the potential matrix element as well as the expressions in Eqs. (3.43) and (3.45) apply also to the T-matrix element given in Eq. (3.54), since these equations result from the nature of the momentum-helicity basis and the invariance properties of the NN potential, which indeed are also possessed by the T-matrix:

$$T_{\Lambda'\Lambda}^{\pi St}(\mathbf{q}', \mathbf{q}) = \sqrt{2} \left(1 - \eta_\pi(-)^{S+t}\right) \langle t | \langle \hat{\mathbf{q}}' S \Lambda' | \langle \mathbf{q}' | T | \mathbf{q} \rangle_\pi | \hat{\mathbf{q}} S \Lambda \rangle | t \rangle \quad (3.55)$$

$$T_{\Lambda'\Lambda}^{\pi St}(\mathbf{q}', \mathbf{q}) = \sqrt{2} \left(1 - \eta_\pi(-)^{S+t}\right) \langle t | \langle \hat{\mathbf{q}}' S \Lambda' |_\pi \langle \mathbf{q}' | T | \mathbf{q} \rangle | \hat{\mathbf{q}} S \Lambda \rangle | t \rangle \quad (3.56)$$

$$T_{-\Lambda', \Lambda}^{\pi St}(\mathbf{q}', \mathbf{q}) = \eta_\pi(-)^S T_{\Lambda'\Lambda}^{\pi St}(-\mathbf{q}', \mathbf{q}) \quad (3.57)$$

$$T_{\Lambda', -\Lambda}^{\pi St}(\mathbf{q}', \mathbf{q}) = \eta_\pi(-)^S T_{\Lambda'\Lambda}^{\pi St}(\mathbf{q}', -\mathbf{q}) \quad (3.58)$$

$$T_{-\Lambda', -\Lambda}^{\pi St}(\mathbf{q}', \mathbf{q}) = T_{\Lambda'\Lambda}^{\pi St}(-\mathbf{q}', -\mathbf{q}). \quad (3.59)$$

Recalling first the LSE given in Eq. (2.7), then using the completeness relation Eq. (3.26) and the definitions in Eq. (3.54) for the T-matrix element and in Eq. (3.42) for the potential matrix element, the LSE for the T-matrix element in momentum-helicity basis takes the following form of an integral equation

$$T_{\Lambda'\Lambda}^{\pi St}(\mathbf{q}', \mathbf{q}) = V_{\Lambda'\Lambda}^{\pi St}(\mathbf{q}', \mathbf{q}) + \frac{1}{4} \sum_{\Lambda''} \int d\mathbf{q}'' V_{\Lambda'\Lambda''}^{\pi St}(\mathbf{q}', \mathbf{q}'') G_0^+(E_q) T_{\Lambda''\Lambda}^{\pi St}(\mathbf{q}'', \mathbf{q}), \quad (3.60)$$

where E_q and $G_0^+(E_q)$ are given in Eq. (2.12). As mentioned there are two total-spin states of the two nucleons, i.e. singlet ($S = 0$) and triplet ($S = 1$) states. For the singlet case the LSE in Eq. (3.60) is one equation

$$T_{00}^{\pi 0t}(\mathbf{q}', \mathbf{q}) = V_{00}^{\pi 0t}(\mathbf{q}', \mathbf{q}) + \frac{1}{4} \int d\mathbf{q}'' V_{00}^{\pi 0t}(\mathbf{q}', \mathbf{q}'') G_0^+(E_q) T_{00}^{\pi 0t}(\mathbf{q}'', \mathbf{q}). \quad (3.61)$$

For the triplet case there are 3 coupled equations to each initial helicity $\Lambda = -1, 0, 1$:

$$T_{1\Lambda}^{\pi 1t}(\mathbf{q}', \mathbf{q}) = V_{1\Lambda}^{\pi 1t}(\mathbf{q}', \mathbf{q}) + \frac{1}{4} \int d\mathbf{q}'' \left\{ V_{11}^{\pi 1t}(\mathbf{q}', \mathbf{q}'') G_0^+(E_q) T_{1\Lambda}^{\pi 1t}(\mathbf{q}'', \mathbf{q}) \right.$$

$$\begin{aligned}
& + V_{10}^{\pi 1t}(\mathbf{q}', \mathbf{q}'') G_0^+(E_q) T_{0\Lambda}^{\pi 1t}(\mathbf{q}'', \mathbf{q}) + V_{-1-1}^{\pi 1t}(\mathbf{q}', \mathbf{q}'') G_0^+(E_q) T_{-1\Lambda}^{\pi 1t}(\mathbf{q}'', \mathbf{q}) \} \\
T_{0\Lambda}^{\pi 1t}(\mathbf{q}', \mathbf{q}) & = V_{0\Lambda}^{\pi 1t}(\mathbf{q}', \mathbf{q}) + \frac{1}{4} \int d\mathbf{q}'' \{ V_{01}^{\pi 1t}(\mathbf{q}', \mathbf{q}'') G_0^+(E_q) T_{1\Lambda}^{\pi 1t}(\mathbf{q}'', \mathbf{q}) \\
& + V_{00}^{\pi 1t}(\mathbf{q}', \mathbf{q}'') G_0^+(E_q) T_{0\Lambda}^{\pi 1t}(\mathbf{q}'', \mathbf{q}) + V_{0-1}^{\pi 1t}(\mathbf{q}', \mathbf{q}'') G_0^+(E_q) T_{-1\Lambda}^{\pi 1t}(\mathbf{q}'', \mathbf{q}) \} \\
T_{-1\Lambda}^{\pi 1t}(\mathbf{q}', \mathbf{q}) & = V_{-1\Lambda}^{\pi 1t}(\mathbf{q}', \mathbf{q}) + \frac{1}{4} \int d\mathbf{q}'' \{ V_{-11}^{\pi 1t}(\mathbf{q}', \mathbf{q}'') G_0^+(E_q) T_{1\Lambda}^{\pi 1t}(\mathbf{q}'', \mathbf{q}) \\
& + V_{-10}^{\pi 1t}(\mathbf{q}', \mathbf{q}'') G_0^+(E_q) T_{0\Lambda}^{\pi 1t}(\mathbf{q}'', \mathbf{q}) + V_{-1-1}^{\pi 1t}(\mathbf{q}', \mathbf{q}'') G_0^+(E_q) T_{-1\Lambda}^{\pi 1t}(\mathbf{q}'', \mathbf{q}) \}.
\end{aligned} \tag{3.62}$$

This coupled set of equations in Eq. (3.62) can be reduced by means of the symmetry properties of the potential and T-matrix elements.

Equations (3.47) and (3.57) change the integral term with $\Lambda'' = -1$ in Eq. (3.60) as

$$\begin{aligned}
& \int d\mathbf{q}'' V_{\Lambda', -1}^{\pi St}(\mathbf{q}', \mathbf{q}'') G_0^+(E_q) T_{-1, \Lambda}^{\pi St}(\mathbf{q}'', \mathbf{q}) \\
& = \int d\mathbf{q}'' \eta_\pi(-)^S V_{\Lambda', 1}^{\pi St}(\mathbf{q}', -\mathbf{q}'') G_0^+(E_q) \eta_\pi(-)^S T_{1, \Lambda}^{\pi St}(-\mathbf{q}'', \mathbf{q}) \\
& = \int d\mathbf{q}'' V_{\Lambda', 1}^{\pi St}(\mathbf{q}', -\mathbf{q}'') G_0^+(E_q) T_{1, \Lambda}^{\pi St}(-\mathbf{q}'', \mathbf{q}) \\
& = \int d\mathbf{q}'' V_{\Lambda', 1}^{\pi St}(\mathbf{q}', \mathbf{q}'') G_0^+(E_q) T_{1, \Lambda}^{\pi St}(\mathbf{q}'', \mathbf{q}).
\end{aligned} \tag{3.63}$$

Thus it can be combined with the integral term with $\Lambda'' = 1$. This leads to

$$\begin{aligned}
T_{\Lambda' \Lambda}^{\pi 1t}(\mathbf{q}', \mathbf{q}) & = V_{\Lambda' \Lambda}^{\pi 1t}(\mathbf{q}', \mathbf{q}) + \frac{1}{2} \int d\mathbf{q}'' V_{\Lambda' 1}^{\pi 1t}(\mathbf{q}', \mathbf{q}'') G_0^+(E_q) T_{1\Lambda}^{\pi 1t}(\mathbf{q}'', \mathbf{q}) \\
& + \frac{1}{4} \int d\mathbf{q}'' V_{\Lambda' 0}^{\pi 1t}(\mathbf{q}', \mathbf{q}'') G_0^+(E_q) T_{0\Lambda}^{\pi 1t}(\mathbf{q}'', \mathbf{q}).
\end{aligned} \tag{3.64}$$

Hence, for the case $S = 1$ one needs only two instead of three coupled equations for $\Lambda' = 1, 0$ for each Λ . In addition Eqs. (3.47) and (3.58) allow us to consider only $\Lambda = 1, 0$.

At this point we would like to summarize that for each isospin (singlet or triplet) the set of the LSE's consists of five equations, i.e. one uncoupled equation for $S = 0$ and two sets ($\Lambda = 1, 0$) of two coupled equations ($\Lambda' = 1, 0$) for $S = 1$. In contrast to the standard partial wave technique the number of the LSE's to be solved is fixed regardless the energy involved in the process. There are 10 equations for np scattering and 5 equations for pp scattering.

The LSE given in Eq. (3.64) is a set of three-dimensional integral equations. This reduced LSE is still subject to further reduction, which makes use of the azimuthal behavior of the potential matrix elements emphasized in the end of the preceding section (Eqs. (3.52) and (3.53)).

We begin by assuming that the azimuthal behavior of the potential matrix elements Eqs. (3.52) and (3.53) are carried over to the T-matrix elements. This is reasonable as

can be seen in the infinite series of the LSE in V

$$T = V + VG_0V + VG_0VG_0V + \dots \quad (3.65)$$

The propagator G_0 has no angular dependence. Thus we make an ansatz for the solution of the LSE given in Eq. (3.60) with $\hat{\mathbf{q}} = \hat{\mathbf{z}}$ as

$$T_{\Lambda'\Lambda}^{\pi St}(\mathbf{q}', q\hat{\mathbf{z}}) = e^{i\Lambda\phi'} T_{\Lambda'\Lambda}^{\pi St}(q', q, \theta'). \quad (3.66)$$

We insert this into the right side of Eq. (3.60) together with Eqs. (3.52) and (3.53) to obtain

$$\begin{aligned} T_{\Lambda'\Lambda}^{\pi St}(\mathbf{q}', q\hat{\mathbf{z}}) &= e^{i\Lambda\phi'} V_{\Lambda'\Lambda}^{\pi St}(q', q, \theta') \\ &\quad + \frac{1}{4} \sum_{\Lambda''} \int d\mathbf{q}'' V_{\Lambda'\Lambda''}^{\pi St} \left\{ e^{iM(\phi' - \phi'')}, \cos(\phi' - \phi''), q', q'' \right\} \\ &\quad \quad \times G_0^+(E_q) e^{i\Lambda\phi''} T_{\Lambda''\Lambda}^{\pi St}(q'', q, \theta'') \\ &= e^{i\Lambda\phi'} V_{\Lambda'\Lambda}^{\pi St}(q', q, \theta') + \frac{1}{4} e^{i\Lambda\phi'} \sum_{\Lambda''} \int_0^\infty dq'' q''^2 \int_{-1}^1 d \cos \theta'' \int_0^{2\pi} d\phi'' \\ &\quad \quad \times V_{\Lambda'\Lambda''}^{\pi St} \left\{ e^{iM(\phi' - \phi'')}, \cos(\phi' - \phi''), q', q'' \right\} \\ &\quad \quad \times G_0^+(E_q) e^{i\Lambda(\phi'' - \phi')} T_{\Lambda''\Lambda}^{\pi St}(q'', q, \theta''). \end{aligned} \quad (3.67)$$

With respect to ϕ'' the integrand is periodical with the period being 2π . Thus we can set $\phi' = 0$ just for the ϕ'' -integration and get

$$\begin{aligned} T_{\Lambda'\Lambda}^{\pi St}(\mathbf{q}', q\hat{\mathbf{z}}) &= e^{i\Lambda\phi'} \left[V_{\Lambda'\Lambda}^{\pi St}(q', q, \theta') + \frac{1}{4} \sum_{\Lambda''} \int_0^\infty dq'' q''^2 \int_{-1}^1 d \cos \theta'' \int_0^{2\pi} d\phi'' \right. \\ &\quad \quad \left. \times V_{\Lambda'\Lambda''}^{\pi St} \left\{ e^{-iM\phi''}, \cos \phi'', q', q'' \right\} G_0^+(E_q) e^{i\Lambda\phi''} T_{\Lambda''\Lambda}^{\pi St}(q'', q, \theta'') \right] \\ &\equiv e^{i\Lambda\phi'} T_{\Lambda'\Lambda}^{\pi St}(q', q, \theta'). \end{aligned} \quad (3.68)$$

This verifies the correctness of the ansatz in Eq. (3.66).

Now we return to Eq. (3.67) and remove the factor $e^{i\Lambda\phi'}$ on both sides of the equation.

This leads to

$$\begin{aligned} T_{\Lambda'\Lambda}^{\pi St}(q', q, \theta') &= V_{\Lambda'\Lambda}^{\pi St}(q', q, \theta') + \frac{1}{4} \sum_{\Lambda''} \int_0^\infty dq'' q''^2 \int_{-1}^1 d \cos \theta'' \int_0^{2\pi} d\phi'' \\ &\quad \quad \times e^{-i\Lambda(\phi' - \phi'')} V_{\Lambda'\Lambda''}^{\pi St}(\mathbf{q}', \mathbf{q}'') G_0^+(E_q) T_{\Lambda''\Lambda}^{\pi St}(q'', q, \theta''), \end{aligned} \quad (3.69)$$

where we restored the original notation $V_{\Lambda'\Lambda''}^{\pi St}(\mathbf{q}', \mathbf{q}'')$ for the potential matrix elements in the integral kernel. This is a LSE for the two-dimensional T-matrix $T_{\Lambda'\Lambda}^{\pi St}(q', q, \theta')$. The solution of this equation has no azimuthal dependence and hence the ϕ'' -integration can be carried out independently. Defining

$$v_{\Lambda'\Lambda''}^{\pi St, \Lambda}(q', q'', \theta', \theta'') \equiv \int_0^{2\pi} d\phi'' e^{-i\Lambda(\phi' - \phi'')} V_{\Lambda'\Lambda''}^{\pi St}(\mathbf{q}', \mathbf{q}''), \quad (3.70)$$

we can write the LSE for the two-dimensional T-matrix as

$$T_{\Lambda'\Lambda}^{\pi St}(q', q, \theta') = V_{\Lambda'\Lambda}^{\pi St}(q', q, \theta') + \frac{1}{4} \sum_{\Lambda''} \int_0^\infty dq'' q''^2 \int_{-1}^1 d \cos \theta'' v_{\Lambda'\Lambda''}^{\pi St, \Lambda}(q', q'', \theta', \theta'') G_0^+(E_q) T_{\Lambda''\Lambda}^{\pi St}(q'', q, \theta''). \quad (3.71)$$

Note that in evaluating the integral in Eq. (3.70) we again set $\phi' = 0$ as explained in the context of Eq. (3.68). The driving term of this equation is a special case of Eq. (3.70) for $q'' = q$, $\theta'' = \phi'' = 0$ and $\Lambda'' = \Lambda$ up to a factor $(2\pi)^{-1}$,

$$v_{\Lambda'\Lambda}^{\pi St, \Lambda}(q', q, \theta', 0) = \int_0^{2\pi} d\phi'' e^{-i\Lambda\phi''} V_{\Lambda'\Lambda}^{\pi St}(\mathbf{q}', q\hat{\mathbf{q}}) = 2\pi V_{\Lambda'\Lambda}^{\pi St}(q', q, \theta'). \quad (3.72)$$

Inserting all these results into Eqs. (3.61) and (3.64) gives

$$\begin{aligned} T_{00}^{\pi 0t}(q', q, \theta') &= V_{00}^{\pi 0t}(q', q, \theta') \\ &\quad + \frac{1}{4} \int_0^\infty dq'' q''^2 \int_{-1}^1 d \cos \theta'' v_{00}^{\pi 0t, 0}(q', q'', \theta', \theta'') G_0^+(E_q) T_{00}^{\pi 0t}(q'', q, \theta'') \\ T_{\Lambda'\Lambda}^{\pi 1t}(q', q, \theta') &= V_{\Lambda'\Lambda}^{\pi 1t}(q', q, \theta') \\ &\quad + \frac{1}{2} \int_0^\infty dq'' q''^2 \int_{-1}^1 d \cos \theta'' v_{\Lambda'1}^{\pi 1t, \Lambda}(q', q'', \theta', \theta'') G_0^+(E_q) T_{1\Lambda}^{\pi 1t}(q'', q, \theta'') \\ &\quad + \frac{1}{4} \int_0^\infty dq'' q''^2 \int_{-1}^1 d \cos \theta'' v_{\Lambda'0}^{\pi 1t, \Lambda}(q', q'', \theta', \theta'') G_0^+(E_q) T_{0\Lambda}^{\pi 1t}(q'', q, \theta''). \end{aligned} \quad (3.73)$$

This is the final form of the set of the LSE's for NN scattering in the momentum-helicity basis.

3.4 Connection to the Physical T-Matrix Representation

In the preceding section we have derived the set of the LSE's Eq. (3.73) for the T-matrix. The T-matrix elements resulting from that equation are in the momentum-helicity basis and therefore not directly appropriate for calculating observables, which are then compared to experimental data. We need the T-matrix elements with respect to the states given as

$$|\nu_1 \nu_2 m_1 m_2 \mathbf{q}\rangle_a \equiv \frac{1}{\sqrt{2}} (1 - P_{12}) |\nu_1 \nu_2 m_1 m_2 \mathbf{q}\rangle, \quad (3.74)$$

where ν_1, ν_2 and m_1, m_2 are the magnetic isospin and spin quantum numbers, respectively. The T-matrix elements in these states are then given as

$$\begin{aligned} {}_a \langle \nu_1 \nu_2 m'_1 m'_2 \mathbf{q}' | T | \nu_1 \nu_2 m_1 m_2 \mathbf{q} \rangle_a &= \frac{1}{2} \langle \nu_1 \nu_2 m'_1 m'_2 \mathbf{q}' | (1 - P_{12}) T (1 - P_{12}) | \nu_1 \nu_2 m_1 m_2 \mathbf{q} \rangle \\ &= \langle \nu_1 \nu_2 m'_1 m'_2 \mathbf{q}' | T (1 - P_{12}) | \nu_1 \nu_2 m_1 m_2 \mathbf{q} \rangle, \end{aligned} \quad (3.75)$$

which we refer to as the physical T-matrix elements. For example, the spin-averaged NN differential cross section is calculated as

$$\frac{d\sigma}{d\Omega} = (2\pi)^4 \left(\frac{m}{2}\right)^2 \frac{1}{4} \sum_{m'_1 m'_2 m_1 m_2} |{}_a \langle \nu_1 \nu_2 m'_1 m'_2 q \hat{\mathbf{q}}' | T | \nu_1 \nu_2 m_1 m_2 \mathbf{q} \rangle_a|^2. \quad (3.76)$$

Thus a connection between the physical T-matrix elements and the T-matrix elements in the momentum-helicity basis is required, especially the one with $\hat{\mathbf{q}} = \hat{\mathbf{z}}$.

The physical T-matrix elements given in Eq. (3.75) have to be expressed in terms of $T_{\Lambda'\Lambda}^{\pi S t}(\mathbf{q}', \mathbf{q})$ by inserting into that equation the completeness relation given in Eq. (3.26) twice. Thus we need the overlap of the momentum-helicity basis state with the state $|\nu_1 \nu_2 m_1 m_2 \mathbf{q}\rangle_a$. This is done in the following:

$$\begin{aligned} & \pi^a \langle \mathbf{q}'; \hat{\mathbf{q}}' S \Lambda'; t | \nu_1 \nu_2 m_1 m_2 \mathbf{q} \rangle_a \\ &= \frac{1}{2} \left(1 - \eta_\pi(-)^{S+t}\right) \langle t |_\pi \langle \mathbf{q}'; \hat{\mathbf{q}}' S \Lambda' | (1 - P_{12}) | \nu_1 \nu_2 m_1 m_2 \mathbf{q} \rangle \\ &= \frac{1}{2\sqrt{2}} \left(1 - \eta_\pi(-)^{S+t}\right) \langle t | (\langle \mathbf{q}' | + \eta_\pi \langle -\mathbf{q}' |) \langle \hat{\mathbf{q}}' S \Lambda' | \\ & \quad \times (|\nu_1 \nu_2 m_1 m_2 \mathbf{q}\rangle - |\nu_2 \nu_1 m_2 m_1 - \mathbf{q}\rangle) \\ &= \frac{1}{2\sqrt{2}} \left(1 - \eta_\pi(-)^{S+t}\right) (\langle \mathbf{q}' | + \eta_\pi \langle -\mathbf{q}' |) \\ & \quad \times (\langle t | \nu_1 \nu_2 \rangle \langle \hat{\mathbf{q}}' S \Lambda' | m_1 m_2 \rangle | \mathbf{q} \rangle - \langle t | \nu_2 \nu_1 \rangle \langle \hat{\mathbf{q}}' S \Lambda' | m_2 m_1 \rangle | -\mathbf{q} \rangle) \\ &= \frac{1}{2\sqrt{2}} \left(1 - \eta_\pi(-)^{S+t}\right) \{ \delta(\mathbf{q}' - \mathbf{q}) \langle t | \nu_1 \nu_2 \rangle \langle \hat{\mathbf{q}}' S \Lambda' | m_1 m_2 \rangle \\ & \quad - \delta(\mathbf{q}' + \mathbf{q}) \langle t | \nu_2 \nu_1 \rangle \langle \hat{\mathbf{q}}' S \Lambda' | m_2 m_1 \rangle + \eta_\pi \delta(\mathbf{q}' + \mathbf{q}) \langle t | \nu_1 \nu_2 \rangle \langle \hat{\mathbf{q}}' S \Lambda' | m_1 m_2 \rangle \\ & \quad - \eta_\pi \delta(\mathbf{q}' - \mathbf{q}) \langle t | \nu_2 \nu_1 \rangle \langle \hat{\mathbf{q}}' S \Lambda' | m_2 m_1 \rangle \}. \end{aligned} \quad (3.77)$$

With the overlap $\langle \hat{\mathbf{q}}' S \Lambda' | m_1 m_2 \rangle$ being

$$\begin{aligned} \langle \hat{\mathbf{q}}' S \Lambda' | m_1 m_2 \rangle &= \sum_{S'} C \left(\frac{1}{2} \frac{1}{2} S'; m_1 m_2 \Lambda_0 \right) \langle \hat{\mathbf{q}}' S \Lambda' | \hat{\mathbf{z}} S' \Lambda_0 \rangle \\ &= \sum_{S'} C \left(\frac{1}{2} \frac{1}{2} S'; m_1 m_2 \Lambda_0 \right) D_{\Lambda_0 \Lambda'}^{S*}(\hat{\mathbf{q}}') \delta_{SS'} \\ &= C \left(\frac{1}{2} \frac{1}{2} S; m_1 m_2 \Lambda_0 \right) e^{i\Lambda_0 \phi'} d_{\Lambda_0 \Lambda'}^S(\theta'), \end{aligned} \quad (3.78)$$

Eq. (3.77) can be evaluated to give

$$\begin{aligned} & \pi^a \langle \mathbf{q}'; \hat{\mathbf{q}}' S \Lambda'; t | \nu_1 \nu_2 m_1 m_2 \mathbf{q} \rangle_a \\ &= \frac{1}{2\sqrt{2}} \left(1 - \eta_\pi(-)^{S+t}\right) C \left(\frac{1}{2} \frac{1}{2} t; \nu_1 \nu_2 \right) C \left(\frac{1}{2} \frac{1}{2} S; m_1 m_2 \Lambda_0 \right) e^{i\Lambda_0 \phi'} d_{\Lambda_0 \Lambda'}^S(\theta') \\ & \quad \times \{ \delta(\mathbf{q}' - \mathbf{q}) - \delta(\mathbf{q}' + \mathbf{q})(-)^{S+t} + \eta_\pi \delta(\mathbf{q}' + \mathbf{q}) - \eta_\pi \delta(\mathbf{q}' - \mathbf{q})(-)^{S+t} \} \\ &= \frac{1}{2\sqrt{2}} \left(1 - \eta_\pi(-)^{S+t}\right) C \left(\frac{1}{2} \frac{1}{2} t; \nu_1 \nu_2 \right) C \left(\frac{1}{2} \frac{1}{2} S; m_1 m_2 \Lambda_0 \right) \end{aligned}$$

$$\begin{aligned}
& \times e^{i\Lambda_0\phi'} d_{\Lambda_0\Lambda'}^S(\theta') \left(1 - \eta_\pi(-)^{S+t}\right) \{\delta(\mathbf{q}' - \mathbf{q}) + \eta_\pi\delta(\mathbf{q}' + \mathbf{q})\} \\
& = \frac{1}{\sqrt{2}} \left(1 - \eta_\pi(-)^{S+t}\right) C\left(\frac{1}{2}\frac{1}{2}t; \nu_1\nu_2\right) C\left(\frac{1}{2}\frac{1}{2}S; m_1m_2\Lambda_0\right) \\
& \times e^{i\Lambda_0\phi'} d_{\Lambda_0\Lambda'}^S(\theta') \{\delta(\mathbf{q}' - \mathbf{q}) + \eta_\pi\delta(\mathbf{q}' + \mathbf{q})\}, \tag{3.79}
\end{aligned}$$

where the following relation for the Clebsch-Gordan coefficient has been used

$$C(j_2j_1j; m_2m_1m) = (-)^{j_1+j_2-j} C(j_1j_2j; m_1m_2m). \tag{3.80}$$

Note that if necessary we write the Clebsch-Gordan coefficient as $C(j_2j_1j; m_2m_1)$ without explicitly show the total magnetic quantum number $m = m_1 + m_2$. For example, in the last equation we have written $C\left(\frac{1}{2}\frac{1}{2}t; \nu_1\nu_2\right)$ instead of $C\left(\frac{1}{2}\frac{1}{2}t; \nu_1\nu_2(\nu_1 + \nu_2)\right)$.

Having the overlap of the momentum-helicity basis state with the state $|\nu_1\nu_2m_1m_2\mathbf{q}\rangle_a$ as given in Eq. (3.79) we derive the expression for the physical T-matrix elements in terms of the T-matrix elements in the momentum-helicity basis as

$$\begin{aligned}
& {}_a\langle \nu_1\nu_2m'_1m'_2\mathbf{q}' | T | \nu_1\nu_2m_1m_2\mathbf{q} \rangle_a \\
& = \left(\frac{1}{4}\right)^2 \sum_{S\Lambda'\pi t\Lambda} \int d\mathbf{q}'' \langle \nu_1\nu_2m'_1m'_2\mathbf{q}' | \mathbf{q}''; \hat{\mathbf{q}}'' S\Lambda'; t \rangle^{\pi a} \\
& \times \int d\mathbf{q}''' \langle \mathbf{q}''; \hat{\mathbf{q}}'' S\Lambda'; t | T | \mathbf{q}'''; \hat{\mathbf{q}}''' S\Lambda; t \rangle^{\pi a} \langle \mathbf{q}'''; \hat{\mathbf{q}}''' S\Lambda; t | \nu_1\nu_2m_1m_2\mathbf{q} \rangle_a \\
& = \left(\frac{1}{4}\right)^2 \sum_{S\Lambda'\pi t\Lambda} \int d\mathbf{q}'' \int d\mathbf{q}''' \langle \nu_1\nu_2m'_1m'_2\mathbf{q}' | \mathbf{q}''; \hat{\mathbf{q}}'' S\Lambda'; t \rangle^{\pi a} \\
& \quad \times T_{\Lambda'\Lambda}^{\pi st}(\mathbf{q}'', \mathbf{q}''')^{\pi a} \langle \mathbf{q}'''; \hat{\mathbf{q}}''' S\Lambda; t | \nu_1\nu_2m_1m_2\mathbf{q} \rangle_a \\
& = \left(\frac{1}{4}\right)^2 \sum_{S\Lambda'\pi t\Lambda} \int d\mathbf{q}'' \int d\mathbf{q}''' \frac{1}{\sqrt{2}} \left(1 - \eta_\pi(-)^{S+t}\right) C\left(\frac{1}{2}\frac{1}{2}t; \nu_1\nu_2\right) C\left(\frac{1}{2}\frac{1}{2}S; m'_1m'_2\Lambda'_0\right) \\
& \quad \times e^{-i\Lambda'_0\phi''} d_{\Lambda'_0\Lambda'}^S(\theta'') \{\delta(\mathbf{q}'' - \mathbf{q}') + \eta_\pi\delta(\mathbf{q}'' + \mathbf{q}')\} T_{\Lambda'\Lambda}^{\pi St}(\mathbf{q}'', \mathbf{q}''') \\
& \quad \times \frac{1}{\sqrt{2}} \left(1 - \eta_\pi(-)^{S+t}\right) C\left(\frac{1}{2}\frac{1}{2}t; \nu_1\nu_2\right) C\left(\frac{1}{2}\frac{1}{2}S; m_1m_2\Lambda_0\right) \\
& \quad \times e^{i\Lambda_0\phi'''} d_{\Lambda_0\Lambda}^S(\theta''') \{\delta(\mathbf{q}''' - \mathbf{q}) + \eta_\pi\delta(\mathbf{q}''' + \mathbf{q})\} \\
& = \left(\frac{1}{4}\right)^2 \sum_{S\Lambda'\pi t\Lambda} \int d\mathbf{q}'' \int d\mathbf{q}''' \left(1 - \eta_\pi(-)^{S+t}\right) C\left(\frac{1}{2}\frac{1}{2}t; \nu_1\nu_2\right)^2 \\
& \quad \times C\left(\frac{1}{2}\frac{1}{2}S; m'_1m'_2\Lambda'_0\right) C\left(\frac{1}{2}\frac{1}{2}S; m_1m_2\Lambda_0\right) \\
& \quad \times e^{-i\Lambda'_0\phi''} d_{\Lambda'_0\Lambda'}^S(\theta'') e^{i\Lambda_0\phi'''} d_{\Lambda_0\Lambda}^S(\theta''') T_{\Lambda'\Lambda}^{\pi St}(\mathbf{q}'', \mathbf{q}''') \\
& \quad \times \{\delta(\mathbf{q}'' - \mathbf{q}') + \eta_\pi\delta(\mathbf{q}'' + \mathbf{q}')\} \{\delta(\mathbf{q}''' - \mathbf{q}) + \eta_\pi\delta(\mathbf{q}''' + \mathbf{q})\} \\
& = \left(\frac{1}{4}\right)^2 \sum_{S\Lambda'\pi t\Lambda} \left(1 - \eta_\pi(-)^{S+t}\right) C\left(\frac{1}{2}\frac{1}{2}t; \nu_1\nu_2\right)^2 C\left(\frac{1}{2}\frac{1}{2}S; m'_1m'_2\Lambda'_0\right) C\left(\frac{1}{2}\frac{1}{2}S; m_1m_2\Lambda_0\right) \\
& \quad \times \left\{ e^{-i\Lambda'_0\phi'} d_{\Lambda'_0\Lambda'}^S(\theta') e^{i\Lambda_0\phi} d_{\Lambda_0\Lambda}^S(\theta) T_{\Lambda'\Lambda}^{\pi St}(\mathbf{q}', \mathbf{q}) \right. \\
& \quad \left. + e^{-i\Lambda'_0(\phi'+\pi)} d_{\Lambda'_0\Lambda'}^S(\pi - \theta') e^{i\Lambda_0(\phi+\pi)} d_{\Lambda_0\Lambda}^S(\pi - \theta) T_{\Lambda'\Lambda}^{\pi St}(-\mathbf{q}', -\mathbf{q}) \right\}
\end{aligned}$$

$$\begin{aligned}
& +\eta_\pi e^{-i\Lambda'_0\phi'} d_{\Lambda'_0\Lambda'}^S(\theta') e^{i\Lambda_0(\phi+\pi)} d_{\Lambda_0\Lambda}^S(\pi-\theta) T_{\Lambda'\Lambda}^{\pi St}(\mathbf{q}', -\mathbf{q}) \\
& + \eta_\pi e^{-i\Lambda'_0(\phi'+\pi)} d_{\Lambda'_0\Lambda'}^S(\pi-\theta') e^{i\Lambda_0\phi} d_{\Lambda_0\Lambda}^S(\theta) T_{\Lambda'\Lambda}^{\pi St}(-\mathbf{q}', \mathbf{q}) \} \\
= & \left(\frac{1}{4}\right)^2 \sum_{S\Lambda'\pi t\Lambda} (1-\eta_\pi(-)^{S+t}) C\left(\frac{1}{2}\frac{1}{2}t; \nu_1\nu_2\right)^2 C\left(\frac{1}{2}\frac{1}{2}S; m'_1m'_2\Lambda'_0\right) C\left(\frac{1}{2}\frac{1}{2}S; m_1m_2\Lambda_0\right) \\
& \times e^{-i\Lambda'_0\phi'} d_{\Lambda'_0\Lambda'}^S(\theta') e^{i\Lambda_0\phi} d_{\Lambda_0\Lambda}^S(\theta) \\
& \times \left\{ T_{\Lambda'\Lambda}^{\pi St}(\mathbf{q}', \mathbf{q}) + e^{-i\Lambda'_0\pi}(-)^{S+\Lambda'_0} e^{i\Lambda_0\pi}(-)^{S+\Lambda_0} T_{-\Lambda',-\Lambda}^{\pi St}(-\mathbf{q}', -\mathbf{q}) \right. \\
& \left. + \eta_\pi e^{i\Lambda_0\pi}(-)^{S+\Lambda_0} T_{\Lambda',-\Lambda}^{\pi St}(\mathbf{q}', -\mathbf{q}) + \eta_\pi e^{-i\Lambda'_0\pi}(-)^{S+\Lambda'_0} T_{-\Lambda',\Lambda}^{\pi St}(-\mathbf{q}', \mathbf{q}) \right\} \\
= & \left(\frac{1}{4}\right)^2 \sum_{S\Lambda'\pi t\Lambda} (1-\eta_\pi(-)^{S+t}) C\left(\frac{1}{2}\frac{1}{2}t; \nu_1\nu_2\right)^2 C\left(\frac{1}{2}\frac{1}{2}S; m'_1m'_2\Lambda'_0\right) C\left(\frac{1}{2}\frac{1}{2}S; m_1m_2\Lambda_0\right) \\
& \times e^{-i\Lambda'_0\phi'} d_{\Lambda'_0\Lambda'}^S(\theta') e^{i\Lambda_0\phi} d_{\Lambda_0\Lambda}^S(\theta) \\
& \times \left\{ T_{\Lambda'\Lambda}^{\pi St}(\mathbf{q}', \mathbf{q}) + T_{-\Lambda',-\Lambda}^{\pi St}(-\mathbf{q}', -\mathbf{q}) \right. \\
& \left. + \eta_\pi(-)^S T_{\Lambda',-\Lambda}^{\pi St}(\mathbf{q}', -\mathbf{q}) + \eta_\pi(-)^S T_{-\Lambda',\Lambda}^{\pi St}(-\mathbf{q}', \mathbf{q}) \right\} \\
= & \frac{1}{4} e^{-i(\Lambda'_0\phi' - \Lambda_0\phi)} \sum_{S\pi t} (1-\eta_\pi(-)^{S+t}) C\left(\frac{1}{2}\frac{1}{2}t; \nu_1\nu_2\right)^2 \\
& \times C\left(\frac{1}{2}\frac{1}{2}S; m'_1m'_2\Lambda'_0\right) C\left(\frac{1}{2}\frac{1}{2}S; m_1m_2\Lambda_0\right) \sum_{\Lambda'} d_{\Lambda'_0\Lambda'}^S(\theta') d_{\Lambda_0\Lambda}^S(\theta) T_{\Lambda'\Lambda}^{\pi St}(\mathbf{q}', \mathbf{q}). \quad (3.81)
\end{aligned}$$

We have used the T-matrix properties given in Eqs. (3.57) - (3.59) and the relation for the d-matrices given in Eq. (3.19) to arrive to this result.

Next using Eq. (3.66) and $d_{\Lambda_0\Lambda}^S(0) = \delta_{\Lambda_0\Lambda}$ we get the expression for the physical T-matrix elements with $\hat{\mathbf{q}} = \hat{\mathbf{z}}$ in terms of $T_{\Lambda'\Lambda_0}^{\pi St}(q', q, \theta')$ given in Eq. (3.73) as

$$\begin{aligned}
{}_a \langle \nu_1\nu_2m'_1m'_2q\hat{\mathbf{q}}' | T | \nu_1\nu_2m_1m_2q\hat{\mathbf{z}} \rangle_a & = \frac{1}{4} e^{-i(\Lambda'_0 - \Lambda_0)\phi'} \sum_{S\pi t} (1-\eta_\pi(-)^{S+t}) C\left(\frac{1}{2}\frac{1}{2}t; \nu_1\nu_2\right)^2 \\
& \times C\left(\frac{1}{2}\frac{1}{2}S; m'_1m'_2\Lambda'_0\right) C\left(\frac{1}{2}\frac{1}{2}S; m_1m_2\Lambda_0\right) \\
& \times \sum_{\Lambda'} d_{\Lambda'_0\Lambda'}^S(\theta') T_{\Lambda'\Lambda_0}^{\pi St}(q, q, \theta'), \quad (3.82)
\end{aligned}$$

where in addition we have set $q' = q$, since observables are measured on-shell.

3.5 Connection to the Standard Partial Wave Representation

After developing a new technique to treat NN scattering it is natural to test and to compare it to the well established, standard partial wave decomposition. Though we can compare our calculations directly to experimental data, it is also interesting to have a comparison on this level. Besides there are not always experimental data available to

compare with. Therefore, we make a connection to the standard partial wave representation. For simplicity we set $q' = q$ from the beginning.

The well known on-shell partial wave projected T-matrix element is defined as

$$T_{l'l}^{Sjt}(q) \equiv \langle q(l'S)jmt | T | q(lS)jmt \rangle, \quad (3.83)$$

where l and l' are the initial and final angular momenta, respectively, and j is the total angular momentum ($\mathbf{J} = \mathbf{L} + \mathbf{S}$). For simplicity we have suppressed the isospin projection m_t along its quantization axis (see the text following Eq. (3.15)). The states $|q(lS)jmt\rangle$, which are called the partial wave basis, are given as

$$|q(lS)jmt\rangle = \sum_{\mu} C(lSj, \mu, m - \mu) |ql\mu\rangle |Sm - \mu\rangle |t\rangle, \quad (3.84)$$

with the standard normalization

$$\langle q'(l'S')j'm't' | q(lS)jmt \rangle = \frac{\delta(q - q')}{q'q} \delta_{l'l} \delta_{S'S} \delta_{j'j} \delta_{m'm} \delta_{t't}. \quad (3.85)$$

The states fulfill the completeness relation

$$\sum_{j'lSmt} \int_0^{\infty} dq q^2 |q(lS)jmt\rangle \langle q(lS)jmt| = 1. \quad (3.86)$$

The idea is to express the partial wave projected T-matrix element $T_{l'l}^{Sjt}(q)$ given in Eq. (3.83) in terms of the T-matrix elements $T_{\Lambda'\Lambda}^{\pi St}(q, q, \theta')$. Then we can compare phase shifts calculated using these partial wave projected T-matrix elements to those resulting from the standard partial wave calculations. Performing a connection the opposite way is difficult, since in obtaining $T_{\Lambda'\Lambda}^{\pi St}(q, q, \theta')$ from $T_{l'l}^{Sjt}(q)$ we need ideally an infinite number of partial waves. Nevertheless we work out both expressions. The first one is the expression for $T_{\Lambda'\Lambda}^{\pi St}(q, q, \theta')$ in terms of $T_{l'l}^{Sjt}(q)$. Using Eq. (3.82) this expression can be verified, since the physical T-matrix elements in the partial wave representation is well known. The second expression is that for $T_{l'l}^{Sjt}(q)$ in terms of $T_{\Lambda'\Lambda}^{\pi St}(q, q, \theta')$, which will be derived from the first expression.

To get the first expression we insert the completeness relation given in Eq. (3.86) twice into Eq. (3.54). It turns out that the overlap $\langle q'(l'S')jm | \mathbf{q}; \hat{\mathbf{q}}S\Lambda \rangle$ need to be worked out first. Using Eqs. (3.18) and (3.84) together with the following projection

$$\langle q'l\mu | \mathbf{q} \rangle = \frac{\delta(q' - q)}{q'q} \langle l\mu | \hat{\mathbf{q}} \rangle = \frac{\delta(q' - q)}{q'q} Y_{l\mu}^*(\hat{\mathbf{q}}) \quad (3.87)$$

this gives

$$\begin{aligned} \langle q'(l'S')jm | \mathbf{q}; \hat{\mathbf{q}}S\Lambda \rangle &= \sum_{\mu} C(lS'j; \mu, m - \mu) \langle q'l\mu | \mathbf{q} \rangle \langle S'm - \mu | \hat{\mathbf{q}}S\Lambda \rangle \\ &= \sum_{\mu} C(lS'j; \mu, m - \mu) \frac{\delta(q' - q)}{q'q} Y_{l\mu}^*(\hat{\mathbf{q}}) \\ &\quad \times \delta_{S'S} e^{-i(m-\mu)\phi} d_{m-\mu, \Lambda}^S(\theta). \end{aligned} \quad (3.88)$$

Now we derive the expression for the on-shell T-matrix $T_{\Lambda'\Lambda}^{\pi St}(q\hat{\mathbf{q}}', \mathbf{q})$ in the momentum-helicity basis in terms of the partial wave projected T-matrix $T_{l'l}^{Sjt}(q)$. We obtain

$$\begin{aligned}
T_{\Lambda'\Lambda}^{\pi St}(q\hat{\mathbf{q}}', \mathbf{q}) &= \pi^a \langle q\hat{\mathbf{q}}'; \hat{\mathbf{q}}' S \Lambda'; t | T | \mathbf{q}; \hat{\mathbf{q}} S \Lambda; t \rangle^{\pi a} \\
&= \frac{1}{2} \left(1 - \eta_\pi(-)^{S+t}\right)^2 \langle t | {}_\pi \langle q\hat{\mathbf{q}}'; \hat{\mathbf{q}}' S \Lambda' | T | \mathbf{q}; \hat{\mathbf{q}} S \Lambda \rangle_\pi | t \rangle \\
&= \left(1 - \eta_\pi(-)^{S+t}\right) \langle t | {}_\pi \langle q\hat{\mathbf{q}}'; \hat{\mathbf{q}}' S \Lambda' | T | \mathbf{q}; \hat{\mathbf{q}} S \Lambda \rangle_\pi | t \rangle \\
&= \left(1 - \eta_\pi(-)^{S+t}\right) \sum_{j'l'S''m't''} \sum_{j'l'S'm't'} \int_0^\infty dq'' q''^2 \int_0^\infty dq' q'^2 \\
&\quad \times \langle t | {}_\pi \langle q\hat{\mathbf{q}}'; \hat{\mathbf{q}}' S \Lambda' | q''(l'S'')j'm't'' \rangle \langle q''(l'S'')j'm't'' | T | q'(lS')jmt' \rangle \\
&\quad \times \langle q'(lS')jmt' | \mathbf{q}; \hat{\mathbf{q}} S \Lambda \rangle_\pi | t \rangle \\
&= \frac{1}{2} \left(1 - \eta_\pi(-)^{S+t}\right) \sum_{l'jm} \langle q(l'S)jmt | T | q(lS)jmt \rangle \\
&\quad \times \left\{ \sum_{\mu'} C(l'Sj; \mu', m - \mu') Y_{l'\mu'}(\hat{\mathbf{q}}') e^{i(m-\mu')\phi'} d_{m-\mu',\Lambda'}^S(\theta') \right. \\
&\quad \left. + \eta_\pi \sum_{\mu'} C(l'Sj; \mu', m - \mu') Y_{l'\mu'}(-\hat{\mathbf{q}}') e^{i(m-\mu')\phi'} d_{m-\mu',\Lambda'}^S(\theta') \right\} \\
&\quad \times \left\{ \sum_{\mu} C(lSj; \mu, m - \mu) Y_{l\mu}^*(\hat{\mathbf{q}}) e^{-i(m-\mu)\phi} d_{m-\mu,\Lambda}^S(\theta) \right. \\
&\quad \left. + \eta_\pi \sum_{\mu} C(lSj; \mu, m - \mu) Y_{l\mu}^*(-\hat{\mathbf{q}}) e^{-i(m-\mu)\phi} d_{m-\mu,\Lambda}^S(\theta) \right\} \\
&= \frac{1}{2} \left(1 - \eta_\pi(-)^{S+t}\right) \sum_{l'jm} T_{l'l}^{Sjt}(q) \left(1 + \eta_\pi(-)^{l'}\right) \left(1 + \eta_\pi(-)^l\right) \\
&\quad \times \sum_{\mu'} C(l'Sj; \mu', m - \mu') Y_{l'\mu'}(\hat{\mathbf{q}}') e^{i(m-\mu')\phi'} d_{m-\mu',\Lambda'}^S(\theta') \\
&\quad \times \sum_{\mu} C(lSj; \mu, m - \mu) Y_{l\mu}^*(\hat{\mathbf{q}}) e^{-i(m-\mu)\phi} d_{m-\mu,\Lambda}^S(\theta), \tag{3.89}
\end{aligned}$$

where in the last equality we have used the relation $Y_{lm}(-\hat{r}) = (-)^l Y_{lm}(\hat{r})$. Inserting $\hat{\mathbf{q}} = \hat{\mathbf{z}}$ and $d_{m-\mu,\Lambda}^S(0) = \delta_{\mu,m-\Lambda}$ into Eq. (3.89) this gives

$$\begin{aligned}
T_{\Lambda'\Lambda}^{\pi St}(q\hat{\mathbf{q}}', q\hat{\mathbf{z}}) &= \frac{1}{2} \left(1 - \eta_\pi(-)^{S+t}\right) \sum_{l'jm} T_{l'l}^{Sjt}(q) \left(1 + \eta_\pi(-)^{l'}\right) \left(1 + \eta_\pi(-)^l\right) \\
&\quad \times \sum_{\mu'} C(l'Sj; \mu', m - \mu') Y_{l'\mu'}(\hat{\mathbf{q}}') e^{i(m-\mu')\phi'} d_{m-\mu',\Lambda'}^S(\theta') \\
&\quad \times C(lSj; m - \Lambda, \Lambda) Y_{l,m-\Lambda}^*(\hat{\mathbf{z}}) \\
&= \frac{1}{2} \left(1 - \eta_\pi(-)^{S+t}\right) \sum_{l'lj} T_{l'l}^{Sjt}(q) \left(1 + \eta_\pi(-)^{l'}\right) \left(1 + \eta_\pi(-)^l\right) \sqrt{\frac{2l+1}{4\pi}} \\
&\quad \times \sum_{\mu'} C(l'Sj; \mu', \Lambda - \mu') Y_{l'\mu'}(\hat{\mathbf{q}}') e^{i(\Lambda-\mu')\phi'} d_{\Lambda-\mu',\Lambda'}^S(\theta') C(lSj; 0, \Lambda). \tag{3.90}
\end{aligned}$$

Using the relations

$$Y_{l'\mu'}(\hat{\mathbf{q}}') = \sqrt{\frac{2l'+1}{4\pi}} D_{\mu',0}^{l'*}(\phi'\theta'0) = \sqrt{\frac{2l'+1}{4\pi}} (-)^{\mu'} D_{-\mu',0}^{l'}(\phi'\theta'0), \quad (3.91)$$

$$d_{m'm}^j(\theta) = (-)^{m'-m} d_{-m',-m}^j(\theta) \quad (3.92)$$

(see Appendix A for the derivation of Eq. (3.92)) and an addition theorem for D-functions

$$D_{\mu_1 m_1}^{j_1} D_{\mu_2 m_2}^{j_2} = \sum_j C(j_1 j_2 j; \mu_1 \mu_2) C(j_1 j_2 j; m_1 m_2) D_{\mu_1 + \mu_2, m_1 + m_2}^j, \quad (3.93)$$

it is straightforward to show that

$$\begin{aligned} & Y_{l'\mu'}(\hat{\mathbf{q}}') e^{i(\Lambda - \mu')\phi'} d_{\Lambda - \mu', \Lambda'}^S(\theta') \\ &= \sqrt{\frac{2l'+1}{4\pi}} (-)^{\Lambda - \Lambda'} D_{-\mu',0}^{l'}(\phi'\theta'0) e^{-i(\mu' - \Lambda)\phi'} d_{\mu' - \Lambda, -\Lambda'}^S(\theta') \\ &= \sqrt{\frac{2l'+1}{4\pi}} (-)^{\Lambda - \Lambda'} D_{-\mu',0}^{l'}(\phi'\theta'0) D_{\mu' - \Lambda, -\Lambda'}^S(\phi'\theta'0) \\ &= \sqrt{\frac{2l'+1}{4\pi}} (-)^{\Lambda - \Lambda'} \sum_j C(l' S j; -\mu', \mu' - \Lambda) C(l' S j; 0, -\Lambda') D_{-\Lambda, -\Lambda'}^j(\phi'\theta'0) \\ &= \sqrt{\frac{2l'+1}{4\pi}} \sum_j C(l' S j; \mu', \Lambda - \mu') C(l' S j; 0 \Lambda') D_{\Lambda \Lambda'}^{j*}(\phi'\theta'0), \end{aligned} \quad (3.94)$$

where in the last step we have applied

$$C(j_1 j_2 j_3; m_1 m_2 m_3) = (-)^{j_1 + j_2 - j_3} C(j_1 j_2 j_3; -m_1, -m_2, -m_3) \quad (3.95)$$

and Eq. (3.92). Thus

$$\begin{aligned} T_{\Lambda' \Lambda}^{\pi S t}(q \hat{\mathbf{q}}', q \hat{\mathbf{z}}) &= \frac{1}{2} (1 - \eta_\pi(-)^{S+t}) \sum_{l' l j} T_{l' l}^{S j t}(q) (1 + \eta_\pi(-)^{l'}) (1 + \eta_\pi(-)^l) \\ &\quad \times \sqrt{\frac{2l'+1}{4\pi}} \sum_{\mu'} C(l' S j; \mu', \Lambda - \mu') \sum_{j'} C(l' S j'; \mu', \Lambda - \mu') C(l' S j'; 0 \Lambda') \\ &\quad \times \sqrt{\frac{2l+1}{4\pi}} D_{\Lambda \Lambda'}^{j*}(\phi'\theta'0) C(l S j; 0, \Lambda) \\ &= \frac{1}{2} (1 - \eta_\pi(-)^{S+t}) \sum_{l' l j} T_{l' l}^{S j t}(q) (1 + \eta_\pi(-)^{l'}) (1 + \eta_\pi(-)^l) \\ &\quad \times \sqrt{\frac{2l'+1}{4\pi}} C(l' S j; 0 \Lambda') D_{\Lambda \Lambda'}^{j*}(\phi'\theta'0) \sqrt{\frac{2l+1}{4\pi}} C(l S j; 0, \Lambda) \\ &= \frac{1}{2} (1 - \eta_\pi(-)^{S+t}) \sum_{l' l j} T_{l' l}^{S j t}(q) (1 + \eta_\pi(-)^{l'}) (1 + \eta_\pi(-)^l) \\ &\quad \times \sqrt{\frac{2l'+1}{4\pi}} C(l' S j; 0 \Lambda') d_{\Lambda \Lambda'}^j(\theta') \sqrt{\frac{2l+1}{4\pi}} C(l S j; 0, \Lambda) e^{i\Lambda\phi'}. \end{aligned} \quad (3.96)$$

Finally, using Eq. (3.66) we obtain the expression for $T_{\Lambda'\Lambda}^{\pi S t}(q, q, \theta')$ in terms of $T_{l'l}^{S j t}(q)$ as

$$\begin{aligned} T_{\Lambda'\Lambda}^{\pi S t}(q, q, \theta') &= \frac{1}{2} \left(1 - \eta_{\pi}(-)^{S+t}\right) \sum_{l'l_j} T_{l'l}^{S j t}(q) \left(1 + \eta_{\pi}(-)^{l'}\right) \left(1 + \eta_{\pi}(-)^l\right) \\ &\quad \times \sqrt{\frac{2l'+1}{4\pi}} C(l' S j; 0 \Lambda') d_{\Lambda\Lambda'}^j(\theta') \sqrt{\frac{2l+1}{4\pi}} C(l S j; 0 \Lambda). \end{aligned} \quad (3.97)$$

Now we perform a test to this expression. We insert this equation into the physical T-matrix elements Eq. (3.82) with the aim to get the partial wave representation for the physical T-matrix elements.

$$\begin{aligned} &{}_a \langle \nu_1 \nu_2 m'_1 m'_2 q \hat{\mathbf{Q}}' | T | \nu_1 \nu_2 m_1 m_2 q \hat{\mathbf{z}} \rangle_a \\ &= \frac{1}{4} e^{-i(\Lambda'_0 - \Lambda_0)\phi'} \sum_{S \pi t} \left(1 - \eta_{\pi}(-)^{S+t}\right) C\left(\frac{1}{2} \frac{1}{2} t; \nu_1 \nu_2\right)^2 \\ &\quad \times C\left(\frac{1}{2} \frac{1}{2} S; m'_1 m'_2 \Lambda'_0\right) C\left(\frac{1}{2} \frac{1}{2} S; m_1 m_2 \Lambda_0\right) \\ &\quad \times \sum_{\Lambda'} d_{\Lambda'_0 \Lambda'}^S(\theta') \frac{1}{2} \left(1 - \eta_{\pi}(-)^{S+t}\right) \sum_{l'l_j} T_{l'l}^{S j t}(q) \left(1 + \eta_{\pi}(-)^{l'}\right) \left(1 + \eta_{\pi}(-)^l\right) \\ &\quad \times \sqrt{\frac{2l'+1}{4\pi}} C(l' S j; 0 \Lambda') d_{\Lambda_0 \Lambda'}^j(\theta') \sqrt{\frac{2l+1}{4\pi}} C(l S j; 0 \Lambda_0) \\ &= \frac{1}{4i\pi\sqrt{\pi}mq} e^{-i(\Lambda'_0 - \Lambda_0)\phi'} \sum_{S t} C\left(\frac{1}{2} \frac{1}{2} t; \nu_1 \nu_2\right)^2 \\ &\quad \times C\left(\frac{1}{2} \frac{1}{2} S; m'_1 m'_2 \Lambda'_0\right) C\left(\frac{1}{2} \frac{1}{2} S; m_1 m_2 \Lambda_0\right) \\ &\quad \times \sum_{l'l_j} \left(1 - (-)^{l'+S+t}\right) \left(1 - (-)^{l+S+t}\right) \left(\delta_{l'l} - S_{l'l}^{S j t}(q)\right) \sqrt{2l+1} C(l S j; 0 \Lambda_0) \\ &\quad \sqrt{\frac{2l'+1}{4\pi}} \sum_{\Lambda'} d_{\Lambda'_0 \Lambda'}^S(\theta') d_{\Lambda_0 \Lambda'}^j(\theta') C(l' S j; 0 \Lambda') \\ &= \frac{1}{4i\pi\sqrt{\pi}mq} \sum_{S t} C\left(\frac{1}{2} \frac{1}{2} t; \nu_1 \nu_2\right)^2 C\left(\frac{1}{2} \frac{1}{2} S; m'_1 m'_2 \Lambda'_0\right) C\left(\frac{1}{2} \frac{1}{2} S; m_1 m_2 \Lambda_0\right) \\ &\quad \times \sum_{l'l_j} \left(1 - (-)^{l'+S+t}\right) \left(1 - (-)^{l+S+t}\right) \left(\delta_{l'l} - S_{l'l}^{S j t}(q)\right) \sqrt{2l+1} C(l S j; 0 \Lambda_0) \\ &\quad \times \sqrt{\frac{2l'+1}{4\pi}} \sum_{\Lambda'} D_{\Lambda'_0 \Lambda'}^S(\phi' \theta' 0) D_{\Lambda_0 \Lambda'}^{j*}(\phi' \theta' 0) C(l' S j; 0 \Lambda') \\ &= \frac{1}{4i\pi\sqrt{\pi}mq} \sum_{S t} C\left(\frac{1}{2} \frac{1}{2} t; \nu_1 \nu_2\right)^2 C\left(\frac{1}{2} \frac{1}{2} S; m'_1 m'_2 \Lambda'_0\right) C\left(\frac{1}{2} \frac{1}{2} S; m_1 m_2 \Lambda_0\right) \\ &\quad \times \sum_{l'l_j} \left(1 - (-)^{l'+S+t}\right) \left(1 - (-)^{l+S+t}\right) \left(\delta_{l'l} - S_{l'l}^{S j t}(q)\right) \sqrt{2l+1} C(l S j; 0 \Lambda_0) \\ &\quad \times \sqrt{\frac{2l'+1}{4\pi}} \sum_{\Lambda'} D_{\Lambda'_0 \Lambda'}^S(\phi' \theta' 0) \sum_n D_{n0}^{l'*}(\phi' \theta' 0) D_{\Lambda_0 - n, \Lambda'}^{S*}(\phi' \theta' 0) C(l' S j; n, \Lambda_0 - n) \\ &= \frac{1}{4i\pi\sqrt{\pi}mq} \sum_{S t} C\left(\frac{1}{2} \frac{1}{2} t; \nu_1 \nu_2\right)^2 C\left(\frac{1}{2} \frac{1}{2} S; m'_1 m'_2 \Lambda'_0\right) C\left(\frac{1}{2} \frac{1}{2} S; m_1 m_2 \Lambda_0\right) \end{aligned}$$

$$\begin{aligned}
& \times \sum_{l'l_j} \left(1 - (-)^{l'+S+t}\right) \left(1 - (-)^{l+S+t}\right) \left(\delta_{l'l} - S_{l'l}^{Sjt}(q)\right) \sqrt{2l+1} C(lSj; 0\Lambda_0) \\
& \times \sqrt{\frac{2l'+1}{4\pi}} D_{\Lambda_0-\Lambda'_0,0}^{l'*}(\phi'\theta'0) C(l'Sj; \Lambda_0 - \Lambda'_0, \Lambda'_0). \tag{3.98}
\end{aligned}$$

Here $S_{l'l}^{Sjt}(q)$ is the partial wave projected S-matrix related to $T_{l'l}^{Sjt}(q)$ as

$$S_{l'l}^{Sjt}(q) = \delta_{l'l} - i\pi m q T_{l'l}^{Sjt}(q). \tag{3.99}$$

In the last two steps of Eq. (3.98) we have used the relation

$$D_{\Lambda_0\Lambda'}^{j*}(\phi'\theta'0) C(l'Sj; 0\Lambda') = \sum_n D_{n0}^{l'*}(\phi'\theta'0) D_{\Lambda_0-n,\Lambda'}^{S*}(\phi'\theta'0) C(l'Sj; n, \Lambda_0 - n) \tag{3.100}$$

and an orthonormality relation of D-functions

$$\sum_{\Lambda'} D_{\Lambda_0\Lambda'}^S(\phi'\theta'0) D_{\Lambda_0-n,\Lambda'}^{S*}(\phi'\theta'0) = \delta_{\Lambda_0,\Lambda_0-n}. \tag{3.101}$$

Using Eq. (3.91) we end up with the standard form of the physical T-matrix elements in the partial wave representation

$$\begin{aligned}
& {}_a \langle \nu_1 \nu_2 m'_1 m'_2 q \hat{\mathbf{q}}' | T | \nu_1 \nu_2 m_1 m_2 q \hat{\mathbf{z}} \rangle_a \\
& = \frac{1}{4} \frac{1}{\sqrt{\pi}} \frac{1}{i\pi m q} \sum_{St} C\left(\frac{1}{2} \frac{1}{2} t; \nu_1 \nu_2\right)^2 C\left(\frac{1}{2} \frac{1}{2} S; m'_1 m'_2 \Lambda'_0\right) C\left(\frac{1}{2} \frac{1}{2} S; m_1 m_2 \Lambda_0\right) \\
& \times \sum_{l'l_j} \left(1 - (-)^{l'+S+t}\right) \left(1 - (-)^{l+S+t}\right) \left(\delta_{l'l} - S_{l'l}^{Sjt}(q)\right) \sqrt{2l+1} C(lSj; 0\Lambda_0) \\
& \times C(l'Sj; \Lambda_0 - \Lambda'_0, \Lambda'_0) Y_{l',\Lambda_0-\Lambda'_0}(\theta', \phi'). \tag{3.102}
\end{aligned}$$

This verifies the expression given in Eq. (3.97).

We work out the reversal expression of Eq. (3.97), which is accomplished in the following way: we perform on the left side of Eq. (3.97) some algebra the effects of which remove all factors and terms on the right side but the partial wave projected T-matrix $T_{l'l}^{Sjt}(q)$. First we make use of the orthogonality relation for the d-matrices

$$\int_{-1}^1 d \cos \theta d_{\mu m}^{j_1}(\theta) d_{\mu m}^{j_2}(\theta) = \frac{2}{2j_1+1} \delta_{j_1 j_2}. \tag{3.103}$$

Applying this relation to Eq. (3.97) cancels the summation over j and removes the d-matrices

$$\begin{aligned}
& \int_{-1}^1 d \cos \theta' d_{\Lambda\Lambda'}^{j'}(\theta') T_{\Lambda'\Lambda}^{\pi S t}(q, q, \theta') \\
& = \frac{1}{2} \left(1 - \eta_\pi(-)^{S+t}\right) \sum_{l'l_j} T_{l'l}^{Sjt}(q) \left(1 + \eta_\pi(-)^{l'}\right) \left(1 + \eta_\pi(-)^l\right) \\
& \times \sqrt{\frac{2l'+1}{4\pi}} C(l'Sj; 0\Lambda') \sqrt{\frac{2l+1}{4\pi}} C(lSj; 0\Lambda) \int_{-1}^1 d \cos \theta' d_{\Lambda\Lambda'}^{j'}(\theta') d_{\Lambda\Lambda'}^j(\theta')
\end{aligned}$$

$$\begin{aligned}
&= \frac{1}{4\pi} \left(1 - \eta_\pi(-)^{S+t}\right) \sum_{l'l} T_{l'l}^{Sj't}(q) \left(1 + \eta_\pi(-)^{l'}\right) \left(1 + \eta_\pi(-)^l\right) \\
&\quad \times \frac{\sqrt{2l'+1}\sqrt{2l+1}}{2j'+1} C(l'Sj'; 0\Lambda') C(lSj'; 0\Lambda). \tag{3.104}
\end{aligned}$$

Next we eliminate the Clebsch-Gordan coefficients and at the same time cancel the double summations over l and l' by means of the orthogonality relation

$$\sum_{m_1} C(j_1 j_2 j; m_1, m - m_1) C(j_1 j_2 j'; m_1, m - m_1) = \delta_{jj'} \tag{3.105}$$

together with another relation for the Clebsch-Gordan coefficients, namely

$$C(j_1 j_2 j; m_1 m_2 m) = (-)^{j_2+m_2} \left(\frac{2j+1}{2j_1+1}\right)^{\frac{1}{2}} C(j_2 j j_1; -m_2, m m_1), \tag{3.106}$$

as can be verified in the following algebra

$$\begin{aligned}
&\sum_{\Lambda'\Lambda} C(\bar{l}' S j'; 0\Lambda') C(\bar{l} S j'; 0\Lambda) \int_{-1}^1 d \cos \theta' d_{\Lambda\Lambda'}^{j'}(\theta') T_{\Lambda'\Lambda}^{\pi S t}(q, q, \theta') \\
&= \frac{1}{4\pi} \left(1 - \eta_\pi(-)^{S+t}\right) \sum_{l'l} T_{l'l}^{Sj't}(q) \left(1 + \eta_\pi(-)^{l'}\right) \left(1 + \eta_\pi(-)^l\right) \frac{\sqrt{2l'+1}\sqrt{2l+1}}{2j'+1} \\
&\quad \times \sum_{\Lambda'\Lambda} C(\bar{l}' S j'; 0\Lambda') C(l' S j'; 0\Lambda') C(\bar{l} S j'; 0\Lambda) C(l S j'; 0\Lambda) \\
&= \frac{1}{4\pi} \left(1 - \eta_\pi(-)^{S+t}\right) \sum_{l'l} T_{l'l}^{Sj't}(q) \left(1 + \eta_\pi(-)^{l'}\right) \left(1 + \eta_\pi(-)^l\right) \frac{\sqrt{2l'+1}\sqrt{2l+1}}{2j'+1} \\
&\quad \times \sum_{\Lambda'} \left(\frac{2j'+1}{2l'+1}\right)^{\frac{1}{2}} C(S j' \bar{l}'; -\Lambda' \Lambda') \left(\frac{2j'+1}{2l'+1}\right)^{\frac{1}{2}} C(S j' l'; -\Lambda' \Lambda') \\
&\quad \times \sum_{\Lambda} \left(\frac{2j'+1}{2l+1}\right)^{\frac{1}{2}} C(S j' \bar{l}; -\Lambda \Lambda) \left(\frac{2j'+1}{2l+1}\right)^{\frac{1}{2}} C(S j' l; -\Lambda \Lambda) \\
&= \frac{1}{4\pi} \left(1 - \eta_\pi(-)^{S+t}\right) T_{\bar{l}l}^{Sj't}(q) \left(1 + \eta_\pi(-)^{\bar{l}}\right) \left(1 + \eta_\pi(-)^l\right) \\
&\quad \times \frac{\sqrt{2l'+1}\sqrt{2l+1}}{2j'+1} \frac{(2j'+1)^2}{(2\bar{l}'+1)(2\bar{l}+1)} \\
&= \frac{1}{4\pi} \left(1 - \eta_\pi(-)^{S+t}\right) \left(1 + \eta_\pi(-)^{\bar{l}}\right) \left(1 + \eta_\pi(-)^l\right) \\
&\quad \times \frac{2j'+1}{\sqrt{2l'+1}\sqrt{2l+1}} T_{\bar{l}l}^{Sj't}(q). \tag{3.107}
\end{aligned}$$

Replacing j' , \bar{l} and \bar{l}' with j , l and l' respectively for better notations this gives the final expression

$$\begin{aligned}
T_{l'l}^{Sj't}(q) &= \frac{\pi \sqrt{2l'+1}\sqrt{2l+1}}{2} \frac{1}{2j+1} \\
&\quad \times \sum_{\Lambda'\Lambda} C(l' S j; 0\Lambda') C(l S j; 0\Lambda) \int_{-1}^1 d \cos \theta' d_{\Lambda\Lambda'}^j(\theta') T_{\Lambda'\Lambda}^{\pi S t}(q, q, \theta'). \tag{3.108}
\end{aligned}$$

We took into account that parity, total spin and isospin are constrained by $\eta_\pi(-)^{S+t} = -1$ and the orbital angular momenta l and l' by $\eta_\pi(-)^{l'} = \eta_\pi(-)^l = 1$.

Once the partial wave projected T-matrix elements are calculated, we can connect them to the partial wave projected S-matrix elements using the relation given in Eq. (3.99). The partial wave projected S-matrix elements are parameterized by the standard partial wave phase shifts [33, 34]. Thus we can calculate phase shifts and compare them with those resulting from the standard partial wave calculations.

Chapter 4

APPLICATION TO NN SCATTERING

In the last chapter we formulated a three-dimensional (3D) approach to calculate NN scattering without employing partial wave (PW) decomposition. The practical application of this formulation includes solving the set of LSE's given in Eq. (3.73) for the T-matrix elements $T_{\Lambda\Lambda}^{\pi St}(q', q, \theta')$. Then we calculate observables, which we compare to experimental data. To check the new 3D formulation for correctness, it is also important to perform a comparison with the standard PW calculations. Here we show results of our calculations and refer to Appendix E for the numerical realization.

For this application we first need to choose NN potential models. These provide the input to the LSE's given in Eq. (3.73), when expressed in the appropriate form. Before showing results of our calculations, we present our choice of NN potentials and show the transformation from the original expressions to the ones indicated by Eq. (3.32). The final expressions can be found in Appendices C and D.

4.1 The NN Potentials

Any NN potential given in operator form can be used for the 3D technique formulated in Chapter 3. We choose two modern realistic NN potentials, each representing a distinct category, namely the one-boson-exchange potential (OBEP) derived from a meson theoretical approach and a phenomenological potential based on the quantum mechanical symmetries of the NN system and the pion exchange. These types of NN potentials are well developed and have been used in few-body nuclear physics for several decades, in the sense that these models give very good quantitative results.

4.1.1 One-Boson-Exchange Potential

Conventionally an OBEP is worked out in the framework of quantum field theory, derived from the Bethe-Salpeter equation, and approximated to a purely spatial form by means of, e.g., the Blankenbecler-Sugar reduction (see Ref. [35, 21]). These potentials can be traced back to Yukawa's suggestion [36] in 1935 that two nucleons interact by exchanging a mediating particle called meson, and supported by the discoveries of π meson (pion) and other heavier mesons. The OBEP's are based on meson-exchanges of pseudoscalar, scalar and vector types, contributing to different parts of the nuclear force. For example, the pseudoscalar mesons contribute to the tensor force. In addition, as suggested by Taketani, Nakamura and Sasaki [37] the nuclear force is divided into three parts corresponding to the long, attractive intermediate and repulsive short range interactions. Hence mesons of different masses are included, since the range of the force can be related to the meson mass. For this purpose, fictitious mesons of mass between 400 - 800 MeV such as σ in Ref.[35] and ϵ in Ref.[38] may be employed to represent the intermediate range attraction. Multiple-meson exchanges between two nucleons are also taken into account [6, 35]. Fortunately, for practical purposes the one-boson-exchange is a qualitatively and quantitatively approximation for the NN force. The parameters of an OBEP are the meson-nucleon coupling constants and the cutoffs, occurring in strong form factors, representing the finite size of the nucleon. The coupling constants are usually extracted from meson decay (see Ref. [39] and <http://pdg.lbl.gov/>) and the cutoffs are fixed to the NN data. In case of the fictitious mesons the masses are also adjusted. A review on the OBEP's is given in Ref. [21].

Among the best OBEP's are the Nijmegen I and II [38] and the CD-Bonn [40] potentials, which are charge-dependent and thus distinguish between pp, nn and np interactions. These potentials are fitted to np as well as pp data below 350 MeV laboratory energy with $\chi^2/\text{datum} \approx 1$. This energy is already above the pion production threshold (≈ 286 MeV laboratory energy). To achieve this close-to-unity χ^2/datum the parameterization is made for each partial wave. Hence, despite their sophistications these potentials cannot be used in the 3D technique.

We choose an OBEP given as tree-level Feynman diagrams and thus a simultaneous parameterization of all partial waves, the Bonn OBEP [35] in the parameterizing of Bonn-B [21]. This potential is well fitted to np data for both 2N total isospin singlet and triplet up to about 325 MeV laboratory energy, in which only the σ -meson mass is different for each isospin. Being fitted only to np data the potential assumes a charge-independent NN interaction.

The Bonn OBEP has the form

$$V(\mathbf{q}', \mathbf{q}) = V^{ps}(\mathbf{q}', \mathbf{q}) + V^s(\mathbf{q}', \mathbf{q}) + V^v(\mathbf{q}', \mathbf{q}), \quad (4.1)$$

where the labels ps , s , v stand for pseudoscalar, scalar and vector, respectively, corresponding to the type of the exchanged mesons. These pseudoscalar, scalar and vector potentials operators are given as

$$V^{ps}(\mathbf{q}', \mathbf{q}) = \frac{g_{ps}^2}{(2\pi)^3} \sqrt{\frac{m}{E'}} \sqrt{\frac{m}{E}} \bar{u}(\mathbf{q}') \gamma^5 u(\mathbf{q}) \bar{u}(-\mathbf{q}') \gamma^5 u(-\mathbf{q}) \frac{F_{ps}^2[(\mathbf{q}' - \mathbf{q})^2]}{(\mathbf{q}' - \mathbf{q})^2 + m_{ps}^2} \quad (4.2)$$

$$V^s(\mathbf{q}', \mathbf{q}) = -\frac{g_s^2}{(2\pi)^3} \sqrt{\frac{m}{E'}} \sqrt{\frac{m}{E}} \bar{u}(\mathbf{q}') u(\mathbf{q}) \bar{u}(-\mathbf{q}') u(-\mathbf{q}) \frac{F_s^2[(\mathbf{q}' - \mathbf{q})^2]}{(\mathbf{q}' - \mathbf{q})^2 + m_s^2} \quad (4.3)$$

$$\begin{aligned} V^v(\mathbf{q}', \mathbf{q}) = & \frac{F_v^2[(\mathbf{q}' - \mathbf{q})^2]}{(\mathbf{q}' - \mathbf{q})^2 + m_v^2} \sqrt{\frac{m}{E'}} \sqrt{\frac{m}{E}} \frac{1}{(2\pi)^3} \left[g_v^2 \bar{u}(\mathbf{q}') \gamma^\mu u(\mathbf{q}) \bar{u}(-\mathbf{q}') \gamma_\mu u(-\mathbf{q}) \right. \\ & + \frac{f_v^2}{4m^2} \left\{ 4m^2 \bar{u}(\mathbf{q}') \gamma^\mu u(\mathbf{q}) \bar{u}(-\mathbf{q}') \gamma_\mu u(-\mathbf{q}) \right. \\ & - 2m \bar{u}(\mathbf{q}') \gamma^\mu u(\mathbf{q}) \bar{u}(-\mathbf{q}') [(E' - E)(g_\mu^0 - \gamma_\mu \gamma^0) + (p_2 + p'_2)_\mu] u(-\mathbf{q}) \\ & - 2m \bar{u}(\mathbf{q}') [(E' - E)(g^{0\mu} - \gamma^\mu \gamma^0) + (p_1 + p'_1)^\mu] u(\mathbf{q}) \bar{u}(-\mathbf{q}') \gamma_\mu u(-\mathbf{q}) \\ & + \bar{u}(\mathbf{q}') [(E' - E)(g^{0\mu} - \gamma^\mu \gamma^0) + (p_1 + p'_1)^\mu] u(\mathbf{q}) \\ & \left. \times \bar{u}(-\mathbf{q}') [(E' - E)(g_\mu^0 - \gamma_\mu \gamma^0) + (p_2 + p'_2)_\mu] u(-\mathbf{q}) \right\} \\ & + \frac{g_v f_v}{2m} \left\{ 4m \bar{u}(\mathbf{q}') \gamma^\mu u(\mathbf{q}) \bar{u}(-\mathbf{q}') \gamma_\mu u(-\mathbf{q}) \right. \\ & - \bar{u}(\mathbf{q}') \gamma^\mu u(\mathbf{q}) \bar{u}(-\mathbf{q}') [(E' - E)(g_\mu^0 - \gamma_\mu \gamma^0) + (p_2 + p'_2)_\mu] u(-\mathbf{q}) \\ & \left. - \bar{u}(\mathbf{q}') [(E' - E)(g^{0\mu} - \gamma^\mu \gamma^0) + (p_1 + p'_1)^\mu] u(\mathbf{q}) \bar{u}(-\mathbf{q}') \gamma_\mu u(-\mathbf{q}) \right\}. \quad (4.4) \end{aligned}$$

Here m stands for the nucleon mass and m_α ($\alpha = ps, s, v$) for the corresponding meson masses. In the vector potential one has 4-momenta $(p_1 + p'_1)^\mu = (E + E', \mathbf{q} + \mathbf{q}')$ and $(p_2 + p'_2)^\mu = (E + E', -\mathbf{q} - \mathbf{q}')$. The form factor $F_\alpha^2[(\mathbf{q}' - \mathbf{q})^2]$ takes the form:

$$F_\alpha^2[(\mathbf{q}' - \mathbf{q})^2] = \left(\frac{\Lambda_\alpha^2 - m_\alpha^2}{\Lambda_\alpha^2 + (\mathbf{q}' - \mathbf{q})^2} \right)^{2n}, \quad (4.5)$$

with the power constant n being 1 for the pseudoscalar and scalar potentials and 2 for the vector potential. The mesons' masses m_α , the coupling constants g_α , f_v and the cutoffs Λ_α are given in Table 4.1, taken from [21].

This OBEP has to be expressed in a form of Eq. (3.32), that is in terms of the Ω_i operators given in Eq. (3.30). This is done as follows. The OBEP's operators are combinations of $\boldsymbol{\sigma}_1 \cdot \hat{\mathbf{q}}$, $\boldsymbol{\sigma}_2 \cdot \hat{\mathbf{q}}$, $\boldsymbol{\sigma}_1 \cdot \hat{\mathbf{q}}'$ and $\boldsymbol{\sigma}_2 \cdot \hat{\mathbf{q}}'$ contained in the Dirac spinors. These operators can be expressed in terms of the \mathbf{W}_i operators given in Eq. (3.29). It turned out that it is easier to express first the \mathbf{W}_i operators in terms $\boldsymbol{\sigma}_1 \cdot \hat{\mathbf{q}}$, $\boldsymbol{\sigma}_2 \cdot \hat{\mathbf{q}}$, $\boldsymbol{\sigma}_1 \cdot \hat{\mathbf{q}}'$ and $\boldsymbol{\sigma}_2 \cdot \hat{\mathbf{q}}'$. One can invert the resulting expressions and apply them to the OBEP. Next by

Table 4.1: Parameters for the Bonn-B potential. The shown σ parameters are for NN total isospin 0. For NN total isospin 1 the parameters are $m_\sigma = 720$ MeV, $\frac{g_\alpha^2}{4\pi} = 18.3773$, $\Lambda_\alpha = 2$ GeV and $n = 1$.

meson	m_α [MeV]	$\frac{g_\alpha^2}{4\pi}$	$\frac{f_\alpha}{q_\alpha}$	Λ_α [GeV]	n
π	138.03	14.4		1.7	1
η	548.8	3		1.5	1
δ	983	2.488		2	1
σ	550	8.9437		1.9	1
ρ	769	0.9	6.1	1.85	2
ω	782.6	24.5	0	1.85	2

means of Eq. (3.31), which relates the \mathbf{W}_i operators with Ω_i operators, the expression of the OBEP in terms of the Ω_i operators will result. For all this purpose one can use symbolic manipulation packages such as Mathematica. In Appendix C the potential final expressions in terms of the \mathbf{W}_i as well as Ω_i operators are presented.

4.1.2 Phenomenological Potential

The development of the phenomenological NN potentials started in the 1950's to provide a simple description of the nuclear force, which then may serve as an input for nuclear calculations [21]. The phenomenological potentials are constructed in terms of operators as combinations of spin, isospin and orbital angular momentum operators (in configuration space) representing processes occurring (or assumed to occur) in the NN interaction. For a fixed isospin state a phenomenological potential is a sum of six independent operator terms, governed by translational, Galilean, rotational, space reflection, time reversal invariances, symmetry condition and hermiticity [41]. The scalar functions multiplying with the operators are different from one potential to another. The appearances of the operators may also be slightly different as shown, for example, in Ref. [38] for Nijmegen Group's potentials and Refs.[9, 20] for the Argonne potentials. However, these sets of operators are related one to another, as demonstrated for instance by the two sets of operators \mathbf{W}_i and Ω_i , given in Eqs. (3.27) and (3.32). Phenomenological potentials also contains the one-pion-exchange (OPE) potential as long range part, since the OPE is a well established concept for the nuclear force. The phenomenological potentials use a larger number of parameters to be fitted to data, compared to the meson theoretical ones.

The charge dependent potentials Reid93 [38] and Argonne 18 (AV18) [20] belong to

the best fitted phenomenological potentials [42]. Both are fitted to pp as well as np data below 350 MeV laboratory energy and showing $\chi^2/\text{datum} \approx 1$. In addition the AV18 potential is fitted also to low-energy nn scattering parameters and deuteron properties. The Reid93 potential is parameterized for each partial wave, whereas the parameterization of the AV18 is given for all partial waves. Hence, we choose the AV18 potential for our calculations.

The AV18 potential is given originally in configuration space and has the general form

$$V(\mathbf{r}) = V^{EM}(\mathbf{r}) + V^\pi(\mathbf{r}) + V^R(\mathbf{r}), \quad (4.6)$$

where \mathbf{r} is the relative position between the two nucleons. The potential $V^{EM}(\mathbf{r})$ represents an electromagnetic part, which is excluded in this work. The charge dependent potentials $V^\pi(\mathbf{r})$ and $V^R(\mathbf{r})$ represent the OPE part and the intermediate- and short-range phenomenological part, respectively. The OPE part has standard spin-spin and tensor operator terms

$$V^\pi(\mathbf{r}) = V_{ss}^\pi(r)\boldsymbol{\sigma}_1 \cdot \boldsymbol{\sigma}_2 + V_t^\pi(r)S_{12}, \quad (4.7)$$

where S_{12} denotes the tensor operator and the radial functions $V_{ss}^\pi(r)$ and $V_t^\pi(r)$ contain exponential cutoffs. The $V^R(\mathbf{r})$ part is expressed as a sum of central, tensor, spin-orbit, L^2 , and quadratic spin-orbit terms abbreviated as c , t , ls , $l2$, $ls2$, respectively, in different spin and iso-spin (St) states:

$$V_{St}^R(\mathbf{r}) = V_{St}^c(r)\mathbf{1} + V_{St}^t(r)S_{12} + V_{St}^{ls}(r)\mathbf{L} \cdot \mathbf{S} + V_{St}^{l2}(r)L^2 + V_{St}^{ls2}(r)(\mathbf{L} \cdot \mathbf{S})^2. \quad (4.8)$$

The coupling constant used in $V^\pi(\mathbf{r})$, the radial functions and the 40 non-zero parameters used in $V^R(\mathbf{r})$ are given in Ref. [20].

For applying this potential in our calculations, we need to have $V^\pi(\mathbf{q}', \mathbf{q})$ and $V^R(\mathbf{q}', \mathbf{q})$ given as

$$V^\pi(\mathbf{q}', \mathbf{q}) = V_{ss}^\pi(\mathbf{q}', \mathbf{q}) + V_t^\pi(\mathbf{q}', \mathbf{q}) \quad (4.9)$$

$$V^R(\mathbf{q}', \mathbf{q}) = V_{St}^c(\mathbf{q}', \mathbf{q}) + V_{St}^t(\mathbf{q}', \mathbf{q}) + V_{St}^{ls}(\mathbf{q}', \mathbf{q}) + V_{St}^{l2}(\mathbf{q}', \mathbf{q}) + V_{St}^{ls2}(\mathbf{q}', \mathbf{q}), \quad (4.10)$$

which are the Fourier transform of $V^\pi(\mathbf{r})$ and $V^R(\mathbf{r})$, respectively. We obtain explicitly

$$V_{ss}^\pi(\mathbf{q}', \mathbf{q}) = \frac{1}{2\pi^2} \boldsymbol{\sigma}_1 \cdot \boldsymbol{\sigma}_2 \int_0^\infty dr r^2 j_0(\rho r) V_{ss}^\pi(r) \quad (4.11)$$

$$V_t^\pi(\mathbf{q}', \mathbf{q}) = \frac{1}{2\pi^2} \left(\frac{-3 \boldsymbol{\sigma}_1 \cdot (\mathbf{q}' - \mathbf{q}) \boldsymbol{\sigma}_2 \cdot (\mathbf{q}' - \mathbf{q})}{\rho^2} + \boldsymbol{\sigma}_1 \cdot \boldsymbol{\sigma}_2 \right) \int_0^\infty dr r^2 j_2(\rho r) V_t^\pi(r) \quad (4.12)$$

$$V_{St}^c(\mathbf{q}', \mathbf{q}) = \frac{1}{2\pi^2} \int_0^\infty dr r^2 j_0(\rho r) V_{St}^c(r) \quad (4.13)$$

$$V_{St}^t(\mathbf{q}', \mathbf{q}) = \frac{1}{2\pi^2} \left(\frac{-3 \boldsymbol{\sigma}_1 \cdot (\mathbf{q}' - \mathbf{q}) \boldsymbol{\sigma}_2 \cdot (\mathbf{q}' - \mathbf{q})}{\rho^2} + \boldsymbol{\sigma}_1 \cdot \boldsymbol{\sigma}_2 \right) \int_0^\infty dr r^2 j_2(\rho r) V_{St}^t(r) \quad (4.14)$$

$$V_{St}^{ls}(\mathbf{q}', \mathbf{q}) = \frac{i}{2\pi^2} \mathbf{S} \cdot (\mathbf{q} \times \mathbf{q}') \frac{1}{\rho} \int_0^\infty dr r^3 j_1(\rho r) V_{St}^{ls}(r) \quad (4.15)$$

$$V_{St}^{l2}(\mathbf{q}', \mathbf{q}) = \frac{1}{2\pi^2} \mathbf{q} \cdot \mathbf{q}' \frac{2}{\rho} \int_0^\infty dr r^3 j_1(\rho r) V_{St}^{l2}(r) - \frac{1}{2\pi^2} [\mathbf{q}'^2 \mathbf{q}^2 (1 - \gamma^2)] \frac{1}{\rho^2} \int_0^\infty dr r^4 j_2(\rho r) V_{St}^{l2}(r) \quad (4.16)$$

$$V_{St}^{ls2}(\mathbf{q}', \mathbf{q}) = \frac{1}{2\pi^2} (\mathbf{S}^2 \mathbf{q} \cdot \mathbf{q}' - \mathbf{S} \cdot \mathbf{q} \mathbf{S} \cdot \mathbf{q}') \frac{1}{\rho} \int_0^\infty dr r^3 j_1(\rho r) V_{St}^{ls2}(r) - \frac{1}{2\pi^2} \left(\frac{1}{2} (\mathbf{q} \times \mathbf{q}')^2 + \frac{1}{2} \boldsymbol{\sigma}_1 \cdot (\mathbf{q} \times \mathbf{q}') \boldsymbol{\sigma}_2 \cdot (\mathbf{q} \times \mathbf{q}') \right) \times \frac{1}{\rho^2} \int_0^\infty dr r^4 j_2(\rho r) V_{St}^{ls2}(r), \quad (4.17)$$

where $\rho \equiv |\mathbf{q}' - \mathbf{q}|$. The resulting operators can be easily represented in terms of the \mathbf{W}_i operators and next by means of Eq. (3.31) in the Ω_i operators. The expressions in these two operators \mathbf{W}_i and Ω_i are given in Appendix D.

4.2 Results and Discussions

In this section we present the results of our calculations for phase shifts, T-matrix elements and observables.

In Subsection 4.2.1 we show some NN phase shifts resulting from our 3D calculations (δ_{3D}) and those from the standard PW calculations (δ_{PW}). The δ_{3D} are obtained from Eq. (3.99) together with Eq. (3.108). Equation (3.99) relates between PW projected S-matrix and T-matrix and Eq. (3.108) connects PW projected T-matrix with T-matrix in the momentum-helicity basis.

In Subsection 4.2.2 we present the 2D half-on-the-energy-shell (half-shell) behavior of the T-matrix elements $T_{\Lambda'\Lambda}^{\pi St}(q', q, \theta')$ in the momentum helicity basis. Two-dimensional behavior means the angular and momentum dependence. We compare this behavior of $T_{\Lambda'\Lambda}^{\pi St}(q', q, \theta')$ resulting from the two chosen NN potential models Bonn-B and AV18, which differ from each other in their nature. The 2D on-the-energy-shell (on-shell) behavior of the T-matrix elements ${}_a \langle \nu_1 \nu_2 m'_1 m'_2 \mathbf{q}' | T | \nu_1 \nu_2 m_1 m_2 \mathbf{q} \rangle_a$ in the physical representation is also shown for a large range of energies up to 1 GeV laboratory energy.

Subsection 4.2.3 serves like Subsection 4.2.1 as a test. First we show comparisons with the standard PW calculations, in which δ_{3D} are used. Next we show comparisons with data at higher energy beyond the π -threshold for NN system as well as beyond the highest energy, where the two NN potentials Bonn-B and AV18 are fitted. We present our calculations together with the partial-wave analyses (PWA) taken from the CNS DAC (<http://gwdac.phys.gwu.edu/>), which is also the source of the experimental data.

4.2.1 Phase Shifts

Here we compare the NN δ_{3D} with the NN δ_{PW} for projectile energies 100 and 300 MeV. For the Bonn-B potential the phase shifts are given in Table 4.2. The agreement between the two calculations, both performed in momentum space, is excellent. For the AV18 potential we give the phase shifts in Table 4.3. In this case the PW calculation is performed in coordinate space [43]. The agreement is also very good, though not as excellent as in the case of Bonn-B. The source of this slight discrepancy is presumably twofold. First, the discrepancy may have been caused by imperfections in the numerical realization of the Fourier-Bessel transformations of the AV18's component functions given in Eqs. (4.11)-(4.17). Second, there probably occur inaccuracies in the solution of the LSE's of Eq. (3.73), described in the following. See also Appendix E Section E.1 for descriptions and values.

Solving the integral equation in Eq. (3.73) requires an evaluation of the potential functions on a grid of size $n_{\phi''} \times (n_{q''} \times n_{\theta''})^2$, where $n_{\phi''}$, $n_{q''}$, $n_{\theta''}$ are the numbers of ϕ'' -, q'' -, θ'' -integration points. For economical reasons we prepare the potential functions once on a fine grid for $\rho = |\mathbf{q}'' - \mathbf{q}'|$ and obtain the value at points actually needed in the calculation via interpolation. The grid is prepared within a range of $0 \leq \rho \leq 300 \text{ fm}^{-1}$, with the resolution being 0.2 fm^{-1} for $0 \leq \rho \leq 10 \text{ fm}^{-1}$, 0.5 fm^{-1} for $10 \leq \rho \leq 50 \text{ fm}^{-1}$ and 2.5 fm^{-1} for $50 \leq \rho \leq 300 \text{ fm}^{-1}$. Using values for the numbers of integration points given in Section E.1 the resolution of actual grid for ρ is roughly 0.1^{-4} fm^{-1} , obtained from $2q_3 / (n_{\phi''} \times (n_{q''} \times n_{\theta''})^2)$, where $q_3 = 150 \text{ fm}^{-1}$ is the upper limit in q'' -integration for the AV18 potential. This resolution is much smaller than the one of the grid for interpolation. Thus, this procedure may leads to larger numerical errors compared to a direct evaluation of the algebraic expressions in the case for Bonn-B. The differences can be clearly seen when comparing Tables 4.2 with 4.3. Note that in both cases a comparable grid for the T-matrix elements is used. For the interpolation one can practically use any reliable method. We use the modified cubic hermite splines [44], which is accurate yet practical.

4.2.2 T-Matrix

Now we show the 2D behavior of the half-shell T-matrix elements $T_{\Lambda'\Lambda}^{\pi St}(q, q_0, \theta)$ as the solution of Eq. (3.73). Here q , θ denote the outgoing momenta in the x-z-plane and q_0 denotes the magnitude of the incoming momentum in the z direction. These are displayed in Figs. 4.1-4.7, all for 300 MeV laboratory energy, corresponding to $q_0 = 375 \text{ MeV}/c$. In the figures $T_{\Lambda'\Lambda}^{\pi St}(q, q_0, \theta)$ are denoted by T for $S = 0$ and by $T_{\Lambda'\Lambda}$ for $S = 1$, where Λ' and Λ take values of 0, 1. Due to the symmetry of the potential, and hence the T-matrix,

Table 4.2: Comparison of the NN phase shifts obtained from our 3D formulation (δ_{3D}) with those from the standard PW calculations in momentum space (δ_{PW}) for the Bonn-B potential at 100 and 300 MeV laboratory energies.

$^{2S+1}L_J$	$E_{lab} = 100 \text{ MeV}$		$E_{lab} = 300 \text{ MeV}$	
	δ_{3D}	δ_{PW}	δ_{3D}	δ_{PW}
1S_0	25.1928	25.1929	-8.1755	-8.1756
3P_0	9.8046	9.8046	-11.4799	-11.4799
1P_1	-16.3131	-16.3451	-28.6946	-28.8747
3P_1	-13.4677	-13.4677	-26.3800	-26.3800
3S_1	41.9858	41.9870	4.0667	4.0676
3D_1	-12.9847	-12.9846	-23.7182	-23.7181
ε_1	-2.2360	-2.2357	-4.0268	-4.0265
1D_2	3.3411	3.3411	7.4888	7.4888
3D_2	17.6710	17.6710	25.3616	25.3617
3P_2	11.7356	11.7356	17.3981	17.3981
3F_2	0.7705	0.7705	0.5236	0.5238
ε_2	2.8402	2.8402	2.0166	2.0166
1F_3	-2.4397	-2.4397	-5.5865	-5.5865
3F_3	-1.6484	-1.6484	-4.0097	-4.0097
3D_3	0.4203	0.4855	2.5719	2.5720
3G_3	-1.0105	-1.0105	-4.4051	-4.4051
ε_3	-3.6604	-3.6604	-7.2233	-7.2233
1G_4	0.4092	0.4092	1.3556	1.3556
3G_4	2.2624	2.2624	7.3000	7.3000
3F_4	0.4203	0.4203	2.4491	2.4491
3H_4	0.1082	0.1082	0.5077	0.5077
ε_4	0.5575	0.5575	1.5509	1.5509

Table 4.3: Comparison of the NN phase shifts obtained from our 3D formulation (δ_{3D}) with those from the standard PW calculations in configuration space (δ_{PW}) [43] for the AV18 potential at 100 and 300 MeV laboratory energies.

$^{2S+1}L_J$	$E_{lab} = 100$ MeV		$E_{lab} = 300$ MeV	
	δ_{3D}	δ_{PW}	δ_{3D}	δ_{PW}
1S_0	25.99	25.94	-4.62	-4.60
3P_0	8.69	8.69	-11.05	-11.06
1P_1	-14.19	-14.20	-26.18	-26.28
3P_1	-13.06	-13.07	-28.38	-28.49
3S_1	43.69	43.56	8.15	8.16
3D_1	-12.08	-12.09	-24.80	-24.90
ε_1	-2.49	-2.49	-4.38	-4.39
1D_2	3.81	3.81	9.45	9.44
3D_2	17.14	17.10	25.11	25.02
3P_2	11.02	11.00	16.96	16.91
3F_2	0.67	0.67	0.77	0.76
ε_2	2.70	2.70	2.21	2.21
1F_3	-2.23	-2.23	-4.87	-4.88
3F_3	-1.35	-1.35	-2.51	-2.51
3D_3	1.61	1.61	5.22	5.21
3G_3	-0.93	-0.93	-4.19	-4.20
ε_3	-3.50	-3.50	-7.17	-7.16
1G_4	0.40	0.40	1.42	1.42
3G_4	2.22	2.22	7.35	7.34
3F_4	0.45	0.45	2.75	2.74
3H_4	0.07	0.07	0.31	0.31
ε_4	0.51	0.51	1.54	1.54

it is sufficient to consider only these two values of helicity. The notations Re and Im have their usual meaning as indicating real and imaginary parts. Figures 4.1-4.5 show the Bonn-B potential and Figs. 4.6-4.7 the AV18 potential cases.

Figure 4.1 shows $T_{\Lambda'\Lambda}^{\pi St}(q, q_0, \theta)$ for $S = 0$. On the left side we see the parity-even and on the right side the parity-odd case, which are distinguished by the symmetric and the antisymmetric angular behavior of the T-matrix elements. The T-matrix elements peak sharply at $q = q_0$ in forward and backward scattering directions, show strong 2D behavior around $q = q_0$ and a very weak momentum dependence for momenta far away from q_0 . The T-matrix elements for parity-even case exhibit a similar behavior as the symmetrized T-matrix elements of the two-boson case studied in Ref. [13].

Figures 4.2-4.5 display $T_{\Lambda'\Lambda}^{\pi St}(q, q_0, \theta)$ for $S = 1$. Coming as two pairs, each showing first the real part and then the imaginary part of the T-matrix elements, the first pair (Figs. 4.2 and 4.3) show the parity-even case and the second pair (Figs. 4.4 and 4.5) the parity-odd case. We see various strong angular and momentum dependence of the T-matrix elements for momenta around q_0 and a very weak one for momenta away from q_0 .

Next we take a look at Figs. 4.6 and 4.7, displaying a few examples of $T_{\Lambda'\Lambda}^{\pi St}(q, q_0, \theta)$ as obtained from the AV18 potential. Thus, we will see how strong the difference is between the half-shell T-matrix elements obtained from the two potentials Bonn-B and AV18. In Fig. 4.6 the real and imaginary parts of $T_{\Lambda'\Lambda}^{\pi St}(q, q_0, \theta)$ for $S = 0$ are shown, where the left side is for parity-even and the right side is for parity-odd case. Compared with Fig. 4.1 along the on-shell line ($q = q_0$) the corresponding T-matrix elements obtained from the two potentials are identical. However, the detailed structures are different, especially the parity-odd T-matrix elements. One sees that at large momenta q the Bonn-B T-matrix elements show a stronger angular behavior than the AV18 ones. For the case $S = 1$ we present only some T-matrix elements, representing the ones which look similar to and those quite different from the corresponding Bonn-B T-matrix elements. The upper part of Fig. 4.7 shows two AV18 T-matrix elements considerably different from the corresponding Bonn-B ones displayed in the upper part of Fig. 4.5. The lower part of Fig. 4.7 shows the ones relatively similar, the figure in the lower left should be compared to that in the lower left of Fig. 4.2 and the figure in the lower right to that in the lower right of Fig. 4.3.

We turn now to the on-shell physical T-matrix elements ${}_a\langle\nu_1\nu_2m'_1m'_2q_0\hat{\mathbf{q}}|T|\nu_1\nu_2m_1m_2\mathbf{q}_0\rangle_a$, simplified in notation as $\langle m'_1m'_2|T|m_1m_2\rangle$, where $m_i, m'_i = \pm$ ($i = 1, 2$) represent the two spin-half states. We are interested in the on-shell T-matrix elements, since these are closely related to observables. Equation (3.76) shows one example of the observables, the spin averaged differential cross section. In the

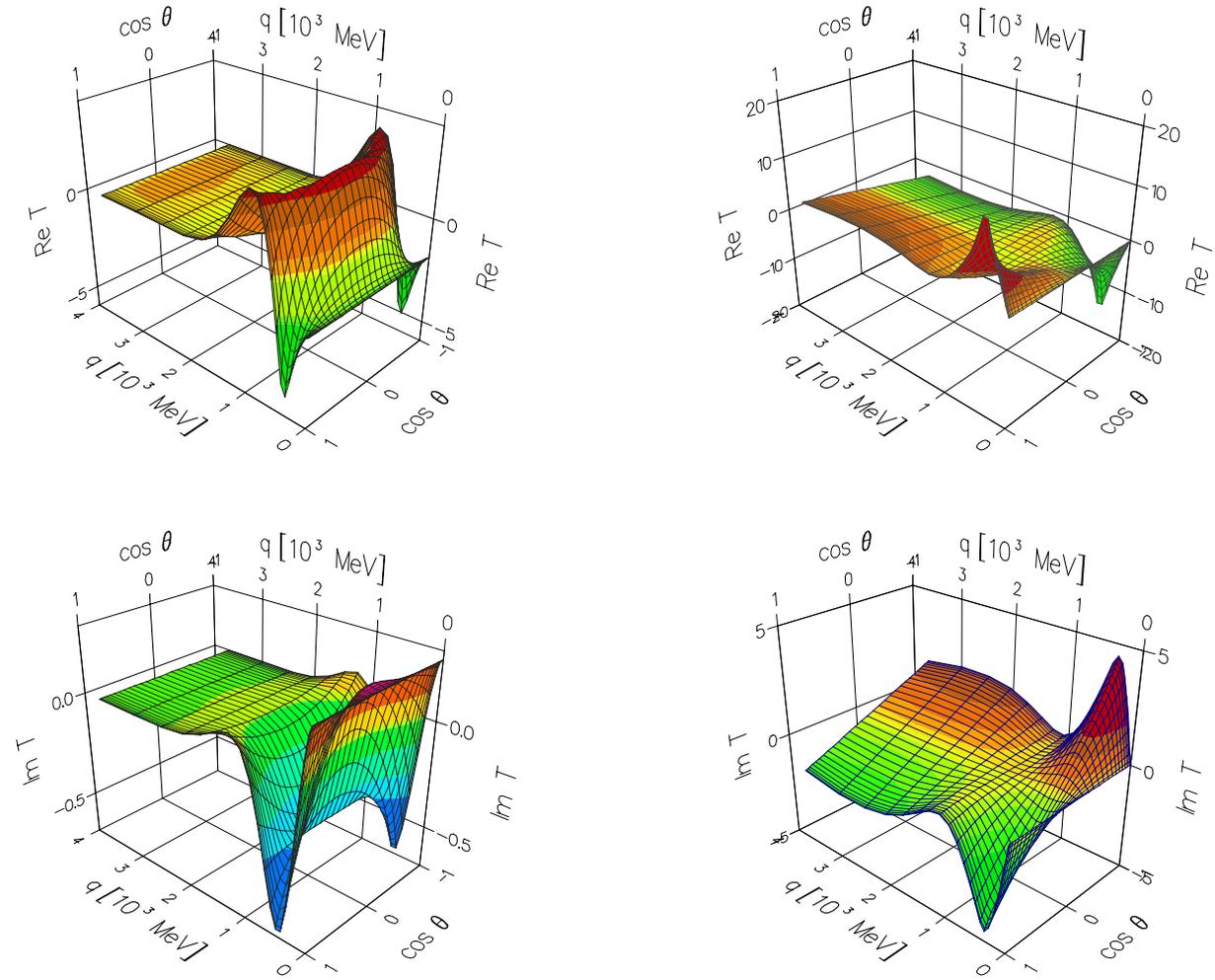


Figure 4.1: $T_{\Lambda'\Lambda}^{\pi St}(q, q_0, \theta)$ for $S = 0$ as function of q and $\cos \theta$ in units 10^{-7} MeV^{-2} , calculated using the Bonn-B potential for $q_0 = 375 \text{ MeV}/c$, corresponding to $E_{lab} = 300 \text{ MeV}$. The left side displays the parity-even and the right side the parity-odd case.

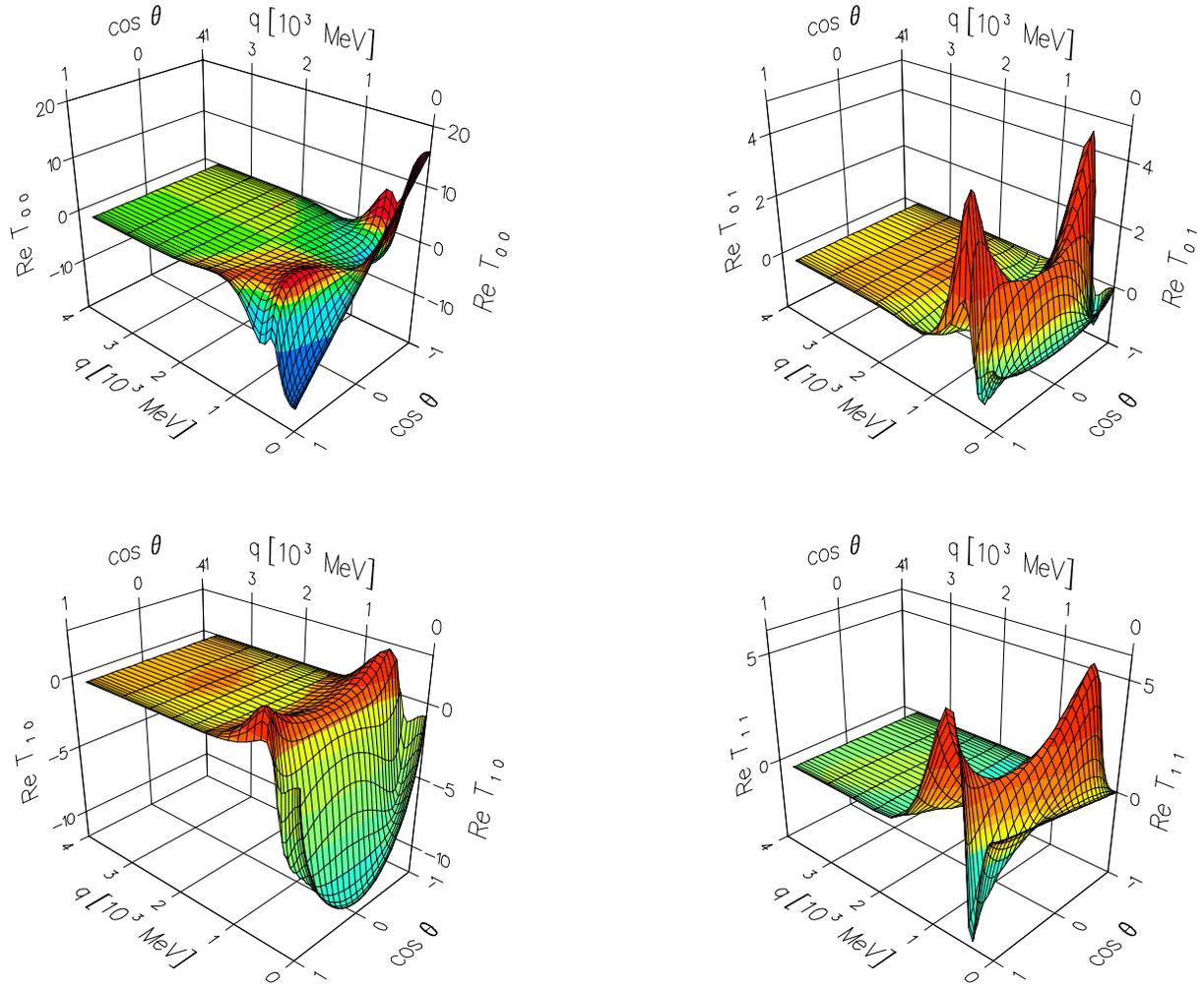


Figure 4.2: The real part of the parity-even $T_{\Lambda\Lambda}^{\pi S t}(q, q_0, \theta)$ for $S = 1$ as a function of q and $\cos \theta$ in units 10^{-7} MeV^{-2} , calculated using the Bonn-B potential for $q_0=375 \text{ MeV}/c$.

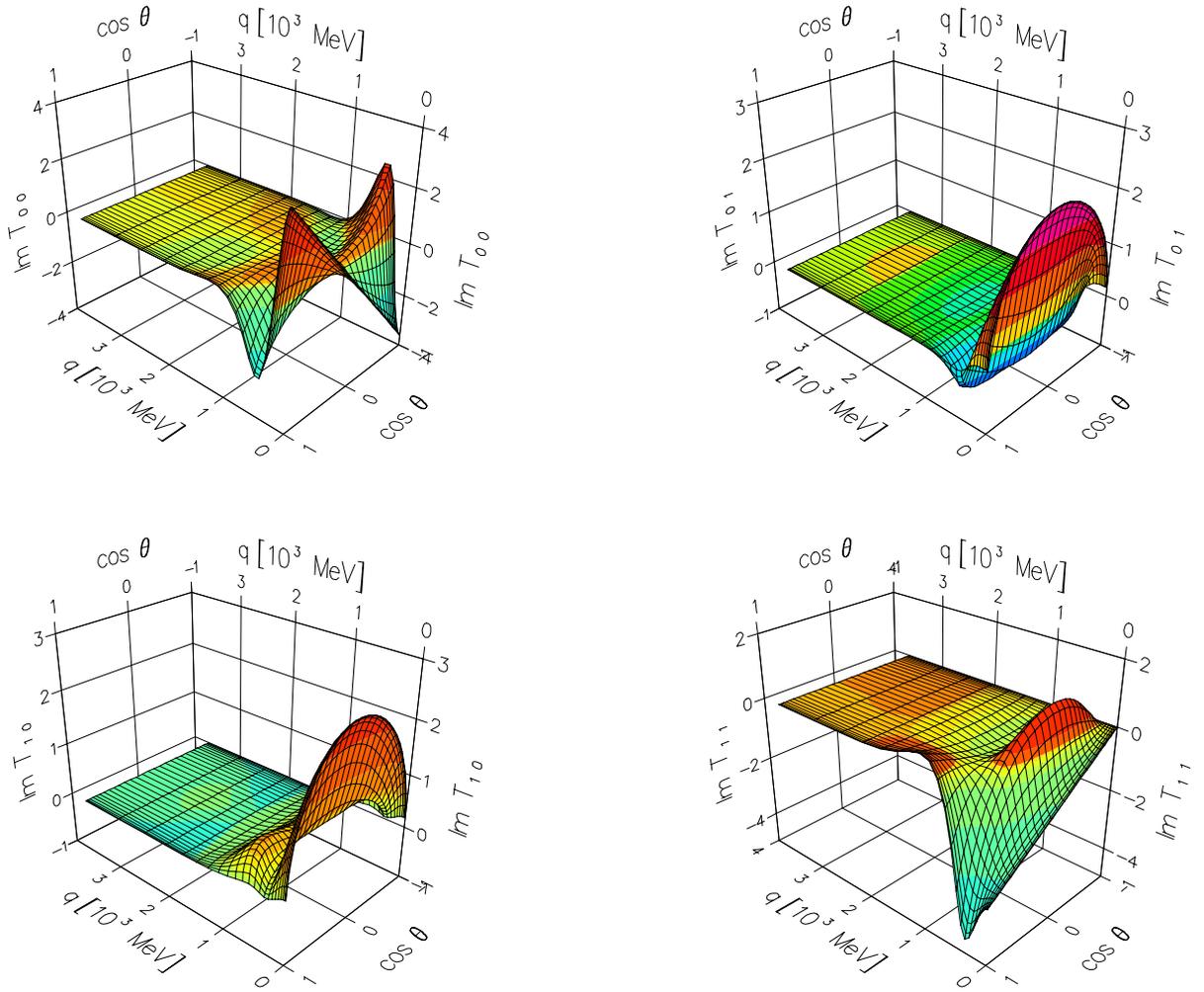


Figure 4.3: Same as Fig. 4.2, but for the imaginary part.

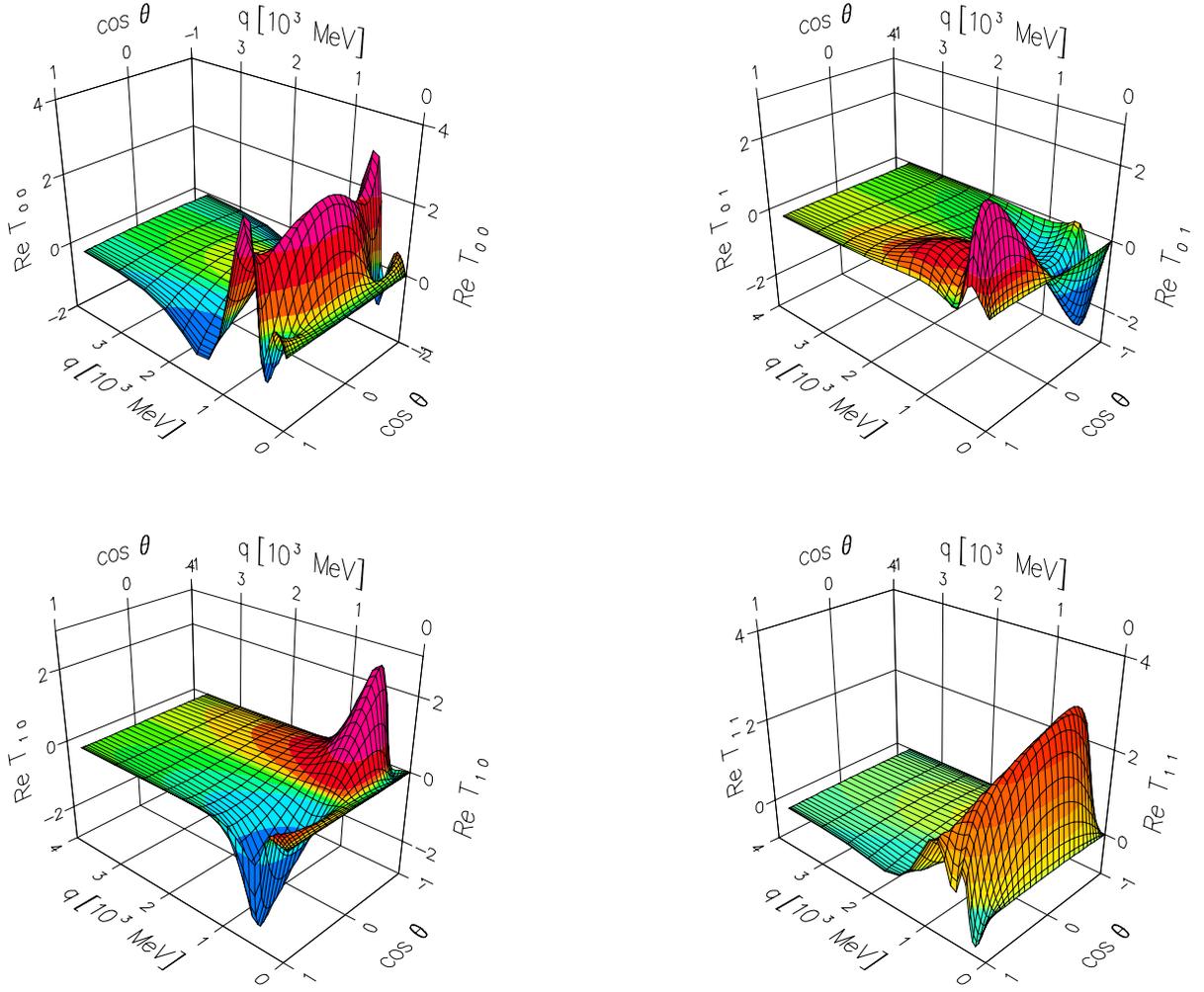


Figure 4.4: The real part of the parity-odd $T_{\Lambda\Lambda}^{\pi S t}(q, q_0, \theta)$ for $S = 1$ as a function of q and $\cos \theta$ in units 10^{-7} MeV^{-2} , calculated using the Bonn-B potential for $q_0=375 \text{ MeV}/c$.

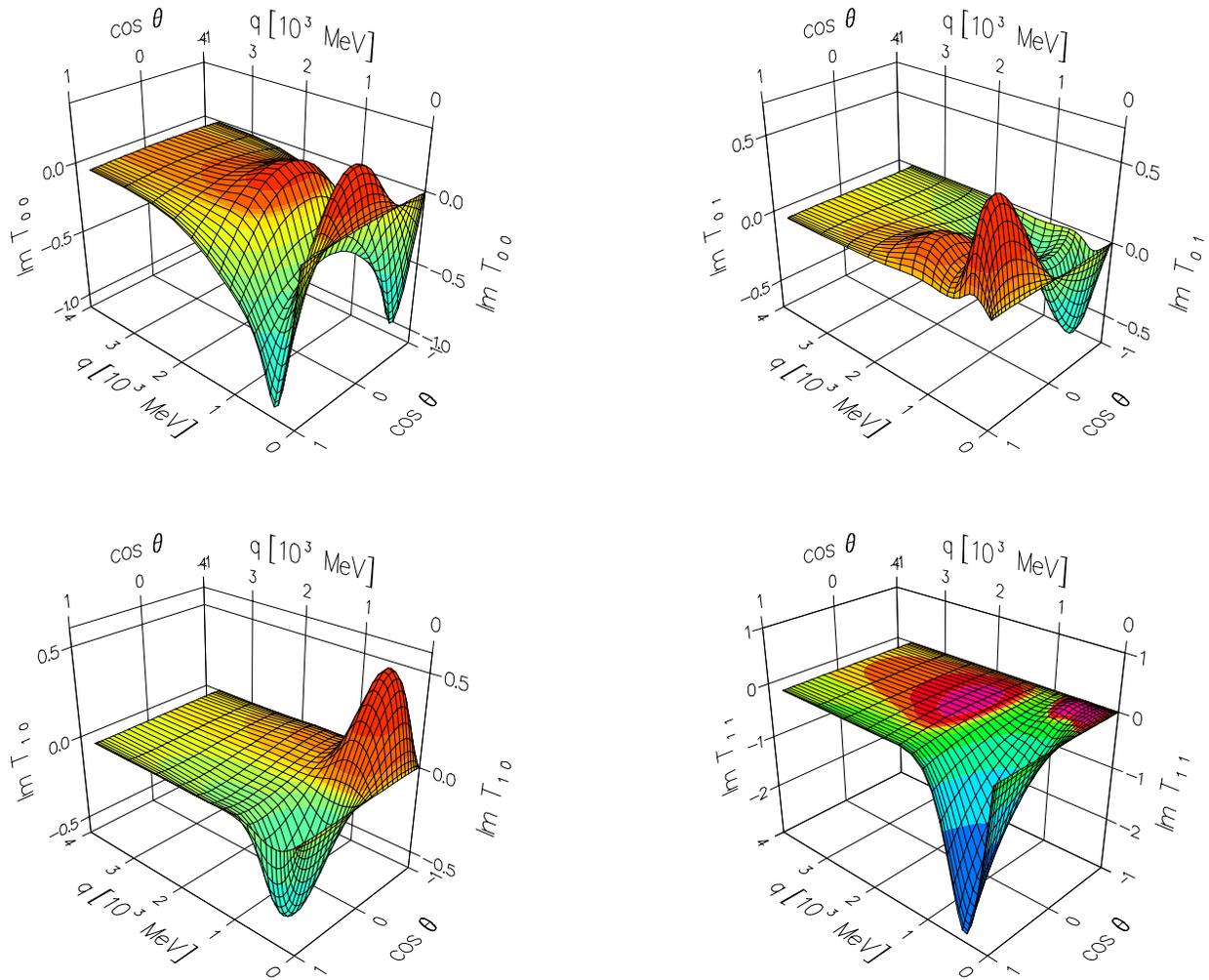


Figure 4.5: Same as Fig. 4.4, but for the imaginary part.

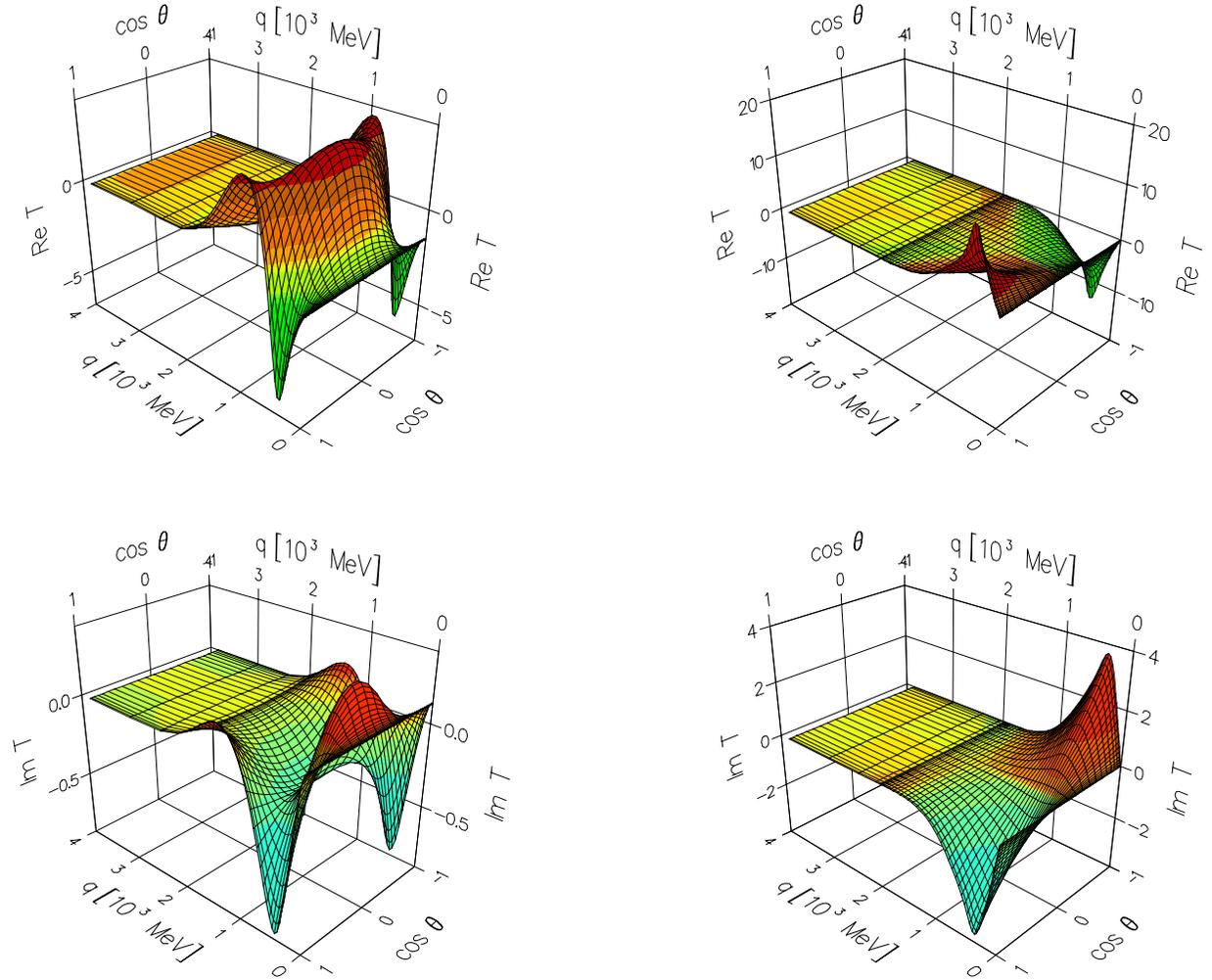


Figure 4.6: $T_{\Lambda'\Lambda}^{\pi S t}(q, q_0, \theta)$ for $S = 0$ as a function of q and $\cos\theta$ in units 10^{-7} MeV^{-2} , calculated using the AV18 potential for $q_0 = 375 \text{ MeV}/c$. The left side displays the parity-even and the right side the parity-odd case.

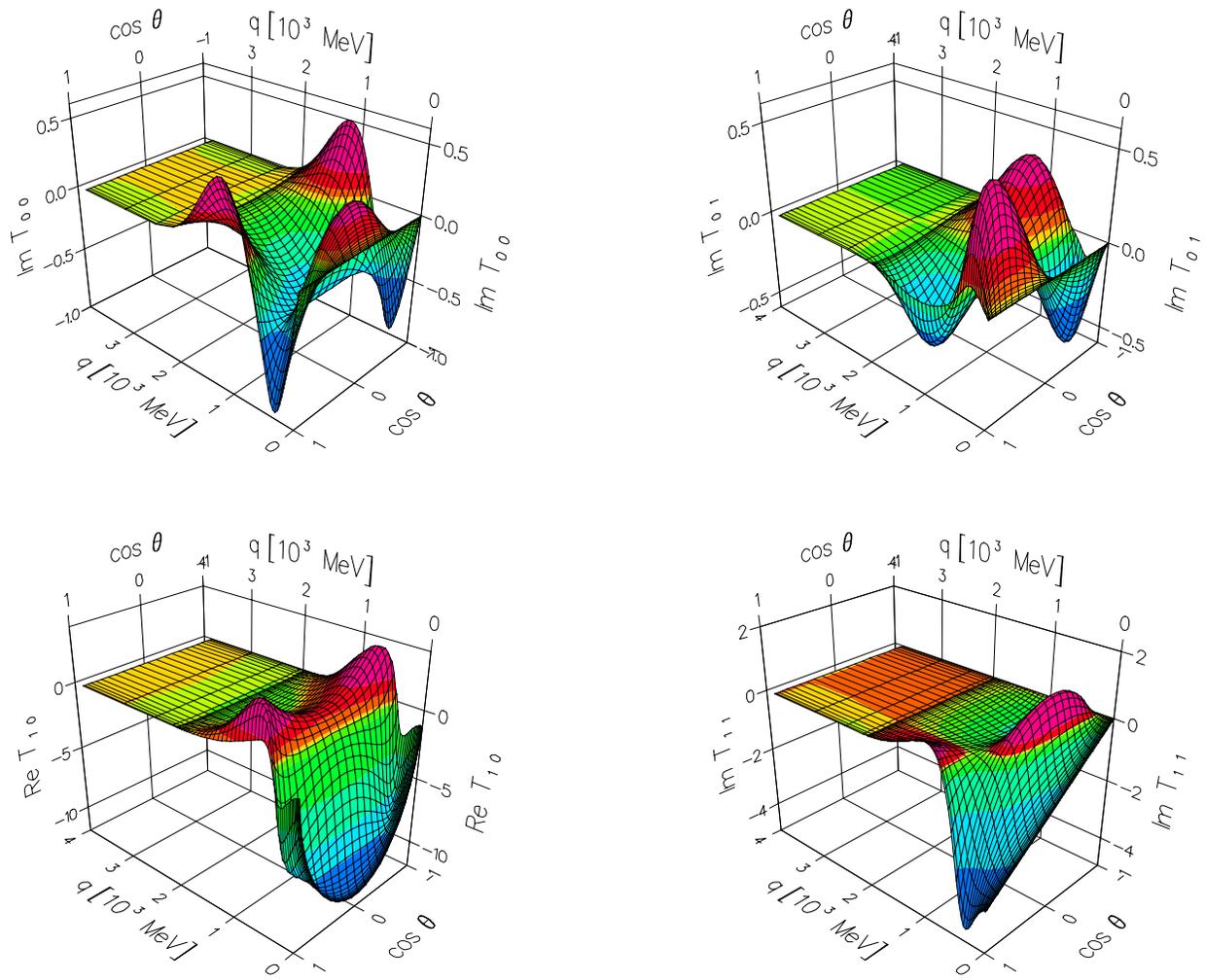


Figure 4.7: Selected $T_{\Lambda'\Lambda}^{\pi S t}(q, q_0, \theta)$ for $S = 1$ as a function of q and $\cos \theta$ in units 10^{-7} MeV^{-2} , calculated from the AV18 potential for $q_0=375$ MeV/c .

following we will use the term amplitudes for the on-shell T-matrix elements.

Considering rotational and parity invariance, one ends up with six independent amplitudes,

$$\begin{aligned}
\langle ++ | T | ++ \rangle &= \langle -- | T | -- \rangle \\
\langle ++ | T | -- \rangle &= \langle -- | T | ++ \rangle \\
\langle +- | T | ++ \rangle &= \langle -+ | T | ++ \rangle = -\langle +- | T | -- \rangle = -\langle -+ | T | -- \rangle \\
\langle ++ | T | +- \rangle &= \langle ++ | T | -+ \rangle = -\langle -- | T | +- \rangle = -\langle -- | T | -+ \rangle \\
\langle +- | T | +- \rangle &= \langle -+ | T | -+ \rangle \\
\langle -+ | T | +- \rangle &= \langle +- | T | -+ \rangle.
\end{aligned} \tag{4.18}$$

Therefore, instead of calculating 16 amplitudes for all possible m_i, m'_i ($i = 1, 2$) combinations one needs only to calculate these six amplitudes. In Figs. 4.8-4.10 we display the squared absolute values of these six amplitudes for the np system as a function of the laboratory energy and the c.m. scattering angle $\cos\theta$, calculated from the Bonn-B potential. We show the amplitudes up to 1 GeV, which is much beyond the energy range, where the Bonn-B as well as the AV18 potentials defined, namely below the π -threshold. At this point we only want to demonstrate that our calculation at higher energies takes the same effort as the one at very low energies. The reason is of course that we do not work with partial waves. We would like to remark that, as indicated in Eq. (3.102), these on-shell amplitudes can also be calculated from the PW projected S-matrix and T-matrix elements. For a numerical test of our formulation we used this relation.

4.2.3 Observables

In this subsection we compare NN scattering observables obtained from our 3D calculations with experimental data. However, at first we compare with results from standard PW calculations.

By definition a 3D calculation contains contributions from all partial waves. Thus, comparing with PW calculations, where increasing maximum total angular momentum j_{max} are taken into account, is instructive. Here we can observe how with increasing j_{max} the PW calculations converge towards the complete sum of all partial waves. We show the spin averaged differential cross section (shortly called the cross section) and two spin observables A_y and D_t for the np system.

Figures 4.11-4.13 display the above given observables for $E_{lab} = 100$ MeV and Figs.4.14-4.16 display them for $E_{lab} = 300$ MeV. All figures show calculations based on the AV18 potential. At $E_{lab} = 100$ MeV $j_{max} = 10$ gives a completely converged result for the cross

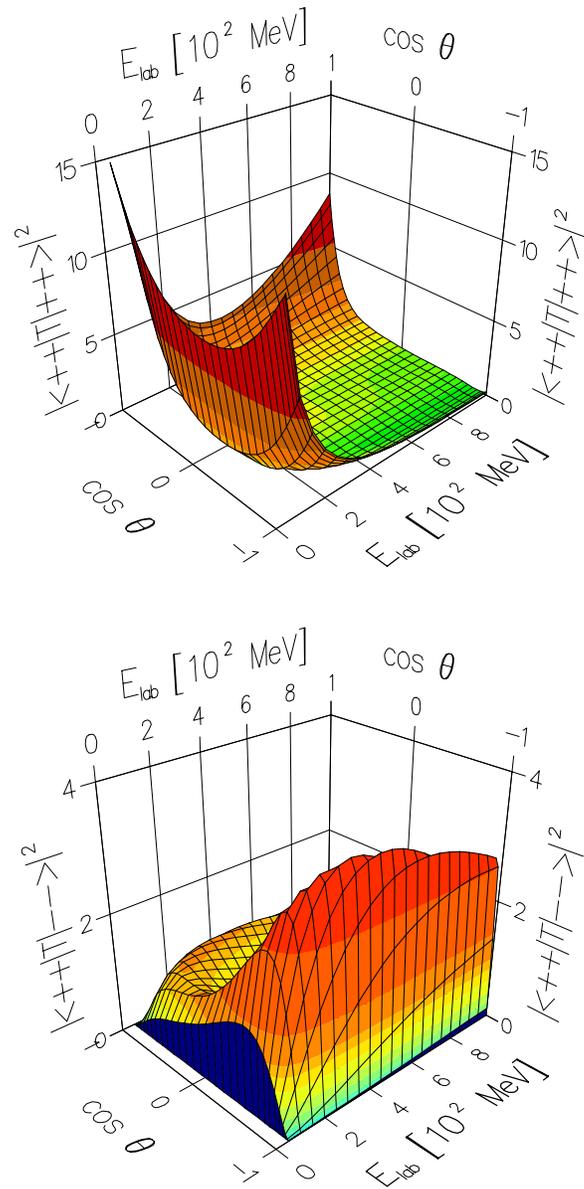


Figure 4.8: The squared absolute value of the on-shell physical T-matrix elements denoted by $|\langle m'_1 m'_2 | T | m_1 m_2 \rangle|^2$ (see text) in units $10^{-14} \text{ MeV}^{-4}$ as a function of E_{lab} and $\cos \theta$.

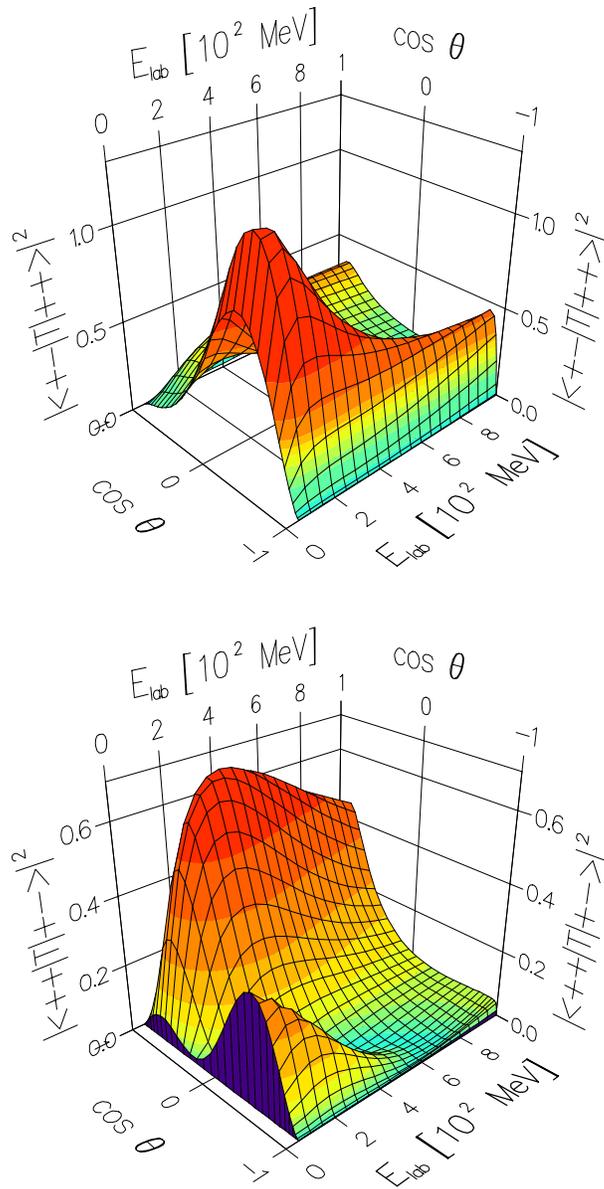


Figure 4.9: Same as Fig. 4.8, but for different m_i, m'_i ($i = 1, 2$) combinations.

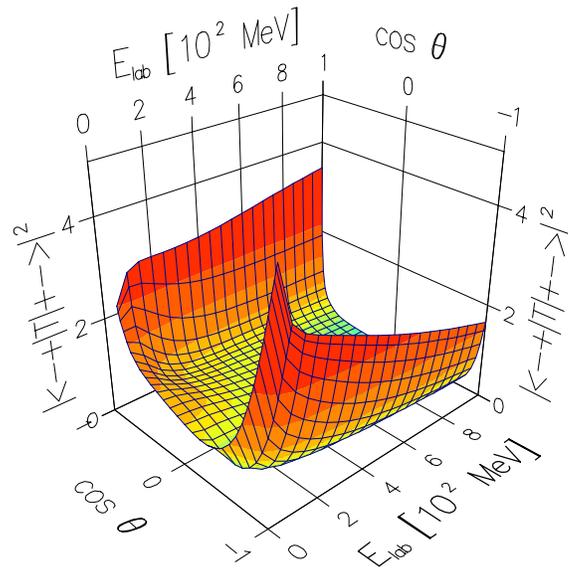
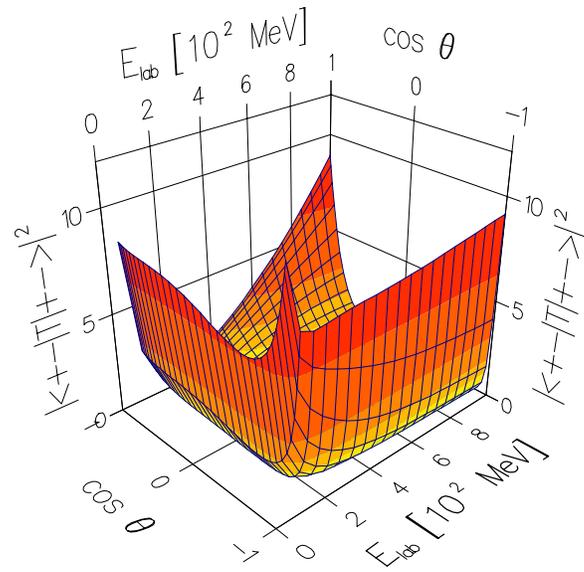


Figure 4.10: Same as Fig. 4.8, but for different m_i, m'_i ($i = 1, 2$) combinations.

section and D_t . For A_y $j_{max} = 8$ is enough. At $E_{lab} = 300$ MeV more partial waves are needed. The cross section and D_t require $j_{max} = 16$ for a converged result, while A_y needs only $j_{max} = 12$. For the cross section, the high values of j_{max} are required to reach convergence at forward and backward directions. These comparisons give us a view of how many LSE's are to be solved in the PW calculations. One characteristic of a PW calculation is also shown in these comparisons, that is its oscillatory behavior. This is observed most obviously in Fig.4.16. A PW calculation of higher order oscillates more rapidly than that of lower order. This behavior reminds us of the Legendre polynomial occurring in the PW expansion of a plane wave.

Next we compare with experimental data. We choose some energies beyond the π -threshold for the NN system, where the potentials are fitted, and at limit of the fit range of the two potentials Bonn-B and AV18. For lower energy we have already seen that our 3D calculations agree with the converged standard PW ones.

The reason of choosing higher energies is the following. First, the 3D formulation is especially advantageous at higher energies. Second, later we consider three-nucleon processes such as the proton-deuteron break-up process. For this reaction data exist at higher energies up to about 500 MeV. The off-the-energy-shell (off-shell) NN T-matrix elements are the input for calculations of this process. Thus, a comparison of our results for the NN observables to data are important.

In Figs. 4.17-4.22 we present various observables from 3D calculations for both potentials Bonn-B and AV18 together with the partial wave analyses (PWA). The PWA and data are taken from CNS DAC (<http://gwdac.phys.gwu.edu/>). In the figure captions we give the individual source of the experimental data. We include also observables for the pp system in this evaluation (see Figs. 4.18 and 4.22), since the proton-deuteron break-up process involve both np and pp sub-systems. In general the figures show a good agreement between our calculations and data as well as the PWA. Even for the pp system in Figs. 4.18 and 4.22 the Bonn-B potential predicts the data reasonably well. In most cases predictions from the AV18 potential and the PWA are close to each other. We conclude from this evaluation that even for these higher energies our 3D calculations using the two NN potentials Bonn-B and AV18 are acceptable.

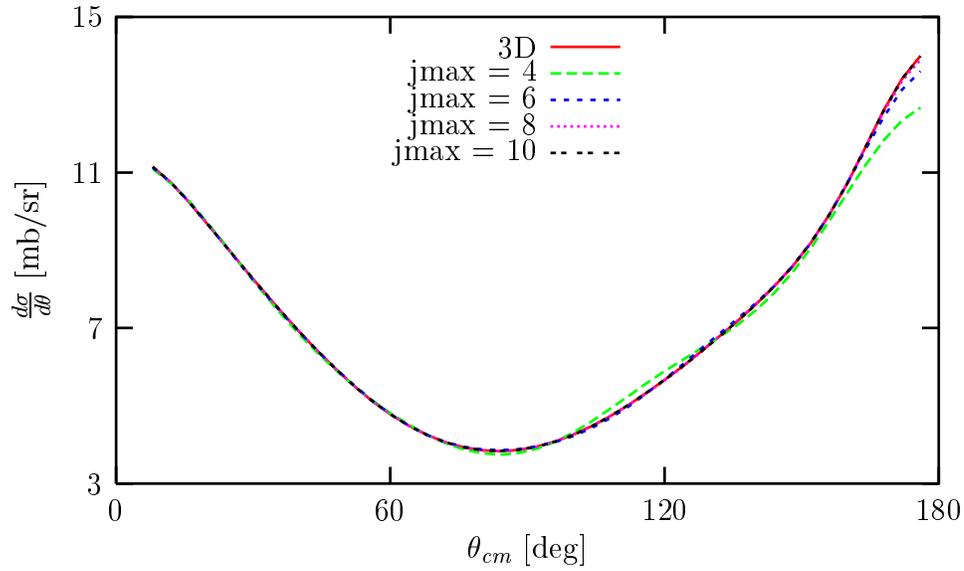


Figure 4.11: np spin averaged differential cross section at $E_{lab} = 100$ MeV. The curve 3D is obtained from the 3D calculation. The other curves are obtained from the PW calculations with indicated maximum NN total angular momentum j_{max} .

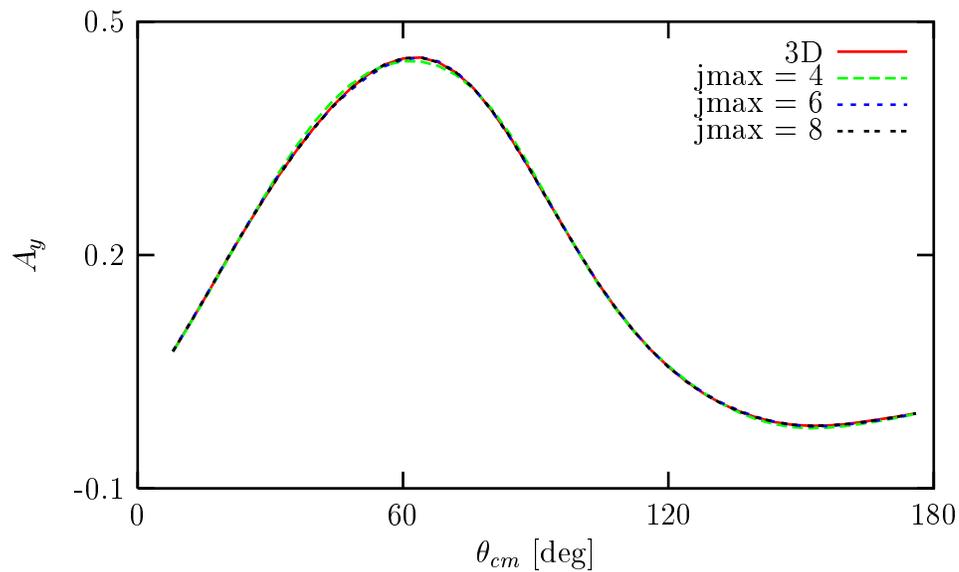


Figure 4.12: Same as Fig.4.11, but for analyzing power A_y .

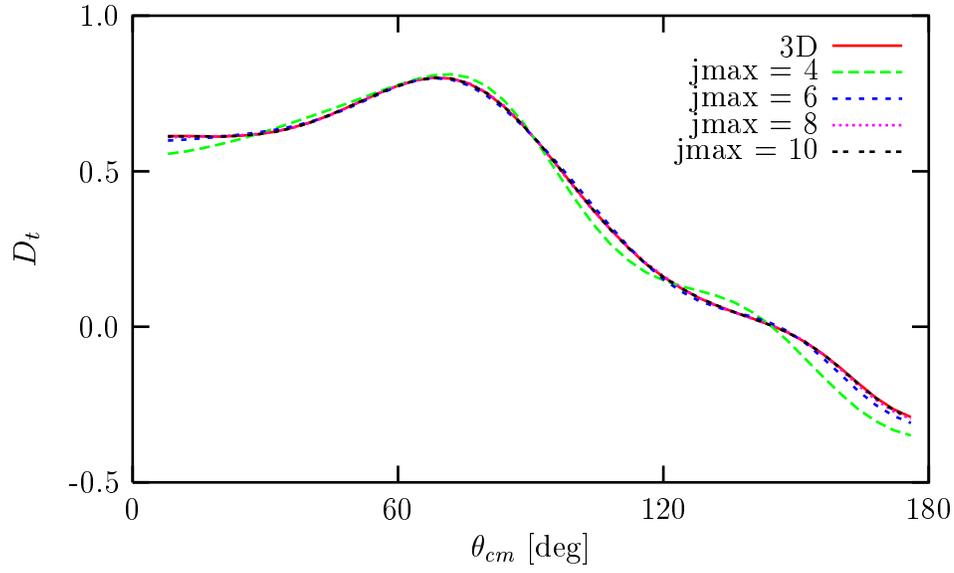


Figure 4.13: Same as Fig.4.11, but for polarization transfer coefficient D_t .

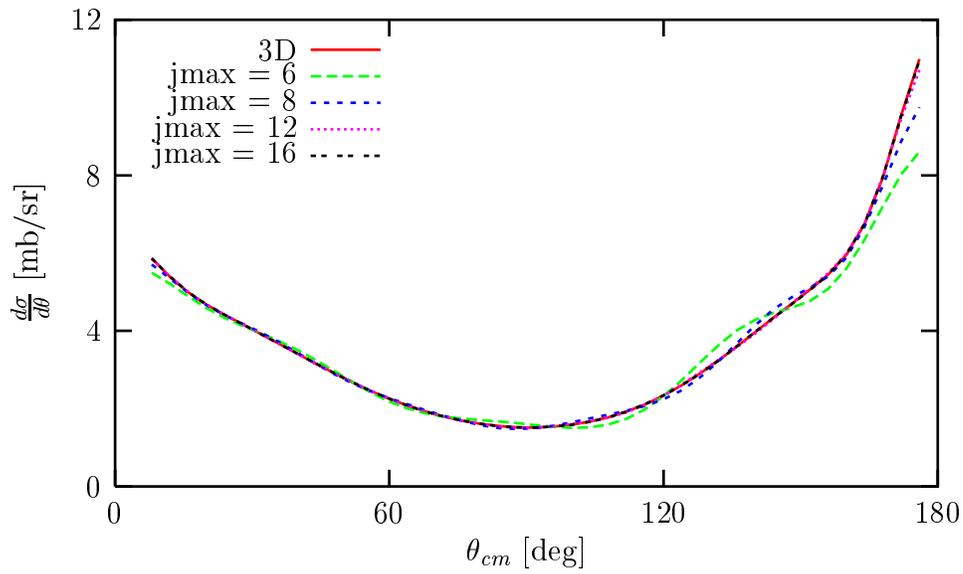


Figure 4.14: Same as Fig.4.11, but for $E_{lab} = 300$ MeV.

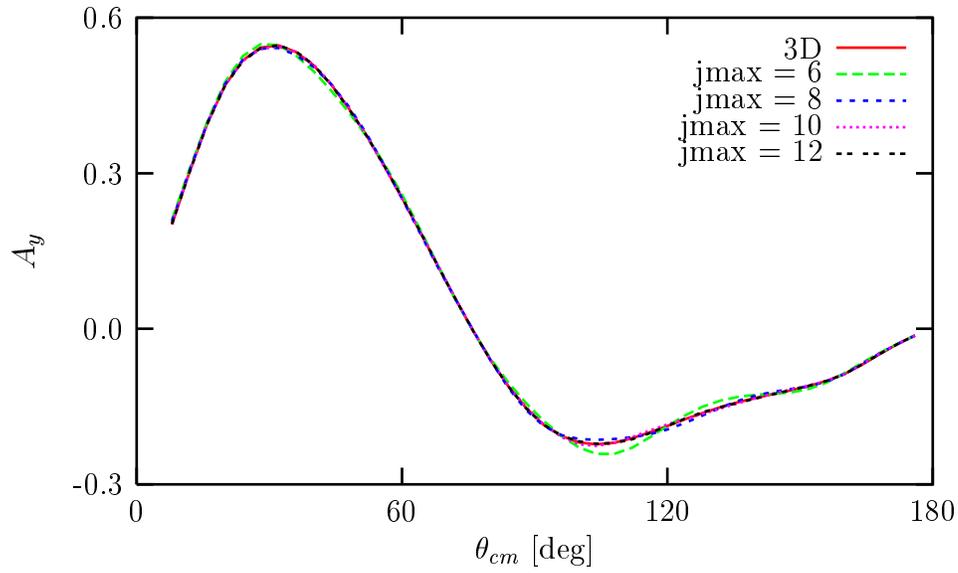


Figure 4.15: Same as Fig.4.12, but for $E_{lab} = 300$ MeV.

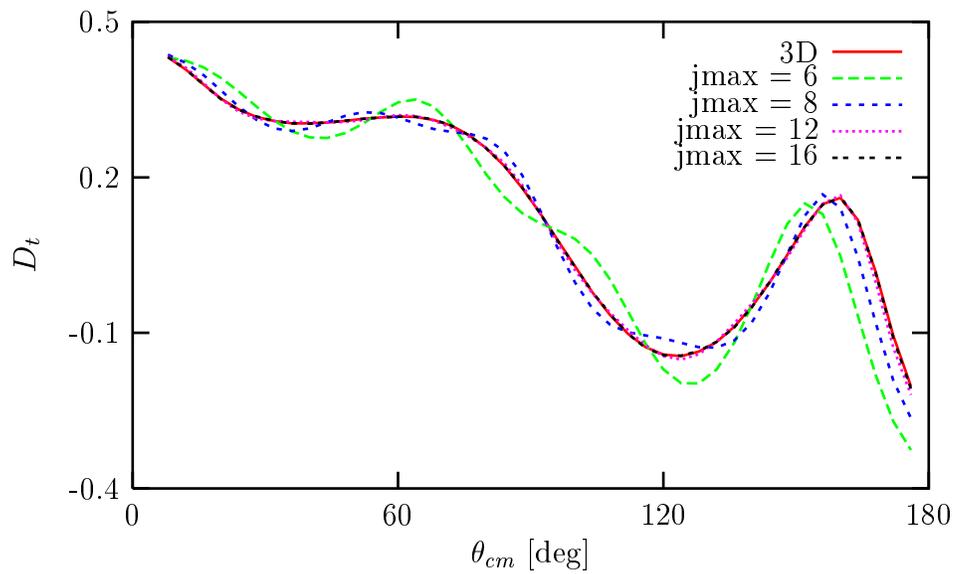


Figure 4.16: Same as Fig.4.13, but for $E_{lab} = 300$ MeV.

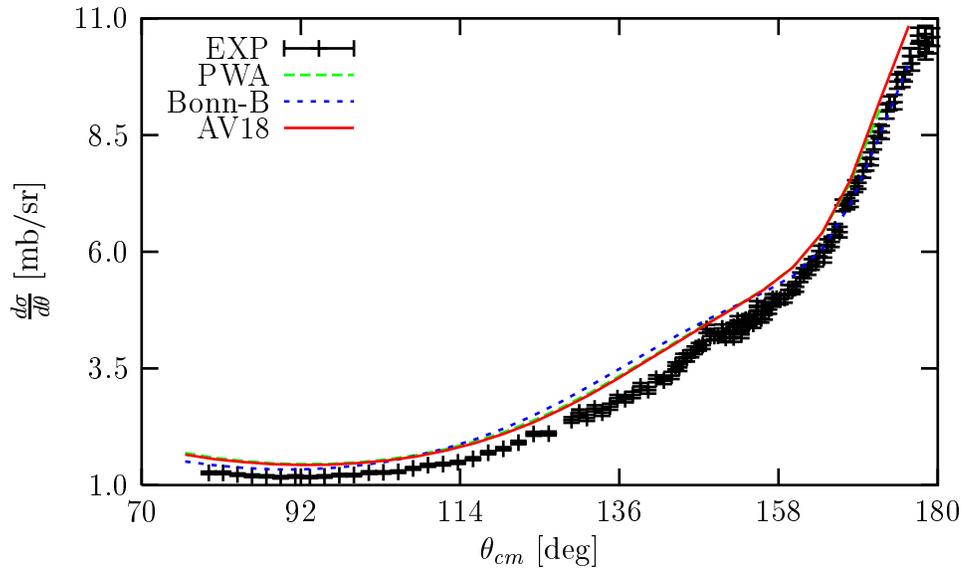


Figure 4.17: np spin averaged differential cross section at $E_{lab} = 340$ MeV. “EXP” are data taken from Franz, PS87, 14 (2000). The curve “PWA” is obtained from partial wave analyses, the curve “Bonn-B” from calculations based on the Bonn-B potential and the curve “AV18” from calculations based on the AV18 potential.

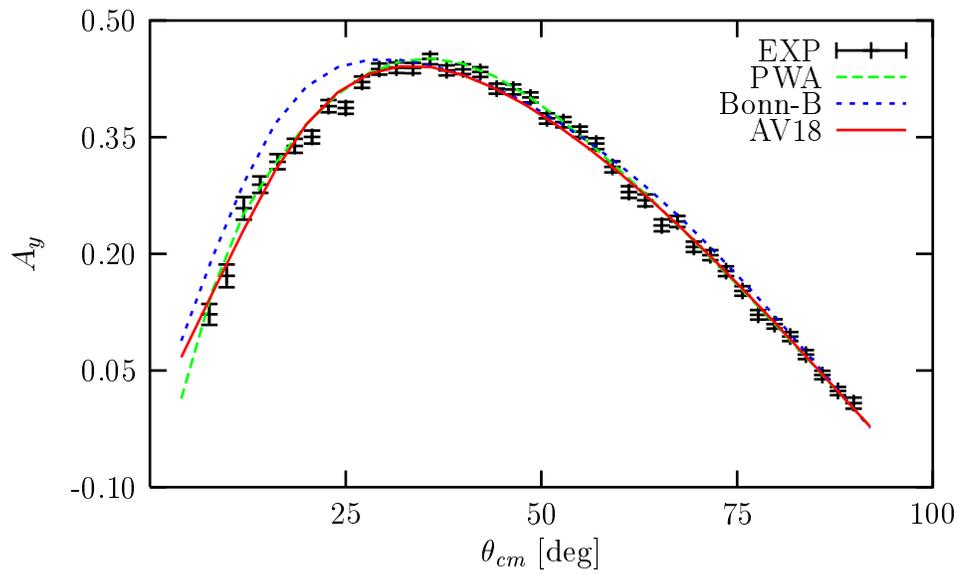


Figure 4.18: Same as Fig. 4.17, but for pp analyzing power A_y at $E_{lab} = 350$ MeV. Data source is Prezwoski, Phys. Rev. **C58**, 1897 (1998).

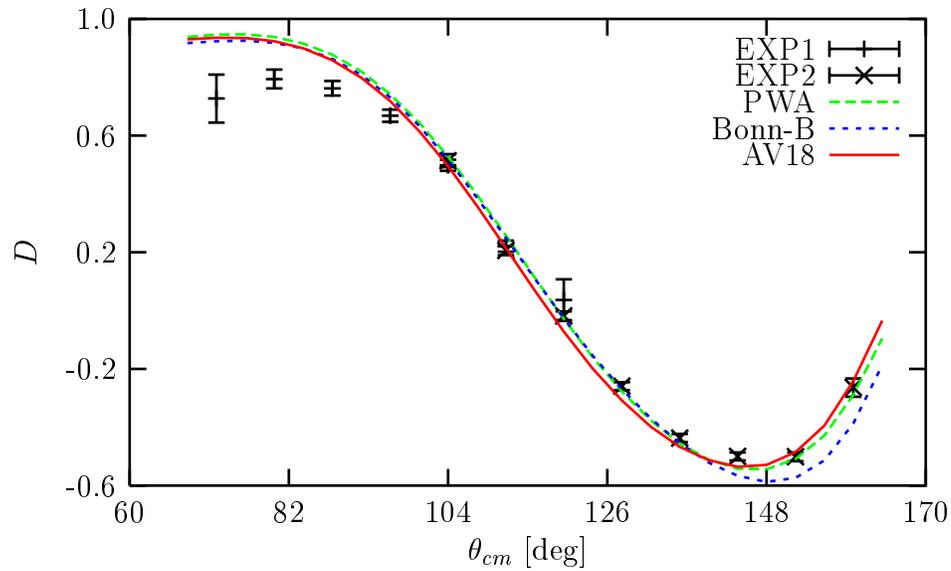


Figure 4.19: Same as Fig. 4.17, but for np depolarization D at $E_{lab} = 380$ MeV. Data source for both “EXP1” and “EXP2” is Arnold, EPJC17, 83 (2000).

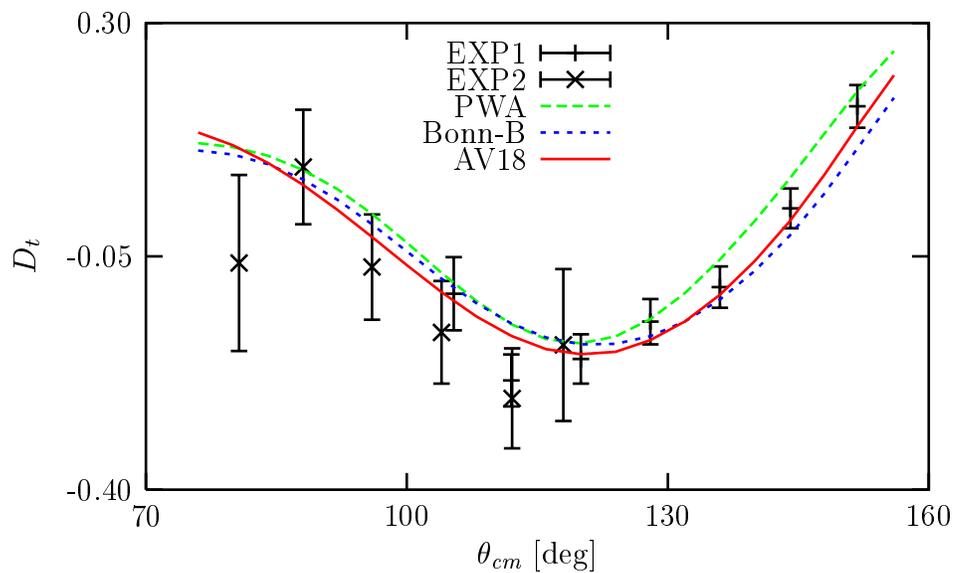


Figure 4.20: Same as Fig. 4.17, but for np polarization transfer coefficient D_t at $E_{lab} = 386$ MeV. Data source for both “EXP1” and “EXP2” is Ahmidouch, EPJC2, 627 (1998).

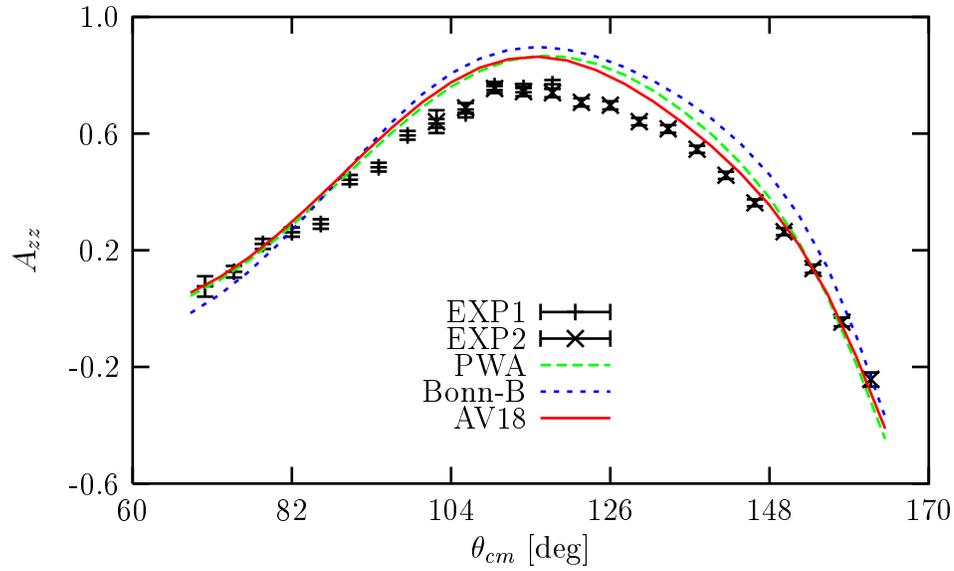


Figure 4.21: Same as Fig. 4.17, but for np spin correlation parameter A_{zz} at $E_{lab} = 380$ MeV. Data source for both “EXP1” and “EXP2” is Arnold, EPJC17, 67 (2000)

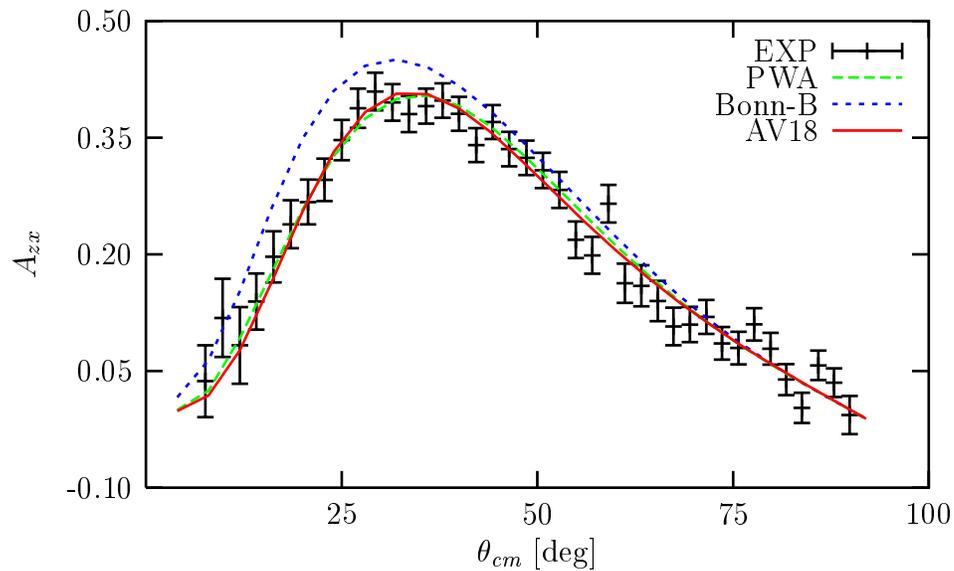


Figure 4.22: Same as Fig. 4.17, but for pp spin correlation parameter A_{zx} at $E_{lab} = 350$ MeV. Data source is Prezwoski, Phys. Rev. **C58**, 1897 (1998).

Chapter 5

THREE-DIMENSIONAL FORMULATION FOR THE DEUTERON

The three-dimensional approach for NN scattering developed in Chapter 3 was started with the creation of the momentum-helicity basis. Once this basis is defined the scattering equation is projected on this basis and the scattering as well as the NN potential matrix elements are calculated in that basis. Thus, it is general and applicable not solely to NN scattering but also to the NN bound system, the deuteron. In this case, the nonrelativistic deuteron equation and the states are projected on the momentum-helicity basis.

The motivation to use directly the relative momentum vector in calculating NN scattering is to avoid the complications which occur in the standard partial wave decomposition, when very many partial waves take part in the process. Since the deuteron state consists of only two partial wave projected components, namely s and d waves, there is no such a complication. However, developing the three-dimensional method leads to the use of a three-dimensional representation of the NN potential, in other words we abolish the partial wave representation of the NN potential. If one wants to use the potential defined in three-dimensional fashion, then it is necessary to apply the three-dimensional method to the deuteron as well. It is also of interest to investigate the deuteron properties in a three-dimensional fashion in momentum space. In configuration space a corresponding three-dimensional investigation on the deuteron wave function and densities based on the NN potential AV18 [20] has been carried out in Ref. [45].

In addition we derive the deuteron wave function in operator form in momentum space. The simple structure of the wave function in spin operators is suitable for the momentum-helicity basis and hence poses no difficulties in projecting the wave function

on this basis. The projection gives analytic expressions of the angular behavior of the deuteron wave function, which are different from the familiar ones. The deuteron wave function in operator form enables to investigate probability densities of various internal spin configurations of the deuteron. The resulting expressions have an analytic angular behavior. In configuration space a corresponding expression of the deuteron wave function can be found in Refs. [46, 47].

We present two formulations for the deuteron in the momentum-helicity basis. The differences of these two formulations emerge from the wave function and show by no means contradictions between the two formulations. In the first formulation we directly project the deuteron state on the momentum-helicity basis, thus introducing the wave function components of the deuteron in this basis. In the second formulation we first derive an operator form of the deuteron wave function and then project it on the momentum-helicity basis. The wave function components obtained in this manner exhibit an analytic angular behavior.

We describe the first formulation in Section 5.1, where we begin with the expansion of the deuteron state in the momentum-helicity basis and at the same time introduce the deuteron wave function components in this basis. We evaluate the normalization of these wave function components as well as the deuteron density. Next we project the deuteron eigenvalue equation on the momentum-helicity basis and end up with a set of two coupled integral equations in two variables, i.e. the magnitude of the relative momentum and the angle between the relative momentum and some arbitrary z-axis. We evaluate the partial wave components, the s and d waves of the deuteron wave function, in terms of the wave function components in the momentum-helicity basis to test the formulation.

The second formulation is described in Section 5.2. We begin with the derivation of the deuteron wave function in operator form, in which we make use of the deuteron partial wave components s and d waves. Next we project the wave function on the momentum-helicity basis. As result we can extract the angular parts of the wave function components, which are analytic. We proceed with further simplifying the deuteron eigenvalue equation obtained in the first formulation, and finally get a set of two coupled integral equations in one variable, i.e. the magnitude of the relative momentum, from which one can get the radial parts (in momentum space) of the deuteron wave function components. We connect these radial parts of the deuteron wave function components to the deuteron s and d waves.

Using the deuteron wave function in operator form we can investigate probability densities of various internal spin configurations of the deuteron. For an overall polarized deuteron there are various possible spin orientations of the two nucleons in the deuteron.

For instance, both nucleons have their spins up, or one nucleon has its spin up and the other down. We derive in Section 5.3 analytic expressions of the corresponding probability densities and display the results.

5.1 Formulation I

5.1.1 Deuteron Wave Function in the Momentum-Helicity Basis

Consider $|\Psi_d^{M_d}\rangle$ as the deuteron state, with M_d being the projection of the total angular momentum along an arbitrary z-axis. The state will be expanded in the momentum-helicity basis $|\mathbf{q}; \hat{\mathbf{q}}S\Lambda; t\rangle^{\pi_a}$ defined in Eq. (3.16). Inserting the completeness relation for the momentum-helicity basis given in Eq. (3.26) gives

$$\begin{aligned} |\Psi_d^{M_d}\rangle &= \frac{1}{4} \sum_{\Lambda=-1}^1 \int d\mathbf{q} |\mathbf{q}; \hat{\mathbf{q}}1\Lambda; 0\rangle^{1a} \langle \mathbf{q}; \hat{\mathbf{q}}1\Lambda; 0 | \Psi_d^{M_d}\rangle \\ &= \frac{1}{4} \int d\mathbf{q} \left\{ |\mathbf{q}; \hat{\mathbf{q}}11; 0\rangle^{1a} \langle \mathbf{q}; \hat{\mathbf{q}}11; 0 | \Psi_d^{M_d}\rangle + |\mathbf{q}; \hat{\mathbf{q}}10; 0\rangle^{1a} \langle \mathbf{q}; \hat{\mathbf{q}}10; 0 | \Psi_d^{M_d}\rangle \right. \\ &\quad \left. + |\mathbf{q}; \hat{\mathbf{q}}1-1; 0\rangle^{1a} \langle \mathbf{q}; \hat{\mathbf{q}}1-1; 0 | \Psi_d^{M_d}\rangle \right\}, \end{aligned} \quad (5.1)$$

in which we have inserted the deuteron properties, i.e. $S = 1$, $t = 0$ and the parity is even. According to Eq. (3.44) the momentum-helicity basis can be written as

$$|\mathbf{q}; \hat{\mathbf{q}}S\Lambda; t\rangle^{\pi_a} = (|\mathbf{q}\rangle + \eta_\pi |-\mathbf{q}\rangle) |\hat{\mathbf{q}}S\Lambda\rangle |t\rangle, \quad (5.2)$$

and this together with Eq. (3.20) gives the following symmetry relation for the momentum-helicity basis

$$\begin{aligned} |\mathbf{q}; \hat{\mathbf{q}}S\Lambda; t\rangle^{\pi_a} &= \eta_\pi (-)^S (|-\mathbf{q}\rangle + \eta_\pi |\mathbf{q}\rangle) |-\hat{\mathbf{q}}S - \Lambda\rangle |t\rangle \\ &= \eta_\pi (-)^S |-\mathbf{q}; -\hat{\mathbf{q}}S - \Lambda; t\rangle^{\pi_a}. \end{aligned} \quad (5.3)$$

Thus, we can simplify Eq. (5.1) to

$$\begin{aligned} |\Psi_d^{M_d}\rangle &= \frac{1}{4} \int d\mathbf{q} \left\{ |\mathbf{q}; \hat{\mathbf{q}}11; 0\rangle^{1a} \langle \mathbf{q}; \hat{\mathbf{q}}11; 0 | \Psi_d^{M_d}\rangle + |\mathbf{q}; \hat{\mathbf{q}}10; 0\rangle^{1a} \langle \mathbf{q}; \hat{\mathbf{q}}10; 0 | \Psi_d^{M_d}\rangle \right. \\ &\quad \left. + |-\mathbf{q}; -\hat{\mathbf{q}}11; 0\rangle^{1a} \langle -\mathbf{q}; -\hat{\mathbf{q}}11; 0 | \Psi_d^{M_d}\rangle \right\} \\ &= \frac{1}{4} \int d\mathbf{q} \left\{ |\mathbf{q}; \hat{\mathbf{q}}11; 0\rangle^{1a} \langle \mathbf{q}; \hat{\mathbf{q}}11; 0 | \Psi_d^{M_d}\rangle + |\mathbf{q}; \hat{\mathbf{q}}10; 0\rangle^{1a} \langle \mathbf{q}; \hat{\mathbf{q}}10; 0 | \Psi_d^{M_d}\rangle \right. \\ &\quad \left. + |\mathbf{q}; \hat{\mathbf{q}}11; 0\rangle^{1a} \langle \mathbf{q}; \hat{\mathbf{q}}11; 0 | \Psi_d^{M_d}\rangle \right\} \\ &= \int d\mathbf{q} \left\{ \frac{1}{2} |\mathbf{q}; \hat{\mathbf{q}}11; 0\rangle^{1a} \langle \mathbf{q}; \hat{\mathbf{q}}11; 0 | \Psi_d^{M_d}\rangle + \frac{1}{4} |\mathbf{q}; \hat{\mathbf{q}}10; 0\rangle^{1a} \langle \mathbf{q}; \hat{\mathbf{q}}10; 0 | \Psi_d^{M_d}\rangle \right\} \\ &\equiv \int d\mathbf{q} \left\{ \frac{1}{2} |\mathbf{q}; \hat{\mathbf{q}}11; 0\rangle^{1a} \varphi_1^{M_d}(\mathbf{q}) + \frac{1}{4} |\mathbf{q}; \hat{\mathbf{q}}10; 0\rangle^{1a} \varphi_0^{M_d}(\mathbf{q}) \right\}. \end{aligned} \quad (5.4)$$

In the last step of Eq. (5.4) we have defined the deuteron wave function component in the momentum-helicity basis as

$$\varphi_{\Lambda}^{M_d}(\mathbf{q}) \equiv {}^{1a} \langle \mathbf{q}; \hat{\mathbf{q}}1\Lambda; 0 | \Psi_d^{M_d} \rangle. \quad (5.5)$$

Since the state $|\mathbf{q}; \hat{\mathbf{q}}S\Lambda\rangle$ is obtained by rotating the state $|q\hat{\mathbf{z}}; \hat{\mathbf{z}}S\Lambda\rangle$ by means of a rotation operator

$$R(\hat{\mathbf{q}}) = \exp -iJ_z\phi \exp -iJ_y\theta, \quad (5.6)$$

as

$$|\mathbf{q}; \hat{\mathbf{q}}S\Lambda\rangle = R(\hat{\mathbf{q}}) |q\hat{\mathbf{z}}; \hat{\mathbf{z}}S\Lambda\rangle, \quad (5.7)$$

where $\mathbf{J} = \mathbf{L} + \mathbf{S}$ is the operator of total angular momentum, it follows that

$$\begin{aligned} {}^{1a} \langle \mathbf{q}; \hat{\mathbf{q}}S\Lambda; t | \Psi_d^{M_d} \rangle &= {}^{1a} \langle q\hat{\mathbf{z}}; \hat{\mathbf{z}}S\Lambda; t | e^{iJ_y\theta} e^{iJ_z\phi} | \Psi_d^{M_d} \rangle \\ &= e^{iM_d\phi} {}^{1a} \langle q\hat{\mathbf{z}}; \hat{\mathbf{z}}S\Lambda; t | e^{iJ_y\theta} | \Psi_d^{M_d} \rangle. \end{aligned} \quad (5.8)$$

In this way, we can pull out the azimuthal dependency of $\varphi_{\Lambda}^{M_d}(\mathbf{q})$ as

$$\varphi_{\Lambda}^{M_d}(\mathbf{q}) \equiv \varphi_{\Lambda}^{M_d}(q, \theta) e^{iM_d\phi}, \quad (5.9)$$

and finally get the expansion of the deuteron state in the momentum-helicity basis as

$$|\Psi_d^{M_d}\rangle = \int d\mathbf{q} \left\{ \frac{1}{2} |\mathbf{q}; \hat{\mathbf{q}}11; 0\rangle^{1a} \varphi_1^{M_d}(q, \theta) + \frac{1}{4} |\mathbf{q}; \hat{\mathbf{q}}10; 0\rangle^{1a} \varphi_0^{M_d}(q, \theta) \right\} e^{iM_d\phi}. \quad (5.10)$$

The normalization of the wave function components $\varphi_{\Lambda}^{M_d}(q, \theta)$ can be determined from the normalization of the deuteron state according to the following equation

$$\begin{aligned} \langle \Psi_d^{M_d} | \Psi_d^{M_d} \rangle &= \int d\mathbf{q}' \int d\mathbf{q} \left\{ \frac{1}{2} {}^{1a} \langle \mathbf{q}'; \hat{\mathbf{q}}'11; 0 | \varphi_1^{M_d*}(q', \theta') + \frac{1}{4} {}^{1a} \langle \mathbf{q}'; \hat{\mathbf{q}}'10; 0 | \varphi_0^{M_d*}(q', \theta') \right\} \\ &\quad \times \left\{ \frac{1}{2} |\mathbf{q}; \hat{\mathbf{q}}11; 0\rangle^{1a} \varphi_1^{M_d}(q, \theta) + \frac{1}{4} |\mathbf{q}; \hat{\mathbf{q}}10; 0\rangle^{1a} \varphi_0^{M_d}(q, \theta) \right\} e^{iM_d(\phi-\phi')} \\ &= \int d\mathbf{q}' \int d\mathbf{q} \left\{ \frac{1}{4} {}^{1a} \langle \mathbf{q}'; \hat{\mathbf{q}}'11; 0 | \mathbf{q}; \hat{\mathbf{q}}11; 0\rangle^{1a} \varphi_1^{M_d*}(q', \theta') \varphi_1^{M_d}(q, \theta) \right. \\ &\quad + \frac{1}{16} {}^{1a} \langle \mathbf{q}'; \hat{\mathbf{q}}'10; 0 | \mathbf{q}; \hat{\mathbf{q}}10; 0\rangle^{1a} \varphi_0^{M_d*}(q', \theta') \varphi_0^{M_d}(q, \theta) \\ &\quad + \frac{1}{8} {}^{1a} \langle \mathbf{q}'; \hat{\mathbf{q}}'11; 0 | \mathbf{q}; \hat{\mathbf{q}}10; 0\rangle^{1a} \varphi_1^{M_d*}(q', \theta') \varphi_0^{M_d}(q, \theta) \\ &\quad \left. + \frac{1}{8} {}^{1a} \langle \mathbf{q}'; \hat{\mathbf{q}}'10; 0 | \mathbf{q}; \hat{\mathbf{q}}11; 0\rangle^{1a} \varphi_0^{M_d*}(q', \theta') \varphi_1^{M_d}(q, \theta) \right\} e^{iM_d(\phi-\phi')} \\ &= \int d\mathbf{q} \left\{ \frac{1}{2} \varphi_1^{M_d*}(q, \theta) \varphi_1^{M_d}(q, \theta) \right. \\ &\quad \left. + \frac{1}{8} \left(\varphi_0^{M_d*}(q, \theta) - (-)^{M_d} \varphi_0^{M_d*}(q, \pi - \theta) \right) \varphi_0^{M_d}(q, \theta) \right\}. \end{aligned} \quad (5.11)$$

In obtaining this equation we have used the orthonormality of the momentum-helicity basis given in Eq. (3.23). To proceed we need to know the symmetry property of $\varphi_{\Lambda}^{M_d}(q, \theta)$.

Using the symmetry relation given in Eq. (5.3) we can find the relation between $\varphi_{\Lambda}^{M_d}(\mathbf{q})$ and $\varphi_{-\Lambda}^{M_d}(-\mathbf{q})$ as

$$\begin{aligned}\varphi_{\Lambda}^{M_d}(\mathbf{q}) &= {}^{1a}\langle \mathbf{q}; \hat{\mathbf{q}}1\Lambda; 0 | \Psi_d^{M_d} \rangle \\ &= -{}^{1a}\langle -\mathbf{q}; -\hat{\mathbf{q}}1-\Lambda; 0 | \Psi_d^{M_d} \rangle \\ &= -\varphi_{-\Lambda}^{M_d}(-\mathbf{q}),\end{aligned}\quad (5.12)$$

and therefore,

$$\varphi_{\Lambda}^{M_d}(q, \theta) = -(-)^{M_d} \varphi_{-\Lambda}^{M_d}(q, \pi - \theta). \quad (5.13)$$

Thus, the normalization of $\varphi_{\Lambda}^{M_d}(q, \theta)$ is determined by the following equation:

$$\langle \Psi_d^{M_d} | \Psi_d^{M_d} \rangle = 2\pi \int_0^{\infty} dq q^2 \int_{-1}^1 d \cos \theta \left\{ \frac{1}{2} |\varphi_1^{M_d}(q, \theta)|^2 + \frac{1}{4} |\varphi_0^{M_d}(q, \theta)|^2 \right\}. \quad (5.14)$$

Now we define the deuteron density $\rho^{M_d}(\mathbf{q})$ as

$$\rho^{M_d}(\mathbf{q}) \equiv \sum_{\Lambda=-1}^1 \langle \Psi_d^{M_d} | \mathbf{q}; \hat{\mathbf{q}}1\Lambda; 0 \rangle^{1a} \frac{1}{4} {}^{1a}\langle \mathbf{q}; \hat{\mathbf{q}}1\Lambda; 0 | \Psi_d^{M_d} \rangle \quad (5.15)$$

such, that the probability to find a deuteron in any possible helicity state and having the relative momentum of the two nucleons between \mathbf{q} and $\mathbf{q} + \Delta\mathbf{q}$ is $\rho^{M_d}(\mathbf{q})\Delta\mathbf{q}$. This definition follows naturally from the following algebra:

$$\begin{aligned}\langle \Psi_d^{M_d} | \Psi_d^{M_d} \rangle &= \sum_{S\Lambda\pi t} \int d\mathbf{q} \langle \Psi_d^{M_d} | \mathbf{q}; \hat{\mathbf{q}}S\Lambda; t \rangle^{\pi a} \frac{1}{4} {}^{\pi a}\langle \mathbf{q}; \hat{\mathbf{q}}S\Lambda; t | \Psi_d^{M_d} \rangle \\ &= \sum_{\Lambda} \int d\mathbf{q} \langle \Psi_d^{M_d} | \mathbf{q}; \hat{\mathbf{q}}1\Lambda; 0 \rangle^{1a} \frac{1}{4} {}^{1a}\langle \mathbf{q}; \hat{\mathbf{q}}1\Lambda; 0 | \Psi_d^{M_d} \rangle \\ &\equiv \int d\mathbf{q} \rho^{M_d}(\mathbf{q})\end{aligned}\quad (5.16)$$

Inserting Eq. (5.10) into Eq. (5.15) this yields

$$\begin{aligned}\rho^{M_d}(\mathbf{q}) &= \frac{1}{4} \sum_{\Lambda=-1}^1 \int d\mathbf{q}' e^{-iM_d\phi'} \left\{ \frac{1}{2} \varphi_1^{M_d*}(q', \theta')^{1a} \langle \mathbf{q}'; \hat{\mathbf{q}}'11; 0 | \mathbf{q}; \hat{\mathbf{q}}1\Lambda; 0 \rangle^{1a} \right. \\ &\quad \left. + \frac{1}{4} \varphi_0^{M_d*}(q', \theta')^{1a} \langle \mathbf{q}'; \hat{\mathbf{q}}'10; 0 | \mathbf{q}; \hat{\mathbf{q}}1\Lambda; 0 \rangle^{1a} \right\} \\ &\quad \times \int d\mathbf{q}'' \left\{ \frac{1}{2} {}^{1a}\langle \mathbf{q}; \hat{\mathbf{q}}1\Lambda; 0 | \mathbf{q}''; \hat{\mathbf{q}}''11; 0 \rangle^{1a} \varphi_1^{M_d}(q'', \theta'') \right. \\ &\quad \left. + \frac{1}{4} {}^{1a}\langle \mathbf{q}; \hat{\mathbf{q}}1\Lambda; 0 | \mathbf{q}''; \hat{\mathbf{q}}''10; 0 \rangle^{1a} \varphi_0^{M_d}(q'', \theta'') \right\} e^{iM_d\phi''} \\ &= \frac{1}{4} \sum_{\Lambda=-1}^1 \left\{ \varphi_1^{M_d*}(q, \theta) e^{-iM_d\phi} \delta_{\Lambda 1} - \varphi_1^{M_d*}(q, \pi - \theta) e^{-iM_d(\phi+\pi)} \delta_{\Lambda, -1} \right. \\ &\quad \left. + \frac{1}{2} \varphi_0^{M_d*}(q, \theta) e^{-iM_d\phi} \delta_{\Lambda 0} - \frac{1}{2} \varphi_0^{M_d*}(q, \pi - \theta) e^{-iM_d(\phi+\pi)} \delta_{\Lambda 0} \right\} \\ &\quad \times \left\{ \varphi_1^{M_d}(q, \theta) e^{iM_d\phi} \delta_{\Lambda 1} - \varphi_1^{M_d}(q, \pi - \theta) e^{iM_d(\phi+\pi)} \delta_{\Lambda, -1} \right\}\end{aligned}$$

$$\begin{aligned}
& + \frac{1}{2} \varphi_0^{M_d}(q, \theta) e^{iM_d \phi} \delta_{\Lambda 0} - \frac{1}{2} \varphi_0^{M_d}(q, \pi - \theta) e^{iM_d(\phi + \pi)} \delta_{\Lambda 0} \Big\} \\
= & \frac{1}{4} \sum_{\Lambda=-1}^1 \left\{ \varphi_1^{M_d^*}(\mathbf{q}) \delta_{\Lambda 1} - \varphi_1^{M_d^*}(-\mathbf{q}) \delta_{\Lambda, -1} + \varphi_0^{M_d^*}(\mathbf{q}) \delta_{\Lambda 0} \right\} \\
& \times \left\{ \varphi_1^{M_d}(\mathbf{q}) \delta_{\Lambda 1} - \varphi_1^{M_d}(-\mathbf{q}) \delta_{\Lambda, -1} + \varphi_0^{M_d}(\mathbf{q}) \delta_{\Lambda 0} \right\}. \tag{5.17}
\end{aligned}$$

Thus, it follows that

$$\begin{aligned}
\rho^{M_d}(\mathbf{q}) & = \frac{1}{4} \left| \varphi_1^{M_d}(\mathbf{q}) \right|^2 + \frac{1}{4} \left| \varphi_0^{M_d}(\mathbf{q}) \right|^2 + \frac{1}{4} \left| \varphi_1^{M_d}(-\mathbf{q}) \right|^2 \\
& = \frac{1}{4} \left| \varphi_1^{M_d}(q, \theta) \right|^2 + \frac{1}{4} \left| \varphi_0^{M_d}(q, \theta) \right|^2 + \frac{1}{4} \left| \varphi_1^{M_d}(q, \pi - \theta) \right|^2. \tag{5.18}
\end{aligned}$$

5.1.2 Two-Dimensional Deuteron Eigenvalue Equation

The deuteron state $|\Psi_d^{M_d}\rangle$ satisfies the eigenvalue equation

$$(H_0 - E_d + V) |\Psi_d^{M_d}\rangle = 0, \tag{5.19}$$

where E_d is the deuteron binding energy. Projecting this eigenvalue equation on the state $|\mathbf{q}; \hat{\mathbf{q}}1\Lambda; 0\rangle^{1a}$ and using the expansion of $|\Psi_d^{M_d}\rangle$ given Eq. (5.10) leads to

$$\begin{aligned}
& {}^{1a} \langle \mathbf{q}; \hat{\mathbf{q}}1\Lambda; 0 | (H_0 - E_d + V) |\Psi_d^{M_d}\rangle \\
& = {}^{1a} \langle \mathbf{q}; \hat{\mathbf{q}}1\Lambda; 0 | (H_0 - E_d) |\Psi_d^{M_d}\rangle \\
& \quad + {}^{1a} \langle \mathbf{q}; \hat{\mathbf{q}}1\Lambda; 0 | V \\
& \quad \times \int d\mathbf{q}' \left\{ \frac{1}{2} |\mathbf{q}'; \hat{\mathbf{q}}'11; 0\rangle^{1a} \varphi_1^{M_d}(q', \theta') + \frac{1}{4} |\mathbf{q}'; \hat{\mathbf{q}}'10; 0\rangle^{1a} \varphi_0^{M_d}(q', \theta') \right\} e^{iM_d \phi'} \\
& = \left(\frac{q^2}{m} - E_d \right) \varphi_{\Lambda}^{M_d}(q, \theta) e^{iM_d \phi} \\
& \quad + \frac{1}{2} \int d\mathbf{q}' {}^{1a} \langle \mathbf{q}; \hat{\mathbf{q}}1\Lambda; 0 | V | \mathbf{q}'; \hat{\mathbf{q}}'11; 0\rangle^{1a} \varphi_1^{M_d}(q', \theta') e^{iM_d \phi'} \\
& \quad + \frac{1}{4} \int d\mathbf{q}' {}^{1a} \langle \mathbf{q}; \hat{\mathbf{q}}1\Lambda; 0 | V | \mathbf{q}'; \hat{\mathbf{q}}'10; 0\rangle^{1a} \varphi_0^{M_d}(q', \theta') e^{iM_d \phi'} \\
& = \left(\frac{q^2}{m} - E_d \right) \varphi_{\Lambda}^{M_d}(q, \theta) e^{iM_d \phi} \\
& \quad + \int d\mathbf{q}' \left\{ \frac{1}{2} V_{\Lambda 1}^{110}(\mathbf{q}, \mathbf{q}') \varphi_1^{M_d}(q', \theta') + \frac{1}{4} V_{\Lambda 0}^{110}(\mathbf{q}, \mathbf{q}') \varphi_0^{M_d}(q', \theta') \right\} e^{iM_d \phi'}, \tag{5.20}
\end{aligned}$$

Hence, the projected eigenvalue equation for the deuteron on the momentum-helicity basis consists of a set of two coupled integral equations

$$\begin{aligned}
& \left(\frac{q^2}{m} - E_d \right) \varphi_{\Lambda}^{M_d}(q, \theta) \\
& \quad + \int d\mathbf{q}' e^{-iM_d(\phi - \phi')} \left\{ \frac{1}{2} V_{\Lambda 1}^{110}(\mathbf{q}, \mathbf{q}') \varphi_1^{M_d}(q', \theta') + \frac{1}{4} V_{\Lambda 0}^{110}(\mathbf{q}, \mathbf{q}') \varphi_0^{M_d}(q', \theta') \right\} = 0, \tag{5.21}
\end{aligned}$$

where $\Lambda = 1, 0$. The wave function components $\varphi_\Lambda^{M_d}(q, \theta)$ have no azimuthal dependence, and therefore the ϕ' -integral in this equation can be carried out independently. Recalling the definition given in Eq. (3.70), the final expression for the deuteron eigenvalue equation is given as

$$\begin{aligned} \left(\frac{q^2}{m} - E_d\right) \varphi_\Lambda^{M_d}(q, \theta) &+ \frac{1}{2} \int_0^\infty dq' q'^2 \int_{-1}^1 d \cos \theta' v_{\Lambda 1}^{110, M_d}(q, q', \theta, \theta') \varphi_1^{M_d}(q', \theta') \\ &+ \frac{1}{4} \int_0^\infty dq' q'^2 \int_{-1}^1 d \cos \theta' v_{\Lambda 0}^{110, M_d}(q, q', \theta, \theta') \varphi_0^{M_d}(q', \theta') = 0. \end{aligned} \quad (5.22)$$

This resulting set of equations for the deuteron, which consists of two coupled two-dimensional integral equations, is consistent with the set of equations for a NN system in scattering states evaluated in Chapter 3 (see Eq. (3.73)). Arriving at this point we would like to give some remarks. The deuteron eigenvalue equation given in Eq. (5.22) and thus the resulting deuteron wave function components from this equation, which are defined in Eq. (5.9), are obtained with the assuming of the deuteron properties, i.e. $S = 1$, $t = 0$ and consequently the parity being even. As a matter of fact this assumption is not necessary. Even if we obtain a set of equations for a NN bound system with any spin, isospin and parity, a calculation using a realistic NN potential will show that the solution of the equations exists only for that certain quantum numbers. In other words, nature will reveal itself without additional assumptions. Therefore, for this approach there is no a priori knowledge needed, the approach will automatically provide full insight into the deuteron.

5.1.3 Deuteron Partial Wave Projected Wave Function

Now we would like to connect the deuteron wave function components $\varphi_\Lambda^{M_d}(q, \theta)$ with the standard partial wave components $\psi_l(q)$ of the deuteron wave function, which are defined as

$$\psi_l(q) \equiv \langle q(l1)jm; 0 | \Psi_d^{M_d} \rangle, \quad (5.23)$$

where $|q(lS)jm; t\rangle$ is the partial wave basis given in Eq. (3.84). Again, for simplicity, we use the already known spin and isospin of the deuteron, but left l , j and m arbitrary, which are the orbital, total and magnetic total angular momentum quantum numbers, respectively.

We begin by inserting into the projection in Eq. (5.23) the expansion of $|\Psi_d^{M_d}\rangle$ given in Eq. (5.10):

$$\begin{aligned} \psi_l(q) &= \frac{1}{2} \int d\mathbf{q}' \langle q(l1)jm; 0 | \mathbf{q}'; \hat{\mathbf{q}}'11; 0 \rangle^{1a} \varphi_1^{M_d}(q', \theta') e^{iM_d\phi'} \\ &+ \frac{1}{4} \int d\mathbf{q}' \langle q(l1)jm; 0 | \mathbf{q}'; \hat{\mathbf{q}}'10; 0 \rangle^{1a} \varphi_0^{M_d}(q', \theta') e^{iM_d\phi'}. \end{aligned} \quad (5.24)$$

Recalling the overlap given in Eq. (3.88) and using Eq. (5.2), the scalar product of the partial wave and momentum-helicity basis is given as

$$\begin{aligned}
\langle q'(lS')jm; t' | \mathbf{q}; \hat{\mathbf{q}}S\Lambda; t \rangle^{\pi a} &= (\langle q'(lS')jm | \mathbf{q} | \hat{\mathbf{q}}S\Lambda \rangle + \eta_\pi \langle q'(lS')jm | -\mathbf{q} | \hat{\mathbf{q}}S\Lambda \rangle) \langle t' | t \rangle \\
&= \frac{\delta(q' - q)}{q'q} \delta_{S'S} \delta_{t't} \sum_\mu C(lSj; \mu, m - \mu, m) \\
&\quad \times \left(Y_{l\mu}^*(\hat{\mathbf{q}}) + \eta_\pi Y_{l\mu}^*(-\hat{\mathbf{q}}) \right) e^{-i(m-\mu)\phi} d_{m-\mu, \Lambda}^S(\theta) \\
&= \left(1 + \eta_\pi (-)^l \right) \frac{\delta(q' - q)}{q'q} \delta_{S'S} \delta_{t't} \\
&\quad \times \sum_\mu C(lSj; \mu, m - \mu, m) Y_{l\mu}^*(\hat{\mathbf{q}}) e^{-i(m-\mu)\phi} d_{m-\mu, \Lambda}^S(\theta) \\
&= \left(1 + \eta_\pi (-)^l \right) \sqrt{\frac{2l+1}{4\pi}} \frac{\delta(q' - q)}{q'q} \delta_{S'S} \delta_{t't} e^{-im\phi} \\
&\quad \times \sum_\mu C(lSj; \mu, m - \mu, m) d_{\mu 0}^l(\theta) d_{m-\mu, \Lambda}^S(\theta) \\
&= \left(1 + \eta_\pi (-)^l \right) \frac{\delta(q' - q)}{q'q} \delta_{S'S} \delta_{t't} \\
&\quad \times \sqrt{\frac{2l+1}{4\pi}} e^{-im\phi} C(lSj; 0\Lambda\Lambda) d_{m\Lambda}^j(\theta), \tag{5.25}
\end{aligned}$$

in which we have used the complex conjugate of the relation given in Eq. (3.91) as well as the complex conjugate of an addition theorem for Wigner's D-functions given in Eq. (3.100). Inserting this scalar product into Eq. (5.24) gives

$$\begin{aligned}
\psi_l(q) &= \left(1 + (-)^l \right) \sqrt{\frac{2l+1}{4\pi}} \int_0^{2\pi} d\phi' e^{-i(m-M_d)\phi'} \\
&\quad \times \int_{-1}^1 d \cos \theta' \left\{ \frac{1}{2} C(l1j; 011) d_{m1}^j(\theta') \varphi_1^{M_d}(q, \theta') + \frac{1}{4} C(l1j; 000) d_{m0}^j(\theta') \varphi_0^{M_d}(q, \theta') \right\} \\
&= \left(1 + (-)^l \right) \sqrt{\pi(2l+1)} \delta_{mM_d} \\
&\quad \times \int_{-1}^1 d \cos \theta' \left\{ \frac{1}{2} C(l1j; 011) d_{m1}^j(\theta') \varphi_1^{M_d}(q, \theta') + \frac{1}{4} C(l1j; 000) d_{m0}^j(\theta') \varphi_0^{M_d}(q, \theta') \right\}. \tag{5.26}
\end{aligned}$$

Equation (5.26) reveals that the partial wave projection of the deuteron state exists only for $m = M_d$ and even l , which demonstrates the even parity of the deuteron. Thus, we obtain

$$\begin{aligned}
\psi_l(q) &= 2\sqrt{\pi(2l+1)} \int_{-1}^1 d \cos \theta' \left\{ \frac{1}{2} C(l1j; 011) d_{M_d 1}^j(\theta') \varphi_1^{M_d}(q, \theta') \right. \\
&\quad \left. + \frac{1}{4} C(l1j; 000) d_{M_d 0}^j(\theta') \varphi_0^{M_d}(q, \theta') \right\}. \tag{5.27}
\end{aligned}$$

Equation (5.27) does not exhibit exactly the well known deuteron quantum numbers l , j and m . These quantum numbers must be determined by explicit calculations, in which

one inserts into Eq. (5.27) the deuteron wave function component $\varphi_{\Lambda}^{M_d}(q, \theta)$ obtained as the solution of Eq. (5.22).

5.1.4 Explicit Solution of the Two-Dimensional Deuteron Eigenvalue Equation

In this section we show results from numerical evaluations of Eq. (5.22). To solve this eigenvalue equation we use the power method [48, 49] and get the deuteron binding energy E_d as well as the deuteron wave function components $\varphi_{\Lambda}^{M_d}(q, \theta)$. A modification to the power method is necessary as described in Ref. [50] to exclude unphysical solutions corresponding to bound states in the repulsive core region of the NN force. The calculations are carried out based on the NN potentials Bonn-B [21] and AV18 [20].

The integrals in Eq. (5.22) are evaluated by means of the Gauss-Legendre quadrature. For both potentials 10 integration points for the ϕ' -integration and 32 integration points for the $\cos \theta'$ -integration are sufficient. The hyperbolic mapping with cut-off (see Appendix E) is employed for the q' -integration. Using the Bonn-B potential we obtain the deuteron binding energy 2.224 MeV, with the q' -integration interval being cut off at 30 fm^{-1} . Using the AV18 potential the resulting deuteron binding energy is 2.225 MeV and the cut off is at 8 fm^{-1} .

In Fig. 5.1 we display the deuteron wave function components $\varphi_{\Lambda}^{M_d}(q, \theta)$ for $M_d = 0$ as functions of q and $\cos \theta$. The figures on the left result from calculations based on the Bonn-B potential and those on the right on the AV18 potential. The results obtained from the two potentials look quite similar. Both drop steeply as the magnitude of the relative momentum between the two nucleons inside the deuteron increases from zero to about $100 \text{ MeV}/c$. The wave function component $\varphi_0^0(q, \theta)$ shows a cosine-like behavior indicated at $q = 0$ by the straight line connecting its maximum at $\theta = 0$ with its minimum at $\theta = 180^\circ$ through zero at $\theta = 90^\circ$. In contrast, the wave function component $\varphi_1^0(q, \theta)$ displays sine-like behavior; it peaks at $\theta = 90^\circ$ and vanishes at $\theta = 0$ and 180° . The figures reveal that the maximum of $\varphi_0^0(q, \theta)$ is larger than that of $\varphi_1^0(q, \theta)$.

Fig. 5.2 displays the deuteron wave function components $\varphi_{\Lambda}^{M_d}(q, \theta)$ for $M_d = 1$ and -1 as functions of q and $\cos \theta$, resulting from calculation based on the Bonn-B potential. Calculations based on the AV18 potential give very much similar results and are therefore not shown here. Similar to those with $M_d = 0$, these wave function components also decay quickly as the relative momentum between the two nucleons inside the deuteron increases from zero to $100 \text{ MeV}/c$. The two figures (a) and (c) depict $\varphi_0^1(q, \theta)$ and $\varphi_0^{-1}(q, \theta)$, respectively. Both vanish at $\theta = 0$ and 180° but differ in sign for the other

θ -values. For instance, while at $\theta = 90^\circ$ $\varphi_0^1(q, \theta)$ reaches its minimum, $\varphi_0^{-1}(q, \theta)$ reaches its maximum. The figures (b) and (d) display $\varphi_1^1(q, \theta)$ and $\varphi_1^{-1}(q, \theta)$, respectively, which show also opposite behavior. $\varphi_1^1(q, \theta)$ peaks at $\theta = 0$ and vanishes at $\theta = 180^\circ$, whereas $\varphi_1^{-1}(q, \theta)$ peaks at $\theta = 180^\circ$ and vanishes at $\theta = 0$. This angular behavior of the two wave function components suggests a relation between the two functions, which will become clear later in Section 5.2.2. It is shown that for $M_d = 1$ and -1 the maximum of $\varphi_1^{M_d}(q, \theta)$ is larger than that of $\varphi_0^{M_d}(q, \theta)$.

Having obtained the deuteron wave function components, it is straightforward to calculate the deuteron densities $\rho^{M_d}(\mathbf{q})$ given in Eq. (5.18). These densities based on the NN potential Bonn-B are displayed in Fig. 5.3. The figures (a) and (b) are for $M_d = 0$, while those figures (c) and (d) are for $M_d = 1$. For $M_d = -1$ the density is the same as that for $M_d = 1$. Calculations based AV18 potential give similar results and are therefore not shown. The figures (a) and (c) displays the two deuteron densities as functions of q and $\cos \theta$, and the figures (b) and (d) depicts them as functions of the Cartesian components of \mathbf{q} , i.e. q_x and q_z . A cut through the q_x - q_z -plane is shown, where each curve represents an equidensity curve. Since the wave functions are invariant under rotations around the q_z -axis, this curve rotated around the q_z -axis will form a three-dimensional equidensity surface of the deuteron. For small q the two densities show uniform distributions along θ , and therefore the equidensity surfaces are spherical. The largest densities at $q = 0$ for all M_d 's means that the most probable configuration for the deuteron is that the two nucleons being at rest with respect to each other.

The connection to the standard partial wave expansion by means of Eq. (5.27) returns the well known s and d wave components of the deuteron wave function. Thus, the deuteron properties are well revealed by this numerical connection.

5.2 Formulation II

5.2.1 Deuteron Wave Function in Operator Form

The deuteron has a neutron and a proton as its constituents. These two nucleons may have their spins pointing in some possible directions even if the deuteron is overall polarized. Therefore, it is interesting to investigate the various possible deuteron internal spin configurations. In order to realize this it would be appropriate if the deuteron wave function is structured such that the deuteron spin state is separated from the other parts. In this way, operators for some spin configurations can be applied to the wave function and their probability densities can be calculated easily. We derive in this section

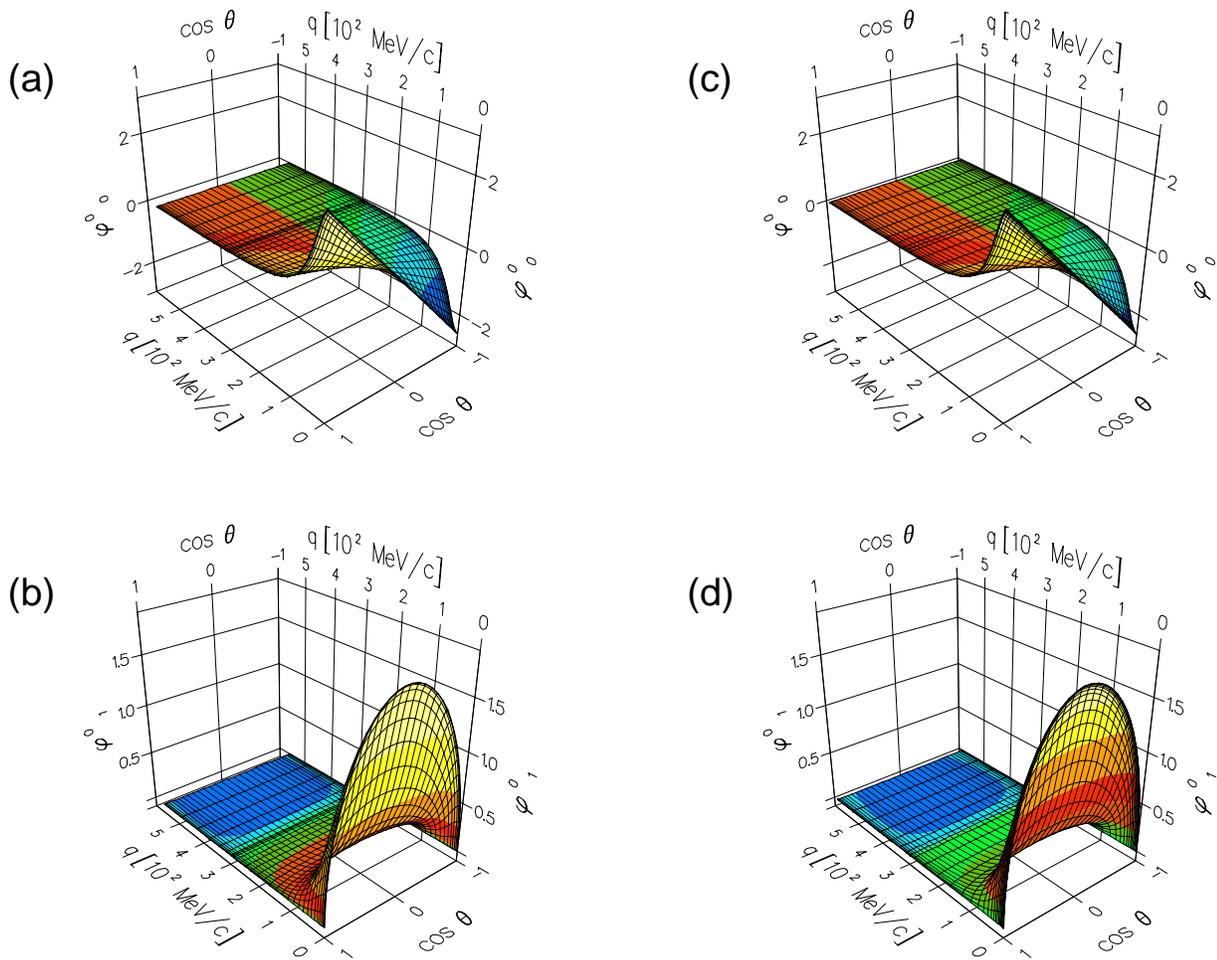


Figure 5.1: The deuteron wave function components for $M_d = 0$ in units $10^{-3} \text{ MeV}^{-1.5}$ as functions of q and $\cos \theta$. The figures (a) and (b) are obtained based on the NN potential Bonn-B and the figures (c) and (d) are obtained based on AV18. Figures (a) and (c) depict $\varphi_0^0(q, \theta)$ whereas figures (b) and (d) display $\varphi_1^0(q, \theta)$.

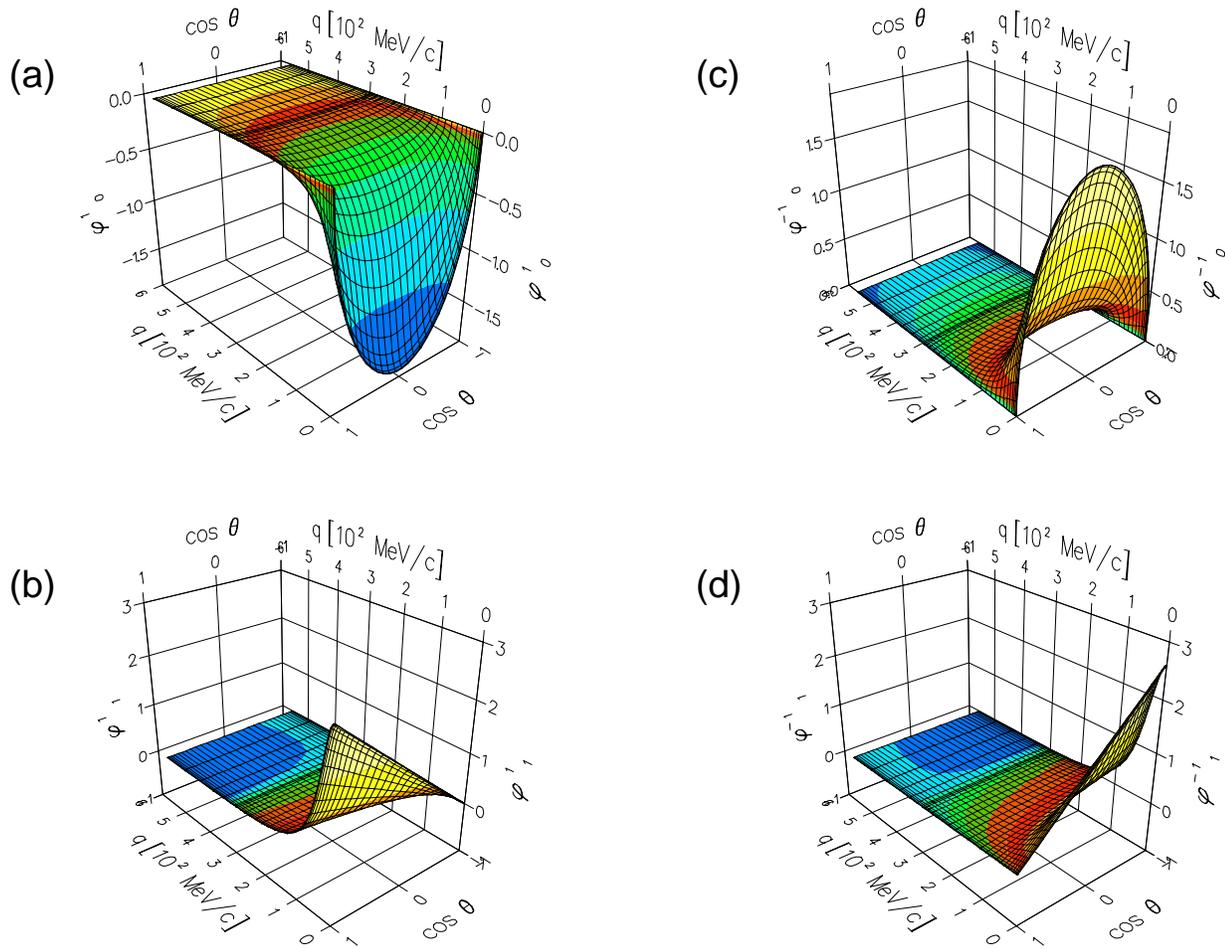


Figure 5.2: The deuteron wave function components based on Bonn-B as functions of q and $\cos \theta$ in units $10^{-3} \text{ MeV}^{-1.5}$: (a) $\varphi_0^1(q, \theta)$, (b) $\varphi_1^1(q, \theta)$, (c) $\varphi_0^{-1}(q, \theta)$ (c) and (d) $\varphi_1^{-1}(q, \theta)$.

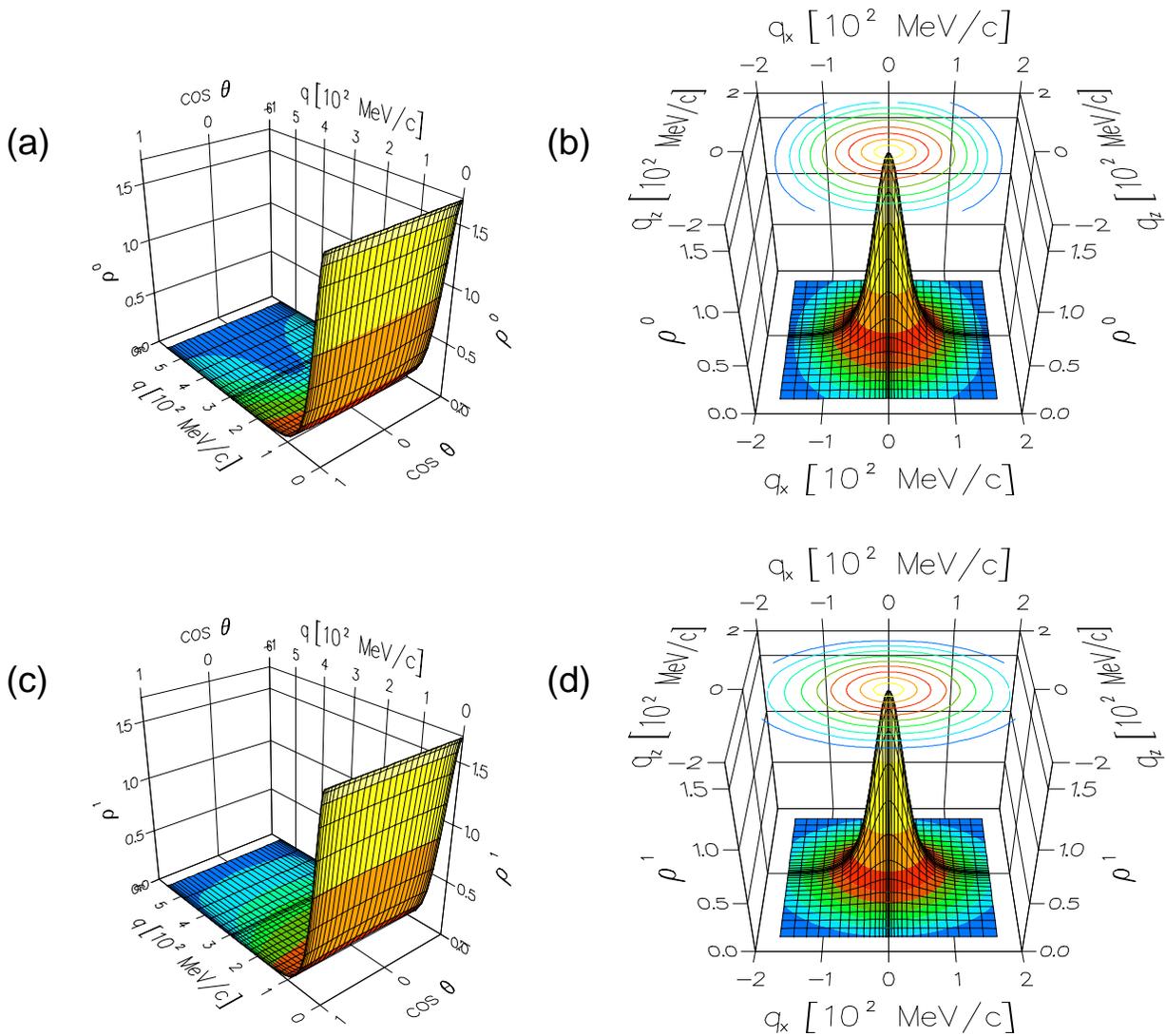


Figure 5.3: The deuteron density based on Bonn-B for $M_d = 0$ ((a) and (b)) and $M_d = 1$ ((c) and (d)) in units 10^{-6} MeV^{-3} , shown as functions of q and $\cos \theta$ on the left side, and of q_x and q_z on the right side. The contours in figures (b) and (d) represent equidensity curves on the q_x - q_z -plane.

the deuteron wave function in momentum space with that structure, evaluate its properties especially its angular behavior and use it to get another set of deuteron eigenvalue equation. The application of this wave function to the evaluations of probability densities for the deuteron internal spin configurations is presented in Section 5.3.

We begin with the partial wave expansion of the deuteron state $|\Psi_d^{M_d}\rangle$:

$$|\Psi_d^{M_d}\rangle = \sum_{l=0,2} \int_0^\infty dq q^2 |q(l1)1M_d; 0\rangle \psi_l(q), \quad (5.28)$$

where $\psi_l(q)$ is defined in Eq. (5.23). The momentum space representation of this expansion results as

$$\begin{aligned} \Psi_d^{M_d}(\mathbf{q}) &\equiv \langle \mathbf{q} | \Psi_d^{M_d} \rangle \\ &= \langle \mathbf{q} | \sum_{l=0,2} \int_0^\infty dq' q'^2 |q'(l1)1M_d; 0\rangle \psi_l(q') \\ &= \langle \mathbf{q} | \sum_{l=0,2} \int_0^\infty dq' q'^2 \sum_{m_s} C(l11; M_d - m_s, m_s M_d) |q'lM_d - m_s\rangle |1m_s\rangle |0\rangle \psi_l(q') \\ &= \sum_{l=0,2} \int_0^\infty dq' q'^2 \frac{\delta(q - q')}{q'q} \\ &\quad \times \sum_{m_s} C(l11; M_d - m_s, m_s M_d) Y_{lM_d - m_s}(\hat{\mathbf{q}}) |1m_s\rangle |0\rangle \psi_l(q') \\ &= |1M_d\rangle \frac{1}{\sqrt{4\pi}} \psi_0(q) |0\rangle \\ &\quad + \{|11\rangle C(211; M_d - 1, 1M_d) Y_{2, M_d - 1}(\hat{\mathbf{q}}) \\ &\quad + |10\rangle C(211; M_d 0 M_d) Y_{2, M_d}(\hat{\mathbf{q}}) \\ &\quad + |1 - 1\rangle C(211; M_d + 1, -1, M_d) Y_{2, M_d + 1}(\hat{\mathbf{q}})\} \psi_2(q) |0\rangle, \end{aligned} \quad (5.29)$$

where we have used the complex conjugate of the projection given in Eq. (3.87). Here $|0\rangle$ denotes the isospin state $|t\rangle$ with $t = 0$.

We would like to simplify this expression so that it has the form

$$\Psi_d^{M_d}(\mathbf{q}) = \{c_0 \psi_0(q) + c_2 \psi_2(q)\} |1M_d\rangle |0\rangle, \quad (5.30)$$

where the deuteron spin state is separated $|1M_d\rangle$, and c_0 and c_2 are operators acting on it. In fact, the operator c_0 is a constant, i.e. $c_0 = \frac{1}{\sqrt{4\pi}}$ (see Eq. (5.29)). The operator c_2 must be scalar under rotation, since the spin state $|1M_d\rangle$ has already the correct transformation property under this rotation. At the same time, according to Eq. (5.29) this operator c_2 must connect the states $|1 - 1\rangle$, $|10\rangle$ and $|11\rangle$ to the state $|1M_d\rangle$. Thus, the operator c_2 has to be formed as combination of the spherical components of the spin operators σ_1 and σ_2 .

To proceed, we choose as example $M_d = 1$. Inserting $M_d = 1$ into Eq. (5.29) gives

$$\begin{aligned} \Psi_d^1(\mathbf{q}) &= |11\rangle \frac{1}{\sqrt{4\pi}} \psi_0(q) |0\rangle \\ &+ \left\{ |11\rangle \sqrt{\frac{1}{10}} Y_{20}(\hat{\mathbf{q}}) - |10\rangle \sqrt{\frac{3}{10}} Y_{21}(\hat{\mathbf{q}}) + |1-1\rangle \sqrt{\frac{3}{5}} Y_{22}(\hat{\mathbf{q}}) \right\} \psi_2(q) |0\rangle. \end{aligned} \quad (5.31)$$

The explicit expressions of the spherical harmonic functions are (see [32] for similar expression in coordinate representation)

$$\begin{aligned} Y_{20}(\hat{\mathbf{q}}) &= \frac{1}{4} \sqrt{\frac{5}{\pi}} (2 \cos^2 \theta - \sin^2 \theta) \\ &= \frac{1}{4q^2} \sqrt{\frac{5}{\pi}} (2q_z^2 - q_x^2 - q_y^2) \\ &= \frac{1}{2q^2} \sqrt{\frac{5}{\pi}} (q_0^2 + q_1 q_{-1}) \end{aligned} \quad (5.32)$$

$$\begin{aligned} Y_{2\pm 1}(\hat{\mathbf{q}}) &= \mp \frac{1}{2} \sqrt{\frac{15}{2\pi}} \cos \theta \sin \theta e^{\pm i\phi} \\ &= \mp \frac{1}{2q^2} \sqrt{\frac{15}{2\pi}} q_z (q_x \pm q_y) \\ &= \frac{1}{2q^2} \sqrt{\frac{15}{\pi}} q_0 q_{\pm 1} \end{aligned} \quad (5.33)$$

$$\begin{aligned} Y_{2\pm 2}(\hat{\mathbf{q}}) &= \frac{1}{4} \sqrt{\frac{15}{2\pi}} \sin^2 \theta e^{\pm 2i\phi} \\ &= \frac{1}{4q^2} \sqrt{\frac{15}{2\pi}} (q_x \pm iq_y)^2 \\ &= \frac{1}{2q^2} \sqrt{\frac{15}{2\pi}} q_{\pm 1}^2, \end{aligned} \quad (5.34)$$

where q_1 , q_0 and q_{-1} are the spherical components of the momentum [31]:

$$q_{\pm 1} = \mp \frac{1}{\sqrt{2}} (q_x \pm iq_z) \quad q_0 = q_z \quad q_0^2 - 2q_1 q_{-1} = q^2 \quad (5.35)$$

Thus, we obtain

$$\begin{aligned} \Psi_d^1(\mathbf{q}) &= |11\rangle \frac{1}{\sqrt{4\pi}} \psi_0(q) |0\rangle \\ &+ \left\{ |11\rangle (q_0^2 + q_1 q_{-1}) - |10\rangle 3q_0 q_1 + |1-1\rangle 3q_1^2 \right\} \frac{1}{2q^2} \sqrt{\frac{1}{2\pi}} \psi_2(q) |0\rangle. \end{aligned} \quad (5.36)$$

To determine c_2 we consider first the combination

$$\boldsymbol{\sigma}_1 \cdot \mathbf{q} \boldsymbol{\sigma}_2 \cdot \mathbf{q} = \left(\sigma_0^{(1)} q_0 - \sigma_1^{(1)} q_{-1} - \sigma_{-1}^{(1)} q_1 \right) \left(\sigma_0^{(2)} q_0 - \sigma_1^{(2)} q_{-1} - \sigma_{-1}^{(2)} q_1 \right), \quad (5.37)$$

and obtain for the sample case $M_d = 1$

$$\begin{aligned}
\boldsymbol{\sigma}_1 \cdot \mathbf{q} \boldsymbol{\sigma}_2 \cdot \mathbf{q} |11\rangle &= \boldsymbol{\sigma}_1 \cdot \mathbf{q} \left| \frac{1}{2} \frac{1}{2} \right\rangle_1 \boldsymbol{\sigma}_2 \cdot \mathbf{q} \left| \frac{1}{2} \frac{1}{2} \right\rangle_2 \\
&= (\sigma_0^{(1)} q_0 - \sigma_1^{(1)} q_{-1} - \sigma_{-1}^{(1)} q_1) \left| \frac{1}{2} \frac{1}{2} \right\rangle_1 (\sigma_0^{(2)} q_0 - \sigma_1^{(2)} q_{-1} - \sigma_{-1}^{(2)} q_1) \left| \frac{1}{2} \frac{1}{2} \right\rangle_2 \\
&= \left(q_0 \left| \frac{1}{2} \frac{1}{2} \right\rangle_1 - \sqrt{2} q_1 \left| \frac{1}{2} - \frac{1}{2} \right\rangle_1 \right) \left(q_0 \left| \frac{1}{2} \frac{1}{2} \right\rangle_2 - \sqrt{2} q_1 \left| \frac{1}{2} - \frac{1}{2} \right\rangle_2 \right) \\
&= q_0^2 \left| \frac{1}{2} \frac{1}{2} \right\rangle_1 \left| \frac{1}{2} \frac{1}{2} \right\rangle_2 - \sqrt{2} q_0 q_1 \left(\left| \frac{1}{2} \frac{1}{2} \right\rangle_1 \left| \frac{1}{2} - \frac{1}{2} \right\rangle_2 + \left| \frac{1}{2} - \frac{1}{2} \right\rangle_1 \left| \frac{1}{2} \frac{1}{2} \right\rangle_2 \right) \\
&\quad + 2q_1^2 \left| \frac{1}{2} - \frac{1}{2} \right\rangle_1 \left| \frac{1}{2} - \frac{1}{2} \right\rangle_2 \\
&= q_0^2 |11\rangle - 2q_0 q_1 |10\rangle + 2q_1^2 |1-1\rangle, \tag{5.38}
\end{aligned}$$

where $\left| \frac{1}{2} \pm \frac{1}{2} \right\rangle_i$ ($i = 1, 2$) are the spin states of the individual nucleons. This equation (5.38) contains actually the $l = 0$ admixture of the deuteron wave function as can be seen by projecting on $Y_{00}(\hat{\mathbf{q}})$. It can be removed by subtracting $\frac{1}{3}q^2 |11\rangle$ from it. This yields

$$\left(\boldsymbol{\sigma}_1 \cdot \mathbf{q} \boldsymbol{\sigma}_2 \cdot \mathbf{q} - \frac{1}{3}q^2 \right) |11\rangle = \frac{2}{3} (q_0^2 + q_1 q_{-1}) |11\rangle - 2q_0 q_1 |10\rangle + 2q_1^2 |1-1\rangle. \tag{5.39}$$

Compared to the corresponding terms in Eq. (5.36) it follows that this tensor operator $\boldsymbol{\sigma}_1 \cdot \mathbf{q} \boldsymbol{\sigma}_2 \cdot \mathbf{q} - \frac{1}{3}q^2$ is already the correct form for c_2 up to some factor. Hence, $\Psi_d^1(\mathbf{q})$ results as

$$\begin{aligned}
\Psi_d^1(\mathbf{q}) &= \left\{ \frac{1}{\sqrt{4\pi}} \psi_0(q) + \left[\boldsymbol{\sigma}_1 \cdot \mathbf{q} \boldsymbol{\sigma}_2 \cdot \mathbf{q} - \frac{1}{3}q^2 \right] \frac{3}{4q^2} \sqrt{\frac{1}{2\pi}} \psi_2(q) \right\} |11\rangle |0\rangle \\
&= \left\{ \bar{\psi}_0(q) + \left[\boldsymbol{\sigma}_1 \cdot \mathbf{q} \boldsymbol{\sigma}_2 \cdot \mathbf{q} - \frac{1}{3}q^2 \right] \bar{\psi}_2(q) \right\} |11\rangle |0\rangle, \tag{5.40}
\end{aligned}$$

where

$$\bar{\psi}_0(q) \equiv \frac{1}{\sqrt{4\pi}} \psi_0(q) \tag{5.41}$$

$$\bar{\psi}_2(q) \equiv \frac{3}{4q^2} \frac{1}{\sqrt{2\pi}} \psi_2(q) \tag{5.42}$$

The expression in Eq. (5.40) was derived for $M_d = 1$. Similar derivations for $M_d = 0$ and $M_d = -1$ show that this form with the corresponding spin state applies also to $M_d = 0, -1$:

$$\begin{aligned}
\Psi_d^0(\mathbf{q}) &= |10\rangle \frac{1}{\sqrt{4\pi}} \psi_0(q) |0\rangle \\
&\quad + \left\{ |11\rangle 3q_0 q_{-1} - |10\rangle 2(q_0^2 + q_1 q_{-1}) + |1-1\rangle 3q_0 q_1 \right\} \frac{1}{2q^2} \sqrt{\frac{1}{2\pi}} \psi_2(q) |0\rangle \\
&= \left\{ \bar{\psi}_0(q) + \left[\boldsymbol{\sigma}_1 \cdot \mathbf{q} \boldsymbol{\sigma}_2 \cdot \mathbf{q} - \frac{1}{3}q^2 \right] \bar{\psi}_2(q) \right\} |10\rangle |0\rangle \tag{5.43}
\end{aligned}$$

$$\begin{aligned}
\Psi_d^{-1}(\mathbf{q}) &= |1-1\rangle \frac{1}{\sqrt{4\pi}} \psi_0(q) |0\rangle \\
&\quad + \left\{ |11\rangle 3q_{-1}^2 - |10\rangle 3q_0 q_{-1} + |1-1\rangle (q_0^2 + q_1 q_{-1}) \right\} \frac{1}{2q^2} \sqrt{\frac{1}{2\pi}} \psi_2(q) |0\rangle \\
&= \left\{ \bar{\psi}_0(q) + \left[\boldsymbol{\sigma}_1 \cdot \mathbf{q} \boldsymbol{\sigma}_2 \cdot \mathbf{q} - \frac{1}{3} q^2 \right] \bar{\psi}_2(q) \right\} |1-1\rangle |0\rangle.
\end{aligned} \tag{5.44}$$

Thus, we obtain the deuteron wave function in operator form in momentum space as

$$\Psi_d^{M_d}(\mathbf{q}) = \left\{ \bar{\psi}_0(q) + \left[\boldsymbol{\sigma}_1 \cdot \mathbf{q} \boldsymbol{\sigma}_2 \cdot \mathbf{q} - \frac{1}{3} q^2 \right] \bar{\psi}_2(q) \right\} |1M_d\rangle |0\rangle. \tag{5.45}$$

In the above expression the positive parity of the deuteron becomes obvious, since $\Psi_d^{M_d}(\mathbf{q}) = \Psi_d^{M_d}(-\mathbf{q})$. A corresponding expression in coordinate space can be found in Ref. [47], which in fact goes back to the work of Rarita and Schwinger in 1941 [46].

We evaluate now the normalization of this deuteron wave function in operator form given in Eq. (5.45). Using

$$\langle 1M_d | \boldsymbol{\sigma}_1 \cdot \mathbf{q} \boldsymbol{\sigma}_2 \cdot \mathbf{q} | 1M_d \rangle = \begin{cases} q_0^2 & , M_d = \pm 1 \\ q^2 - 2q_0^2 & , M_d = 0 \end{cases} \tag{5.46}$$

and

$$\int d\hat{\mathbf{q}} \langle 1M_d | \boldsymbol{\sigma}_1 \cdot \mathbf{q} \boldsymbol{\sigma}_2 \cdot \mathbf{q} | 1M_d \rangle = \frac{4\pi}{3} q^2, \tag{5.47}$$

we obtain

$$\begin{aligned}
\langle \Psi_d^{M_d} | \Psi_d^{M_d} \rangle &= \int d\mathbf{q} |\Psi_d^{M_d}(\mathbf{q})|^2 \\
&= \int d\mathbf{q} \langle 0 | \langle 1M_d | \left\{ \bar{\psi}_0(q) + \left[\boldsymbol{\sigma}_1 \cdot \mathbf{q} \boldsymbol{\sigma}_2 \cdot \mathbf{q} - \frac{1}{3} q^2 \right] \bar{\psi}_2(q) \right\} \\
&\quad \times \left\{ \bar{\psi}_0(q) + \left[\boldsymbol{\sigma}_1 \cdot \mathbf{q} \boldsymbol{\sigma}_2 \cdot \mathbf{q} - \frac{1}{3} q^2 \right] \bar{\psi}_2(q) \right\} | 1M_d \rangle | 0 \rangle \\
&= \int d\mathbf{q} \left\{ \bar{\psi}_0^2(q) + \bar{\psi}_2^2(q) \langle 1M_d | \left[\boldsymbol{\sigma}_1 \cdot \mathbf{q} \boldsymbol{\sigma}_2 \cdot \mathbf{q} - \frac{1}{3} q^2 \right]^2 | 1M_d \rangle \right. \\
&\quad \left. + 2 \bar{\psi}_0(q) \bar{\psi}_2(q) \langle 1M_d | \left[\boldsymbol{\sigma}_1 \cdot \mathbf{q} \boldsymbol{\sigma}_2 \cdot \mathbf{q} - \frac{1}{3} q^2 \right] | 1M_d \rangle \right\} \\
&= \int d\mathbf{q} \left\{ \bar{\psi}_0^2(q) \right. \\
&\quad \left. + \bar{\psi}_2^2(q) \langle 1M_d | \left[(\boldsymbol{\sigma}_1 \cdot \mathbf{q} \boldsymbol{\sigma}_2 \cdot \mathbf{q})^2 - \frac{2}{3} q^2 \boldsymbol{\sigma}_1 \cdot \mathbf{q} \boldsymbol{\sigma}_2 \cdot \mathbf{q} + \frac{1}{9} q^4 \right] | 1M_d \rangle \right. \\
&\quad \left. + 2 \bar{\psi}_0(q) \bar{\psi}_2(q) \langle 1M_d | \left[\boldsymbol{\sigma}_1 \cdot \mathbf{q} \boldsymbol{\sigma}_2 \cdot \mathbf{q} - \frac{1}{3} q^2 \right] | 1M_d \rangle \right\} \\
&= \int d\mathbf{q} \left\{ \bar{\psi}_0^2(q) + \bar{\psi}_2^2(q) \langle 1M_d | \left[q^4 - \frac{2}{3} q^2 \boldsymbol{\sigma}_1 \cdot \mathbf{q} \boldsymbol{\sigma}_2 \cdot \mathbf{q} + \frac{1}{9} q^4 \right] | 1M_d \rangle \right. \\
&\quad \left. + 2 \bar{\psi}_0(q) \bar{\psi}_2(q) \langle 1M_d | \left[\boldsymbol{\sigma}_1 \cdot \mathbf{q} \boldsymbol{\sigma}_2 \cdot \mathbf{q} - \frac{1}{3} q^2 \right] | 1M_d \rangle \right\}
\end{aligned}$$

$$\begin{aligned}
&= \int d\mathbf{q} \left\{ \bar{\psi}_0^2(q) + \frac{10}{9}q^4\bar{\psi}_2^2(q) - \frac{2}{3}q^2\bar{\psi}_0(q)\bar{\psi}_2(q) \right. \\
&\quad \left. + 2 \left[\bar{\psi}_0(q)\bar{\psi}_2(q) - \frac{1}{3}q^2\bar{\psi}_2^2(q) \right] \langle 1M_d | \boldsymbol{\sigma}_1 \cdot \mathbf{q} \boldsymbol{\sigma}_2 \cdot \mathbf{q} | 1M_d \rangle \right\} \\
&= 4\pi \int_0^\infty dq q^2 \left\{ \bar{\psi}_0^2(q) + \frac{10}{9}q^4\bar{\psi}_2^2(q) - \frac{2}{3}q^2\bar{\psi}_0(q)\bar{\psi}_2(q) \right. \\
&\quad \left. + \left[\bar{\psi}_0(q)\bar{\psi}_2(q) - \frac{1}{3}q^2\bar{\psi}_2^2(q) \right] \frac{2}{3}q^2 \right\} \\
&= 4\pi \int_0^\infty dq q^2 \left\{ \bar{\psi}_0^2(q) + \frac{8}{9}q^4\bar{\psi}_2^2(q) \right\} \\
&= \int_0^\infty dq q^2 \left\{ \psi_0^2(q) + \psi_2^2(q) \right\}. \tag{5.48}
\end{aligned}$$

Thus, we get the standard normalization of the partial wave components of the deuteron wave function.

5.2.2 Analytic Angular Behavior of the Deuteron Wave Function

In this section we would like to reevaluate the deuteron wave function components $\varphi_\Lambda^{M_d}(\mathbf{q})$ defined in Eq. (5.5) by making use of the momentum representation $\Psi_d^{M_d}(\mathbf{q})$ of the deuteron state given in Eq. (5.45). The operator $\boldsymbol{\sigma}_1 \cdot \mathbf{q} \boldsymbol{\sigma}_2 \cdot \mathbf{q}$ in Eq. (5.45) can be expressed in terms of the total helicity operator $\mathbf{S} \cdot \mathbf{q}$, which is more appropriate for the momentum-helicity basis $|\mathbf{q}; \hat{\mathbf{q}}S\Lambda; t\rangle^{\pi_a}$, as

$$\boldsymbol{\sigma}_1 \cdot \mathbf{q} \boldsymbol{\sigma}_2 \cdot \mathbf{q} = 2(\mathbf{S} \cdot \mathbf{q})^2 - q^2. \tag{5.49}$$

Thus, the deuteron wave function components in the momentum-helicity basis are given as

$$\begin{aligned}
\varphi_\Lambda^{M_d}(\mathbf{q}) &\equiv {}^{1a} \langle \mathbf{q}; \hat{\mathbf{q}}1\Lambda; 0 | \Psi_d^{M_d} \rangle \\
&= \langle 0 | \langle \hat{\mathbf{q}}1\Lambda | (\langle \mathbf{q} | + \langle -\mathbf{q} |) \Psi_d^{M_d} \rangle \\
&= 2 \langle 0 | \langle \hat{\mathbf{q}}1\Lambda | \Psi_d^{M_d}(\mathbf{q}) \\
&= 2 \langle 0 | \langle \hat{\mathbf{q}}1\Lambda | \left\{ \bar{\psi}_0(q) + \left[\boldsymbol{\sigma}_1 \cdot \mathbf{q} \boldsymbol{\sigma}_2 \cdot \mathbf{q} - \frac{1}{3}q^2 \right] \bar{\psi}_2(q) \right\} | 1M_d \rangle | 0 \rangle \\
&= 2 \langle \hat{\mathbf{q}}1\Lambda | \left\{ \bar{\psi}_0(q) + \left[2(\mathbf{S} \cdot \mathbf{q})^2 - \frac{4}{3}q^2 \right] \bar{\psi}_2(q) \right\} | 1M_d \rangle \\
&= 2 \left\{ \bar{\psi}_0(q) + \left[2\Lambda^2 - \frac{4}{3} \right] q^2 \bar{\psi}_2(q) \right\} \langle \hat{\mathbf{q}}1\Lambda | 1M_d \rangle \\
&= 2 \left\{ \bar{\psi}_0(q) + \left[2\Lambda^2 - \frac{4}{3} \right] q^2 \bar{\psi}_2(q) \right\} D_{M_d\Lambda}^{1*}(\phi\theta 0) \\
&= 2 \left\{ \bar{\psi}_0(q) + \left[2\Lambda^2 - \frac{4}{3} \right] q^2 \bar{\psi}_2(q) \right\} e^{iM_d\phi} d_{M_d\Lambda}^1(\theta), \tag{5.50}
\end{aligned}$$

with the analytic angular behavior $e^{iM_d\phi}d_{M_d\Lambda}^1(\theta)$, where the d-matrix is explicitly given as [31]

$$d_{M_d\Lambda}^1(\theta) = \begin{pmatrix} \frac{1+\cos\theta}{2} & -\frac{\sin\theta}{\sqrt{2}} & \frac{1-\cos\theta}{2} \\ \frac{\sin\theta}{\sqrt{2}} & \cos\theta & -\frac{\sin\theta}{\sqrt{2}} \\ \frac{1-\cos\theta}{2} & \frac{\sin\theta}{\sqrt{2}} & \frac{1+\cos\theta}{2} \end{pmatrix}. \quad (5.51)$$

We define for the radial parts of the wave function components an angle independent function $\Phi_\Lambda(q)$ as

$$\begin{aligned} \Phi_\Lambda(q) &\equiv \bar{\psi}_0(q) + \left[2\Lambda^2 - \frac{4}{3}\right] q^2 \bar{\psi}_2(q) \\ &= \frac{1}{\sqrt{4\pi}}\psi_0(q) + \left[3\Lambda^2 - 2\right] \frac{1}{\sqrt{8\pi}}\psi_2(q). \end{aligned} \quad (5.52)$$

(From now on we call this function the amplitude $\Phi_\Lambda(q)$.) Hence, the deuteron wave function components in the momentum-helicity basis can be expressed as

$$\begin{aligned} \varphi_\Lambda^{M_d}(\mathbf{q}) &= 2\Phi_\Lambda(q)e^{iM_d\phi}d_{M_d\Lambda}^1(\theta) \\ &= \varphi_\Lambda^{M_d}(q, \theta)e^{iM_d\phi}. \end{aligned} \quad (5.53)$$

The factor of 2 is kept in the expression for later convenience, and $\varphi_\Lambda^{M_d}(q, \theta)$ are the two-dimensional wave function components defined in Eq. (5.9). The normalization of this amplitude $\Phi_\Lambda(q)$ can be obtained by inserting Eq. (5.53) into Eq. (5.14):

$$\begin{aligned} \langle \Psi_d^{M_d} | \Psi_d^{M_d} \rangle &= 2\pi \int_0^\infty dq q^2 \int_{-1}^1 d\cos\theta \left\{ 2\Phi_1^2(q)d_{M_d1}^1(\theta)d_{M_d1}^1(\theta) + \Phi_0^2(q)d_{M_d0}^1(\theta)d_{M_d0}^1(\theta) \right\} \\ &= \frac{4\pi}{3} \int_0^\infty dq q^2 \left\{ 2\Phi_1^2(q) + \Phi_0^2(q) \right\}, \end{aligned} \quad (5.54)$$

which agrees with Eq. (5.48). In the last step of Eq. (5.54) we have used the orthogonality property of the d-matrices:

$$\int_{-1}^1 d\cos\theta d_{\mu_1 m_1}^{j_1}(\theta)d_{\mu_2 m_2}^{j_2}(\theta) = \frac{2}{2j_1+1}\delta_{j_1 j_2}\delta_{\mu_1 \mu_2}\delta_{m_1 m_2}. \quad (5.55)$$

Let us now return to Section 5.1.4 to evaluate some behavior of the results displayed in that section.

The wave function components $\varphi_\Lambda^{M_d}(q, \theta)$ obtained from numerically solving of Eq. (5.22) display an angular behavior, which should be compared to the analytic one. With the help of Eqs. (5.53) and (5.51) we can express $\varphi_\Lambda^{M_d}(q, \theta)$ showing their analytic angular behavior as

$$M_d = 0 \quad : \quad \varphi_0^0(q, \theta) = 2\Phi_0(q) \cos\theta \quad (5.56)$$

$$\varphi_1^0(q, \theta) = \sqrt{2}\Phi_1(q) \sin \theta \quad (5.57)$$

$$M_d = 1 : \varphi_0^1(q, \theta) = -\sqrt{2}\Phi_0(q) \sin \theta \quad (5.58)$$

$$\varphi_1^1(q, \theta) = \Phi_1(q)(1 + \cos \theta) \quad (5.59)$$

$$M_d = -1 : \varphi_0^{-1}(q, \theta) = \sqrt{2}\Phi_0(q) \sin \theta \quad (5.60)$$

$$\varphi_1^{-1}(q, \theta) = \Phi_1(q)(1 - \cos \theta). \quad (5.61)$$

Clearly, the numerical angular behavior displayed in Figs. 5.1 and 5.2 agrees with the analytic one.

At small q , where the maxima of $|\varphi_{\Lambda}^{M_d}(q, \theta)|$ occur, the amplitude $\Phi_{\Lambda}(q)$ are determined dominantly by the s-wave. Therefore, the d-matrix determines how the maxima change with Λ and M_d . This explains why the maximum of $|\varphi_{M_d}^{M_d}(q, \theta)|$ is larger than that of $|\varphi_{\Lambda \neq M_d}^{M_d}(q, \theta)|$. The expressions in Eqs. (5.56)-(5.61) show that the ratio $|\varphi_{M_d}^{M_d}(q, \theta)_{max} / \varphi_{\Lambda \neq M_d}^{M_d}(q, \theta)_{max}|$ is exactly $\sqrt{2}$.

Using Eqs. (5.56)-(5.61) the analytic angular behavior of the deuteron densities given in Eq. (5.18) can now be derived. We find for $M_d = 0, 1$

$$\begin{aligned} \rho^0(\mathbf{q}) &= \frac{1}{2}\Phi_1^2(q) \sin^2 \theta + \Phi_0^2(q) \cos^2 \theta + \frac{1}{2}\Phi_1^2(q) \sin^2(\pi - \theta) \\ &= \Phi_1^2(q) \sin^2 \theta + \Phi_0^2(q) \cos^2 \theta \end{aligned} \quad (5.62)$$

$$\begin{aligned} \rho^1(\mathbf{q}) &= \frac{1}{4}\Phi_1^2(q)(1 + \cos \theta)^2 + \frac{1}{2}\Phi_0^2(q) \sin^2 \theta + \frac{1}{4}\Phi_1^2(q)(1 + \cos(\pi - \theta))^2 \\ &= \frac{1}{4}\Phi_1^2(q)(1 + \cos \theta)^2 + \frac{1}{2}\Phi_0^2(q) \sin^2 \theta + \frac{1}{4}\Phi_1^2(q)(1 - \cos \theta)^2 \\ &= \frac{1}{2}\Phi_1^2(q)(1 + \cos^2 \theta) + \frac{1}{2}\Phi_0^2(q) \sin^2 \theta \end{aligned} \quad (5.63)$$

$$\begin{aligned} \rho^{-1}(\mathbf{q}) &= \frac{1}{4}\Phi_1^2(q)(1 - \cos \theta)^2 + \frac{1}{2}\Phi_0^2(q) \sin^2 \theta + \frac{1}{4}\Phi_1^2(q)(1 - \cos(\pi - \theta))^2 \\ &= \frac{1}{4}\Phi_1^2(q)(1 - \cos \theta)^2 + \frac{1}{2}\Phi_0^2(q) \sin^2 \theta + \frac{1}{4}\Phi_1^2(q)(1 + \cos \theta)^2 \\ &= \rho^1(\mathbf{q}). \end{aligned} \quad (5.64)$$

For small q , where $\Phi_0(q)$ and $\Phi_1(q)$ are almost identical, $\rho^0(\mathbf{q})$ and $\rho^{\pm 1}(\mathbf{q})$ are very much the same to each other and are perfect spheres. For larger q these spheres are deformed according to the ratio $|\Phi_0(q)/\Phi_1(q)|$.

5.2.3 One-Dimensional Deuteron Eigenvalue Equation

Recalling the derivation of the deuteron eigenvalue equation given in Eq. (5.22), we notice that there we have been able to separate out the azimuthal integration. Since we now know

the angular behavior of the deuteron wave function components, we see that analytically the equation is separable into the angular and the radial parts. Finally we need to solve only the radial part of that deuteron eigenvalue equation.

Inserting Eq. (5.53) into Eq. (5.21) gives

$$\begin{aligned} & \left(\frac{q^2}{m} - E_d \right) \Phi_\Lambda(q) d_{M_d \Lambda}^1(\theta) \\ & + \int d\mathbf{q}' e^{-iM_d(\phi-\phi')} \left\{ \frac{1}{2} V_{\Lambda 1}^{110}(\mathbf{q}, \mathbf{q}') \Phi_1(q') d_{M_d 1}^1(\theta') + \frac{1}{4} V_{\Lambda 0}^{110}(\mathbf{q}, \mathbf{q}') \Phi_0(q') d_{M_d 0}^1(\theta') \right\} = 0. \end{aligned} \quad (5.65)$$

This is an equation, which is valid for any direction of \mathbf{q} . For $\hat{\mathbf{q}} = \hat{\mathbf{z}}$ the azimuthal dependencies of the potential can be factored out similarly as in Eq. (3.53) to give

$$V_{\Lambda \Lambda'}^{\pi S t}(q \hat{\mathbf{z}}, \mathbf{q}') \equiv e^{-i\Lambda \phi'} V_{\Lambda \Lambda'}^{\pi S t}(q, q', \theta'), \quad (5.66)$$

and therefore, the equation is simplified by choosing this direction:

$$\begin{aligned} & \left(\frac{q^2}{m} - E_d \right) \Phi_\Lambda(q) \delta_{M_d \Lambda} \\ & + \int d\mathbf{q}' e^{i(M_d - \Lambda)\phi'} \left\{ \frac{1}{2} V_{\Lambda 1}^{110}(q, q', \theta') \Phi_1(q') d_{M_d 1}^1(\theta') + \frac{1}{4} V_{\Lambda 0}^{110}(q, q', \theta') \Phi_0(q') d_{M_d 0}^1(\theta') \right\} = 0. \end{aligned} \quad (5.67)$$

Equation (5.67) survives for $M_d = \Lambda$, and this leads to

$$\begin{aligned} & \left(\frac{q^2}{m} - E_d \right) \Phi_{M_d}(q) \\ & + \pi \int_0^\infty dq' q'^2 \int_{-1}^1 d \cos \theta' \left\{ V_{M_d 1}^{110}(q, q', \theta') \Phi_1(q') d_{M_d 1}^1(\theta') \right. \\ & \quad \left. + \frac{1}{2} V_{M_d 0}^{110}(q, q', \theta') \Phi_0(q') d_{M_d 0}^1(\theta') \right\} = 0. \end{aligned} \quad (5.68)$$

This condition $M_d = \Lambda$ for the equation to survive does not exclude the existence of its solution for $M_d \neq \Lambda$. In fact, the solution for $M_d \neq \Lambda$ at this specific direction $\hat{\mathbf{q}} = \hat{\mathbf{z}}$ vanishes, as displayed in Section 5.1.4. By choosing $M_d = 1$ and 0 we have a closed system of two coupled equations for the amplitudes Φ_1 and Φ_0 .

The $\cos \theta'$ integration can be worked out separately and independent of the amplitudes $\Phi_\Lambda(q')$. Defining

$$V_{M_d \Lambda'}^{110}(q, q') \equiv \int_{-1}^1 d \cos \theta' V_{M_d \Lambda'}^{110}(q, q', \theta') d_{M_d \Lambda'}^1(\theta'), \quad (5.69)$$

equation (5.68) is reduced to a set of two coupled equations in one variable, namely q :

$$\left(\frac{q^2}{m} - E_d \right) \Phi_{M_d}(q) + \pi \int_0^\infty dq' q'^2 \left\{ V_{M_d 1}^{110}(q, q') \Phi_1(q') + \frac{1}{2} V_{M_d 0}^{110}(q, q') \Phi_0(q') \right\} = 0. \quad (5.70)$$

As in the evaluations of Eq. (5.22) in Section 5.1.4 we employ the power method to solve this set of Eq. (5.70). We also take the same Gaussian-Legendre quadrature points for the q' - and $\cos \theta'$ -integrations. For the NN potential Bonn-B we obtain the deuteron binding energy 2.224 MeV and for the AV18 potential 2.225 MeV. The amplitudes $\Phi_0(q)$ and $\Phi_1(q)$ are displayed in Fig. 5.4 for the Bonn-B and in Fig. 5.5 for the AV18. The figures show that for small q the amplitudes $\Phi_0(q)$ and $\Phi_1(q)$ are of the same magnitude, and both fall from their largest values by about one order of magnitude at $q \approx 200$ MeV/ c . The amplitude $\Phi_1(q)$ has its first node at $q \approx 300$ MeV/ c , whereas $\Phi_0(q)$ has its own first node at $q \approx 900$ MeV/ c for the Bonn-B and at $q \approx 1000$ MeV/ c for the AV18. Within the momentum range shown the magnitude of $\Phi_0(q)$ and $\Phi_1(q)$ for the Bonn-B in general fall off with the same rates, whereas for the AV18 the magnitude of $\Phi_1(q)$ decreases slower than that of $\Phi_0(q)$.

5.2.4 Connection to the Standard Partial Wave Representation

In Section 5.1.3 we have started to connect the deuteron wave function components in the momentum-helicity basis to the partial wave projected components of the deuteron state. We have obtained Eq. (5.27), which left the determination of some deuteron quantum numbers for numerical calculation. With the analytic angular behavior of $\varphi_\Lambda(q, \theta)$ given, we can continue deriving the connection and find the remaining quantum numbers. Inserting Eq. (5.53) into Eq. (5.27) yields

$$\begin{aligned} \psi_l(q) &= 2\sqrt{\pi(2l+1)} \int_{-1}^1 d \cos \theta' \left\{ C(l1j; 011) d_{M_{d1}}^j(\theta') \Phi_1(q) d_{M_{d1}}^1(\theta') \right. \\ &\quad \left. + \frac{1}{2} C(l1j; 000) d_{M_{d0}}^j(\theta') \Phi_0(q) d_{M_{d0}}^1(\theta') \right\} \\ &= \frac{4}{3} \delta_{j1} \sqrt{\pi(2l+1)} \left\{ C(l1j; 011) \Phi_1(q) + \frac{1}{2} C(l1j; 000) \Phi_0(q) \right\}, \end{aligned} \quad (5.71)$$

in which we have used the orthogonality property of the d-matrices given in Eq. (5.55). It turns out that the connection exists only for a total angular momentum $j = 1$, and the Clebsch-Gordon coefficients allow only $l = 0$ and $l = 2$. Thus, we obtain for the s and d waves

$$\psi_0(q) = \frac{2}{3} \sqrt{\pi} \{ 2\Phi_1(q) + \Phi_0(q) \} \quad (5.72)$$

$$\psi_2(q) = \frac{2}{3} \sqrt{2\pi} \{ \Phi_1(q) - \Phi_0(q) \}, \quad (5.73)$$

which is consistent with Eq. (5.52).

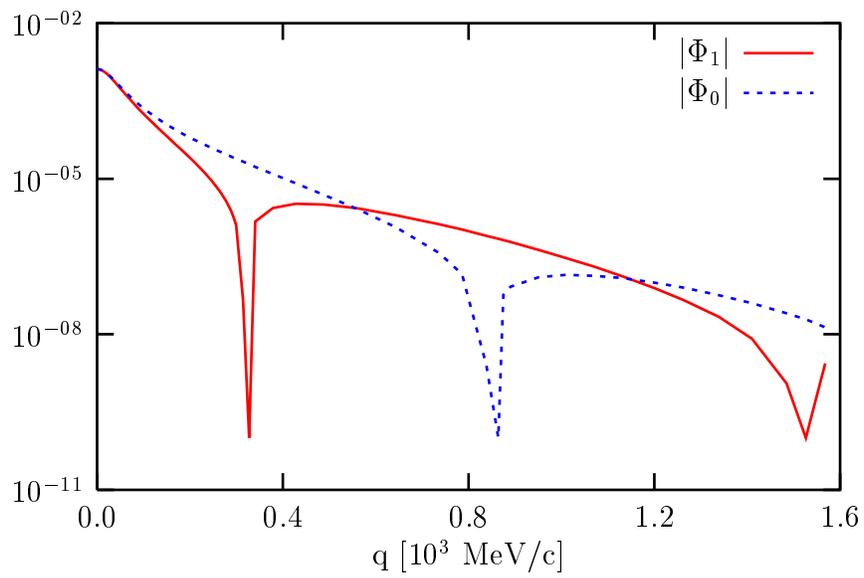


Figure 5.4: The absolute values of the amplitudes $\Phi_0(q)$ and $\Phi_1(q)$ in units $\text{MeV}^{-1.5}$ for Bonn-B.

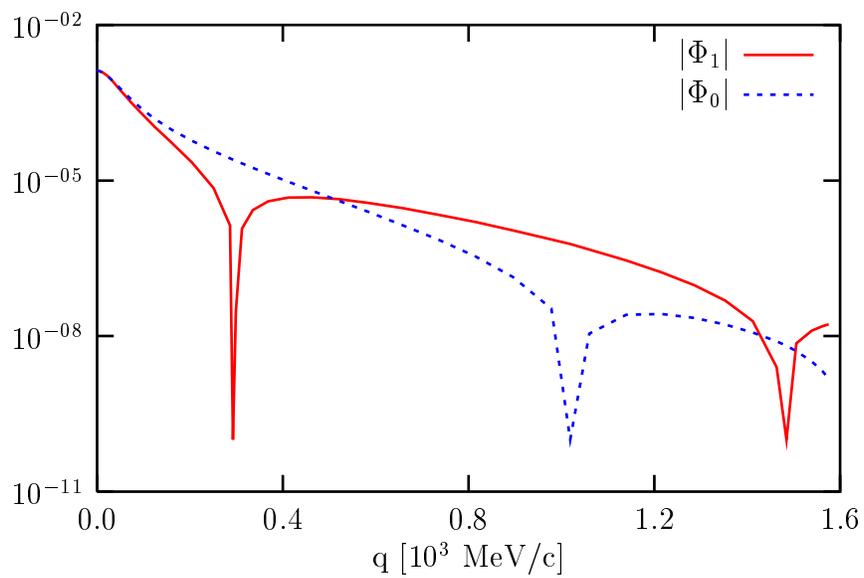


Figure 5.5: Same as Fig. 5.4, but for AV18.

5.3 Probability Densities for Different Spin Configurations

In this section we describe the internal spin configuration of the deuteron with the help of the deuteron wave function in operator form given in Eq. (5.45). As example we choose an overall polarized deuteron with $M_d = 1$. Cases of interest are if (1) both nucleons have their spins up, (2) both nucleons have their spins down, (3) one nucleon has spin up and the other has spin down, (4) one nucleon has spin up and the other has arbitrary spin orientation and (5) one nucleon has spin down and the other has arbitrary spin orientation. The probability densities for these five cases are given below in terms of the deuteron s and d waves.

1. probability density for both nucleons having their spins up:

$$\begin{aligned}
\rho_{\uparrow\uparrow}^1(\mathbf{q}) &= \Psi_d^{1*}(\mathbf{q}) \frac{1}{2} [1 + \sigma_z^{(1)}] \frac{1}{2} [1 + \sigma_z^{(2)}] \Psi_d^1(\mathbf{q}) \\
&= \frac{1}{4} \langle 11 | \left\{ \bar{\psi}_0(q) + \left[\boldsymbol{\sigma}_1 \cdot \mathbf{q} \boldsymbol{\sigma}_2 \cdot \mathbf{q} - \frac{1}{3} q^2 \right] \bar{\psi}_2(q) \right\} \\
&\quad \times [1 + \sigma_z^{(1)}] [1 + \sigma_z^{(2)}] \left\{ \bar{\psi}_0(q) + \left[\boldsymbol{\sigma}_1 \cdot \mathbf{q} \boldsymbol{\sigma}_2 \cdot \mathbf{q} - \frac{1}{3} q^2 \right] \bar{\psi}_2(q) \right\} | 11 \rangle \\
&= \frac{1}{4} \bar{\psi}_0^2(q) \langle 11 | [1 + \sigma_z^{(1)}] [1 + \sigma_z^{(2)}] | 11 \rangle \\
&\quad + \frac{1}{4} \bar{\psi}_0(q) \bar{\psi}_2(q) \langle 11 | [1 + \sigma_z^{(1)}] [1 + \sigma_z^{(2)}] \left[\boldsymbol{\sigma}_1 \cdot \mathbf{q} \boldsymbol{\sigma}_2 \cdot \mathbf{q} - \frac{1}{3} q^2 \right] | 11 \rangle \\
&\quad + \frac{1}{4} \bar{\psi}_2(q) \bar{\psi}_0(q) \langle 11 | \left[\boldsymbol{\sigma}_1 \cdot \mathbf{q} \boldsymbol{\sigma}_2 \cdot \mathbf{q} - \frac{1}{3} q^2 \right] [1 + \sigma_z^{(1)}] [1 + \sigma_z^{(2)}] | 11 \rangle \\
&\quad + \frac{1}{4} \bar{\psi}_2^2(q) \langle 11 | \left[\boldsymbol{\sigma}_1 \cdot \mathbf{q} \boldsymbol{\sigma}_2 \cdot \mathbf{q} - \frac{1}{3} q^2 \right] [1 + \sigma_z^{(1)}] \\
&\quad \times [1 + \sigma_z^{(2)}] \left[\boldsymbol{\sigma}_1 \cdot \mathbf{q} \boldsymbol{\sigma}_2 \cdot \mathbf{q} - \frac{1}{3} q^2 \right] | 11 \rangle \\
&= \bar{\psi}_0^2(q) + 2q^2 \left(\cos^2 \theta - \frac{1}{3} \right) \bar{\psi}_0(q) \bar{\psi}_2(q) + q^4 \left(\cos^2 \theta - \frac{1}{3} \right)^2 \bar{\psi}_2^2(q) \\
&= \frac{1}{4\pi} \left\{ \psi_0^2(q) + \frac{3}{\sqrt{2}} \left(\cos^2 \theta - \frac{1}{3} \right) \psi_0(q) \psi_2(q) + \frac{9}{8} \left(\cos^2 \theta - \frac{1}{3} \right)^2 \psi_2^2(q) \right\} \\
&= \frac{1}{4\pi} \left\{ \psi_0^2(q) + 2\sqrt{\frac{2\pi}{5}} Y_{20}(\hat{\mathbf{q}}) \psi_0(q) \psi_2(q) + \frac{2\pi}{5} Y_{20}^2(\hat{\mathbf{q}}) \psi_2^2(q) \right\}. \tag{5.74}
\end{aligned}$$

2. probability density for both nucleons having their spins down:

$$\begin{aligned}
\rho_{\downarrow\downarrow}^1(\mathbf{q}) &= \Psi_d^{1*}(\mathbf{q}) \frac{1}{2} [1 - \sigma_z^{(1)}] \frac{1}{2} [1 - \sigma_z^{(2)}] \Psi_d^1(\mathbf{q}) \\
&= \frac{1}{4} \langle 11 | \left\{ \bar{\psi}_0(q) + \left[\boldsymbol{\sigma}_1 \cdot \mathbf{q} \boldsymbol{\sigma}_2 \cdot \mathbf{q} - \frac{1}{3} q^2 \right] \bar{\psi}_2(q) \right\} \\
&\quad \times [1 - \sigma_z^{(1)}] [1 - \sigma_z^{(2)}] \left\{ \bar{\psi}_0(q) + \left[\boldsymbol{\sigma}_1 \cdot \mathbf{q} \boldsymbol{\sigma}_2 \cdot \mathbf{q} - \frac{1}{3} q^2 \right] \bar{\psi}_2(q) \right\} | 11 \rangle
\end{aligned}$$

$$\begin{aligned}
&= \frac{1}{4} \bar{\psi}_0^2(q) \langle 11 | [1 - \sigma_z^{(1)}] [1 - \sigma_z^{(2)}] | 11 \rangle \\
&\quad + \frac{1}{4} \bar{\psi}_0(q) \bar{\psi}_2(q) \langle 11 | [1 - \sigma_z^{(1)}] [1 - \sigma_z^{(2)}] \left[\boldsymbol{\sigma}_1 \cdot \mathbf{q} \boldsymbol{\sigma}_2 \cdot \mathbf{q} - \frac{1}{3} q^2 \right] | 11 \rangle \\
&\quad + \frac{1}{4} \bar{\psi}_2(q) \bar{\psi}_0(q) \langle 11 | \left[\boldsymbol{\sigma}_1 \cdot \mathbf{q} \boldsymbol{\sigma}_2 \cdot \mathbf{q} - \frac{1}{3} q^2 \right] [1 - \sigma_z^{(1)}] [1 - \sigma_z^{(2)}] | 11 \rangle \\
&\quad + \frac{1}{4} \bar{\psi}_2^2(q) \langle 11 | \left[\boldsymbol{\sigma}_1 \cdot \mathbf{q} \boldsymbol{\sigma}_2 \cdot \mathbf{q} - \frac{1}{3} q^2 \right] [1 - \sigma_z^{(1)}] \\
&\quad \quad \times [1 - \sigma_z^{(2)}] \left[\boldsymbol{\sigma}_1 \cdot \mathbf{q} \boldsymbol{\sigma}_2 \cdot \mathbf{q} - \frac{1}{3} q^2 \right] | 11 \rangle \\
&= q^4 \sin^4 \theta \bar{\psi}_2^2(q) \\
&= \frac{9}{32\pi} \sin^4 \theta \psi_2^2(q) \\
&= \frac{3}{5} Y_{22}(\hat{\mathbf{q}}) Y_{2-2}(\hat{\mathbf{q}}) \psi_2^2(q). \tag{5.75}
\end{aligned}$$

3. probability density for one nucleon having spin up and the other having spin down:

$$\begin{aligned}
\rho_{\uparrow\downarrow}^1(\mathbf{q}) &= \Psi_d^{1*}(\mathbf{q}) \frac{1}{2} [1 + \sigma_z^{(1)}] \frac{1}{2} [1 - \sigma_z^{(2)}] \Psi_d^1(\mathbf{q}) \\
&= \frac{1}{4} \langle 11 | \left\{ \bar{\psi}_0(q) + \left[\boldsymbol{\sigma}_1 \cdot \mathbf{q} \boldsymbol{\sigma}_2 \cdot \mathbf{q} - \frac{1}{3} q^2 \right] \bar{\psi}_2(q) \right\} \\
&\quad \times [1 + \sigma_z^{(1)}] [1 - \sigma_z^{(2)}] \left\{ \bar{\psi}_0(q) + \left[\boldsymbol{\sigma}_1 \cdot \mathbf{q} \boldsymbol{\sigma}_2 \cdot \mathbf{q} - \frac{1}{3} q^2 \right] \bar{\psi}_2(q) \right\} | 11 \rangle \\
&= \frac{1}{4} \bar{\psi}_0^2(q) \langle 11 | [1 + \sigma_z^{(1)}] [1 - \sigma_z^{(2)}] | 11 \rangle \\
&\quad + \frac{1}{4} \bar{\psi}_0(q) \bar{\psi}_2(q) \langle 11 | [1 + \sigma_z^{(1)}] [1 - \sigma_z^{(2)}] \left[\boldsymbol{\sigma}_1 \cdot \mathbf{q} \boldsymbol{\sigma}_2 \cdot \mathbf{q} - \frac{1}{3} q^2 \right] | 11 \rangle \\
&\quad + \frac{1}{4} \bar{\psi}_2(q) \bar{\psi}_0(q) \langle 11 | \left[\boldsymbol{\sigma}_1 \cdot \mathbf{q} \boldsymbol{\sigma}_2 \cdot \mathbf{q} - \frac{1}{3} q^2 \right] [1 + \sigma_z^{(1)}] [1 - \sigma_z^{(2)}] | 11 \rangle \\
&\quad + \frac{1}{4} \bar{\psi}_2^2(q) \langle 11 | \left[\boldsymbol{\sigma}_1 \cdot \mathbf{q} \boldsymbol{\sigma}_2 \cdot \mathbf{q} - \frac{1}{3} q^2 \right] [1 + \sigma_z^{(1)}] \\
&\quad \quad \times [1 - \sigma_z^{(2)}] \left[\boldsymbol{\sigma}_1 \cdot \mathbf{q} \boldsymbol{\sigma}_2 \cdot \mathbf{q} - \frac{1}{3} q^2 \right] | 11 \rangle \\
&= q^4 \cos^2 \theta \sin^2 \theta \bar{\psi}_2^2(q) \\
&= \frac{9}{32\pi} \cos^2 \theta \sin^2 \theta \psi_2^2(q) \\
&= -\frac{3}{20} Y_{21}(\hat{\mathbf{q}}) Y_{2-1}(\hat{\mathbf{q}}) \psi_2^2(q). \tag{5.76}
\end{aligned}$$

4. probability density for one nucleon having spin up and the other having arbitrary spin orientation:

$$\begin{aligned}
\rho_{\uparrow(1)}^1(\mathbf{q}) &= \Psi_d^{1*}(\mathbf{q}) \frac{1}{2} [1 + \sigma_z^{(1)}] \Psi_d^1(\mathbf{q}) \\
&= \frac{1}{2} \langle 11 | \left\{ \bar{\psi}_0(q) + \left[\boldsymbol{\sigma}_1 \cdot \mathbf{q} \boldsymbol{\sigma}_2 \cdot \mathbf{q} - \frac{1}{3} q^2 \right] \bar{\psi}_2(q) \right\} \\
&\quad \times [1 + \sigma_z^{(1)}] \left\{ \bar{\psi}_0(q) + \left[\boldsymbol{\sigma}_1 \cdot \mathbf{q} \boldsymbol{\sigma}_2 \cdot \mathbf{q} - \frac{1}{3} q^2 \right] \bar{\psi}_2(q) \right\} | 11 \rangle
\end{aligned}$$

$$\begin{aligned}
&= \frac{1}{2} \bar{\psi}_0^2(q) \langle 11 | [1 + \sigma_z^{(1)}] | 11 \rangle \\
&\quad + \frac{1}{2} \bar{\psi}_0(q) \bar{\psi}_2(q) \langle 11 | [1 + \sigma_z^{(1)}] \left[\boldsymbol{\sigma}_1 \cdot \mathbf{q} \boldsymbol{\sigma}_2 \cdot \mathbf{q} - \frac{1}{3} q^2 \right] | 11 \rangle \\
&\quad + \frac{1}{2} \bar{\psi}_2(q) \bar{\psi}_0(q) \langle 11 | \left[\boldsymbol{\sigma}_1 \cdot \mathbf{q} \boldsymbol{\sigma}_2 \cdot \mathbf{q} - \frac{1}{3} q^2 \right] [1 + \sigma_z^{(1)}] | 11 \rangle \\
&\quad + \frac{1}{2} \bar{\psi}_2^2(q) \langle 11 | \left[\boldsymbol{\sigma}_1 \cdot \mathbf{q} \boldsymbol{\sigma}_2 \cdot \mathbf{q} - \frac{1}{3} q^2 \right] [1 + \sigma_z^{(1)}] \left[\boldsymbol{\sigma}_1 \cdot \mathbf{q} \boldsymbol{\sigma}_2 \cdot \mathbf{q} - \frac{1}{3} q^2 \right] | 11 \rangle \\
&= \bar{\psi}_0^2(q) + 2q^2 \left(\cos^2 \theta - \frac{1}{3} \right) \bar{\psi}_0(q) \bar{\psi}_2(q) \\
&\quad + q^4 \left\{ \left(\cos^2 \theta - \frac{1}{3} \right)^2 + \cos^2 \theta \sin^2 \theta \right\} \bar{\psi}_2^2(q) \\
&= \frac{1}{4\pi} \left[\psi_0^2(q) + \frac{3}{\sqrt{2}} \left(\cos^2 \theta - \frac{1}{3} \right) \psi_0(q) \psi_2(q) \right. \\
&\quad \left. + \frac{9}{8} \left\{ \left(\cos^2 \theta - \frac{1}{3} \right)^2 + \cos^2 \theta \sin^2 \theta \right\} \psi_2^2(q) \right] \\
&= \rho_{\uparrow\uparrow}^1(\mathbf{q}) + \rho_{\uparrow\downarrow}^1(\mathbf{q}). \tag{5.77}
\end{aligned}$$

5. probability density for one nucleon having spin down and the other having arbitrary spin orientation:

$$\begin{aligned}
\rho_{\downarrow(1)}^1(\mathbf{q}) &= \Psi_d^{1*}(\mathbf{q}) \frac{1}{2} [1 - \sigma_z^{(1)}] \Psi_d^1(\mathbf{q}) \\
&= \frac{1}{2} \langle 11 | \left\{ \bar{\psi}_0(q) + \left[\boldsymbol{\sigma}_1 \cdot \mathbf{q} \boldsymbol{\sigma}_2 \cdot \mathbf{q} - \frac{1}{3} q^2 \right] \bar{\psi}_2(q) \right\} \\
&\quad \times [1 - \sigma_z^{(1)}] \left\{ \bar{\psi}_0(q) + \left[\boldsymbol{\sigma}_1 \cdot \mathbf{q} \boldsymbol{\sigma}_2 \cdot \mathbf{q} - \frac{1}{3} q^2 \right] \bar{\psi}_2(q) \right\} | 11 \rangle \\
&= \frac{1}{2} \bar{\psi}_0^2(q) \langle 11 | [1 - \sigma_z^{(1)}] | 11 \rangle \\
&\quad + \frac{1}{2} \bar{\psi}_0(q) \bar{\psi}_2(q) \langle 11 | [1 - \sigma_z^{(1)}] \left[\boldsymbol{\sigma}_1 \cdot \mathbf{q} \boldsymbol{\sigma}_2 \cdot \mathbf{q} - \frac{1}{3} q^2 \right] | 11 \rangle \\
&\quad + \frac{1}{2} \bar{\psi}_2(q) \bar{\psi}_0(q) \langle 11 | \left[\boldsymbol{\sigma}_1 \cdot \mathbf{q} \boldsymbol{\sigma}_2 \cdot \mathbf{q} - \frac{1}{3} q^2 \right] [1 - \sigma_z^{(1)}] | 11 \rangle \\
&\quad + \frac{1}{2} \bar{\psi}_2^2(q) \langle 11 | \left[\boldsymbol{\sigma}_1 \cdot \mathbf{q} \boldsymbol{\sigma}_2 \cdot \mathbf{q} - \frac{1}{3} q^2 \right] [1 - \sigma_z^{(1)}] \left[\boldsymbol{\sigma}_1 \cdot \mathbf{q} \boldsymbol{\sigma}_2 \cdot \mathbf{q} - \frac{1}{3} q^2 \right] | 11 \rangle \\
&= q^4 \sin^2 \theta \bar{\psi}_2^2(q) \\
&= \frac{9}{32\pi} \sin^2 \theta \psi_2^2(q) \\
&= \rho_{\uparrow\downarrow}^1(\mathbf{q}) + \rho_{\downarrow\downarrow}^1(\mathbf{q}). \tag{5.78}
\end{aligned}$$

The angular dependencies of all these functions result from terms containing the deuteron d-wave, which is obvious since the s-wave is spherically symmetric. Thus, these probability densities for five different internal spin configurations of the deuteron exhibit

combinations of angular behavior owned by the spherical harmonics functions of orbital angular momentum $l = 0$ and $l = 2$. These probability densities are shown in Figs. 5.6-5.11. In Figs. 5.6, 5.8 and 5.10 the left side displays the probability densities as functions of q and $\cos \theta$, whereas the right side displays them as functions of q_x and q_z . The contours in the the figures on the right side represent equidensity curves in the q_x - q_z -plane, which rotated around the q_z -axis form three-dimensional images of the equidensity surfaces. All the figures shown results from the calculations based on the Bonn-B potential. Since the AV18 potential produces results of similar shapes they are not displayed.

Fig. 5.6 shows the probability densities for the first two cases. The figures (a) and (b) display $\rho_{\uparrow\uparrow}^1(\mathbf{q})$, while those figures (c) and (d) display $\rho_{\downarrow\downarrow}^1(\mathbf{q})$. The probability density $\rho_{\uparrow\uparrow}^1(\mathbf{q})$ has its maximum at $\mathbf{q} = 0$, telling that the configuration where both nucleon have their spin up occurs most probably when the nucleons are at rest with respect to each other. In the momentum range shown $\rho_{\uparrow\uparrow}^1(\mathbf{q})$ has a spherical shape, since according to Eq. (5.74) it is dominated by the s-wave. The probability density $\rho_{\downarrow\downarrow}^1(\mathbf{q})$ has a different shape. It vanishes at $\mathbf{q}=0$ and reaches two maxima at $|q_{max}| \approx 100$ MeV/c along the q_x -axis ($\theta = \frac{\pi}{2}$). This tells that for the case where the two nucleons have their spin down they have most probable momenta back to back and right to the polarization axis of the deuteron. If the equidensity curves in Fig. 5.6(d) are rotated around the q_z -axis they will exhibit a toroidal shape of the equidensity surfaces of this probability density, as shown illustratively in Fig. 5.7, where two equidensity surfaces are displayed.

In Fig. 5.8 we show the probability density given in Eq. (5.76) for the case where the two nucleons have opposite spin directions to each other. This probability density is given solely by the d-wave and a function of the angle θ . Thus, $\rho_{\downarrow\uparrow}^1(\mathbf{q})$ has four peaks of equal height in each quadrant of the $q_x - q_z$ -plane at $|q_x| = |q_z| = q_{max} \cos(\frac{\pi}{4})$. Hence, for this spin configuration it is most probable that the two nucleons have momenta back to back and pointing at $\theta = 45^\circ$. The rotated contours in the q_x - q_z -plane around the q_z -axis lead to double toroidal structures. This is shown illustratively in Fig. 5.9, where two equidensity surfaces are picked and displayed. The inner tubes represent surfaces of higher density compared to the outer ones.

Fig. 5.10 shows the probability densities for the last two configurations given in Eqs. (5.77) and (5.78). The figures (a) and (b) display $\rho_{\uparrow(1)}^1(\mathbf{q})$, whereas the figures (c) and (d) depict $\rho_{\downarrow(1)}^1(\mathbf{q})$. For the momentum range shown $\rho_{\uparrow(1)}^1(\mathbf{q})$ behaves very similarly as $\rho_{\uparrow\uparrow}^1(\mathbf{q})$ displayed in the figures (a) and (b) of Fig. 5.6. This can be understood as that $\rho_{\uparrow\uparrow}^1(\mathbf{q})$ is larger than $\rho_{\uparrow\downarrow}^1(\mathbf{q})$ and thus dominates. The probability density $\rho_{\downarrow(1)}^1(\mathbf{q})$ has the same maxima as that of $\rho_{\downarrow\downarrow}^1(\mathbf{q})$ shown in the figures (c) and (d) of Fig. 5.6(d), but a slightly different angular behavior. For a fixed q the changes of $\rho_{\downarrow(1)}^1(\mathbf{q})$ with θ are

slower than that of $\rho_{\downarrow\downarrow}^{\downarrow}(\mathbf{q})$. The 3D-image of $\rho_{\downarrow(1)}^{\downarrow}(\mathbf{q})$ is presented in Fig. 5.11, which looks similar to the one shown in Fig. 5.7.

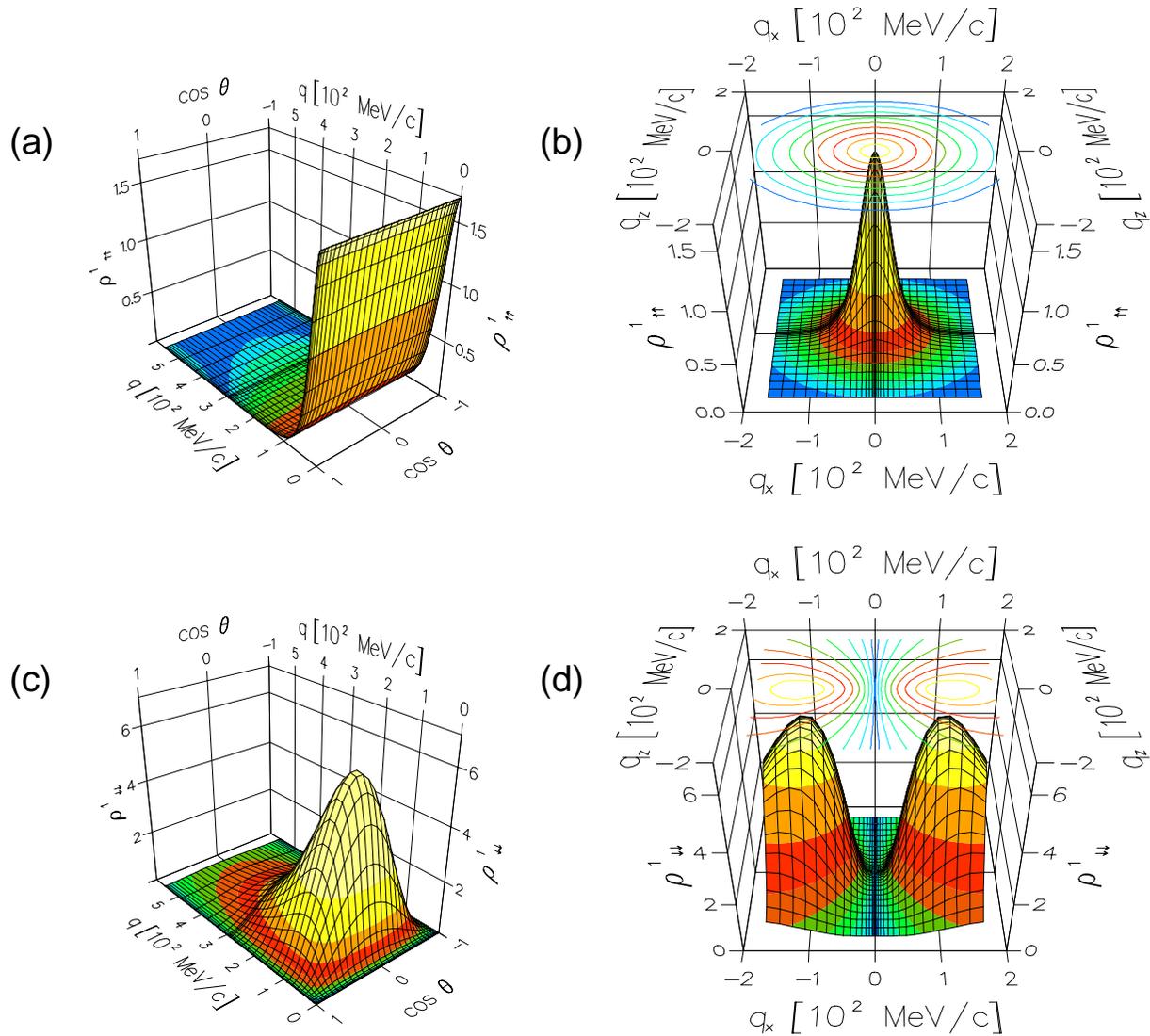


Figure 5.6: The probability densities $\rho_{\uparrow\uparrow}^1(\mathbf{q})$ in units 10^{-6} MeV^{-3} ((a) and (b)) and $\rho_{\downarrow\downarrow}^1(\mathbf{q})$ in units $10^{-10} \text{ MeV}^{-3}$ ((c) and (d)). The contours represent equidensity curves in the q_x - q_z -plane.



Figure 5.7: Two selected equidensity surfaces of $\rho_{\downarrow\downarrow}^1(\mathbf{q})$. The image is created by rotating two of the equidensity curves of Fig. 5.6(d) around the q_z -axis. Note that the q_z -axis is stretched out with respect to the other two axes.

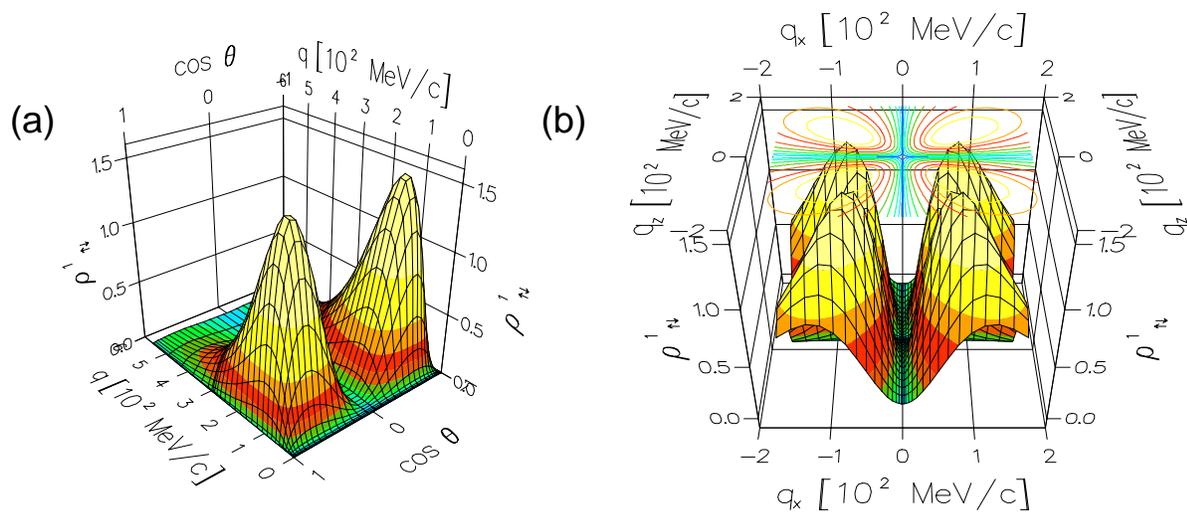


Figure 5.8: The probability density $\rho_{\uparrow\downarrow}^1(\mathbf{q})$ in units $10^{-10} \text{ MeV}^{-3}$. The contours represent equidensity curves in the q_x - q_z -plane.

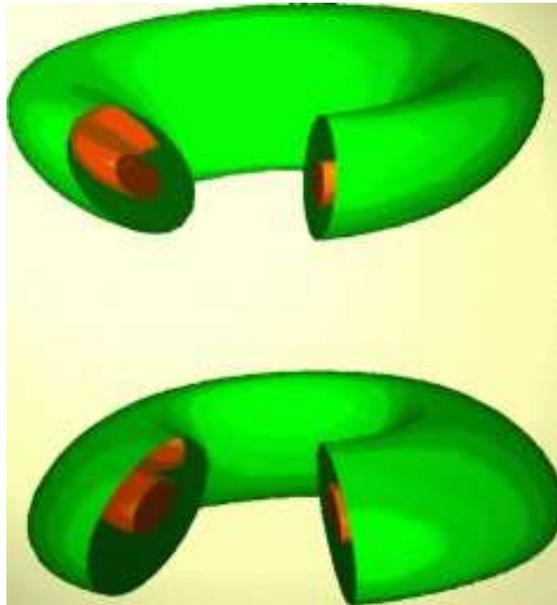


Figure 5.9: Two selected equidensity surfaces of $\rho_{\uparrow\downarrow}^1(\mathbf{q})$. The image is created by rotating two of the equidensity curves of Fig. 5.8(b) around the q_z -axis. Note that the q_z -axis is stretched out with respect to the other two axes.

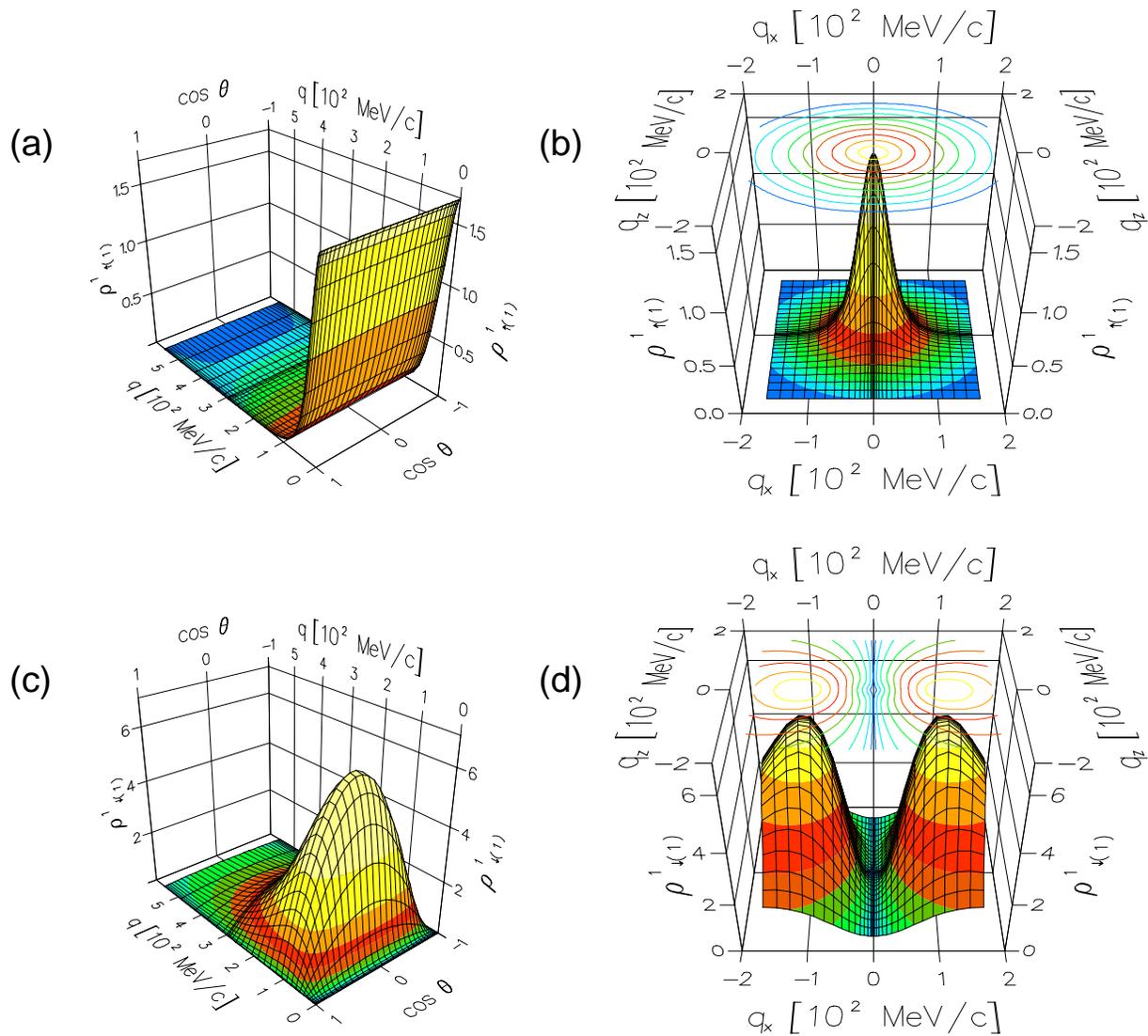


Figure 5.10: The probability densities $\rho_{\uparrow(1)}^1(\mathbf{q})$ in units 10^{-6} MeV^{-3} ((a) and (b)) and $\rho_{\downarrow(1)}^1(\mathbf{q})$ in units $10^{-10} \text{ MeV}^{-3}$ ((c) and (d)). The contours represent equidensity curves in the q_x - q_z -plane.

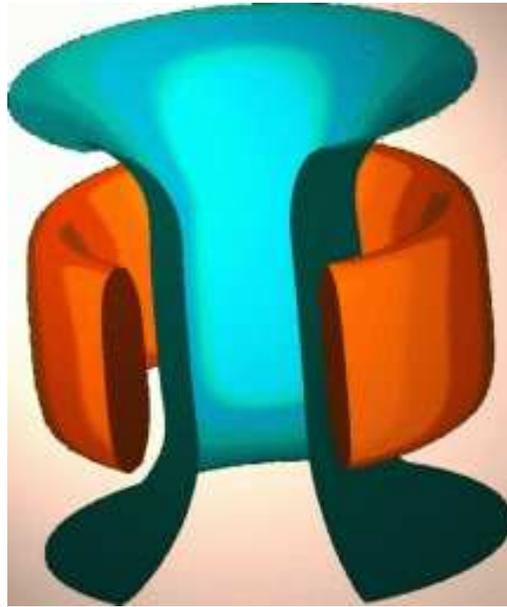


Figure 5.11: Two selected equidensity surfaces of $\rho_{\downarrow(1)}^1(\mathbf{q})$. The image is created by rotating two of the equidensity curves of Fig. 5.10(d) around the q_z -axis. Note that the q_z -axis is stretched out with respect to the other two axes.

Chapter 6

THREE-DIMENSIONAL FORMULATION FOR THE NUCLEON-DEUTERON BREAK-UP PROCESS

In the previous chapters we described the 2N system treated in a 3D formulation as derived in Chapter 3. The applications in Chapter 4 for NN scattering and in Chapter 5 for the deuteron agree with experimental data and standard PW calculations. The 3D formulation allows to calculate at lower as well as at higher energies with a fixed number of LSE's, whereas in a formulation based on partial waves the number of LSE's increases with the energy.

In this chapter we extend the 3D formulation without partial wave decomposition to three-nucleon (3N) scattering. This can briefly be summarized as follows. Calculations of 3N scattering take as input the off-shell NN T-matrix elements corresponding to the process in the 2N subsystems. These off-shell NN T-matrix elements are given through the 3D approach presented in Chapter 3. Finally, the amplitude for the 3N scattering can be calculated directly as a function of Jacobi momenta describing the relative motion of the three nucleons. We take the Faddeev's scheme [1] for this purpose, which is derived for handling a three-particle system. Moreover we use only the lowest order of the multiple scattering series provided by the Faddeev equations.

We choose one of the 3N scattering channels, the nucleon-deuteron (Nd) break-up process. We begin with a brief review on this process. As in the 2N case, this review is meant to give a short summary of necessary formulas and definitions of some terminologies and quantities used in the following text.

We consider only the leading term of the break-up amplitude, since we are interested in higher energies and would like to see then whether the leading term is sufficient to describe the process. From now on we mean by the break-up amplitude (or simply the amplitude) the leading term and by the full break-up amplitude (the full amplitude) the leading term plus the rescattering terms. After the brief review on the process we derive the expression for the break-up amplitude in terms of the T-matrix elements in the momentum-helicity basis.

Up to this point the formulation is nonrelativistic. But in calculating higher energies it is natural to expect some relativistic effects. Therefore, we proceed with including relativistic correction in our formulation by introducing relativistic kinematics, which is based on the work in Ref. [51].

6.1 Review on the Nucleon-Deuteron Break-Up Process

This brief review covers kinematics, the amplitude, the Faddeev's equation and observables of the nucleon-deuteron process. These are given in more detail in, for example, Refs. [5].

6.1.1 Kinematics of the Three-Nucleon System in Laboratory and Center of Mass Reference Frames

In momentum space a 3N system can be described by using Jacobi momenta as illustrated in Fig.6.1(a). The Jacobi momenta \mathbf{p}_1 and \mathbf{q}_1 describe a 3N system in the c.m. frame and together with the laboratory momentum \mathbf{K} of the 3N center of mass describe the system in the laboratory frame. Figure 6.1(b) shows the cyclic behavior of Jacobi momenta \mathbf{p}_i and \mathbf{q}_i ($i = 1, 2, 3$), which all describe the same 3N system.

For a 3N system, that is a system of three equal mass particles, Jacobi momenta \mathbf{p}_i and \mathbf{q}_i are given as

$$\mathbf{p}_i = \frac{1}{2}(\mathbf{k}_j - \mathbf{k}_k) \quad \mathbf{q}_i = \frac{2}{3} \left[\mathbf{k}_i - \frac{1}{2}(\mathbf{k}_j + \mathbf{k}_k) \right] \quad i, j, k = \{1, 2, 3\} = \text{cyclic}, \quad (6.1)$$

where \mathbf{k}_i is the laboratory momentum of the i^{th} nucleon. Thus, \mathbf{p}_i is the relative momentum for the 2N subsystem of nucleons j and k (jk -subsystem) and \mathbf{q}_i is the relative momentum of nucleon i to the jk -subsystem. These three pairs of $\mathbf{p}_i, \mathbf{q}_i$ describe the same state. Hence,

$$|\mathbf{p}_1 \mathbf{q}_1 \alpha\rangle = |\mathbf{p}_2 \mathbf{q}_2 \alpha\rangle = |\mathbf{p}_3 \mathbf{q}_3 \alpha\rangle, \quad (6.2)$$

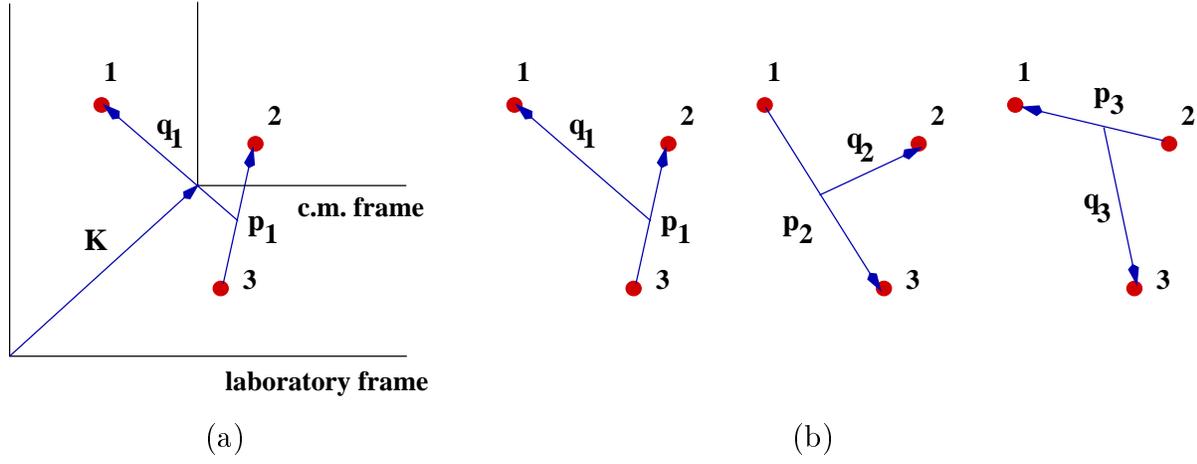


Figure 6.1: (a) A 3N system in momentum space can be described in the c.m. frame using Jacobi momenta \mathbf{p}_1 and \mathbf{q}_1 and in the laboratory frame using the same Jacobi momenta together with laboratory momentum \mathbf{K} of the 3N center of mass. (b) Jacobi momenta are cyclic and all describe the same system.

where $|\mathbf{p}_i, \mathbf{q}_i, \alpha\rangle$ is defined as the free 3N state and α stands for the discrete quantum numbers of the three nucleons. The relations between different pairs of \mathbf{p}_i , \mathbf{q}_i can be derived to be

$$\begin{aligned} \mathbf{p}_j &= -\frac{1}{2}\mathbf{p}_i - \frac{3}{4}\mathbf{q}_i & \mathbf{p}_k &= -\frac{1}{2}\mathbf{p}_i + \frac{3}{4}\mathbf{q}_i & i, j, k &= \{1, 2, 3\} = \text{cyclic.} \\ \mathbf{q}_j &= \mathbf{p}_i - \frac{1}{2}\mathbf{q}_i & \mathbf{q}_k &= -\mathbf{p}_i - \frac{1}{2}\mathbf{q}_i \end{aligned} \quad (6.3)$$

In the Nd break-up process one has in the final state three free nucleons, and in the initial state the deuteron being at rest and a nucleon coming with laboratory momentum \mathbf{k}_{lab} , corresponding to its laboratory nonrelativistic kinetic energy E_{lab} as

$$k_{lab} = \sqrt{2mE_{lab}}. \quad (6.4)$$

Let us choose without loss of generality this incoming nucleon as nucleon 1. Conservations of total momentum and total energy in the laboratory frame are given by

$$\mathbf{k}_{lab} = \mathbf{k}_1 + \mathbf{k}_2 + \mathbf{k}_3 \quad (6.5)$$

$$\frac{k_{lab}^2}{6m} + \frac{3q_0^2}{4m} + E_d = \frac{(\mathbf{k}_1 + \mathbf{k}_2 + \mathbf{k}_3)^2}{6m} + \frac{3q^2}{4m} + \frac{p^2}{m}, \quad (6.6)$$

where E_d is the deuteron binding energy, \mathbf{q}_0 the relative momentum of the incoming nucleon to the deuteron, \mathbf{p} the relative momentum for the 23-subsystem and \mathbf{q} the relative momentum of nucleon 1 to the 23-subsystem:

$$\mathbf{q}_0 = \frac{2}{3}\mathbf{k}_{lab} \quad (6.7)$$

$$\mathbf{p} = \frac{1}{2}(\mathbf{k}_2 - \mathbf{k}_3) \quad (6.8)$$

$$\begin{aligned} \mathbf{q} &= \frac{2}{3} \left[\mathbf{k}_1 - \frac{1}{2}(\mathbf{k}_2 + \mathbf{k}_3) \right] \\ &= \frac{2}{3} \left[\mathbf{k}_1 - \frac{1}{2}(\mathbf{k}_{lab} - \mathbf{k}_1) \right] \\ &= \mathbf{k}_1 - \frac{1}{3}\mathbf{k}_{lab}. \end{aligned} \quad (6.9)$$

In both sides of Eq. (6.6) the first term is the kinetic energy of the 3N center of mass, which is equal to $\frac{1}{3}E_{lab}$. The other terms sum up to the conserved total energy E_{cm} in the c.m. frame. Thus,

$$E_{cm} = \frac{3q_0^2}{4m} + E_d = \frac{3q^2}{4m} + \frac{p^2}{m}. \quad (6.10)$$

This Eq. (6.10) also provides the relation between q and p .

We will consider the inclusive break-up process, where only one nucleon is detected in the final state, which is in this case nucleon 1. In the experiment the detector is placed at a certain position and hence the scattering angle θ_{lab} is fixed. This scattering angle θ_{lab} determines the maximum value $k_{1,max}$ of the magnitude of the momentum \mathbf{k}_1 of the detected nucleon. Equation (6.9) leads to a quadratic equation in k_1 , with one of the solutions being

$$k_1 = \frac{1}{3}k_{lab} \cos \theta_{lab} + \sqrt{q^2 - \frac{1}{9}k_{lab}^2 \sin^2 \theta_{lab}} \quad . \quad (6.11)$$

The other solution with negative square-root term is not considered, since it is not appropriate to find $k_{1,max}$. Inserting into Eq. (6.11) the maximum value for q according to Eq. (6.10) gives

$$k_{1,max} = \frac{1}{3}k_{lab} \cos \theta_{lab} + \sqrt{\frac{1}{9}k_{lab}^2 (3 + \cos^2 \theta_{lab}) + \frac{4}{3}mE_d} \quad . \quad (6.12)$$

6.1.2 Break-up Amplitude and the Faddeev's Equation

Let us define U_0^{full} as the full Nd break-up operator. For a system of identical particles the full break-up operator can be written as

$$U_0^{full} = (1 + P)T_F. \quad (6.13)$$

Here P is a permutation operator defined as

$$P \equiv P_{12}P_{23} + P_{13}P_{23}. \quad (6.14)$$

The first term performs a cyclic permutation, which changes the nucleons' labels, for example from (123) to (231), and the second term an anticyclic permutation operator,

which changes the nucleons' labels from (123) to (312). That notation T_F in Eq. (6.13) stands for the Faddeev operator obeying the Faddeev equation for the break-up process [1]:

$$T_F = TP + TG_0PT_F. \quad (6.15)$$

Here T is NN T-matrix and G_0 the free 3N propagator given as

$$G_0 \left(\frac{3q_0^2}{4m} + E_d \right) = \frac{1}{\frac{3q_0^2}{4m} + E_d - H_0}, \quad (6.16)$$

where H_0 is the free 3N hamiltonian in the c.m. frame and we have applied the c.m. energy given in the previous subsection.

Now we consider only the leading term of the full break-up amplitude. This means we take only the first term of the Faddeev operator given in Eq. (6.15). Defining U_0 as the break-up operator for this special case, we have

$$U_0 = (1 + P)TP. \quad (6.17)$$

The Nd break-up amplitude $U_0(\mathbf{p}, \mathbf{q})$ is then defined as

$$\begin{aligned} U_0(\mathbf{p}, \mathbf{q}) &\equiv \left\langle \mathbf{p}\mathbf{q}m_{s_1}m_{s_2}m_{s_3}\tau_1\tau_2\tau_3 \left| U_0 \right| \mathbf{q}_0m_{s_1}^0\tau_1^0\Psi_d^{M_d} \right\rangle \\ &= \left\langle \mathbf{p}\mathbf{q}m_{s_1}m_{s_2}m_{s_3}\tau_1\tau_2\tau_3 \left| (1 + P)TP \right| \mathbf{q}_0m_{s_1}^0\tau_1^0\Psi_d^{M_d} \right\rangle. \end{aligned} \quad (6.18)$$

Here

$$|\mathbf{p}\mathbf{q}m_{s_1}m_{s_2}m_{s_3}\tau_1\tau_2\tau_3\rangle \equiv |\mathbf{q}m_{s_1}\tau_1\rangle |\mathbf{p}m_{s_2}m_{s_3}\tau_2\tau_3\rangle \quad (6.19)$$

is the final not-antisymmetrized free state,

$$|\mathbf{q}_0m_{s_1}^0\tau_1^0\Psi_d^{M_d}\rangle \equiv |\mathbf{q}_0m_{s_1}^0\tau_1^0\rangle |\Psi_d^{M_d}\rangle \quad (6.20)$$

the initial state, in which only the deuteron state is antisymmetrized, m_{s_i}, τ_i ($i = 1, 2, 3$) final spins and isospins of the three nucleons, $m_{s_1}^0, \tau_1^0$ initial spin and isospin of nucleon 1 and $|\Psi_d^{M_d}\rangle$ the deuteron state with M_d being the projection of its total angular momentum along an arbitrary z-axis. In the amplitude $U_0(\mathbf{p}, \mathbf{q})$ we suppress the initial quantum numbers as well as the final discrete quantum numbers for simplicity.

6.1.3 Cross Section and Spin Observables

Similarly to Eq. (2.21) for the NN system, the expression for the expectation value $\langle \sigma_\alpha^{(1)} \sigma_\beta^{(2)} \sigma_\gamma^{(3)} \rangle_f$ of a general spin observable for the Nd break-up process is given as

$$I \langle \sigma_\alpha^{(1)} \sigma_\beta^{(2)} \sigma_\gamma^{(3)} \rangle_f = \frac{1}{6} \sum_{\lambda\rho} \langle \sigma_\lambda^{(1)} S_\rho \rangle_i Tr \{ M \sigma_\lambda^{(1)} S_\rho M^\dagger \sigma_\alpha^{(1)} \sigma_\beta^{(2)} \sigma_\gamma^{(3)} \}, \quad (6.21)$$

where

$$I = \frac{1}{6} \sum_{\lambda\rho} \langle \sigma_\lambda^{(1)} S_\rho \rangle_i \text{Tr} \{ M \sigma_\lambda^{(1)} S_\rho M^\dagger \} \quad (6.22)$$

is related to the differential cross section summed over all possible final spin states. For the break-up process the scattering amplitude M is U_0 . Here σ_α ($\alpha = 0, 1, 2, 3$) are the 2×2 matrices given in Eq. (2.16) and S_ρ ($\rho = 0, 1, \dots, 8$) the 3×3 matrices of the general spin observables for spin-1 particles, in this case the target deuteron. They are combinations of the matrices of the Cartesian components S_x, S_y, S_z of angular momentum $S = 1$

$$S_x = \frac{1}{\sqrt{2}} \begin{pmatrix} 0 & 1 & 0 \\ 1 & 0 & 1 \\ 0 & 1 & 0 \end{pmatrix} \quad S_y = \frac{1}{\sqrt{2}} \begin{pmatrix} 0 & -i & 0 \\ i & 0 & -i \\ 0 & i & 0 \end{pmatrix} \quad S_z = \begin{pmatrix} 1 & 0 & 0 \\ 0 & 0 & 0 \\ 0 & 0 & -1 \end{pmatrix}. \quad (6.23)$$

(See Ref. [52] for more details.) For the inclusive break-up process one has to sum over all directions of the relative momentum \mathbf{p} , thus,

$$\langle \sigma_\alpha^{(1)} \sigma_\beta^{(2)} \sigma_\gamma^{(3)} \rangle_f = \sum_{\lambda\rho} \langle \sigma_\lambda^{(1)} S_\rho \rangle_i \frac{\int d\hat{\mathbf{p}} \text{Tr} \{ M \sigma_\lambda^{(1)} S_\rho M^\dagger \sigma_\alpha^{(1)} \sigma_\beta^{(2)} \sigma_\gamma^{(3)} \}}{6 \int d\hat{\mathbf{p}} I}. \quad (6.24)$$

We consider cases where the deuteron is unpolarized, hence, $S_\rho = S_0 \delta_{\rho 0} = \delta_{\rho 0}$.

Now we take a look at the spin averaged differential cross section and some spin observables, i.e. polarization, analyzing power and polarization transfer coefficients. Data for these observables are given in the laboratory frame. Hence, we have to calculate these observables in the laboratory frame. Though we can first calculate observables in the c.m. frame and later connect them with the ones in the laboratory frame, we choose to calculate directly in the laboratory frame. This poses no difficulty. Ref. [53] give the relations between polarization transfer coefficients in the c.m. and in the laboratory frames, including the ones with relativistic kinematics.

We use the unit vectors $\hat{\mathbf{I}}, \hat{\mathbf{n}}, \hat{\mathbf{s}}, \hat{\mathbf{l}}', \hat{\mathbf{n}}', \hat{\mathbf{s}}'$ in the laboratory frame defined in Eqs. (2.26)-(2.30), with changes in notations such that \hat{k}_1 is replaced by \hat{k}_{lab} and \hat{k}'_1 by \hat{k}_1 . Note that the relation with the unit vectors in the c.m. frame shown in Eqs. (2.26)-(2.30) is not valid for the 3N scattering. See Ref. [53] for the general formulae. Choosing $\hat{k}_{lab} = \hat{z}$ and \hat{k}_1 in the xz-plane, the laboratory unit vectors in a Cartesian coordinate system are given by Eq. (2.31).

The spin averaged differential cross section in the c.m. frame for the inclusive break-up process is given by [5]

$$\frac{d^3\sigma}{dq d\hat{\mathbf{q}}} = (2\pi)^4 \frac{m^2 p q^2}{3q_0} \int d\hat{\mathbf{p}} I_0, \quad (6.25)$$

with

$$I_0 \equiv \frac{1}{6} Tr \{ MM^\dagger \} = \frac{1}{6} \sum_{m_{s1} m_{s2} m_{s3} m_{s1}^0 M_d} |U_0(\mathbf{p}, \mathbf{q})|^2. \quad (6.26)$$

In order to compare with experimental data we need to calculate the cross section in the laboratory frame, written as a function of the nucleon's outgoing kinetic energy $E_1 = \frac{k_1^2}{2m}$ and scattering angle θ_{lab} . Using Eq. (6.9) we get $d\mathbf{q} = d\mathbf{k}_1$. Hence, the cross section in the laboratory frame is obtained as

$$\frac{d^5\sigma}{dE_1 d\hat{\mathbf{k}}_1} = (2\pi)^4 \frac{m^3 p k_1}{2k_{lab}} \frac{1}{6} \sum_{m_{s1} m_{s2} m_{s3} m_{s1}^0 M_d} \int d\hat{\mathbf{p}} |U_0(\mathbf{p}, \mathbf{k}_1)|^2. \quad (6.27)$$

It should be pointed out that p is not independent, but determined by \mathbf{k}_1 via Eqs. (6.10) and (6.9).

In the following we give the polarization P_0 of the outgoing nucleon, the analyzing power A_y and polarization transfer coefficients $D_{ij} \equiv \frac{1}{6I_0} Tr \{ M(\boldsymbol{\sigma} \cdot \hat{\mathbf{j}}) M^\dagger(\boldsymbol{\sigma} \cdot \hat{\mathbf{i}}) \}$, where we suppress the integration over $\hat{\mathbf{p}}$:

$$\begin{aligned} P_0 &= \frac{1}{6I_0} Tr \{ MM^\dagger(\boldsymbol{\sigma} \cdot \hat{\mathbf{n}}) \} \\ &= \frac{1}{6I_0} Tr \{ MM^\dagger \sigma_y \} \end{aligned} \quad (6.28)$$

$$\begin{aligned} A_y &= \frac{1}{6I_0} Tr \{ M(\boldsymbol{\sigma} \cdot \hat{\mathbf{n}}) M^\dagger \} \\ &= \frac{1}{6I_0} Tr \{ M \sigma_y M^\dagger \} \end{aligned} \quad (6.29)$$

$$\begin{aligned} D_{n'n} &= \frac{1}{6I_0} Tr \{ M(\boldsymbol{\sigma} \cdot \hat{\mathbf{n}}) M^\dagger(\boldsymbol{\sigma} \cdot \hat{\mathbf{n}}') \} \\ &= \frac{1}{6I_0} Tr \{ M \sigma_y M^\dagger \sigma_y \} \end{aligned} \quad (6.30)$$

$$\begin{aligned} D_{s's} &= \frac{1}{6I_0} Tr \{ M(\boldsymbol{\sigma} \cdot \hat{\mathbf{s}}) M^\dagger(\boldsymbol{\sigma} \cdot \hat{\mathbf{s}}') \} \\ &= \frac{1}{6I_0} Tr \{ M \sigma_x M^\dagger (\sigma_x \cos \theta_{lab} - \sigma_z \sin \theta_{lab}) \} \end{aligned} \quad (6.31)$$

$$\begin{aligned} D_{l's} &= \frac{1}{6I_0} Tr \{ M(\boldsymbol{\sigma} \cdot \hat{\mathbf{s}}) M^\dagger(\boldsymbol{\sigma} \cdot \hat{\mathbf{l}}') \} \\ &= \frac{1}{6I_0} Tr \{ M \sigma_x M^\dagger (\sigma_x \sin \theta_{lab} + \sigma_z \cos \theta_{lab}) \} \end{aligned} \quad (6.32)$$

$$\begin{aligned} D_{s'l} &= \frac{1}{6I_0} Tr \{ M(\boldsymbol{\sigma} \cdot \hat{\mathbf{l}}) M^\dagger(\boldsymbol{\sigma} \cdot \hat{\mathbf{s}}') \} \\ &= \frac{1}{6I_0} Tr \{ M \sigma_z M^\dagger (\sigma_x \cos \theta_{lab} - \sigma_z \sin \theta_{lab}) \} \end{aligned} \quad (6.33)$$

$$\begin{aligned} D_{l'l} &= \frac{1}{6I_0} Tr \{ M(\boldsymbol{\sigma} \cdot \hat{\mathbf{l}}) M^\dagger(\boldsymbol{\sigma} \cdot \hat{\mathbf{l}}') \} \\ &= \frac{1}{6I_0} Tr \{ M \sigma_z M^\dagger (\sigma_x \sin \theta_{lab} + \sigma_z \cos \theta_{lab}) \}. \end{aligned} \quad (6.34)$$

In obtaining Eqs. (6.28)-(6.34) we have applied Eq. (2.31), which gives the laboratory unit vectors in a Cartesian coordinate system.

6.2 Three-Dimensional Nucleon-Deuteron Break-Up Amplitude

In this section we derive an expression for the Nd break-up amplitude. Returning to Eq. (6.18) the amplitude can be written in three terms as

$$U_0(\mathbf{p}, \mathbf{q}) = U_0^{(1)}(\mathbf{p}, \mathbf{q}) + U_0^{(2)}(\mathbf{p}, \mathbf{q}) + U_0^{(3)}(\mathbf{p}, \mathbf{q}), \quad (6.35)$$

with

$$U_0^{(1)}(\mathbf{p}, \mathbf{q}) \equiv \langle \mathbf{p}\mathbf{q}m_{s_1}m_{s_2}m_{s_3}\tau_1\tau_2\tau_3 | TP | \mathbf{q}_0m_{s_1}^0\tau_1^0\Psi_d^{M_d} \rangle \quad (6.36)$$

$$U_0^{(2)}(\mathbf{p}, \mathbf{q}) \equiv \langle \mathbf{p}\mathbf{q}m_{s_1}m_{s_2}m_{s_3}\tau_1\tau_2\tau_3 | P_{12}P_{23}TP | \mathbf{q}_0m_{s_1}^0\tau_1^0\Psi_d^{M_d} \rangle \quad (6.37)$$

$$U_0^{(3)}(\mathbf{p}, \mathbf{q}) \equiv \langle \mathbf{p}\mathbf{q}m_{s_1}m_{s_2}m_{s_3}\tau_1\tau_2\tau_3 | P_{13}P_{23}TP | \mathbf{q}_0m_{s_1}^0\tau_1^0\Psi_d^{M_d} \rangle. \quad (6.38)$$

For clarity let us label the free 3N states as

$$\begin{aligned} |\mathbf{p}\mathbf{q}\alpha\rangle_i &= \text{being the free 3N state, where nucleons } j \text{ and } k \text{ form a 2N } jk\text{-subsystem,} \\ &\text{discrete quantum numbers listed in } \alpha \text{ are to be understood in} \\ &\text{nucleons' order } i, j, k \text{ and } i,j,k = 1,2,3 \text{ are cyclic.} \end{aligned} \quad (6.39)$$

If there is no label, that means the label is 1. Now we consider $U_0^{(2)}(\mathbf{p}, \mathbf{q})$. We apply the permutation operator $P_{12}P_{23}$ in Eq. (6.37) to the final state. This gives

$$\begin{aligned} U_0^{(2)}(\mathbf{p}, \mathbf{q}) &= {}_1 \left\langle \mathbf{p}\mathbf{q}m_{s_1}m_{s_2}m_{s_3}\tau_1\tau_2\tau_3 \left| P_{12}P_{23}TP \right| \mathbf{q}_0m_{s_1}^0\tau_1^0\Psi_d^{M_d} \right\rangle \\ &= {}_1 \left\langle P_{23}P_{12}\mathbf{p}\mathbf{q}m_{s_1}m_{s_2}m_{s_3}\tau_1\tau_2\tau_3 \left| TP \right| \mathbf{q}_0m_{s_1}^0\tau_1^0\Psi_d^{M_d} \right\rangle \\ &= {}_3 \left\langle \mathbf{p}\mathbf{q}m_{s_1}m_{s_2}m_{s_3}\tau_1\tau_2\tau_3 \left| TP \right| \mathbf{q}_0m_{s_1}^0\tau_1^0\Psi_d^{M_d} \right\rangle. \end{aligned} \quad (6.40)$$

In Eq. (6.40) the final state represents a free 3N system, where nucleons 1 and 2 form the 12-subsystem. Now we want to have the final state representing a system, where nucleons 2 and 3 form the 23-subsystem. We use the relation for Jacobi momenta given in Eq. (6.3) and obtain

$$|\mathbf{p}\mathbf{q}m_{s_1}m_{s_2}m_{s_3}\tau_1\tau_2\tau_3\rangle_3 = \left| \left(-\frac{1}{2}\mathbf{p} - \frac{3}{4}\mathbf{q} \right) \left(\mathbf{p} - \frac{1}{2}\mathbf{q} \right) m_{s_2}m_{s_3}m_{s_1}\tau_2\tau_3\tau_1 \right\rangle_1. \quad (6.41)$$

Hence,

$$U_0^{(2)}(\mathbf{p}, \mathbf{q}) = \left\langle \left(-\frac{1}{2}\mathbf{p} - \frac{3}{4}\mathbf{q} \right) \left(\mathbf{p} - \frac{1}{2}\mathbf{q} \right) m_{s_2}m_{s_3}m_{s_1}\tau_2\tau_3\tau_1 \left| TP \right| \mathbf{q}_0m_{s_1}^0\tau_1^0\Psi_d^{M_d} \right\rangle. \quad (6.42)$$

Similarly for $U_0^{(3)}(\mathbf{p}, \mathbf{q})$ we get

$$U_0^{(3)}(\mathbf{p}, \mathbf{q}) = \left\langle \left(-\frac{1}{2}\mathbf{p} + \frac{3}{4}\mathbf{q} \right) \left(-\mathbf{p} - \frac{1}{2}\mathbf{q} \right) m_{s_3} m_{s_1} m_{s_2} \tau_3 \tau_1 \tau_2 \left| TP \left| \mathbf{q}_0 m_{s_1}^0 \tau_1^0 \Psi_d^{M_d} \right. \right. \right\rangle. \quad (6.43)$$

Thus, $U_0^{(1)}(\mathbf{p}, \mathbf{q})$, $U_0^{(2)}(\mathbf{p}, \mathbf{q})$ and $U_0^{(3)}(\mathbf{p}, \mathbf{q})$ all have the same form and differ from each other only in values of their variables. Therefore, it is sufficient to work out a 3D expression for one of them, which we choose $U_0^{(1)}(\mathbf{p}, \mathbf{q})$. The following replacements have to be applied to get $U_0^{(2)}(\mathbf{p}, \mathbf{q})$ and $U_0^{(3)}(\mathbf{p}, \mathbf{q})$:

$$\text{for } U_0^{(2)}(\mathbf{p}, \mathbf{q}) : \{ \tau, m \}_{\{1,2,3\}} \rightarrow \{ \tau, m \}_{\{2,3,1\}} \quad \mathbf{p} \rightarrow -\frac{1}{2}\mathbf{p} - \frac{3}{4}\mathbf{q} \quad \mathbf{q} \rightarrow \mathbf{p} - \frac{1}{2}\mathbf{q} \quad (6.44)$$

$$\text{for } U_0^{(3)}(\mathbf{p}, \mathbf{q}) : \{ \tau, m \}_{\{1,2,3\}} \rightarrow \{ \tau, m \}_{\{3,1,2\}} \quad \mathbf{p} \rightarrow -\frac{1}{2}\mathbf{p} + \frac{3}{4}\mathbf{q} \quad \mathbf{q} \rightarrow -\mathbf{p} - \frac{1}{2}\mathbf{q}. \quad (6.45)$$

We begin by inserting twice the following completeness relation for the free 3N system

$$\sum_{m_{s_1} \tau_1} \sum_{m_{s_2} m_{s_3} \tau_2 \tau_3} \int d\mathbf{p} \int d\mathbf{q} |\mathbf{p}\mathbf{q} m_{s_1} m_{s_2} m_{s_3} \tau_1 \tau_2 \tau_3\rangle \langle \mathbf{p}\mathbf{q} m_{s_1} m_{s_2} m_{s_3} \tau_1 \tau_2 \tau_3| = 1 \quad (6.46)$$

into Eq. (6.36). This gives

$$\begin{aligned} U_0^{(1)}(\mathbf{p}, \mathbf{q}) &= \sum_{m'_{s_1} \tau'_1} \sum_{m'_{s_2} m'_{s_3} \tau'_2 \tau'_3} \int d\mathbf{p}' \int d\mathbf{q}' \langle \mathbf{p}\mathbf{q} m_{s_1} m_{s_2} m_{s_3} \tau_1 \tau_2 \tau_3 | T | \mathbf{p}'\mathbf{q}' m'_{s_1} m'_{s_2} m'_{s_3} \tau'_1 \tau'_2 \tau'_3 \rangle \\ &\quad \times \sum_{m''_{s_1} \tau''_1} \sum_{m''_{s_2} m''_{s_3} \tau''_2 \tau''_3} \int d\mathbf{p}'' \int d\mathbf{q}'' \\ &\quad \times \langle \mathbf{p}'\mathbf{q}' m'_{s_1} m'_{s_2} m'_{s_3} \tau'_1 \tau'_2 \tau'_3 | P | \mathbf{p}''\mathbf{q}'' m''_{s_1} m''_{s_2} m''_{s_3} \tau''_1 \tau''_2 \tau''_3 \rangle \\ &\quad \times \langle \mathbf{p}''\mathbf{q}'' m''_{s_1} m''_{s_2} m''_{s_3} \tau''_1 \tau''_2 \tau''_3 | \mathbf{q}_0 m_{s_1}^0 \tau_1^0 \Psi_d^{M_d} \rangle \\ &= \sum_{m'_{s_1} \tau'_1} \sum_{m'_{s_2} m'_{s_3} \tau'_2 \tau'_3} \int d\mathbf{p}' \int d\mathbf{q}' \langle \mathbf{q} m_{s_1} \tau_1 | \mathbf{q}' m'_{s_1} \tau'_1 \rangle \\ &\quad \times \langle \mathbf{p} m_{s_2} m_{s_3} \tau_2 \tau_3 | T(E_p) | \mathbf{p}' m'_{s_2} m'_{s_3} \tau'_2 \tau'_3 \rangle \\ &\quad \times \sum_{m''_{s_1} \tau''_1} \sum_{m''_{s_2} m''_{s_3} \tau''_2 \tau''_3} \int d\mathbf{p}'' \int d\mathbf{q}'' \\ &\quad \times \langle \mathbf{p}' m'_{s_2} m'_{s_3} \tau'_2 \tau'_3 | \langle \mathbf{q}' m'_{s_1} \tau'_1 | P | \mathbf{q}'' m''_{s_1} \tau''_1 \rangle | \mathbf{p}'' m''_{s_2} m''_{s_3} \tau''_2 \tau''_3 \rangle \\ &\quad \times \langle \mathbf{q}'' m''_{s_1} \tau''_1 | \mathbf{q}_0 m_{s_1}^0 \tau_1^0 \rangle \langle \mathbf{p}'' m''_{s_2} m''_{s_3} \tau''_2 \tau''_3 | \Psi_d^{M_d} \rangle \\ &= \sum_{m'_{s_2} m'_{s_3} \tau'_2 \tau'_3} \int d\mathbf{p}' \langle \mathbf{p} m_{s_2} m_{s_3} \tau_2 \tau_3 | T(E_p) | \mathbf{p}' m'_{s_2} m'_{s_3} \tau'_2 \tau'_3 \rangle \\ &\quad \times \sum_{m''_{s_2} m''_{s_3} \tau''_2 \tau''_3} \int d\mathbf{p}'' \langle \mathbf{p}' m'_{s_2} m'_{s_3} \tau'_2 \tau'_3 | \langle \mathbf{q} m_{s_1} \tau_1 | P | \mathbf{q}_0 m_{s_1}^0 \tau_1^0 \rangle | \mathbf{p}'' m''_{s_2} m''_{s_3} \tau''_2 \tau''_3 \rangle \\ &\quad \times \langle \mathbf{p}'' m''_{s_2} m''_{s_3} \tau''_2 \tau''_3 | \Psi_d^{M_d} \rangle. \end{aligned} \quad (6.47)$$

The NN T-matrix is calculated at energy E_p :

$$E_p \equiv \frac{p^2}{m} = \frac{3}{4m}(q_0^2 - q^2) + E_d, \quad (6.48)$$

which does not necessarily corresponds to the intermediate relative momenta \mathbf{p}' .

The permutation part of Eq. (6.47) is worked out as follows with the help of the relations for Jacobi momenta given in Eq. (6.3):

$$\begin{aligned}
& \langle \mathbf{p}' m'_{s_2} m'_{s_3} \tau'_2 \tau'_3 | \langle \mathbf{q} m_{s_1} \tau_1 | P | \mathbf{q}_0 m_{s_1}^0 \tau_1^0 \rangle | \mathbf{p}'' m''_{s_2} m''_{s_3} \tau''_2 \tau''_3 \rangle \\
&= \langle \mathbf{p}' | \langle \mathbf{q} | P | \mathbf{q}_0 \rangle | \mathbf{p}'' \rangle \langle m_{s_1} m'_{s_2} m'_{s_3} \tau_1 \tau'_2 \tau'_3 | P | m_{s_1}^0 m''_{s_2} m''_{s_3} \tau_1^0 \tau''_2 \tau''_3 \rangle \\
&= {}_1 \langle \mathbf{p}' | \langle \mathbf{q} | \mathbf{q}_0 \rangle | \mathbf{p}'' \rangle {}_2 \langle m_{s_1} m'_{s_2} m'_{s_3} \tau_1 \tau'_2 \tau'_3 | m_{s_1}^0 m''_{s_2} m''_{s_3} \tau_1^0 \tau''_2 \tau''_3 \rangle {}_2 \\
&\quad + {}_1 \langle \mathbf{p}' | \langle \mathbf{q} | \mathbf{q}_0 \rangle | \mathbf{p}'' \rangle {}_3 \langle m_{s_1} m'_{s_2} m'_{s_3} \tau_1 \tau'_2 \tau'_3 | m_{s_1}^0 m''_{s_2} m''_{s_3} \tau_1^0 \tau''_2 \tau''_3 \rangle {}_3 \\
&= {}_1 \langle \mathbf{p}' | \langle \mathbf{q} | -\mathbf{p}'' - \frac{1}{2} \mathbf{q}_0 \rangle | -\frac{1}{2} \mathbf{p}'' + \frac{3}{4} \mathbf{q}_0 \rangle {}_1 \langle m_{s_1} m'_{s_2} m'_{s_3} \tau_1 \tau'_2 \tau'_3 | m''_{s_3} m_{s_1}^0 m''_{s_2} \tau''_3 \tau_1^0 \tau''_2 \rangle {}_1 \\
&\quad + {}_1 \langle \mathbf{p}' | \langle \mathbf{q} | \mathbf{p}'' - \frac{1}{2} \mathbf{q}_0 \rangle | -\frac{1}{2} \mathbf{p}'' - \frac{3}{4} \mathbf{q}_0 \rangle {}_1 \langle m_{s_1} m'_{s_2} m'_{s_3} \tau_1 \tau'_2 \tau'_3 | m''_{s_2} m''_{s_3} m_{s_1}^0 \tau''_2 \tau''_3 \tau_1^0 \rangle {}_1 \\
&= \delta \left(\mathbf{p}' + \frac{1}{2} \mathbf{p}'' - \frac{3}{4} \mathbf{q}_0 \right) \delta \left(\mathbf{q} + \mathbf{p}'' + \frac{1}{2} \mathbf{q}_0 \right) \delta_{m_{s_1} m''_{s_3}} \delta_{m'_{s_2} m_{s_1}^0} \delta_{m'_{s_3} m''_{s_2}} \delta_{\tau_1 \tau''_3} \delta_{\tau'_2 \tau_1^0} \delta_{\tau'_3 \tau''_2} \\
&\quad + \delta \left(\mathbf{p}' + \frac{1}{2} \mathbf{p}'' + \frac{3}{4} \mathbf{q}_0 \right) \delta \left(\mathbf{q} - \mathbf{p}'' + \frac{1}{2} \mathbf{q}_0 \right) \delta_{m_{s_1} m''_{s_2}} \delta_{m'_{s_2} m''_{s_3}} \delta_{m'_{s_3} m_{s_1}^0} \delta_{\tau_1 \tau''_2} \delta_{\tau'_2 \tau''_3} \delta_{\tau'_3 \tau_1^0} \\
&= \delta \left(\mathbf{p}' - \frac{1}{2} \mathbf{q} - \mathbf{q}_0 \right) \delta \left(\mathbf{p}'' + \mathbf{q} + \frac{1}{2} \mathbf{q}_0 \right) \delta_{m_{s_1} m''_{s_3}} \delta_{m'_{s_2} m_{s_1}^0} \delta_{m'_{s_3} m''_{s_2}} \delta_{\tau_1 \tau''_3} \delta_{\tau'_2 \tau_1^0} \delta_{\tau'_3 \tau''_2} \\
&\quad + \delta \left(\mathbf{p}' + \frac{1}{2} \mathbf{q} + \mathbf{q}_0 \right) \delta \left(\mathbf{p}'' - \mathbf{q} - \frac{1}{2} \mathbf{q}_0 \right) \delta_{m_{s_1} m''_{s_2}} \delta_{m'_{s_2} m''_{s_3}} \delta_{m'_{s_3} m_{s_1}^0} \delta_{\tau_1 \tau''_2} \delta_{\tau'_2 \tau''_3} \delta_{\tau'_3 \tau_1^0}. \quad (6.49)
\end{aligned}$$

In the last equality we have arranged the delta functions, in such a fashion that it contains only one integration variable. Next defining

$$\boldsymbol{\pi} \equiv \frac{1}{2} \mathbf{q} + \mathbf{q}_0 \quad \boldsymbol{\pi}' \equiv -\mathbf{q} - \frac{1}{2} \mathbf{q}_0 \quad (6.50)$$

we get

$$\begin{aligned}
& \langle \mathbf{p}' m'_{s_2} m'_{s_3} \tau'_2 \tau'_3 | \langle \mathbf{q} m_{s_1} \tau_1 | P | \mathbf{q}_0 m_{s_1}^0 \tau_1^0 \rangle | \mathbf{p}'' m''_{s_2} m''_{s_3} \tau''_2 \tau''_3 \rangle \\
&= \delta(\mathbf{p}' - \boldsymbol{\pi}) \delta(\mathbf{p}'' - \boldsymbol{\pi}') \delta_{m_{s_1} m''_{s_3}} \delta_{m'_{s_2} m_{s_1}^0} \delta_{m'_{s_3} m''_{s_2}} \delta_{\tau_1 \tau''_3} \delta_{\tau'_2 \tau_1^0} \delta_{\tau'_3 \tau''_2} \\
&\quad + \delta(\mathbf{p}' + \boldsymbol{\pi}) \delta(\mathbf{p}'' + \boldsymbol{\pi}') \delta_{m_{s_1} m''_{s_2}} \delta_{m'_{s_2} m''_{s_3}} \delta_{m'_{s_3} m_{s_1}^0} \delta_{\tau_1 \tau''_2} \delta_{\tau'_2 \tau''_3} \delta_{\tau'_3 \tau_1^0}, \quad (6.51)
\end{aligned}$$

Now we insert Eq. (6.51) into $U_0^{(1)}(\mathbf{p}, \mathbf{q})$ in Eq. (6.47), and get

$$\begin{aligned}
U_0^{(1)}(\mathbf{p}, \mathbf{q}) &= \sum_{m'_{s_2} m'_{s_3} \tau'_2 \tau'_3} \int d\mathbf{p}' \langle \mathbf{p} m_{s_2} m_{s_3} \tau_2 \tau_3 | T(E_p) | \mathbf{p}' m'_{s_2} m'_{s_3} \tau'_2 \tau'_3 \rangle \\
&\quad \times \sum_{m''_{s_2} m''_{s_3} \tau''_2 \tau''_3} \int d\mathbf{p}'' \\
&\quad \times \left\{ \delta(\mathbf{p}' - \boldsymbol{\pi}) \delta(\mathbf{p}'' - \boldsymbol{\pi}') \delta_{m_{s_1} m''_{s_3}} \delta_{m'_{s_2} m_{s_1}^0} \delta_{m'_{s_3} m''_{s_2}} \delta_{\tau_1 \tau''_3} \delta_{\tau'_2 \tau_1^0} \delta_{\tau'_3 \tau''_2} \right. \\
&\quad \left. + \delta(\mathbf{p}' + \boldsymbol{\pi}) \delta(\mathbf{p}'' + \boldsymbol{\pi}') \delta_{m_{s_1} m''_{s_2}} \delta_{m'_{s_2} m''_{s_3}} \delta_{m'_{s_3} m_{s_1}^0} \delta_{\tau_1 \tau''_2} \delta_{\tau'_2 \tau''_3} \delta_{\tau'_3 \tau_1^0} \right\} \\
&\quad \times \langle \mathbf{p}'' m''_{s_2} m''_{s_3} \tau''_2 \tau''_3 | \Psi_d^{M_d} \rangle
\end{aligned}$$

$$\begin{aligned}
&= \sum_{m'_{s3}\tau'_3} \left\langle \mathbf{p}m_{s2}m_{s3}\tau_2\tau_3 \mid T(E_p) \mid \boldsymbol{\pi}m_{s1}^0m'_{s3}\tau_1^0\tau'_3 \right\rangle \left\langle \boldsymbol{\pi}'m'_{s3}m_{s1}\tau'_3\tau_1 \mid \Psi_d^{M_d} \right\rangle \\
&\quad + \sum_{m'_{s2}\tau'_2} \left\langle \mathbf{p}m_{s2}m_{s3}\tau_2\tau_3 \mid T(E_p) \mid -\boldsymbol{\pi}m'_{s2}m_{s1}^0\tau'_2\tau_1^0 \right\rangle \left\langle -\boldsymbol{\pi}'m_{s1}m'_{s2}\tau_1\tau'_2 \mid \Psi_d^{M_d} \right\rangle \\
&= \sum_{m'_s\tau'} \left\{ \left\langle \mathbf{p}m_{s2}m_{s3}\tau_2\tau_3 \mid T(E_p) \mid \boldsymbol{\pi}m_{s1}^0m'_s\tau_1^0\tau' \right\rangle \left\langle \boldsymbol{\pi}'m'_sm_{s1}\tau'\tau_1 \mid \Psi_d^{M_d} \right\rangle \right. \\
&\quad \left. + \left\langle \mathbf{p}m_{s2}m_{s3}\tau_2\tau_3 \mid T(E_p)P_{23} \mid \boldsymbol{\pi}m_{s1}^0m'_s\tau_1^0\tau' \right\rangle \left\langle \boldsymbol{\pi}'m'_sm_{s1}\tau'\tau_1 \mid P_{23}^{-1} \mid \Psi_d^{M_d} \right\rangle \right\} \\
&= \sum_{m'_s\tau'} \left\langle \mathbf{p}m_{s2}m_{s3}\tau_2\tau_3 \mid T(E_p)(1 - P_{23}) \mid \boldsymbol{\pi}m_{s1}^0m'_s\tau_1^0\tau' \right\rangle \\
&\quad \times \left\langle \boldsymbol{\pi}'m'_sm_{s1}\tau'\tau_1 \mid \Psi_d^{M_d} \right\rangle. \tag{6.52}
\end{aligned}$$

In the last equality we made use of the antisymmetry of the deuteron state $\left| \Psi_d^{M_d} \right\rangle$.

The projection $\left\langle \boldsymbol{\pi}'m'_sm_{s1}\tau'\tau_1 \mid \Psi_d^{M_d} \right\rangle$ in Eq. (6.52) is worked out in the following, where the deuteron state is expanded in partial waves. We recall the partial wave components $\psi_l(p)$ of the deuteron wave function, defined in Eq. (5.23).

$$\begin{aligned}
\left\langle \boldsymbol{\pi}'m'_sm_{s1}\tau'\tau_1 \mid \Psi_d^{M_d} \right\rangle &= \sum_l \int dp' p'^2 \left\langle \boldsymbol{\pi}'m'_sm_{s1}\tau'\tau_1 \mid p'(l1)1M_d; 0 \right\rangle \psi_l(p') \\
&= \left\langle \tau'\tau_1 \mid 0 \right\rangle \sum_l \int dp' p'^2 \left\langle \boldsymbol{\pi}'m'_sm_{s1} \mid p'(l1)1M_d \right\rangle \psi_l(p') \\
&= \sum_\tau C \left(\frac{1}{2} \frac{1}{2} \tau; \tau'\tau_1 \right) \left\langle \tau \mid 0 \right\rangle \sum_l \int dp' p'^2 \left\langle \boldsymbol{\pi}'m'_sm_{s1} \mid p'(l1)1M_d \right\rangle \psi_l(p') \\
&= C \left(\frac{1}{2} \frac{1}{2} 0; \tau'\tau_1 \right) \sum_l \int dp' p'^2 \left\langle \boldsymbol{\pi}'m'_sm_{s1} \mid p'(l1)1M_d \right\rangle \psi_l(p') \\
&= C \left(\frac{1}{2} \frac{1}{2} 0; \tau'\tau_1 \right) \sum_{l\mu} C(l11; \mu, M_d - \mu) \\
&\quad \times \int dp' p'^2 \left\langle \boldsymbol{\pi}' \mid p'l\mu \right\rangle \left\langle m'_sm_{s1} \mid 1, M_d - \mu \right\rangle \psi_l(p') \\
&= C \left(\frac{1}{2} \frac{1}{2} 0; \tau'\tau_1 \right) \sum_{l\mu} C(l11; \mu, M_d - \mu) Y_{l\mu}(\hat{\boldsymbol{\pi}}') \\
&\quad \times \left\langle m'_sm_{s1} \mid 1, M_d - \mu \right\rangle \psi_l(\boldsymbol{\pi}') \\
&= C \left(\frac{1}{2} \frac{1}{2} 0; \tau'\tau_1 \right) \sum_{l\mu} C(l11; \mu, M_d - \mu) \\
&\quad \times \sum_S C \left(\frac{1}{2} \frac{1}{2} S; m'_sm_{s1} \right) Y_{l\mu}(\hat{\boldsymbol{\pi}}') \left\langle S, m'_s + m_{s1} \mid 1, M_d - \mu \right\rangle \psi_l(\boldsymbol{\pi}') \\
&= C \left(\frac{1}{2} \frac{1}{2} 0; \tau'\tau_1 \right) \sum_{l\mu} C(l11; \mu, M_d - \mu) \\
&\quad \times C \left(\frac{1}{2} \frac{1}{2} 1; m'_sm_{s1}, M_d - \mu \right) Y_{l\mu}(\hat{\boldsymbol{\pi}}') \psi_l(\boldsymbol{\pi}') \delta_{m'_s+m_{s1}, M_d-\mu} \\
&= C \left(\frac{1}{2} \frac{1}{2} 0; \tau'\tau_1 \right) C \left(\frac{1}{2} \frac{1}{2} 1; m'_sm_{s1} \right) \\
&\quad \times \sum_l C(l11; M_d - m'_s - m_{s1}, m'_s + m_{s1})
\end{aligned}$$

$$\times Y_{l, M_d - m'_s - m_{s1}}(\hat{\boldsymbol{\pi}}') \psi_l(\boldsymbol{\pi}'). \quad (6.53)$$

Now we have the first part $U_0^{(1)}(\mathbf{p}, \mathbf{q})$ of the Nd break-up amplitude as

$$\begin{aligned} U_0^{(1)}(\mathbf{p}, \mathbf{q}) &= \sum_{m'_s \tau'} \left\langle \mathbf{p} m_{s2} m_{s3} \tau_2 \tau_3 \mid T(E_p)(1 - P_{23}) \mid \boldsymbol{\pi} m_{s1}^0 m'_s \tau_1^0 \tau' \right\rangle \\ &\quad \times C\left(\frac{1}{2} \frac{1}{2} 0; \tau' \tau_1\right) C\left(\frac{1}{2} \frac{1}{2} 1; m'_s m_{s1}\right) \\ &\quad \times \sum_l C(l11; M_d - m'_s - m_{s1}, m'_s + m_{s1}) Y_{l, M_d - m'_s - m_{s1}}(\hat{\boldsymbol{\pi}}') \psi_l(\boldsymbol{\pi}') \\ &= \frac{(-)^{\frac{1}{2} + \tau_1}}{\sqrt{2}} \sum_{m'_s} C\left(\frac{1}{2} \frac{1}{2} 1; m'_s m_{s1}\right)_a \langle \tau_2 \tau_3 m_{s2} m_{s3} \mathbf{p} \mid T(E_p) \mid \tau_1^0, -\tau_1 m_{s1}^0 m'_s \boldsymbol{\pi} \rangle_a \\ &\quad \times \sum_l C(l11; M_d - m'_s - m_{s1}, m'_s + m_{s1}) Y_{l, M_d - m'_s - m_{s1}}(\hat{\boldsymbol{\pi}}') \psi_l(\boldsymbol{\pi}'). \quad (6.54) \end{aligned}$$

Here we meet the physical representation ${}_a \langle \tau_2 \tau_3 m_{s2} m_{s3} \mathbf{p} \mid T(E_p) \mid \tau_1^0, -\tau_1 m_{s1}^0 m'_s \boldsymbol{\pi} \rangle_a$ of the NN T-matrix, defined in Eq. (3.75). These T-matrix elements are connected with the ones in the momentum-helicity basis, namely $T_{\Lambda\Lambda'}^{\pi S t}(\mathbf{p}, \boldsymbol{\pi}; E_p)$, as given in Eq. (3.81). Here we rewrite it again, inserting a Kronecker delta to ensure charge conservation.

$$\begin{aligned} &{}_a \langle \tau_2 \tau_3 m_{s2} m_{s3} \mathbf{p} \mid T(E_p) \mid \tau_1^0, -\tau_1 m_{s1}^0 m'_s \boldsymbol{\pi} \rangle_a \\ &= \frac{1}{4} \delta_{\tau_2 + \tau_3, \tau_1^0 - \tau_1} e^{-i(\Lambda_0 \phi_p - \Lambda'_0 \phi_\pi)} \sum_{S \pi t} (1 - \eta_\pi(-)^{S+t}) C\left(\frac{1}{2} \frac{1}{2} t; \tau_2 \tau_3\right) C\left(\frac{1}{2} \frac{1}{2} t; \tau_1^0, -\tau_1\right) \\ &\quad \times C\left(\frac{1}{2} \frac{1}{2} S; m_{s2} m_{s3} \Lambda_0\right) C\left(\frac{1}{2} \frac{1}{2} S; m_{s1}^0 m'_s \Lambda'_0\right) \\ &\quad \times \sum_{\Lambda\Lambda'} d_{\Lambda_0 \Lambda}^S(\theta_p) d_{\Lambda'_0 \Lambda'}^S(\theta_\pi) T_{\Lambda\Lambda'}^{\pi S t}(\mathbf{p}, \boldsymbol{\pi}; E_p). \quad (6.55) \end{aligned}$$

Hence, we obtained $U_0^{(1)}(\mathbf{p}, \mathbf{q})$ expressed in terms of NN T-matrix elements $T_{\Lambda\Lambda'}^{\pi S t}(\mathbf{p}, \boldsymbol{\pi}; E_p)$ in the momentum-helicity basis as

$$\begin{aligned} U_0^{(1)}(\mathbf{p}, \mathbf{q}) &= \frac{(-)^{\frac{1}{2} + \tau_1}}{4\sqrt{2}} \delta_{\tau_2 + \tau_3, \tau_1^0 - \tau_1} \sum_{m'_s} e^{-i(\Lambda_0 \phi_p - \Lambda'_0 \phi_\pi)} C\left(\frac{1}{2} \frac{1}{2} 1; m'_s m_{s1}\right) \\ &\quad \times \sum_l C(l11; M_d - m'_s - m_{s1}, m'_s + m_{s1}) Y_{l, M_d - m'_s - m_{s1}}(\hat{\boldsymbol{\pi}}') \psi_l(\boldsymbol{\pi}') \\ &\quad \times \sum_{S \pi t} (1 - \eta_\pi(-)^{S+t}) C\left(\frac{1}{2} \frac{1}{2} t; \tau_2 \tau_3\right) C\left(\frac{1}{2} \frac{1}{2} t; \tau_1^0, -\tau_1\right) \\ &\quad \times C\left(\frac{1}{2} \frac{1}{2} S; m_{s2} m_{s3} \Lambda_0\right) C\left(\frac{1}{2} \frac{1}{2} S; m_{s1}^0 m'_s \Lambda'_0\right) \\ &\quad \times \sum_{\Lambda\Lambda'} d_{\Lambda_0 \Lambda}^S(\theta_p) d_{\Lambda'_0 \Lambda'}^S(\theta_\pi) T_{\Lambda\Lambda'}^{\pi S t}(\mathbf{p}, \boldsymbol{\pi}; E_p). \quad (6.56) \end{aligned}$$

These NN T-matrix elements $T_{\Lambda\Lambda'}^{\pi S t}(\mathbf{p}, \boldsymbol{\pi}; E_p)$ are not the solution of our final LSE's in Eq. (3.73). The solution of Eq. (3.73) would be $T_{\Lambda\Lambda'}^{\pi S t}(p, \pi, \theta_p; E_p)$, which are T-matrix elements in the momentum-helicity basis with initial momentum in the z-direction and

without its azimuthal dependence. Therefore, $T_{\Lambda\Lambda'}^{\pi St}(\mathbf{p}, \boldsymbol{\pi}; E_p)$ have to be connected to $T_{\Lambda\Lambda'}^{\pi St}(p, \pi, \theta_p; E_p)$. This is done as follows. Let us regard T-matrix elements $T_{\Lambda\Lambda'}^{\pi St}(\mathbf{p}, \mathbf{p}'; E_p)$. We rotate $T_{\Lambda\Lambda'}^{\pi St}(\mathbf{p}, \mathbf{p}'; E_p)$ so that the initial momentum points in the z-direction, i.e. \mathbf{p}' becomes $p'\hat{\mathbf{z}}$:

$$\begin{aligned} T_{\Lambda\Lambda'}^{\pi St}(\mathbf{p}, \mathbf{p}'; E_p) &= \pi^a \langle \mathbf{p}; \hat{\mathbf{p}}S\Lambda; t | T(E_p) | \mathbf{p}'; \hat{\mathbf{p}}'S\Lambda'; t \rangle^{\pi a} \\ &= \pi^a \langle \mathbf{p}; \hat{\mathbf{p}}S\Lambda; t | T(E_p) R(\hat{\mathbf{p}}') | p'\hat{\mathbf{z}}; \hat{\mathbf{z}}S\Lambda'; t \rangle^{\pi a} \\ &= \pi^a \langle \mathbf{p}; \hat{\mathbf{p}}S\Lambda; t | R(\hat{\mathbf{p}}') T(E_p) | p'\hat{\mathbf{z}}; \hat{\mathbf{z}}S\Lambda'; t \rangle^{\pi a} \\ &= \pi^a \langle R^\dagger(\hat{\mathbf{p}}') \mathbf{p}; \hat{\mathbf{p}}S\Lambda; t | T(E_p) | p'\hat{\mathbf{z}}; \hat{\mathbf{z}}S\Lambda'; t \rangle^{\pi a}. \end{aligned} \quad (6.57)$$

The action of $R^\dagger(\hat{\mathbf{p}}')$ on state $|\mathbf{p}; \hat{\mathbf{p}}S\Lambda\rangle$ leads to two successive rotations as

$$R^\dagger(\hat{\mathbf{p}}') |\mathbf{p}; \hat{\mathbf{p}}S\Lambda\rangle = R(0, -\theta', -\phi') R(\phi\theta) |p\hat{\mathbf{z}}; \hat{\mathbf{z}}S\Lambda\rangle. \quad (6.58)$$

This is evaluated in detail in Appendix F. Here we give only the results:

$$\begin{aligned} R^\dagger(\hat{\mathbf{p}}') |\mathbf{p}; \hat{\mathbf{p}}S\Lambda\rangle &= e^{i\Lambda\Omega} R(\phi''\theta''0) |p\hat{\mathbf{z}}; \hat{\mathbf{z}}S\Lambda\rangle \\ &= e^{i\Lambda\Omega} |\mathbf{p}''; \hat{\mathbf{p}}''S\Lambda\rangle, \end{aligned} \quad (6.59)$$

with

$$\cos \theta'' = \cos \theta \cos \theta' + \sin \theta \sin \theta' \cos(\phi - \phi') \quad (6.60)$$

$$\sin \theta'' e^{i\phi''} = -\cos \theta \sin \theta' + \sin \theta \cos \theta' \cos(\phi - \phi') + i \sin \theta \sin(\phi - \phi') \quad (6.61)$$

$$e^{i\Lambda\Omega} = \frac{\sum_{N=-S}^S D_{N\Lambda'}^{S*}(\phi'\theta'0) D_{N\Lambda}^S(\phi\theta0)}{D_{\Lambda'\Lambda}^S(\phi''\theta''0)}. \quad (6.62)$$

Thus,

$$\begin{aligned} T_{\Lambda\Lambda'}^{\pi St}(\mathbf{p}, \mathbf{p}'; E_p) &= e^{-i\Lambda\Omega} \pi^a \langle \mathbf{p}''; \hat{\mathbf{p}}''S\Lambda; t | T(E_p) | p'\hat{\mathbf{z}}; \hat{\mathbf{z}}S\Lambda'; t \rangle^{\pi a} \\ &= e^{-i\Lambda\Omega} T_{\Lambda\Lambda'}^{\pi St}(\mathbf{p}'', p'\hat{\mathbf{z}}; E_p) \\ &= e^{i(\Lambda'\phi'' - \Lambda\Omega)} T_{\Lambda\Lambda'}^{\pi St}(p, p', \cos \theta''; E_p), \end{aligned} \quad (6.63)$$

where in the last equality we have applied the relation in Eq. (3.66). The exponential factor $e^{i(\Lambda'\phi'' - \Lambda\Omega)}$ can be calculated as

$$\begin{aligned} e^{i(\Lambda'\phi'' - \Lambda\Omega)} &= e^{i\Lambda'\phi''} \frac{\sum_{N=-S}^S D_{N\Lambda}^{S*}(\phi\theta0) D_{N\Lambda'}^S(\phi'\theta'0)}{D_{\Lambda'\Lambda}^{S*}(\phi''\theta''0)} \\ &= e^{i\Lambda'\phi''} \frac{\sum_{N=-S}^S e^{iN(\phi-\phi')} d_{N\Lambda}^S(\theta) d_{N\Lambda'}^S(\theta')}{e^{i\Lambda'\phi''} d_{\Lambda'\Lambda}^S(\theta'')} \\ &= \frac{\sum_{N=-S}^S e^{iN(\phi-\phi')} d_{N\Lambda}^S(\theta) d_{N\Lambda'}^S(\theta')}{d_{\Lambda'\Lambda}^S(\theta'')}. \end{aligned} \quad (6.64)$$

By inserting the relation Eq. (6.63) for $T_{\Lambda\Lambda'}^{\pi St}(\mathbf{p}, \boldsymbol{\pi}; E_p)$ into Eq. (6.56) we arrive at our final expression for $U_0^{(1)}(\mathbf{p}, \mathbf{q})$ as

$$\begin{aligned}
U_0^{(1)}(\mathbf{p}, \mathbf{q}) &= \frac{(-)^{\frac{1}{2}+\tau_1}}{4\sqrt{2}} \delta_{\tau_2+\tau_3, \tau_1^0-\tau_1} \sum_{m'_s} e^{-i(\Lambda_0\phi_p - \Lambda'_0\phi_\pi)} C\left(\frac{1}{2}\frac{1}{2}1; m'_s m_{s1}\right) \\
&\times \sum_l C(l11; M_d - m'_s - m_{s1}, m'_s + m_{s1}) Y_{l, M_d - m'_s - m_{s1}}(\hat{\boldsymbol{\pi}}') \psi_l(\pi') \\
&\times \sum_{S\pi t} \left(1 - \eta_\pi(-)^{S+t}\right) C\left(\frac{1}{2}\frac{1}{2}t; \tau_2\tau_3\right) C\left(\frac{1}{2}\frac{1}{2}t; \tau_1^0, -\tau_1\right) \\
&\times C\left(\frac{1}{2}\frac{1}{2}S; m_{s2}m_{s3}\Lambda_0\right) C\left(\frac{1}{2}\frac{1}{2}S; m_{s1}^0 m'_s \Lambda'_0\right) \\
&\times \sum_{\Lambda\Lambda'} d_{\Lambda_0\Lambda}^S(\theta_p) d_{\Lambda'_0\Lambda'}^S(\theta_\pi) e^{i(\Lambda'\phi' - \Lambda\Omega)} T_{\Lambda\Lambda'}^{\pi St}(p, \pi, \cos\theta'; E_p), \tag{6.65}
\end{aligned}$$

with

$$\cos\theta' = \cos\theta_p \cos\theta_\pi + \sin\theta_p \sin\theta_\pi \cos(\phi_p - \phi_\pi) \tag{6.66}$$

$$e^{i(\Lambda'\phi' - \Lambda\Omega)} = \frac{\sum_{N=-S}^S e^{iN(\phi_p - \phi_\pi)} d_{N\Lambda}^S(\theta_p) d_{N\Lambda'}^S(\theta_\pi)}{d_{\Lambda'\Lambda}^S(\theta')}. \tag{6.67}$$

6.3 Relativistic Kinematics

In this section we introduce relativistic kinematics into the formulation given in the previous sections. Thus, we reevaluate the maximum value $k_{1,max}$ of magnitude of the nucleon's outgoing momentum and the Jacobi momenta \mathbf{p} and \mathbf{q} . We derive S-matrix elements for the break-up process and the spin averaged differential cross section. We adopt a formulation in Ref. [51], which is given for an arbitrary two-particle system. Note that in this section energy means relativistic energy, i.e. $E = \sqrt{m^2 + k^2}$, however, we do not use a 4-vector notation. Thus, here k is the magnitude of a 3-vector \mathbf{k} . This is in contrast to Ref. [51], where k is a 4-vector and \mathbf{k} is its 3-vector component.

6.3.1 Maximum of Magnitude of Nucleon's Outgoing Momentum

Conservations of total energy and total momentum for the Nd break-up process are given by

$$m_d + E_{lab} = E_1 + E_2 + E_3 \equiv E_1 + E_{23} \tag{6.68}$$

$$\mathbf{k}_{lab} = \mathbf{k}_1 + \mathbf{k}_2 + \mathbf{k}_3 \equiv \mathbf{k}_1 + \mathbf{k}_{23}, \tag{6.69}$$

where m_d is the deuteron rest mass and E_i ($i = lab, 1, 2, 3$) relativistic energies corresponding to \mathbf{k}_i ($i = lab, 1, 2, 3$). In Eqs. (6.68) and (6.69) we define E_{23} as total

energy and \mathbf{k}_{23} as total momentum of the 23-subsystem in the laboratory frame. The quantities E_{23} and \mathbf{k}_{23} are connected by

$$E_{23}^2 - \mathbf{k}_{23}^2 \equiv M_{23}^2 \geq 4m^2, \quad (6.70)$$

which is Lorentz invariant. Here M_{23} is called the invariant mass of the 23-subsystem, equal to the total energy of the 23-subsystem in its c.m. frame. The minimal value of M_{23} is $2m$, where the two nucleons are at rest in the c.m. frame of the 23-subsystem. Together these three equations (6.68), (6.69) and (6.70) determine the maximum value $k_{1,max}$ of the magnitude of the nucleon's outgoing momentum as shown in the following.

Inserting Eqs. (6.68) and (6.69) into Eq. (6.70) leads to

$$\begin{aligned} (E_{lab} + m_d - E_1)^2 - (\mathbf{k}_{lab} - \mathbf{k}_1)^2 &\geq 4m^2 \\ (E_{lab} + m_d)^2 + E_1^2 - 2(E_{lab} + m_d)E_1 \\ &\quad - k_{lab}^2 - k_1^2 + 2k_{lab}k_1 \cos \theta_{lab} \geq 4m^2 \\ (E_{lab} + m_d)^2 + m^2 - 2(E_{lab} + m_d)\sqrt{m^2 + k_1^2} \\ &\quad - k_{lab}^2 + 2k_{lab}k_1 \cos \theta_{lab} \geq 4m^2 \\ (E_{lab} + m_d)^2 - 3m^2 - k_{lab}^2 + 2k_{lab}k_1 \cos \theta_{lab} &\geq 2(E_{lab} + m_d)\sqrt{m^2 + k_1^2} \\ \{(E_{lab} + m_d)^2 - 3m^2 - k_{lab}^2\}^2 + 4k_{lab}^2 k_1^2 \cos^2 \theta_{lab} \\ + 4k_{lab}k_1 \cos \theta_{lab} \{(E_{lab} + m_d)^2 - 3m^2 - k_{lab}^2\} &\geq 4(E_{lab} + m_d)^2 (m^2 + k_1^2) \\ 4\{k_{lab}^2 \cos^2 \theta_{lab} - (E_{lab} + m_d)^2\} k_1^2 \\ + 4k_{lab} \cos \theta_{lab} \{(E_{lab} + m_d)^2 - 3m^2 - k_{lab}^2\} k_1 \\ + \{(E_{lab} + m_d)^2 - 3m^2 - k_{lab}^2\}^2 - 4(E_{lab} + m_d)^2 m^2 &\geq 0. \end{aligned} \quad (6.71)$$

This is a quadratic equations in k_1

$$Ak_1^2 + Bk_1 + C \geq 0, \quad (6.72)$$

with

$$A = 4\{k_{lab}^2 \cos^2 \theta_{lab} - (E_{lab} + m_d)^2\} < 0 \quad (6.73)$$

$$B = 4k_{lab} \cos \theta_{lab} \{(E_{lab} + m_d)^2 - 3m^2 - k_{lab}^2\} \quad (6.74)$$

$$C = \{(E_{lab} + m_d)^2 - 3m^2 - k_{lab}^2\}^2 - 4(E_{lab} + m_d)^2 m^2 > 0. \quad (6.75)$$

Equation (6.72) is sketched in Fig. 6.2. Thus, $k_{1,max}$ occurs where Eq. (6.72) equals zero and is obtained as

$$k_{1,max} = \frac{-B - \sqrt{B^2 - 4AC}}{2A}. \quad (6.76)$$

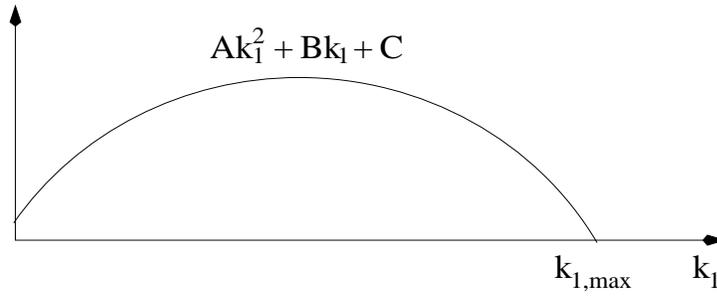


Figure 6.2: A sketch of Eq. (6.72).

6.3.2 Jacobi Momenta

A system described by (E, \mathbf{k}) in one frame can be described in other frame by (E', \mathbf{k}') by means of a Lorentz transformation $L(\mathbf{v})$, where \mathbf{v} is the relative velocity of the new frame to the old frame. Thus [51],

$$(E', \mathbf{k}') \equiv L(\mathbf{v})(E, \mathbf{k}), \quad (6.77)$$

where

$$\mathbf{k}' = \mathbf{k} + (\gamma - 1)(\mathbf{k} \cdot \hat{\mathbf{v}})\hat{\mathbf{v}} - \gamma E \mathbf{v} \quad (6.78)$$

$$E' = \gamma(E - \mathbf{k} \cdot \mathbf{v}) \quad (6.79)$$

$$\gamma \equiv \frac{1}{\sqrt{1 - v^2}}. \quad (6.80)$$

Using Eqs. (6.77)-(6.80) with the appropriate velocity $\mathbf{v} = \mathbf{u}$ we can transform our 3N system from the laboratory frame to the c.m. frame and find the corresponding Jacobi momenta \mathbf{p} and \mathbf{q} .

First we take the 23-subsystem and derive \mathbf{p} . We bring the 23-subsystem from the laboratory frame to its c.m. frame (the 23-frame) by the following Lorentz transformation

$$\mathbf{u} = \frac{\mathbf{k}_{23}}{E_{23}} \quad (6.81)$$

$$(E'_2, \mathbf{p}) \equiv (E'_2, \mathbf{k}'_2) = L(\mathbf{u})(E_2, \mathbf{k}_2) \quad (6.82)$$

$$(E'_2, -\mathbf{p}) \equiv (E'_3, \mathbf{k}'_3) = L(\mathbf{u})(E_3, \mathbf{k}_3). \quad (6.83)$$

Here \mathbf{k}'_i and E'_i ($i = 2, 3$) are momenta and energies of nucleons 2 and 3 in the 23-frame. According to Eq. (6.78) the Jacobi momentum \mathbf{p} , defined by the transformation given in Eqs. (6.82)-(6.83), is given by the following two equations

$$\begin{aligned} \mathbf{p} &= \mathbf{k}_2 + \frac{\mathbf{k}_{23}}{M_{23}} \frac{(E_{23} - M_{23})}{k_{23}^2} (\mathbf{k}_2 \cdot \mathbf{k}_{23}) - \frac{\mathbf{k}_{23}}{M_{23}} E_2 \\ &= \mathbf{k}_2 + \frac{\mathbf{k}_{23}}{M_{23}} \left(\frac{\mathbf{k}_2 \cdot \mathbf{k}_{23}}{E_{23} + M_{23}} - E_2 \right) \end{aligned} \quad (6.84)$$

$$\begin{aligned}
-\mathbf{p} &= \mathbf{k}_3 + \frac{\mathbf{k}_{23}}{M_{23}} \frac{(E_{23} - M_{23})}{k_{23}^2} (\mathbf{k}_3 \cdot \mathbf{k}_{23}) - \frac{\mathbf{k}_{23}}{M_{23}} E_3 \\
&= \mathbf{k}_3 + \frac{\mathbf{k}_{23}}{M_{23}} \left(\frac{\mathbf{k}_3 \cdot \mathbf{k}_{23}}{E_{23} + M_{23}} - E_3 \right), \tag{6.85}
\end{aligned}$$

where we have used

$$\gamma = \frac{1}{\sqrt{1 - \left(\frac{\mathbf{k}_{23}}{E_{23}}\right)^2}} = \frac{E_{23}}{M_{23}}. \tag{6.86}$$

Instead of two expressions defining \mathbf{p} we want to have one expression as a combination of Eqs. (6.84) and (6.85). Subtracting Eq. (6.85) from Eq. (6.84) leads to

$$\mathbf{p} = \frac{1}{2}(\mathbf{k}_2 - \mathbf{k}_3) + \frac{\mathbf{k}_{23}}{2M_{23}} \left(\frac{(\mathbf{k}_2 - \mathbf{k}_3) \cdot \mathbf{k}_{23}}{E_{23} + M_{23}} - (E_2 - E_3) \right). \tag{6.87}$$

Next using

$$(\mathbf{k}_2 - \mathbf{k}_3) \cdot \mathbf{k}_{23} = k_2^2 - k_3^2 = E_2^2 - E_3^2 = (E_2 - E_3)E_{23} \tag{6.88}$$

we get the final expression for \mathbf{p} as

$$\begin{aligned}
\mathbf{p} &= \frac{1}{2}(\mathbf{k}_2 - \mathbf{k}_3) + \frac{(E_2 - E_3)\mathbf{k}_{23}}{2M_{23}} \left(\frac{E_{23}}{E_{23} + M_{23}} - 1 \right) \\
&= \frac{1}{2}(\mathbf{k}_2 - \mathbf{k}_3) - \frac{1}{2}\mathbf{k}_{23} \left(\frac{E_2 - E_3}{E_{23} + M_{23}} \right). \tag{6.89}
\end{aligned}$$

Thus, \mathbf{p} in Eq. (6.89) consists of a nonrelativistic part (the first term) and a relativistic correction (the second term), which nonrelativistically vanishes ($E_2 = E_3 \simeq m$).

The energies E'_2 and E'_3 are given as

$$E'_2 = \sqrt{m^2 + k_2'^2} = \sqrt{m^2 + p^2} = \sqrt{m^2 + k_3'^2} = E'_3. \tag{6.90}$$

We obtain the total energy M_{23} in the 23-frame as

$$M_{23} = E'_2 + E'_3 = 2E'_2 = 2\sqrt{m^2 + p^2}. \tag{6.91}$$

Using Eqs. (6.91) and (6.68)-(6.70) the magnitude of \mathbf{p} can be calculated as

$$\begin{aligned}
p &= \sqrt{\frac{M_{23}^2}{4} - m^2} \\
&= \sqrt{\frac{1}{4}(E_{23}^2 - k_{23}^2) - m^2} \\
&= \sqrt{\frac{1}{4}\{(E_{lab} + m_d - E_1)^2 - (\mathbf{k}_{lab} - \mathbf{k}_1)^2\} - m^2} \\
&= \sqrt{\frac{1}{4}\{E_{lab}^2 + m_d^2 + E_1^2 + 2m_d(E_{lab} - E_1) - 2E_{lab}E_1 - k_{lab}^2 - k_1^2 + 2k_{lab}k_1 \cos \theta_{lab}\} - m^2} \\
&= \frac{1}{2}\sqrt{m_d^2 - 2m^2 + 2m_d(E_{lab} - E_1) - 2E_{lab}E_1 + 2k_{lab}k_1 \cos \theta_{lab}}. \tag{6.92}
\end{aligned}$$

Here we would like to give some remarks. Since we consider the inclusive Nd break-up process, we sum over all directions of \mathbf{p} , which are independent of the kinematics (E_1, \mathbf{k}_1) of the single detected nucleon. Therefore, a vectorial expression of \mathbf{p} , such as the one in Eq. (6.89), is not required. It is the expression given in Eq. (6.92) for the magnitude of \mathbf{p} , which is needed. We have nevertheless worked out Eq. (6.89) to complete the presentation.

Now we derive the Jacobi momentum \mathbf{q} in a similar way as we derived \mathbf{p} . First we define some notation, namely \mathbf{k}'_1 and E'_1 be the momentum and the energy of nucleon 1 in the c.m. frame, \mathbf{k}'_{23} and E'_{23} the momentum and the energy of the 23-subsystem in the c.m. frame. E_0 is the total energy in the laboratory frame given by

$$E_0 \equiv m_d + E_{lab} = E_1 + E_{23}. \quad (6.93)$$

Here we also define M_0 as the total energy in the c.m. frame or the invariant mass of the system

$$M_0 \equiv E'_1 + E'_{23}, \quad (6.94)$$

which is connected to the total energy E_0 and the total momentum \mathbf{k}_{lab} in the laboratory frame as given by the following Lorentz invariant relation

$$E_0^2 - \mathbf{k}_{lab}^2 = M_0^2 \geq 9m^2. \quad (6.95)$$

Thus, with given E_0 and \mathbf{k}_{lab} one can calculate M_0 as given by

$$\begin{aligned} M_0 &= \sqrt{E_0^2 - k_{lab}^2} \\ &= \sqrt{(m_d + E_{lab})^2 - k_{lab}^2} \\ &= \sqrt{m^2 + m_d^2 + 2m_d E_{lab}}, \end{aligned} \quad (6.96)$$

which is conserved.

To bring the system from the laboratory frame to the c.m. frame we apply the following Lorentz transformation

$$\mathbf{u} = \frac{\mathbf{k}_{lab}}{E_0} \quad (6.97)$$

$$(E'_1, \mathbf{q}) \equiv (E'_1, \mathbf{k}'_1) = L(\mathbf{u})(E_1, \mathbf{k}_1) \quad (6.97)$$

$$(E'_{23}, -\mathbf{q}) \equiv (E'_{23}, \mathbf{k}'_{23}) = L(\mathbf{u})(E_{23}, \mathbf{k}_{23}), \quad (6.98)$$

with the corresponding γ factor

$$\gamma = \frac{1}{\sqrt{1 - \left(\frac{\mathbf{k}_{lab}}{E_0}\right)^2}} = \frac{E_0}{M_0}. \quad (6.99)$$

The Jacobi momentum \mathbf{q} is given by two equations

$$\begin{aligned}\mathbf{q} &= \mathbf{k}_1 + \frac{\mathbf{k}_{lab}}{M_0} \frac{(E_0 - M_0)}{k_{lab}^2} (\mathbf{k}_1 \cdot \mathbf{k}_{lab}) - \frac{\mathbf{k}_{lab}}{M_0} E_1 \\ &= \mathbf{k}_1 + \frac{\mathbf{k}_{lab}}{M_0} \left(\frac{\mathbf{k}_1 \cdot \mathbf{k}_{lab}}{E_0 + M_0} - E_1 \right)\end{aligned}\quad (6.100)$$

$$\begin{aligned}-\mathbf{q} &= \mathbf{k}_{23} + \frac{\mathbf{k}_{lab}}{M_0} \frac{(E_0 - M_0)}{k_{lab}^2} (\mathbf{k}_{23} \cdot \mathbf{k}_{lab}) - \frac{\mathbf{k}_{lab}}{M_0} E_{23} \\ &= \mathbf{k}_{23} + \frac{\mathbf{k}_{lab}}{M_0} \left(\frac{\mathbf{k}_{23} \cdot \mathbf{k}_{lab}}{E_0 + M_0} - E_{23} \right)\end{aligned}\quad (6.101)$$

and the energies E'_1 , E'_{23} and M_0 in the c.m. frame are given in terms of the magnitudes of Jacobi momenta \mathbf{p} and \mathbf{q} as

$$E'_1 = \sqrt{m^2 + k_1'^2} = \sqrt{m^2 + q^2} \quad (6.102)$$

$$E'_{23} = \sqrt{M_{23}^2 + k_{23}'^2} = \sqrt{4(m^2 + p^2) + q^2} \quad (6.103)$$

$$M_0 = E'_1 + E'_{23} = \sqrt{m^2 + q^2} + \sqrt{4(m^2 + p^2) + q^2}. \quad (6.104)$$

As in case of \mathbf{p} , we want to have one expression for \mathbf{q} as a combination of Eqs. (6.100) and (6.101). Here a vectorial expression of \mathbf{q} is needed, since \mathbf{q} depends on the kinematics (E_1, \mathbf{k}_1) of the detected nucleon.

Subtracting Eq. (6.101) from Eq. (6.100) leads to

$$\mathbf{q} = \frac{1}{2}(\mathbf{k}_1 - \mathbf{k}_{23}) + \frac{\mathbf{k}_{lab}}{2M_0} \left(\frac{(\mathbf{k}_1 - \mathbf{k}_{23}) \cdot \mathbf{k}_{lab}}{E_0 + M_0} - (E_1 - E_{23}) \right). \quad (6.105)$$

Using Eqs. (6.93)-(6.95) and (6.102)-(6.104) we get

$$\begin{aligned}(\mathbf{k}_1 - \mathbf{k}_{23}) \cdot \mathbf{k}_{lab} &= k_1^2 - k_{23}^2 \\ &= E_1^2 - E_{23}^2 - m^2 + M_{23}^2 \\ &= (E_1 - E_{23})E_0 - \{m^2 + q^2 - (M_{23}^2 + q^2)\} \\ &= (E_1 - E_{23})E_0 - (E_1'^2 - E_{23}'^2) \\ &= (E_1 - E_{23})E_0 - (E_1' - E_{23}')M_0.\end{aligned}\quad (6.106)$$

We insert Eq. (6.106) into Eq. (6.105) and obtain the final expression for \mathbf{q} as

$$\begin{aligned}\mathbf{q} &= \frac{1}{2}(\mathbf{k}_1 - \mathbf{k}_{23}) + \frac{\mathbf{k}_{lab}}{2M_0} \left(\frac{(E_1 - E_{23})E_0 - (E_1' - E_{23}')M_0}{E_0 + M_0} - (E_1 - E_{23}) \right) \\ &= \frac{1}{2}(\mathbf{k}_1 - \mathbf{k}_{23}) + \frac{(E_1 - E_{23})\mathbf{k}_{lab}}{2M_0} \left(\frac{E_0}{E_0 + M_0} - 1 \right) - \frac{1}{2}\mathbf{k}_{lab} \frac{(E_1' - E_{23}')}{(E_0 + M_0)} \\ &= \frac{1}{2}(\mathbf{k}_1 - \mathbf{k}_{23}) - \frac{1}{2}\mathbf{k}_{lab} \left(\frac{E_1 - E_{23} + E_1' - E_{23}'}{E_0 + M_0} \right) \\ &= \mathbf{k}_1 - \mathbf{k}_{lab} \left(\frac{E_1 + E_1'}{E_0 + M_0} \right).\end{aligned}\quad (6.107)$$

In the last equality we have applied total momentum conservation given in Eq. (6.69).

The magnitude of \mathbf{q} is calculated using Eq. (6.104) as follows:

$$\begin{aligned}
M_0^2 &= \left\{ \sqrt{m^2 + q^2} + \sqrt{4(m^2 + p^2) + q^2} \right\}^2 \\
&= 5m^2 + 4p^2 + 2q^2 \\
&\quad + 2\sqrt{4m^2(m^2 + p^2) + (5m^2 + 4p^2)q^2 + q^4} \\
M_0^2 - (5m^2 + 4p^2) - 2q^2 &= 2\sqrt{4m^2(m^2 + p^2) + (5m^2 + 4p^2)q^2 + q^4} \\
\left\{ M_0^2 - (5m^2 + 4p^2) \right\}^2 + 4q^4 & \\
-4 \left\{ M_0^2 - (5m^2 + 4p^2) \right\} q^2 &= 4 \left\{ 4m^2(m^2 + p^2) + (5m^2 + 4p^2)q^2 + q^4 \right\} \\
\left\{ M_0^2 - (5m^2 + 4p^2) \right\}^2 - 4M_0^2 q^2 &= 16m^2(m^2 + p^2). \tag{6.108}
\end{aligned}$$

Thus,

$$q = \frac{1}{2M_0} \sqrt{\left\{ M_0^2 - (5m^2 + 4p^2) \right\}^2 - 16m^2(m^2 + p^2)}, \tag{6.109}$$

where M_0 is given in Eq. (6.96). Equation (6.109) also shows the relation between q and p , if relativity is taken into account.

Now let us consider the initial situation and find out the Jacobi momentum \mathbf{q}_0 , the energies E'_{lab} of the incoming nucleon and E'_d of the deuteron in the c.m. frame. Replacing in Eq. (6.105) \mathbf{k}_1 with \mathbf{k}_{lab} , E_1 with E_{lab} , \mathbf{k}_{23} with zero and E_{23} with m_d the Jacobi momentum \mathbf{q}_0 is given as

$$\begin{aligned}
\mathbf{q}_0 &= \frac{1}{2}\mathbf{k}_{lab} + \frac{\mathbf{k}_{lab}}{2M_0} \left(\frac{k_{lab}^2}{E_0 + M_0} - (E_{lab} - m_d) \right) \\
&= \frac{1}{2}\mathbf{k}_{lab} + \frac{\mathbf{k}_{lab}}{2M_0} \left(\frac{E_0^2 - M_0^2}{E_0 + M_0} - (E_{lab} - m_d) \right) \\
&= \frac{1}{2}\mathbf{k}_{lab} + \frac{\mathbf{k}_{lab}}{2M_0} (E_0 - M_0 - (E_{lab} - m_d)) \\
&= \frac{1}{2}\mathbf{k}_{lab} + \frac{\mathbf{k}_{lab}}{2M_0} (2m_d - M_0) \\
&= \frac{m_d}{M_0} \mathbf{k}_{lab}. \tag{6.110}
\end{aligned}$$

Using Eq. (6.79) E'_{lab} and E'_d are given as

$$\begin{aligned}
E'_{lab} &= \frac{E_0}{M_0} (E_{lab} - \frac{k_{lab}^2}{E_0}) \\
&= \frac{1}{M_0} (E_{lab}^2 + m_d E_{lab} - k_{lab}^2) \\
&= \frac{1}{M_0} (m^2 + m_d E_{lab}) \tag{6.111}
\end{aligned}$$

$$\begin{aligned}
E'_d &= \frac{E_0}{M_0} m_d \\
&= \frac{1}{M_0} (E_{lab} + m_d) m_d. \tag{6.112}
\end{aligned}$$

Hence, E'_{lab} and E'_d sum up to $M_0 = E'_1 + E'_{23}$ as required by total energy conservation in the c.m. frame.

6.3.3 S-Matrix and Cross Section

Here we derive S-matrix elements in the lab frame by using relativistic kinematics and connect with the Nd break-up amplitude. We neglect the boost effects on the magnetic spin quantum numbers, in other words we do not take Wigner rotation into account. From the S-matrix elements we derive the spin averaged differential cross section by using the standard relativistic time-dependent scattering theory.

Suppressing all discrete quantum numbers we define S-matrix elements in the laboratory frame as

$$S(\mathbf{k}_1, \mathbf{k}_2, \mathbf{k}_3) \equiv \langle \mathbf{k}_1 \mathbf{k}_2 \mathbf{k}_3 | S | \mathbf{k}_{lab} \mathbf{k}_d \rangle \quad (6.113)$$

and in the c.m. frame as

$$S(\mathbf{p}, \mathbf{q}) \equiv \langle \mathbf{p} \mathbf{q} | S | \mathbf{q}_0 \rangle \equiv \langle \mathbf{p} \mathbf{q} | S | \mathbf{q}_0 \rangle. \quad (6.114)$$

One has to bear in mind that there is the deuteron state $|\Psi_d\rangle$ in the initial state in the c.m. frame, which is here suppressed. The deuteron laboratory momentum \mathbf{k}_d is given for clarity though it has a value of zero. In Eq. (6.114) \mathbf{p} , \mathbf{q} , \mathbf{q}_0 are the Jacobi momenta given in Eqs. (6.89), (6.107), (6.110), respectively. The state $|\mathbf{k}_1 \mathbf{k}_2 \mathbf{k}_3\rangle$ is related to $|\mathbf{p} \mathbf{q}\rangle$, and the state $|\mathbf{k}_{lab} \mathbf{k}_d\rangle$ to $|\mathbf{q}_0\rangle$, as

$$\begin{aligned} |\mathbf{k}_1 \mathbf{k}_2 \mathbf{k}_3\rangle &\equiv |\mathbf{k}_1\rangle |\mathbf{k}_2 \mathbf{k}_3\rangle \\ &= J^{-\frac{1}{2}}(\mathbf{k}_2, \mathbf{k}_3) |\mathbf{k}_1\rangle |\mathbf{p} \mathbf{k}_{23}\rangle \\ &= J^{-\frac{1}{2}}(\mathbf{k}_2, \mathbf{k}_3) J^{-\frac{1}{2}}(\mathbf{k}_1, \mathbf{k}_{23}) |\mathbf{p} \mathbf{q}(\mathbf{k}_1 + \mathbf{k}_{23})\rangle \\ &\equiv J^{-\frac{1}{2}}(\mathbf{k}_2, \mathbf{k}_3) J^{-\frac{1}{2}}(\mathbf{k}_1, \mathbf{k}_{23}) |\mathbf{p} \mathbf{q}\rangle |\mathbf{k}_1 + \mathbf{k}_{23}\rangle \end{aligned} \quad (6.115)$$

$$\begin{aligned} |\mathbf{k}_{lab} \mathbf{k}_d\rangle &= J^{-\frac{1}{2}}(\mathbf{k}_{lab}, \mathbf{k}_d) |\mathbf{q}_0 \mathbf{k}_{lab}\rangle \\ &\equiv J^{-\frac{1}{2}}(\mathbf{k}_{lab}, \mathbf{k}_d) |\mathbf{q}_0\rangle |\mathbf{k}_{lab}\rangle. \end{aligned} \quad (6.116)$$

The Jacobian $J(\mathbf{k}_2, \mathbf{k}_3)$ of the transformation in Eq. (6.115) from variables $(\mathbf{k}_2, \mathbf{k}_3)$ to $(\mathbf{p}, \mathbf{k}_{23})$ is given as [51]

$$J(\mathbf{k}_2, \mathbf{k}_3) = \left| \frac{\partial(\mathbf{k}_2, \mathbf{k}_3)}{\partial(\mathbf{p}, \mathbf{k}_{23})} \right| = \frac{E_2 E_3}{E_{23}} \frac{M_{23}}{E'_2 E'_3} = \frac{4E_2 E_3}{E_{23} M_{23}}, \quad (6.117)$$

where the last equality results by means of Eq. (6.91) for M_{23} . Similarly, the Jacobians $J(\mathbf{k}_1, \mathbf{k}_{23})$ in Eq. (6.115) and $J(\mathbf{k}_{lab}, \mathbf{k}_d)$ in Eq. (6.116) are given as

$$J(\mathbf{k}_1, \mathbf{k}_{23}) = \left| \frac{\partial(\mathbf{k}_1, \mathbf{k}_{23})}{\partial(\mathbf{q}, \mathbf{k}_1 + \mathbf{k}_{23})} \right| = \frac{E_1 E_{23}}{E_0} \frac{M_0}{E'_1 E'_{23}} \quad (6.118)$$

$$J(\mathbf{k}_{lab}, \mathbf{k}_d) = \left| \frac{\partial(\mathbf{k}_{lab}, \mathbf{k}_d)}{\partial(\mathbf{q}_0, \mathbf{k}_{lab})} \right| = \frac{E_{lab} m_d}{E_0} \frac{M_0}{E'_{lab} E'_d}. \quad (6.119)$$

One therefore arrives at the relation between $S(\mathbf{k}_1, \mathbf{k}_2, \mathbf{k}_3)$ and $S(\mathbf{p}, \mathbf{q})$ as

$$\begin{aligned} S(\mathbf{k}_1, \mathbf{k}_2, \mathbf{k}_3) &= \langle \mathbf{k}_1 \mathbf{k}_2 \mathbf{k}_3 | S | \mathbf{k}_{lab} \mathbf{k}_d \rangle \\ &= J^{-\frac{1}{2}}(\mathbf{k}_2, \mathbf{k}_3) J^{-\frac{1}{2}}(\mathbf{k}_1, \mathbf{k}_{23}) J^{-\frac{1}{2}}(\mathbf{k}_{lab}, \mathbf{k}_d) \langle \mathbf{k}_1 + \mathbf{k}_{23} | \langle \mathbf{p} \mathbf{q} | S | \mathbf{q}_0 \rangle | \mathbf{k}_{lab} \rangle \\ &= \delta(\mathbf{k}_1 + \mathbf{k}_{23} - \mathbf{k}_{lab}) \{ J(\mathbf{k}_2, \mathbf{k}_3) J(\mathbf{k}_1, \mathbf{k}_{23}) J(\mathbf{k}_{lab}, \mathbf{k}_d) \}^{-\frac{1}{2}} S(\mathbf{p}, \mathbf{q}) \end{aligned} \quad (6.120)$$

where the delta function ensures total momentum conservation.

We proceed to connect $S(\mathbf{k}_1, \mathbf{k}_2, \mathbf{k}_3)$ with the amplitude $U_0(\mathbf{p}, \mathbf{q})$, defined in Eq. (6.18). In fact $U_0(\mathbf{p}, \mathbf{q})$ is the T-matrix element for the Nd break-up process, which is related to $S(\mathbf{p}, \mathbf{q})$ as given in Eq. (2.5), but without the first term. Thus,

$$S(\mathbf{p}, \mathbf{q}) = -2\pi i \delta(E'_1 + E'_{23} - E'_{lab} - E'_d) U_0(\mathbf{p}, \mathbf{q}). \quad (6.121)$$

Inserting Eq. (6.121) into Eq. (6.120) leads to

$$\begin{aligned} S(\mathbf{k}_1, \mathbf{k}_2, \mathbf{k}_3) &= -2\pi i \delta(\mathbf{k}_1 + \mathbf{k}_{23} - \mathbf{k}_{lab}) \delta(E'_1 + E'_{23} - E'_{lab} - E'_d) \\ &\quad \times \{ J(\mathbf{k}_2, \mathbf{k}_3) J(\mathbf{k}_1, \mathbf{k}_{23}) J(\mathbf{k}_{lab}, \mathbf{k}_d) \}^{-\frac{1}{2}} U_0(\mathbf{p}, \mathbf{q}). \end{aligned} \quad (6.122)$$

Next we insert into Eq. (6.122) the identity¹

$$\begin{aligned} &\delta(\mathbf{k}_1 + \mathbf{k}_{23} - \mathbf{k}_{lab}) \delta(E'_1 + E'_{23} - E'_{lab} - E'_d) \\ &= \delta(\mathbf{k}_1 + \mathbf{k}_{23} - \mathbf{k}_{lab}) \delta(E_1 + E_{23} - E_{lab} - m_d) \\ &\quad \times \frac{E'_1 + E'_{23} + E'_{lab} + E'_d}{E_1 + E_{23} + E_{lab} + m_d}, \end{aligned} \quad (6.123)$$

¹The identity in Eq. (6.123) can be proven as follows. Take E' and E as total energies in the laboratory frame, \mathbf{K}' and \mathbf{K} the corresponding total momenta, M' and M total energies in the c.m. frame, related as

$$E'^2 - \mathbf{K}'^2 = M'^2 \quad E^2 - \mathbf{K}^2 = M^2.$$

The energies E' , E , M' and M are required to be positive. Hence, $\delta(M'^2 - M^2)$ can be evaluated as

$$\delta(M'^2 - M^2) = \delta((M' - M)(M' + M)) = \frac{\delta(M' - M)}{M' + M} + \frac{\delta(M' + M)}{|M' - M|} = \frac{\delta(M' - M)}{M' + M},$$

and similarly

$$\delta(E'^2 - E^2) = \frac{\delta(E' - E)}{E' + E}.$$

Using $\delta(\mathbf{K}' - \mathbf{K})$ to fix the momenta to be $\mathbf{K}' = \mathbf{K}$ one obtains

$$\begin{aligned} \delta(\mathbf{K}' - \mathbf{K}) \delta(M' - M) &= \delta(\mathbf{K}' - \mathbf{K}) \delta(M'^2 - M^2) (M' + M) \\ &= \delta(\mathbf{K}' - \mathbf{K}) \delta(E'^2 - \mathbf{K}'^2 - (E^2 - \mathbf{K}^2)) (M' + M) \\ &= \delta(\mathbf{K}' - \mathbf{K}) \delta(E'^2 - E^2) (M' + M) \\ &= \delta(\mathbf{K}' - \mathbf{K}) \delta(E' - E) \frac{M' + M}{E' + E}, \end{aligned}$$

which proves the identity given in Eq. (6.123).

and this gives

$$\begin{aligned}
S(\mathbf{k}_1, \mathbf{k}_2, \mathbf{k}_3) &= -2\pi i \delta(\mathbf{k}_1 + \mathbf{k}_{23} - \mathbf{k}_{lab}) \delta(E_1 + E_{23} - E_{lab} - m_d) \\
&\quad \times \frac{E'_1 + E'_{23} + E'_{lab} + E'_d}{E_1 + E_{23} + E_{lab} + m_d} \\
&\quad \times \{J(\mathbf{k}_2, \mathbf{k}_3)J(\mathbf{k}_1, \mathbf{k}_{23})J(\mathbf{k}_{lab}, \mathbf{k}_d)\}^{-\frac{1}{2}} U_0(\mathbf{p}, \mathbf{q}). \tag{6.124}
\end{aligned}$$

As the final step to simplify the expression we define a function $\Gamma(\mathbf{p}, \mathbf{q})$ as

$$\begin{aligned}
\Gamma(\mathbf{p}, \mathbf{q}) &\equiv \frac{E'_1 + E'_{23} + E'_{lab} + E'_d}{E_1 + E_{23} + E_{lab} + m_d} \{J(\mathbf{k}_2, \mathbf{k}_3)J(\mathbf{k}_1, \mathbf{k}_{23})J(\mathbf{k}_{lab}, \mathbf{k}_d)\}^{-\frac{1}{2}} \\
&= \frac{2M_0}{2E_0} \left(\frac{4E_2E_3}{E_{23}M_{23}} \frac{E_1E_{23}}{E_0} \frac{M_0}{E'_1E'_{23}} \frac{E_{lab}m_d}{E_0} \frac{M_0}{E'_{lab}E'_d} \right)^{-\frac{1}{2}} \\
&= \sqrt{\frac{M_{23}E'_1E'_{23}E'_{lab}E'_d}{4E_1E_2E_3E_{lab}m_d}}, \tag{6.125}
\end{aligned}$$

and thus obtain the relation between $S(\mathbf{k}_1, \mathbf{k}_2, \mathbf{k}_3)$ and $U_0(\mathbf{p}, \mathbf{q})$ as

$$S(\mathbf{k}_1, \mathbf{k}_2, \mathbf{k}_3) = -2\pi i \delta(\mathbf{k}_1 + \mathbf{k}_{23} - \mathbf{k}_{lab}) \delta(E_1 + E_{23} - E_{lab} - m_d) \Gamma(\mathbf{p}, \mathbf{q}) U_0(\mathbf{p}, \mathbf{q}). \tag{6.126}$$

At this point let us return to $U_0(\mathbf{p}, \mathbf{q})$, which has been derived in Section 6.2 nonrelativistically. To achieve more consistency with the relativistic kinematics being introduced, the amplitude $U_0(\mathbf{p}, \mathbf{q})$ is calculated using relativistic values of its kinematics variables. These variables are the Jacobi momenta \mathbf{p} , \mathbf{q} , \mathbf{q}_0 and the energy, for which the NN T-matrix elements are calculated. This is the kinetic energy in the 23-subsystem. Take for example $U_0^{(1)}(\mathbf{p}, \mathbf{q})$, given in Eq. (6.65). The Jacobi momenta \mathbf{p} , \mathbf{q} , \mathbf{q}_0 are given in Eqs. (6.89), (6.107), (6.110), respectively. The energy E_p , for which $T_{\Lambda\Lambda'}^{\pi St}(p, \pi, \cos \theta'; E_p)$ is calculated, is given as

$$E_p = M_{23} - 2m = 2\sqrt{m^2 + p^2} - 2m, \tag{6.127}$$

different from the nonrelativistic one, given in Eq. (6.48). In Eq. (6.127) $2m$ is the rest mass of the 23-subsystem, thus, E_p is the kinetic energy in the 23-subsystem.

Now we derive the cross section using the standard relativistic scattering theory. The delta functions in Eq. (6.126) can be evaluated, with the arguments being zero, as

$$\begin{aligned}
&\delta(\mathbf{k}_1 + \mathbf{k}_{23} - \mathbf{k}_{lab}) \delta(E_1 + E_{23} - E_{lab} - m_d) \\
&= \frac{1}{(2\pi)^3} \int_{\mathcal{V}} d\mathbf{x} e^{-i(\mathbf{k}_1 + \mathbf{k}_{23} - \mathbf{k}_{lab}) \cdot \mathbf{x}} \frac{1}{2\pi} \int_{\mathcal{T}} dt e^{i(E_1 + E_{23} - E_{lab} - m_d)t} \\
&= \frac{1}{(2\pi)^4} \int_{\mathcal{V}} d\mathbf{x} \int_{\mathcal{T}} dt \\
&\equiv \frac{\mathcal{V}\mathcal{T}}{(2\pi)^4}, \tag{6.128}
\end{aligned}$$

where \mathcal{V} and \mathcal{T} stand for the whole normal space volume and time. Hence, the squared absolute value of the S-matrix element $S(\mathbf{k}_1, \mathbf{k}_2, \mathbf{k}_3)$ is given as

$$\begin{aligned} |S(\mathbf{k}_1, \mathbf{k}_2, \mathbf{k}_3)|^2 &= (2\pi)^{-2} \delta(\mathbf{k}_1 + \mathbf{k}_{23} - \mathbf{k}_{lab}) \delta(E_1 + E_{23} - E_{lab} - m_d) \\ &\quad \times \Gamma^2(\mathbf{p}, \mathbf{q}) |U_0(\mathbf{p}, \mathbf{q})|^2 \mathcal{V} \mathcal{T}, \end{aligned} \quad (6.129)$$

and the transition rate W from initial to final state per unit volume results as

$$\begin{aligned} W &= \frac{|S(\mathbf{k}_1, \mathbf{k}_2, \mathbf{k}_3)|^2}{\mathcal{V} \mathcal{T}} \\ &= (2\pi)^{-2} \delta(\mathbf{k}_1 + \mathbf{k}_{23} - \mathbf{k}_{lab}) \delta(E_1 + E_{23} - E_{lab} - m_d) \Gamma^2(\mathbf{p}, \mathbf{q}) |U_0(\mathbf{p}, \mathbf{q})|^2. \end{aligned} \quad (6.130)$$

The outgoing flux dN , which is the number of outgoing nucleons per unit area and time, with momenta within a range of $d\mathbf{k}_1 d\mathbf{k}_2 d\mathbf{k}_3$ is given as

$$\begin{aligned} dN &= W d\mathbf{k}_1 d\mathbf{k}_2 d\mathbf{k}_3 \\ &= (2\pi)^{-2} \delta(\mathbf{k}_1 + \mathbf{k}_{23} - \mathbf{k}_{lab}) \delta(E_1 + E_{23} - E_{lab} - m_d) \\ &\quad \times \Gamma^2(\mathbf{p}, \mathbf{q}) |U_0(\mathbf{p}, \mathbf{q})|^2 d\mathbf{k}_1 d\mathbf{k}_2 d\mathbf{k}_3, \end{aligned} \quad (6.131)$$

while the incoming flux j is given as

$$\begin{aligned} j &= \frac{1}{(2\pi)^3} \frac{\sqrt{(E_{lab} m_d - \mathbf{k}_{lab} \cdot \mathbf{k}_d)^2 - (m m_d)^2}}{E_{lab} m_d} \\ &= \frac{1}{(2\pi)^3} \frac{\sqrt{(E_{lab}^2 - m^2) m_d^2}}{E_{lab} m_d} \\ &= \frac{1}{(2\pi)^3} \frac{k_{lab}}{E_{lab}}. \end{aligned} \quad (6.132)$$

The target density is $j_0 = (2\pi)^{-3}$. Thus, the differential cross section $d\sigma$ is obtained as

$$\begin{aligned} d\sigma &= \frac{dN}{j j_0} \\ &= (2\pi)^4 \frac{E_{lab}}{k_{lab}} \delta(\mathbf{k}_1 + \mathbf{k}_{23} - \mathbf{k}_{lab}) \delta(E_1 + E_{23} - E_{lab} - m_d) \\ &\quad \times \Gamma^2(\mathbf{p}, \mathbf{q}) |U_0(\mathbf{p}, \mathbf{q})|^2 d\mathbf{k}_1 d\mathbf{k}_2 d\mathbf{k}_3. \end{aligned} \quad (6.133)$$

For the inclusive Nd break-up process the differential cross section is calculated as a function of the kinetic energy $E_{k,1}$ and direction $\hat{\mathbf{k}}_1$ of the detected nucleon. The kinetic energy $E_{k,1}$ is given as

$$E_{k,1} = E_1 - m, \quad (6.134)$$

and thus,

$$d\mathbf{k}_1 = dk_1 k_1^2 d\hat{\mathbf{k}}_1 = E_1 k_1 dE_1 d\hat{\mathbf{k}}_1 = E_1 k_1 dE_{k,1} d\hat{\mathbf{k}}_1. \quad (6.135)$$

We insert Eq. (6.135) into Eq. (6.133), and end up with

$$\begin{aligned}
\frac{d\sigma}{dE_{k,1}d\hat{\mathbf{k}}_1} &= (2\pi)^4 \frac{E_{lab}E_1k_1}{k_{lab}} \\
&\quad \times \int d\mathbf{k}_2d\mathbf{k}_3\delta(\mathbf{k}_1 + \mathbf{k}_{23} - \mathbf{k}_{lab})\delta(E_1 + E_{23} - E_{lab} - m_d)\Gamma^2(\mathbf{p}, \mathbf{q})|U_0(\mathbf{p}, \mathbf{q})|^2 \\
&= (2\pi)^4 \frac{E_{lab}E_1k_1}{k_{lab}} \\
&\quad \times \int d\mathbf{k}_{23}d\mathbf{p}J(\mathbf{k}_2, \mathbf{k}_3)\delta(\mathbf{k}_1 + \mathbf{k}_{23} - \mathbf{k}_{lab})\delta(E_1 + E_{23} - E_{lab} - m_d) \\
&\quad \times \Gamma^2(\mathbf{p}, \mathbf{q})|U_0(\mathbf{p}, \mathbf{q})|^2 \\
&= (2\pi)^4 \frac{E_{lab}E_1k_1}{k_{lab}} \\
&\quad \times \int d\hat{\mathbf{p}}dp p^2 \frac{4E_2E_3}{E_{23}M_{23}}\delta(E_1 + E_{23} - E_{lab} - m_d)\Gamma^2(\mathbf{p}, \mathbf{q})|U_0(\mathbf{p}, \mathbf{q})|^2 \\
&= (2\pi)^4 \frac{E_{lab}E_1k_1p}{k_{lab}M_{23}} \int d\hat{\mathbf{p}}E_2E_3\Gamma^2(\mathbf{p}, \mathbf{q})|U_0(\mathbf{p}, \mathbf{q})|^2. \tag{6.136}
\end{aligned}$$

In arriving to Eq. (6.136) we have used Eq. (6.117) for $J(\mathbf{k}_2, \mathbf{k}_3)$ and

$$\begin{aligned}
dE_{23} &= d\sqrt{M_{23}^2 + k_{23}^2} \\
&= d\sqrt{4(m^2 + p^2) + k_{23}^2} \\
&= \frac{4p}{E_{23}}dp. \tag{6.137}
\end{aligned}$$

We define a function $\rho(p, q)$ as

$$\begin{aligned}
\rho(p, q) &\equiv \frac{2E_{lab}E_1E_2E_3}{M_{23}}\Gamma^2(\mathbf{p}, \mathbf{q}) \\
&= \frac{2E_{lab}E_1E_2E_3}{M_{23}} \frac{M_{23}E'_1E'_{23}E'_{lab}E'_d}{4E_1E_2E_3E_{lab}m_d} \\
&= \frac{E'_1E'_{23}E'_{lab}E'_d}{2m_d}, \tag{6.138}
\end{aligned}$$

allowing the differential cross section to be written in a similar fashion as the nonrelativistic one in Eq. (6.27), that is

$$\frac{d\sigma}{dE_{k,1}d\hat{\mathbf{k}}_1} = (2\pi)^4 \frac{\rho(p, q)pk_1}{2k_{lab}} \frac{1}{6} \sum_{m_{s1}m_{s2}m_{s3}m_{s1}^0M_d} \int d\hat{\mathbf{p}} |U_0(\mathbf{p}, \mathbf{q})|^2, \tag{6.139}$$

where we have restored the summation over final spins and the averaging over initial spins states. Nonrelativistically the function $\rho(p, q)$ reduces to m^3 , and the differential cross section to the nonrelativistic expression in Eq. (6.27).

Chapter 7

APPLICATION TO THE PROTON-NEUTRON CHARGE EXCHANGE REACTION

In this chapter we apply the 3D formulation derived in the last chapter for the Nd break-up process to the (p,n) charge exchange reaction and show numerical results together with comparisons to experiment. We consider the pd break-up process, in which a proton is directed towards an unpolarized deuteron target. The deuteron is then broken up into a neutron and a proton, and finally two protons and one neutron scatter in directions, which are constrained by energy and momentum conservation. In the experiments we are going to analyze, the neutron is detected, while the two protons are not detected. Hence, in calculating the observables all possible directions of the two protons are taken into account. In fact, energy and momentum conservations allow to sum over the relative directions $\hat{\mathbf{p}}$ between the two protons and not over the exact directions of their motions. We calculate the spin averaged differential cross section and some spin observables, which are the neutron polarization P_0 , the analyzing power A_y and the polarization transfer coefficients D_{ij} . The observables P_0 , A_y and D_{ij} are given in Eqs. (6.28)-(6.34), where the integration over $\hat{\mathbf{p}}$ is suppressed. The spin averaged differential cross section is given in Eqs. (6.27) and (6.139), where in the latter relativistic kinematics is used. Corresponding to each observable, we use the following notation

$$d(p, n)pp \quad \text{corresponds to} \quad \text{spin averaged differential cross section} \quad (7.1)$$

$$d(p, \vec{n})pp \quad \text{corresponds to} \quad P_0 \quad (7.2)$$

$$d(\vec{p}, n)pp \quad \text{corresponds to} \quad A_y \quad (7.3)$$

$$d(\vec{p}, \vec{n})pp \quad \text{corresponds to} \quad D_{ij}. \quad (7.4)$$

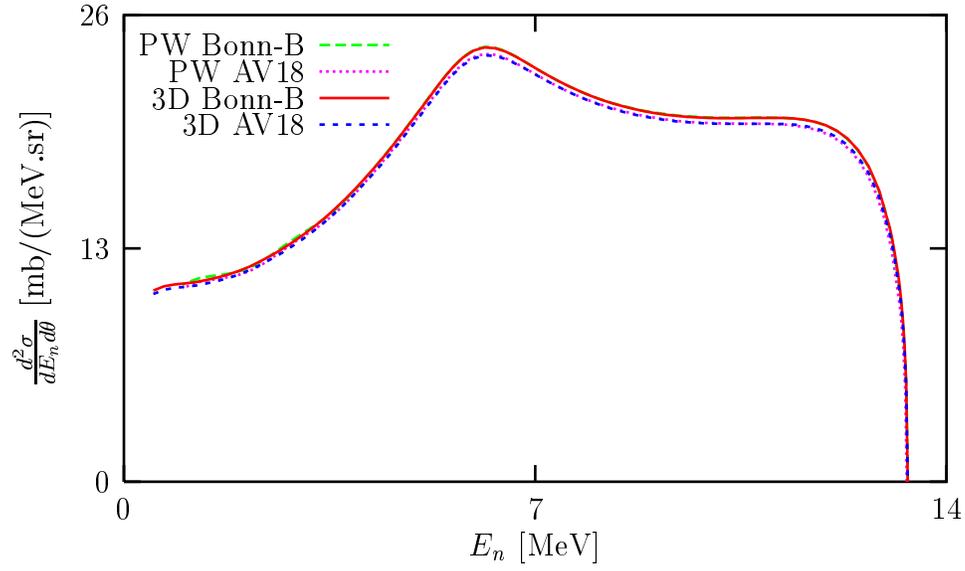
Here the arrows mean that either the particle is polarized or the polarization of the particle is measured. The calculations are performed using the NN potentials Bonn-B and AV18. The numerical realization is described in Appendix G.

We show the results in the following order. Firstly we compare our 3D calculations with PW calculations of the first order term. Next we compare with the PW calculations, which take the full break-up amplitude into account. We recall that we use the term "full break-up amplitude" for the leading term plus the rescattering terms and the term "break-up amplitude" for only the leading term. Thus, here one can see the effects of multiple scattering in the process. Last we compare between 3D calculations with nonrelativistic kinematics and the ones, which use relativistic kinematics. This will show the effects of relativity. Finally we compare with data at various energies.

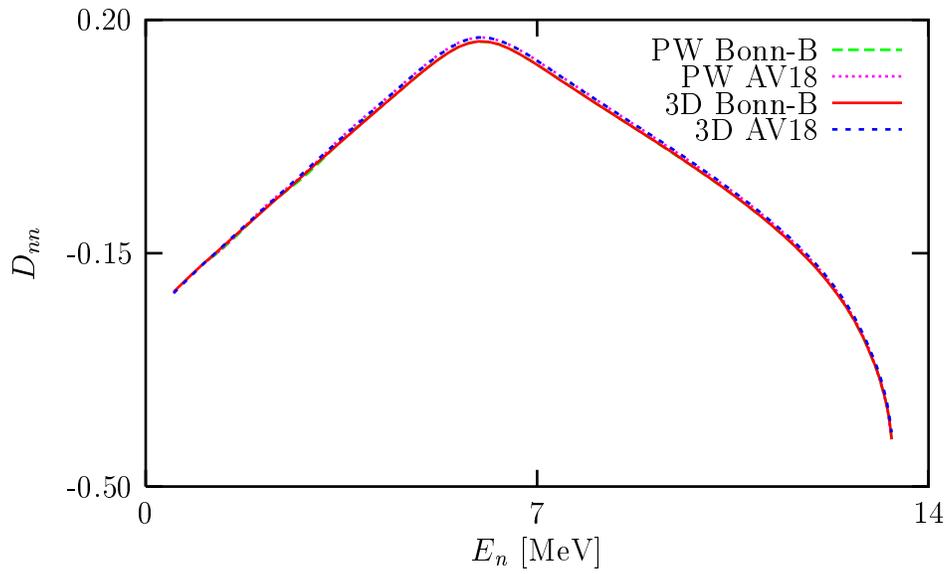
7.1 Comparison with Partial-Wave Calculations

For a 3N scattering using partial waves one has to check convergence in two different places. The first is the 2N-subsystem, for which the NN T-matrix is calculated. The second is the 3N system itself. The NN T-matrix is calculated by including 2N states up to a NN total angular momentum j . Then using the NN T-matrix as input the Nd break-up amplitude is calculated by including 3N states up to a 3N total angular momentum J . In this section we compare our 3D calculations to PW calculations [54, 55]. The 3D calculations can be regarded as the ideal PW calculations, which include an infinite number of partial waves.

In Figs. 7.1-7.4 we show the 3D calculations and the PW calculations with $j = 5$ and $J = 31/2$ for the pd break-up process at $E_{lab} = 16$ MeV and neutron laboratory scattering angle $\theta_{lab} = 13^\circ$. The calculations are based on the NN potentials Bonn-B and AV18. Figures 7.1(a) and 7.1(b) show the spin averaged differential cross section (abbreviated cross section) and the polarization transfer coefficient D_{nn} , respectively, over the neutron outgoing energies E_n . Figures 7.2(a) and 7.2(b) display the analyzing power A_y and the neutron polarization P_0 . Figures 7.3(a) and 7.3(b) show the polarization transfer coefficients D_{ll} and D_{ss} . Figures 7.4(a) and 7.4(b) show the polarization transfer coefficients D_{sl} and D_{ls} . At $E_{lab} = 16$ MeV the 3D and the PW calculations agree with each other. There is an exception for A_y around $E_n = 3$ MeV, where the curves of the PW calculations oscillate over the smooth curves of the 3D calculations. Now we go to a higher energy. In Figs. 7.5-7.8 the same set of observables is shown for the same scattering angle $\theta_{lab} = 13^\circ$ but at a higher energy $E_{lab} = 197$ MeV. At this energy the 3D calculations disagree with the PW calculations, which again take



(a)



(b)

Figure 7.1: The 3D and the PW calculations ($j = 5$, $J = 31/2$) for (a) the spin averaged differential cross section and (b) the polarization transfer coefficient D_{nn} in the pd break-up process at $E_{lab} = 16$ MeV and neutron laboratory scattering angle $\theta_{lab} = 13^\circ$. The NN potentials used are Bonn-B and AV18.

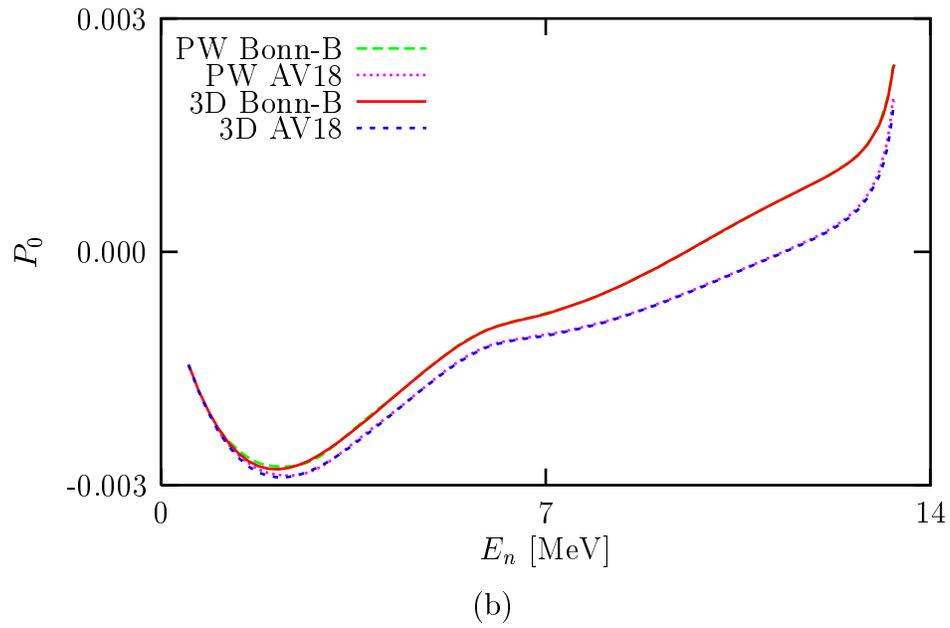
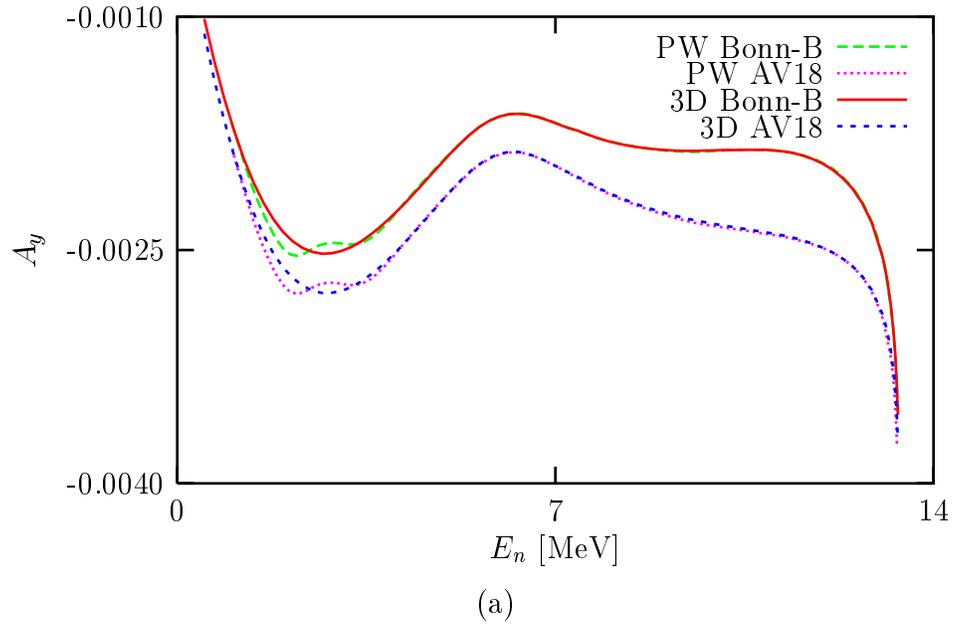


Figure 7.2: Same as in Fig. 7.1, but for (a) the analyzing power A_y and (b) the neutron polarization P_0 .

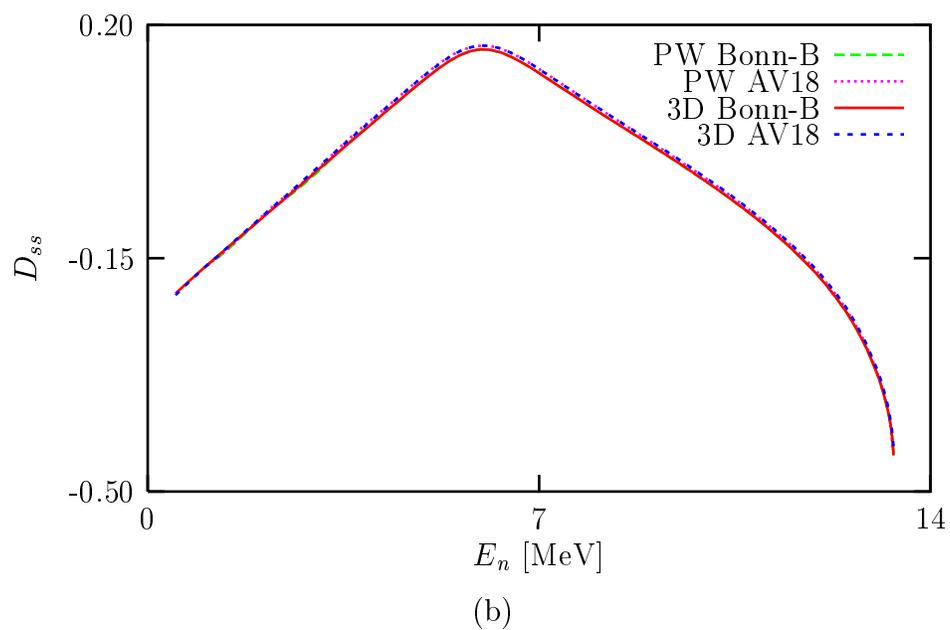
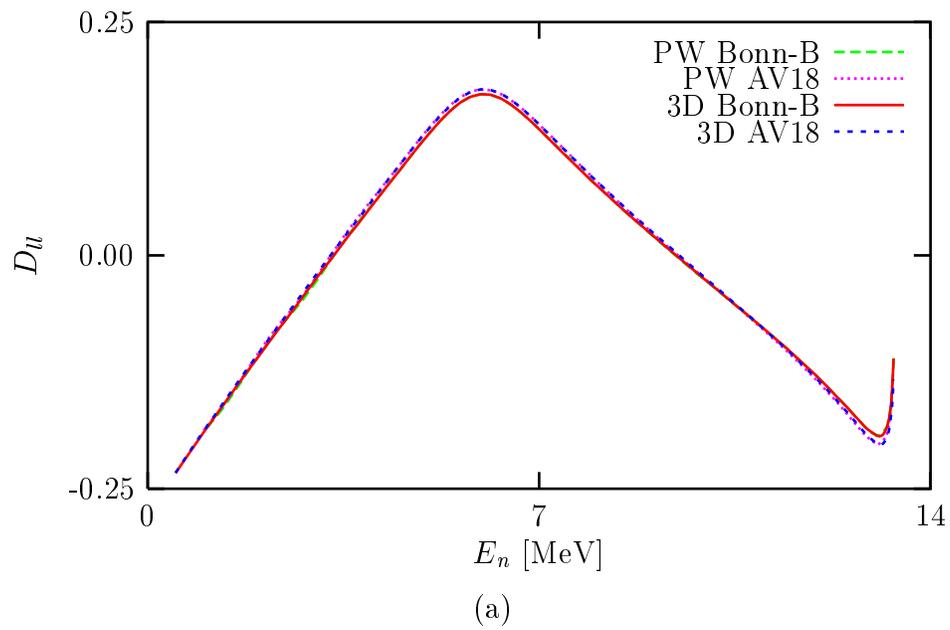


Figure 7.3: Same as in Fig. 7.1, but for the polarization transfer coefficients (a) D_u and (b) D_{ss} .

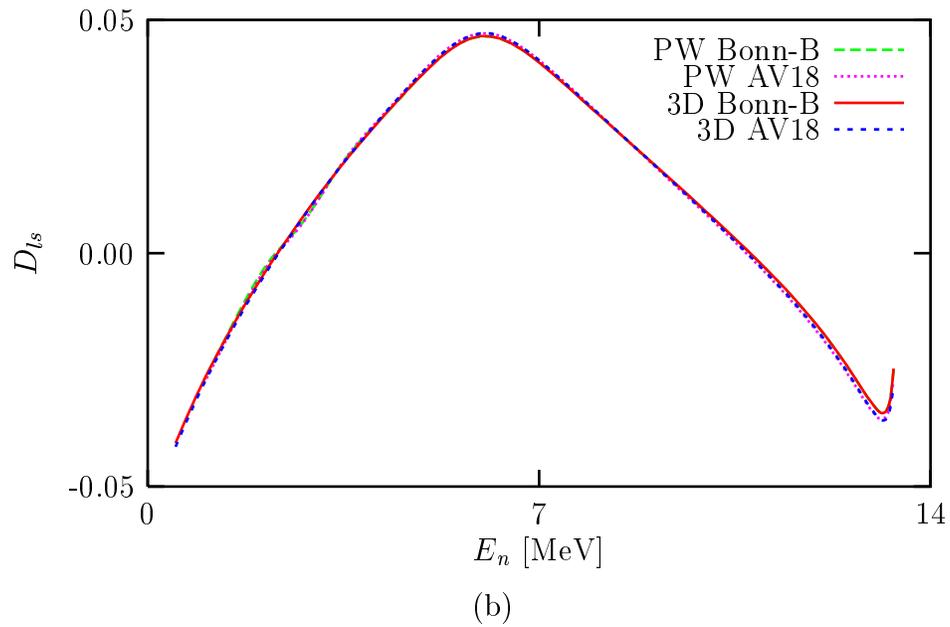
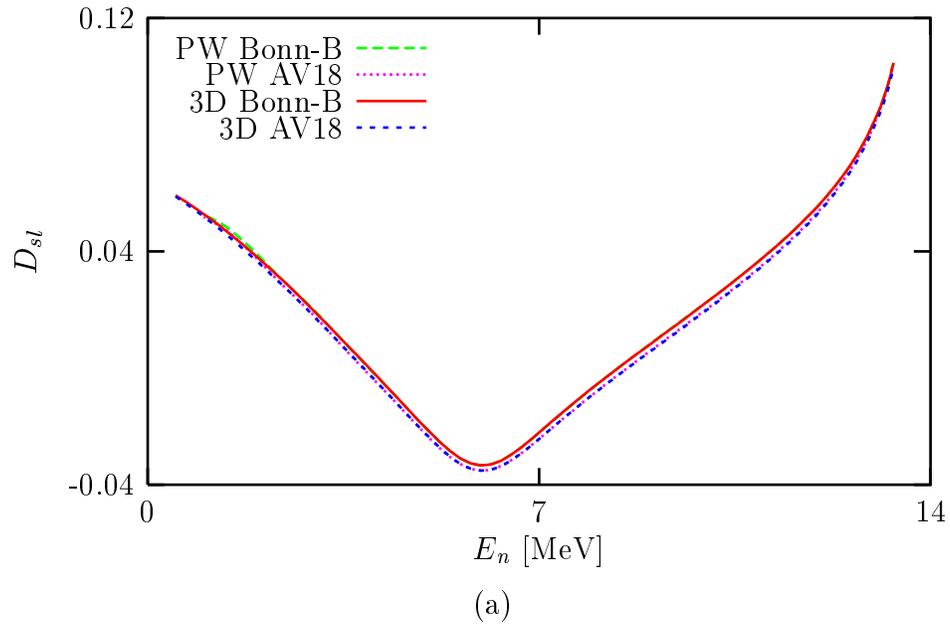


Figure 7.4: Same as in Fig. 7.1, but for the polarization transfer coefficients (a) D_{sl} and (b) D_{ls} .

$j = 5$ and $J = 31/2$. In Fig. 7.5(a) the height of the cross section peak in the PW calculation for the Bonn-B is about 14% lower than that in the 3D calculation and about 8% for the AV18. Figure 7.5(b) shows disagreements between the 3D and the PW calculations for D_{nn} , which become more visible as E_n increases ($E_n > 100$ MeV). And this behavior is also seen for the other polarization transfer coefficients in Figs. 7.7 and 7.8 except for D_{ss} in Fig. 7.7(b). For A_y and P_0 in Fig. 7.6 the disagreements occur mostly for E_n between 70 and 130 MeV, that is around the middle of the E_n -range for $E_{lab} = 197$ MeV and $\theta_{lab} = 13^\circ$. To give more examples in Figs. 7.9-7.12 we show again the same set of observables at $E_{lab} = 197$ MeV but for a larger scattering angle $\theta_{lab} = 24^\circ$. Again we see disagreements between the 3D and the PW calculations, which take $j = 5$ and $J = 31/2$. Here the cross section peak in the PW calculation for the Bonn-B is about 2% higher than the corresponding peak in the 3D calculation and about 4% for the AV18. Now at this angle one also sees in Fig. 7.11(b) disagreements between the 3D and the PW calculations for D_{ss} . As at $\theta_{lab} = 13^\circ$ the disagreements for the polarization transfer coefficients D_{ij} occur mostly for the second half of the E_n -range, if one goes from lower E_n to higher E_n . For A_y and P_0 in Fig. 7.10 the disagreements occur near the middle and the maximum of the E_n -range. All these indicate that at $E_{lab} = 197$ MeV the PW calculations with $j = 5$ and $J = 31/2$ have not converged to the ideal PW calculations, which include all partial waves, as represented by the 3D calculations.

In order to check the converging process of the PW calculations at $E_{lab} = 197$ MeV we compare to some PW calculations with increasing j and J , even up to $j = 7$. Figures 7.13 and 7.16 show such comparisons at $\theta_{lab} = 13^\circ$ for the Bonn-B. Here we show only for regions of E_n , where the converging processes are better seen. For the E_n -region shown the PW calculation with $j = 7$ and $J = 31/2$ can be considered to have already converged for D_{ss} in Fig. 7.15(b). But for the other observables even with $j = 7$ and $J = 31/2$ the PW calculations do not converge to the 3D calculations. Next we see that increasing j improves the PW calculations to reach the 3D calculations faster than increasing J . For A_y (Fig. 7.14(a)) and the polarization transfer coefficients D_{nn} (Fig. 7.13(b)), D_{ll} (Fig. 7.15(a)), D_{sl} (Fig. 7.16(a)) and D_{ls} (Fig. 7.16(b)) the convergences of the PW calculations to the 3D calculations at $E_{lab} = 197$ MeV may be achieved with $j = 9$, but unfortunately this would not be the case for the cross section (Fig. 7.13(a)) and P_0 (Fig. 7.14(b)). For P_0 and moreover the cross section the converging processes are much slower than those for A_y , D_{nn} , D_{ll} , D_{sl} and D_{ls} . Let us take a look at the cross section in Fig. 7.13(a). With $j = 7$ and $J = 31/2$ the cross section peak is raised to be about 6% higher than the one resulting from the PW calculation with $j = 5$, $J = 31/2$, but still it is about 9% lower than the cross section peak from the 3D calculation. If by

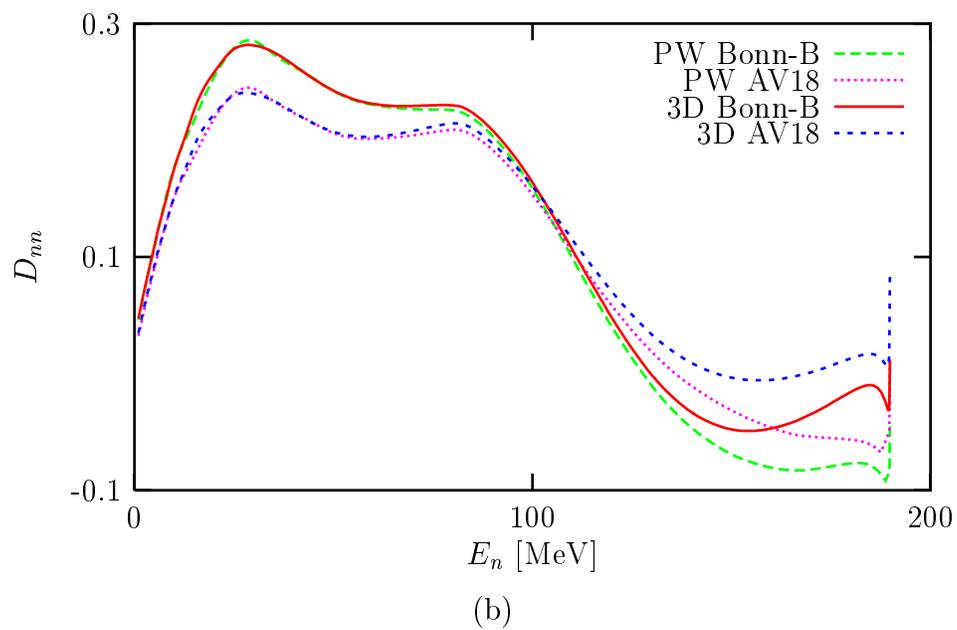
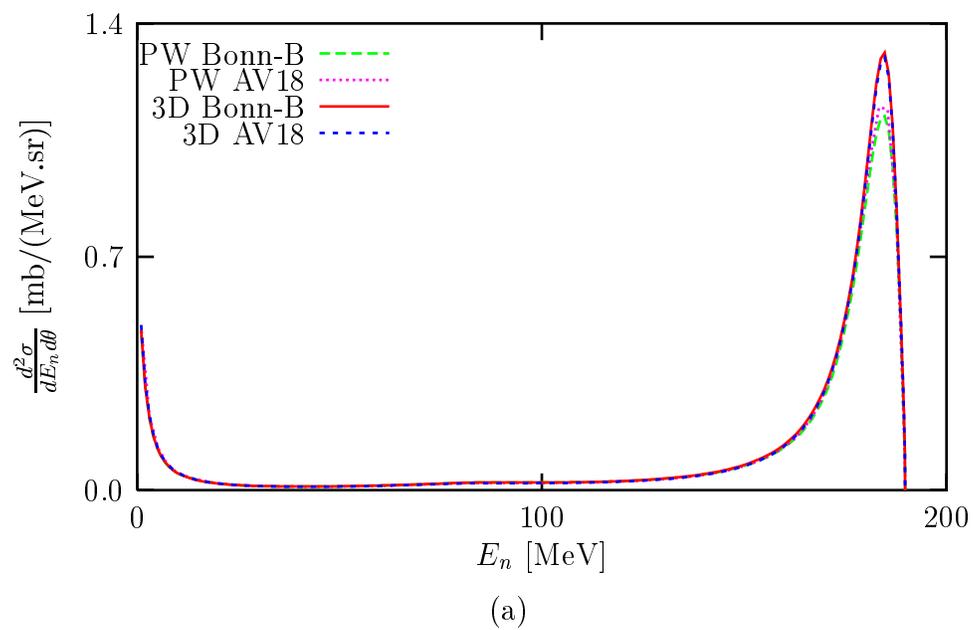


Figure 7.5: Same as in Fig. 7.1, but at $E_{lab} = 197$ MeV and $\theta_{lab} = 13^\circ$.

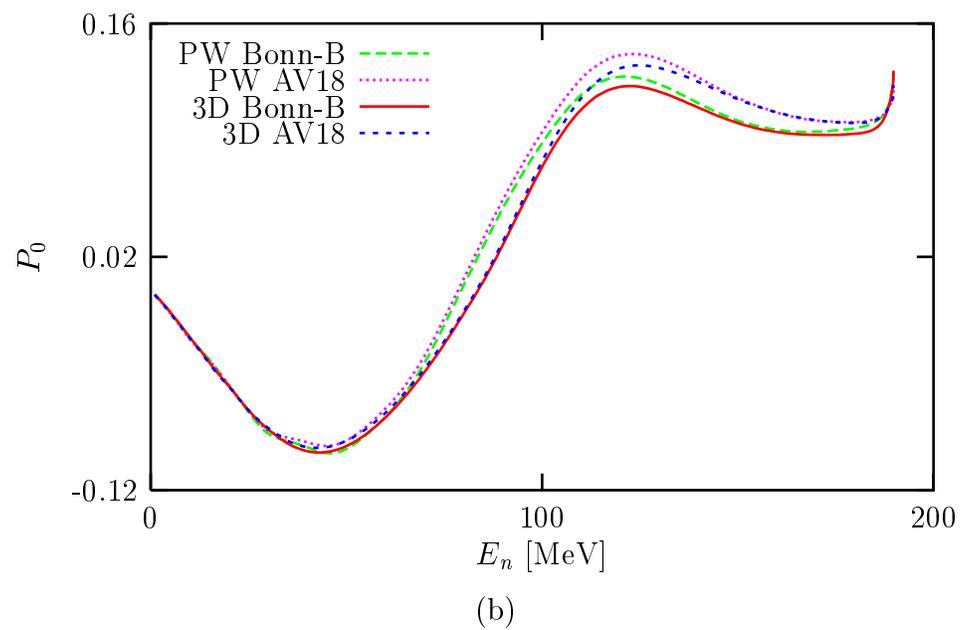
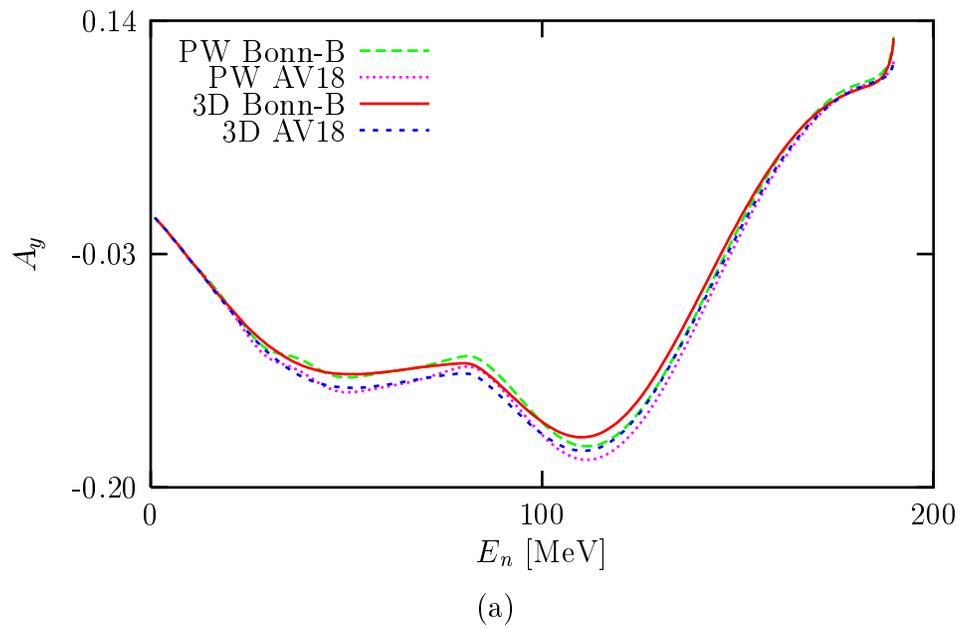


Figure 7.6: Same as in Fig. 7.5, but for (a) the analyzing power A_y and (b) the neutron polarization P_0 .

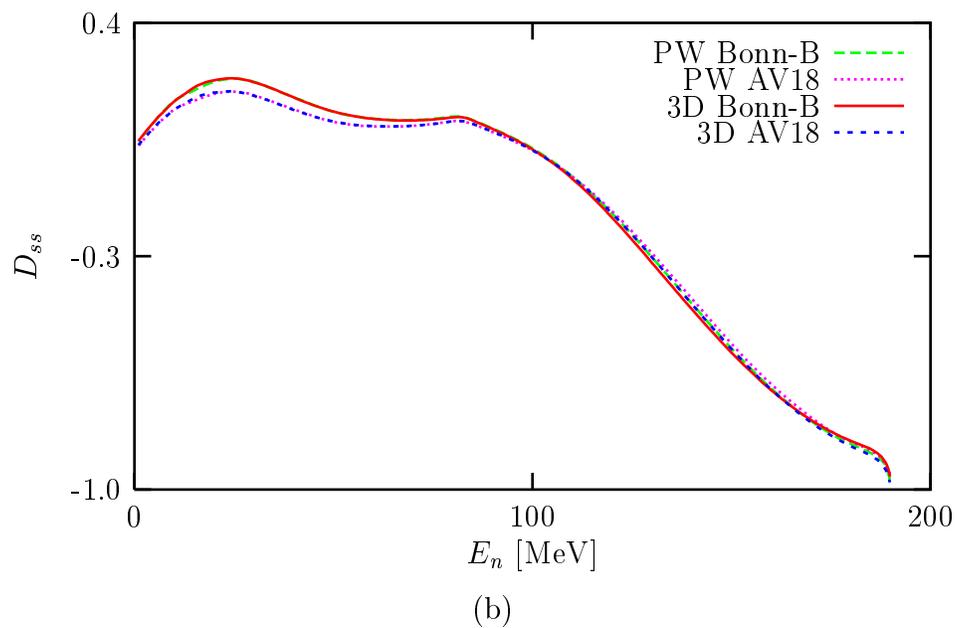
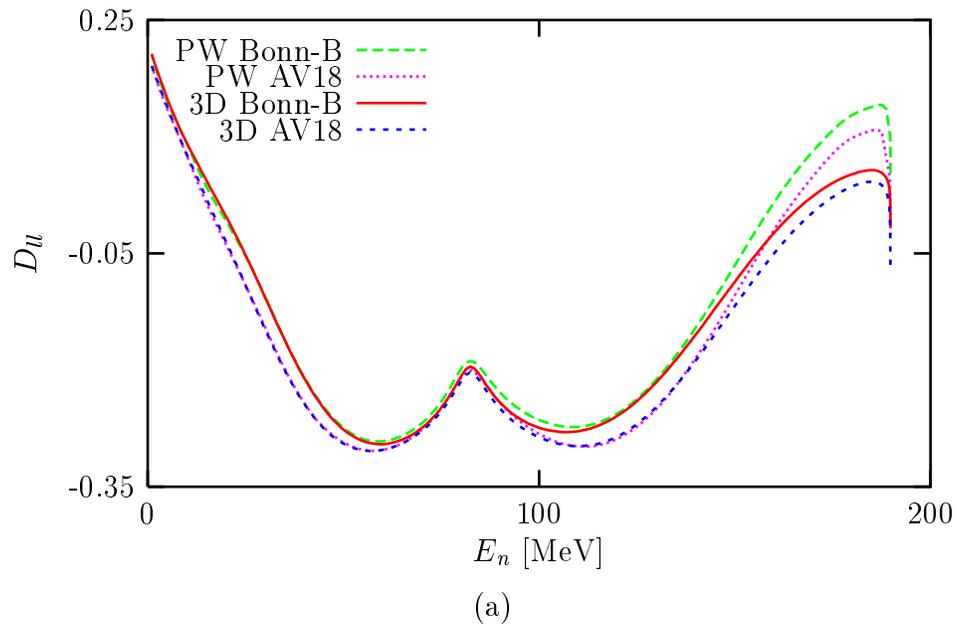


Figure 7.7: Same as in Fig. 7.5, but for the polarization transfer coefficients (a) D_u and (b) D_{ss} .

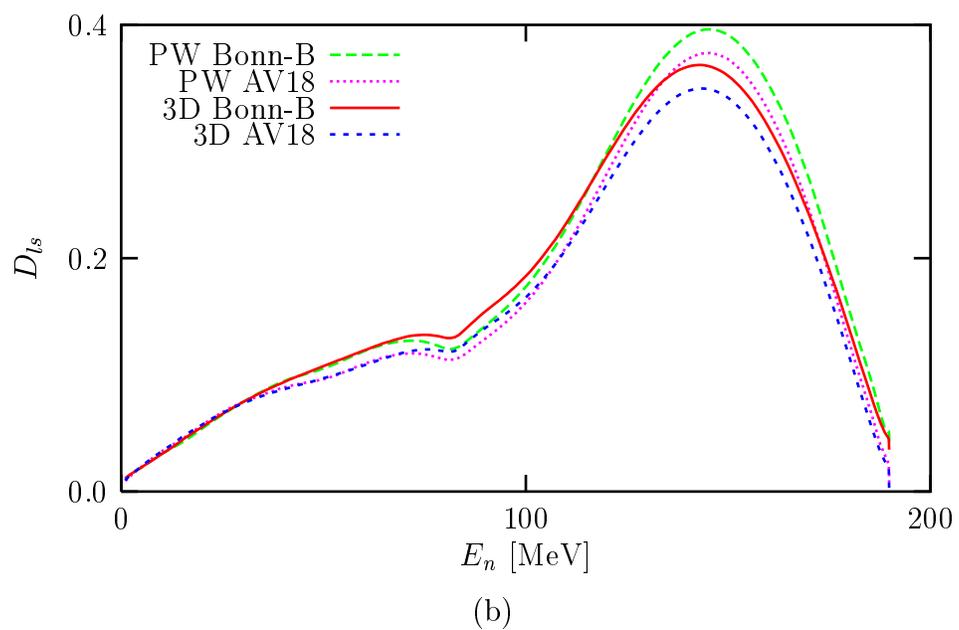
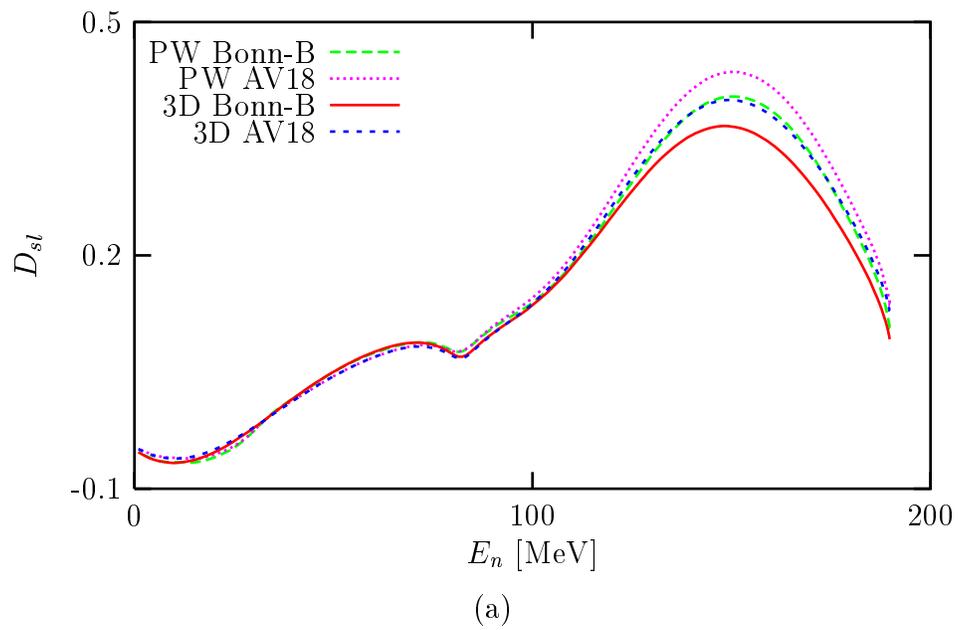
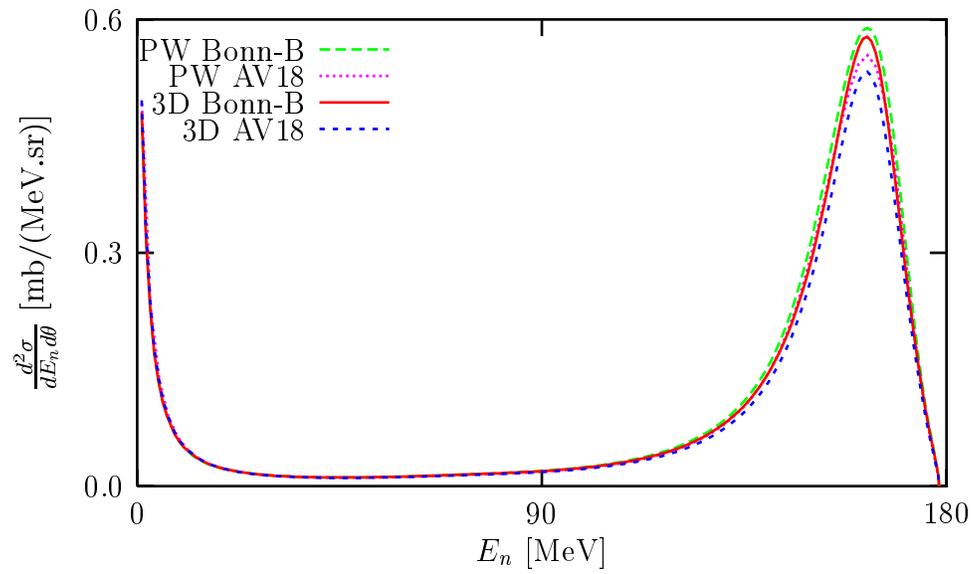
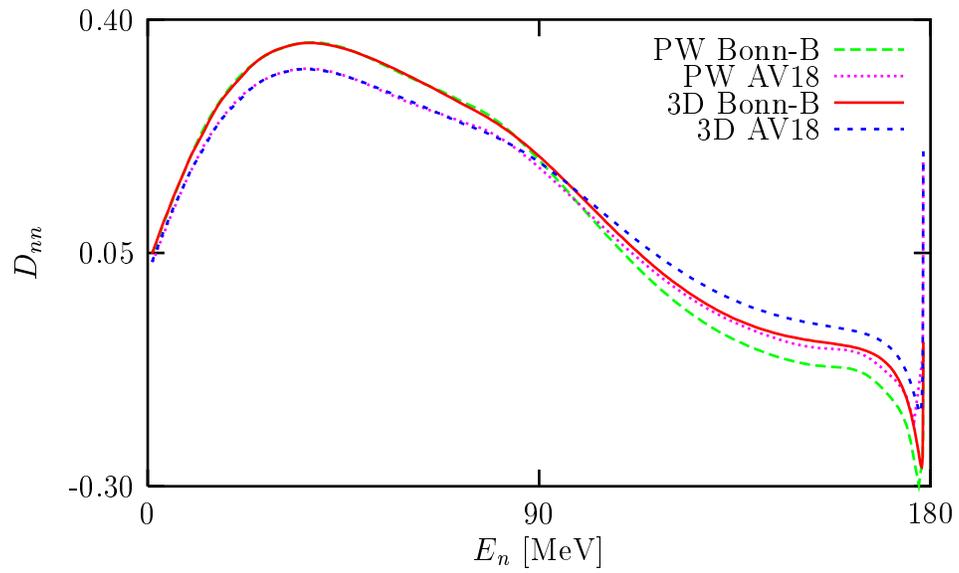


Figure 7.8: Same as in Fig. 7.5, but for the polarization transfer coefficients (a) D_{sl} and (b) D_{ls} .



(a)



(b)

Figure 7.9: Same as in Fig. 7.5, but at $\theta_{lab} = 24^\circ$.

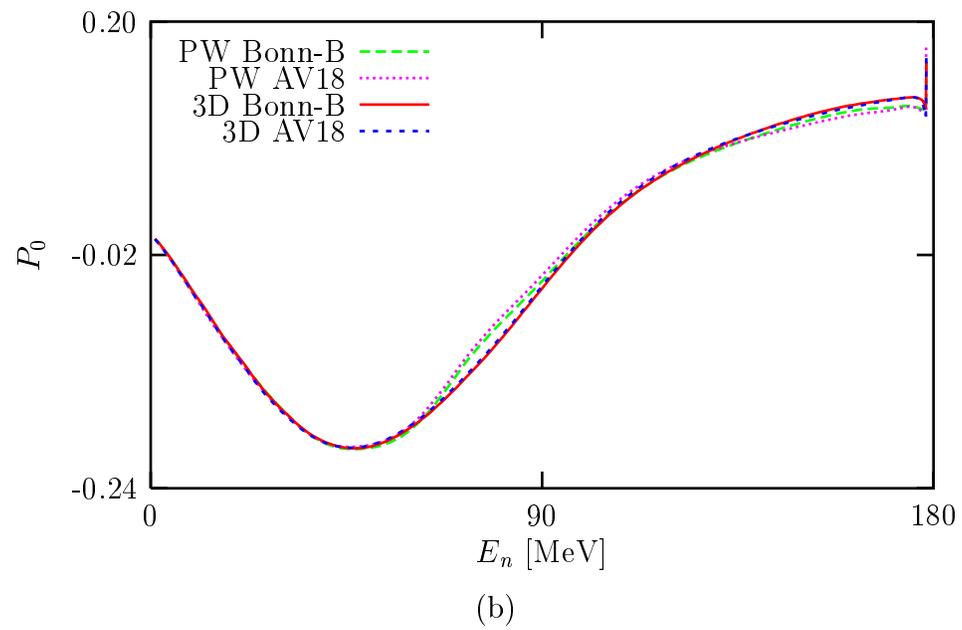
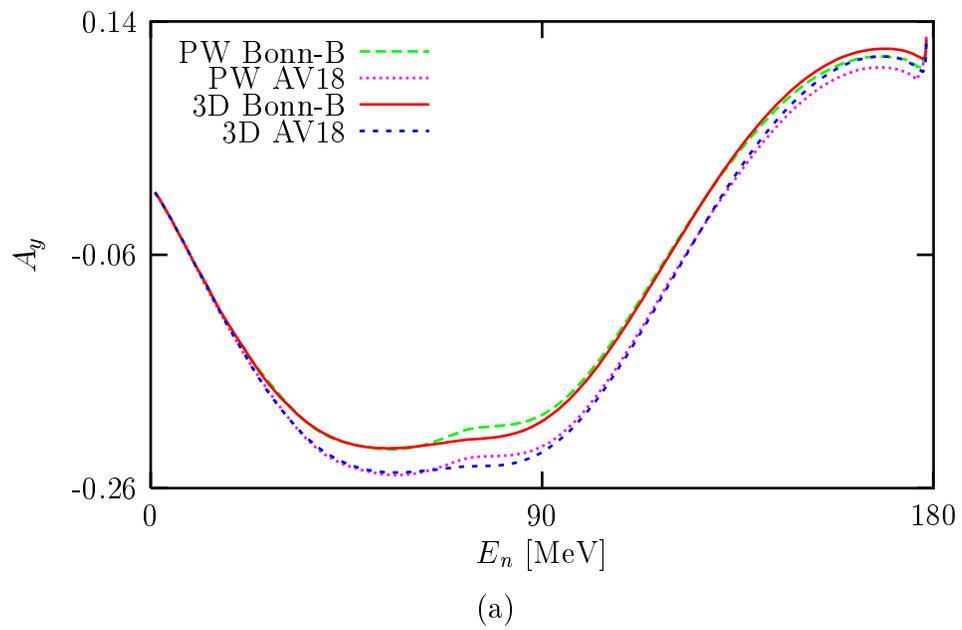
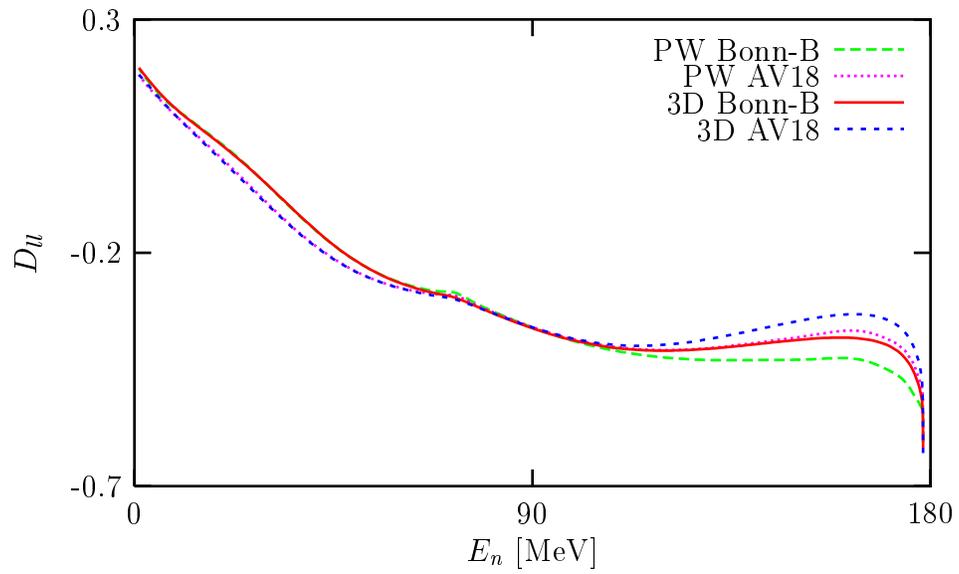
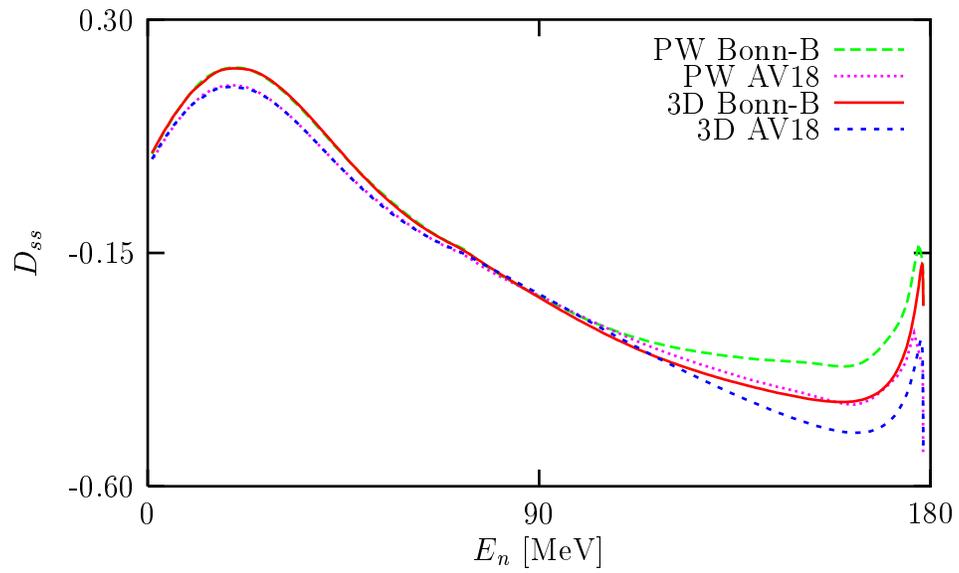


Figure 7.10: Same as in Fig. 7.6, but at $\theta_{lab} = 24^\circ$.



(a)



(b)

Figure 7.11: Same as in Fig. 7.7, but at $\theta_{lab} = 24^\circ$.

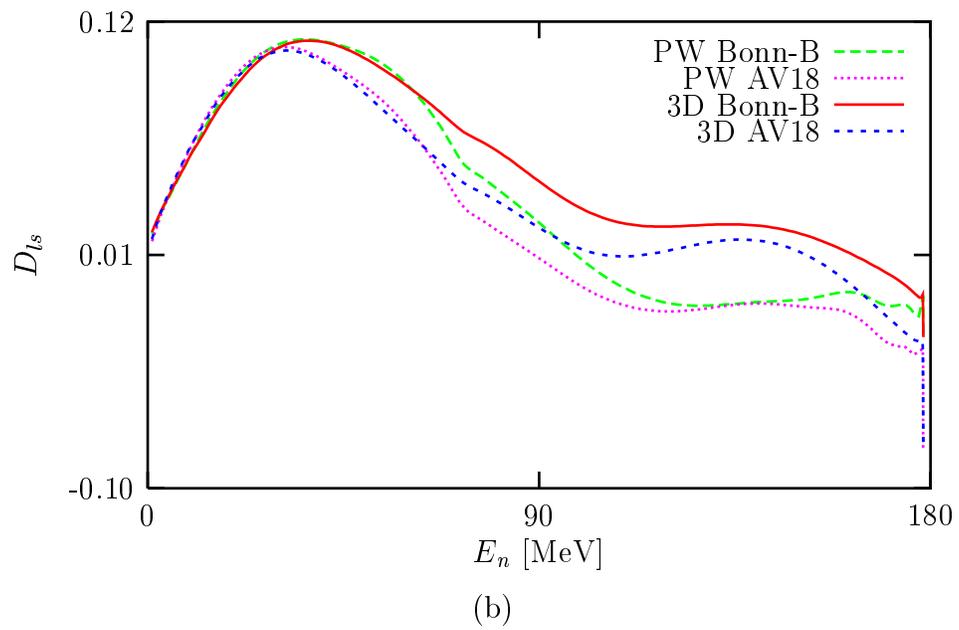
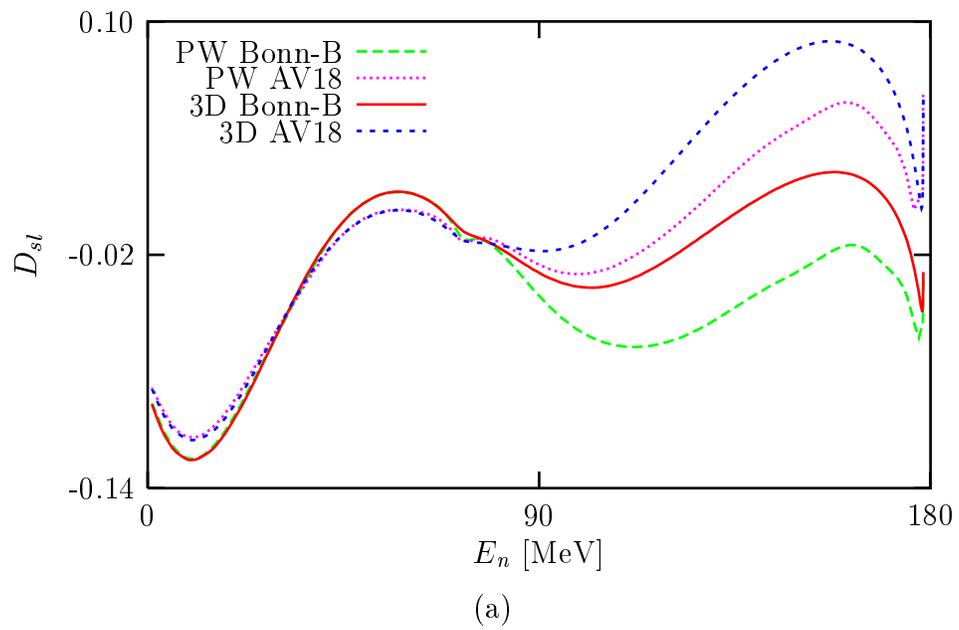


Figure 7.12: Same as in Fig. 7.8, but at $\theta_{lab} = 24^\circ$.

taking $j = 9$, $J = 31/2$ one would expect to have the cross section peak further raised by at most 6%, then it is still about 4% lower than the peak from the 3D calculation. In fact one should take into account that as one continuously increases the number of partial waves the improvement is getting less and less, otherwise the calculation will not converge. Therefore, it is unlikely for the cross section that by always increasing $j > 7$ the PW calculations will soon converge to the 3D calculation. It is worthy to mention that with $j = 5$ and $J = 31/2$ one has actually reached the nowadays limits of the PW calculations. Therefore, for energies around 200 MeV and higher it is not feasible to perform a PW calculation, which converges to the corresponding 3D calculation.

Now we go to energies below 200 MeV to see where 3D calculations start to appreciably disagree with PW calculations. We choose the PW calculations, which take $j = 7$, $J = 31/2$ and are based on the NN potential Bonn-B. From the investigation for $E_{lab} = 197$ we know that for the cross section the PW calculation converges slowliest than for other observables. Therefore, we shall look at the disagreement for the cross section peak. Nevertheless, we will show all the investigated observables. In Figs. 7.17-7.20 we display the 3D and the PW calculations for $E_{lab} = 65$ MeV and $\theta_{lab} = 13^\circ$. At this energy one can hardly see disagreements between the 3D and the PW calculations. There is an exception for A_y in Fig. 7.18(a) around $E_n = 10$ MeV, to which a similar disagreement is also seen at $E_{lab} = 16$ MeV around $E_n = 3$ MeV (see Fig. 7.2(a)). At $E_{lab} = 65$ MeV the height of the cross section peak in Fig. 7.17(a) from the PW calculation is about 0.5% lower than the one from the 3D calculation. In Figs. 7.21-7.24 we show the calculations for $E_{lab} = 100$ MeV and $\theta_{lab} = 13^\circ$. For the polarization transfer coefficients D_{ij} one can hardly see disagreements between the 3D and the PW calculations. For A_y in Fig. 7.22(a) one sees around $E_n = 20$ MeV similar disagreements to the ones occurring at $E_{lab} = 65$ MeV and $E_n = 10$ MeV (see Fig. 7.18(a)). At $E_{lab} = 100$ MeV the disagreement for the cross section peak in Fig. 7.21(a) between the two calculations is about 1.7%, thus, it is more than three times larger than the disagreement at $E_{lab} = 65$ MeV. Now if E_{lab} is getting higher than 100 MeV the disagreement for the cross section peak will quickly increase. We conclude that for $E_{lab} = 100$ MeV and lower PW calculations with $j = 7$, $J = 31/2$ can be used to describe Nd break-up process reasonably well, but for $E_{lab} > 100$ MeV the calculations are inadequate. But with $j = 7$, $J = 31/2$ this means that one has to pay much effort to perform the calculations up to the limits. Thus, according to this insight for $E_{lab} > 100$ MeV PW calculations cannot be used to well describe the Nd break-up process.

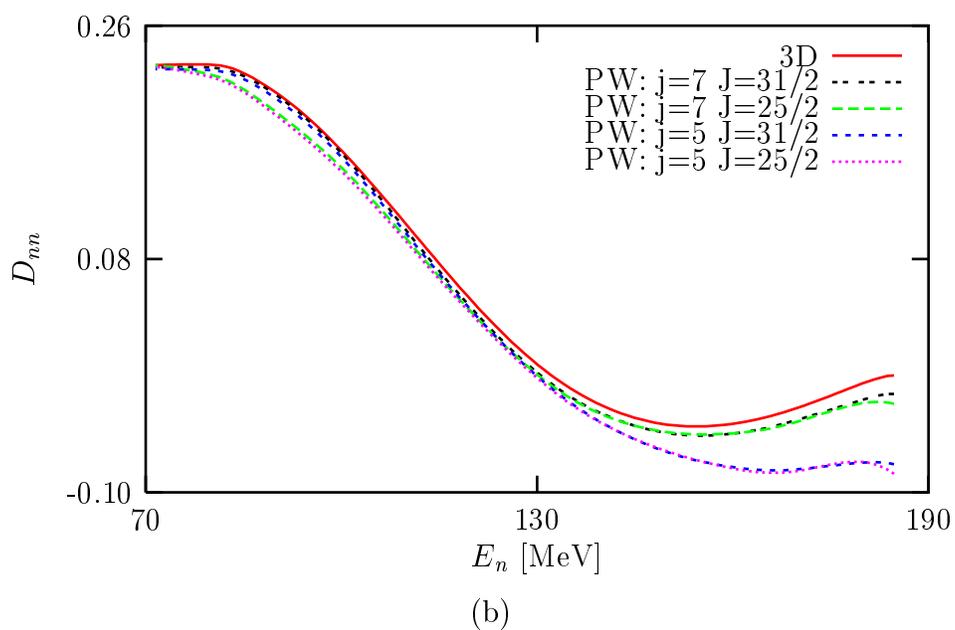
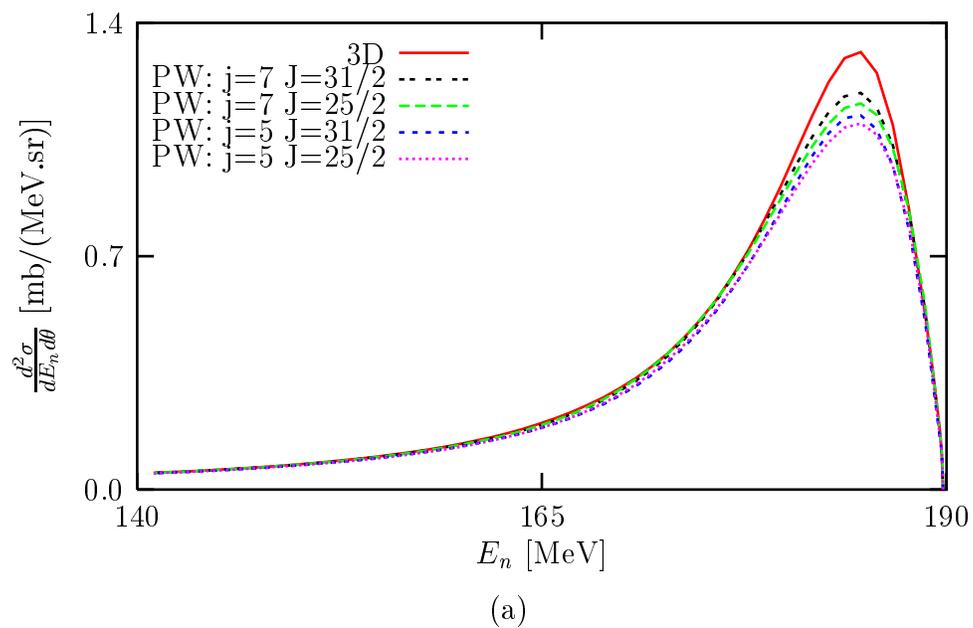
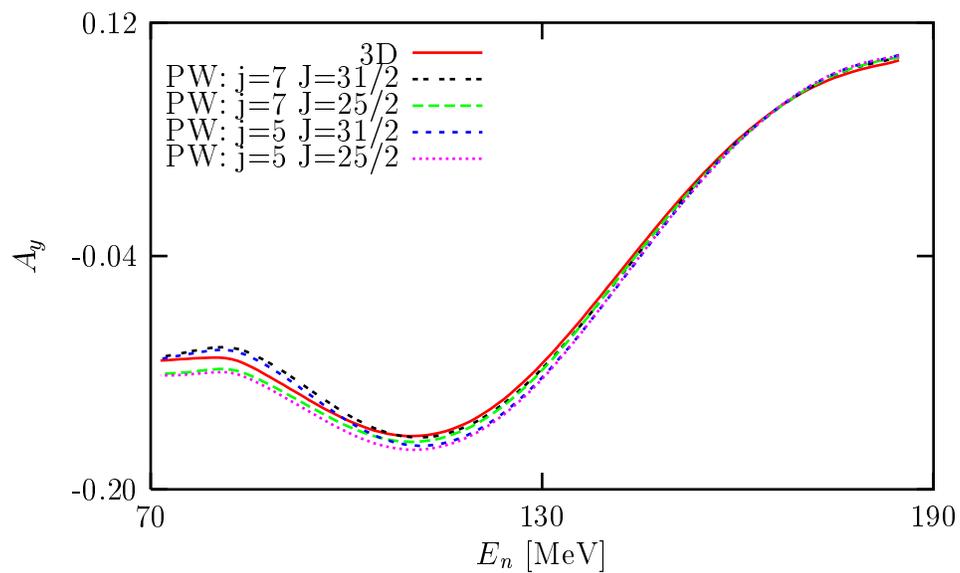
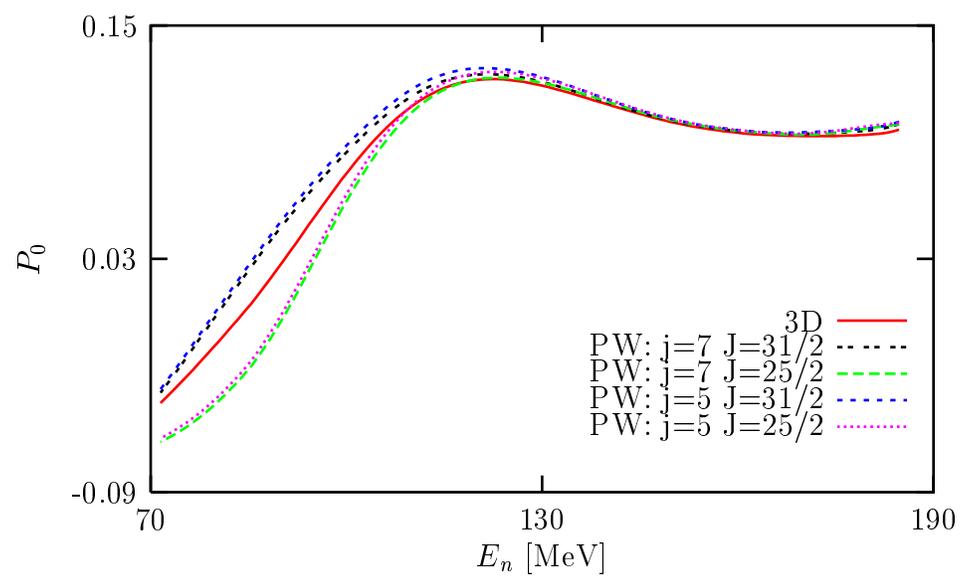


Figure 7.13: Convergence tests of the PW calculations for (a) the spin averaged cross section and (b) the polarization transfer coefficient D_{nn} in the pd break-up process at $E_{lab} = 197$ MeV and $\theta_{lab} = 13^\circ$. The NN potential used is Bonn-B.

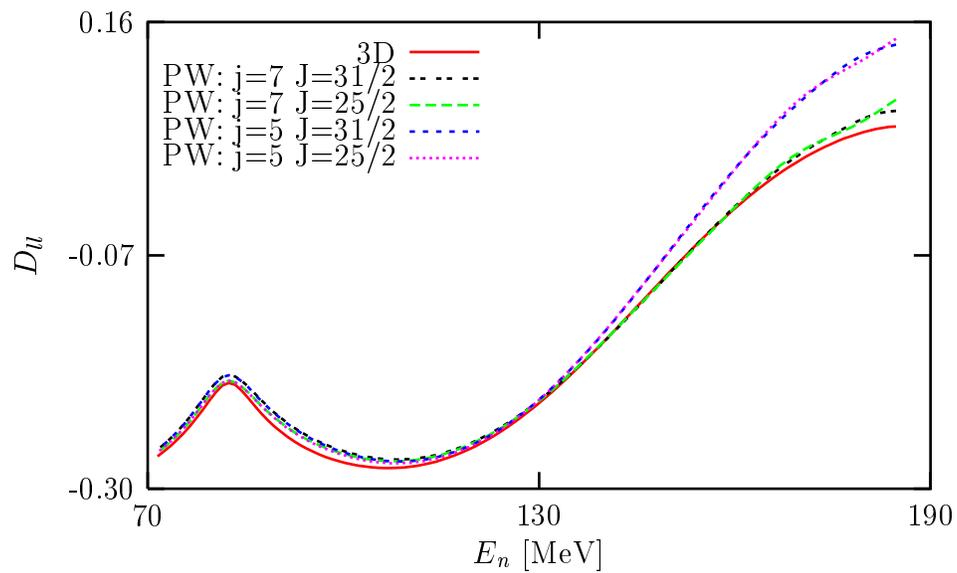


(a)

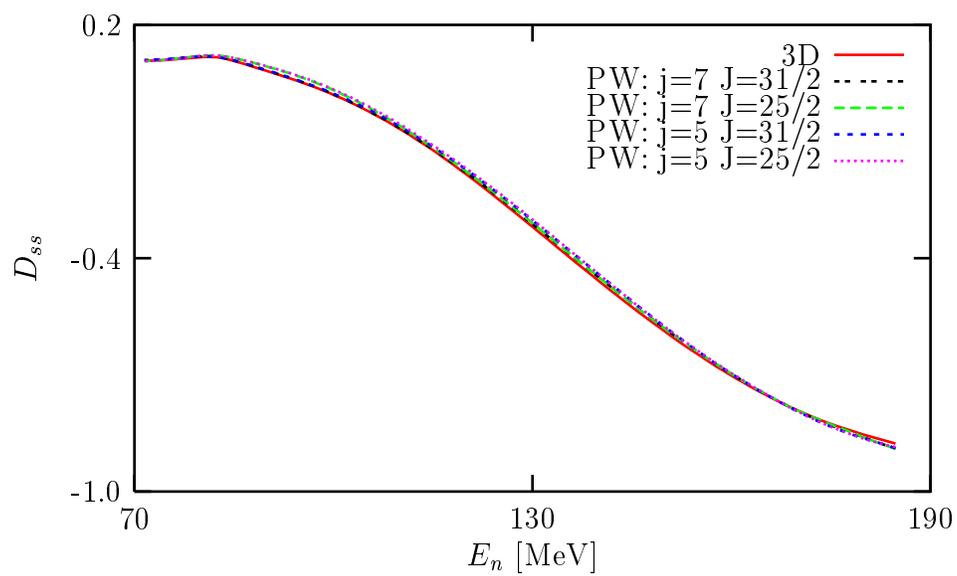


(b)

Figure 7.14: Same as in Fig. 7.13, but for (a) the analyzing power A_y and (b) the neutron polarization P_0 .



(a)



(b)

Figure 7.15: Same as in Fig 7.13, but for the polarization transfer coefficients (a) D_{ll} and (b) D_{ss} .

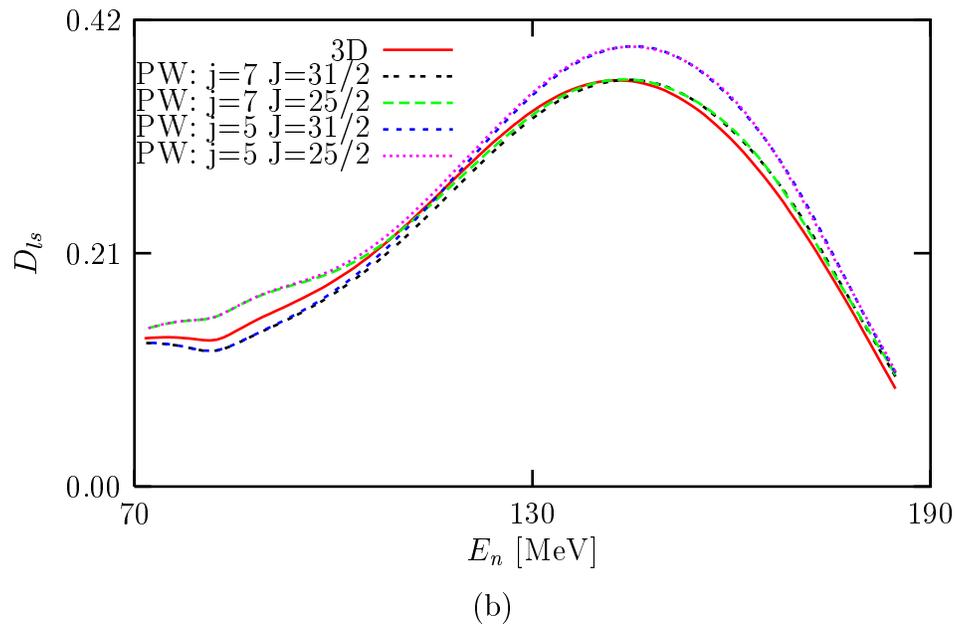
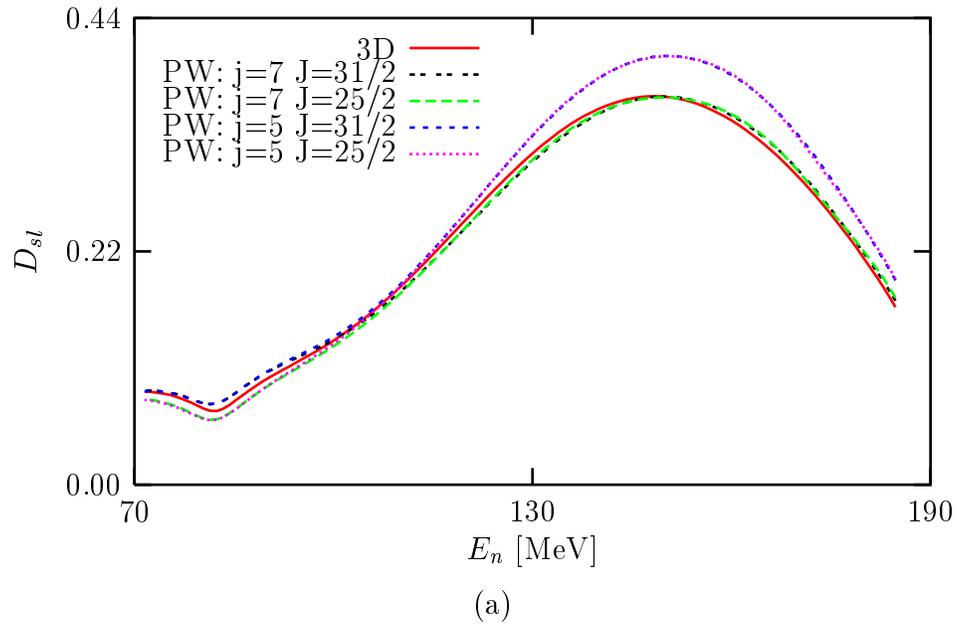
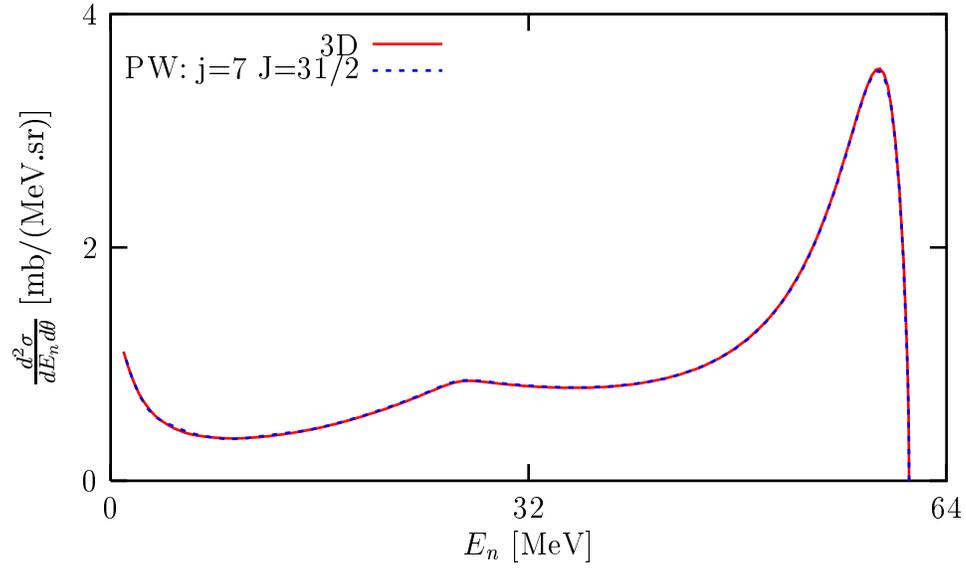
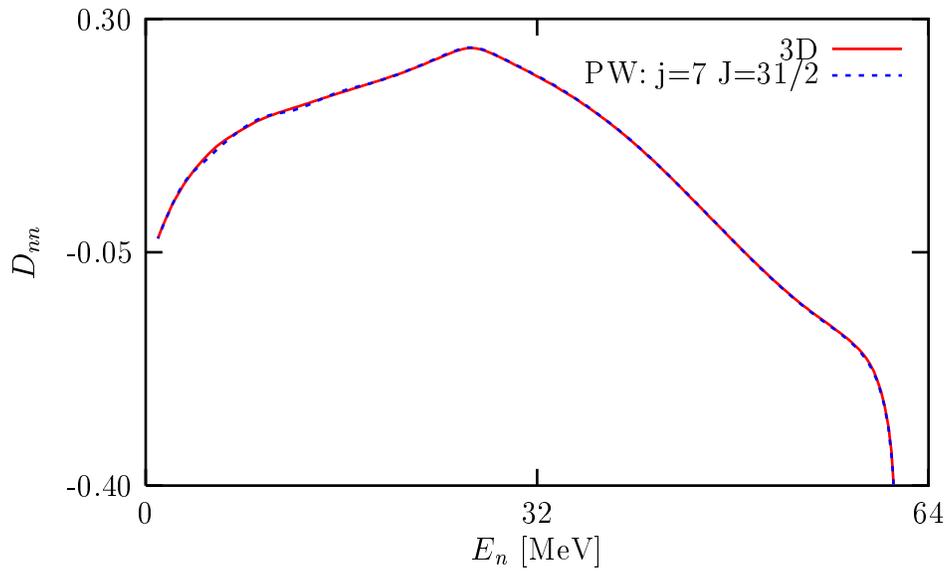


Figure 7.16: Same as in Fig 7.13, but for the polarization transfer coefficients (a) D_{sl} and (b) D_{ls} .



(a)



(b)

Figure 7.17: The 3D and PW calculations for (a) the spin averaged differential cross section and (b) the polarization transfer coefficient D_{nn} in the pd break-up process at $E_{lab} = 65$ MeV and $\theta_{lab} = 13^\circ$. The NN potential used is Bonn-B. The PW calculations take $j = 7$, $J = 31/2$.

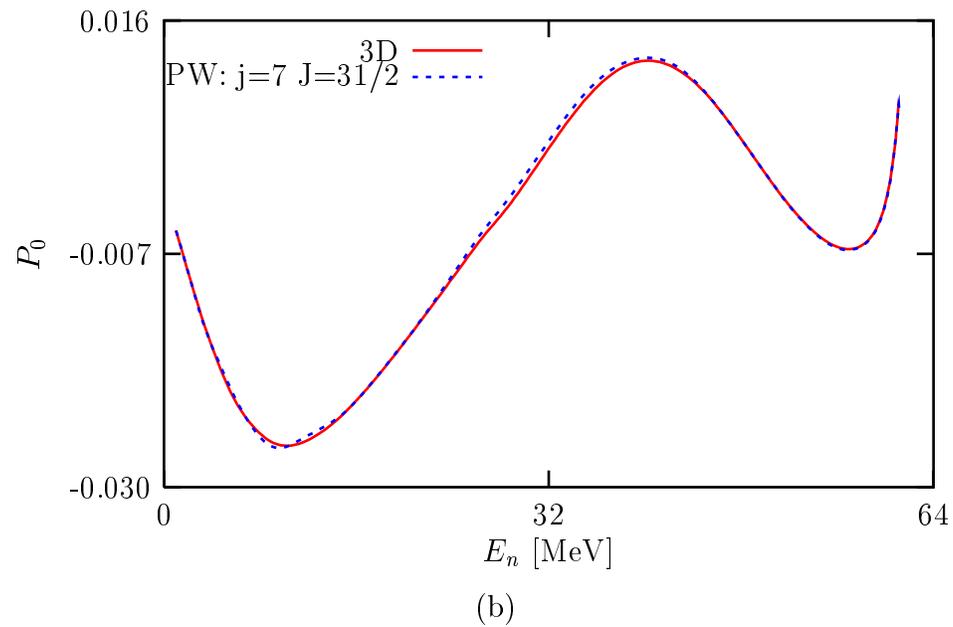
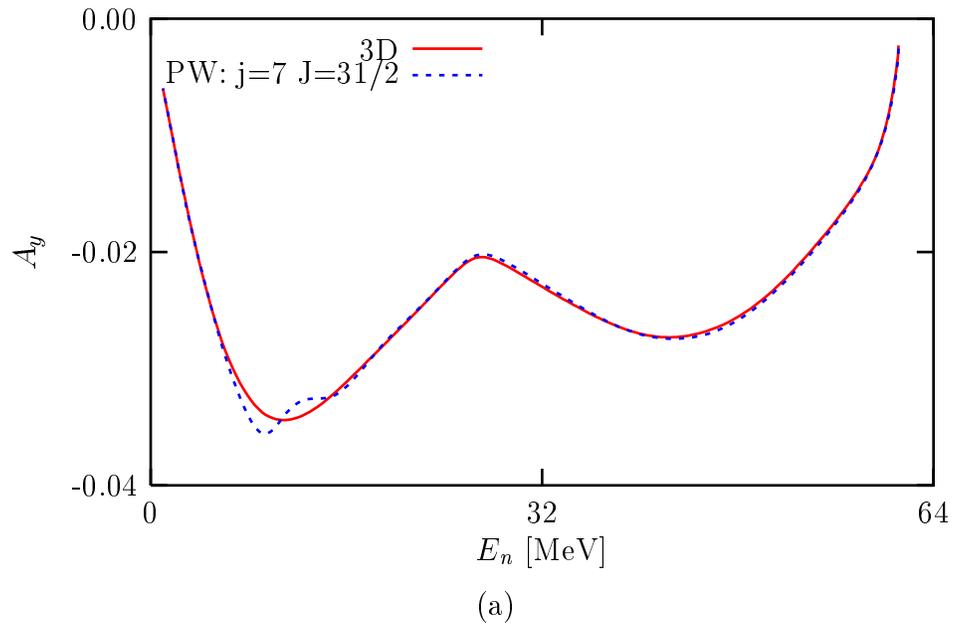


Figure 7.18: Same as in Fig. 7.17, but for (a) the analyzing power A_y and (b) the neutron polarization P_0 .

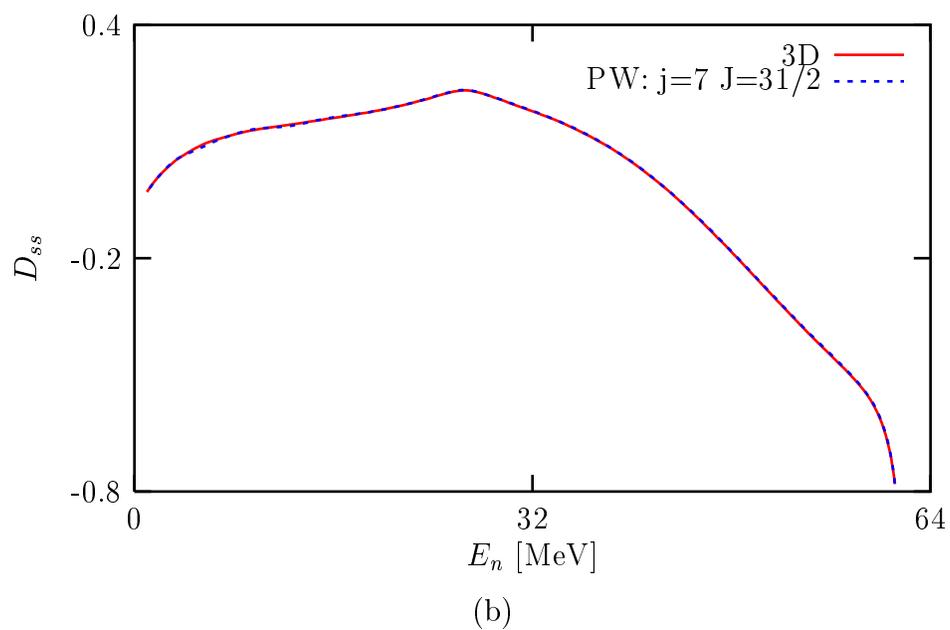
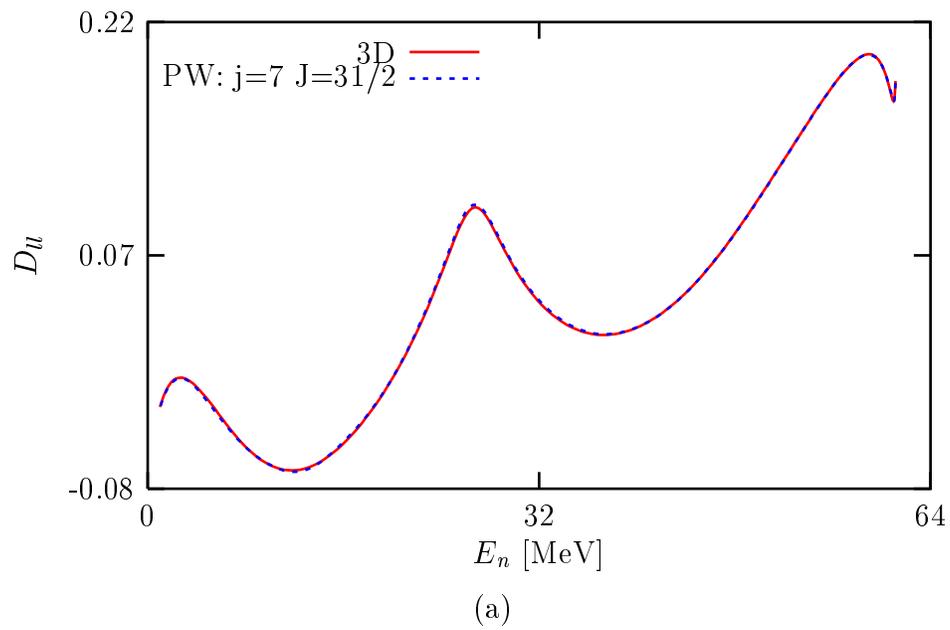


Figure 7.19: Same as in Fig. 7.17, but for the polarization transfer coefficients (a) D_u and (b) D_{ss} .

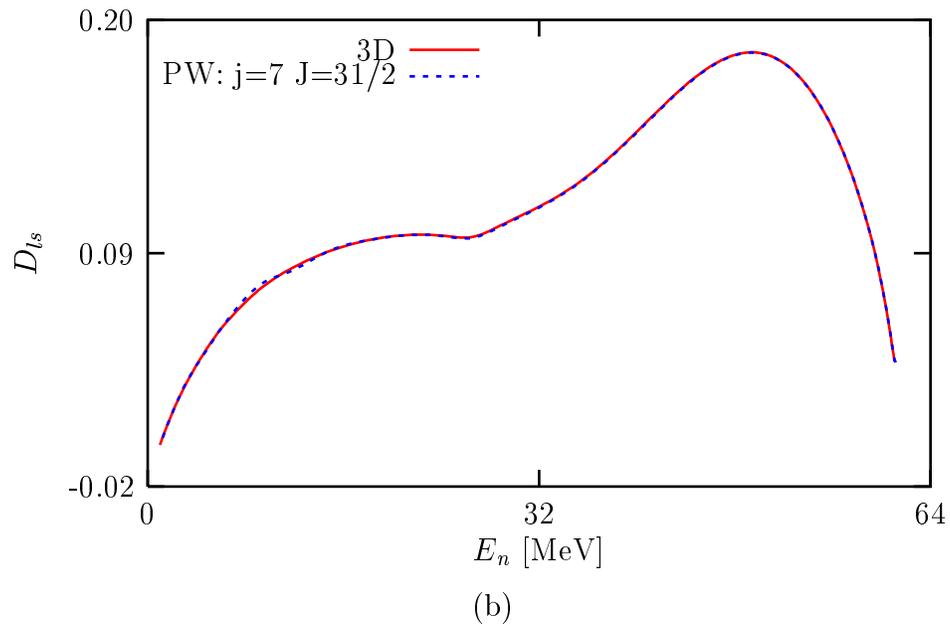
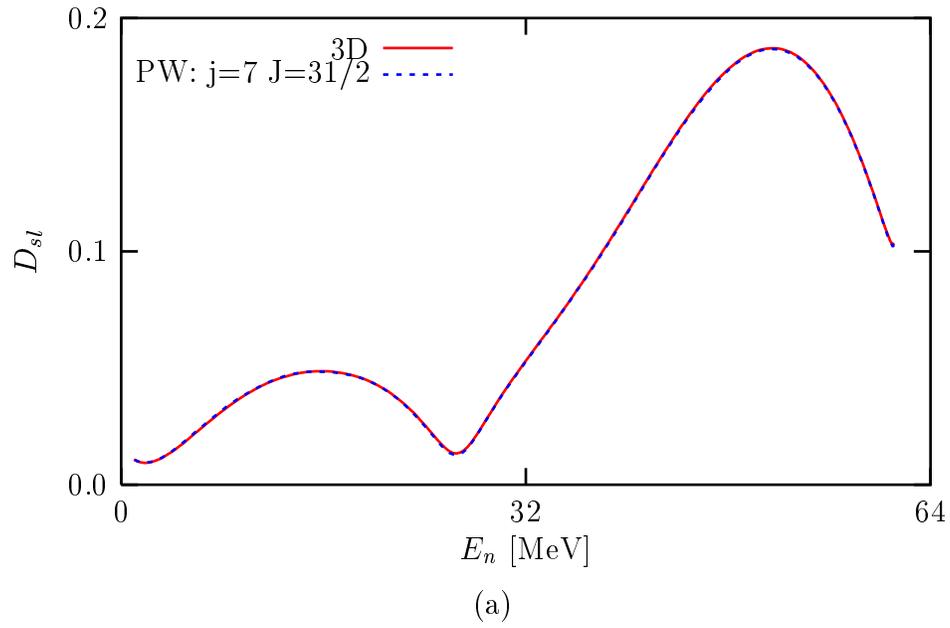


Figure 7.20: Same as in Fig. 7.17, but for the polarization transfer coefficients (a) D_{sl} and (b) D_{ts} .

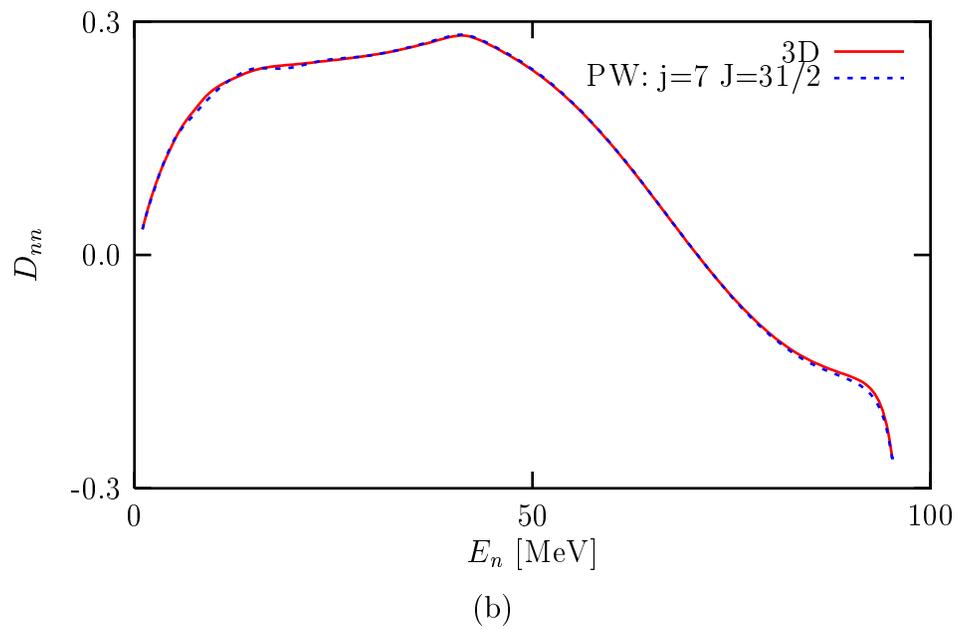
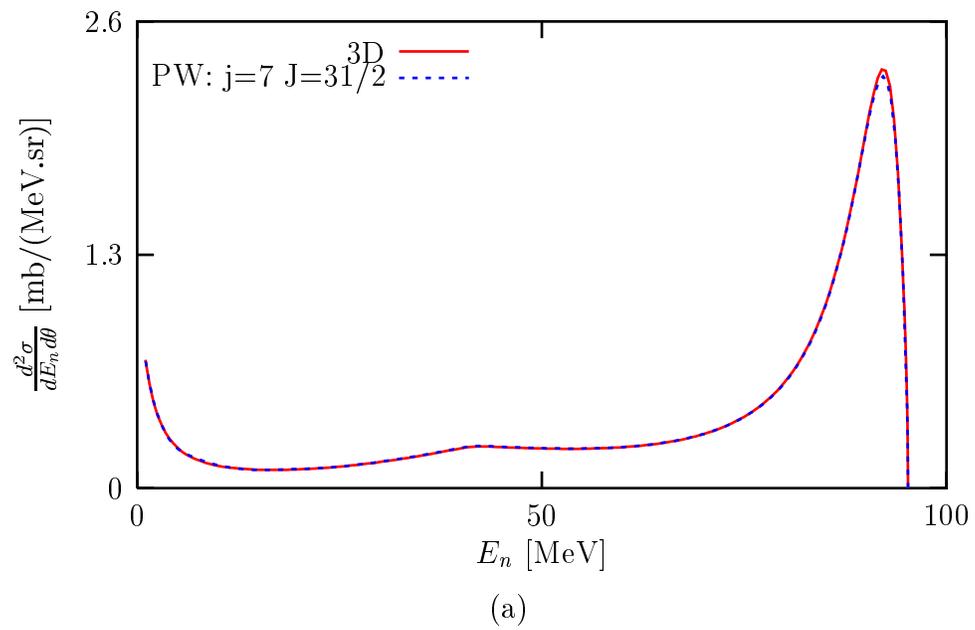


Figure 7.21: Same as in Fig. 7.17, but at $E_{lab} = 100$ MeV and $\theta_{lab} = 13^\circ$.

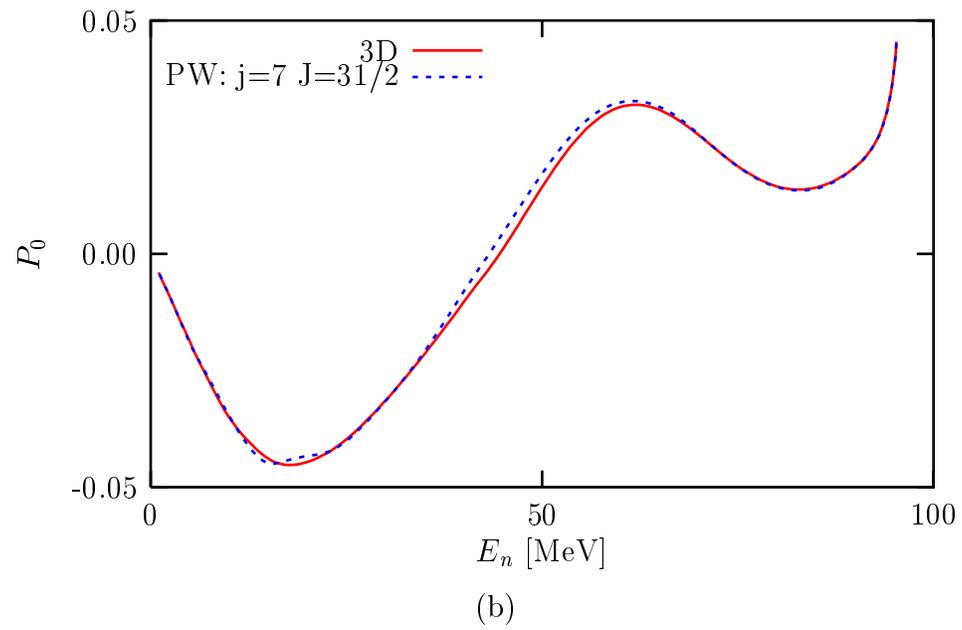
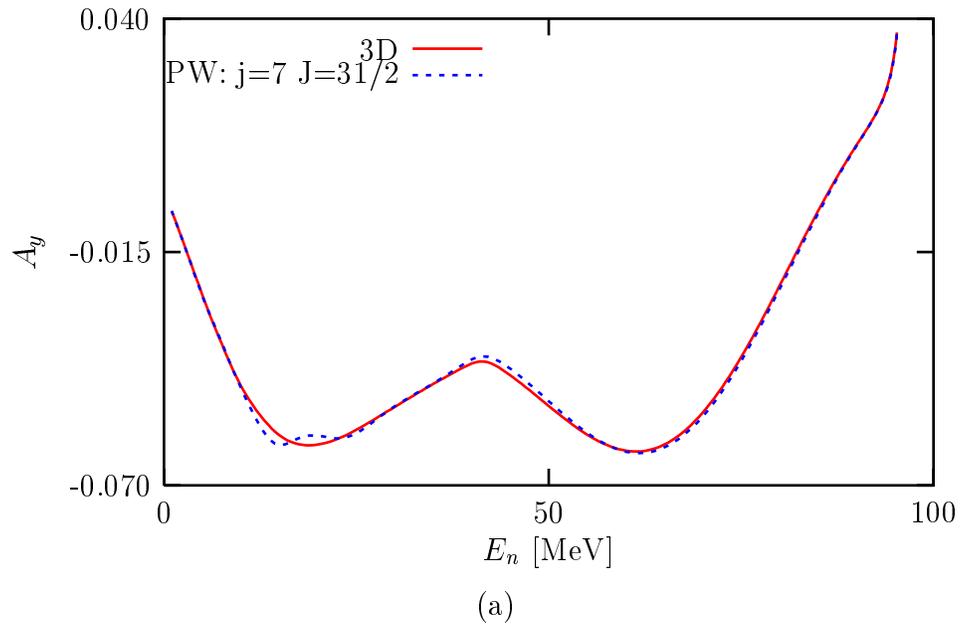


Figure 7.22: Same as in Fig. 7.21, but for (a) the analyzing power A_y and (b) the neutron polarization P_0 .

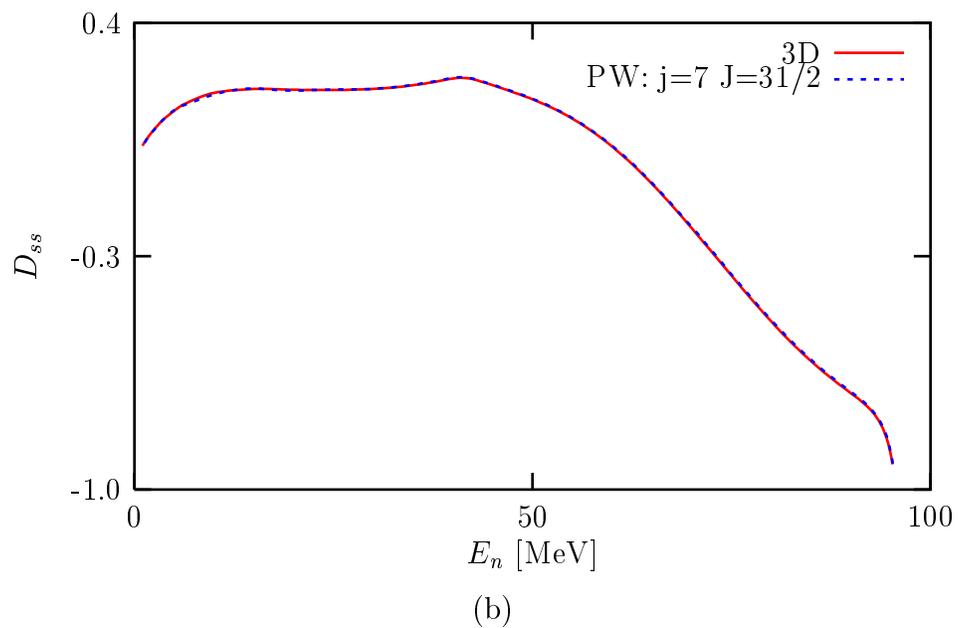
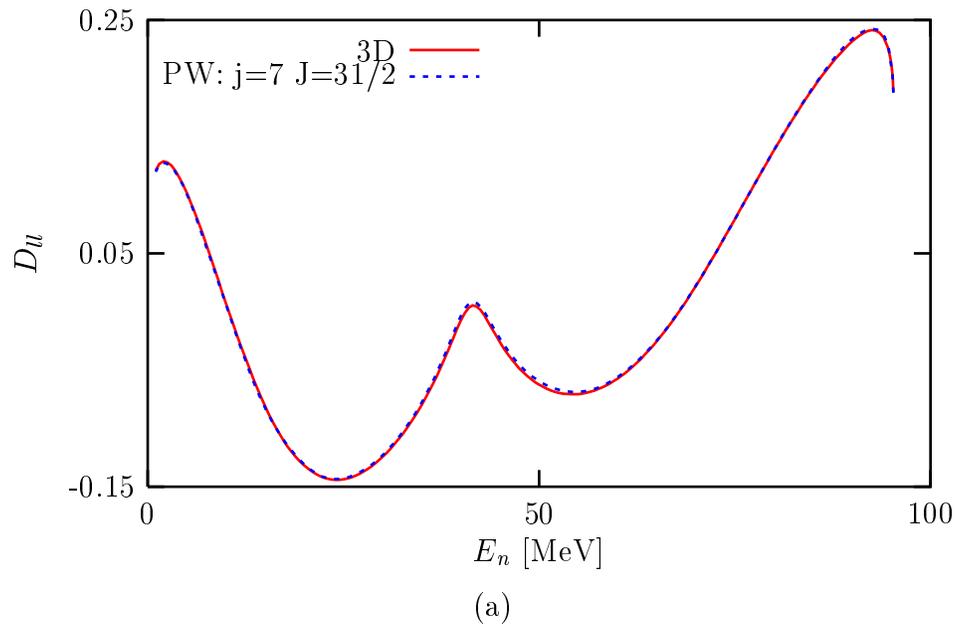


Figure 7.23: Same as in Fig. 7.21, but for the polarization transfer coefficients (a) D_u and (b) D_{ss} .

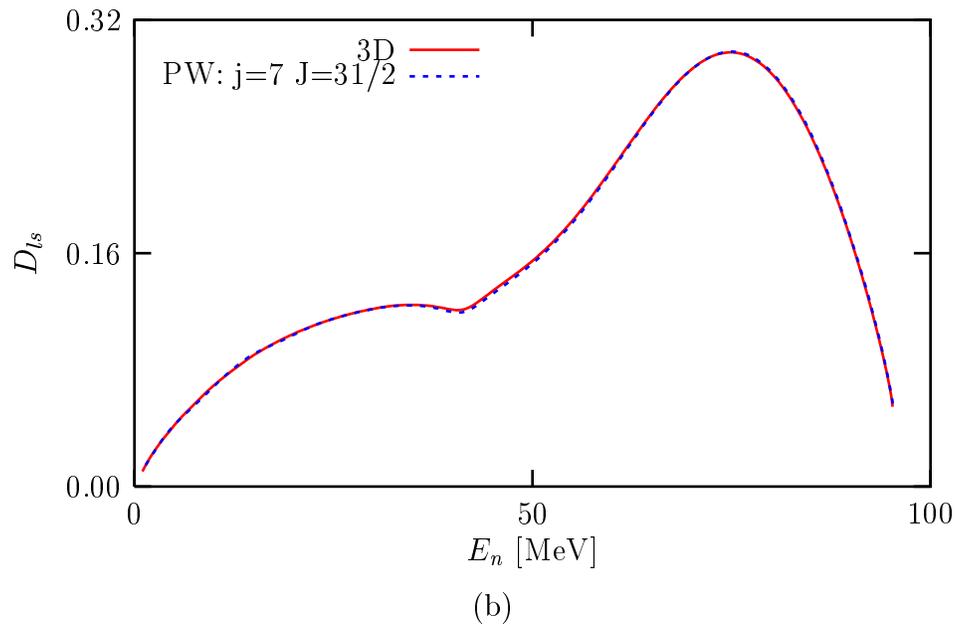
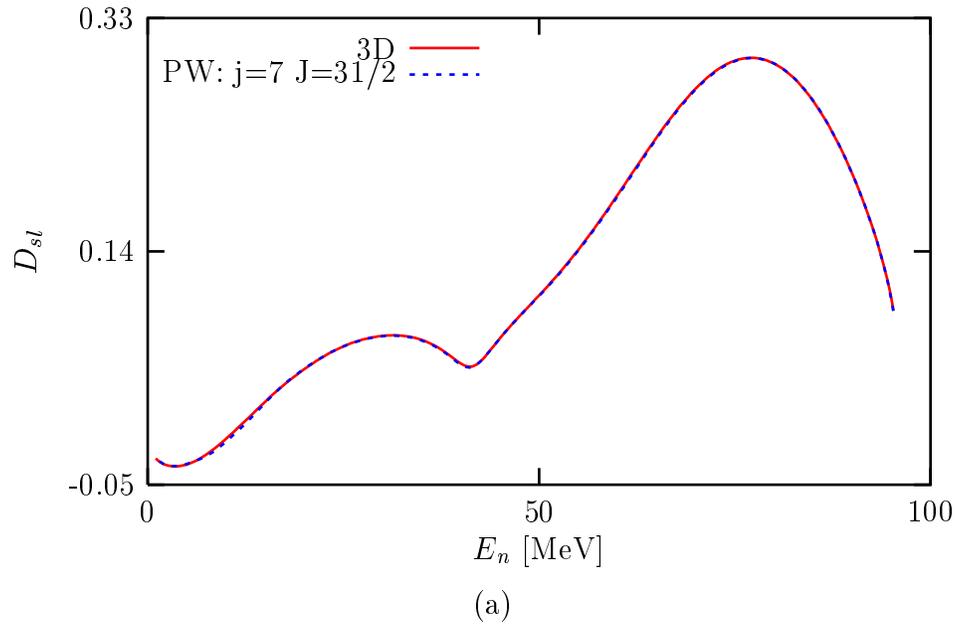


Figure 7.24: Same as in Fig. 7.21, but for the polarization transfer coefficients (a) D_{sl} and (b) D_{ts} .

7.2 Contributions from the Rescattering Terms

In the present work we include only the leading term of the full Faddeev Nd break-up amplitude and leave out the rescattering terms. It can be expected that with increasing energy the importance of the rescattering terms will have decreased. This can, however, depend on the kinematical regime. Now unfortunately a 3D full Faddeev calculation does not yet exist to compare with. Thus, we are forced to compare with existing PW full Faddeev calculations, which actually can be expected to be reliable only below $E_{lab} \simeq 100$ MeV as inferred from our comparisons in the last section in first order in the NN T-matrix. Nevertheless the comparisons with the PW full Faddeev calculations at some higher energies will provide some hints about the importance of rescattering effects. This insight will then be some orientation about the usefulness of comparing our 3D calculations in first order in the NN T-matrix with data. Since now we shall also show experimental data, it is necessary to discuss the NN potentials Bonn-B and AV18, before we continue to discuss multiple scattering effects. As already mentioned in Chapter 4 the two NN potentials are defined below 350 MeV NN laboratory energy. This corresponds to the NN c.m. energy of 175 MeV. In the Nd break-up process and in our approximations of keeping the NN T-matrix in first order only the energy for the NN T-matrix is fixed in terms of the final nucleon's laboratory momenta and the projectile's energy. Thus, we can determine the maximum NN c.m. energy occurring in the 2N subsystem. At $E_{lab} \simeq 200$ MeV the maximum NN c.m. energy occurring in the 2N-subsystem is about 133.4 MeV (refer to Section G.4). Therefore, for the Nd break-up process at $E_{lab} \simeq 200$ MeV the NN T-matrix elements obtained from the two NN potentials are reasonably correct. It will be interesting to see the effects from the off-shell part of the NN T-matrices, which are somewhat different between the two NN potential as shown in Chapter 4. In a more complete dynamical picture one would have to add also a proper 3N force. Thus, contributions from the off-shell behavior of the NN T-matrix and the 3N force would balance each other and the results should be invariant under exchange of the models [56]. Here in our restricted dynamical input we can only get insight, whether the NN potentials Bonn-B and AV18 yield essentially the same results or different ones. For E_{lab} higher than 263 MeV the maximum NN c.m. energy is higher than 175 MeV, thus, beyond the energy range, where the NN potentials Bonn-B and AV18 are defined. Therefore, this can be one source of deficiencies in describing the Nd break-up process at $E_{lab} > 263$ MeV.

In Figs. 7.25-7.40 we show the 3D calculations, the PW full Faddeev calculations [54] and experimental data [18] at $E_{lab} = 197$ MeV and various scattering angles θ_{lab} for the investigated observables in the pd break-up process. The PW full Faddeev calculations

take $j = 5$, $J = 31/2$ for the NN potential AV18 and $j = 4$, $J = 31/2$ for the NN potential Bonn-B. In the last section we have seen that at $E_{lab} \simeq 100$ MeV one has already reached the limits of the PW calculations to get converged results. In that investigation the case was simpler, since one took only the leading term of the full Faddeev Nd break-up amplitude. Thus, one could include partial waves up to $j = 7$, $J = 31/2$. Now the case is more complex, since the rescattering terms are also included. Hence, we are provided with the PW calculations only with a lower number of partial waves. Nevertheless, it is sufficient to qualitatively see multiple scattering effects. Let us take a look at Figs. 7.25-7.28, which show the observables at $\theta_{lab} = 13^\circ$. Figure 7.25(a) displays the cross section. The sharp peak in the PW calculations close to the highest neutron energy E_n is due to the final state interaction (FSI) between the two protons, which are not detected. The FSI takes place if the two protons are moving together in the same direction. Thus, the relative momentum between the two protons is zero and this happens if the neutron takes most of the energy. The FSI is not taken into account in the 3D calculation and the peak is not detected in the experiment due to the E_n -resolution. Therefore, here we can put the FSI aside. The figure shows that the inclusion of the rescattering terms lowers the theoretical predictions for the cross section. Now among the spin observables the analyzing power A_y turns out to be suitable to see rescattering effects in the pd break-up process. The inclusion of the rescattering terms for A_y in Fig. 7.26(a) greatly improves the theoretical predictions to match the experimental data better. The effect is as if it tilts A_y by raising its one end at lower E_n . For the other spin observables the inclusion of the rescattering terms leads to smaller effects than for A_y . In some cases like, for example, for D_{ll} in Fig. 7.27(a) at lower E_n it improves the theoretical predictions. But in some other cases like for D_{ss} in Fig. 7.27(b) it causes worse agreements with the data. Next in Figs. 7.29-7.32 we show the same set of observables at a different scattering angle $\theta_{lab} = 24^\circ$. Again for the cross section in Fig. 7.29(a) we see the rescattering effects as lowering the theoretical cross section peak. Now the theoretical cross section peaks overlap with the data. For A_y in Fig. 7.30(a) we also see the similar rescattering effects as at $\theta_{lab} = 13^\circ$, which is like a tilt of A_y by raising its one end at lower E_n . In addition we also see at E_n towards its maximum that the inclusion of the rescattering terms drops A_y . For other observables we see some various changes caused by the rescattering terms. At other scattering angles $\theta_{lab} = 37^\circ$ in Figs. 7.33-7.36 and $\theta_{lab} = 48^\circ$ in Figs. 7.37-7.40 we see a similar situation for the investigated observables. At this point we have to conclude that at $E_{lab} \simeq 200$ MeV the rescattering terms still give much contributions to the full pd break-up amplitude and hence cannot be neglected.

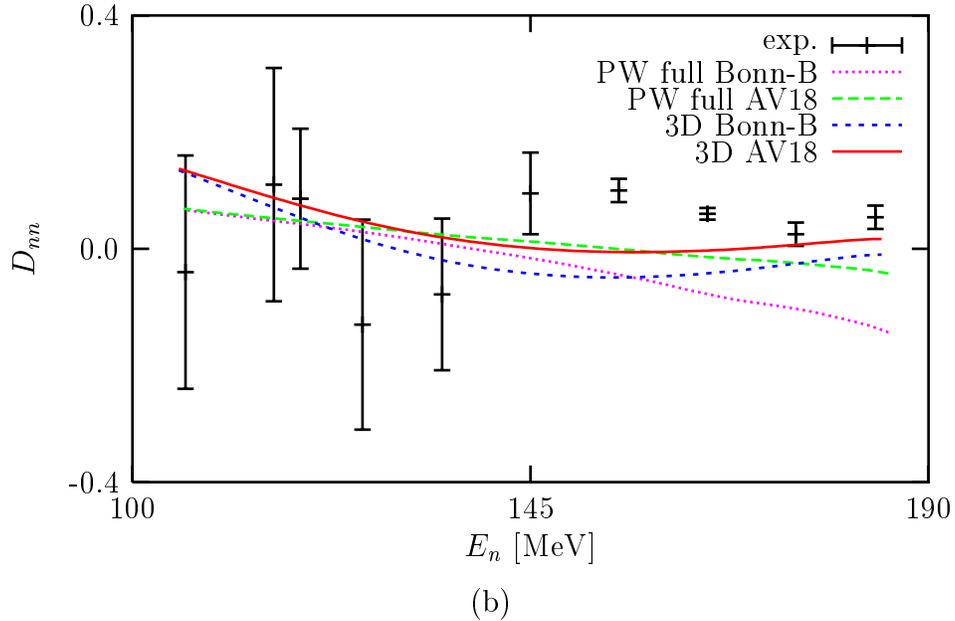
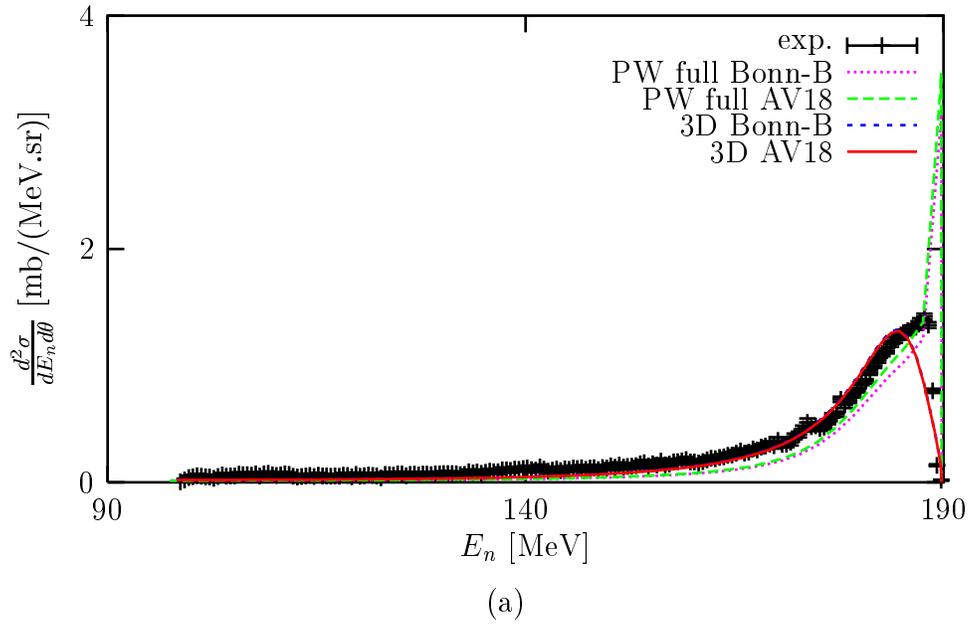


Figure 7.25: The 3D and the PW calculations for (a) the spin averaged differential cross section and (b) the polarization transfer coefficient D_{nn} in the pd break-up process at $E_{lab} = 197$ MeV and $\theta_{lab} = 13^\circ$. The NN potentials used are Bonn-B and AV18. The 3D calculations take the pd break-up amplitude, while the PW calculations take the full pd break-up amplitude. The experimental data are taken from Ref. [18]. The sharp peak in the PW calculations for the cross section close to the highest neutron outgoing energy E_n is due to the final state interaction between the two proton, which are not detected. See text for more details.

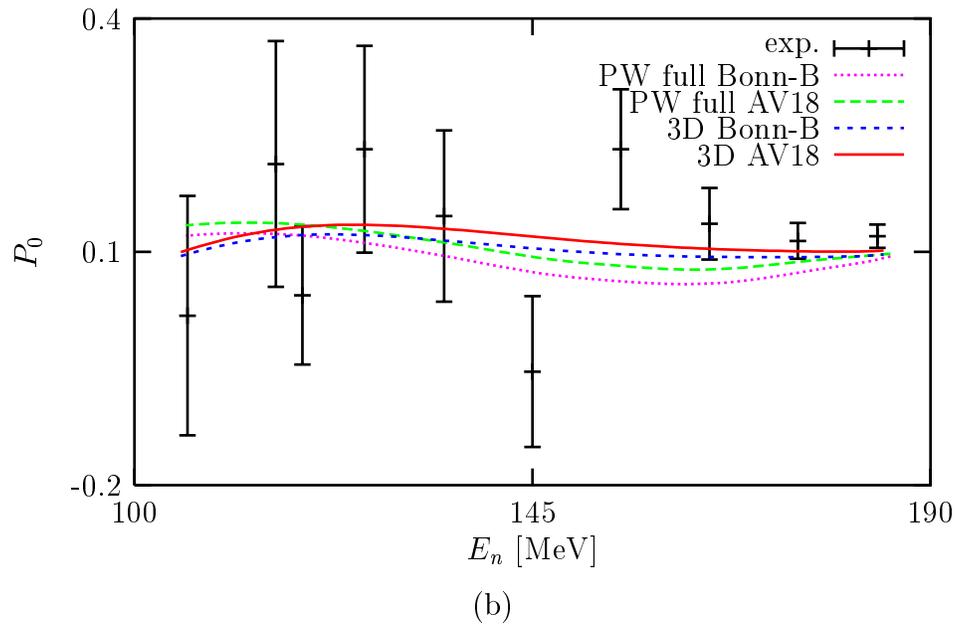
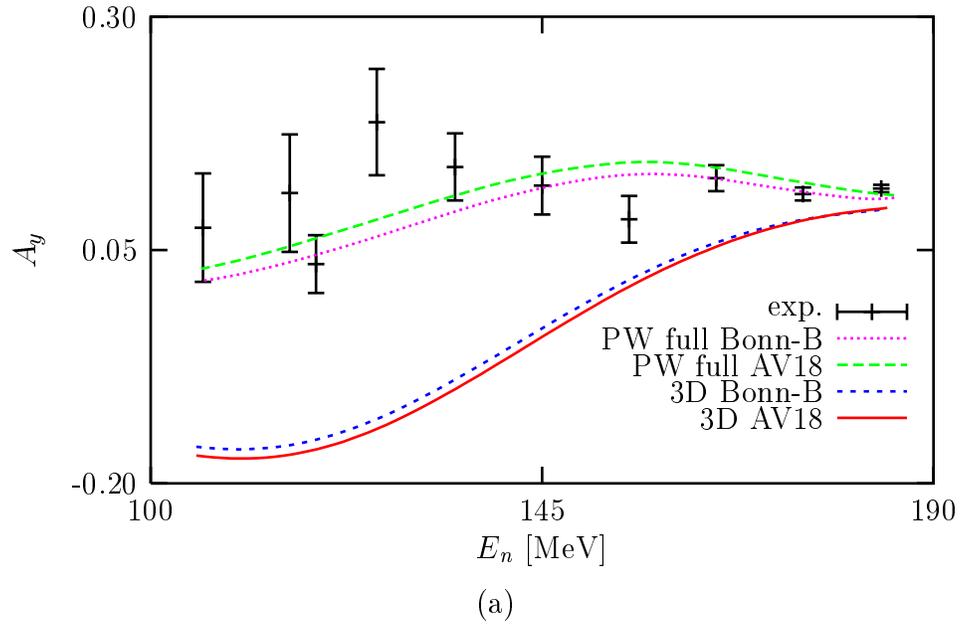


Figure 7.26: Same as in Fig. 7.25, but for (a) the analyzing power A_y and (b) the neutron polarization P_0 .

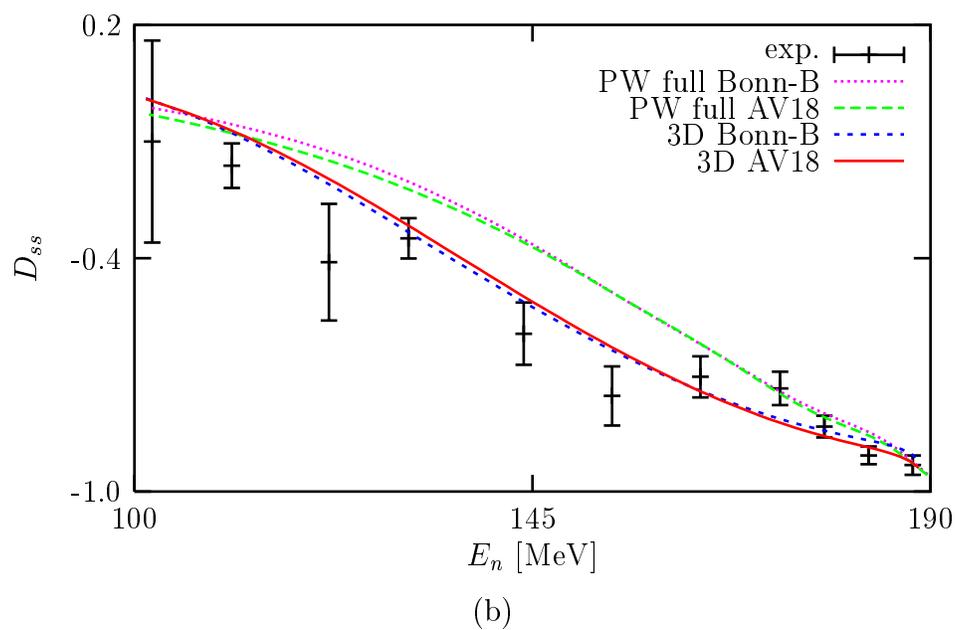
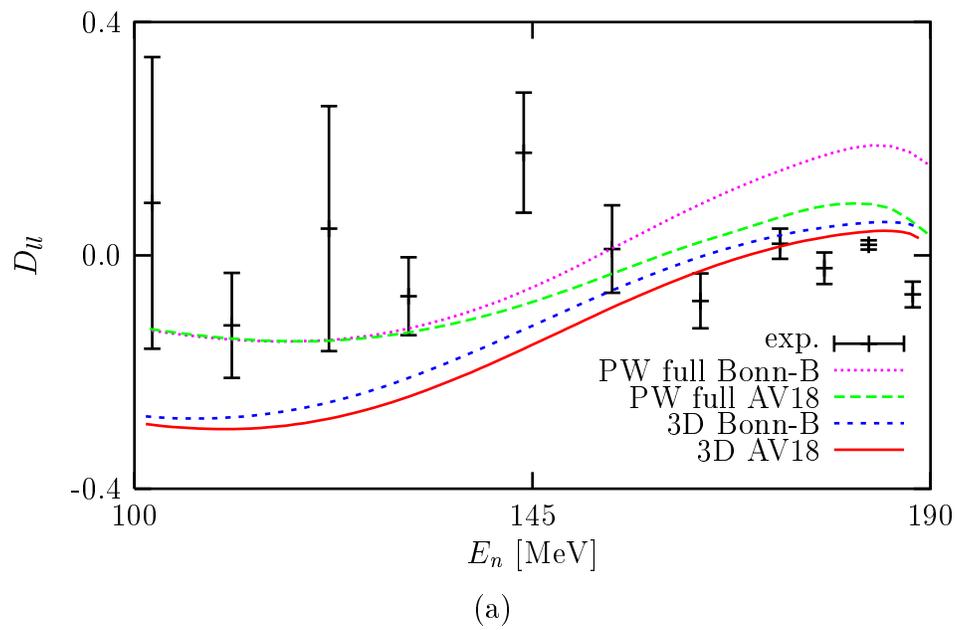


Figure 7.27: Same as in Fig. 7.25, but for the polarization transfer coefficients (a) D_u and (b) D_{ss} .

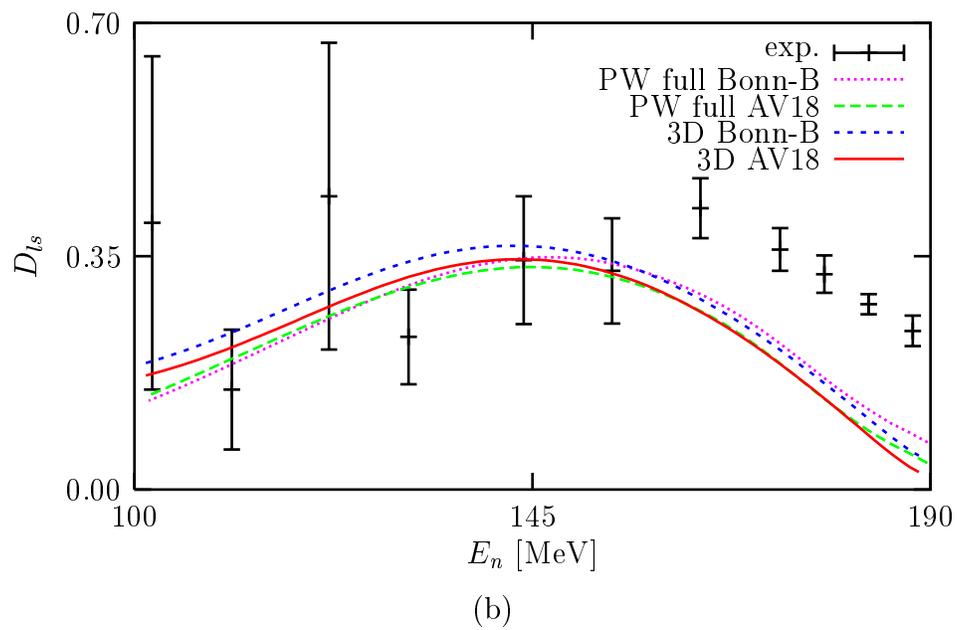
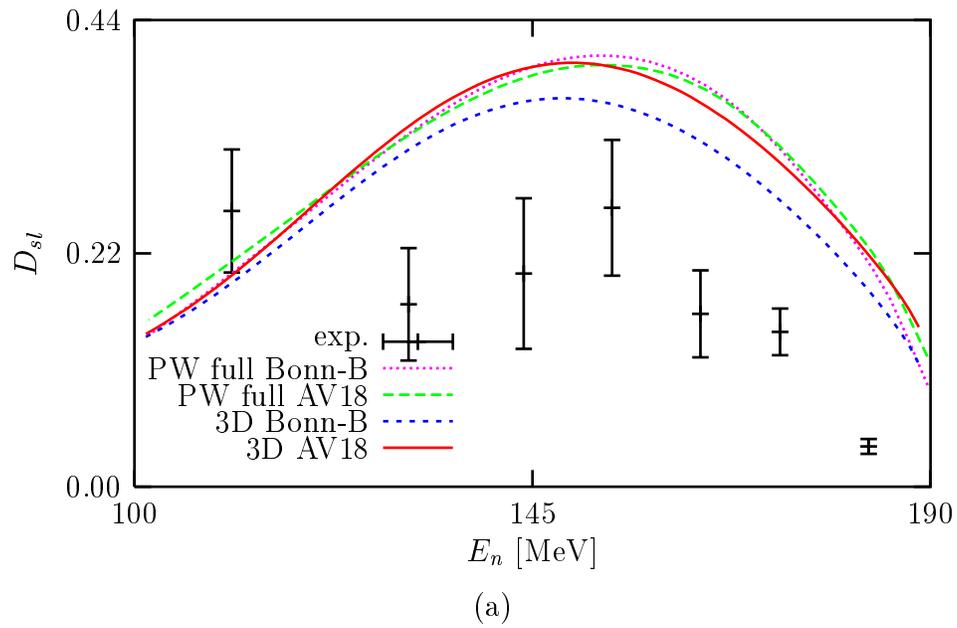
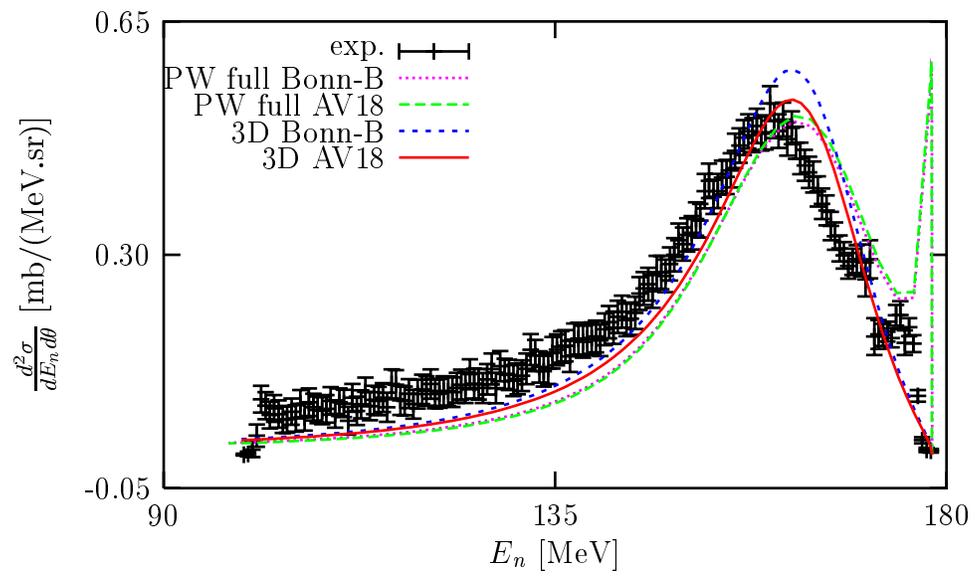
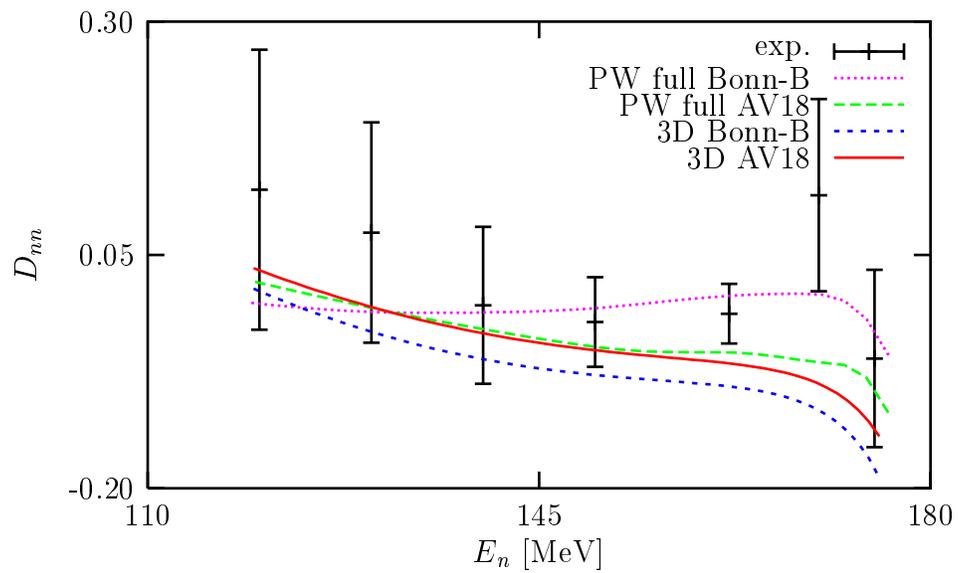


Figure 7.28: Same as in Fig. 7.25, but for the polarization transfer coefficients (a) D_{sl} and (b) D_{ts} .



(a)



(b)

Figure 7.29: Same as in Fig. 7.25, but at $\theta_{lab} = 24^\circ$.

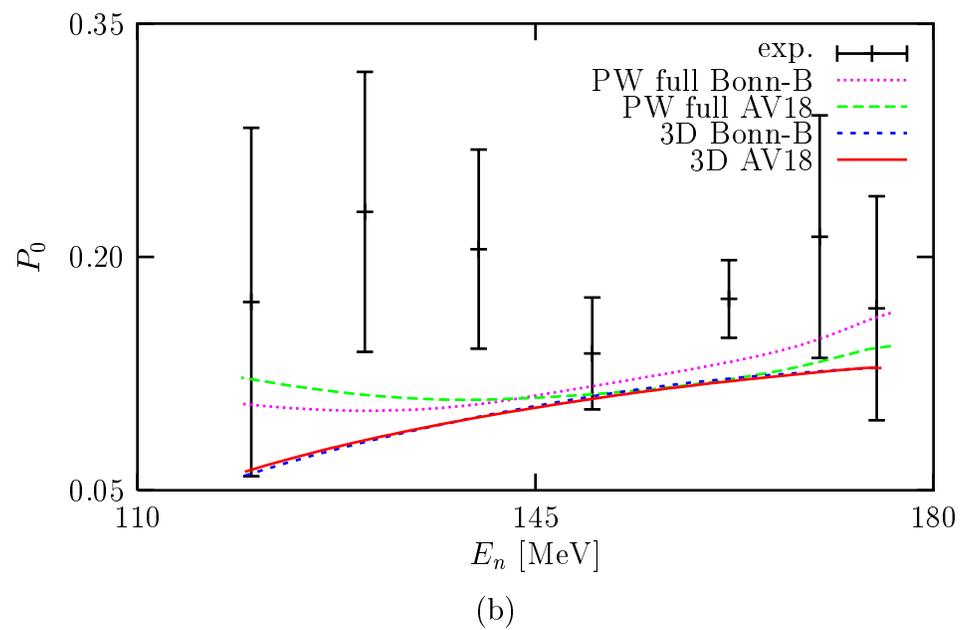
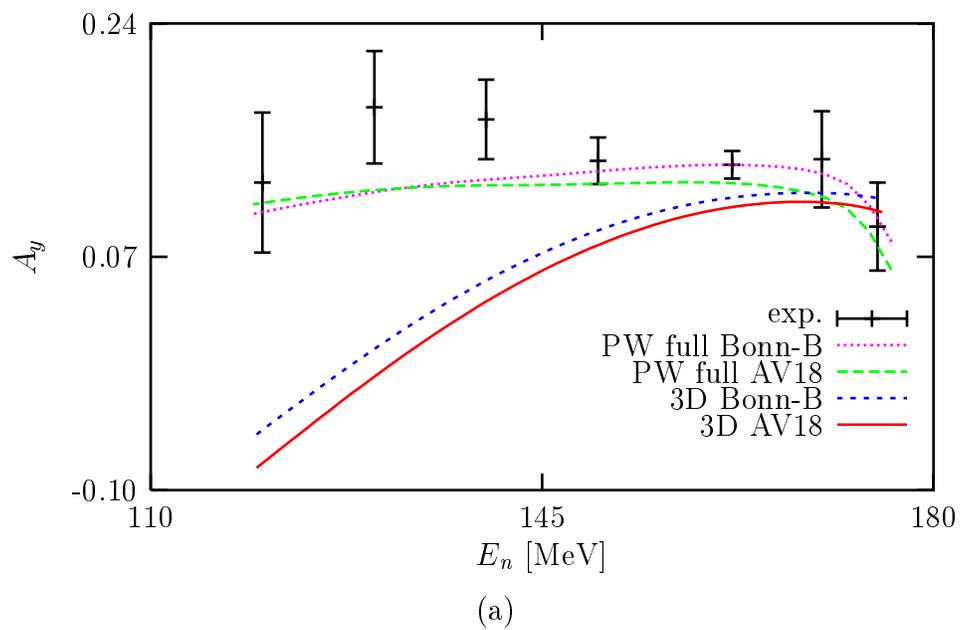
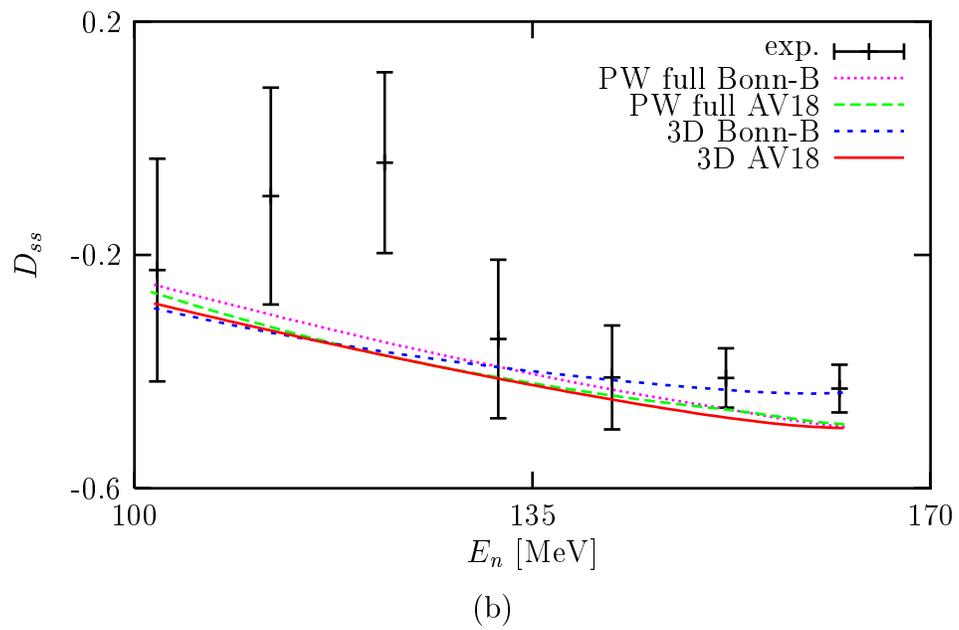
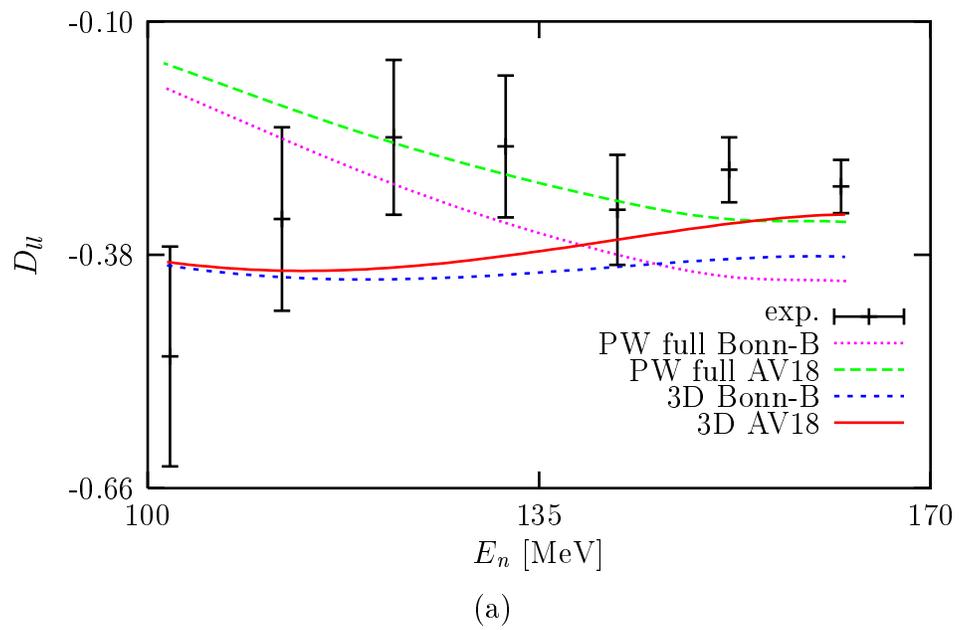


Figure 7.30: Same as in Fig. 7.26, but at $\theta_{lab} = 24^\circ$.

Figure 7.31: Same as in Fig. 7.27, but at $\theta_{lab} = 24^\circ$.

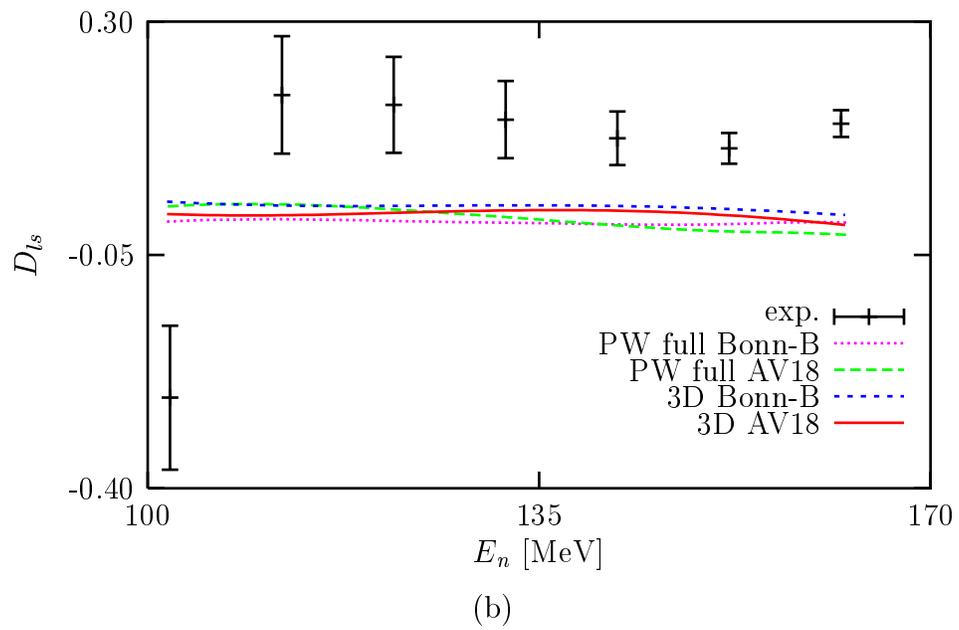
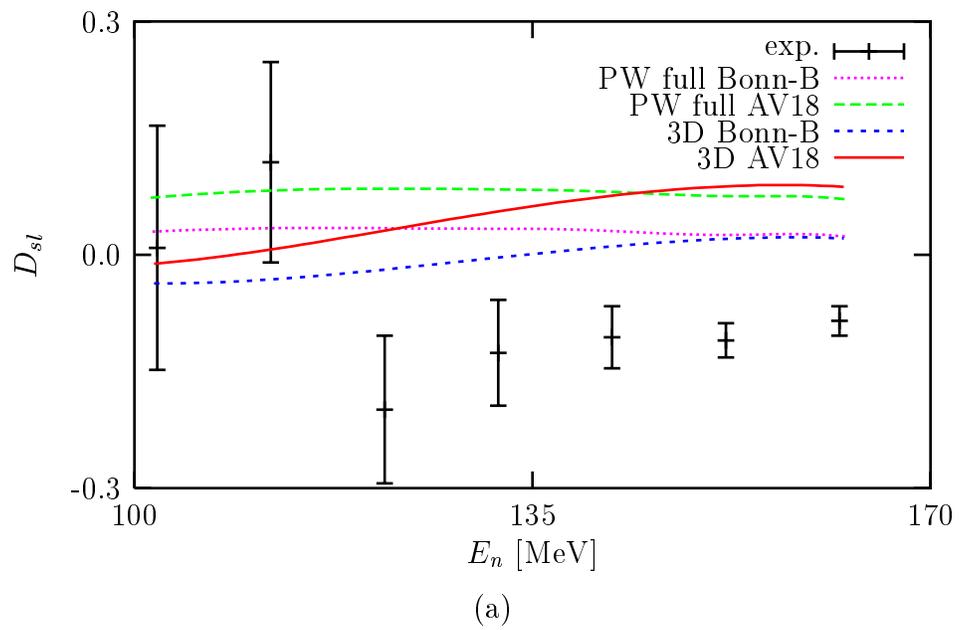
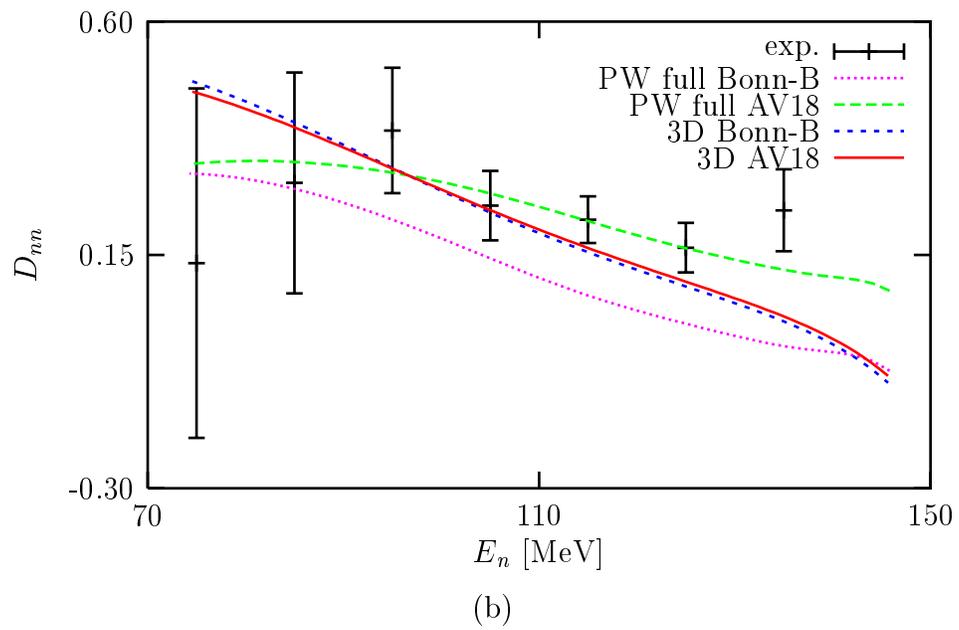
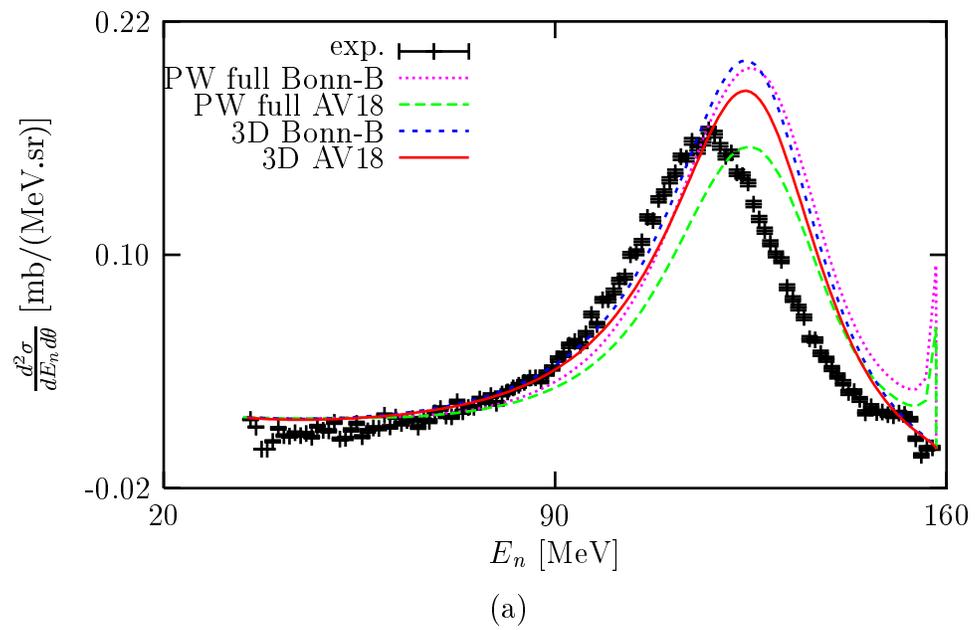


Figure 7.32: Same as in Fig. 7.28, but at $\theta_{lab} = 24^\circ$.

Figure 7.33: Same as in Fig. 7.25, but at $\theta_{lab} = 37^\circ$.

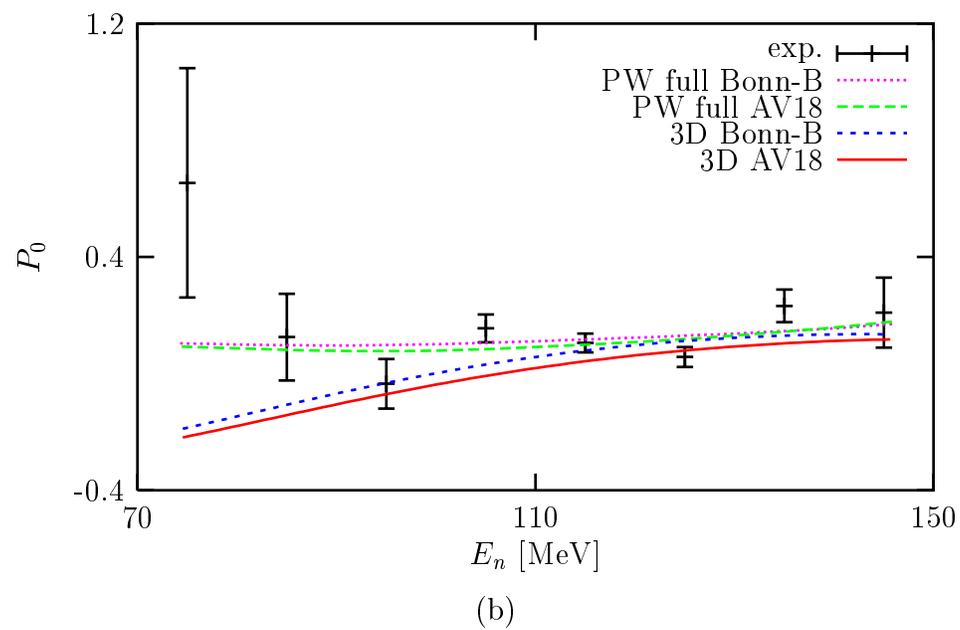
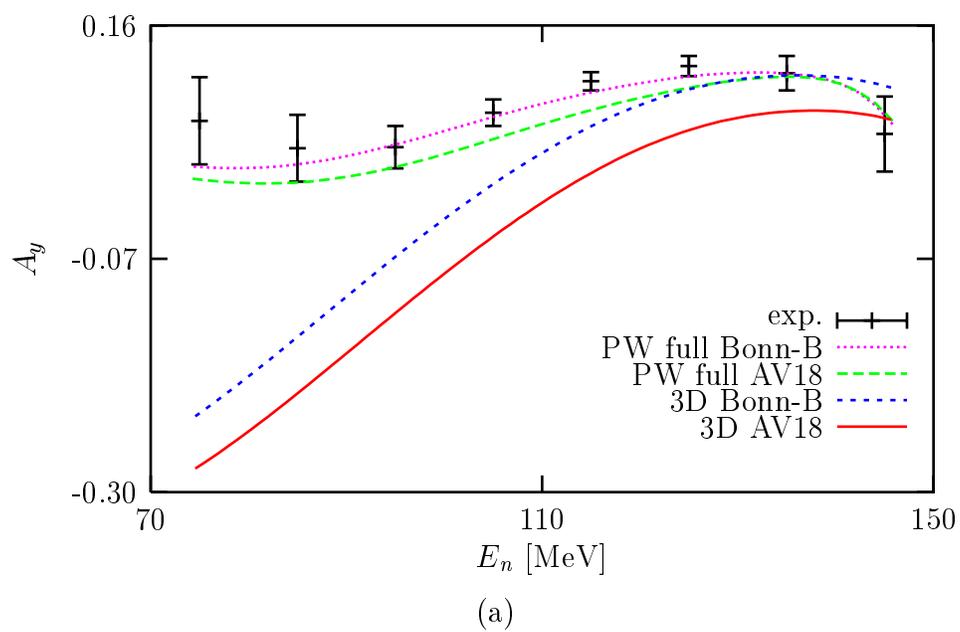
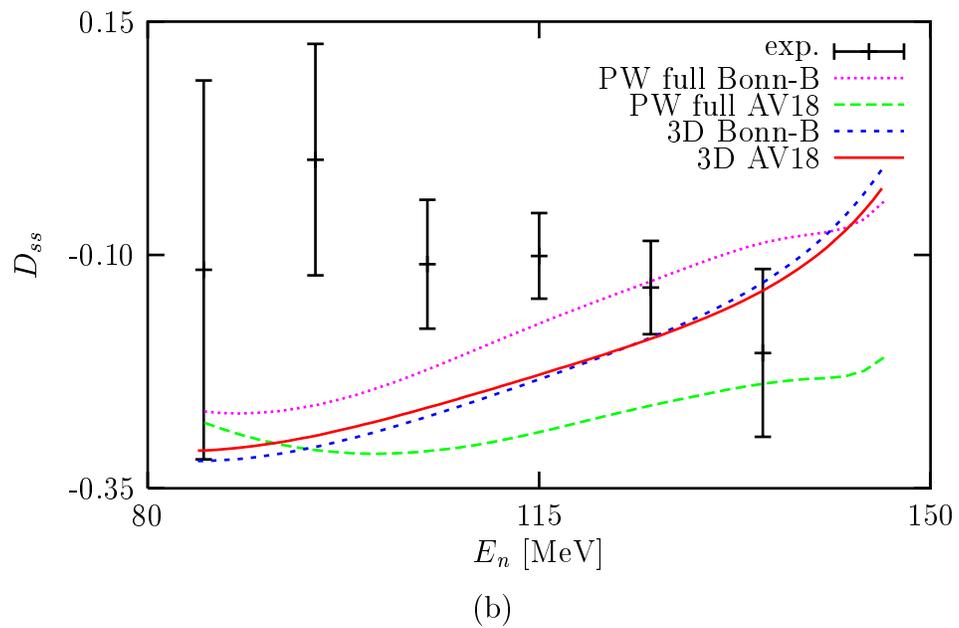
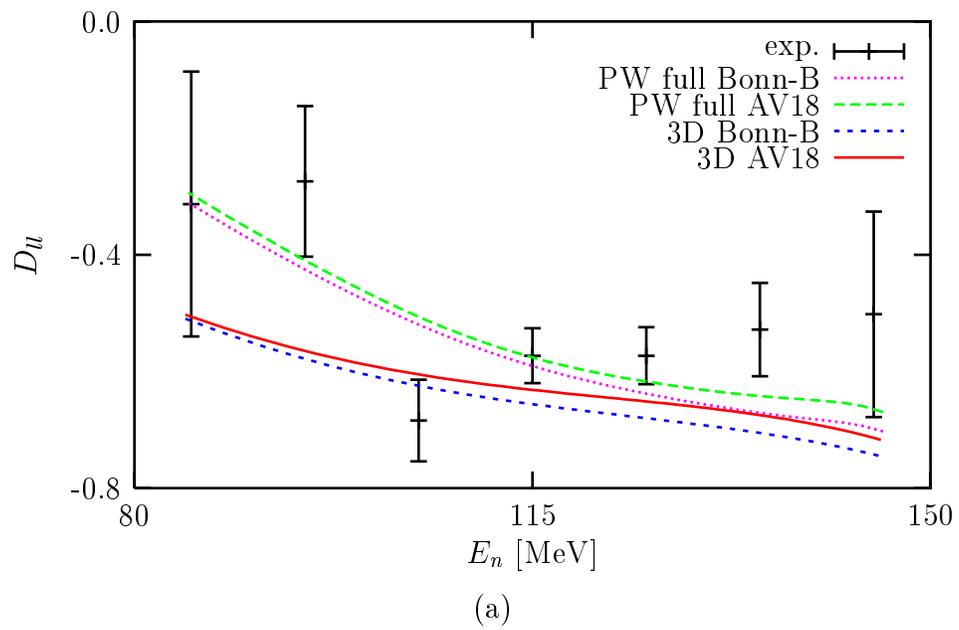


Figure 7.34: Same as in Fig. 7.26, but at $\theta_{lab} = 37^\circ$.

Figure 7.35: Same as in Fig. 7.27, but at $\theta_{lab} = 37^\circ$.

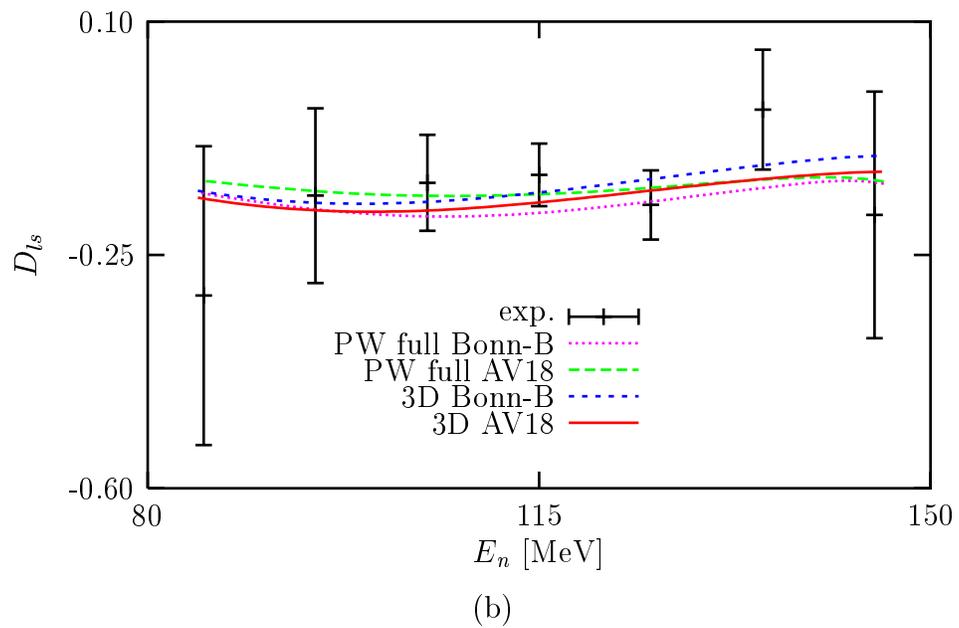
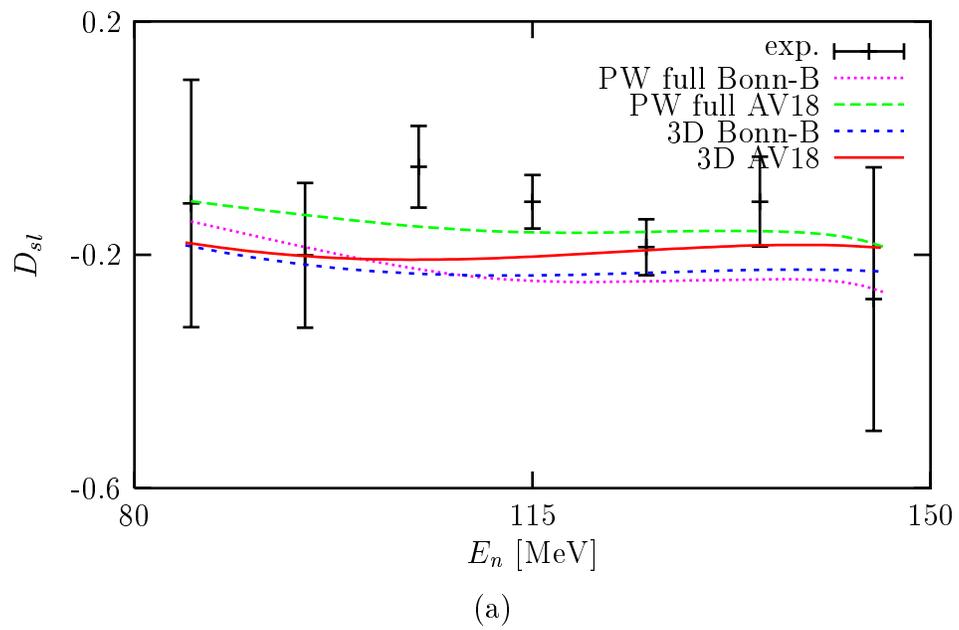
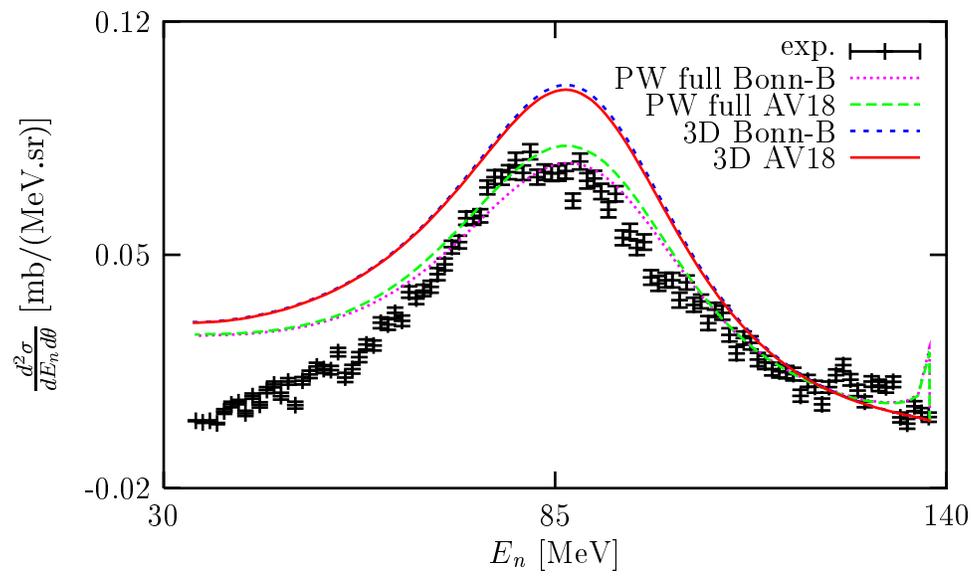
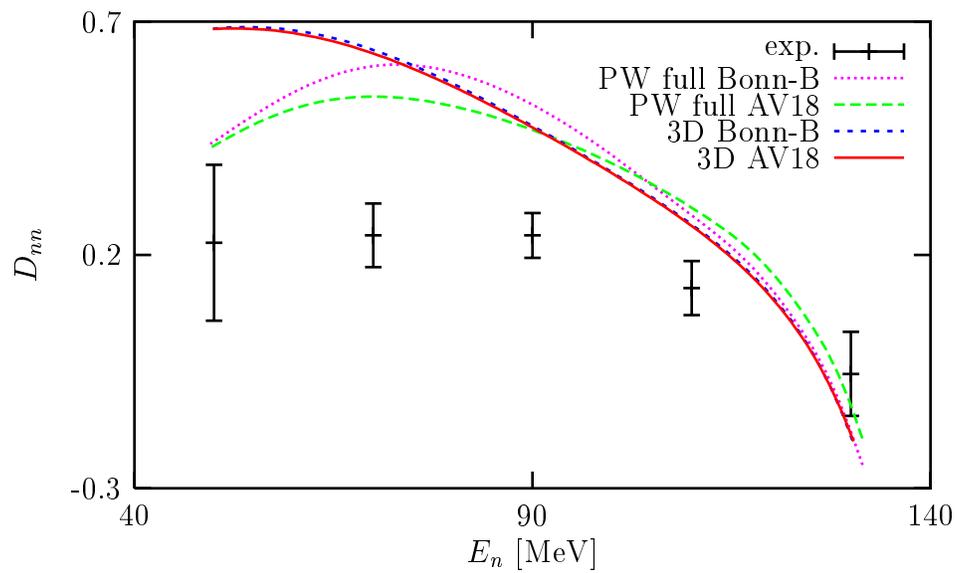


Figure 7.36: Same as in Fig. 7.28, but at $\theta_{lab} = 37^\circ$.

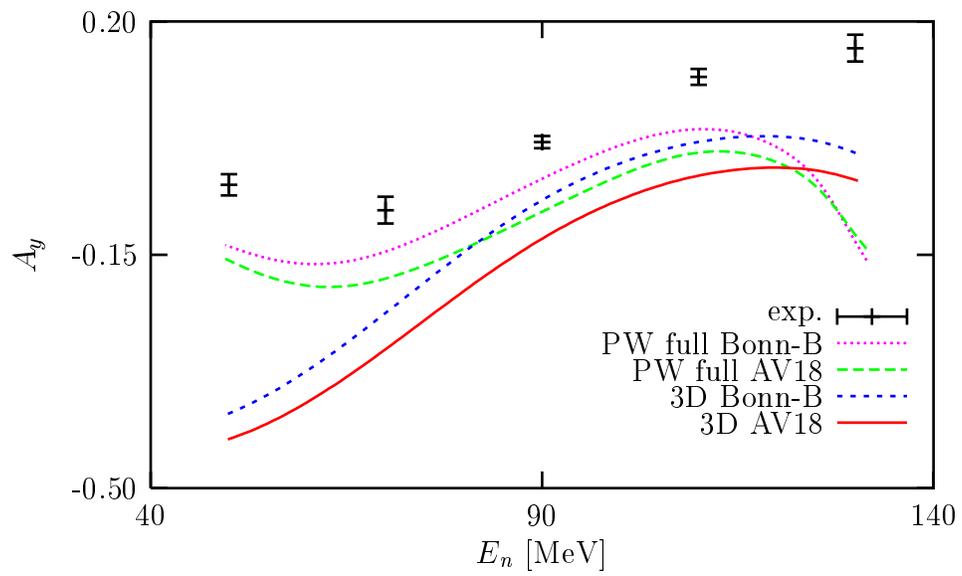


(a)

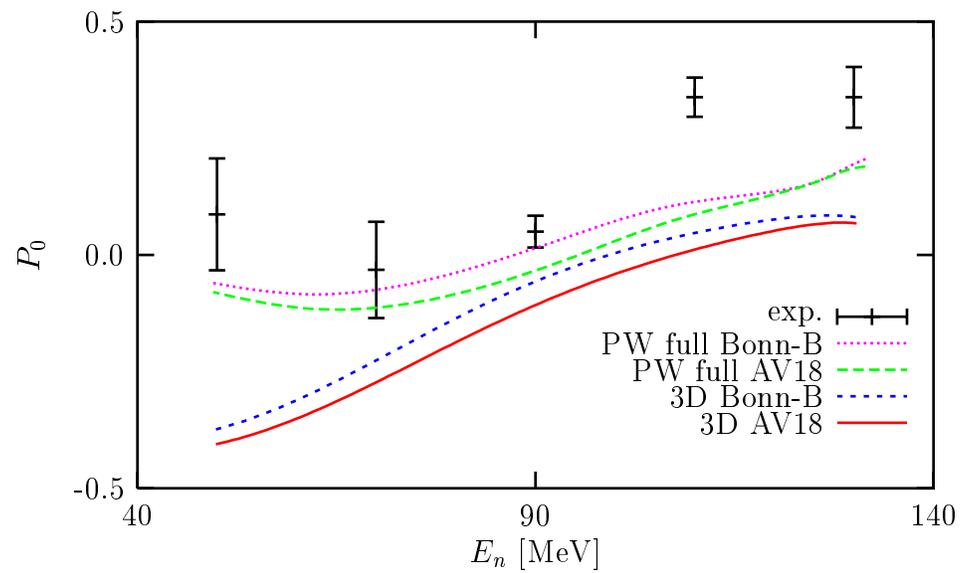


(b)

Figure 7.37: Same as in Fig. 7.25, but at $\theta_{lab} = 48^\circ$.

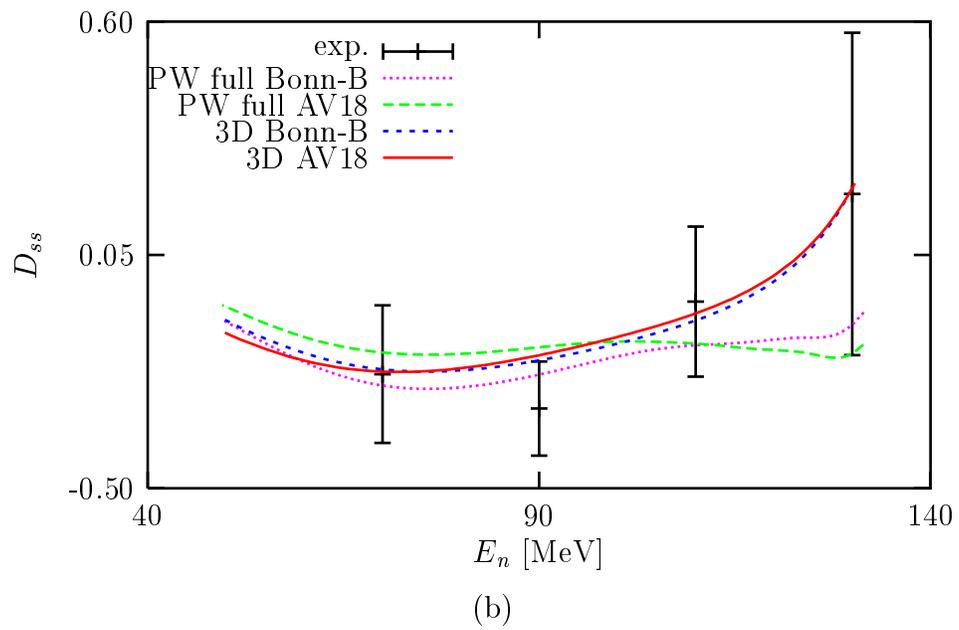
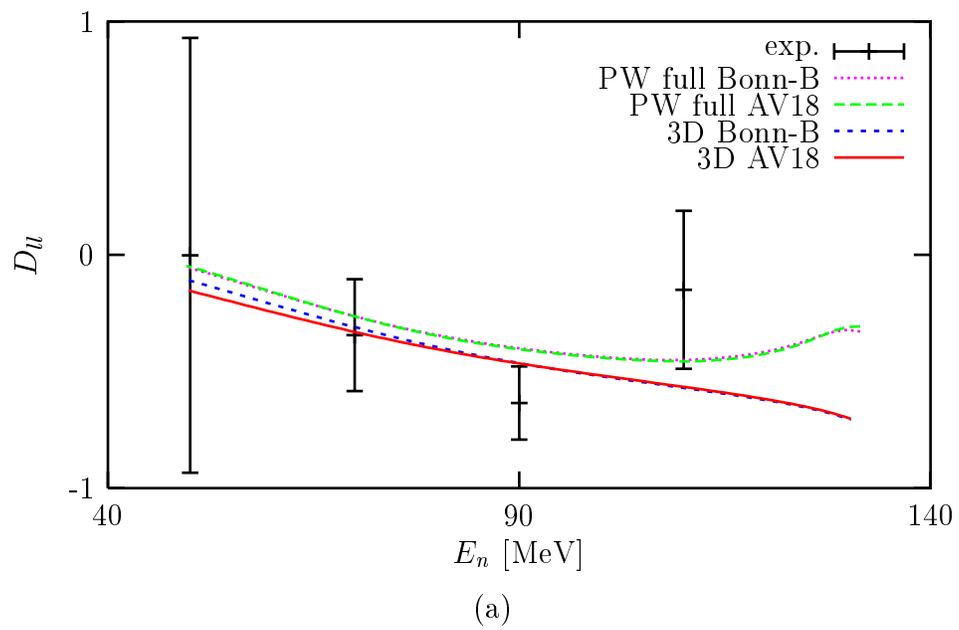


(a)



(b)

Figure 7.38: Same as in Fig. 7.26, but at $\theta_{lab} = 48^\circ$.

Figure 7.39: Same as in Fig. 7.27, but at $\theta_{lab} = 48^\circ$.

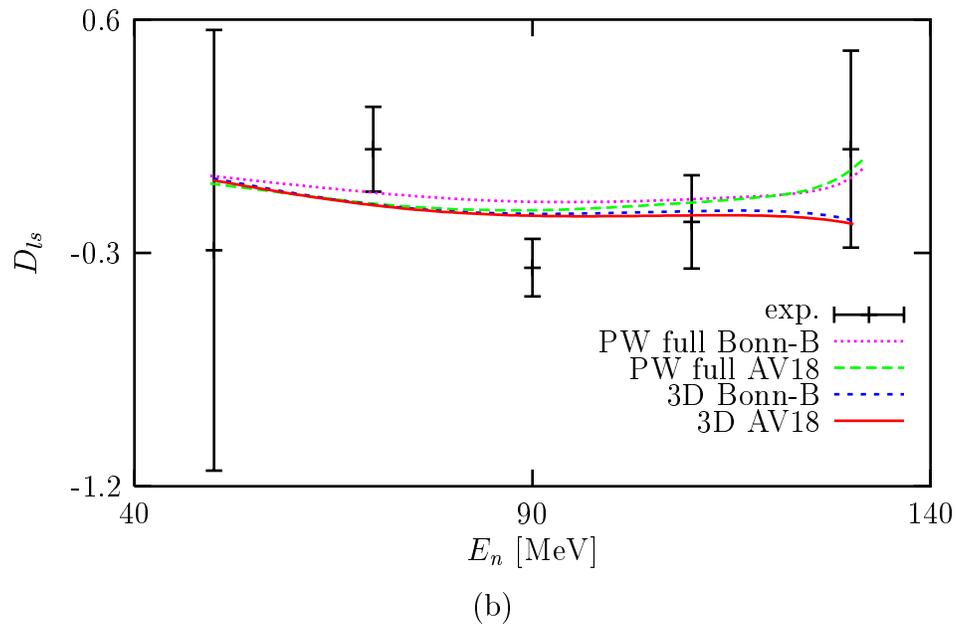
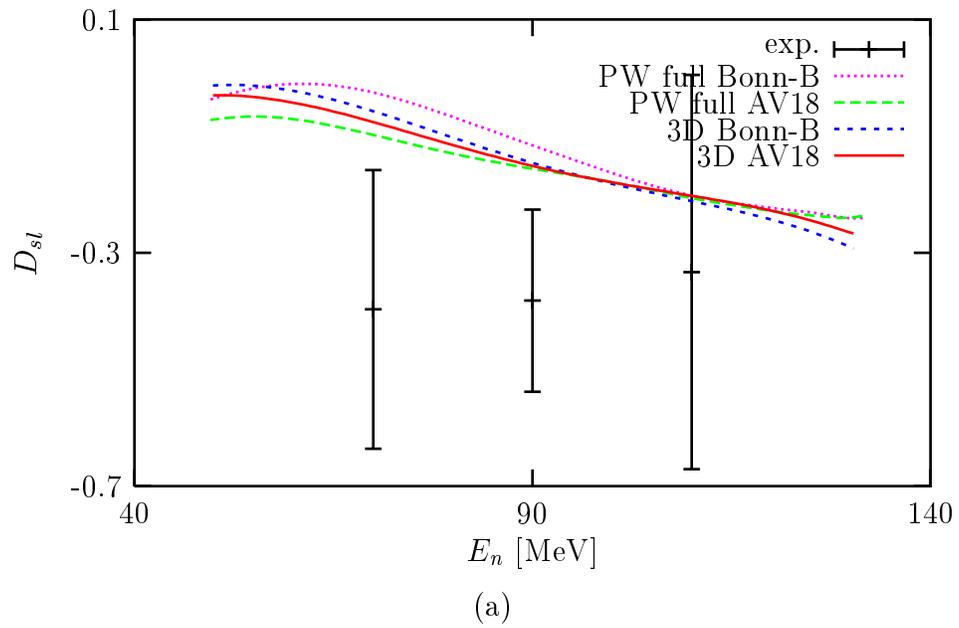


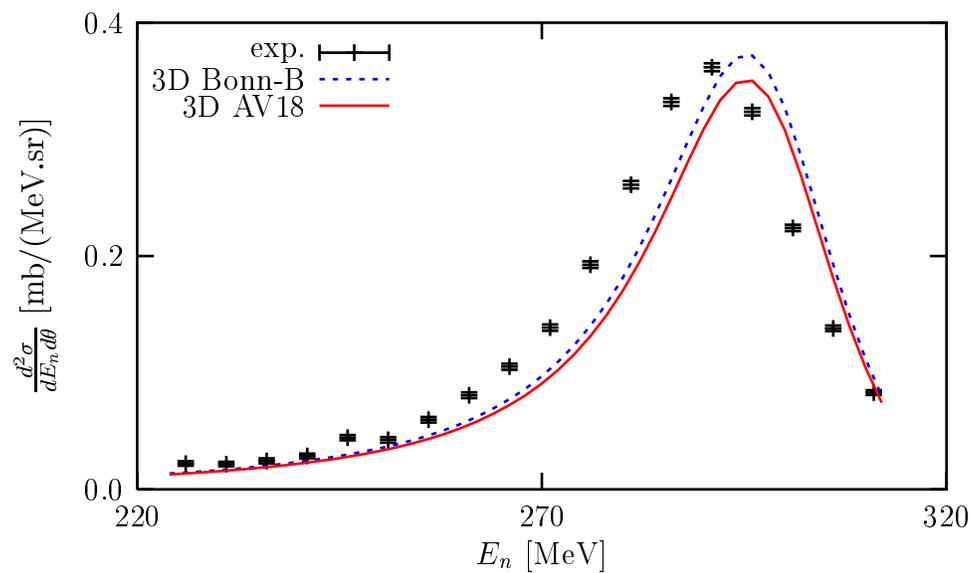
Figure 7.40: Same as in Fig. 7.28, but at $\theta_{lab} = 48^\circ$.

Now we go to higher energies than 200 MeV. There are experimental data at $E_{lab} = 346$ MeV [19]. Unfortunately there exists no full Faddeev calculation for this energy. Hence, we can compare only with data. In Figs. 7.41-7.44 we show the cross section and the spin observables in the pd break-up process at $E_{lab} = 346$ MeV and $\theta_{lab} = 22^\circ$. The calculations agree only qualitatively with the data. In Fig. 7.41(a) the theoretical peak of the cross section for the NN potential Bonn-B is higher than the data, but on the contrary for the NN potential AV18 it is lower than the data. We recall the discussion for $E_{lab} = 197$ MeV that the multiple scattering lowers the cross section. If this process is not negligible at $E_{lab} = 346$ MeV that means that by including the rescattering terms the theoretical prediction based on the NN potential Bonn-B may be improved but the one based on the NN potential AV18 is getting worse. Now regardless the height of the peak, the position of the theoretical peak is shifted to a higher neutron energy E_n , compared to the data. This is actually already seen at $E_{lab} = 197$ MeV and it cannot be fixed by including the rescattering terms. Therefore, other processes are responsible to shift back the cross section peak along E_n to the right position. These dynamical ingredients together with the multiple scattering may also determine the height of the peak or the whole parts of the cross section. For A_y in Fig. 7.42(a) the rescattering terms seem to be required to tilt the theoretical prediction to be closer to the data, if we recall the similar improvement of the theoretical prediction at $E_{lab} = 197$ MeV by including the rescattering terms. Thus, at this energy $E_{lab} = 346$ MeV one can argue that the rescattering terms are still important to be included.

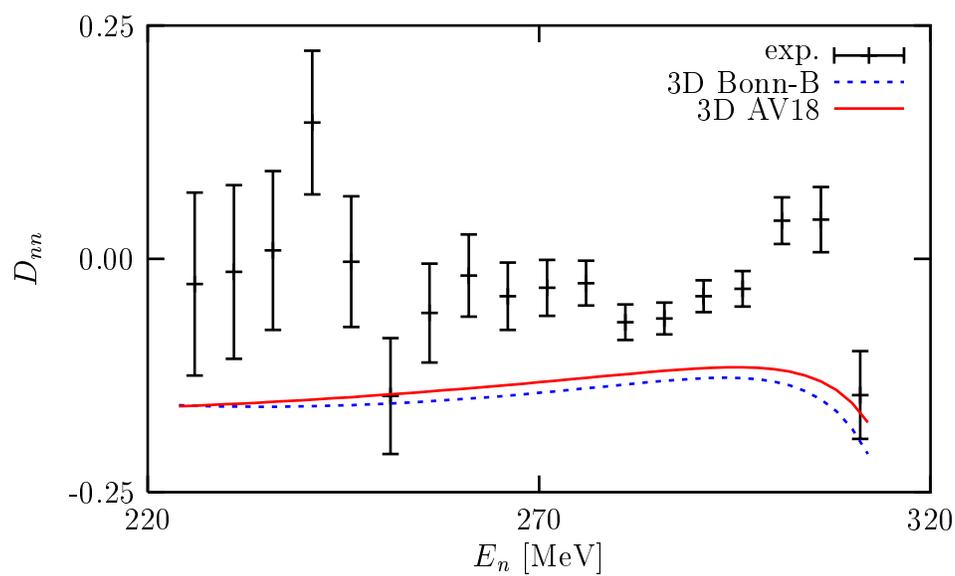
Lastly we go on to $E_{lab} \simeq 500$ MeV. We compare with experimental data at $E_{lab} = 495$ MeV [57]. Again at this energy there is no full Faddeev calculation. In Figs. 7.45-7.48 we show the observables at $E_{lab} = 495$ MeV and $\theta_{lab} = 18^\circ$. We see in Fig. 7.45(a) that the calculations overestimate the cross section at the peak and that the theoretical peak is shifted to a higher neutron energy E_n , compared to the data. In Fig. 7.46(a) the theoretical predictions for the analyzing power A_y are somewhat below the experimental data but not at E_n close to its maximum. Similar as in the case at $E_{lab} = 346$ MeV one can conjecture that at $E_{lab} = 495$ MeV the rescattering terms are necessary to be taken into account.

7.3 Effects of Relativity

We saw in the last section that compared to data the theoretical peaks of the cross sections are shifted to higher neutron energies in comparisons with the data. The shifts are getting larger as the energy E_{lab} increases and cannot be fixed by including the rescattering terms



(a)



(b)

Figure 7.41: Same as in Fig. 7.25, but with no PW full Faddeev calculation, at $E_{lab} = 346$ MeV, $\theta_{lab} = 22^\circ$. The experimental data are taken from Ref. [19].

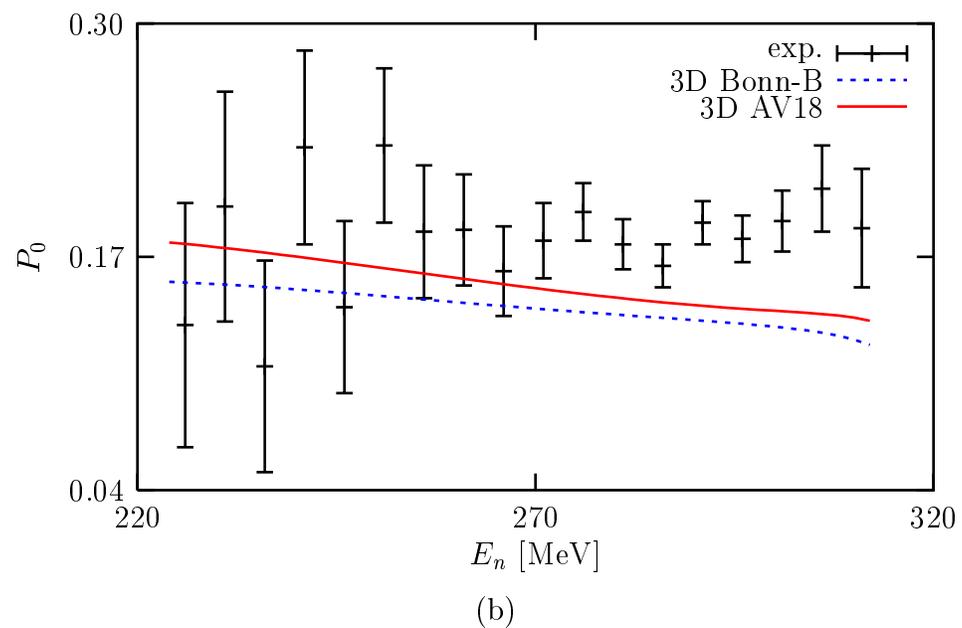
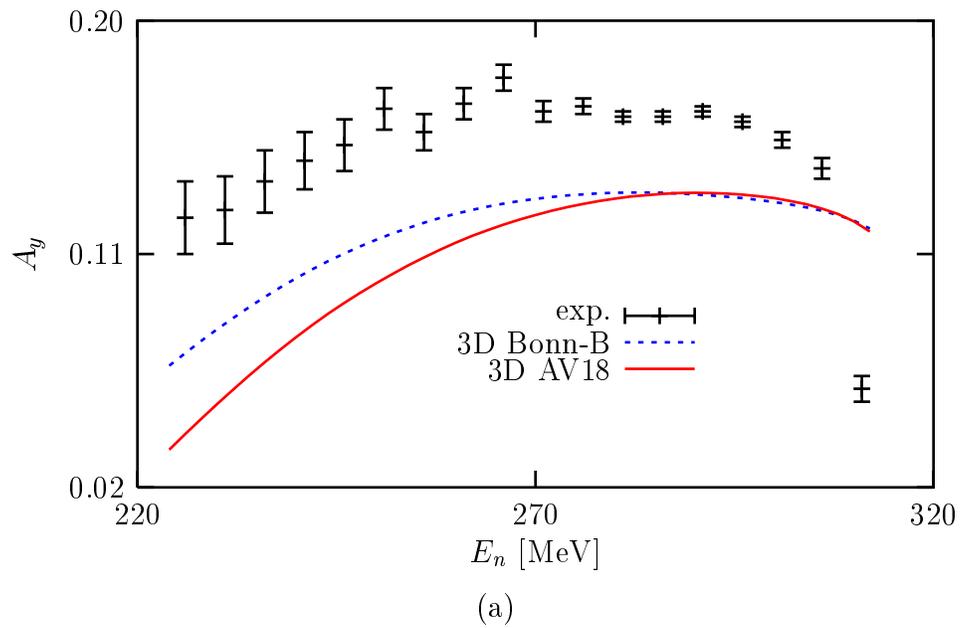
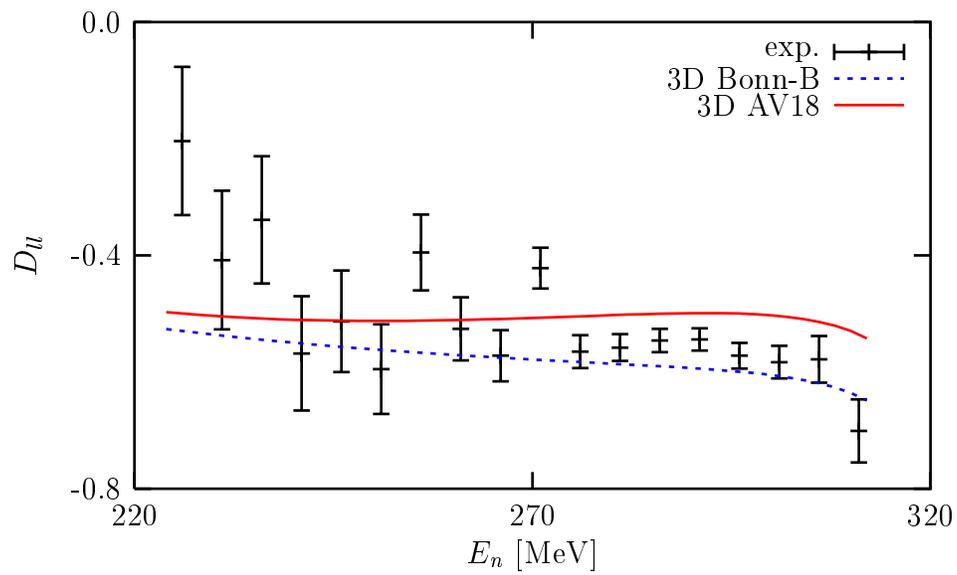
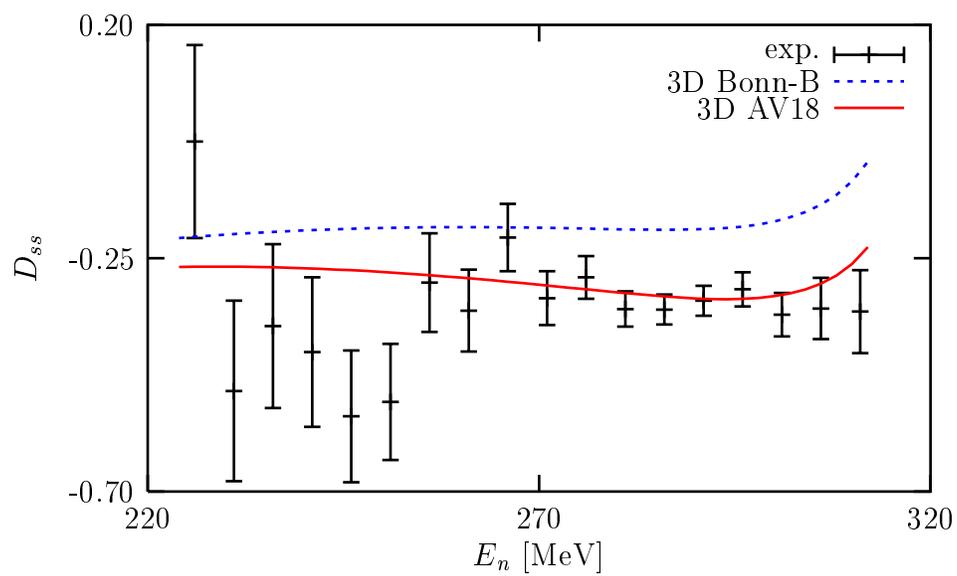


Figure 7.42: Same as in Fig. 7.41, but for (a) the analyzing power A_y and (b) the neutron polarization P_0 .



(a)



(b)

Figure 7.43: Same as in Fig. 7.41, but for the polarization transfer coefficients (a) D_u and (b) D_{ss} .

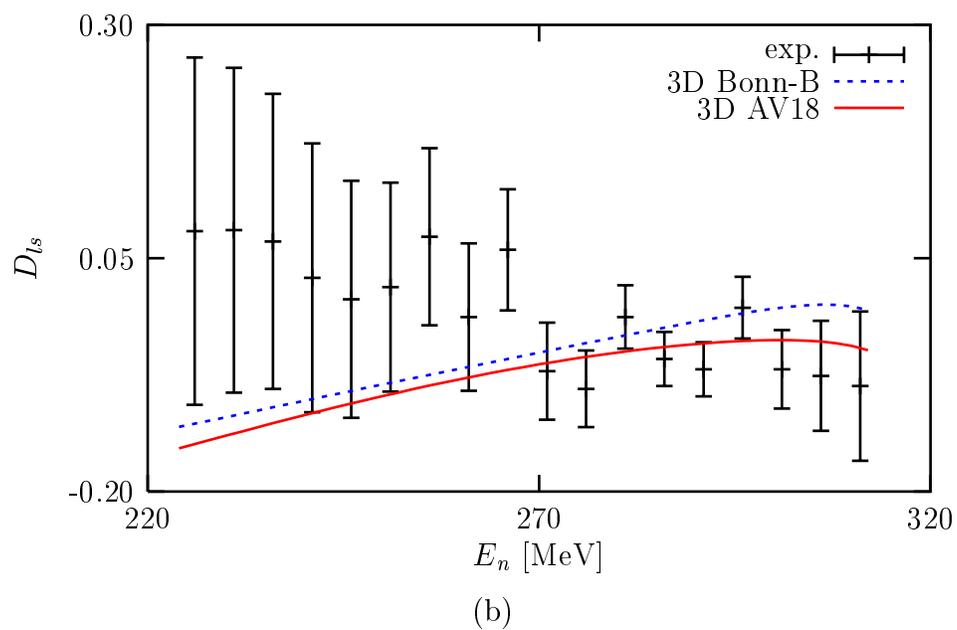
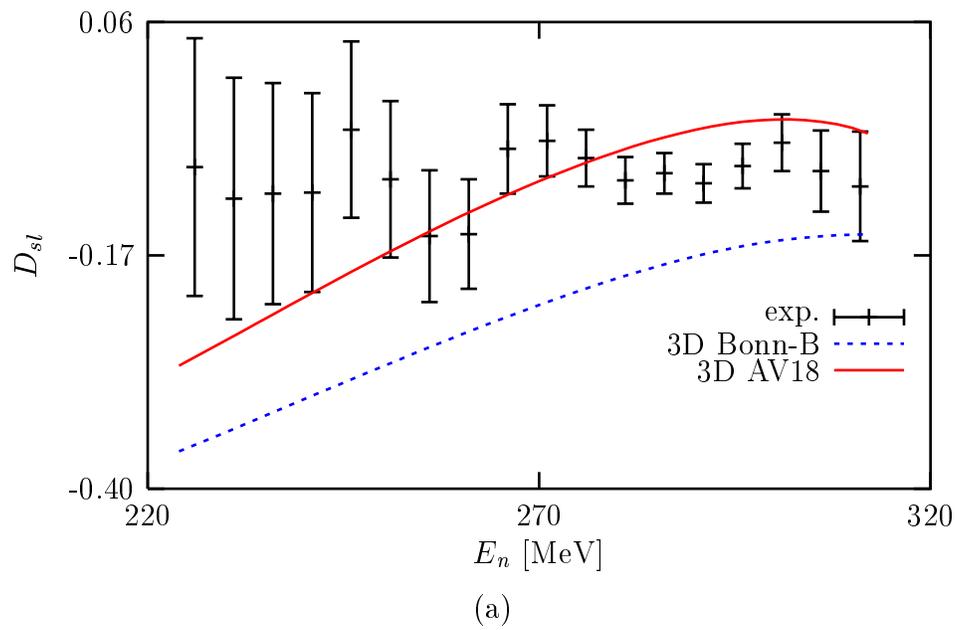


Figure 7.44: Same as in Fig. 7.41, but for the polarization transfer coefficients (a) D_{sl} and (b) D_{ts} .

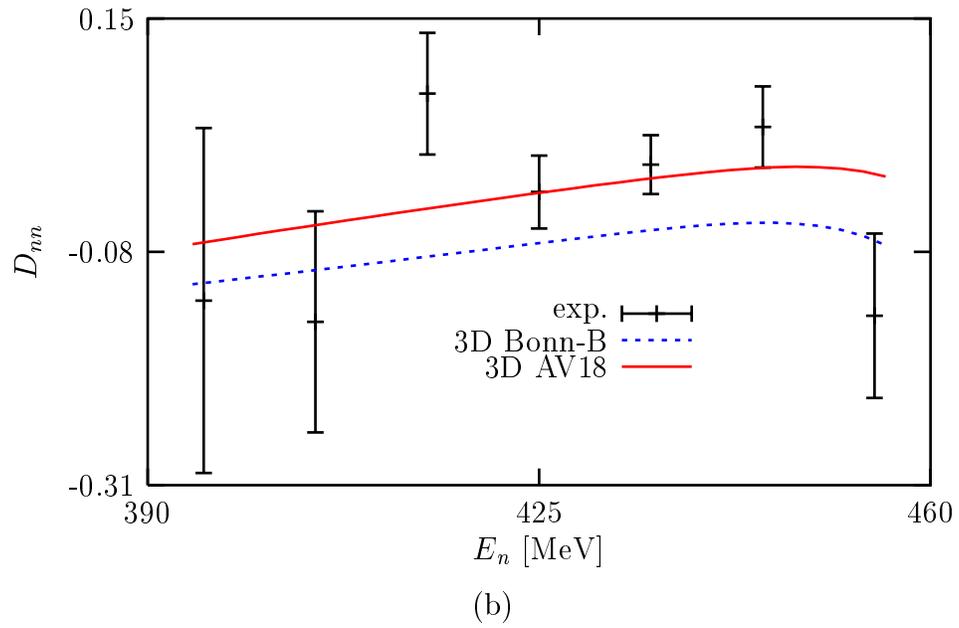
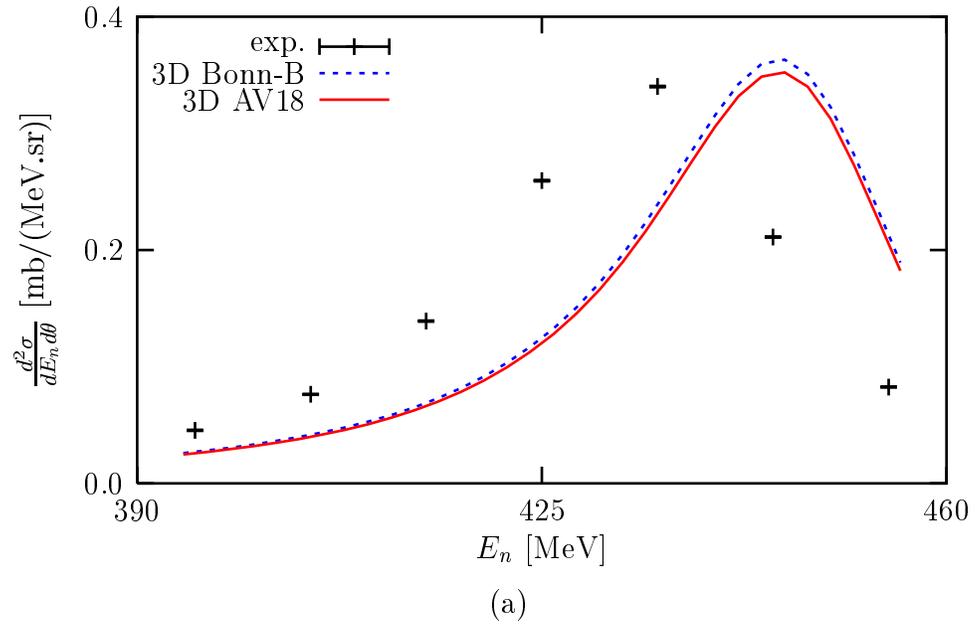


Figure 7.45: Same as in Fig. 7.41, but at $E_{lab} = 495$ MeV and $\theta_{lab} = 18^\circ$. The experimental data are taken from Ref. [57].

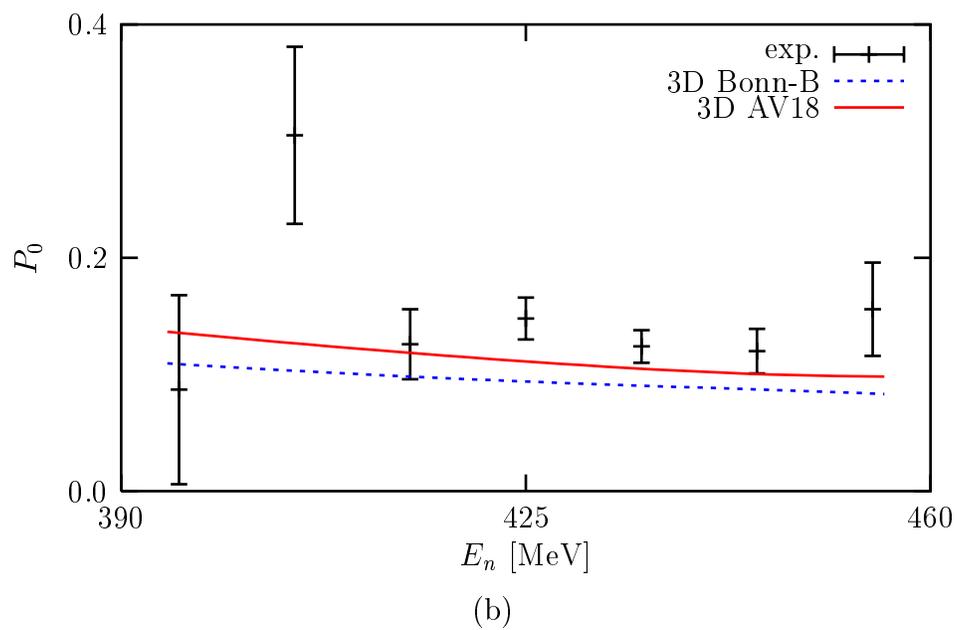
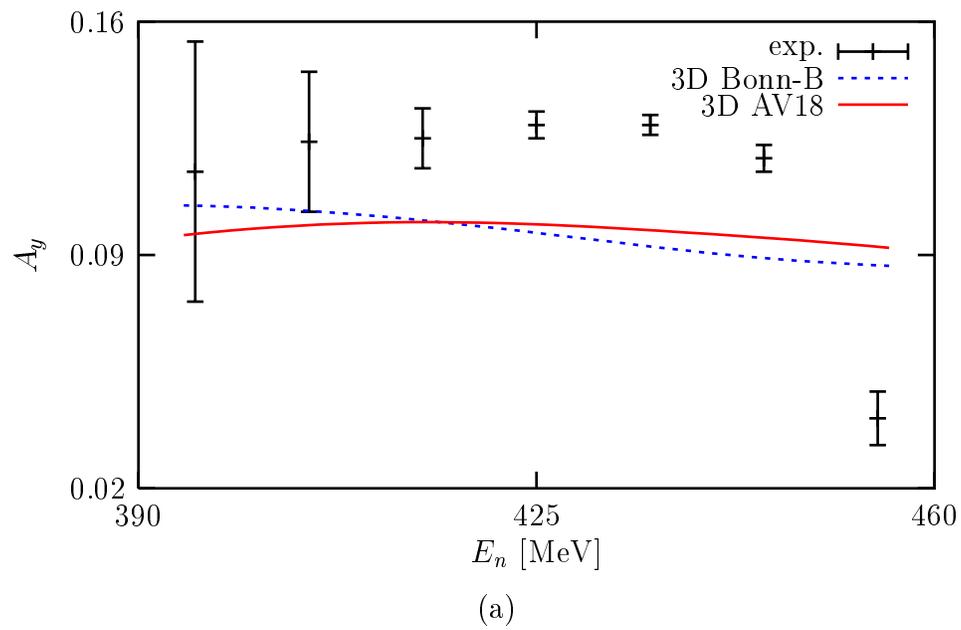


Figure 7.46: Same as in Fig. 7.45, but for (a) the analyzing power A_y and (b) the polarization P_0 .

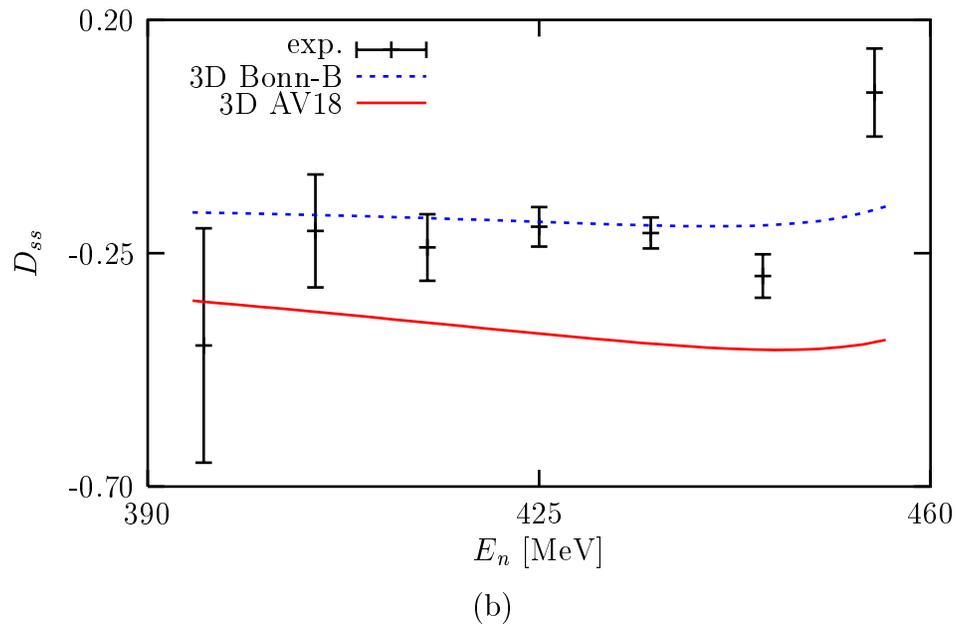
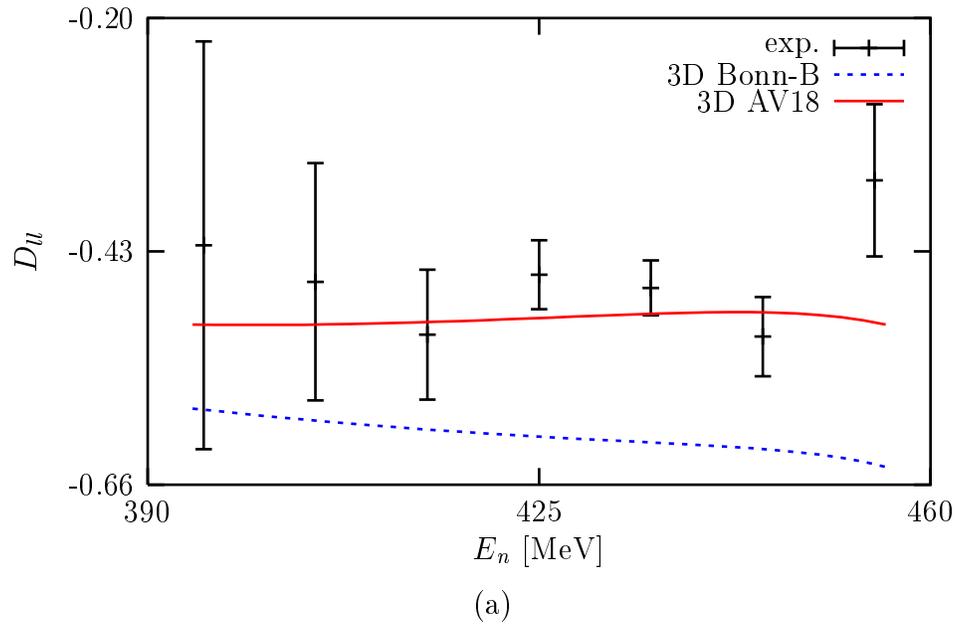
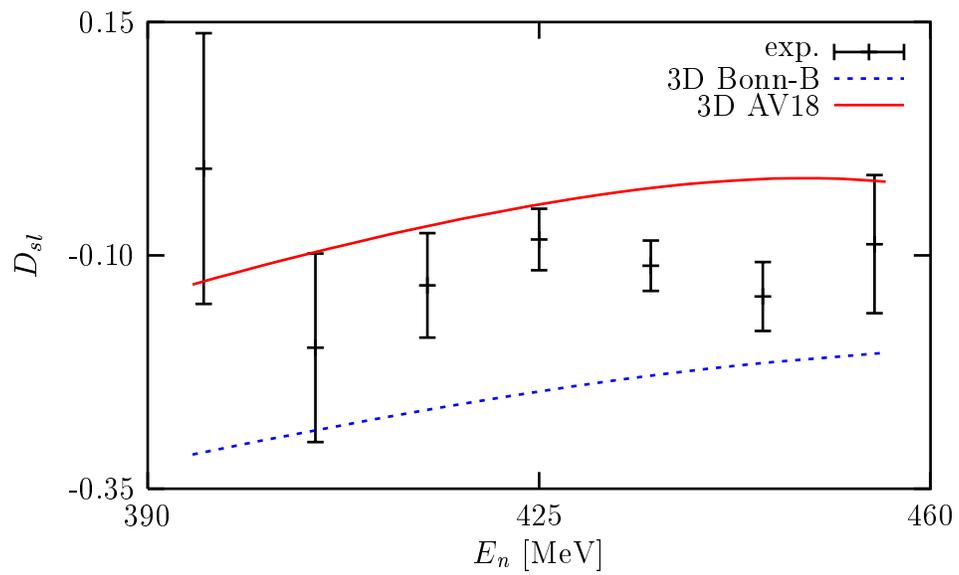
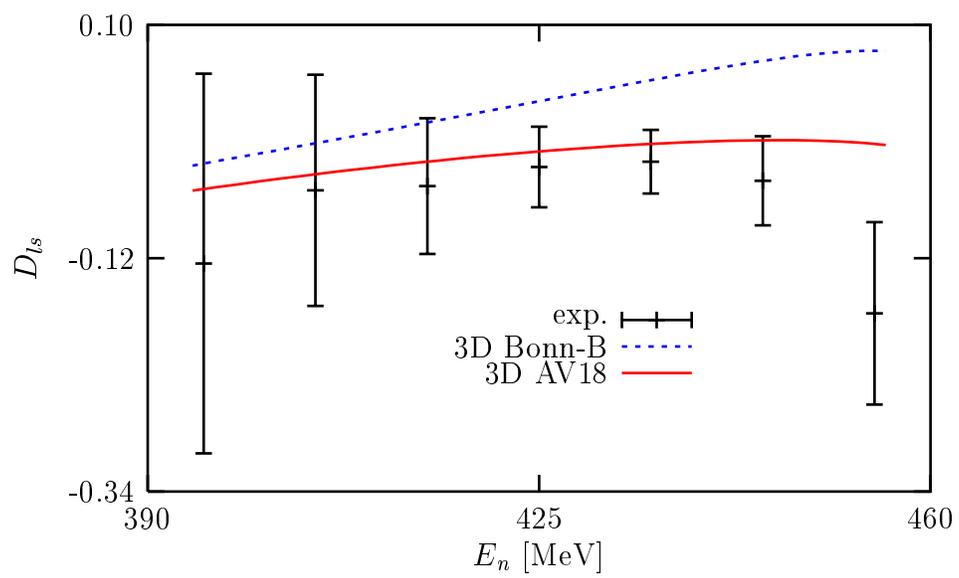


Figure 7.47: Same as in Fig. 7.45, but for the polarization transfer coefficients (a) D_u and (b) D_{ss} .



(a)



(b)

Figure 7.48: Same as in Fig. 7.45, but for the polarization transfer coefficients (a) D_{sl} and (b) D_{ts} .

of the full Faddeev Nd break-up amplitude. Therefore, another process (or processes) must also be taken into account to bring the theoretical peak to the right position. The process should become more important as the energy E_{lab} increases. Since we are observing the pd break-up process at higher energies, we consider to include relativity in our calculations. The formulation derived in Chapter 6 for the cross section is fully relativistic, but in practise there we were still forced to approximate the relativistic S-matrix. We restricted ourselves just to relativistic kinematics. This includes, however, not only the changes of the phase-space factor but also the S-matrix elements. The latter is due to the relativistic momenta, which enter as arguments of the NN T-matrix and the deuteron wave function components. We have to leave further steps for future investigations. These further steps are boosting the NN T-matrix [58] and Wigner's rotation [59], which are still under debate in the literature.

Let us more closely look at the position of the cross section peak. In the inclusive Nd break-up process without consideration of the FSI the cross section peak occurs at a point along the energy E_1 of the detected nucleon, where after the break-up one of the two undetected nucleons is at rest. Thus, in the investigated pd break-up process the cross section peak occurs at a point along E_n , where one of the two protons is at rest after the break-up. Then in the final state two nucleons carry most of the energy of the process. The process then happens as if one of the three nucleons acts just as a spectator, while the other two collide upon each other. The process is called the quasi-free scattering (QFS) and the cross section peak under discussion the QFS-peak. The position of the QFS-peak can be determined by means of the energy and the momentum conservations, while setting the final momentum of one of the two undetected nucleons to be zero. Using nonrelativistic kinematics we obtain the QFS-peak position E_1^{QFS} as

$$E_1^{QFS} = \frac{1}{2}E_{lab} \cos^2 \theta_{lab} + \frac{1}{2}E_d + \frac{1}{2}\sqrt{E_{lab} \cos^2 \theta_{lab}(E_{lab} \cos^2 \theta_{lab} + 2E_d)}, \quad (7.5)$$

and using relativistic kinematics we obtain the QFS-peak position $E_1^{QFS,rel}$ as

$$E_1^{QFS,rel} = \frac{-B \pm \sqrt{B^2 - 4AC}}{2A}, \quad (7.6)$$

with

$$A = 4((2m + E_{lab})E_{lab} \cos^2 \theta_{lab} - (2m + E_{lab} + E_d)^2) \quad (7.7)$$

$$B = 4(2(2m + E_{lab})mE_{lab} \cos^2 \theta_{lab} + E_d(2m + E_{lab} + E_d)(2m + 2E_{lab} + E_d)) \quad (7.8)$$

$$C = -E_d^2(2m + 2E_{lab} + E_d)^2. \quad (7.9)$$

Note that in Eqs. (7.5), (7.7)-(7.9) E_{lab} is the kinetic energy of the projectile and not its

total energy.¹ In Table 7.1 we show E_1^{QFS} and $E_1^{QFS,rel}$ at some energies and scattering angles, at which data for the pd break-up process exist and have been shown in the previous section. We see in the table that $E_1^{QFS,rel}$ is less than E_1^{QFS} . Thus, relativity brings the QFS-peak position to a lower energy of the detected nucleon, compared to the one obtained from a nonrelativistic calculation. Later we shall compare the QFS-peak positions shown in Table 7.1 with data as we also check other relativistic effects in the pd break-up process. In the table we see at $E_{lab} = 197$ MeV that the difference between E_1^{QFS} and $E_1^{QFS,rel}$ is getting larger as the scattering angle θ_{lab} increases. It is also indicated in the table that the difference between E_1^{QFS} and $E_1^{QFS,rel}$ is getting larger as the projectile energy E_{lab} increases, which is something that one would expect from a relativistic effect.

Table 7.1: The QFS-peak positions E_1^{QFS} and $E_1^{QFS,rel}$ for the pd break-up process at some energies and scattering angles.

E_{lab} [MeV]	θ_{lab}	E_1^{QFS} [MeV]	$E_1^{QFS,rel}$ [MeV]
197	13°	184.8	183.8
197	24°	162.2	159.3
197	37°	123.4	118.7
197	48°	86.0	81.0
346	22°	295.2	287.6
495	18°	445.5	434.4

¹Here we sketch out how to arrive at Eqs. (7.5) and (7.6). To obtain E_1^{QFS} in Eq. (7.5) we begin with the energy and the momentum conservations for the Nd break-up process, which are given as:

$$E_{lab} + E_d = E_1 + E_2 + E_3 \quad (7.10)$$

$$\mathbf{k}_{lab} = \mathbf{k}_1 + \mathbf{k}_2 + \mathbf{k}_3. \quad (7.11)$$

Next we choose in the final state that nucleon 3 is at rest, thus, \mathbf{k}_3 is equal to zero. Under this condition Eqs. (7.10) and (7.11) lead to a quadratic equation in $\sqrt{E_1}$ given as

$$2E_1 + E_{lab} - 2\sqrt{E_1 E_{lab}} \cos \theta_{lab} - E_{lab} - E_d = 0. \quad (7.12)$$

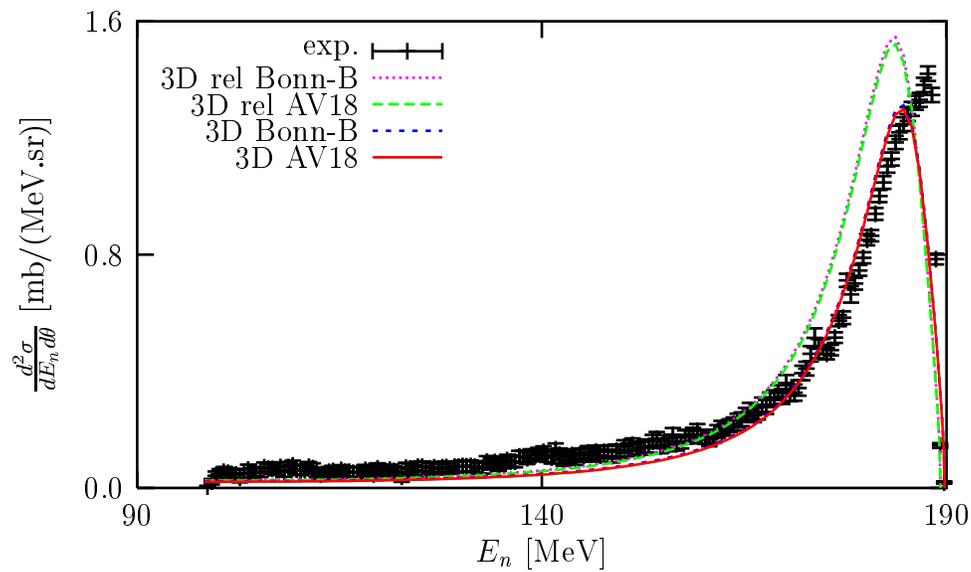
The solution of Eq. (7.12) leads to E_1^{QFS} as given in Eq. (7.5). Now to obtain $E_1^{QFS,rel}$ in Eq. (7.6) we start with the same momentum conservation given in Eq. (7.11) and the relativistic energy conservation for the Nd break-up process, which is given as

$$E_{lab} + m_d - 2m = E_1 + E_2 + E_3. \quad (7.13)$$

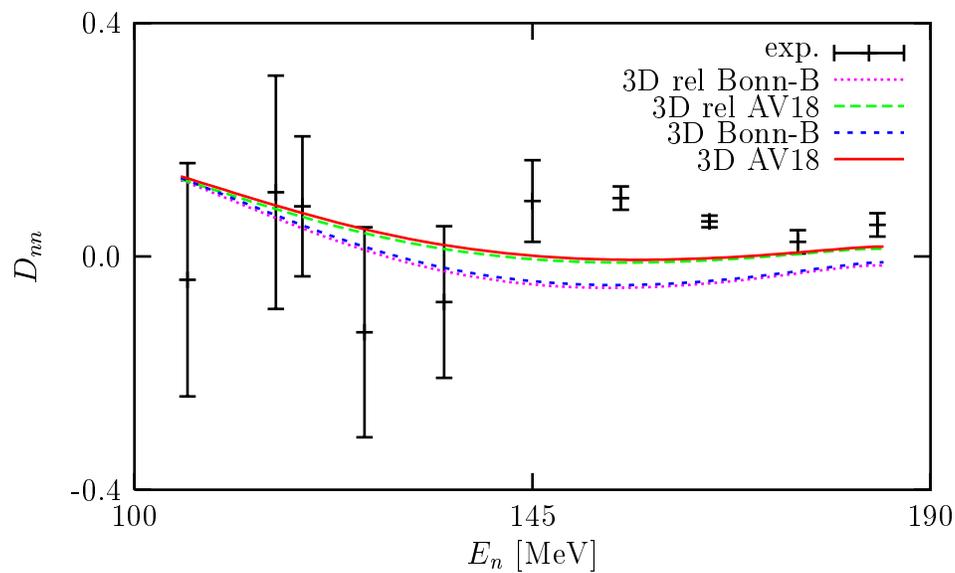
Next we set \mathbf{k}_3 to be zero, and then Eqs. (7.11) and (7.13) lead to a quadratic equation, of which one of the solutions is $E_1^{QFS,rel}$ as given in Eq. (7.6).

Now we continue to compare between the calculations with and without the relativistic correction as well as experimental data for the pd break-up process at various energies and scattering angles. In Figs. 7.49-7.64 we show the comparisons at $E_{lab} = 197$ MeV. The nonrelativistic and the relativistic QFS-peaks in Figs. 7.49(a), 7.53(a), 7.57(a) and 7.61(a) occur at E_1^{QFS} and $E_1^{QFS,rel}$, respectively, as given in Table 7.1. Encouragingly the relativistic correction brings the QFS-peaks at $\theta_{lab} = 24^\circ$ in Fig. 7.53(a), at $\theta_{lab} = 37^\circ$ in Fig. 7.57(a) and at $\theta_{lab} = 48^\circ$ in Fig. 7.61(a) to the correct positions along the neutron energy E_n , where also the data occur. But it also raises the heights of the peaks to be higher than the data. At $\theta_{lab} = 13^\circ$ in Fig. 7.49(a) the relativistic correction shifts the QFS-peaks in the same direction as at other θ_{lab} 's. The result is that now the peaks occur at lower E_n , compared to the data. To understand this let us return to Fig. 7.25(a), which shows the PW full Faddeev calculations for the cross section at $E_{lab} = 197$ MeV and $\theta_{lab} = 13^\circ$. In Fig. 7.25(a) we see that the FSI is very important at this energy and scattering angle as indicated by the very high peaks in the PW full Faddeev calculations at the maximum of E_n . In addition the FSI-peak occurs very close to the QFS-peak. Thus, at $E_{lab} = 197$ MeV, $\theta_{lab} = 13^\circ$ the height and the position of the cross section peak is also determined strongly by the FSI. Since we do not include the FSI, we obtain the results as shown in Fig. 7.49(a) that the calculations predict the cross section peaks occurring at a shifted position to lower E_n . For the spin observables the relativistic correction leads to various effects. In some cases the effects are getting larger as E_n increases towards its maximum. This is seen, for example, for A_y in Figs. 7.54(a) ($\theta_{lab} = 24^\circ$), 7.58(a) ($\theta_{lab} = 37^\circ$), 7.62(a) ($\theta_{lab} = 48^\circ$) and for D_{ss} in Figs. 7.55(b) ($\theta_{lab} = 24^\circ$), 7.59(b) ($\theta_{lab} = 37^\circ$), 7.63(b) ($\theta_{lab} = 48^\circ$). There at E_n towards its maximum the relativistic correction lowers the theoretical predictions for A_y and increases the ones for D_{ss} . In any case we can state that at $E_{lab} = 197$ MeV the relativistic correction is clearly required to correctly place the cross section peak along the neutron energy.

Similar comparisons are shown in Figs. 7.65-7.68 for $E_{lab} = 346$ MeV, $\theta_{lab} = 22^\circ$ and in Figs. 7.69-7.72 for $E_{lab} = 495$ MeV, $\theta_{lab} = 18^\circ$. The nonrelativistic and the relativistic QFS-peaks in Figs. 7.65(a) and 7.69(a) occur at E_1^{QFS} and $E_1^{QFS,rel}$ as given in Table 7.1. As at $E_{lab} = 197$ MeV the relativistic correction brings the QFS-peaks in Figs. 7.65(a) and 7.69(a) to where the data occur along E_n . It also increases the heights of the peaks. We would like to point out that at $E_{lab} = 346$ MeV the relativistic QFS-peak in Fig. 7.65(a) is surprisingly shifted to the left, compared to the data. The origin of this little discrepancy between the calculations and the data can be traced back to the experiment. In the experiment there is an uncertainty of the energy, at which the pd break-up process exactly occurs. For example, due to the thickness of the target

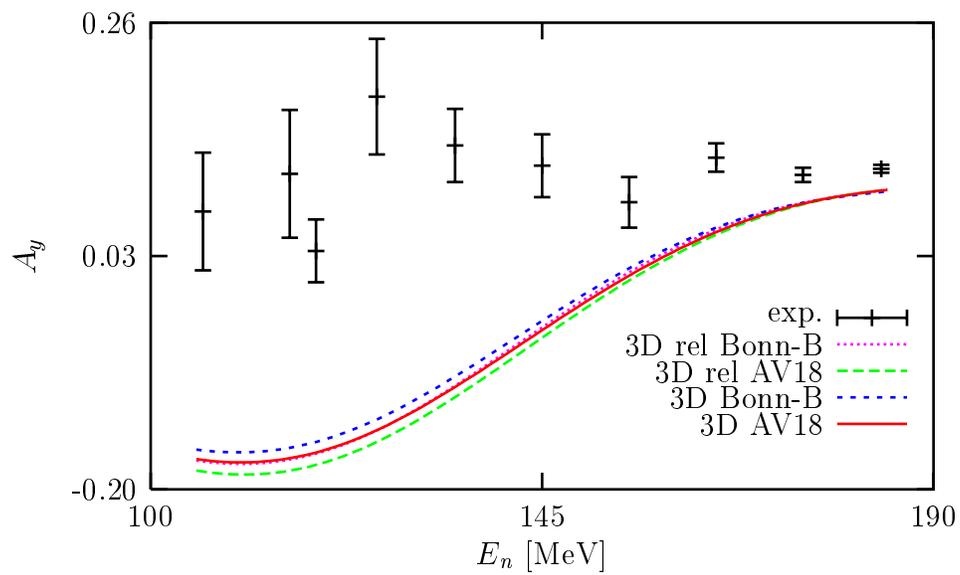


(a)

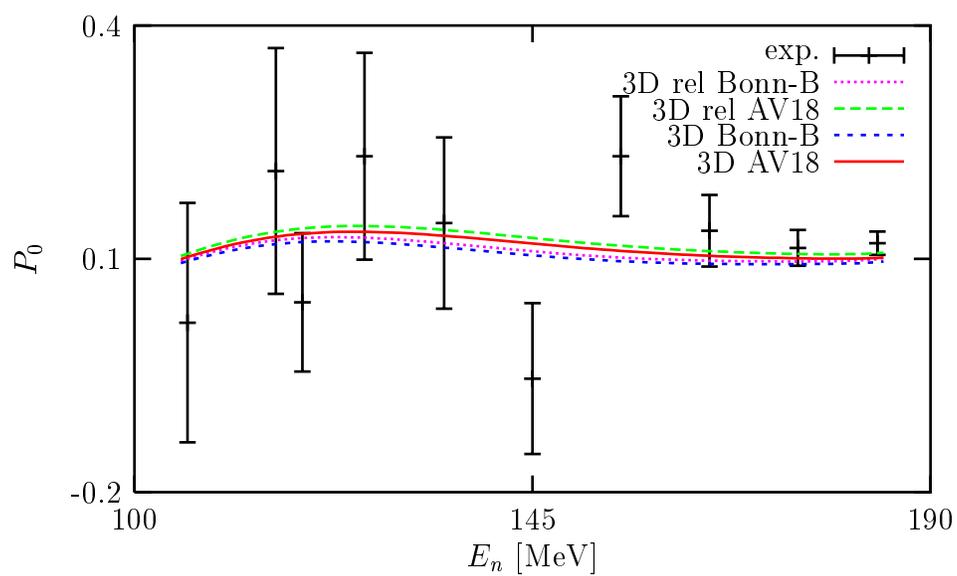


(b)

Figure 7.49: The 3D calculations for (a) the spin averaged differential cross section and (b) the polarization transfer coefficient D_{nn} in the pd break-up process at $E_{lab} = 197$ MeV and $\theta_{lab} = 13^\circ$. The NN potentials used are Bonn-B and AV18. The word “rel” in the curves’ labels means that the corresponding calculations include relativistic kinematic. The experimental data are taken from Ref. [18].



(a)



(b)

Figure 7.50: Same as in Fig. 7.49, but for (a) the analyzing power A_y and (b) the neutron polarization P_0 .

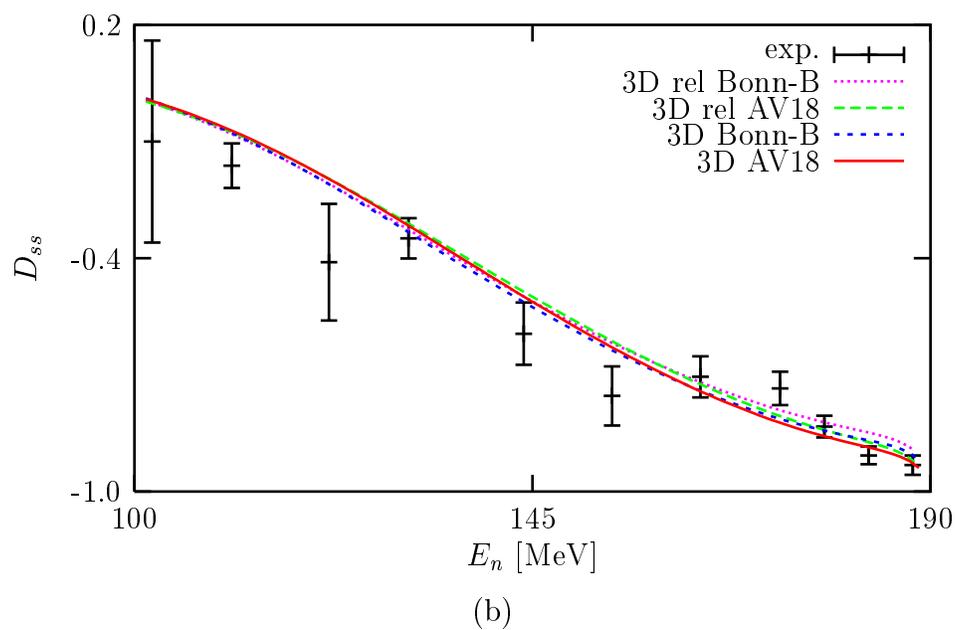
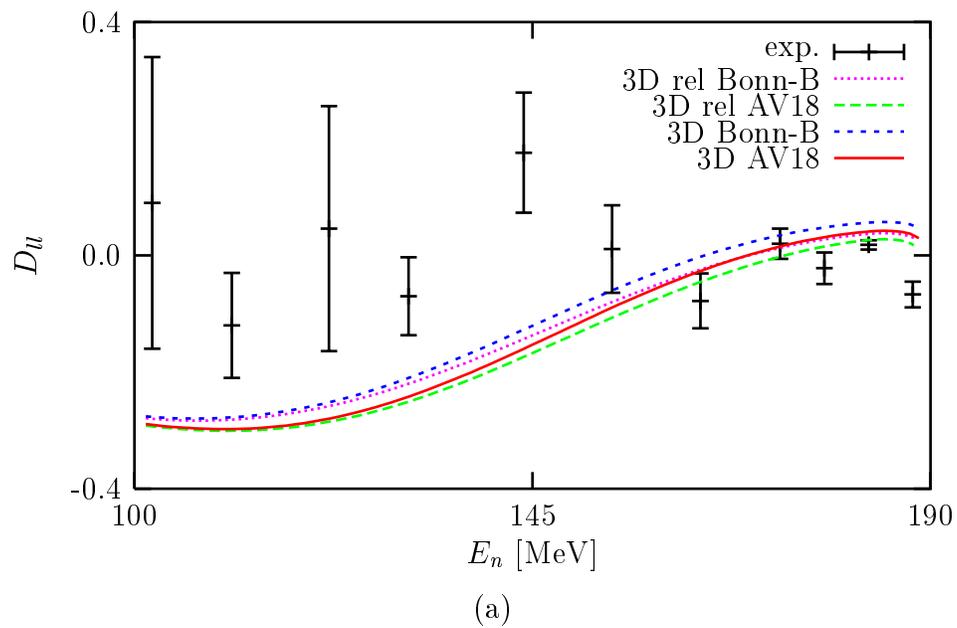


Figure 7.51: Same as in Fig. 7.49, but for the polarization transfer coefficients (a) D_u and (b) D_{ss} .

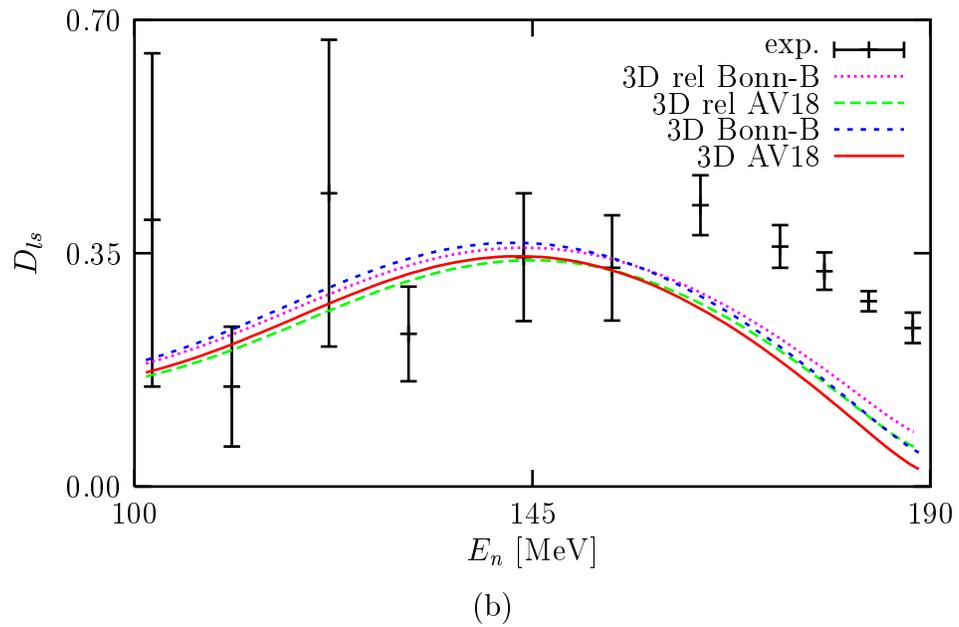
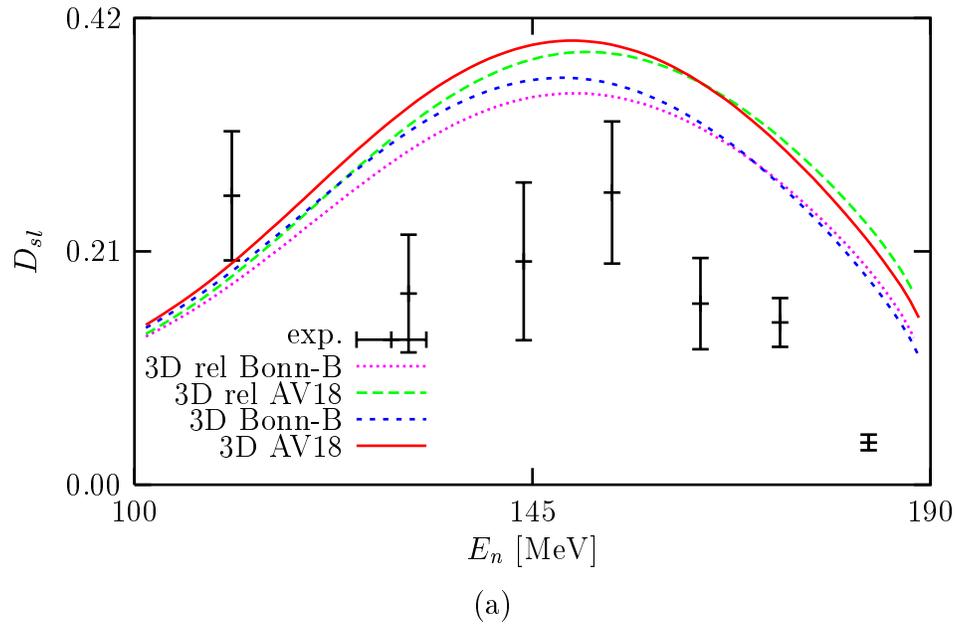


Figure 7.52: Same as in Fig. 7.49, but for the polarization transfer coefficients (a) D_{sl} and (b) D_{ts} .

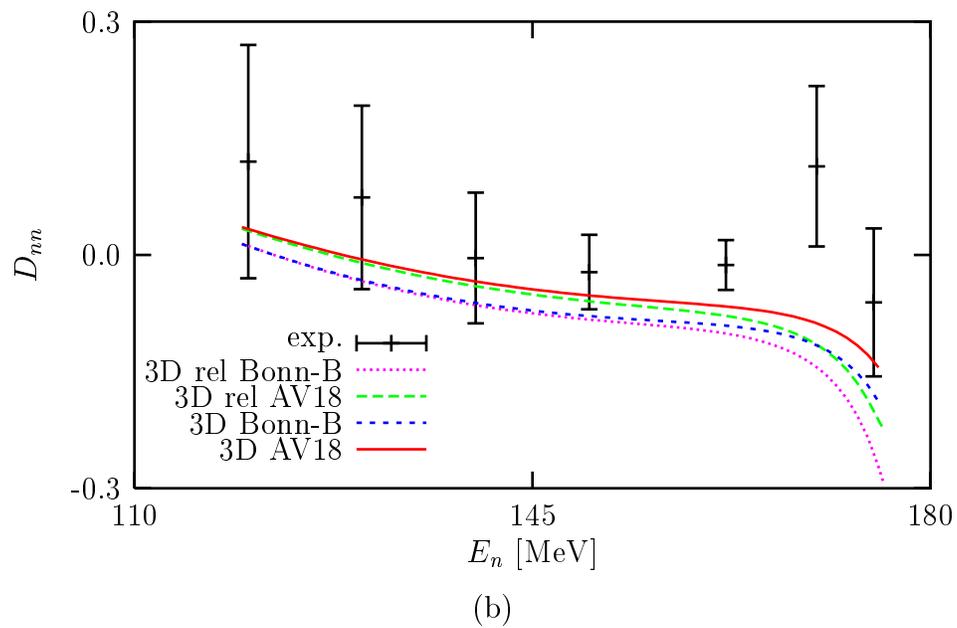
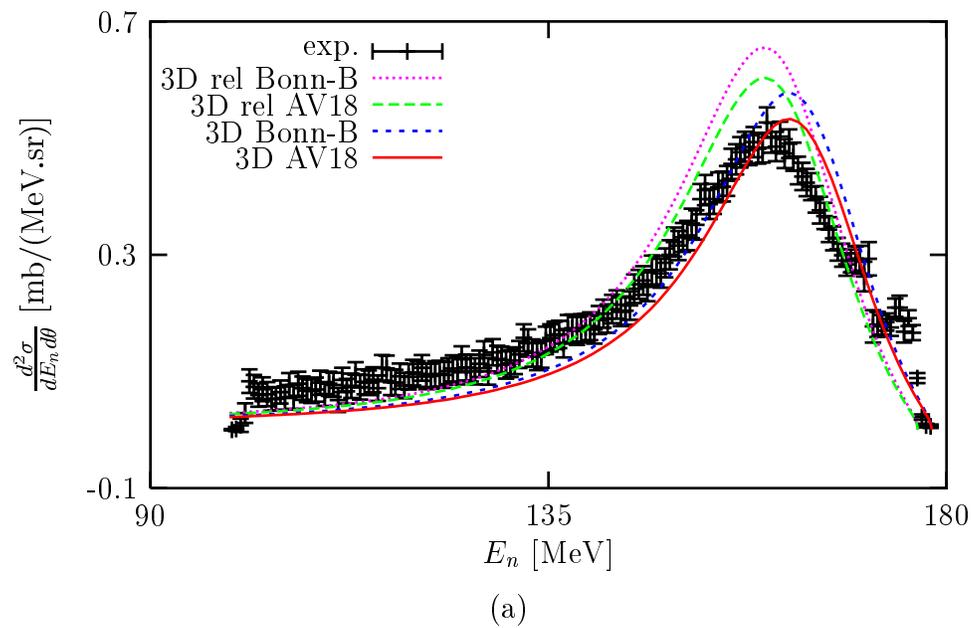


Figure 7.53: Same as in Fig. 7.49, but at $\theta_{lab} = 24^\circ$.

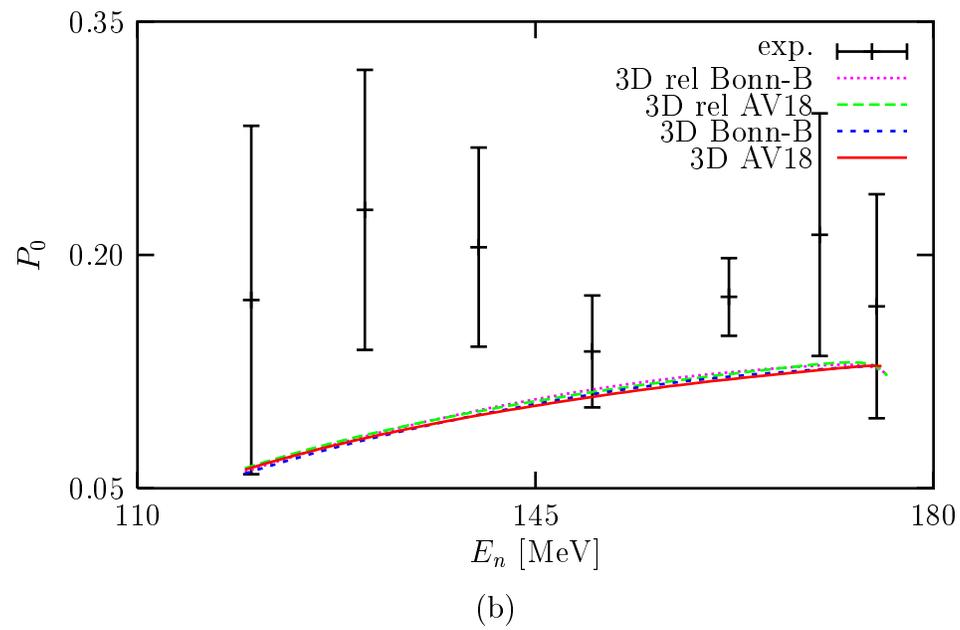
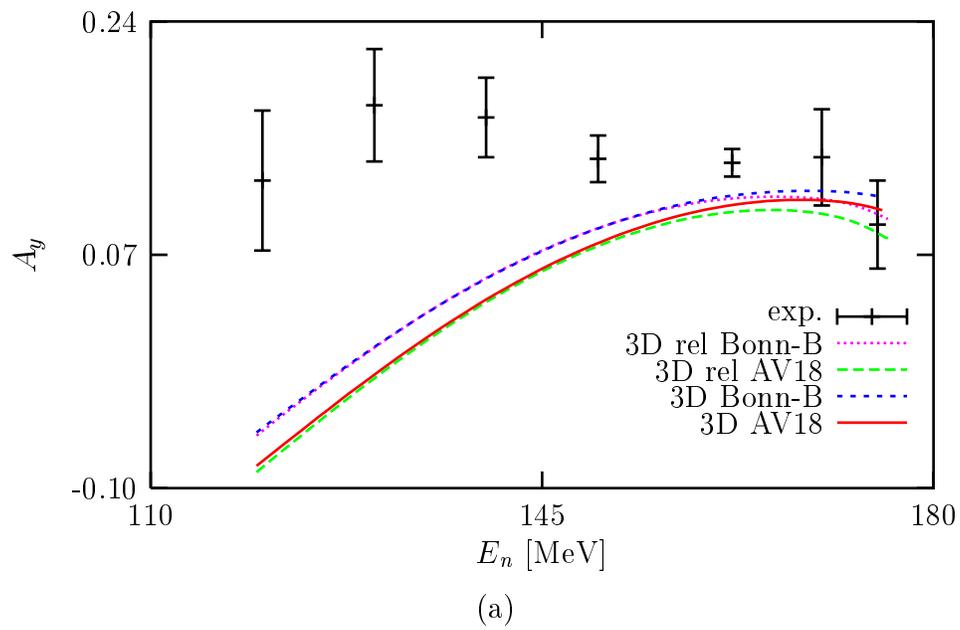


Figure 7.54: Same as in Fig. 7.50, but at $\theta_{lab} = 24^\circ$.

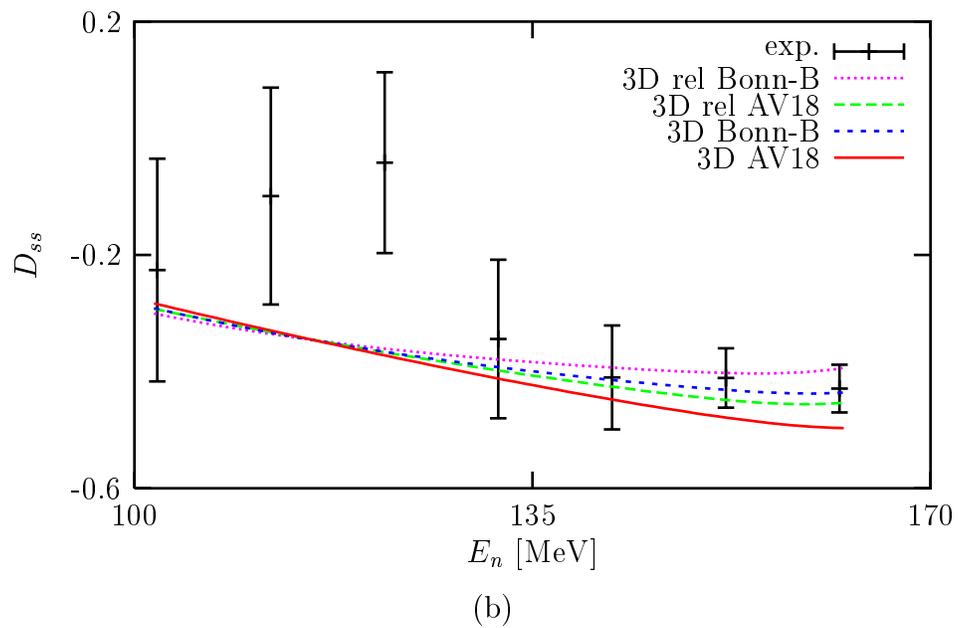
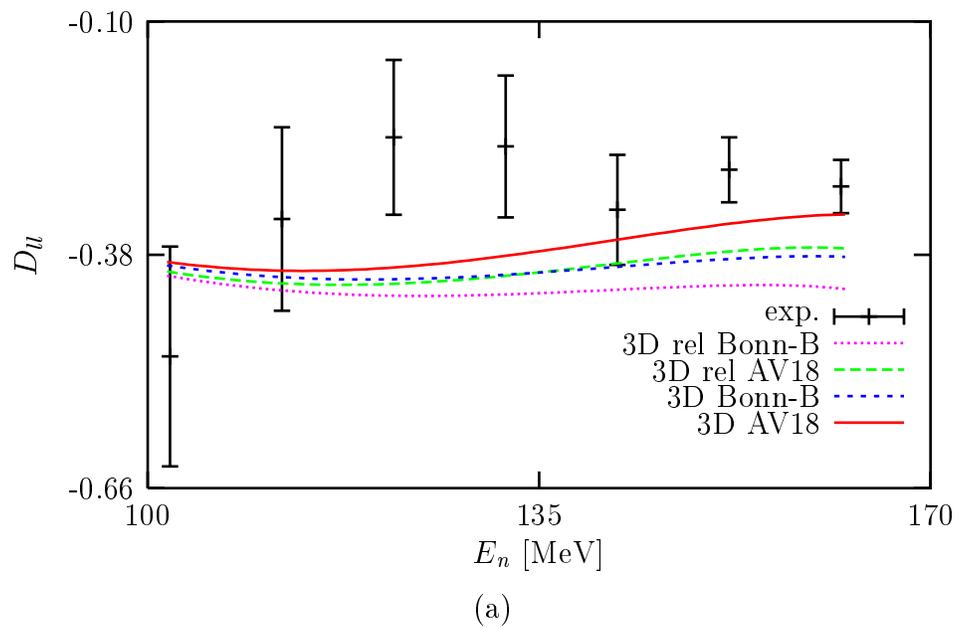


Figure 7.55: Same as in Fig. 7.51, but at $\theta_{lab} = 24^\circ$.

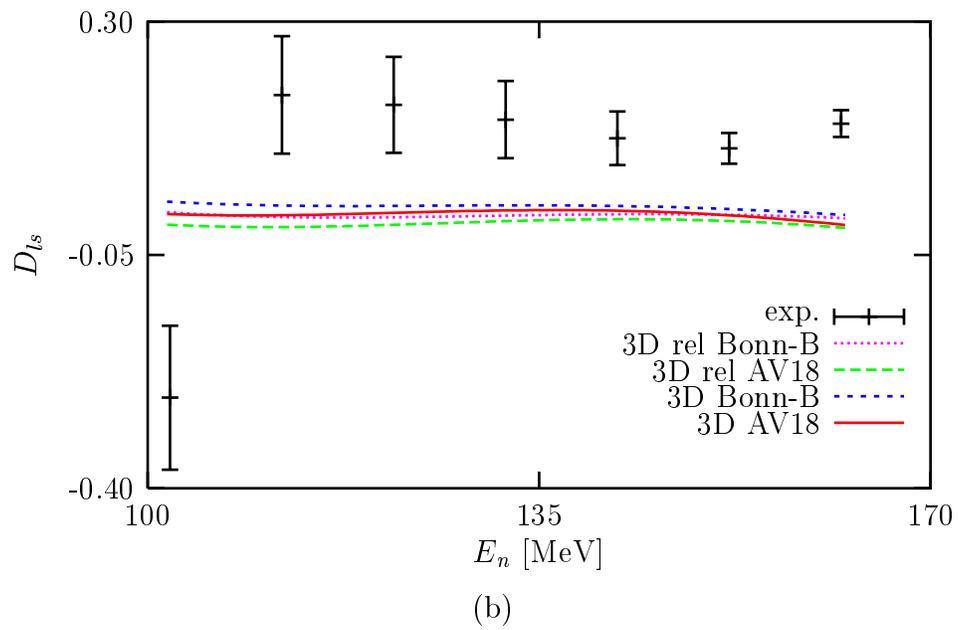
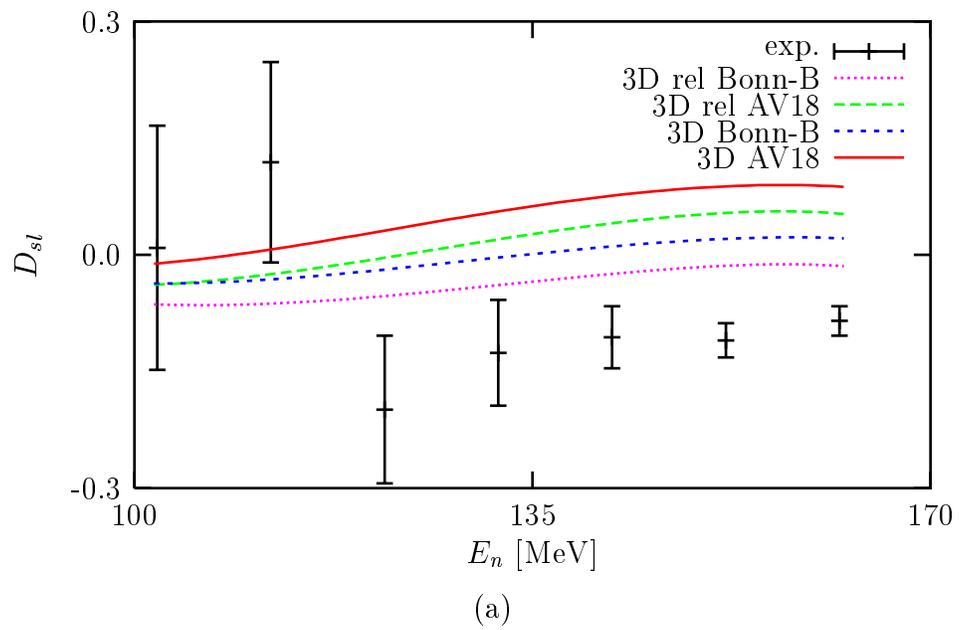


Figure 7.56: Same as in Fig. 7.52, but at $\theta_{lab} = 24^\circ$.

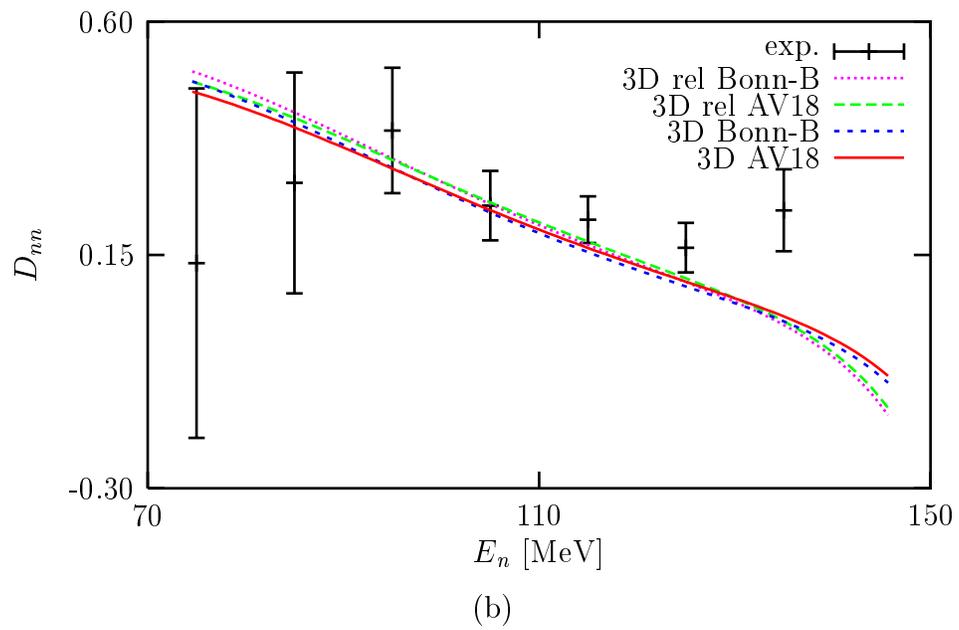
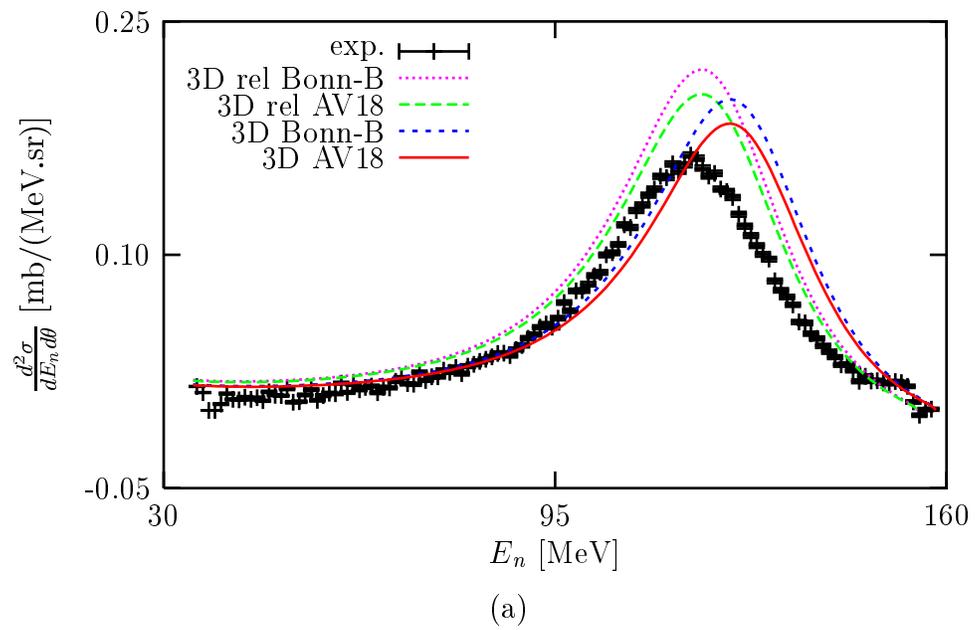


Figure 7.57: Same as in Fig. 7.49, but at $\theta_{lab} = 37^\circ$.

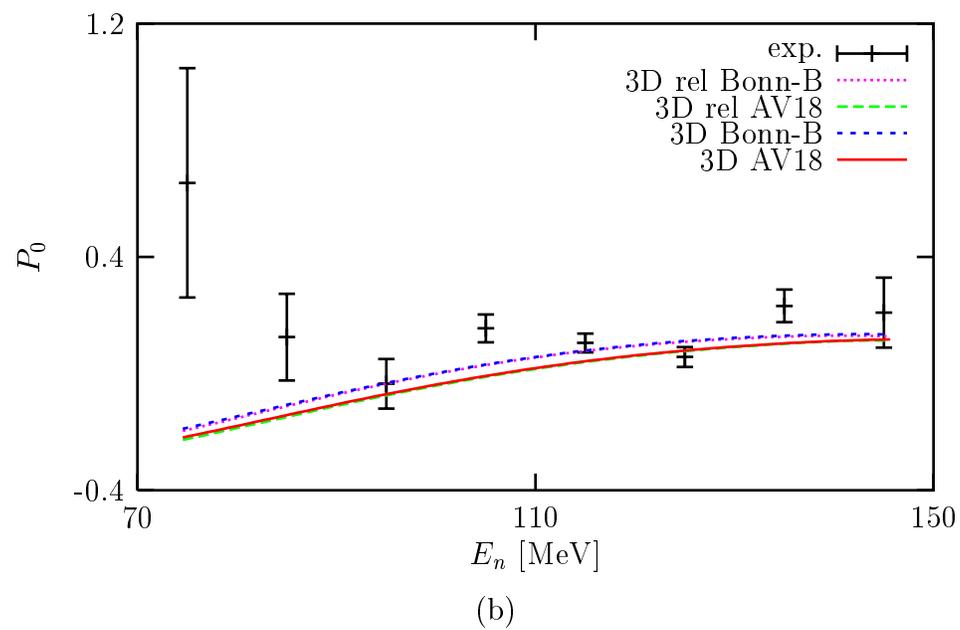
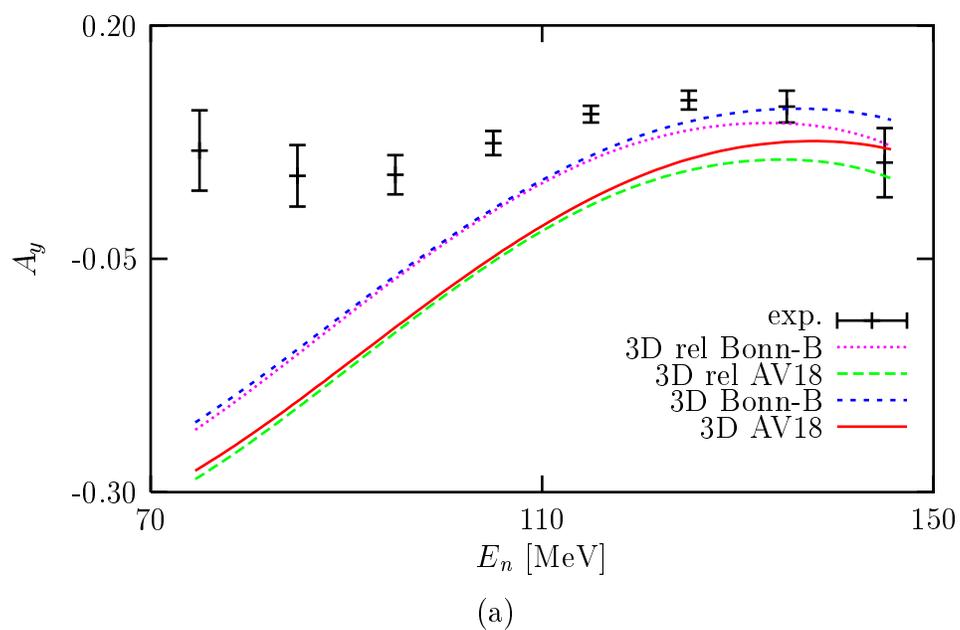
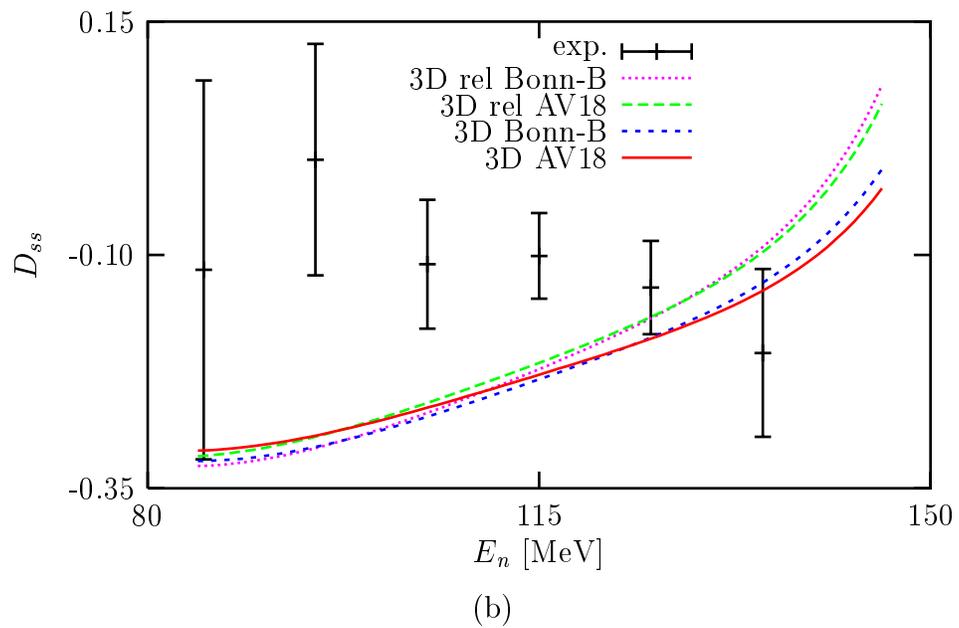
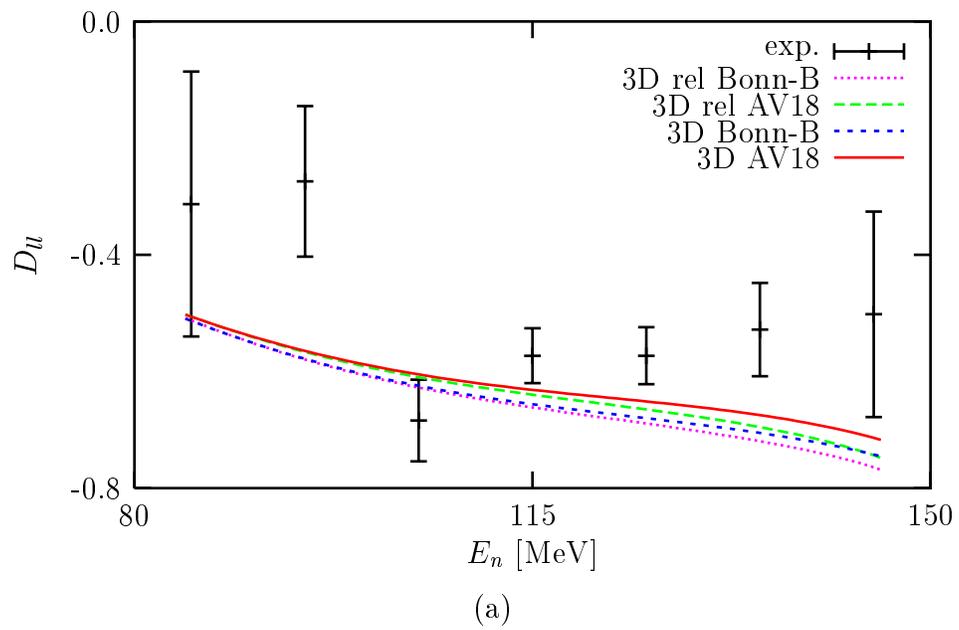


Figure 7.58: Same as in Fig. 7.50, but at $\theta_{lab} = 37^\circ$.

Figure 7.59: Same as in Fig. 7.51, but at $\theta_{lab} = 37^\circ$.

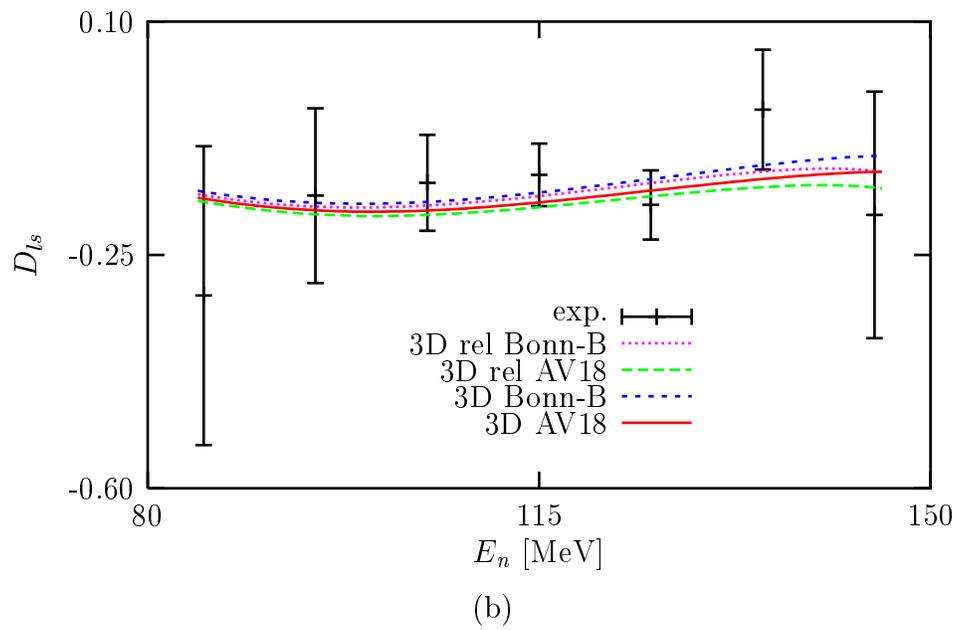
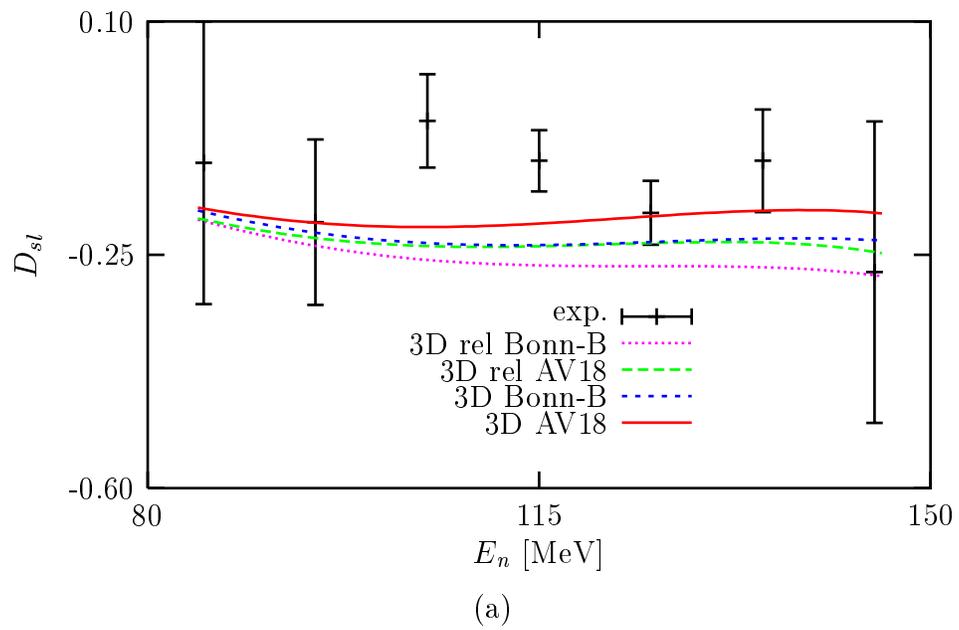
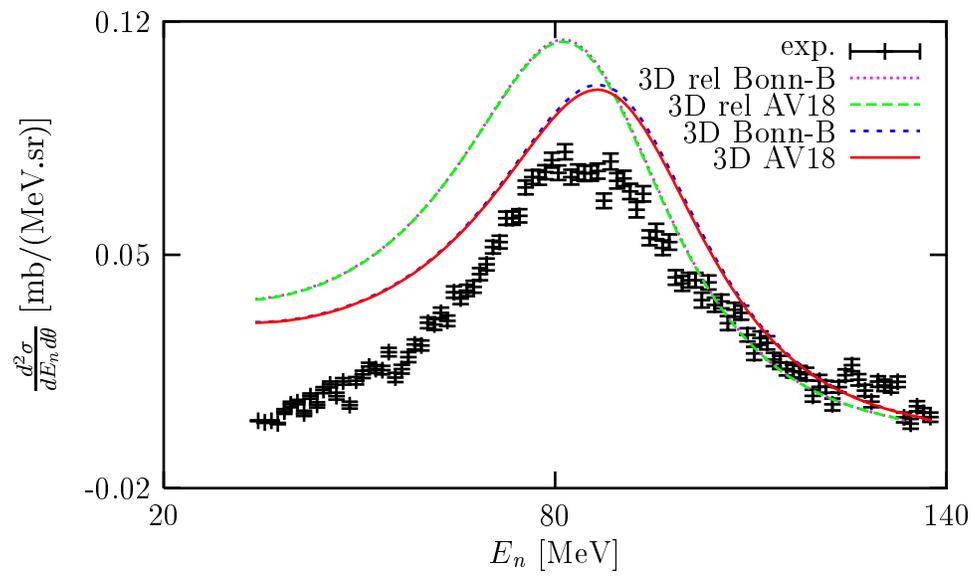
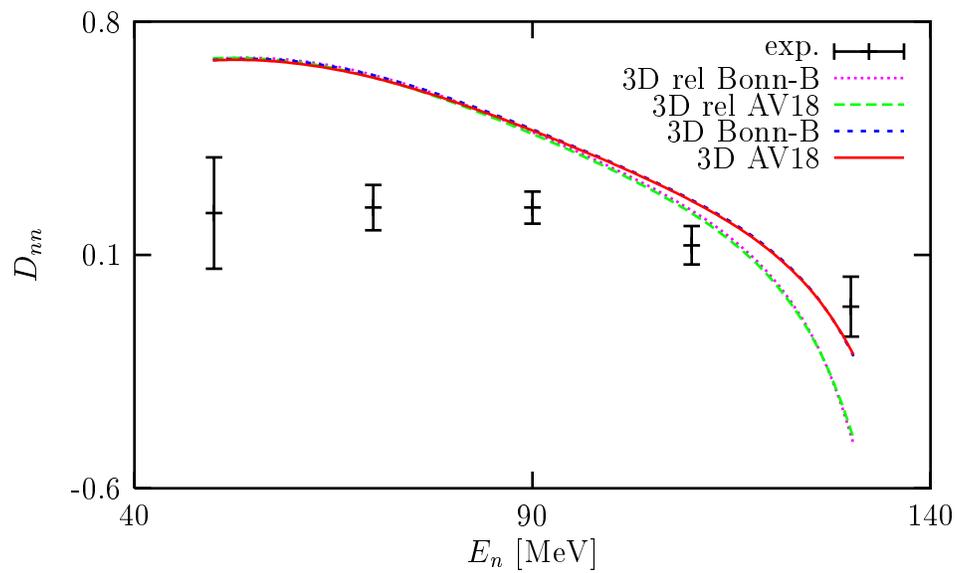


Figure 7.60: Same as in Fig. 7.52, but at $\theta_{lab} = 37^\circ$.



(a)



(b)

Figure 7.61: Same as in Fig. 7.49, but at $\theta_{lab} = 48^\circ$.

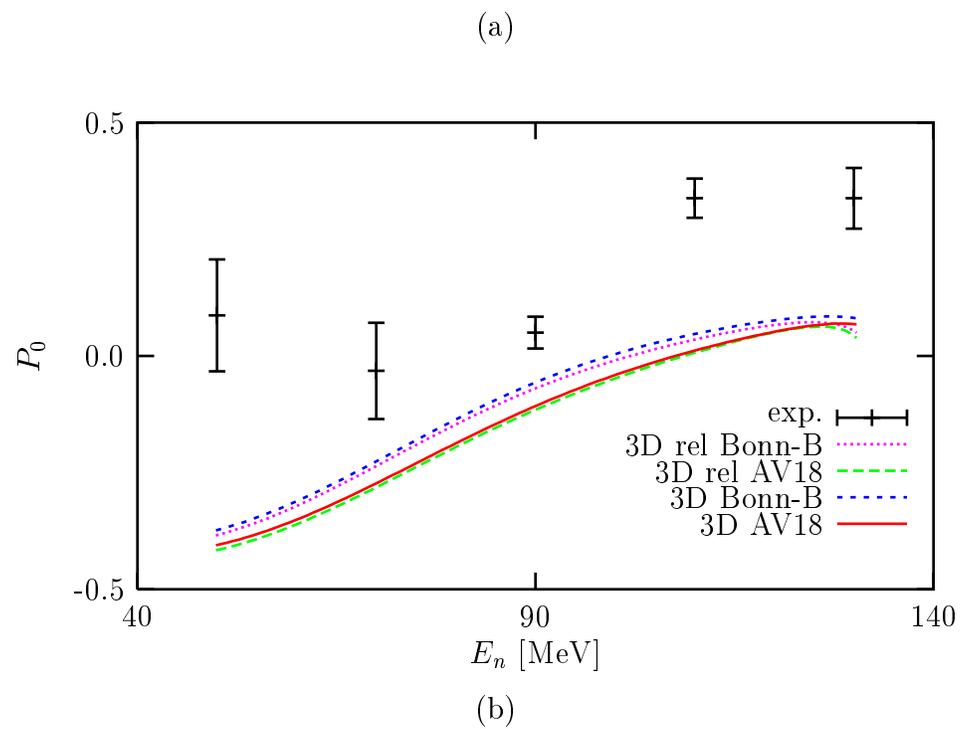
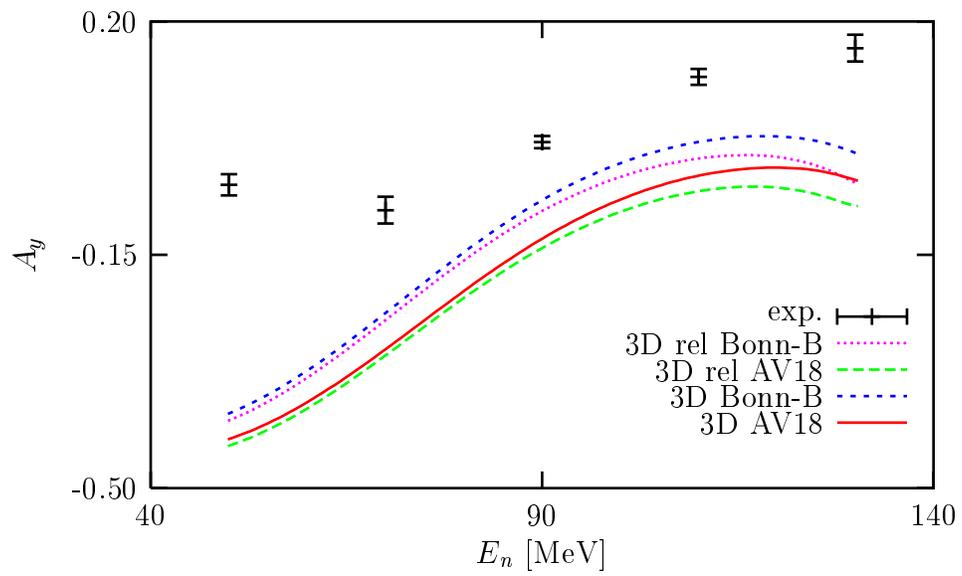


Figure 7.62: Same as in Fig. 7.50, but at $\theta_{lab} = 48^\circ$.

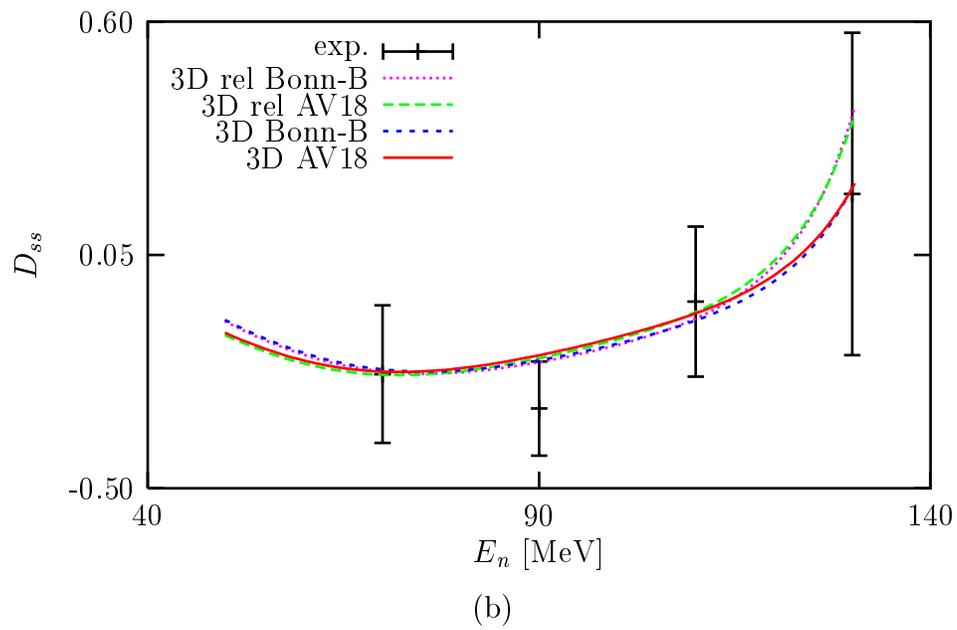
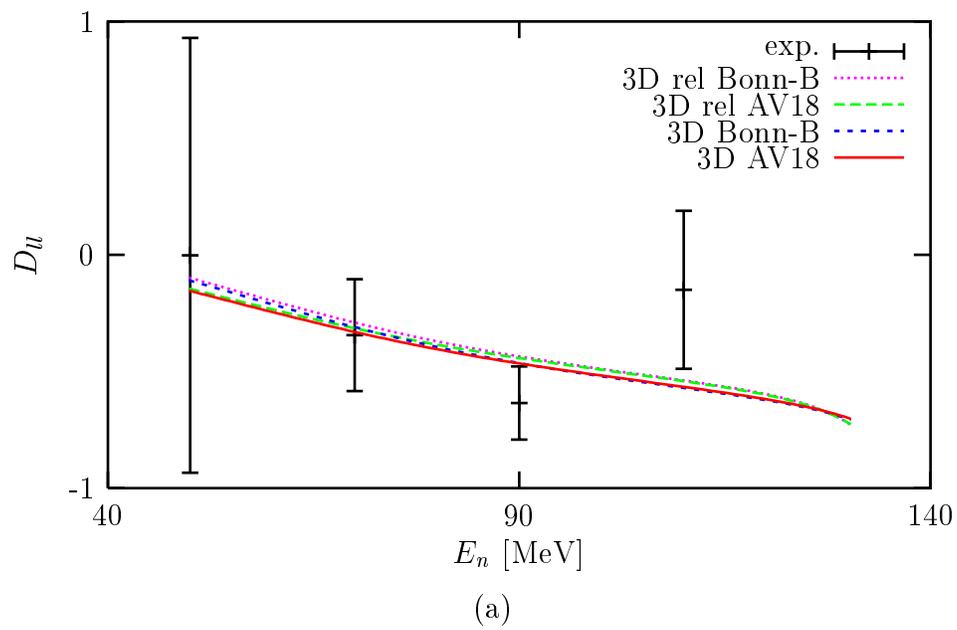


Figure 7.63: Same as in Fig. 7.51, but at $\theta_{lab} = 48^\circ$.

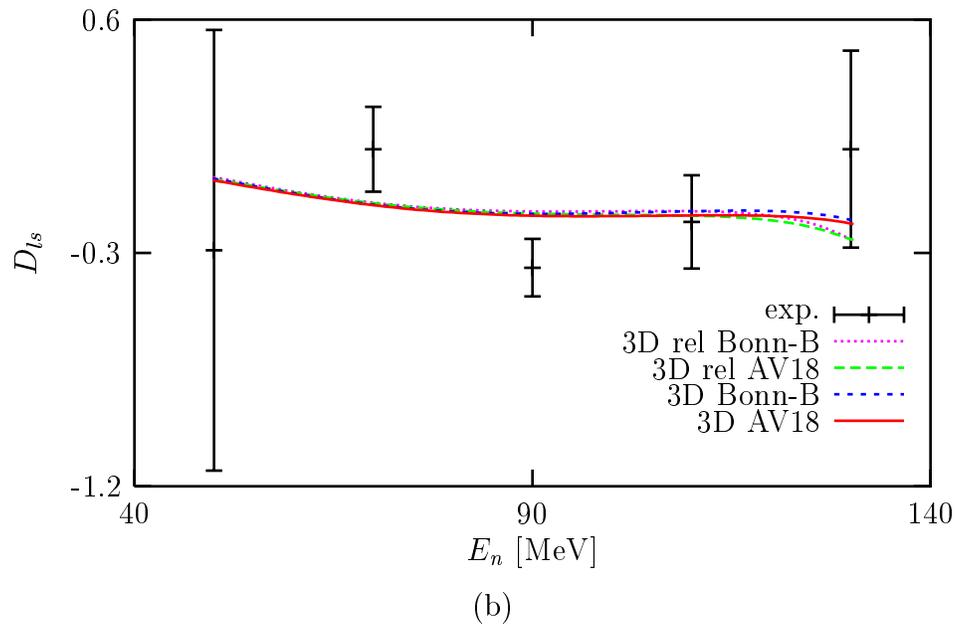
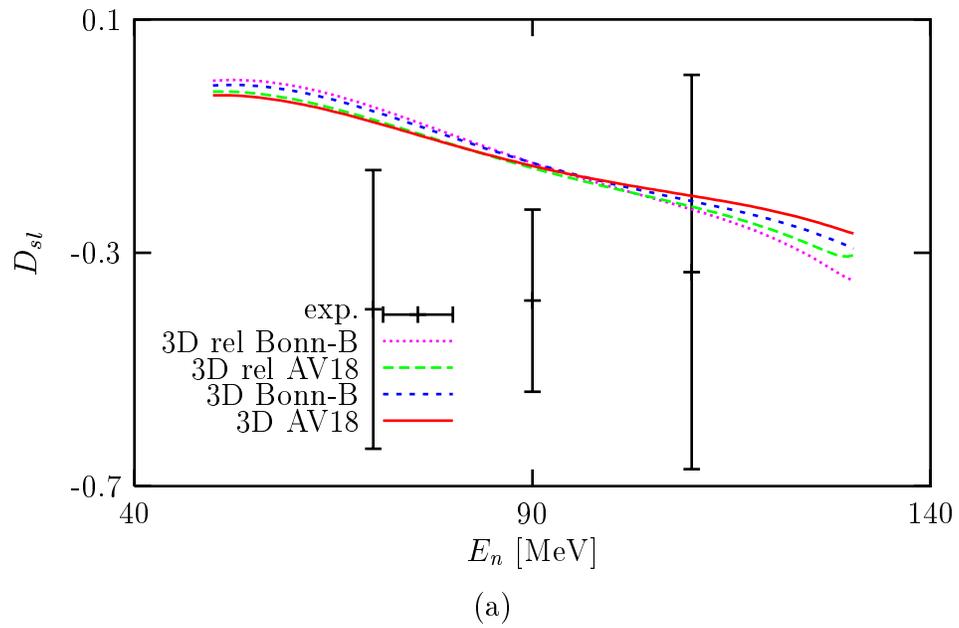
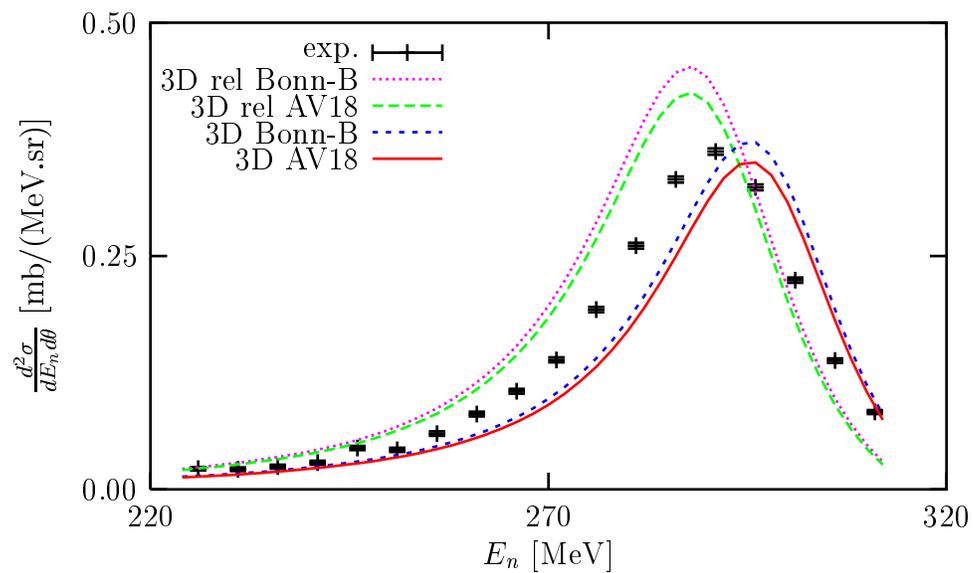


Figure 7.64: Same as in Fig. 7.52, but at $\theta_{lab} = 48^\circ$.

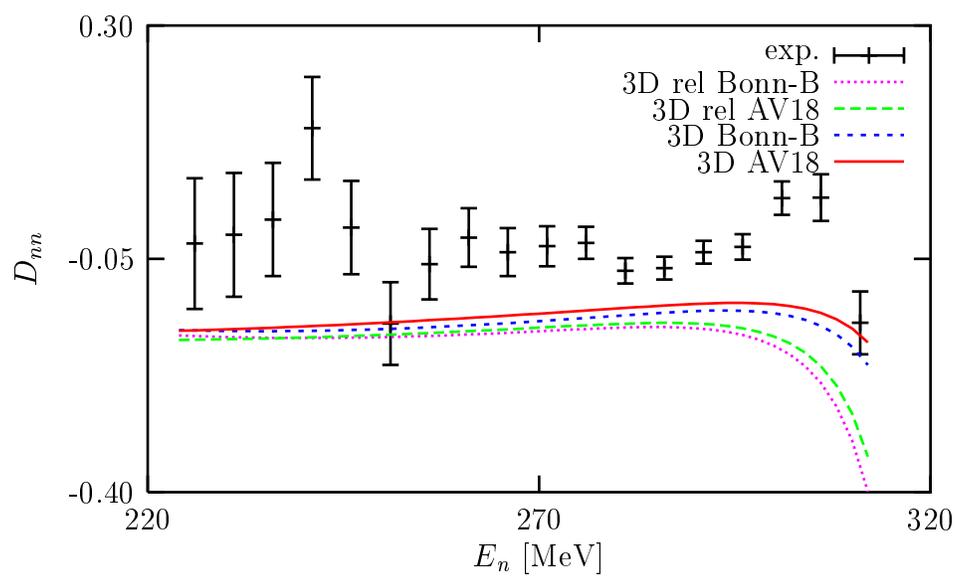
the proton may have lost some of its energy before it hits and breaks the deuteron apart [54]. In this case the process occurs at some energy, which deviates from the considered one. At $E_{lab} = 346$ and 495 MeV one sees more clearly than at $E_{lab} = 197$ MeV that for the spin observables the relativistic effects become larger as E_n increases and mostly at E_n towards its maximum. For A_y at $E_{lab} = 346$ MeV in Fig. 7.66(a) we see a similar tilting effect as the one seen in the last section, when we investigated the rescattering process. Clearly at higher energies relativity is getting more important. Therefore, the relativistic correction leads to more changes as the energy increases.

Now we tentatively discuss the relativistic correction in connection with the inclusion of the rescattering terms of the full Faddeev Nd break-up amplitude. In the last section it was shown that the multiple scattering decreases the pd break-up cross section, which is especially visible around the peak. Compared to the data the theoretical peak is, however, shifted to a higher neutron energy E_n . Here in this section we see that the relativistic correction shifts the theoretical peak back to the correct position along E_n , but increases its height. Therefore, one could conjecture that including both, the rescattering terms and the relativistic correction, will move the theoretical prediction for the cross section peak towards the data. For the analyzing power A_y the multiple scattering improves the theoretical prediction by the effect like tilting A_y . Thus, it lifts A_y at lower E_n and drops A_y at E_n close to its maximum. An almost similar effect is again caused by the relativistic correction, which can best be observed in Fig. 7.66(a). Therefore, including the rescattering terms and the relativistic correction will very likely improve the theoretical prediction. Thus, for the higher energies we considered, say from $\simeq 200$ MeV to 500 MeV, we conjecture that both multiple scattering and relativity must be taken into account.

After the observations at higher energies we go to energies lower than $E_{lab} \simeq 200$ MeV and seek for relativistic effects. In Figs. 7.73-7.76 we show the cross section and the spin observables at $E_{lab} = 16$ MeV, $\theta_{lab} = 13^\circ$ and in Figs. 7.77-7.80 at $E_{lab} = 65$ MeV, $\theta_{lab} = 13^\circ$. At $E_{lab} = 16$ MeV we see for the cross section in Fig. 7.73(a) only small relativistic effects. The cross sections obtained from the relativistic calculations are larger than the ones from the nonrelativistic calculations, that is about 1.4% at the peak around $E_n = 6$ MeV. For the spin observables relativistic effects are hardly seen at $E_{lab} = 16$ MeV. At $E_{lab} = 65$ MeV in Fig. 7.77(a) the cross section peaks around $E_n = 58$ MeV arising from the relativistic calculations are already clearly seen to be shifted to lower E_n , compared to the ones from the nonrelativistic calculations. The heights of the cross section peaks from the relativistic calculations are about 6% higher than those from the nonrelativistic calculations. At $E_{lab} = 65$ MeV relativistic effects for the spin observables

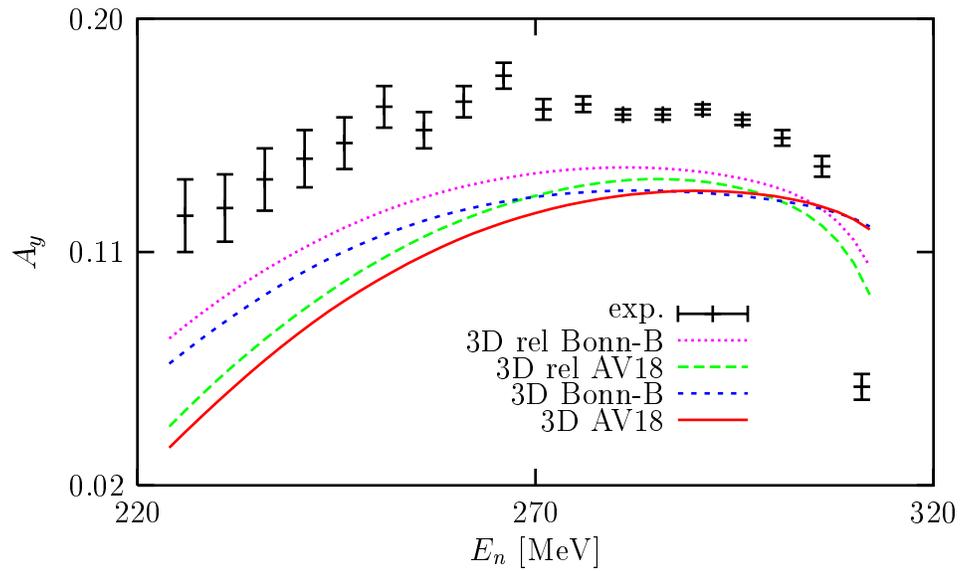


(a)

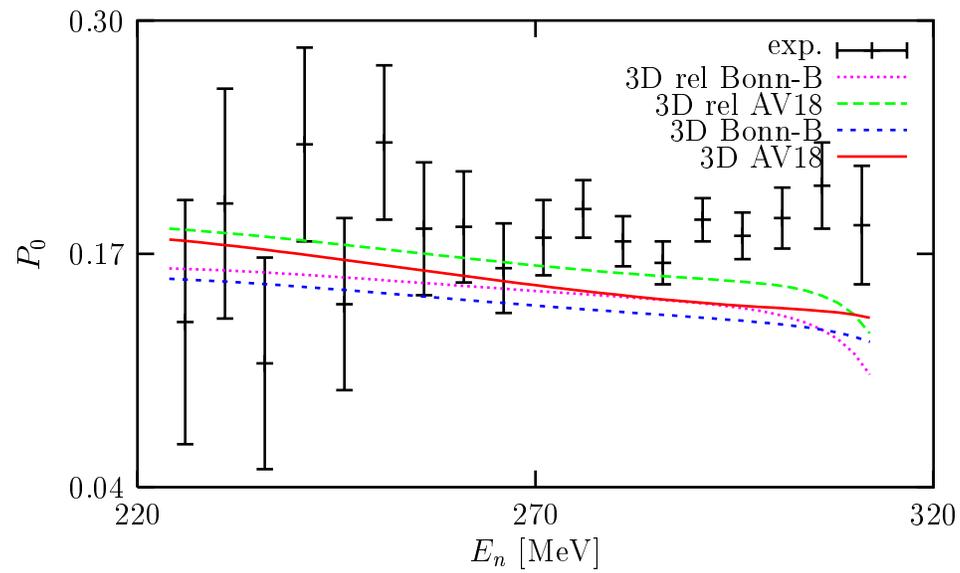


(b)

Figure 7.65: Same as in Fig. 7.49, but at $E_{lab} = 346$ MeV and $\theta_{lab} = 22^\circ$. The experimental data are taken from Ref. [19].

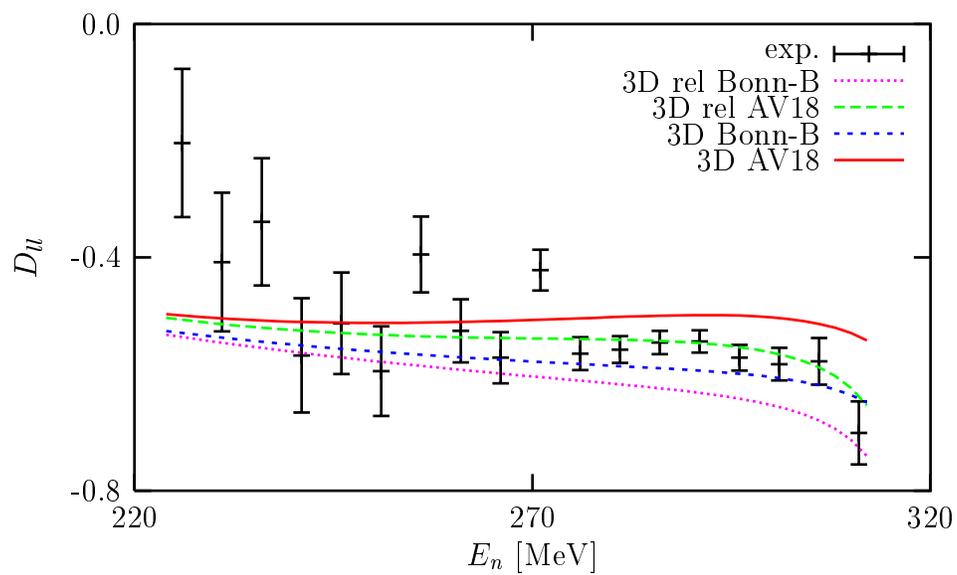


(a)

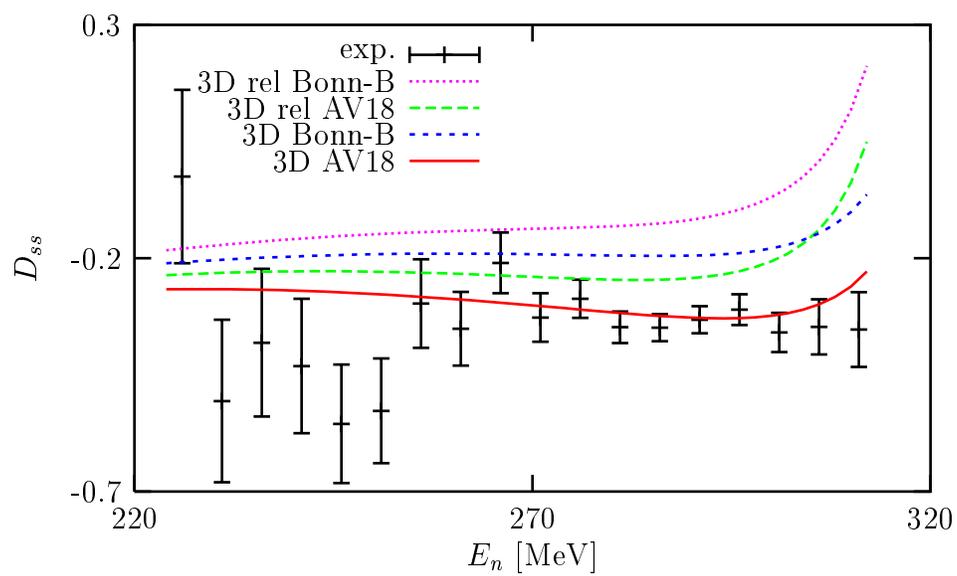


(b)

Figure 7.66: Same as in Fig. 7.65, but for (a) the analyzing power A_y and (b) the neutron polarization P_0 .

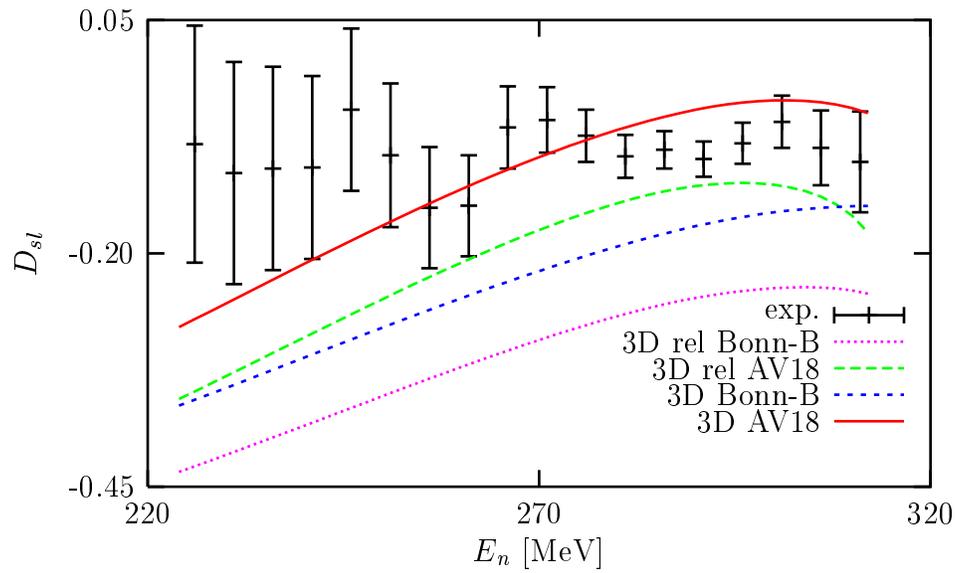


(a)

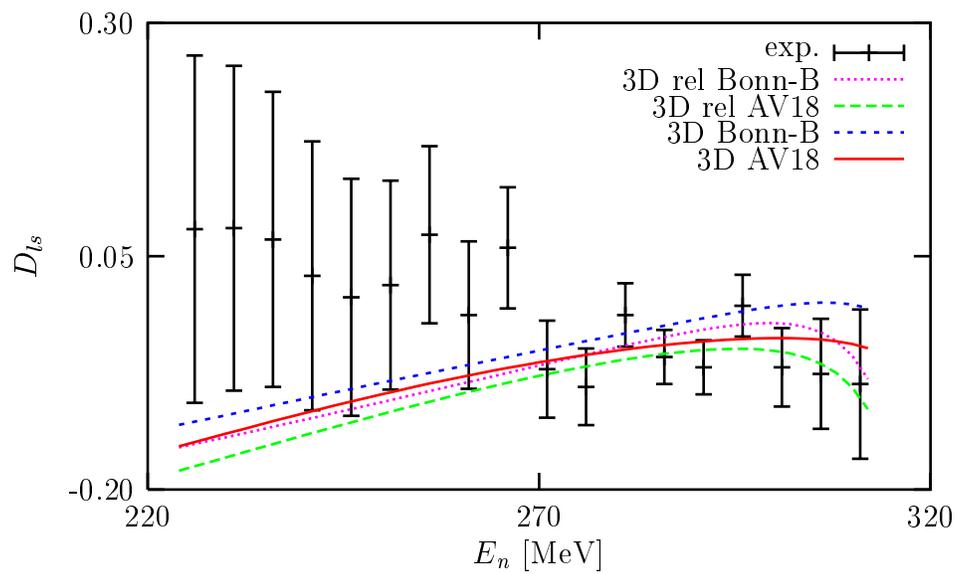


(b)

Figure 7.67: Same as in Fig. 7.65, but for the polarization transfer coefficients (a) D_u and (b) D_{ss} .

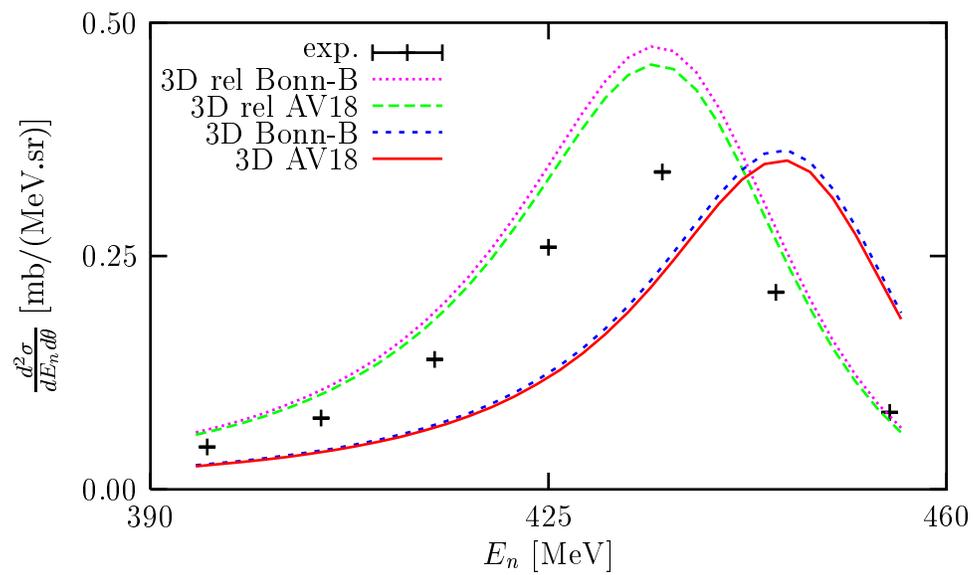


(a)

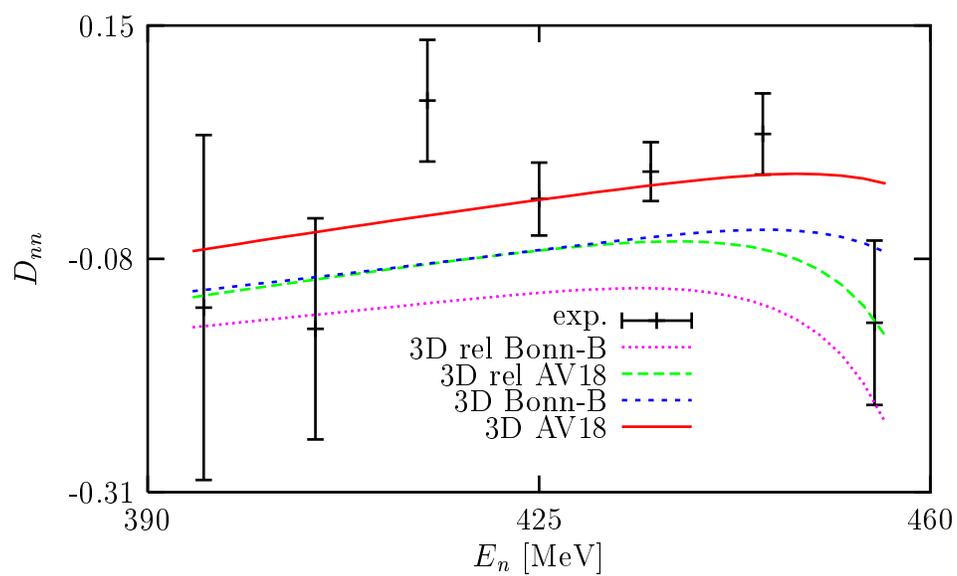


(b)

Figure 7.68: Same as in Fig. 7.65, but for the polarization transfer coefficients (a) D_{sl} and (b) D_{ts} .



(a)



(b)

Figure 7.69: Same as in Fig. 7.65, but at $E_{lab} = 495$ MeV and $\theta_{lab} = 18^\circ$. The experimental data are taken from Ref. [57].

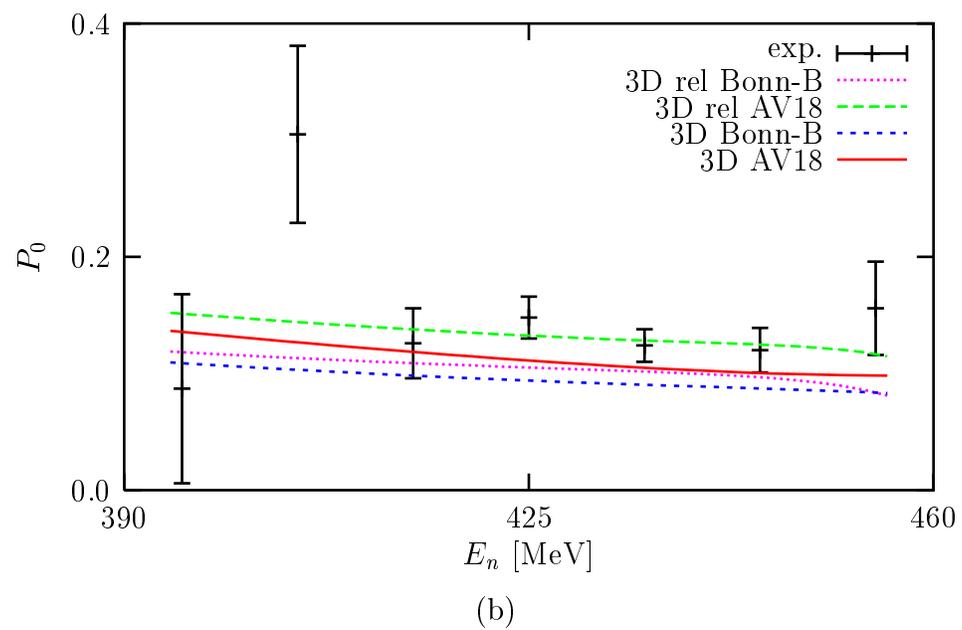
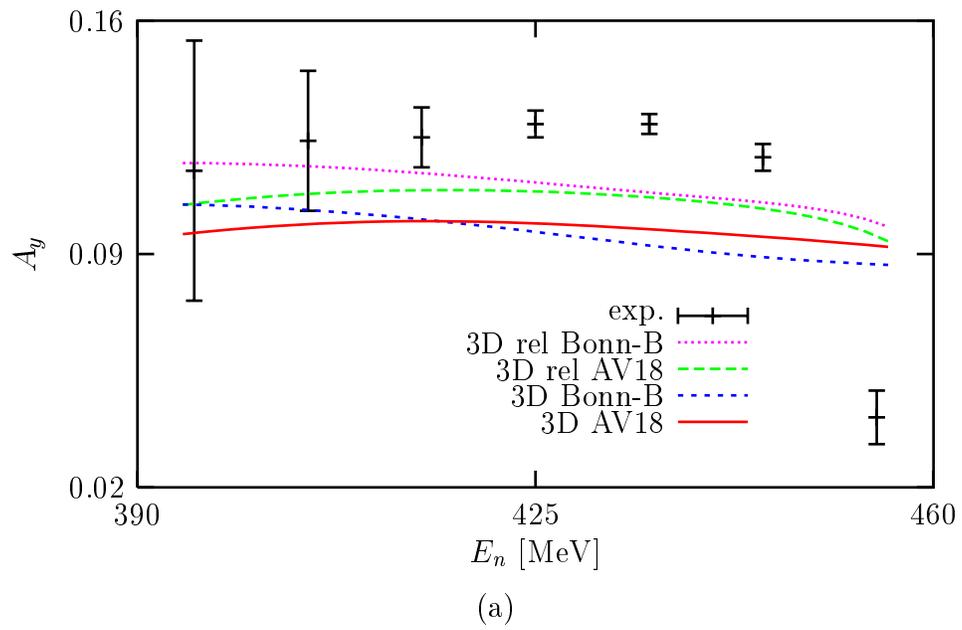
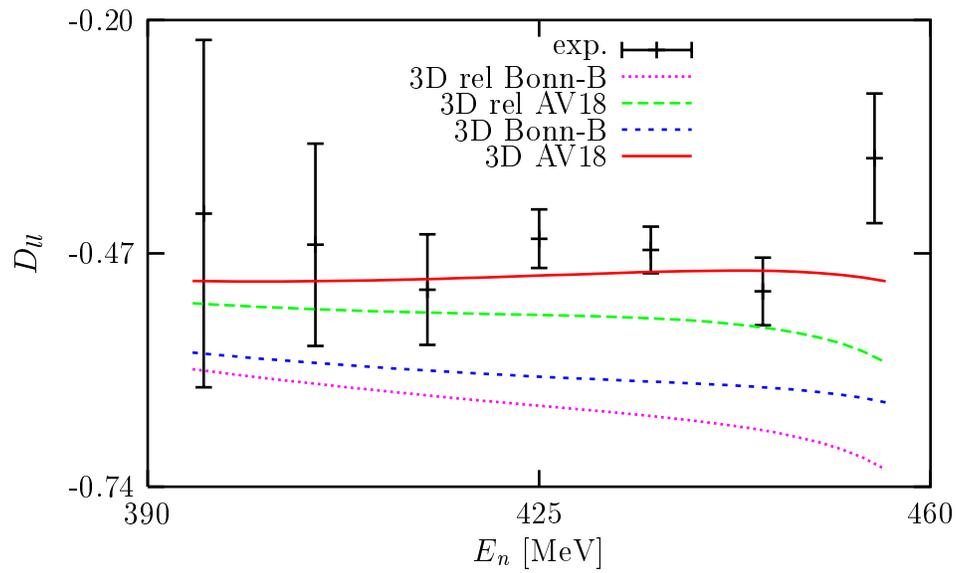
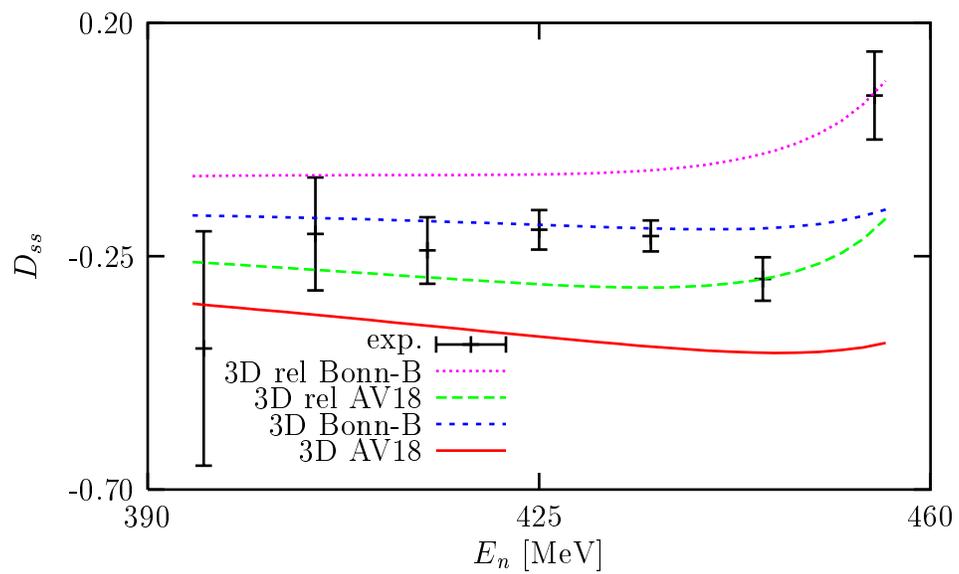


Figure 7.70: Same as in Fig. 7.69, but for (a) the analyzing power A_y and (b) the neutron polarization P_0 .

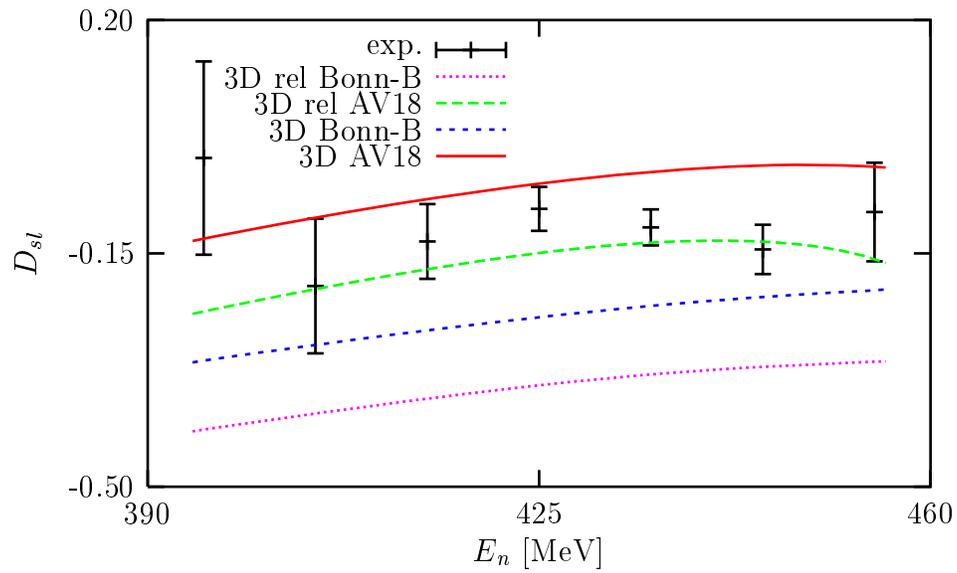


(a)

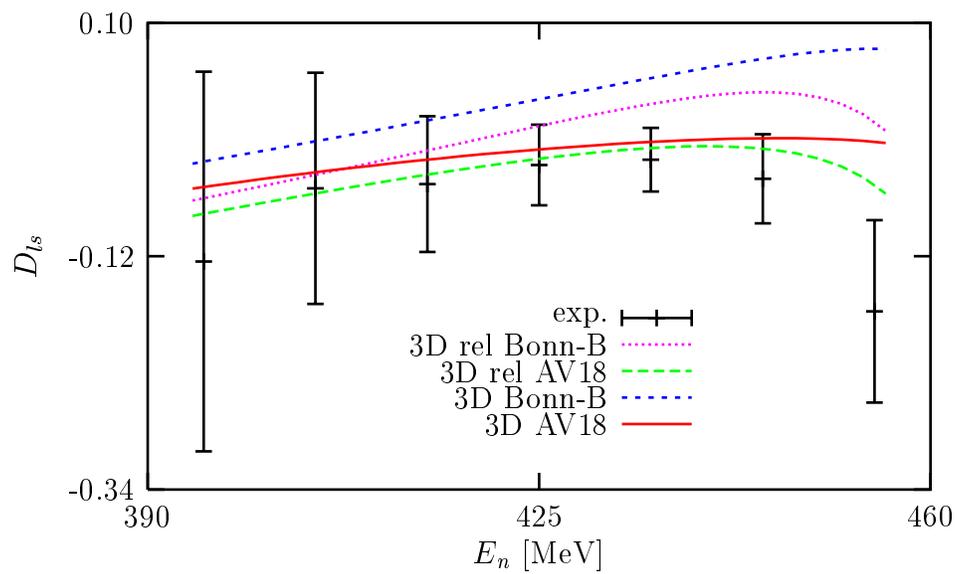


(b)

Figure 7.71: Same as in Fig. 7.69, but for the polarization transfer coefficients (a) D_u and (b) D_{ss} .



(a)



(b)

Figure 7.72: Same as in Fig. 7.69, but for the polarization transfer coefficients (a) D_{sl} and (b) D_{ts} .

can be seen, for example, in Fig. 7.78(a) for A_y . The effects are about 4% around $E_n = 42$ MeV. Therefore, at $E_{lab} = 65$ MeV the relativity has already begun to be important.

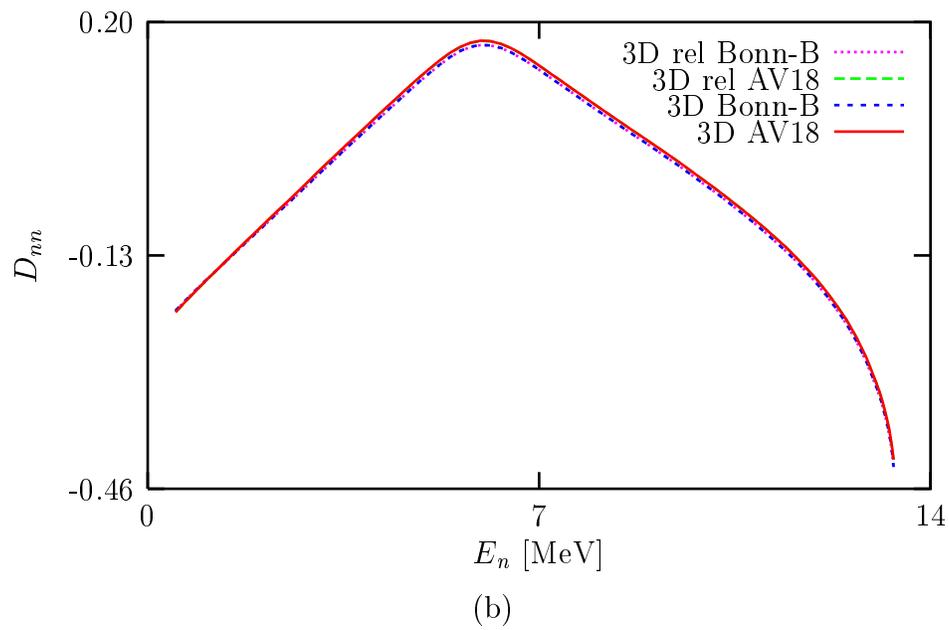
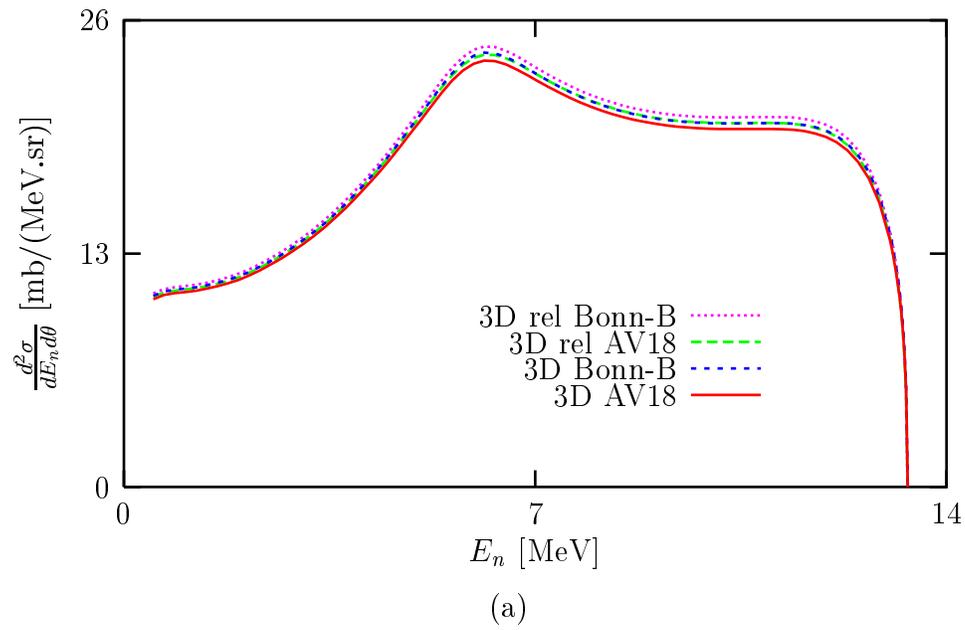
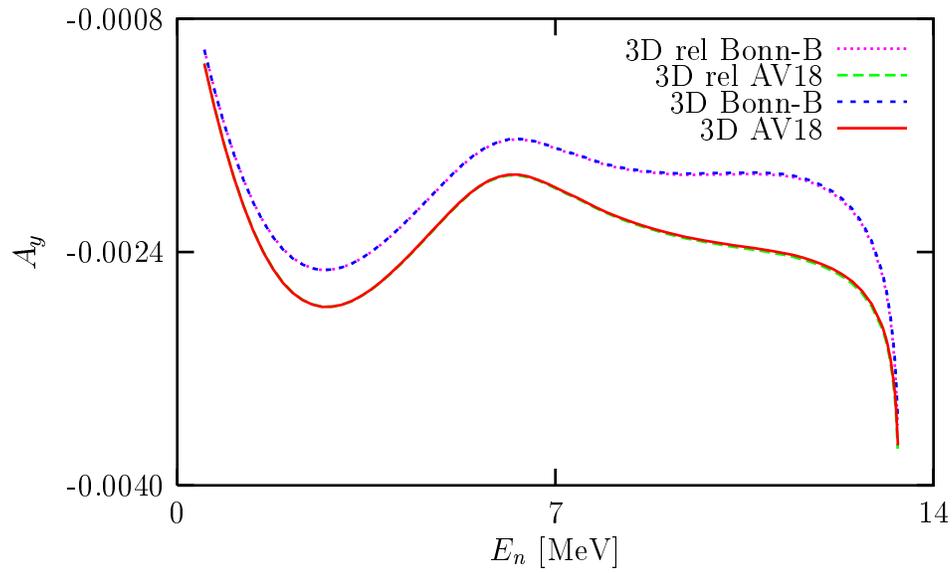
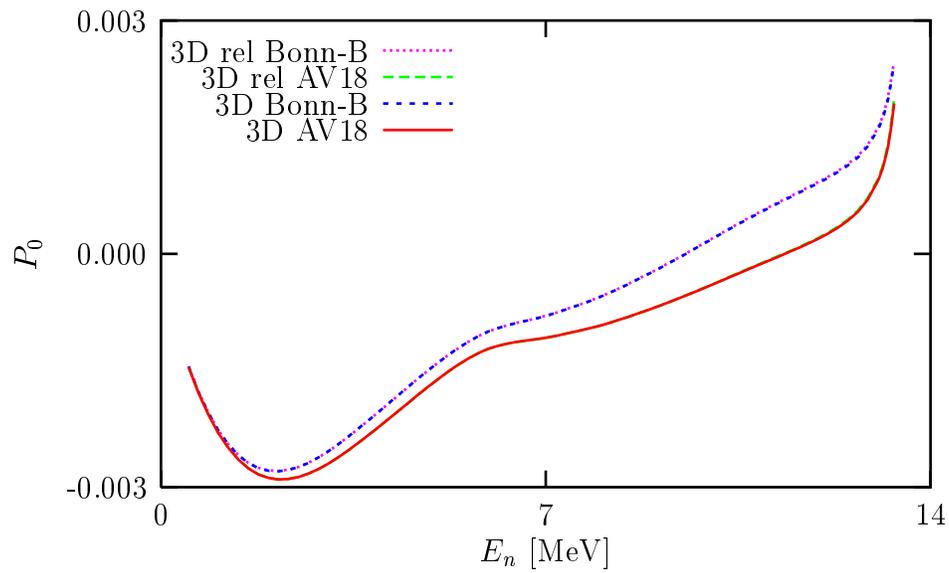


Figure 7.73: Same as in Fig. 7.69, but with no experimental data, at $E_{lab} = 16$ MeV and $\theta_{lab} = 13^\circ$.

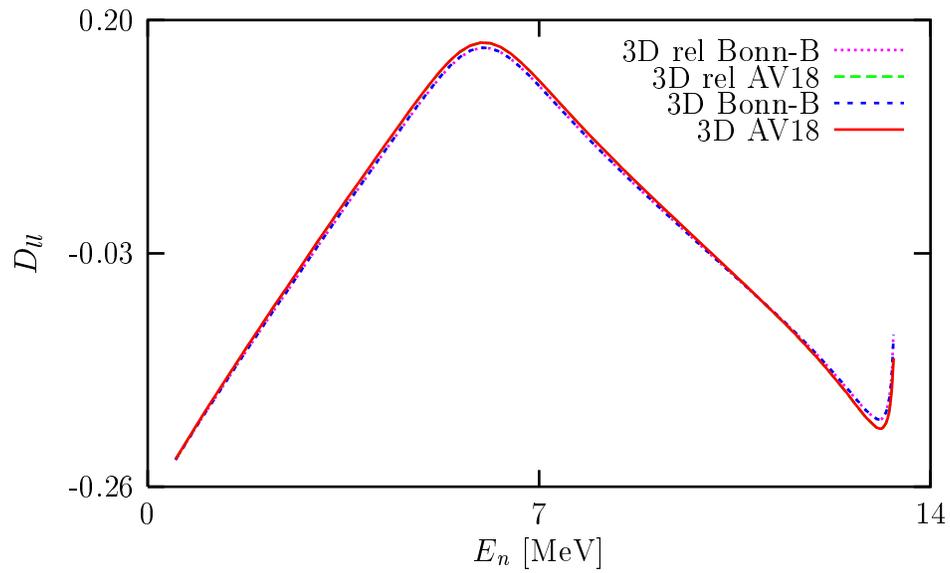


(a)

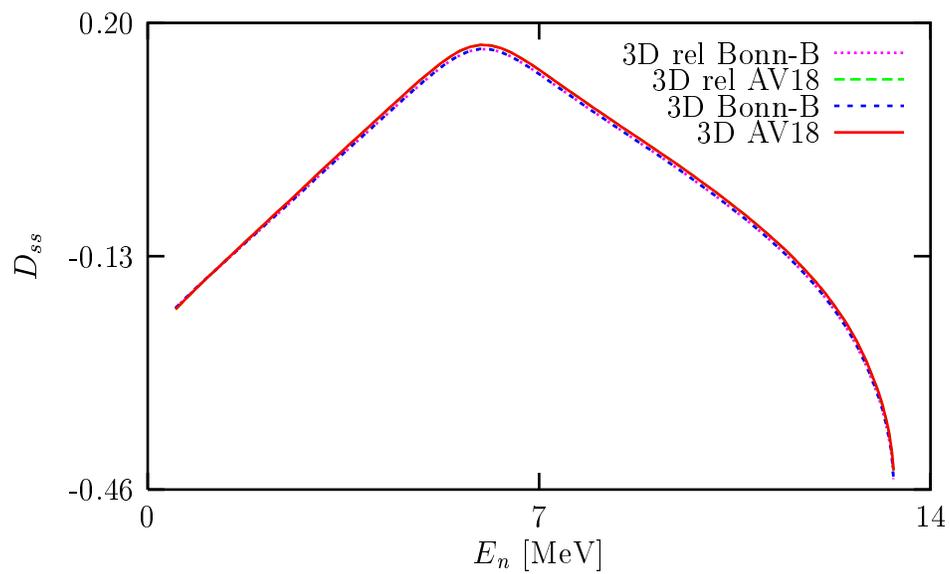


(b)

Figure 7.74: Same as in Fig. 7.73, but for (a) the analyzing power A_y and (b) the neutron polarization P_0 .



(a)



(b)

Figure 7.75: Same as in Fig. 7.73, but for the polarization transfer coefficients (a) D_u and (b) D_{ss} .

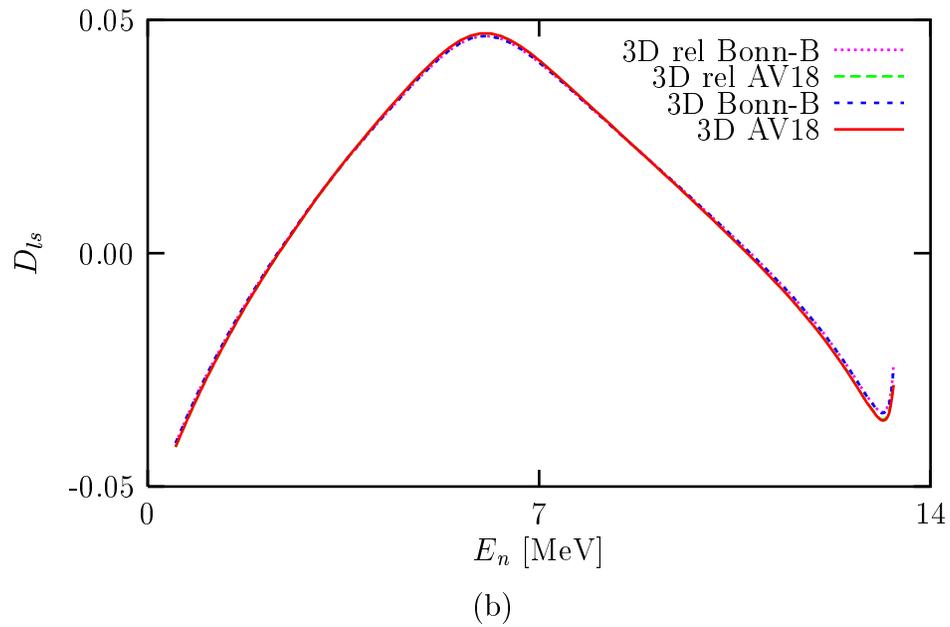
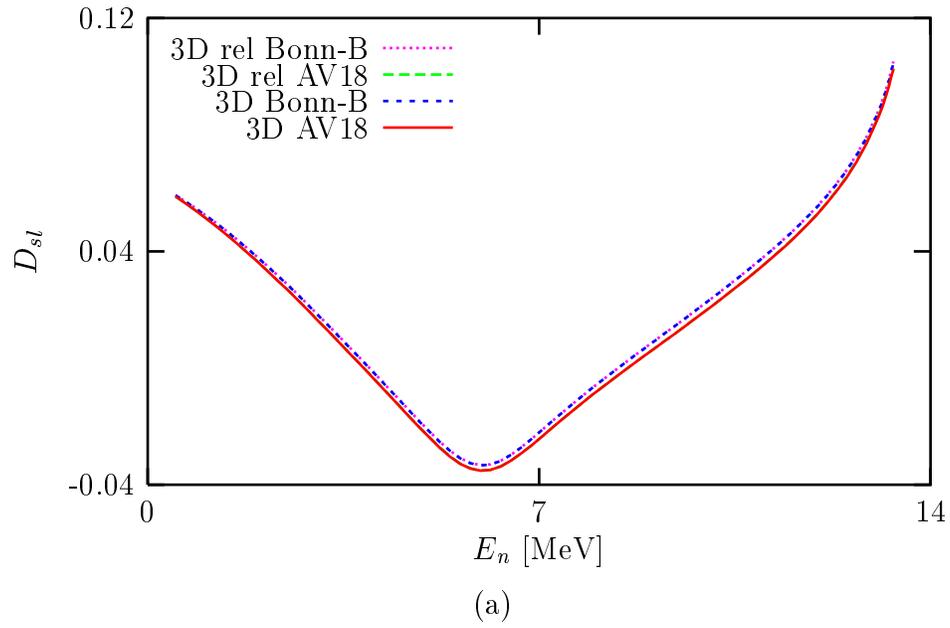
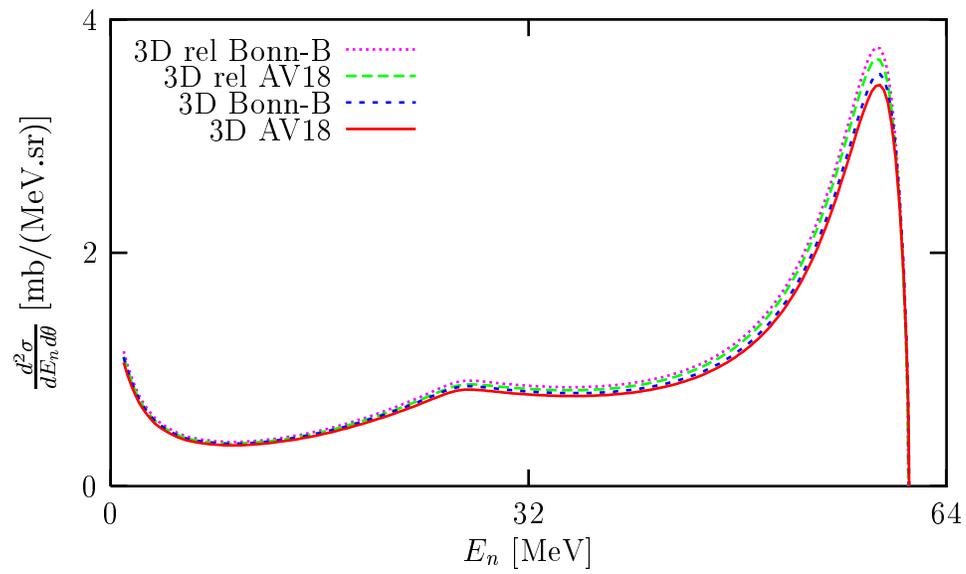
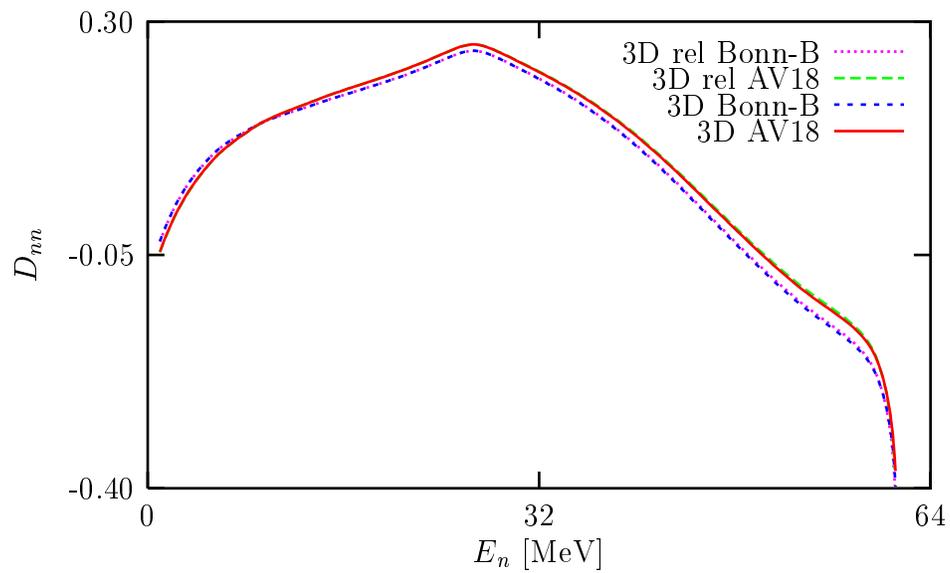


Figure 7.76: Same as in Fig. 7.73, but for the polarization transfer coefficients (a) D_{sl} and (b) D_{ts} .



(a)



(b)

Figure 7.77: Same as in Fig. 7.73, but at $E_{lab} = 65$ MeV and $\theta_{lab} = 13^\circ$.

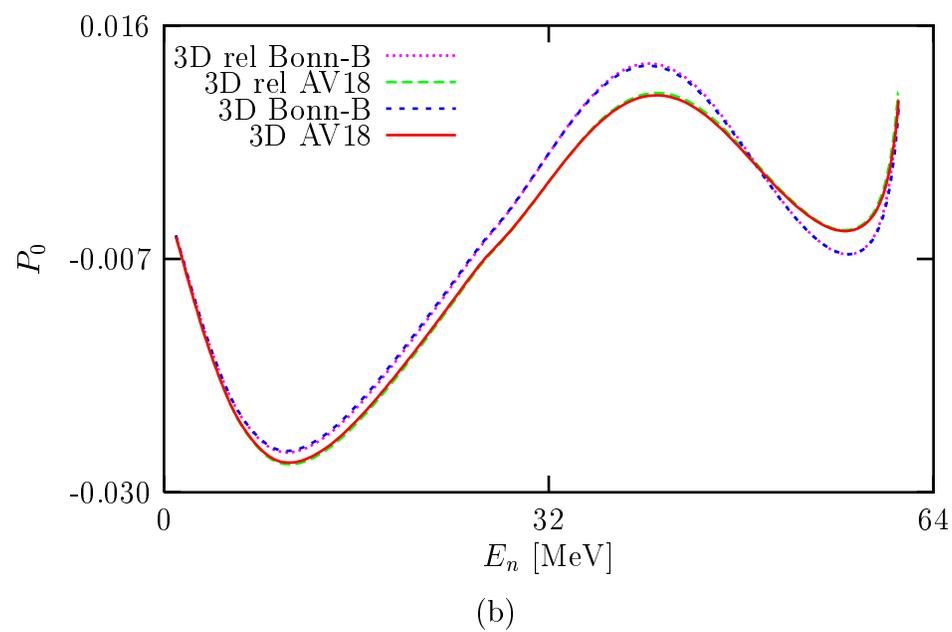
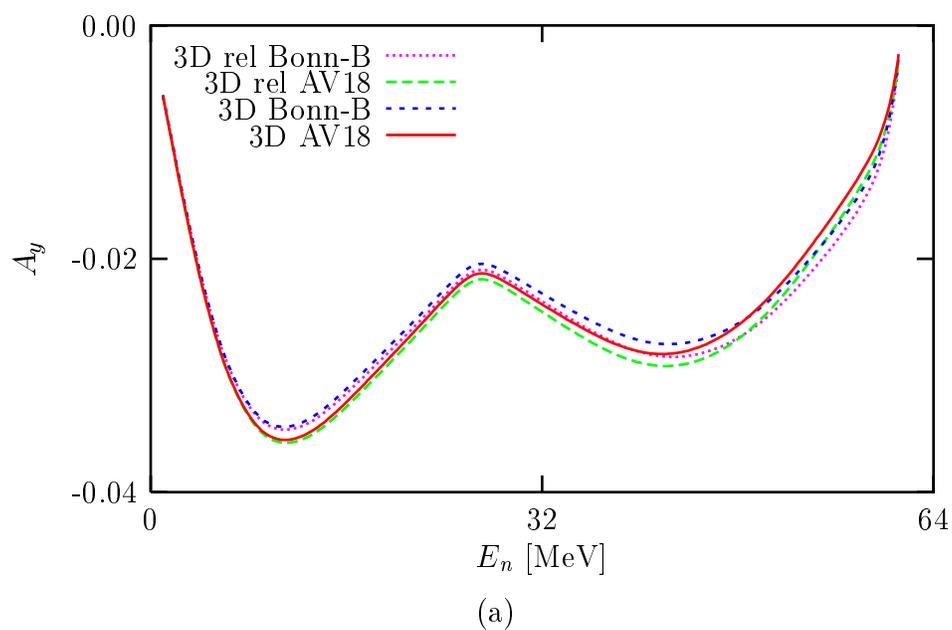
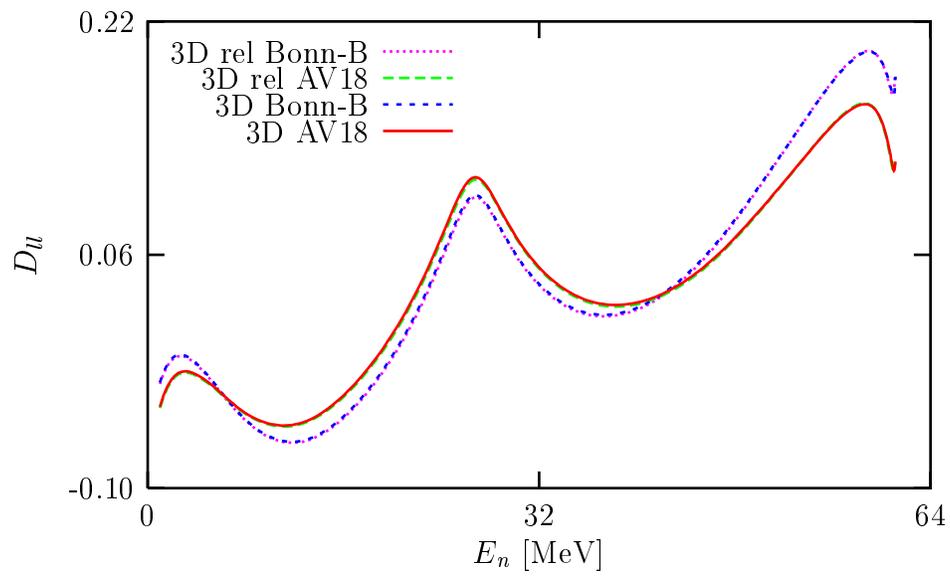
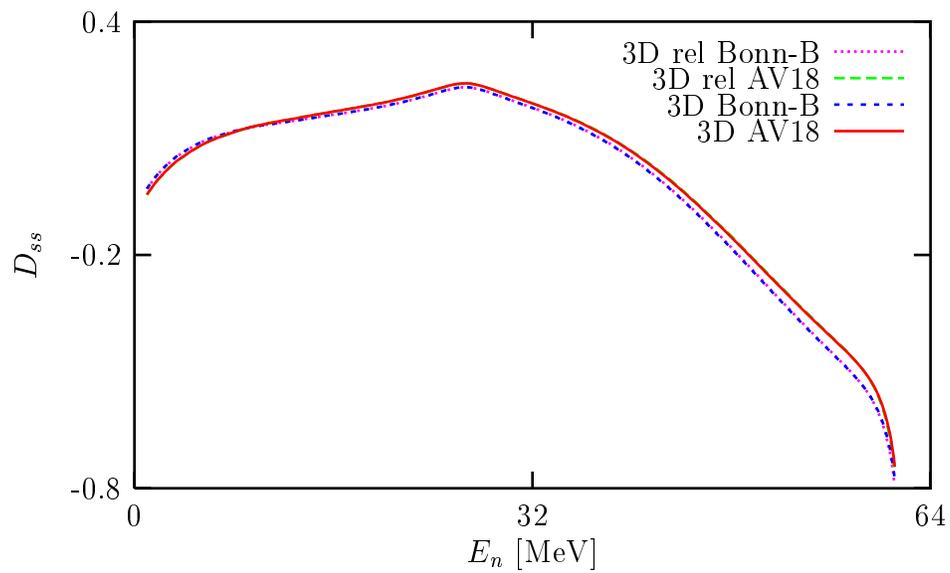


Figure 7.78: Same as in Fig. 7.74, but at $E_{lab} = 65$ MeV and $\theta_{lab} = 13^\circ$.



(a)



(b)

Figure 7.79: Same as in Fig. 7.75, but at $E_{lab} = 65$ MeV and $\theta_{lab} = 13^\circ$.

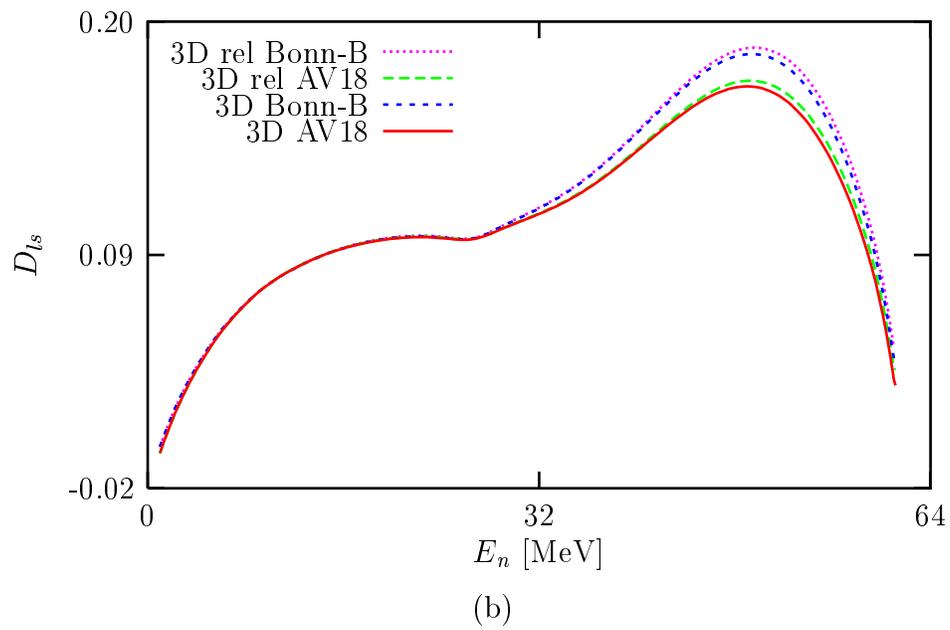
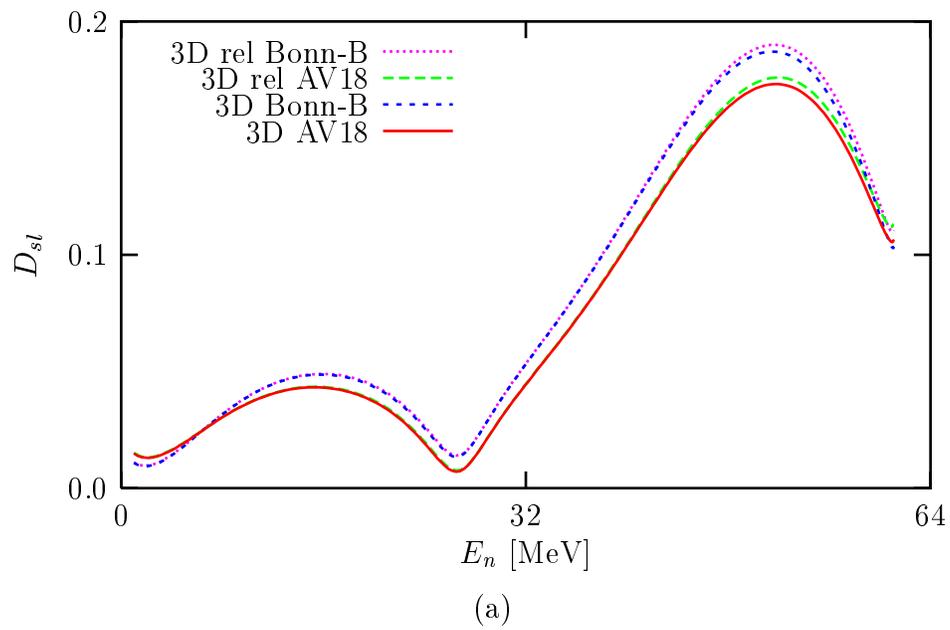


Figure 7.80: Same as in Fig. 7.77, but at $E_{lab} = 65$ MeV and $\theta_{lab} = 13^\circ$.

Chapter 8

SUMMARY AND OUTLOOK

We have developed a technique to perform few-nucleon calculations in momentum space without employing partial wave decompositions. We call this the 3D technique. We began with the NN system and continued to 3N scattering, which was the Nd break-up process in first order. The 3D technique has been intended to be a viable alternative to the successful PW technique. At higher energies the 3D technique should be better suited than a PW based one. Here we summarize how we developed our 3D technique for the NN system and the Nd break-up process. The calculations in this work were carried out based on the NN potentials AV18 [20] and Bonn-B [21]. Finally we give an outlook for further investigations as well as developments of the 3D technique.

NN Scattering

To develop the 3D technique it was necessary to start with NN scattering, since the NN T-matrix is input to calculations of more complex few-nucleon systems. The first step was to define basis states for the NN system. We defined momentum-helicity basis states being antisymmetric under exchange of the two nucleons in momentum, spin and isospin space. As reflected by the name the momentum-helicity basis states were constructed using momentum vectors states and helicity states of NN total spin. The NN total spin was chosen instead of individual spins of the two nucleons to allow obtaining a smaller number of LSE's to be solved. The symmetry properties of the T-matrix and the NN potential matrix elements in the momentum-helicity basis states allow the reduction of the number of the LSE's for the NN T-matrix from 10 to 5 for each NN total isospin state. All LSE's in the 3D technique are integral equations in two variables, the magnitude of the relative momentum between the two nucleons and the scattering angle.

The NN potential is expressed in a set of six independent operators, Ω . We defined the

Ω operators to be suitable for the momentum-helicity basis states and thus, allow for very simple evaluations of the NN potential matrix elements. We derived a relation between the set of the Ω operators and the set of six operators known as the Wolfenstein operators [26]. This is possible due to the invariances, symmetry conditions and the hermiticity of the NN potential [41]. We want to point out that any NN potential given in operator form can be used in the 3D technique. Representative potentials are the AV18 and Bonn-B potentials, which were used in this work.

In order to calculate observables and compare them with NN data we connected the T-matrix elements in the momentum-helicity basis states to the ones in a physical representation. The physical representation uses spins and isospins of the individual nucleons, where the spins are quantized along an arbitrary but fixed z axis. Hence, the physical representation is closely connected to the experimental set up of NN scattering. We also expanded the T-matrix elements in the momentum-helicity basis states into partial waves and compared the resulting NN phase shifts to the ones from standard PW calculations. The agreement with the PW calculations for the NN phase shifts as well as for the NN observables is perfect. The comparisons for NN observables showed that especially for higher energies many partial waves are needed in the PW calculations to converge to the 3D calculations. For example, at $E_{lab} = 300$ MeV the PW calculation for the np differential cross section must take at least $j_{max} = 16$ corresponding to 98 LSE's. We also compared our 3D calculations to observables based on the phase shifts determined in a partial wave analysis (PWA) as well as directly to NN data for laboratory energies higher than 300 MeV. Later, when we calculated the Nd break-up process at various energies, we needed the NN T-matrix for those energies. Since the 3D technique is applicable with equal performance for any energy, the comparisons were intended to check the implementations of the two NN potentials AV18 and Bonn-B in the 3D technique at higher energies. Though these two parameterized NN potentials have been fitted to NN data only for energies below 350 MeV, the comparisons with the PWA results and NN data showed nevertheless rather good agreements.

The Deuteron

Conventionally the deuteron has always been calculated as a set of coupled equations for orbital angular momenta $l = 0$ and $l = 2$. It was interesting to investigate, if we can use the momentum-helicity basis states for a solution of the NN bound state. To achieve this we projected the deuteron state and the eigenvalue equation onto this basis. Thus, we defined the deuteron wave function components, which are three-dimensional, in the

momentum-helicity basis states. We also defined deuteron probability densities in the momentum-helicity basis states. We derived the deuteron equations in the momentum-helicity basis states as two coupled integral equations in two variables, the magnitude of the relative momenta between the two nucleons and an angle referring to an arbitrary z direction. We related the deuteron wave function components in the momentum-helicity basis states to the ones in the PW basis states. This connection allows to calculate the PW projected deuteron wave function components in s and d waves from the deuteron wave function components in the momentum-helicity basis states. Comparisons with the PW calculations for the deuteron s and d waves showed good agreements.

Next, using the momentum-helicity basis states, again we formulated the deuteron equation and the deuteron wave function components in a different way. At first we kept the deuteron state being expanded in partial waves, and then derived an operator form for the deuteron wave function in momentum space. By means of the momentum-helicity basis states the deuteron wave function in operator form led to the deuteron wave function components in the momentum-helicity basis states, but now with analytic angular behavior. This analytic angular behavior confirmed the numerical one obtained in the first formulation. This allowed us to derive the deuteron equation in one variable only, namely the magnitude of the relative momentum between the two nucleons. We solved this equation and obtained the same results as those in the first formulation. Again we connected to the standard PW decomposition and obtained good agreements for the PW projected deuteron wave function components in s and d waves. Finally by means of the deuteron wave function in operator form we investigated in a 3D fashion the probability densities for some spin configurations of the two nucleons inside the deuteron for an overall polarized deuteron.

The Nd Break-Up Process

Finally we stepped to a 3N system and extended the 3D technique for the Nd break-up process. We are interested in higher energies and decided to consider only the leading order term of the full Nd break-up amplitude. Thus, we wanted to see if the leading term alone could describe the Nd break-up process for the higher energies being considered, which were beyond $\simeq 200$ MeV nucleon laboratory energy. We used the Faddeev's scheme to treat the Nd break-up process. For simplicity we kept the deuteron state being expanded in partial waves. This was a natural step, since the deuteron wave function has only two partial wave components, s and d waves. We started with deriving the leading term of the full Nd break-up amplitude in the 3N basis states, which were in a physical representation.

As in the NN scattering case the physical representation uses spins and isospins of the individual nucleons, where the spins are quantized along an arbitrary but fixed z axis. The kinematics of the three nucleons were described by two Jacobi momenta such, that the 3N system was considered as consisting of one nucleon and a 2N subsystem. Symmetry properties under exchange of the three nucleons were introduced to the leading term of the full Nd break-up amplitude by means of permutation operators. As a result we obtained an expression for the leading term in terms of the NN T-matrix elements in the physical representation. Using the previously derived physical representation of the NN T-matrix elements it was straightforward to obtain the leading term of the full Nd break-up amplitude in terms of the NN T-matrix elements in the momentum-helicity basis states. In the resulting expression the initial 2N relative momenta as arguments of the NN T-matrix elements in the momentum-helicity basis states were pointing in arbitrary directions. To solve the NN LSE's for the NN T-matrix we choose a fixed, say z , direction as the directions of the initial NN relative momenta. Therefore, as a final step we rotated the NN T-matrix elements in the momentum-helicity basis states such, that the initial 2N relative momenta were pointing into a fixed z direction. The rotation then led to an intricate additional phase factor.

With this leading term of the full Nd break-up amplitude in the momentum-helicity basis states we calculated observables. Since for higher energies one also has to expect relativistic effects to be important, we took a further step, namely included relativistic kinematics. Here we restricted ourselves to a very first and necessary step, namely to replace the nonrelativistic Jacobi momenta and energy arguments of the nonrelativistic leading term with the relativistic expressions. Finally we derived the cross section using the standard relativistic scattering theory. Thus, the leading term and the phase space factor of the cross section changed compared to the one obtained using nonrelativistic scattering theory.

We applied the formulation for the Nd break-up process in a 3D approach to the (p,n) charge exchange reaction in the inclusive pd break-up process. In this process a proton is directed towards a deuteron, which then breaks up, and finally the neutron is detected, while the two protons are not detected. We calculated the spin averaged differential cross section (shortly called cross section) and some spin observables, which were the neutron polarization, the proton analyzing power and the polarization transfer coefficients. We discussed three different aspects of our calculations. First, we compared our calculations to the PW calculations for proton laboratory energies E_{lab} up to 197 MeV. It turned out that up to $E_{lab} = 100$ MeV our calculations still agreed with the PW calculations. There was, however, already a discrepancy of about 1.7% for the cross section peak at

100 MeV, where the PW calculations took 2N states of 2N total angular momenta $j \leq 7$ and 3N states of 3N total angular momenta $J \leq 31/2$. In fact, by taking so many angular momentum states one has already reached the present limits of PW calculations. At $E_{lab} = 197$ MeV our calculations disagreed with the PW calculations with $j \leq 7$ and $J \leq 31/2$, since the PW calculations did not sufficiently converge. A convergence test also showed that the 2N total angular momentum states are more important than those of the 3N total angular momentum for the PW calculations to achieve convergence. For the same number of total angular momentum states taken into account disagreement between our calculations and the PW calculations grows rapidly as the energy increases. We concluded that for $E_{lab} > 100$ MeV PW calculations cannot be used safely to accurately describe the Nd break-up process.

Secondly, we wanted to show the importance of rescattering effects. Thus, we compared our calculations at $E_{lab} = 197$ MeV to the PW full Faddeev calculations, which included not only the leading term but also the rescattering terms of the full pd break-up amplitude. The comparisons showed that at this energy rescattering effect do occur and mostly show up in the cross section and the analyzing power. For these two observables inclusions of rescattering terms led to results closer to the data. We concluded that at $E_{lab} = 197$ MeV rescattering terms of the full Nd break-up amplitude still have to be considered.

For energies higher than 197 MeV we had no PW full Faddeev calculations to compare with. Therefore, we compared directly to the data at $E_{lab} = 346$ and 495 MeV. For these energies we could only conjecture that rescattering terms may be necessary, since discrepancies to the data were visible.

At last, we studied the effect of relativistic kinematics in our calculations. For this purpose we compared our 3D calculations with and without relativistic kinematics to each other for energies of 197, 346 and 495 MeV, at which we also had the experimental data. At these energies we observed relativistic effects mostly in the cross sections and the analyzing powers. For these two observables relativistic kinematics led to better results in relation to the data. The effects grew larger with increasing energy, as one might expect. In comparisons to the data the observed relativistic effects together with the previously seen rescattering effects led to a conjecture that to better describe the pd break-up process at higher energies, say $\simeq 200$ MeV to 500 MeV, one needs to include both, the rescattering terms and the relativistic corrections. In order to find out at which energy relativistic effects appear already to be important we compared our calculations with and without relativistic ingredients to each other at 16 and 65 MeV. We found that at $E_{lab} = 65$ MeV relativistic effects started to be visible.

Finally we would like to summarize our work within one paragraph. We have developed a 3D technique for NN scattering, the deuteron and the Nd break-up process. The 3D technique has proven to be a good alternative to the PW decomposition and appears to be necessary at higher energies. In contrast to the PW decomposition the 3D technique requires much less algebraic work. For lower energies, where the PW calculations are still reliable, the 3D calculations show perfect agreements with the PW calculations.

Outlook

It is clear that after finishing this work, there are still many investigations left on few-nucleon systems to pursue using the 3D technique. For the NN system it is interesting to implement in the 3D technique new NN potentials such as the ones [60] based on the chiral perturbation theory. For few-nucleon bound systems with nucleon numbers greater than 2 the 3D technique should necessarily be employed, since unlike for the deuteron the triton [61, 62, 63], the α -particle [64, 65] and other more complex few-nucleon bound systems involve very many angular momentum states. For 3N scattering we have not yet solved the full Faddeev equation, which has been shown to be important. We also have not yet included three nucleon forces (3NF's), which may play a more predominant role at higher energies. In appreciating relativity we only considered relativistic kinematics. We have not taken into account the boost of the NN T-matrix [58] and the Wigner rotations [59]. These will be interesting and challenging investigations to carry out in the future. Especially in incorporating dynamical features of relativity a 3D formulation will be rewarding. From our point of view the next step will be to include the rescattering terms of the full Nd break-up amplitude and 3NF's. This will enter a domain at higher energies, which up to now has not yet been investigated thoroughly.

APPENDICES

Appendix A

THE ROTATION MATRIX

In this appendix we give derivations of the two relations for $d_{m'm}^j$ which we used in the main text. See Ref. [31, 32] for a more detailed description of $d_{m'm}^j$.

Wigner's definition for $d_{m'm}^j$ is

$$\begin{aligned}
 d_{m'm}^j(\beta) &= \left[(j+m)!(j-m)!(j+m')!(j-m')! \right]^{\frac{1}{2}} \\
 &\times \sum_n \frac{(-)^n}{(j-m'-n)!(j+m-n)!(n+m'-m)!n!} \\
 &\times \left(\cos \frac{\beta}{2} \right)^{2j+m-m'-2n} \left(-\sin \frac{\beta}{2} \right)^{m'-m+2n}.
 \end{aligned} \tag{A.1}$$

It is obvious from this definition that $d_{m'm}^j$ is real.

The first relation is

$$d_{m'm}^j(\pi - \beta) = (-)^{j+m'} d_{m'-m}^j(\beta). \tag{A.2}$$

Using the definition given in Eq. (A.1) this relation can be derived as

$$\begin{aligned}
 d_{m'm}^j(\pi - \beta) &= \left[(j+m)!(j-m)!(j+m')!(j-m')! \right]^{\frac{1}{2}} \\
 &\times \sum_n \frac{(-)^n}{(j-m'-n)!(j+m-n)!(n+m'-m)!n!} \\
 &\times \left(\cos \frac{\pi - \beta}{2} \right)^{2j+m-m'-2n} \left(-\sin \frac{\pi - \beta}{2} \right)^{m'-m+2n} \\
 &= (-)^{2j} \left[(j+m)!(j-m)!(j+m')!(j-m')! \right]^{\frac{1}{2}} \\
 &\times \sum_n \frac{(-)^n}{(j-m'-n)!(j+m-n)!(n+m'-m)!n!} \\
 &\times \left(\cos \frac{\beta}{2} \right)^{m'-m+2n} \left(-\sin \frac{\beta}{2} \right)^{2j+m-m'-2n}
 \end{aligned}$$

$$\begin{aligned}
&= (-)^{2j} [(j+m)!(j-m)!(j+m')!(j-m')!]^{\frac{1}{2}} \\
&\quad \times \sum_u \frac{(-)^{j-m'-u}}{u!(u+m'+m)!(j-m-u)!(j-m'-u)!} \\
&\quad \times \left(\cos \frac{\beta}{2}\right)^{2j-m-m'-2u} \left(-\sin \frac{\beta}{2}\right)^{m'+m+2u} \\
&= (-)^{2j} (-)^{j-m'} d_{m'-m}^j(\beta) \\
&= (-)^{2(j-m')} (-)^{j+m'} d_{m'-m}^j(\beta) \\
&= (-)^{j+m'} d_{m'-m}^j(\beta). \tag{A.3}
\end{aligned}$$

Similarly we can also have the following relation

$$d_{m'm}^j(\pi - \beta) = (-)^{j-m} d_{-m'm}^j(\beta), \tag{A.4}$$

which is obtained if we insert $u = j + m - n$ instead of $u = j - m' - n$ in the third equality of Eq. (A.3):

$$\begin{aligned}
d_{m'm}^j(\pi - \beta) &= (-)^{2j} [(j+m)!(j-m)!(j+m')!(j-m')!]^{\frac{1}{2}} \\
&\quad \times \sum_u \frac{(-)^{j+m-u}}{(u-m'-m)!u!(j+m'-u)!(j+m-u)!} \\
&\quad \times \left(\cos \frac{\beta}{2}\right)^{2j+m+m'-2u} \left(-\sin \frac{\beta}{2}\right)^{-m'-m+2u} \\
&= (-)^{2j} (-)^{j+m} d_{-m'm}^j(\beta) \\
&= (-)^{2(j+m)} (-)^{j-m} d_{-m'm}^j(\beta) \\
&= (-)^{j-m} d_{-m'm}^j(\beta).
\end{aligned}$$

The second relation is

$$d_{m'm}^j(\theta) = (-)^{m'-m} d_{-m',-m}^j(\theta). \tag{A.5}$$

This can be derived using Eqs. (A.2) and (A.4) as

$$\begin{aligned}
d_{m'm}^j(\theta) &= (-)^{j+m'} d_{m',-m}^j(\pi - \theta) \\
&= (-)^{j+m'} (-)^{j+m} d_{-m',-m}^j(\theta) \\
&= (-)^{2j+m'+m} d_{-m',-m}^j(\theta) \\
&= (-)^{2(j+m)} (-)^{m'-m} d_{-m',-m}^j(\theta) \\
&= (-)^{m'-m} d_{-m',-m}^j(\theta).
\end{aligned}$$

Appendix B

THE Ω OPERATORS

The general structure of a NN potential has the following form

$$V(\mathbf{q}', \mathbf{q}) = \sum_{i,j=1}^6 v_i(q', q, \gamma) A_{ij} \Omega_j, \quad (\text{B.1})$$

where the Ω_i operators are defined as

$$\begin{aligned} \Omega_1 &= 1 & \Omega_2 &= \mathbf{S}^2 & \Omega_3 &= \mathbf{S} \cdot \hat{\mathbf{q}}' \mathbf{S} \cdot \hat{\mathbf{q}}' \\ \Omega_4 &= \mathbf{S} \cdot \hat{\mathbf{q}}' \mathbf{S} \cdot \hat{\mathbf{q}} & \Omega_5 &= (\mathbf{S} \cdot \hat{\mathbf{q}}')^2 (\mathbf{S} \cdot \hat{\mathbf{q}})^2 & \Omega_6 &= \mathbf{S} \cdot \hat{\mathbf{q}} \mathbf{S} \cdot \hat{\mathbf{q}} \end{aligned} \quad (\text{B.2})$$

Note that the Ω_i operators are composed of helicity operators in the directions of $\hat{\mathbf{q}}$ and $\hat{\mathbf{q}}'$. These operators are related to the Wolfenstein \mathbf{W}_i operators given in Eq. (3.29) as

$$W_i = \sum_j A_{ij} \Omega_j, \quad (\text{B.3})$$

where the transformation matrix $A = \{A_{ij}\}$ is given as

$$A = \begin{pmatrix} 1 & 0 & 0 & 0 & 0 & 0 \\ 0 & \frac{ia}{\gamma} & \frac{-2i}{\gamma a} & \frac{2i}{a} & \frac{2i}{\gamma a} & \frac{-2i}{\gamma a} \\ -1 & 1 & 0 & \frac{2\gamma}{a^2} & \frac{-2}{a^2} & 0 \\ -1 & \frac{-q'qa^2}{\gamma c} & \frac{2q'(q'\gamma+q)}{\gamma c} & \frac{2q'q}{c} & \frac{-2q'q}{\gamma c} & \frac{2q(q\gamma+q')}{\gamma c} \\ -1 & \frac{q'qa^2}{\gamma b} & \frac{2q'(q'\gamma-q)}{\gamma b} & \frac{-2q'q}{b} & \frac{2q'q}{\gamma b} & \frac{2q(q\gamma-q')}{\gamma b} \\ \frac{-2(q'^2-q^2)}{e} & 0 & \frac{4q'^2}{e} & 0 & 0 & \frac{-4q^2}{e} \end{pmatrix}, \quad (\text{B.4})$$

with

$$\begin{aligned} a &= \sqrt{1 - \gamma^2} & b &= q'^2 + q^2 - 2q'q\gamma & c &= q'^2 + q^2 + 2q'q\gamma \\ e &= \sqrt{(q'^2 + q^2)^2 - 4q'^2q^2\gamma^2} & f &= \frac{1}{q'^2} + \frac{1}{q^2} & g &= \frac{1}{q'^2} - \frac{1}{q^2} \end{aligned}.$$

This was derived by means of Mathematica. Obviously the matrix elements A_{ij} are scalar functions and depend only on q , q' and γ , which is the angle between \mathbf{q}' and \mathbf{q} . We

calculate the determinant of the matrix A and get

$$\det A = \frac{-i2^9}{\gamma\sqrt{1-\gamma^2}} \left(\frac{qq'}{|\mathbf{q}' + \mathbf{q}||\mathbf{q}' - \mathbf{q}|} \right)^3, \quad (\text{B.5})$$

and find the inverse matrix A^{-1} to be

$$A^{-1} = \begin{pmatrix} 1 & 0 & 0 & 0 & 0 & 0 \\ \frac{3}{2} & 0 & \frac{1}{2} & \frac{e^2}{8a^2q'^2q^2} & \frac{e^2}{8a^2q'^2q^2} & \frac{-(q'^2-q^2)e}{8a^2q'^2q^2} \\ \frac{1}{2} & 0 & 0 & \frac{c}{8q'^2} & \frac{b}{8q'^2} & \frac{e}{8q'^2} \\ \frac{\gamma}{2} & \frac{-ia}{4} & 0 & \frac{c}{8q'q} & \frac{-b}{8q'q} & 0 \\ \frac{1+\gamma^2}{4} & \frac{-ia\gamma}{4} & \frac{-a^2}{4} & \frac{fc}{16} & \frac{fb}{16} & \frac{ge}{16} \\ \frac{1}{2} & 0 & 0 & \frac{c}{8q^2} & \frac{b}{8q^2} & \frac{-e}{8q^2} \end{pmatrix}. \quad (\text{B.6})$$

In the transformation matrix A given in Eq. (B.4) there are terms of γ^{-1} , $(1-\gamma^2)^{-\frac{1}{2}}$ and $(1-\gamma^2)^{-1}$ which seem to cause singularities for $\gamma = 0, 1$. If we insert this matrix A into Eq. (B.3) we find those terms appear as

$$\frac{1}{\gamma}(\Omega_2 - 2\Omega_3 + 2\Omega_5 - 2\Omega_6) \quad \text{in} \quad \mathbf{W}_2, \mathbf{W}_4, \mathbf{W}_5 \quad (\text{B.7})$$

$$\frac{1}{\sqrt{1-\gamma^2}} \left\{ 2\Omega_4 - \gamma\Omega_2 + \frac{1}{\gamma}(\Omega_2 - 2\Omega_3 - 2\Omega_6 + 2\Omega_5) \right\} \quad \text{in} \quad \mathbf{W}_2 \quad (\text{B.8})$$

$$\frac{1}{1-\gamma^2} (-2\Omega_5 + 2\gamma\Omega_4) \quad \text{in} \quad \mathbf{W}_3. \quad (\text{B.9})$$

We show in the following that these terms do not cause singularities.

Multiplied with a factor 2 (just for convenience), the numerator in Eq. (B.7) gives

$$\begin{aligned} 2(\Omega_2 - 2\Omega_3 + 2\Omega_5 - 2\Omega_6) &= 2\mathbf{S}^2 - 4(\mathbf{S} \cdot \hat{\mathbf{q}}')^2 + 4(\mathbf{S} \cdot \hat{\mathbf{q}}')^2 (\mathbf{S} \cdot \hat{\mathbf{q}})^2 - 4(\mathbf{S} \cdot \hat{\mathbf{q}})^2 \\ &= 3 + \boldsymbol{\sigma}_1 \cdot \boldsymbol{\sigma}_2 - 2 - 2\boldsymbol{\sigma}_1 \cdot \hat{\mathbf{q}}' \boldsymbol{\sigma}_2 \cdot \hat{\mathbf{q}}' \\ &\quad + (1 + \boldsymbol{\sigma}_1 \cdot \hat{\mathbf{q}}' \boldsymbol{\sigma}_2 \cdot \hat{\mathbf{q}}')(1 + \boldsymbol{\sigma}_1 \cdot \hat{\mathbf{q}} \boldsymbol{\sigma}_2 \cdot \hat{\mathbf{q}}) \\ &\quad - 2 - 2\boldsymbol{\sigma}_1 \cdot \hat{\mathbf{q}} \boldsymbol{\sigma}_2 \cdot \hat{\mathbf{q}} \\ &= \boldsymbol{\sigma}_1 \cdot \boldsymbol{\sigma}_2 - \boldsymbol{\sigma}_1 \cdot \hat{\mathbf{q}}' \boldsymbol{\sigma}_2 \cdot \hat{\mathbf{q}}' - \boldsymbol{\sigma}_1 \cdot \hat{\mathbf{q}} \boldsymbol{\sigma}_2 \cdot \hat{\mathbf{q}} \\ &\quad + \boldsymbol{\sigma}_1 \cdot \hat{\mathbf{q}}' \boldsymbol{\sigma}_2 \cdot \hat{\mathbf{q}}' \boldsymbol{\sigma}_1 \cdot \hat{\mathbf{q}} \boldsymbol{\sigma}_2 \cdot \hat{\mathbf{q}} \\ &= \boldsymbol{\sigma}_1 \cdot \boldsymbol{\sigma}_2 - \boldsymbol{\sigma}_1 \cdot \hat{\mathbf{q}}' \boldsymbol{\sigma}_2 \cdot \hat{\mathbf{q}}' - \boldsymbol{\sigma}_1 \cdot \hat{\mathbf{q}} \boldsymbol{\sigma}_2 \cdot \hat{\mathbf{q}} \\ &\quad + \{\gamma + i\boldsymbol{\sigma}_1 \cdot (\hat{\mathbf{q}}' \times \hat{\mathbf{q}})\} \{\gamma + i\boldsymbol{\sigma}_2 \cdot (\hat{\mathbf{q}}' \times \hat{\mathbf{q}})\} \\ &= \boldsymbol{\sigma}_1 \cdot \boldsymbol{\sigma}_2 - \boldsymbol{\sigma}_1 \cdot \hat{\mathbf{q}}' \boldsymbol{\sigma}_2 \cdot \hat{\mathbf{q}}' - \boldsymbol{\sigma}_1 \cdot \hat{\mathbf{q}} \boldsymbol{\sigma}_2 \cdot \hat{\mathbf{q}} + \gamma^2 \\ &\quad + i\gamma(\boldsymbol{\sigma}_1 + \boldsymbol{\sigma}_2) \cdot (\hat{\mathbf{q}}' \times \hat{\mathbf{q}}) - \boldsymbol{\sigma}_1 \cdot (\hat{\mathbf{q}}' \times \hat{\mathbf{q}}) \boldsymbol{\sigma}_2 \cdot (\hat{\mathbf{q}}' \times \hat{\mathbf{q}}) \\ &= \frac{\boldsymbol{\sigma}_1 \cdot (\hat{\mathbf{q}}' + \hat{\mathbf{q}}) \boldsymbol{\sigma}_2 \cdot (\hat{\mathbf{q}}' + \hat{\mathbf{q}})}{|\hat{\mathbf{q}}' + \hat{\mathbf{q}}|^2} + \frac{\boldsymbol{\sigma}_1 \cdot (\hat{\mathbf{q}}' - \hat{\mathbf{q}}) \boldsymbol{\sigma}_2 \cdot (\hat{\mathbf{q}}' - \hat{\mathbf{q}})}{|\hat{\mathbf{q}}' - \hat{\mathbf{q}}|^2} \end{aligned}$$

$$\begin{aligned}
& + \frac{\boldsymbol{\sigma}_1 \cdot (\hat{\mathbf{q}}' \times \hat{\mathbf{q}}) \boldsymbol{\sigma}_2 \cdot (\hat{\mathbf{q}}' \times \hat{\mathbf{q}})}{|\hat{\mathbf{q}}' \times \hat{\mathbf{q}}|^2} - \boldsymbol{\sigma}_1 \cdot \hat{\mathbf{q}}' \boldsymbol{\sigma}_2 \cdot \hat{\mathbf{q}}' \\
& - \boldsymbol{\sigma}_1 \cdot \hat{\mathbf{q}} \boldsymbol{\sigma}_2 \cdot \hat{\mathbf{q}} + \gamma^2 + i\gamma(\boldsymbol{\sigma}_1 + \boldsymbol{\sigma}_2) \cdot (\hat{\mathbf{q}}' \times \hat{\mathbf{q}}) \\
& - \boldsymbol{\sigma}_1 \cdot (\hat{\mathbf{q}}' \times \hat{\mathbf{q}}) \boldsymbol{\sigma}_2 \cdot (\hat{\mathbf{q}}' \times \hat{\mathbf{q}}) \\
= & \frac{\boldsymbol{\sigma}_1 \cdot \hat{\mathbf{q}}' \boldsymbol{\sigma}_2 \cdot \hat{\mathbf{q}}'}{|\hat{\mathbf{q}}' + \hat{\mathbf{q}}|^2} + \frac{\boldsymbol{\sigma}_1 \cdot \hat{\mathbf{q}} \boldsymbol{\sigma}_2 \cdot \hat{\mathbf{q}}}{|\hat{\mathbf{q}}' + \hat{\mathbf{q}}|^2} + \frac{\boldsymbol{\sigma}_1 \cdot \hat{\mathbf{q}}' \boldsymbol{\sigma}_2 \cdot \hat{\mathbf{q}}}{|\hat{\mathbf{q}}' + \hat{\mathbf{q}}|^2} \\
& + \frac{\boldsymbol{\sigma}_1 \cdot \hat{\mathbf{q}} \boldsymbol{\sigma}_2 \cdot \hat{\mathbf{q}}'}{|\hat{\mathbf{q}}' + \hat{\mathbf{q}}|^2} + \frac{\boldsymbol{\sigma}_1 \cdot \hat{\mathbf{q}}' \boldsymbol{\sigma}_2 \cdot \hat{\mathbf{q}}'}{|\hat{\mathbf{q}}' - \hat{\mathbf{q}}|^2} + \frac{\boldsymbol{\sigma}_1 \cdot \hat{\mathbf{q}} \boldsymbol{\sigma}_2 \cdot \hat{\mathbf{q}}}{|\hat{\mathbf{q}}' - \hat{\mathbf{q}}|^2} \\
& - \frac{\boldsymbol{\sigma}_1 \cdot \hat{\mathbf{q}}' \boldsymbol{\sigma}_2 \cdot \hat{\mathbf{q}}}{|\hat{\mathbf{q}}' - \hat{\mathbf{q}}|^2} - \frac{\boldsymbol{\sigma}_1 \cdot \hat{\mathbf{q}} \boldsymbol{\sigma}_2 \cdot \hat{\mathbf{q}}'}{|\hat{\mathbf{q}}' - \hat{\mathbf{q}}|^2} - \boldsymbol{\sigma}_1 \cdot \hat{\mathbf{q}}' \boldsymbol{\sigma}_2 \cdot \hat{\mathbf{q}}' \\
& - \boldsymbol{\sigma}_1 \cdot \hat{\mathbf{q}} \boldsymbol{\sigma}_2 \cdot \hat{\mathbf{q}} + \gamma^2 + i\gamma(\boldsymbol{\sigma}_1 + \boldsymbol{\sigma}_2) \cdot (\hat{\mathbf{q}}' \times \hat{\mathbf{q}}) \\
& - \boldsymbol{\sigma}_1 \cdot (\hat{\mathbf{q}}' \times \hat{\mathbf{q}}) \boldsymbol{\sigma}_2 \cdot (\hat{\mathbf{q}}' \times \hat{\mathbf{q}}) \left(1 - \frac{1}{|\hat{\mathbf{q}}' \times \hat{\mathbf{q}}|^2} \right),
\end{aligned}$$

where we have used the identity relation

$$\begin{aligned}
\boldsymbol{\sigma}_1 \cdot \boldsymbol{\sigma}_2 = & \frac{\boldsymbol{\sigma}_1 \cdot (\hat{\mathbf{q}}' + \hat{\mathbf{q}}) \boldsymbol{\sigma}_2 \cdot (\hat{\mathbf{q}}' + \hat{\mathbf{q}})}{|\hat{\mathbf{q}}' + \hat{\mathbf{q}}|^2} + \frac{\boldsymbol{\sigma}_1 \cdot (\hat{\mathbf{q}}' - \hat{\mathbf{q}}) \boldsymbol{\sigma}_2 \cdot (\hat{\mathbf{q}}' - \hat{\mathbf{q}})}{|\hat{\mathbf{q}}' - \hat{\mathbf{q}}|^2} \\
& + \frac{\boldsymbol{\sigma}_1 \cdot (\hat{\mathbf{q}} \times \hat{\mathbf{q}}') \boldsymbol{\sigma}_2 \cdot (\hat{\mathbf{q}} \times \hat{\mathbf{q}}')}{|\hat{\mathbf{q}} \times \hat{\mathbf{q}}'|^2}.
\end{aligned} \tag{B.10}$$

For $\gamma = 0$

$$\begin{aligned}
|\hat{\mathbf{q}}' \times \hat{\mathbf{q}}| & = 1 \\
|\hat{\mathbf{q}}' + \hat{\mathbf{q}}| & = |\hat{\mathbf{q}}' - \hat{\mathbf{q}}| = \sqrt{2},
\end{aligned}$$

therefore the numerator in Eq. (B.7) vanishes.

For $\gamma = 1$

$$\begin{aligned}
\Omega_3 = \Omega_4 = \Omega_6 & = (\mathbf{S} \cdot \hat{\mathbf{q}})^2 = \frac{1}{4} \\
\Omega_5 & = (\mathbf{S} \cdot \hat{\mathbf{q}})^4 = \frac{1}{4}.
\end{aligned}$$

Therefore, the numerators in Eqs. (B.8) and (B.9) vanish.

In the inverse A^{-1} of the transformation matrix given in Eq. (B.6) there occur the $(1 - \gamma^2)^{-1}$ terms. Inverting the relation given in Eq. (B.3) this term appears only in Ω_2 as

$$\frac{\{(q'^2 + q^2)^2 - 4q'^2 q^2 \gamma^2\} (\mathbf{W}_4 + \mathbf{W}_5) - (q'^2 - q^2) \sqrt{(q'^2 + q^2)^2 - 4q'^2 q^2 \gamma^2} \mathbf{W}_6}{1 - \gamma^2}. \tag{B.11}$$

For $\gamma = 1$ the numerator of this term vanishes as can be shown here

$$\{(q'^2 + q^2)^2 - 4q'^2 q^2\} (\mathbf{W}_4 + \mathbf{W}_5) - (q'^2 - q^2) \sqrt{(q'^2 + q^2)^2 - 4q'^2 q^2} \mathbf{W}_6$$

$$\begin{aligned}
&= (q' + q)^2(q' - q)^2(\mathbf{W}_4 + \mathbf{W}_5) - (q'^2 - q^2)(q' + q)(q' - q)\mathbf{W}_6 \\
&= 2(q' + q)^2(q' - q)^2\boldsymbol{\sigma}_1 \cdot \hat{\mathbf{q}}\boldsymbol{\sigma}_2 \cdot \hat{\mathbf{q}} - 2(q'^2 - q^2)(q' + q)(q' - q)\boldsymbol{\sigma}_1 \cdot \hat{\mathbf{q}}\boldsymbol{\sigma}_2 \cdot \hat{\mathbf{q}} \\
&= 2(q' + q)(q' - q)[(q' + q)(q' - q) - (q'^2 - q^2)]\boldsymbol{\sigma}_1 \cdot \hat{\mathbf{q}}\boldsymbol{\sigma}_2 \cdot \hat{\mathbf{q}} \\
&= 2(q' + q)(q' - q)(q'^2 - q^2 - q'^2 + q^2)\boldsymbol{\sigma}_1 \cdot \hat{\mathbf{q}}\boldsymbol{\sigma}_2 \cdot \hat{\mathbf{q}} \\
&= 0.
\end{aligned}$$

Appendix C

THE BONN ONE-BOSON-EXCHANGE POTENTIAL

The pseudoscalar, scalar and vector part of the Bonn one-boson-exchange potential (OBEP) takes the following form:

$$V_{ps}(\mathbf{q}', \mathbf{q}) = \frac{g_{ps}^2}{(2\pi)^3 4m^2} \sqrt{\frac{m}{E'}} \sqrt{\frac{m}{E}} \frac{F_{ps}^2[(\mathbf{q}' - \mathbf{q})^2]}{(\mathbf{q}' - \mathbf{q})^2 + m_{ps}^2} \frac{\hat{O}_{ps}}{W'W} \quad (\text{C.1})$$

$$V_s(\mathbf{q}', \mathbf{q}) = \frac{g_s^2}{(2\pi)^3 4m^2} \sqrt{\frac{m}{E'}} \sqrt{\frac{m}{E}} \frac{F_s^2[(\mathbf{q}' - \mathbf{q})^2]}{(\mathbf{q}' - \mathbf{q})^2 + m_s^2} \frac{\hat{O}_s}{W'W} \quad (\text{C.2})$$

$$V_v(\mathbf{q}', \mathbf{q}) = \frac{1}{(2\pi)^3 4m^2} \sqrt{\frac{m}{E'}} \sqrt{\frac{m}{E}} \frac{F_v^2[(\mathbf{q}' - \mathbf{q})^2]}{(\mathbf{q}' - \mathbf{q})^2 + m_v^2} \frac{(g_v^2 \hat{O}_{vv} + 2g_v f_v \hat{O}_{vt} + f_v^2 \hat{O}_{tt})}{W'W}, \quad (\text{C.3})$$

where m denotes the nucleon mass, m_α ($\alpha = ps, s, v$) the meson's mass, $E = \sqrt{m^2 + \mathbf{q}^2}$ and $W = m + E$. The form factor $F_\alpha^2[(\mathbf{q}' - \mathbf{q})^2]$ is given as

$$F_\alpha^2[(\mathbf{q}' - \mathbf{q})^2] = \left(\frac{\Lambda_\alpha^2 - m_\alpha^2}{\Lambda_\alpha^2 + (\mathbf{q}' - \mathbf{q})^2} \right)^{2n}, \quad (\text{C.4})$$

with Λ_α being the cutoff. In the propagator one has

$$(\mathbf{q}' - \mathbf{q})^2 = q'^2 + q^2 - 2q'q\gamma \quad (\text{C.5})$$

$$\gamma = \hat{\mathbf{q}}' \cdot \hat{\mathbf{q}} = \cos \theta' \cos \theta + \sin \theta' \sin \theta \cos(\phi' - \phi). \quad (\text{C.6})$$

The \hat{O}_β operators ($\beta = ps, s, vv, vt, tt$) take a form of a combination of $\boldsymbol{\sigma}_1 \cdot \hat{\mathbf{q}}$, $\boldsymbol{\sigma}_2 \cdot \hat{\mathbf{q}}$, $\boldsymbol{\sigma}_1 \cdot \hat{\mathbf{q}}'$ and $\boldsymbol{\sigma}_2 \cdot \hat{\mathbf{q}}'$. These \hat{O}_β operators have to be expressed in terms of the Ω_i operators given in Eq. (3.30), accomplished in the following. First, the \hat{O}_β operators are written in terms of the \mathbf{W}_i operators given in Eq. (3.29). An easy way to do this is that one rewrites

the \mathbf{W}_i operators as combinations of $\boldsymbol{\sigma}_1 \cdot \hat{\mathbf{q}}$, $\boldsymbol{\sigma}_2 \cdot \hat{\mathbf{q}}$, $\boldsymbol{\sigma}_1 \cdot \hat{\mathbf{q}}'$ and $\boldsymbol{\sigma}_2 \cdot \hat{\mathbf{q}}'$, then inverts the expressions and applies them to the \hat{O}_β operators. This gives

$$\begin{aligned} \hat{O}_{ps} = & -\frac{1}{4} \left[(W' - W)^2 (q'^2 + q^2 + 2q'q\gamma) \mathbf{W}_4 + (W' + W)^2 (q'^2 + q^2 - 2q'q\gamma) \mathbf{W}_5 \right. \\ & \left. - (W'^2 - W^2) \sqrt{(q'^2 + q^2)^2 - 4q'^2q^2\gamma^2} \mathbf{W}_6 \right] \end{aligned} \quad (\text{C.7})$$

$$\begin{aligned} \hat{O}_s = & -(W'W - q'q\gamma)^2 \mathbf{W}_1 - i(W'W - q'q\gamma)q'q\sqrt{1 - \gamma^2} \mathbf{W}_2 \\ & + q'^2q^2(1 - \gamma^2) \mathbf{W}_3 \end{aligned} \quad (\text{C.8})$$

$$\begin{aligned} \hat{O}_{vv} = & (W'^2W^2 + q'^2q^2\gamma^2 + 4W'Wq'q\gamma + W'^2q^2 + W^2q'^2) \mathbf{W}_1 \\ & - i(3W'W + q'q\gamma)q'q\sqrt{1 - \gamma^2} \mathbf{W}_2 \\ & - \left[q'^2q^2(1 - \gamma^2) + W'^2q^2 + W^2q'^2 - 2W'Wq'q\gamma \right] \mathbf{W}_3 \\ & + \left[W'^2 + W^2 - 2W'W - \frac{(q'^2 + q^2 - 2q'q\gamma)}{q'^2q^2(1 - \gamma^2)} (W'^2q^2 + W^2q'^2 - 2W'Wq'q\gamma) \right] \\ & \times \frac{1}{4} (q'^2 + q^2 + 2q'q\gamma) \mathbf{W}_4 \\ & + \left[W'^2 + W^2 + 2W'W - \frac{(q'^2 + q^2 + 2q'q\gamma)}{q'^2q^2(1 - \gamma^2)} (W'^2q^2 + W^2q'^2 - 2W'Wq'q\gamma) \right] \\ & \times \frac{1}{4} (q'^2 + q^2 - 2q'q\gamma) \mathbf{W}_5 \\ & - \left[W'^2 - W^2 - \frac{(q'^2 - q^2)}{q'^2q^2(1 - \gamma^2)} (W'^2q^2 + W^2q'^2 - 2W'Wq'q\gamma) \right] \\ & \times \frac{1}{4} \sqrt{(q'^2 + q^2)^2 - 4q'^2q^2\gamma^2} \mathbf{W}_6 \end{aligned} \quad (\text{C.9})$$

$$\begin{aligned} \hat{O}_{vt} = & \left[\frac{(2m - E' - E)}{m} W'^2W^2 + \frac{(W' + W)}{m} q'^2q^2\gamma^2 + 2q'qW'W\gamma \right. \\ & \left. + \frac{(2m - E' + E)}{2m} W'^2q^2 + \frac{(2m + E' - E)}{2m} W^2q'^2 \right] \mathbf{W}_1 \\ & - i \left[\frac{(W' + W)}{m} q'q\gamma + 2W'W \right] q'q\sqrt{1 - \gamma^2} \mathbf{W}_2 \\ & - \left\{ \frac{(W' + W)}{m} q'^2q^2(1 - \gamma^2) \right. \\ & \left. + \left[\frac{(2m - E' + E)}{2m} W'^2q^2 + \frac{(2m + E' - E)}{2m} W^2q'^2 - 2W'Wq'q\gamma \right] \right\} \mathbf{W}_3 \\ & + \frac{1}{4} (q'^2 + q^2 + 2q'q\gamma) \left\{ \frac{(2m - E' + E)}{2m} W'^2 + \frac{(2m + E' - E)}{2m} W^2 - 2W'W \right. \\ & \left. - \left[\frac{(2m - E' + E)}{2m} \frac{W'^2}{q'^2} + \frac{(2m + E' - E)}{2m} \frac{W^2}{q^2} - 2W'W \frac{\gamma}{q'q} \right] \right. \\ & \left. \times \frac{(q'^2 + q^2 - 2q'q\gamma)}{(1 - \gamma^2)} \right\} \mathbf{W}_4 \end{aligned}$$

$$\begin{aligned}
& + \frac{1}{4} (q'^2 + q^2 - 2q'q\gamma) \left\{ \frac{(2m - E' + E)}{2m} W'^2 + \frac{(2m + E' - E)}{2m} W^2 + 2W'W \right. \\
& - \left. \left[\frac{(2m - E' + E)}{2m} \frac{W'^2}{q'^2} + \frac{(2m + E' - E)}{2m} \frac{W^2}{q^2} - 2W'W \frac{\gamma}{q'q} \right] \right. \\
& \times \left. \frac{(q'^2 + q^2 + 2q'q\gamma)}{(1 - \gamma^2)} \right\} \mathbf{W}_5 \\
& - \frac{1}{4} \sqrt{(q'^2 + q^2)^2 - 4q'^2 q^2 \gamma^2} \left\{ \frac{(2m - E' + E)}{2m} W'^2 - \frac{(2m + E' - E)}{2m} W^2 \right. \\
& - \left. \left[\frac{(2m - E' + E)}{2m} \frac{W'^2}{q'^2} + \frac{(2m + E' - E)}{2m} \frac{W^2}{q^2} - 2W'W \frac{\gamma}{q'q} \right] \right. \\
& \times \left. \frac{(q'^2 - q^2)}{(1 - \gamma^2)} \right\} \mathbf{W}_6 \tag{C.10}
\end{aligned}$$

$$\begin{aligned}
\hat{O}_{tt} = & \left\{ [5m^2 - 4m(E' + E) + 3E'E + q'q\gamma] W'^2 W^2 \right. \\
& + [5m^2 + 4m(E' + E) + 3E'E + q'q\gamma] q'^2 q^2 \gamma^2 \\
& + (2m^2 - 4E'E - E'^2 - E^2 - 2q'q\gamma) W'W q'q\gamma \\
& + \left. \frac{1}{2} [(2m - E' + E)^2 q^2 W'^2 + (2m + E' - E)^2 q'^2 W^2] \right\} \frac{1}{2m^2} \mathbf{W}_1 \\
& - i \left\{ (3m^2 - E'E - E'^2 - E^2 - q'q\gamma) W'W \right. \\
& + [5m^2 + 4m(E' + E) + 3E'E + q'q\gamma] q'q\gamma \left. \frac{q'q}{2m^2} \sqrt{1 - \gamma^2} \right\} \mathbf{W}_2 \\
& - \left\{ [10m^2 + 8m(E' + E) + 6E'E + 2q'q\gamma] q'^2 q^2 (1 - \gamma^2) \right. \\
& + [(2m - E' + E)^2 W'^2 q^2 + (2m + E' - E)^2 W^2 q'^2 \\
& - 2 [4m^2 - (E' - E)^2] W'W q'q\gamma \left. \right\} \frac{\mathbf{W}_3}{4m^2} \\
& + \left\{ (2m - E' + E)^2 W'^2 + (2m + E' - E)^2 W^2 - 2 [4m^2 - (E' - E)^2] W'W \right. \\
& - \left. \left[(2m - E' + E)^2 \frac{W'^2}{q'^2} + (2m + E' - E)^2 \frac{W^2}{q^2} - 2 [4m^2 - (E' - E)^2] W'W \frac{\gamma}{q'q} \right] \right. \\
& \times \left. \frac{(q'^2 + q^2 - 2q'q\gamma)}{(1 - \gamma^2)} \right\} \frac{(q'^2 + q^2 + 2q'q\gamma)}{16m^2} \mathbf{W}_4 \\
& + \left\{ (2m - E' + E)^2 W'^2 + (2m + E' - E)^2 W^2 + 2 [4m^2 - (E' - E)^2] W'W \right. \\
& - \left. \left[(2m - E' + E)^2 \frac{W'^2}{q'^2} + (2m + E' - E)^2 \frac{W^2}{q^2} - 2 [4m^2 - (E' - E)^2] W'W \frac{\gamma}{q'q} \right] \right. \\
& \times \left. \frac{(q'^2 + q^2 + 2q'q\gamma)}{(1 - \gamma^2)} \right\} \frac{(q'^2 + q^2 - 2q'q\gamma)}{16m^2} \mathbf{W}_5 \\
& - \left\{ (2m - E' + E)^2 W'^2 - (2m + E' - E)^2 W^2 \right.
\end{aligned}$$

$$\begin{aligned}
& - \left[(2m - E' + E)^2 \frac{W'^2}{q'^2} + (2m + E' - E)^2 \frac{W^2}{q^2} - 2 \left[4m^2 - (E' - E)^2 \right] W'W \frac{\gamma}{q'q} \right] \\
& \times \frac{(q'^2 - q^2)}{(1 - \gamma^2)} \left\} \frac{\sqrt{(q'^2 + q^2)^2 - 4q'^2 q^2 \gamma^2}}{16m^2} \mathbf{W}_6. \tag{C.11}
\end{aligned}$$

Next using the transformation given in Eq. (3.31) and discussed in detail in Appendix B the expression for the \hat{O}_β operators in terms of the Ω_i operators are obtained as

$$\begin{aligned}
\hat{O}_{ps} &= W^2 q'^2 (\Omega_1 - 2\Omega_3) + W'^2 q^2 (\Omega_1 - 2\Omega_6) + 2W'W q'q \Omega_4 \\
& - W'W q'q \gamma (2\Omega_1 - \Omega_2) - W'W q'q \frac{1}{\gamma} (\Omega_2 - 2\Omega_3 - 2\Omega_6 + 2\Omega_5) \tag{C.12}
\end{aligned}$$

$$\begin{aligned}
\hat{O}_s &= -W'^2 W^2 \Omega_1 - q'^2 q^2 (\Omega_1 - 2\Omega_3 - 2\Omega_6 + 4\Omega_5) + 2W'W q'q \Omega_4 \\
& + W'W q'q \gamma (2\Omega_1 - \Omega_2) + W'W q'q \frac{1}{\gamma} (\Omega_2 - 2\Omega_3 - 2\Omega_6 + 2\Omega_5) \tag{C.13}
\end{aligned}$$

$$\begin{aligned}
\hat{O}_{vv} &= W'^2 W^2 \Omega_1 + q'^2 q^2 (\Omega_1 - 2\Omega_3 - 2\Omega_6 + 4\Omega_5) \\
& + W'^2 q^2 (3\Omega_1 - 2\Omega_2 + 2\Omega_6) + W^2 q'^2 (3\Omega_1 - 2\Omega_2 + 2\Omega_3) \\
& + 4W'W q'q \Omega_4 + 4W'W q'q \frac{1}{\gamma} (\Omega_2 - 2\Omega_3 - 2\Omega_6 + 2\Omega_5) \tag{C.14}
\end{aligned}$$

$$\begin{aligned}
\hat{O}_{vt} &= \frac{W' + W}{m} q'^2 q^2 (\Omega_1 - 2\Omega_3 - 2\Omega_6 + 4\Omega_5) - W'^2 W^2 \Omega_1 \frac{E' + E - 2m}{m} + 2W'W q'q \Omega_4 \\
& + W'^2 q^2 (3\Omega_1 - 2\Omega_2 + 2\Omega_6) \frac{(2m - E' + E)}{2m} \\
& + W^2 q'^2 (3\Omega_1 - 2\Omega_2 + 2\Omega_3) \frac{(2m + E' - E)}{2m} \\
& + W'W q'q \gamma (\Omega_2 - 2\Omega_1) + 3W'W q'q \frac{1}{\gamma} (\Omega_2 - 2\Omega_3 - 2\Omega_6 + 2\Omega_5) \tag{C.15}
\end{aligned}$$

$$\begin{aligned}
\hat{O}_{tt} &= W'^2 W^2 \Omega_1 \frac{1}{2m^2} \left[5m^2 - 4m(E' + E) + 3E'E \right] \\
& + q'^2 q^2 \frac{1}{2m^2} \left[5m^2 + 4m(E' + E) + 3E'E \right] (\Omega_1 - 2\Omega_3 - 2\Omega_6 + 4\Omega_5) \\
& - W'W q'^2 q^2 \frac{1}{2m^2} (\Omega_2 - 2\Omega_3 - 2\Omega_6 + 2\Omega_5) \\
& + W'^2 q^2 \frac{1}{4m^2} (2m - E' + E)^2 (3\Omega_1 - 2\Omega_2 + 2\Omega_6) \\
& + W^2 q'^2 \frac{1}{4m^2} (2m + E' - E)^2 (3\Omega_1 - 2\Omega_2 + 2\Omega_3) \\
& + W'W q'q \frac{1}{2m^2} \left[2m^2 - (E' - E)^2 - 6E'E \right] \Omega_4 \\
& + q'q \gamma \frac{1}{2m^2} \left\{ W'^2 W^2 \Omega_1 + q'^2 q^2 (\Omega_1 - 2\Omega_3 - 2\Omega_6 + 4\Omega_5) \right. \\
& \left. + W'W \left[3m^2 - \frac{1}{2}(E' - E)^2 + 3E'E \right] (\Omega_2 - 2\Omega_1) - 2W'W q'q \Omega_4 \right\} \\
& + W'W q'q \frac{1}{2m^2 \gamma} \left[5m^2 - \frac{3}{2}(E' - E)^2 - 3E'E \right] (\Omega_2 - 2\Omega_3 - 2\Omega_6 + 2\Omega_5)
\end{aligned}$$

$$+W'Wq'^2q^2\gamma^2\frac{1}{2m^2}(\Omega_2 - 2\Omega_1). \quad (\text{C.16})$$

This task can also be done with help of symbolic manipulation packages, such as *mathematica*.

One sees that the azimuthal behavior of the matrix elements $V_{\Lambda'\Lambda}^{\pi St}(\mathbf{q}', \mathbf{q})$ of the potentials in Eqs. (C.1)-(C.3) in the momentum-helicity basis is just the one described in Eq. (3.52). As shown in Chapter 3 this behavior leads to simplification in solving the LSE.

Appendix D

THE ARGONNE AV18 POTENTIAL

The OPE part $V^\pi(\mathbf{q}', \mathbf{q})$ and intermediate- and short-range part $V^R(\mathbf{q}', \mathbf{q})$ of the Argonne AV18 potential are given as

$$V^\pi(\mathbf{q}', \mathbf{q}) = V_{ss}^\pi(\mathbf{q}', \mathbf{q}) + V_t^\pi(\mathbf{q}', \mathbf{q}) \quad (\text{D.1})$$

$$V^R(\mathbf{q}', \mathbf{q}) = V_{St}^c(\mathbf{q}', \mathbf{q}) + V_{St}^t(\mathbf{q}', \mathbf{q}) + V_{St}^{ls}(\mathbf{q}', \mathbf{q}) + V_{St}^{l2}(\mathbf{q}', \mathbf{q}) + V_{St}^{ls2}(\mathbf{q}', \mathbf{q}), \quad (\text{D.2})$$

where

$$V_{ss}^\pi(\mathbf{q}', \mathbf{q}) = \frac{1}{2\pi^2} \hat{O}_{ss} \int_0^\infty dr r^2 j_0(\rho r) V_{ss}^\pi(r) \quad (\text{D.3})$$

$$V_t^\pi(\mathbf{q}', \mathbf{q}) = \frac{1}{2\pi^2} \hat{O}_t \int_0^\infty dr r^2 j_2(\rho r) V_t^\pi(r) \quad (\text{D.4})$$

$$V_{St}^c(\mathbf{q}', \mathbf{q}) = \frac{1}{2\pi^2} \hat{O}_{ss} \int_0^\infty dr r^2 j_0(\rho r) V_{St}^c(r) \quad (\text{D.5})$$

$$V_{St}^t(\mathbf{q}', \mathbf{q}) = \frac{1}{2\pi^2} \hat{O}_t \int_0^\infty dr r^2 j_2(\rho r) V_{St}^t(r) \quad (\text{D.6})$$

$$V_{St}^{ls}(\mathbf{q}', \mathbf{q}) = \frac{1}{2\pi^2} \hat{O}_{ls} \int_0^\infty dr r^3 j_1(\rho r) V_{St}^{ls}(r) \quad (\text{D.7})$$

$$V_{St}^{l2}(\mathbf{q}', \mathbf{q}) = \frac{1}{2\pi^2} \hat{O}_{l2}^{(1)} \int_0^\infty dr r^3 j_1(\rho r) V_{St}^{l2}(r) - \frac{1}{2\pi^2} \hat{O}_{l2}^{(2)} \int_0^\infty dr r^4 j_2(\rho r) V_{St}^{l2}(r) \quad (\text{D.8})$$

$$V_{St}^{ls2}(\mathbf{q}', \mathbf{q}) = \frac{1}{2\pi^2} \hat{O}_{ls2}^{(1)} \int_0^\infty dr r^3 j_1(\rho r) V_{St}^{ls2}(r) - \frac{1}{2\pi^2} \hat{O}_{ls2}^{(2)} \int_0^\infty dr r^4 j_2(\rho r) V_{St}^{ls2}(r), \quad (\text{D.9})$$

where $\rho \equiv |\mathbf{q}' - \mathbf{q}|$. As shown in Eqs. (4.11)-(4.17) the \hat{O}_β operators ($\beta = ss, t, ls, l2, ls2$) are combinations of projected-spin operators along some axes, for example $\sigma \cdot \hat{\mathbf{q}}$. These \hat{O}_β operators have to be expressed in the Ω_i operators. In similar way to that for the Bonn OBEP, first we rewrite the \hat{O}_β operators in terms of the \mathbf{W}_i operators. We obtain

$$\hat{O}_{ss} = \mathbf{W}_1 \quad (\text{D.10})$$

$$\begin{aligned} \hat{O}_t &= \mathbf{W}_3 - \frac{1}{4} \frac{(\mathbf{q}' - \mathbf{q})^2 (\mathbf{q}' + \mathbf{q})^2}{q'^2 q^2 (\gamma^2 - 1)} \mathbf{W}_4 - \frac{1}{4} \frac{(q'^4 + 8q'^2 q^2 \gamma^2 - 10q'^2 q^2 + q^4)}{q'^2 q^2 (\gamma^2 - 1)} \mathbf{W}_5 \\ &\quad + \frac{1}{4} \frac{\sqrt{(q'^2 + q^2)^2 - 4q'^2 q^2 \gamma^2} (q'^2 - q^2)}{q'^2 q^2 (\gamma^2 - 1)} \mathbf{W}_6 \end{aligned} \quad (\text{D.11})$$

$$\hat{O}_{ls} = \frac{i}{2\rho} q' q \sqrt{1 - \gamma^2} \mathbf{W}_2 \quad (\text{D.12})$$

$$\hat{O}_{l2}^{(1)} = \frac{2q' q \gamma}{\rho} \mathbf{W}_1 \quad (\text{D.13})$$

$$\hat{O}_{l2}^{(2)} = \frac{q'^2 q^2 (1 - \gamma^2)}{\rho^2} \mathbf{W}_1 \quad (\text{D.14})$$

$$\begin{aligned} \hat{O}_{ls2}^{(1)} &= \frac{1}{\rho} \left[q' q \gamma \mathbf{W}_1 - \frac{i}{4} q' q \sqrt{1 - \gamma^2} \mathbf{W}_2 + \frac{1}{2} q' q \gamma \mathbf{W}_3 - \frac{1}{8} \frac{(\mathbf{q}' + \mathbf{q})^2 (q' - \gamma q) (q' \gamma - q)}{q' q (\gamma^2 - 1)} \mathbf{W}_4 \right. \\ &\quad \left. - \frac{1}{8} \frac{(\mathbf{q}' - \mathbf{q})^2 (q' + q \gamma) (q + q' \gamma)}{q' q (\gamma^2 - 1)} \mathbf{W}_5 \right. \\ &\quad \left. + \frac{1}{8} \frac{\gamma (q'^2 - q^2) \sqrt{(q'^2 + q^2)^2 - 4q'^2 q^2 \gamma^2}}{q' q (\gamma^2 - 1)} \mathbf{W}_6 \right] \end{aligned} \quad (\text{D.15})$$

$$\hat{O}_{ls2}^{(2)} = \frac{q'^2 q^2}{2\rho^2} (1 - \gamma^2) (\mathbf{W}_1 + \mathbf{W}_3), \quad (\text{D.16})$$

with

$$(\mathbf{q}' - \mathbf{q})^2 = q'^2 + q^2 - 2q' q \gamma \quad (\text{D.17})$$

$$\gamma = \hat{\mathbf{q}}' \hat{\mathbf{q}} = \cos \theta' \cos \theta + \sin \theta' \sin \theta \cos(\phi' - \phi). \quad (\text{D.18})$$

Next by means of the transformation given in Eq. (3.31) and discussed in detail in Appendix B we get the expressions for the \hat{O}_β operators in terms of the Ω_i operators as

$$\hat{O}_{ss} = \Omega_1 \quad (\text{D.19})$$

$$\begin{aligned} \hat{O}_t &= \frac{1}{\rho^2} \left[6q' q \Omega_4 + 2q'^2 (\Omega_2 - 3\Omega_3) + 2q^2 (\Omega_2 - 3\Omega_6) \right. \\ &\quad \left. - q' q \gamma \Omega_2 - 3q' q \frac{1}{\gamma} (\Omega_2 - 2\Omega_3 - 2\Omega_6 + 2\Omega_5) \right] \end{aligned} \quad (\text{D.20})$$

$$\hat{O}_{ls} = \frac{q' q}{2\rho} \left[\gamma \Omega_2 - 2\Omega_4 - \frac{1}{\gamma} (\Omega_2 - 2\Omega_3 - 2\Omega_6 + 2\Omega_5) \right] \quad (\text{D.21})$$

$$\hat{O}_{l2}^{(1)} = \frac{2q' q \gamma}{\rho} \Omega_1 \quad (\text{D.22})$$

$$\hat{O}_{l2}^{(2)} = \frac{1}{\rho^2} [q'^2 q^2 (1 - \gamma^2)] \Omega_1 \quad (\text{D.23})$$

$$\hat{O}_{ls2}^{(1)} = \frac{q' q}{2\rho} \left[\gamma \Omega_2 + \frac{1}{\gamma} (\Omega_2 + 2\Omega_5 - 2\Omega_3 - 2\Omega_6) \right] \quad (\text{D.24})$$

$$\hat{O}_{ls2}^{(2)} = \frac{q'^2 q^2}{2\rho^2} [(1 - \gamma^2) \Omega_2 + 2\gamma \Omega_4 - 2\Omega_5]. \quad (\text{D.25})$$

Concerning azimuthal behavior one can check that the matrix elements $V_{\Lambda'\Lambda}^{\pi St}(\mathbf{q}', \mathbf{q})$ of the potential given in Eqs. (D.3)-(D.9) in the momentum-helicity basis have azimuthal behavior as described by Eq. (3.52).

Appendix E

NUMERICAL REALIZATION FOR NN SCATTERING

In this appendix we describe the evaluation of integrals, the way we treat the principal value singularity and solve the LSE's given in Eq. (3.73). We make also a note on the numerical method in performing the Fourier-Bessel transformations given in Eqs. (4.11)-(4.17).

E.1 Integration

In solving the LSE's in Eq. (3.73) altogether we have integrals in three variables q'' , θ'' and ϕ'' . However, the integral in the variable ϕ'' , which is given in Eq. (3.70), can be evaluated independently. Therefore, the LSE's to be solved are two-dimensional (2D) integral equations in the variables q'' and θ'' . We evaluate these integrals by means of a numerical integration (known also as quadrature) method. In our case Gauss-Legendre quadrature [66] is most suitable. For clarity of description all integrals in this subsection will be written as

$$I = \int_a^b dx f(x).$$

The integration points and weights of the Gauss-Legendre quadrature are defined for an integration within an interval $[-1, 1]$. Therefore, these points and weights must be mapped onto the interval $[a, b]$ of the evaluated integral, as described in the following equation

$$\begin{aligned} I &= \int_a^b dx f(x) = \int_{-1}^1 dy f(y) \\ &= \sum_i w_i f(x_i) = \sum_i v_i f(y_i), \end{aligned} \tag{E.1}$$

where the y_i 's and v_i 's are points and weights of the Gauss-Legendre quadrature, and the x_i 's and w_i 's must be the corresponding points and weights for the evaluated integral, respectively. For the θ'' - and ϕ'' -integrations we use a linear mapping given as

$$x_i = \frac{b-a}{2}y_i + \frac{b+a}{2} \quad w_i = \frac{1}{2}(b-a)v_i. \quad (\text{E.2})$$

For the q'' -integration, which is within the interval $[0, \infty]$, we use two different mapping schemes for the Bonn-B and the AV18 potentials presented in the next paragraphs. The Gauss-Legendre quadrature points are more dense at both ends than in the middle of the interval. This is of special advantage for the θ'' -integrations, since the T-matrix behaves more peaked around forward and backward directions.

For the q'' -integration in case of the Bonn-B potential the y_i 's and v_i 's are mapped onto the interval $[0, \infty]$ in steps described as follows:

$$\begin{aligned} I &= \int_0^\infty dx f(x) = \int_0^1 dz f(z) = \int_{-1}^1 dy f(y) \\ &= \sum_i w_i f(x_i) = \sum_i u_i f(z_i) = \sum_i v_i f(y_i), \end{aligned} \quad (\text{E.3})$$

where the z_i 's and u_i 's are points and weights of the integral with the interval $[0, 1]$. In the rightmost equalities a linear mapping is applied. Next the z_i 's and u_i 's are mapped onto the interval $[0, \infty]$ by employing the following mapping

$$x_i = k \tan\left(\frac{\pi}{2}z_i\right) \quad w_i = k \frac{\pi}{2} \frac{u_i}{\cos^2\left(\frac{\pi}{2}z_i\right)}. \quad (\text{E.4})$$

With this mapping the integration points are distributed such that the density decreases as the momentum increases, since the T-matrix is getting smoother and falls off at higher momenta. This behavior of the integration point density is controlled by the constant k . Smaller k increases the density of points at lower momenta. The typical value of k is 1000 MeV/c or 5.068 fm^{-1} , depending on the units used.

For the AV18 potential the q'' -integration is terminated at a certain point q_3 . This termination is unavoidable since the potential is obtained by performing a numerical Fourier-Bessel transformation of the AV18 potential in configuration space, which is difficult to realize for very high momenta. We found out that the integral interval can be safely cut off at $q_3 = 150 \text{ fm}^{-1}$. The interval $[0, q_3]$ is splitted into two intervals $[0, q_2]$ and $[q_2, q_3]$ representing lower and higher momentum regions, respectively. In the higher momenta interval $[q_2, q_3]$ we use a linear mapping as given in Eq. (E.2), with a, b being replaced by q_2, q_3 . In the lower momenta interval $[0, q_2]$ a hyperbolic mapping given in the following is employed:

$$x_i = \frac{1 + y_i}{\frac{1}{q_1} - \left(\frac{1}{q_1} - \frac{2}{q_2}\right) y_i} \quad w_i = \frac{\left(\frac{2}{q_1} - \frac{2}{q_2}\right) v_i}{\left\{\frac{1}{q_1} - \left(\frac{1}{q_1} - \frac{2}{q_2}\right) y_i\right\}^2}. \quad (\text{E.5})$$

Here q_1 is the momentum, where the interval $[0, q_2]$ is splitted into two intervals $[0, q_1]$ and $[q_1, q_2]$ of equal number of points. The typical values for q_1 and q_2 are 3 fm^{-1} and 10 fm^{-1} , respectively.

For performing the above mentioned numerical Fourier-Bessel transformation to obtain the AV18 potential in momentum space we employ Filon's quadrature method [67]. This method is proven to be accurate for integrations of strong oscillatory functions such as the ones in Eqs. (4.11)- (4.17) for large values of ρ . And compared to another powerful method, for example the Simpson's rule, it needs less integration points. For small ρ and $\rho = 0$ we use the Gauss-Legendre quadrature with linear mapping.

Now we would like to give the number of integration points for all the q'' -, θ'' - and ϕ'' -integrations we have. To obtain these numbers we check for some lower partial waves up to $j = 4$ the convergence of phase shifts. The numbers of integration points mentioned in the following are sufficient to achieve a convergence within four digits after the decimal point. This means the large phase shifts converge within 6 significant figures and the small ones 4 significant figures.

The original ϕ'' -integration within an interval $[0, 2\pi]$ is rewritten within an interval $[0, \frac{\pi}{2}]$ as shown in the following notation:

$$\begin{aligned}
 I &= \int_0^{2\pi} d\phi'' f(\cos(\phi' - \phi'')) e^{im(\phi' - \phi'')} \\
 &= \int_0^{2\pi} d\phi'' f(\cos \phi'') e^{im\phi''} \\
 &= \int_0^{\pi} d\phi'' \left\{ f(\cos \phi'') e^{im\phi''} + f(-\cos \phi'') e^{im(\phi'' + \pi)} \right\} \\
 &= \int_0^{\frac{\pi}{2}} d\phi'' \left\{ f(\cos \phi'') \left(e^{im\phi''} + e^{im(2\pi - \phi'')} \right) \right. \\
 &\quad \left. + f(-\cos \phi'') \left(e^{im(\phi'' + \pi)} + e^{im(\pi - \phi'')} \right) \right\}. \tag{E.6}
 \end{aligned}$$

The second equality is justified by the periodicity of the integrand within 2π . In this way the number of integration points can be reduced. For both potentials Bonn-B and AV18 ten integrations points are sufficient. In case of the θ'' -integration it turns out that for the Bonn-B potential one needs at least 32 integration points, whereas for the AV18 potential one can take 24 integration points. The q'' -integration for the Bonn-B potential requires 72 integration points in the $S = 0$ case and 48 points in the $S = 1$ case. For the AV18 potential both in the $S = 0$ and $S = 1$ cases 50 integration points are required for the lower momenta interval $[0, q_2]$ and 22 points for the higher momenta interval $[q_2, q_3]$. Clearly one needs more integration points at lower momenta, where the T-matrix is not smooth.

E.2 Principal Value Singularity

The free propagator $G_0^+(E_q)$ given in Eq. (2.12) for an outgoing wave can be written as

$$G_0^+(E_q) = \lim_{\epsilon \rightarrow 0} \frac{1}{E_q + i\epsilon - E_{q''}} = \frac{\mathcal{P}}{E_q - E_{q''}} - i\pi\delta(E_q - E_{q''}), \quad (\text{E.7})$$

where \mathcal{P} in the first term in the last equality stands for the principal value part. This term is singular at $E_{q''} = E_q$. In the q'' -integration of Eq. (3.73) this singularity occurs at $q'' = q$. We treat the singularity problem by employing a reduction method [68] described in the following.

Consider the following principal value integral

$$I = \int_0^\infty dx \frac{\mathcal{P}x^2 f(x)}{a^2 - x^2}, \quad (\text{E.8})$$

where the integrand is singular at $x = a$. This integral can be rewritten as

$$I = \int_0^\infty dx \frac{\mathcal{P}x^2 f(x)}{a^2 - x^2} - \int_0^\infty dx \frac{a^2 f(a)}{a^2 - x^2}, \quad (\text{E.9})$$

since the second term equals zero. Next we treat the singularity by evaluating the integral as

$$I = \int_0^\infty dx \frac{x^2 f(x) - a^2 f(a)}{a^2 - x^2}. \quad (\text{E.10})$$

Thus, the numerator vanishes at $x = a$ and the integrand is well defined at $x = a$. In case of the AV18 potential, where we do not integrate to ∞ , the integral is evaluated as

$$I = \int_0^M dx \frac{x^2 f(x) - a^2 f(a)}{a^2 - x^2} - \frac{1}{2} a f(a) \ln \left(\frac{M - a}{M + a} \right), \quad (\text{E.11})$$

where the second term results from

$$- \int_M^\infty dx \frac{a^2 f(a)}{a^2 - x^2}.$$

E.3 Solving the Lippmann-Schwinger Equation for the T-Matrix

In this subsection we describe how the LSE's given in Eq. (3.73) are solved to obtain the T-matrix elements $T_{\Lambda'\Lambda}^{\pi S t}(\mathbf{q}', \mathbf{q})$. For $S = 0$ the LSE is an uncoupled equation and for $S = 1$ we have for each initial helicity $\Lambda = 1, 0$ two coupled equations for final helicities $\Lambda' = 1, 0$. In favor of simplicity we express the LSE in the following notation:

$$T_{q'\theta'\Lambda'} = V_{q'\theta'\Lambda'} + \lim_{\epsilon \rightarrow 0} \sum_{\Lambda''} \int_0^\pi d\theta'' \int_0^M dq'' q''^2 \frac{m F_{q'\theta'\Lambda' q''\theta''\Lambda''}}{q^2 + i\epsilon - q''^2} T_{q''\theta''\Lambda''}, \quad (\text{E.12})$$

suppressing all the parameters: spin S , isospin t and parity η_π as well as the initial variables: helicity Λ and the momentum's magnitude q , except the one in the propagator. We choose the interval for the q'' -integration as $[0, M]$ instead of $[0, \infty]$ to make it more general, since for the AV18 potential the integration is terminated at $M = q_3$.

We write Eq. (E.12) in terms of a principal value part and a delta function and then treat the principal value singularity by the method given in the previous subsection:

$$\begin{aligned}
T_{q'\theta'\Lambda'} &= V_{q'\theta'\Lambda'} \\
&+ \sum_{\Lambda''} \int_0^\pi d\theta'' \int_0^M dq'' q''^2 \left(\frac{\mathcal{P}}{q^2 - q''^2} - i\pi\delta(q^2 - q''^2) \right) mF_{q'\theta'\Lambda'q''\theta''\Lambda''} T_{q''\theta''\Lambda''} \\
&= V_{q'\theta'\Lambda'} \\
&+ \sum_{\Lambda''} \int_0^\pi d\theta'' \left[\int_0^M dq'' \frac{q''^2 mF_{q'\theta'\Lambda'q''\theta''\Lambda''} T_{q''\theta''\Lambda''} - q^2 mF_{q'\theta'\Lambda'q\theta''\Lambda''} T_{q\theta''\Lambda''}}{q^2 - q''^2} \right. \\
&\quad \left. - \frac{1}{2} \left\{ \ln \left(\frac{M - q}{M + q} \right) + i\pi \right\} q mF_{q'\theta'\Lambda'q\theta''\Lambda''} T_{q\theta''\Lambda''} \right]. \tag{E.13}
\end{aligned}$$

Numerically this equation is evaluated as

$$\begin{aligned}
T_{q'\theta'\Lambda'} &= V_{q'\theta'\Lambda'} \\
&+ \sum_{\Lambda''} \sum_{\theta''} w_{\theta''} \left[\sum_{q''} w_{q''} \frac{q''^2 mF_{q'\theta'\Lambda'q''\theta''\Lambda''} T_{q''\theta''\Lambda''} - q^2 mF_{q'\theta'\Lambda'q\theta''\Lambda''} T_{q\theta''\Lambda''}}{q^2 - q''^2} \right. \\
&\quad \left. - \frac{1}{2} \left\{ \ln \left(\frac{M - q}{M + q} \right) + i\pi \right\} q mF_{q'\theta'\Lambda'q\theta''\Lambda''} T_{q\theta''\Lambda''} \right] \\
&= V_{q'\theta'\Lambda'} \\
&+ \sum_{\Lambda''} \sum_{\theta''} \sum_{q'' \neq q} w_{\theta''} w_{q''} \frac{q''^2 mF_{q'\theta'\Lambda'q''\theta''\Lambda''} T_{q''\theta''\Lambda''} - q^2 mF_{q'\theta'\Lambda'q\theta''\Lambda''} T_{q\theta''\Lambda''}}{q^2 - q''^2} \\
&\quad - \sum_{\Lambda''} \sum_{\theta''} w_{\theta''} \frac{1}{2} \left\{ \ln \left(\frac{M - q}{M + q} \right) + i\pi \right\} q mF_{q'\theta'\Lambda'q\theta''\Lambda''} T_{q\theta''\Lambda''} \\
&= V_{q'\theta'\Lambda'} \\
&+ \sum_{\Lambda''} \sum_{\theta''} \sum_{q'' \neq q} \frac{w_{\theta''} w_{q''} q''^2 mF_{q'\theta'\Lambda'q''\theta''\Lambda''} T_{q''\theta''\Lambda''}}{q^2 - q''^2} \\
&\quad - \sum_{\Lambda''} \sum_{\theta''} w_{\theta''} \left\{ \sum_{q'' \neq q} \frac{w_{q''} q}{q^2 - q''^2} + \frac{1}{2} \ln \left(\frac{M - q}{M + q} \right) + \frac{1}{2} i\pi \right\} q mF_{q'\theta'\Lambda'q\theta''\Lambda''} T_{q\theta''\Lambda''} \\
&= V_{q'\theta'\Lambda'} \\
&+ \sum_{\Lambda''} \sum_{\theta''} \sum_{q''} \left[\bar{\delta}_{q''q} \frac{w_{q''} q''}{q^2 - q''^2} - \delta_{q''q} \left\{ \sum_{q''' \neq q} \frac{w_{q'''} q}{q^2 - q'''^2} + \frac{1}{2} \ln \left(\frac{M - q}{M + q} \right) + \frac{1}{2} i\pi \right\} \right] \\
&\quad \times w_{\theta''} q'' mF_{q'\theta'\Lambda'q''\theta''\Lambda''} T_{q''\theta''\Lambda''}, \tag{E.14}
\end{aligned}$$

where $w_{\theta''}$ and $w_{q''}$ are the weights for the θ'' - and q'' -integrations, respectively, and $\bar{\delta}_{q''q} \equiv (1 - \delta_{q''q})$. Let us now simplify the notations, define α for the combination $q'\theta'\Lambda'$,

β for $q''\theta''\Lambda''$ and Σ_β for $\Sigma_{\Lambda''}\Sigma_{\theta''}\Sigma_{q''}$. Next resolving Eq. (E.14) with respect to $V_{q''\theta''\Lambda''}$ gives

$$\sum_{\beta} A_{\alpha\beta} T_{\beta} = V_{\alpha}, \quad (\text{E.15})$$

with

$$A_{\alpha\beta} \equiv \delta_{\alpha\beta} - \left[\bar{\delta}_{q''q} \frac{w_{q''} q''}{q^2 - q''^2} - \delta_{q''q} \left\{ \sum_{q''' \neq q} \frac{w_{q'''} q}{q^2 - q'''^2} + \frac{1}{2} \ln \left(\frac{M - q}{M + q} \right) + \frac{1}{2} i\pi \right\} \right] w_{\theta''} q'' m F_{\alpha\beta}. \quad (\text{E.16})$$

Equation (E.15) is a matrix representation of a system of linear equation, with the size of the symmetric matrix A being $(n_{q''} \times n_{\theta''})^2$, where $n_{q''}$ and $n_{\theta''}$ are the numbers of q'' - and θ'' -integration points. A system of linear equations can be solved using methods like the Gaussian elimination and the LU decomposition, which is better than the former one [66]. Some ready-to-use routines collected as a library such as Lapack and NAG libraries are also available at computing centers, which proved to be powerful. The Lapack routines can also be downloaded from the site <http://www.netlib.org/>. In our calculations we use one of the Lapack routines called ZGESV.

Appendix F

TWO SUCCESSIVE ROTATIONS

In Chapter 6 we faced two successive rotations, applied to the momentum-helicity states. Here we evaluate two successive rotations in momentum space and in spin space. But we firstly give a few basic definitions and relations required in this appendix. See Refs.[32, 31] for more details.

A rotation of a system (a state) is performed by means of a rotation operator $R(\hat{\mathbf{p}})$ defined as

$$R(\hat{\mathbf{p}}) = R(\phi\theta) = e^{-iJ_z\phi}e^{-iJ_y\theta}, \quad (\text{F.1})$$

where J_z, J_y are the z- and y-components of the angular momentum operator \mathbf{J} and (θ, ϕ) the rotation angles and the direction of \mathbf{p} as well. The rotation operator $R(\hat{\mathbf{p}})$ works on the angular momentum state $|\hat{\mathbf{z}}jm\rangle$ as

$$R(\hat{\mathbf{p}})|\hat{\mathbf{z}}jm\rangle = |\hat{\mathbf{p}}jm\rangle. \quad (\text{F.2})$$

Here $|\hat{\mathbf{p}}jm\rangle$ is the rotated angular momentum state (shorted as the rotated state), given as

$$\begin{aligned} |\hat{\mathbf{p}}jm\rangle &= R(\hat{\mathbf{p}})|\hat{\mathbf{z}}jm\rangle \\ &= \sum_{j'm'} |\hat{\mathbf{z}}j'm'\rangle \langle \hat{\mathbf{z}}j'm'|R(\hat{\mathbf{p}})|\hat{\mathbf{z}}jm\rangle \\ &\equiv \sum_{m'} D_{m'm}^j(\hat{\mathbf{p}})|\hat{\mathbf{z}}jm'\rangle, \end{aligned} \quad (\text{F.3})$$

where

$$D_{m'm}^j(\hat{\mathbf{p}}) = D_{m'm}^j(\phi\theta) = \langle \hat{\mathbf{z}}jm'|R(\hat{\mathbf{p}})|\hat{\mathbf{z}}jm\rangle, \quad (\text{F.4})$$

which we call the Wigner D-function. We see that $R(\hat{\mathbf{p}})$ conserves j . In the following text we use $R_L(\hat{\mathbf{p}})$ and $R_S(\hat{\mathbf{p}})$ for rotations in momentum space and in spin space, with \mathbf{J} being replaced by \mathbf{L} and \mathbf{S} , respectively. Thus,

$$R_L(\hat{\mathbf{p}}) = R_L(\phi\theta) = e^{-iL_z\phi}e^{-iL_y\theta} \quad R_S(\hat{\mathbf{p}}) = R_S(\phi\theta) = e^{-iS_z\phi}e^{-iS_y\theta}. \quad (\text{F.5})$$

A rotation $R(\alpha\beta\gamma)$ of a state $|\hat{\mathbf{z}}jm\rangle$ corresponds to a change of the Cartesian coordinates \mathbf{r} describing the state through a rotation matrix $M(\alpha\beta\gamma)$. The new Cartesian coordinates \mathbf{r}' are related to the old ones \mathbf{r} as

$$\mathbf{r}' = M(\alpha\beta\gamma)\mathbf{r}. \quad (\text{F.6})$$

The rotation matrix $M(\alpha\beta\gamma)$ is given as

$$M(\alpha\beta\gamma)\mathbf{r} \equiv M_{z''}(\gamma)M_{y'}(\beta)M_z(\alpha)\mathbf{r}, \quad (\text{F.7})$$

with

$$M_z(\alpha) = \begin{pmatrix} \cos \alpha & \sin \alpha & 0 \\ -\sin \alpha & \cos \alpha & 0 \\ 0 & 0 & 1 \end{pmatrix} \quad M_{y'}(\beta) = \begin{pmatrix} \cos \beta & 0 & -\sin \beta \\ 0 & 1 & 0 \\ \sin \beta & 0 & \cos \beta \end{pmatrix} \quad (\text{F.8})$$

$$M_{z''}(\gamma) = \begin{pmatrix} \cos \gamma & \sin \gamma & 0 \\ -\sin \gamma & \cos \gamma & 0 \\ 0 & 0 & 1 \end{pmatrix}.$$

Here $M_z(\alpha)$ represents a rotation of the coordinate system O through an angle α around the z -axis, $M_{y'}(\beta)$ a rotation of the rotated coordinate system O' through an angle β around the rotated y' -axis, $M_{z''}(\gamma)$ a rotation of the rotated coordinate system O'' through an angle γ around the rotated z'' -axis. Thus, the rotation matrix $M(\alpha\beta\gamma)$ represents three successive rotations, which bring the old coordinate system O to the new one O''' . It follows that

$$M(\alpha\beta\gamma) = \begin{pmatrix} \cos \alpha \cos \beta \cos \gamma - \sin \alpha \sin \gamma & \sin \alpha \cos \beta \cos \gamma + \cos \alpha \sin \gamma & -\sin \beta \cos \gamma \\ -\cos \alpha \cos \beta \sin \gamma - \sin \alpha \cos \gamma & -\sin \alpha \cos \beta \sin \gamma + \cos \alpha \cos \gamma & \sin \beta \sin \gamma \\ \cos \alpha \sin \beta & \sin \alpha \sin \beta & \cos \beta \end{pmatrix}. \quad (\text{F.9})$$

F.1 Two Successive Rotations in Momentum Space

Let us consider a momentum state $|\mathbf{p}\rangle$ with $\hat{\mathbf{p}}$ pointing in (θ, ϕ) direction, expanded in partial waves as

$$|\mathbf{p}\rangle = \sum_{lm} |plm\rangle Y_{lm}^*(\theta, \phi), \quad (\text{F.10})$$

where $|plm\rangle$ is defined to be quantized along the z-axis. Now take a special direction $\hat{\mathbf{p}} = \hat{\mathbf{z}}$. The momentum state $|p\hat{\mathbf{z}}\rangle$ is given as

$$|p\hat{\mathbf{z}}\rangle = \sum_{lm} |plm\rangle Y_{lm}^*(0, 0) = \sum_l |pl0\rangle \sqrt{\frac{2l+1}{4\pi}}. \quad (\text{F.11})$$

Applying to the state $|p\hat{\mathbf{z}}\rangle$ a rotation operator $R_L(\hat{\mathbf{p}})$ given in Eq. (F.5) leads to

$$\begin{aligned} R_L(\hat{\mathbf{p}})|p\hat{\mathbf{z}}\rangle &= R_L(\phi\theta 0) \sum_l |pl0\rangle \sqrt{\frac{2l+1}{4\pi}} \\ &= \sum_l \sum_{l'm} |pl'm\rangle \langle \hat{\mathbf{z}}l'm | R_L(\phi\theta 0) | \hat{\mathbf{z}}l0 \rangle \sqrt{\frac{2l+1}{4\pi}} \\ &= \sum_{lm} |plm\rangle D_{m0}^l(\phi\theta 0) \sqrt{\frac{2l+1}{4\pi}} \\ &= \sum_{lm} |plm\rangle Y_{lm}^*(\theta, \phi) \\ &= |\mathbf{p}\rangle, \end{aligned} \quad (\text{F.12})$$

where we have used the relation between the spherical harmonics and the Wigner D-functions given as

$$Y_{lm}^*(\theta, \phi) = \sqrt{\frac{2l+1}{4\pi}} D_{m0}^l(\phi\theta 0). \quad (\text{F.13})$$

Thus, $R_L(\hat{\mathbf{p}})$ rotates the state $|p\hat{\mathbf{z}}\rangle$ to become the state $|\mathbf{p}\rangle$.

Next we apply to the state $|\mathbf{p}\rangle$ an inverse rotation operator $R_L^{-1}(\hat{\mathbf{p}}') = R_L^\dagger(\hat{\mathbf{p}}') = R_L(0, -\theta', -\phi')$. We firstly take a look at the definition of the spherical harmonics $Y_{l'm'}(\theta'', \phi'')$:

$$\begin{aligned} Y_{l'm'}(\theta'', \phi'') &\equiv \langle \hat{\mathbf{p}}'' | \hat{\mathbf{z}}l'm' \rangle \\ &= \langle \hat{\mathbf{p}}'' | R_L^\dagger(\hat{\mathbf{p}}') R_L(\hat{\mathbf{p}}') | \hat{\mathbf{z}}l'm' \rangle \\ &= \langle R_L(\hat{\mathbf{p}}') \hat{\mathbf{p}}'' | R_L(\hat{\mathbf{p}}') | \hat{\mathbf{z}}l'm' \rangle \\ &\equiv \langle \hat{\mathbf{p}} | \hat{\mathbf{p}}'l'm' \rangle, \end{aligned} \quad (\text{F.14})$$

where we have defined the $\hat{\mathbf{p}}$ direction as to be connected to the $\hat{\mathbf{p}}''$ direction according to

$$|\hat{\mathbf{p}}''\rangle = R_L^\dagger(\hat{\mathbf{p}}') |\hat{\mathbf{p}}\rangle. \quad (\text{F.15})$$

Hence, the spherical harmonics $Y_{l'm'}(\theta'', \phi'')$ can be obtained as a representation in $\hat{\mathbf{p}}$ of the angular momentum state $|\hat{\mathbf{p}}'l'm'\rangle$ with the quantization axis in the $\hat{\mathbf{p}}'$ direction. Using Eq. (F.14) we obtain¹

$$R_L^\dagger(\hat{\mathbf{p}}') |\mathbf{p}\rangle = R_L(0, -\theta', -\phi') \sum_{lm} |plm\rangle Y_{lm}^*(\theta, \phi)$$

¹In obtaining Eq. (F.19) one can also use the following equation [31]

$$Y_{l'm'}(\theta', \phi') = \sum_m D_{mm'}^l(\alpha\beta\gamma) Y_{lm}(\theta, \phi), \quad (\text{F.16})$$

$$\begin{aligned}
&= \sum_{lm} \sum_{l'm'} |pl'm'\rangle \langle \hat{z}l'm' | R_L(0, -\theta', -\phi') | \hat{z}lm \rangle Y_{lm}^*(\theta, \phi) \\
&= \sum_{lm} \sum_{l'm'} |pl'm'\rangle \langle \hat{z}l'm' | R_L(0, -\theta', -\phi') | \hat{z}lm \rangle \langle \hat{z}lm | \hat{\mathbf{p}} \rangle \\
&= \sum_{l'm'} |pl'm'\rangle \langle \hat{z}l'm' | R_L(0, -\theta', -\phi') | \hat{\mathbf{p}} \rangle \\
&= \sum_{l'm'} |pl'm'\rangle \langle R_L(\phi'\theta'0) \hat{z}l'm' | \hat{\mathbf{p}} \rangle \\
&= \sum_{l'm'} |pl'm'\rangle \langle \hat{\mathbf{p}}'l'm' | \hat{\mathbf{p}} \rangle \\
&\equiv \sum_{l'm'} |pl'm'\rangle Y_{l'm'}^*(\theta'', \phi'') \\
&= R_L(\hat{\mathbf{p}}'') |p\hat{\mathbf{z}}\rangle. \tag{F.19}
\end{aligned}$$

Inserting Eq. (F.12) into Eq. (F.19) leads to

$$R_L^\dagger(\hat{\mathbf{p}}') R_L(\hat{\mathbf{p}}) |p\hat{\mathbf{z}}\rangle = R_L(\hat{\mathbf{p}}'') |p\hat{\mathbf{z}}\rangle. \tag{F.20}$$

Hence, we obtain that the two successive rotations $R_L^\dagger(\hat{\mathbf{p}}') R_L(\hat{\mathbf{p}})$ applied to the state $|p\hat{\mathbf{z}}\rangle$ can be replaced by the rotation $R_L(\hat{\mathbf{p}}'')$. Consequently any number of successive rotations in momentum space can always be replaced by one rotation with the right rotation angles. The angles (θ'', ϕ'') of $\hat{\mathbf{p}}''$ are determined by the angles (θ, ϕ) of $\hat{\mathbf{p}}$ and (θ', ϕ') of $\hat{\mathbf{p}}'$ as

$$\cos \theta'' = \cos \theta \cos \theta' + \sin \theta \sin \theta' \cos(\phi - \phi') \tag{F.21}$$

$$\sin \theta'' e^{i\phi''} = -\cos \theta \sin \theta' + \sin \theta \cos \theta' \cos(\phi - \phi') + i \sin \theta \sin(\phi - \phi'). \tag{F.22}$$

Equations (F.21) and (F.22) are obtained from the rotation matrices of the Cartesian coordinates, which correspond to the rotations in Eq. (F.20). Such a rotation matrix $M(\alpha\beta\gamma)$ corresponding to $R(\alpha\beta\gamma)$ is given in Eq. (F.9).

which is obtained by applying the formal expression for a rotation of an angular momentum state given in Eq. (F.2) to the spherical harmonics, which are eigenstates of the orbital angular momentum operator \mathbf{L} . The angles (θ', ϕ') are connected to (θ, ϕ) according to

$$|\hat{\mathbf{p}}'\rangle = R_L(\alpha\beta\gamma) |\hat{\mathbf{p}}\rangle. \tag{F.17}$$

Thus,

$$\begin{aligned}
R_L^\dagger(\hat{\mathbf{p}}') |\mathbf{p}\rangle &= R_L^\dagger(\phi'\theta'0) \sum_{lm} |plm\rangle Y_{lm}^*(\theta, \phi) \\
&= \sum_{lm} \sum_{l'm'} |pl'm'\rangle \langle \hat{z}l'm' | R_L^\dagger(\phi'\theta'0) | \hat{z}lm \rangle Y_{lm}^*(\theta, \phi) \\
&= \sum_{l'm'} |pl'm'\rangle \sum_m D_{mm'}^{l'm'}(\phi'\theta'0) Y_{l'm}^*(\theta, \phi) \\
&= \sum_{l'm'} |pl'm'\rangle Y_{l'm'}^*(\theta'', \phi'') \\
&= R_L(\hat{\mathbf{p}}'') |p\hat{\mathbf{z}}\rangle. \tag{F.18}
\end{aligned}$$

F.2 Two Successive Rotations in Spin Space

One may think that analogously the rotation identity given in Eq. (F.20) also applies in spin space. But this must be checked, since analogies do not always lead to correct conclusions. Therefore, we evaluate two successive rotations in spin space, independent of the evaluation in momentum space in the previous section. We use the rotation operator $R_S(\hat{\mathbf{p}})$ given in Eq. (F.5). Thus, we compare the rotated spin state or the helicity state $|\hat{\mathbf{p}}''S\Lambda\rangle_1$ given as

$$|\hat{\mathbf{p}}''S\Lambda\rangle_1 = R_S(\hat{\mathbf{p}}'')|\hat{\mathbf{z}}S\Lambda\rangle \quad (\text{F.23})$$

with the rotated spin state $|\hat{\mathbf{p}}''S\Lambda\rangle_2$ given as

$$|\hat{\mathbf{p}}''S\Lambda\rangle_2 = R_S^\dagger(\hat{\mathbf{p}}')R_S(\hat{\mathbf{p}})|\hat{\mathbf{z}}S\Lambda\rangle. \quad (\text{F.24})$$

Note that here the relation between (θ'', ϕ'') , (θ', ϕ') and (θ, ϕ) given in Eqs. (F.21) and (F.22) is still valid, since this relation results from the transformation of the Cartesian coordinates, which is the same in both momentum space and spin space.

The state $|\hat{\mathbf{p}}''S\Lambda\rangle_1$ is eigenstate of the helicity operator $\mathbf{S} \cdot \hat{\mathbf{p}}''$ with eigenvalue Λ , as can be shown as follows:

$$\begin{aligned} \mathbf{S} \cdot \hat{\mathbf{p}}''|\hat{\mathbf{p}}''S\Lambda\rangle_1 &= R_S(\hat{\mathbf{p}}'')\mathbf{S} \cdot \hat{\mathbf{z}}R_S^\dagger(\hat{\mathbf{p}}'')R_S(\hat{\mathbf{p}}'')|\hat{\mathbf{z}}S\Lambda\rangle \\ &= R_S(\hat{\mathbf{p}}'')\mathbf{S} \cdot \hat{\mathbf{z}}|\hat{\mathbf{z}}S\Lambda\rangle \\ &= \Lambda R_S(\hat{\mathbf{p}}'')|\hat{\mathbf{z}}S\Lambda\rangle \\ &= \Lambda|\hat{\mathbf{p}}''S\Lambda\rangle_1. \end{aligned} \quad (\text{F.25})$$

Similarly it can be shown that the state $|\hat{\mathbf{p}}''S\Lambda\rangle_2$ is also eigenstate of the helicity operator $\mathbf{S} \cdot \hat{\mathbf{p}}''$ with eigenvalue Λ :

$$\begin{aligned} \mathbf{S} \cdot \hat{\mathbf{p}}''|\hat{\mathbf{p}}''S\Lambda\rangle_2 &= R_S^\dagger(\hat{\mathbf{p}}')R_S(\hat{\mathbf{p}})\mathbf{S} \cdot \hat{\mathbf{z}}R_S^\dagger(\hat{\mathbf{p}})R_S(\hat{\mathbf{p}})R_S^\dagger(\hat{\mathbf{p}}')R_S(\hat{\mathbf{p}})|\hat{\mathbf{z}}S\Lambda\rangle \\ &= R_S^\dagger(\hat{\mathbf{p}}')R_S(\hat{\mathbf{p}})\mathbf{S} \cdot \hat{\mathbf{z}}|\hat{\mathbf{z}}S\Lambda\rangle \\ &= \Lambda R_S^\dagger(\hat{\mathbf{p}}')R_S(\hat{\mathbf{p}})|\hat{\mathbf{z}}S\Lambda\rangle \\ &= \Lambda|\hat{\mathbf{p}}''S\Lambda\rangle_2. \end{aligned} \quad (\text{F.26})$$

Moreover a scalar product of two states is rotationally invariant. Thus,

$${}_1\langle\hat{\mathbf{p}}''S\Lambda'|\hat{\mathbf{p}}''S\Lambda\rangle_1 = {}_2\langle\hat{\mathbf{p}}''S\Lambda'|\hat{\mathbf{p}}''S\Lambda\rangle_2 = \langle\hat{\mathbf{z}}S\Lambda'|\hat{\mathbf{z}}S\Lambda\rangle. \quad (\text{F.27})$$

Therefore, it remains to find out whether the two helicity states $|\hat{\mathbf{p}}''S\Lambda\rangle_1$ and $|\hat{\mathbf{p}}''S\Lambda\rangle_2$ are just the same or are distinguished from each other by merely a phase factor.

The helicity states $|\hat{\mathbf{p}}''S\Lambda\rangle_1$ and $|\hat{\mathbf{p}}''S\Lambda\rangle_2$ are expanded in the spin states $|\hat{\mathbf{z}}S\Lambda\rangle$ as

$$\begin{aligned} |\hat{\mathbf{p}}''S\Lambda\rangle_1 &= R_S(\hat{\mathbf{p}}'')|\hat{\mathbf{z}}S\Lambda\rangle \\ &= \sum_{\Lambda'} |\hat{\mathbf{z}}S\Lambda'\rangle \langle \hat{\mathbf{z}}S\Lambda' | R_S(\phi''\theta''0) | \hat{\mathbf{z}}S\Lambda\rangle \\ &= \sum_{\Lambda'} |\hat{\mathbf{z}}S\Lambda'\rangle D_{\Lambda'\Lambda}^S(\phi''\theta''0) \end{aligned} \quad (\text{F.28})$$

$$\begin{aligned} |\hat{\mathbf{p}}''S\Lambda\rangle_2 &= R_S^\dagger(\hat{\mathbf{p}}')R_S(\hat{\mathbf{p}})|\hat{\mathbf{z}}S\Lambda\rangle \\ &= \sum_N R_S^\dagger(\phi'\theta'0)|\hat{\mathbf{z}}SN\rangle \langle \hat{\mathbf{z}}SN | R_S(\phi\theta0) | \hat{\mathbf{z}}S\Lambda\rangle \\ &= \sum_{\Lambda'N} |\hat{\mathbf{z}}S\Lambda'\rangle \langle \hat{\mathbf{z}}S\Lambda' | R_S^\dagger(\phi'\theta'0) | \hat{\mathbf{z}}SN\rangle D_{N\Lambda}^S(\phi\theta0) \\ &= \sum_{\Lambda'} |\hat{\mathbf{z}}S\Lambda'\rangle \sum_N D_{N\Lambda'}^{S*}(\phi'\theta'0) D_{N\Lambda}^S(\phi\theta0) \\ &\equiv \sum_{\Lambda'} |\hat{\mathbf{z}}S\Lambda'\rangle X_{\Lambda'\Lambda}^S(\phi''\theta''0), \end{aligned} \quad (\text{F.29})$$

where

$$X_{\Lambda'\Lambda}^S(\phi''\theta''0) \equiv \sum_N D_{N\Lambda'}^{S*}(\phi'\theta'0) D_{N\Lambda}^S(\phi\theta0). \quad (\text{F.30})$$

Therefore, instead of comparing $|\hat{\mathbf{p}}''S\Lambda\rangle_1$ with $|\hat{\mathbf{p}}''S\Lambda\rangle_2$ we compare $D_{\Lambda'\Lambda}^S(\phi''\theta''0)$ with $X_{\Lambda'\Lambda}^S(\phi''\theta''0)$, since these are known functions. We have two spin cases $S = 0$ and $S = 1$. For $S = 0$ the spin state is rotationally invariant and thus

$$X_{00}^0(\phi''\theta''0) = D_{00}^0(\phi''\theta''0) = 1 \quad |\hat{\mathbf{p}}''00\rangle_1 = |\hat{\mathbf{p}}''00\rangle_2 = |\hat{\mathbf{z}}00\rangle. \quad (\text{F.31})$$

The Wigner D-functions obey a symmetry relation given as

$$D_{m'm}^{j*}(\alpha\beta\gamma) = (-)^{m'-m} D_{-m',-m}^j(\alpha\beta\gamma). \quad (\text{F.32})$$

Therefore, for $S = 1$ the case with initial helicity $\Lambda = -1$ can be left out and we consider only six cases with $\Lambda' = 1, 0, -1$ and $\Lambda = 1, 0$.

The Wigner D-function $D_{\Lambda'\Lambda}^1(\phi\theta0)$ is given as

$$D^1(\phi\theta0) = \begin{pmatrix} e^{-i\phi} \frac{1+\cos\theta}{2} & -e^{-i\phi} \frac{\sin\theta}{\sqrt{2}} & e^{-i\phi} \frac{1-\cos\theta}{2} \\ \frac{\sin\theta}{\sqrt{2}} & \cos\theta & -\frac{\sin\theta}{\sqrt{2}} \\ e^{i\phi} \frac{1-\cos\theta}{2} & e^{i\phi} \frac{\sin\theta}{\sqrt{2}} & e^{i\phi} \frac{1+\cos\theta}{2} \end{pmatrix}. \quad (\text{F.33})$$

For $\Lambda = 0$ it follows

$$\begin{aligned} X_{10}^1(\phi''\theta''0) &= -e^{i\phi'} \frac{1+\cos\theta'}{2} e^{-i\phi} \frac{\sin\theta}{\sqrt{2}} + \frac{\sin\theta'}{\sqrt{2}} \cos\theta + e^{-i\phi'} \frac{1-\cos\theta'}{2} e^{i\phi} \frac{\sin\theta}{\sqrt{2}} \\ &= -\frac{1}{\sqrt{2}} \{-\cos\theta \sin\theta' + \sin\theta \cos\theta' \cos(\phi-\phi') - i \sin\theta \sin(\phi-\phi')\} \\ &= -e^{-i\phi''} \frac{\sin\theta''}{\sqrt{2}} \end{aligned}$$

$$= D_{10}^1(\phi''\theta''0) \quad (\text{F.34})$$

$$\begin{aligned} X_{00}^1(\phi''\theta''0) &= e^{i\phi'} \frac{\sin \theta'}{\sqrt{2}} e^{-i\phi} \frac{\sin \theta}{\sqrt{2}} + \cos \theta' \cos \theta + e^{-i\phi'} \frac{\sin \theta'}{\sqrt{2}} e^{i\phi} \frac{\sin \theta}{\sqrt{2}} \\ &= \{\cos \theta \cos \theta' + \sin \theta \sin \theta' \cos(\phi - \phi')\} \\ &= \cos \theta'' \end{aligned}$$

$$= D_{00}^1(\phi''\theta''0) \quad (\text{F.35})$$

$$\begin{aligned} X_{-10}^1(\phi''\theta''0) &= -e^{i\phi'} \frac{1 - \cos \theta'}{2} e^{-i\phi} \frac{\sin \theta}{\sqrt{2}} - \frac{\sin \theta'}{\sqrt{2}} \cos \theta + e^{-i\phi'} \frac{1 + \cos \theta'}{2} e^{i\phi} \frac{\sin \theta}{\sqrt{2}} \\ &= \frac{1}{\sqrt{2}} \{-\cos \theta \sin \theta' + \sin \theta \cos \theta' \cos(\phi - \phi') + i \sin \theta \sin(\phi - \phi')\} \\ &= e^{i\phi''} \frac{\sin \theta''}{\sqrt{2}} \\ &= D_{-10}^1(\phi''\theta''0). \end{aligned} \quad (\text{F.36})$$

Thus,

$$X_{\Lambda'0}^1(\phi''\theta''0) = D_{\Lambda'0}^1(\phi''\theta''0) \quad |\hat{\mathbf{p}}''10\rangle_1 = |\hat{\mathbf{p}}''10\rangle_2. \quad (\text{F.37})$$

For $\Lambda = 1$ we obtain

$$\begin{aligned} X_{11}^1(\phi''\theta''0) &= e^{i\phi'} \frac{1 + \cos \theta'}{2} e^{-i\phi} \frac{1 + \cos \theta}{2} + \frac{\sin \theta'}{\sqrt{2}} \frac{\sin \theta}{\sqrt{2}} + e^{-i\phi'} \frac{1 - \cos \theta'}{2} e^{i\phi} \frac{1 - \cos \theta}{2} \\ &= \frac{1}{2} \{(1 + \cos \theta \cos \theta') \cos(\phi - \phi') + \sin \theta \sin \theta'\} \\ &\quad - \frac{i}{2} (\cos \theta + \cos \theta') \sin(\phi - \phi') \end{aligned} \quad (\text{F.38})$$

$$\begin{aligned} X_{01}^1(\phi''\theta''0) &= -e^{i\phi'} \frac{\sin \theta'}{\sqrt{2}} e^{-i\phi} \frac{1 + \cos \theta}{2} + \cos \theta' \frac{\sin \theta}{\sqrt{2}} + e^{-i\phi'} \frac{\sin \theta'}{\sqrt{2}} e^{i\phi} \frac{1 - \cos \theta}{2} \\ &= \frac{1}{\sqrt{2}} \{-\cos \theta \sin \theta' \cos(\phi - \phi') + \sin \theta \cos \theta'\} \\ &\quad + \frac{i}{\sqrt{2}} \sin \theta' \sin(\phi - \phi') \end{aligned} \quad (\text{F.39})$$

$$\begin{aligned} X_{-11}^1(\phi''\theta''0) &= e^{i\phi'} \frac{1 - \cos \theta'}{2} e^{-i\phi} \frac{1 + \cos \theta}{2} - \frac{\sin \theta'}{\sqrt{2}} \frac{\sin \theta}{\sqrt{2}} + e^{-i\phi'} \frac{1 + \cos \theta'}{2} e^{i\phi} \frac{1 - \cos \theta}{2} \\ &= \frac{1}{2} \{(1 - \cos \theta \cos \theta') \cos(\phi - \phi') - \sin \theta \sin \theta'\} \\ &\quad - \frac{i}{2} (\cos \theta - \cos \theta') \sin(\phi - \phi'). \end{aligned} \quad (\text{F.40})$$

Hence, for $\Lambda = 1$ apparently we have

$$X_{\Lambda'1}^1(\phi''\theta''0) \neq D_{\Lambda'1}^1(\phi''\theta''0) \quad |\hat{\mathbf{p}}''11\rangle_1 \neq |\hat{\mathbf{p}}''11\rangle_2. \quad (\text{F.41})$$

The difference between Eq. (F.37) and Eq. (F.41) is at the value of Λ . And from Eq. (F.27) we know that

$$|X_{\Lambda'\Lambda}^1(\phi''\theta''0)|^2 = |D_{\Lambda'\Lambda}^1(\phi''\theta''0)|^2, \quad (\text{F.42})$$

which we also have checked using Eqs. (F.33) and (F.38)-(F.40). Therefore, we can be sure that $X_{\Lambda'\Lambda}^1(\phi''\theta''0)$ is related to $D_{\Lambda'\Lambda}^1(\phi''\theta''0)$ by a phase factor. The phase factor must depend on Λ and the set of angles $(\phi, \theta, \phi', \theta')$, and is independent of Λ' . The latter can be understood as we see in Eqs. (F.23) and (F.24) that there is no Λ' . We choose the phase factor such that

$$X_{\Lambda'\Lambda}^1(\phi''\theta''0) = e^{i\Omega\Lambda} D_{\Lambda'\Lambda}^1(\phi''\theta''0), \quad (\text{F.43})$$

where Ω depends on the set of angles $(\phi, \theta, \phi', \theta')$ and is given through its tangential as

$$\tan \Omega = \frac{\text{Im}\{X_{01}^1(\phi''\theta''0)\}}{\text{Re}\{X_{01}^1(\phi''\theta''0)\}} = \frac{\sin \theta' \sin(\phi - \phi')}{-\cos \theta \sin \theta' \cos(\phi - \phi') + \sin \theta \cos \theta'}. \quad (\text{F.44})$$

The Ω calculated in Eq. (F.44) is also valid for other combinations of Λ' and Λ , since Ω is independent of Λ' and Λ . Equation (F.43) agrees with Eqs. (F.37), (F.41) and (F.42) as well as Eq. (F.31) for $S = 0$. A further check shows that

$$X_{11}^1(\phi''\theta''0)X_{-11}^1(\phi''\theta''0) = \frac{1}{2}X_{01}^{1\ 2}(\phi''\theta''0) \quad (\text{F.45})$$

$$D_{11}^1(\phi''\theta''0)D_{-11}^1(\phi''\theta''0) = \frac{1}{2}D_{01}^{1\ 2}(\phi''\theta''0), \quad (\text{F.46})$$

which is consistent with Eq. (F.43) as

$$\begin{aligned} X_{11}^1(\phi''\theta''0)X_{-11}^1(\phi''\theta''0) &= e^{2i\Omega\Lambda} D_{11}^1(\phi''\theta''0)D_{-11}^1(\phi''\theta''0) \\ \frac{1}{2}X_{01}^{1\ 2}(\phi''\theta''0) &= \frac{1}{2}e^{2i\Omega\Lambda} D_{01}^{1\ 2}(\phi''\theta''0). \end{aligned} \quad (\text{F.47})$$

After all these evaluations we summarize that

$$R_S^\dagger(\hat{\mathbf{p}}')R_S(\hat{\mathbf{p}})|\hat{\mathbf{z}}S\Lambda\rangle = e^{i\Omega\Lambda}R_S(\hat{\mathbf{p}}'')|\hat{\mathbf{z}}S\Lambda\rangle \quad (\text{F.48})$$

$$e^{i\Omega\Lambda} = \frac{\sum_{N=-S}^S D_{N\Lambda'}^{S*}(\phi'\theta'0)D_{N\Lambda}^S(\phi\theta0)}{D_{\Lambda'\Lambda}^S(\phi''\theta''0)}. \quad (\text{F.49})$$

We have restored the spin notation S , since Eqs. (F.48) and (F.49) are general and hence apply to arbitrary spin S , including $S = 0$.

Appendix G

NUMERICAL REALIZATION FOR THE PROTON-NEUTRON CHARGE EXCHANGE REACTION

In this appendix we describe how to numerically calculate the Nd break-up amplitude $U_0(\mathbf{p}, \mathbf{q})$. As a reminder, the amplitude consists of three parts $U_0^{(1)}(\mathbf{p}, \mathbf{q})$, $U_0^{(2)}(\mathbf{p}, \mathbf{q})$ and $U_0^{(3)}(\mathbf{p}, \mathbf{q})$ as

$$U_0(\mathbf{p}, \mathbf{q}) = U_0^{(1)}(\mathbf{p}, \mathbf{q}) + U_0^{(2)}(\mathbf{p}, \mathbf{q}) + U_0^{(3)}(\mathbf{p}, \mathbf{q}). \quad (\text{G.1})$$

These three parts are related to each other through permutations of the nucleons. The first part $U_0^{(1)}(\mathbf{p}, \mathbf{q})$ is given as

$$\begin{aligned} U_0^{(1)}(\mathbf{p}, \mathbf{q}) &= \frac{(-)^{\frac{1}{2}+\tau_1}}{4\sqrt{2}} \delta_{\tau_2+\tau_3, \tau_1^0-\tau_1} \sum_{m'_s} e^{-i(\Lambda_0\phi_p - \Lambda'_0\phi_\pi)} C\left(\frac{1}{2} \frac{1}{2} 1; m'_s m_{s1}\right) \\ &\times \sum_l C(l 1 1; M_d - m'_s - m_{s1}, m'_s + m_{s1}) Y_{l, M_d - m'_s - m_{s1}}(\hat{\boldsymbol{\pi}}') \psi_l(\pi') \\ &\times \sum_{S\pi t} \left(1 - \eta_\pi(-)^{S+t}\right) C\left(\frac{1}{2} \frac{1}{2} t; \tau_2 \tau_3\right) C\left(\frac{1}{2} \frac{1}{2} t; \tau_1^0, -\tau_1\right) \\ &\times C\left(\frac{1}{2} \frac{1}{2} S; m_{s2} m_{s3} \Lambda_0\right) C\left(\frac{1}{2} \frac{1}{2} S; m_{s1}^0 m'_s \Lambda'_0\right) \\ &\times \sum_{\Lambda\Lambda'} d_{\Lambda_0\Lambda}^S(\theta_p) d_{\Lambda'_0\Lambda'}^S(\theta_\pi) e^{i(\Lambda'\phi' - \Lambda\Omega)} T_{\Lambda\Lambda'}^{\pi S t}(p, \pi, \cos\theta'; E_p), \end{aligned} \quad (\text{G.2})$$

with

$$\begin{aligned} \psi_l(\pi') &= \text{the deuteron partial wave projected wave function} \\ T_{\Lambda\Lambda'}^{\pi S t}(p, \pi, \cos\theta'; E_p) &= \text{the NN T-matrix elements} \end{aligned}$$

$$\boldsymbol{\pi} = \frac{1}{2}\mathbf{q} + \mathbf{q}_0 \quad (\text{G.3})$$

$$\boldsymbol{\pi}' = -\mathbf{q} - \frac{1}{2}\mathbf{q}_0 \quad (\text{G.4})$$

$$\cos \theta' = \cos \theta_p \cos \theta_\pi + \sin \theta_p \sin \theta_\pi \cos(\phi_p - \phi_\pi) \quad (\text{G.5})$$

$$e^{i(\Lambda'\phi' - \Lambda\Omega)} = \frac{\sum_{N=-S}^S e^{iN(\phi_p - \phi_\pi)} d_{N\Lambda}^S(\theta_p) d_{N\Lambda'}^S(\theta_\pi)}{d_{\Lambda'\Lambda}^S(\theta')} \quad (\text{G.6})$$

The other parts $U_0^{(2)}(\mathbf{p}, \mathbf{q})$ and $U_0^{(3)}(\mathbf{p}, \mathbf{q})$ are obtained from Eqs. (G.2)-(G.6) by applying the following replacements

$$\text{for } U_0^{(2)}(\mathbf{p}, \mathbf{q}) : \{\tau, m\}_{\{1,2,3\}} \rightarrow \{\tau, m\}_{\{2,3,1\}} \quad \mathbf{p} \rightarrow -\frac{1}{2}\mathbf{p} - \frac{3}{4}\mathbf{q} \quad \mathbf{q} \rightarrow \mathbf{p} - \frac{1}{2}\mathbf{q} \quad (\text{G.7})$$

$$\text{for } U_0^{(3)}(\mathbf{p}, \mathbf{q}) : \{\tau, m\}_{\{1,2,3\}} \rightarrow \{\tau, m\}_{\{3,1,2\}} \quad \mathbf{p} \rightarrow -\frac{1}{2}\mathbf{p} + \frac{3}{4}\mathbf{q} \quad \mathbf{q} \rightarrow -\mathbf{p} - \frac{1}{2}\mathbf{q}. \quad (\text{G.8})$$

G.1 Momentum Addition

There are several additions of momenta in the formulation, see for example Eqs. (G.3), (G.4), (G.7) and (G.8). Thus, one has to find out the resulting momenta from these additions by calculating their components. Since we are working with a spherical coordinate systems these components are the magnitude, the angles θ to the z-axis and the azimuthal angle ϕ . It is straightforward to obtain these components of the momenta as shown in the following.

Consider a momentum addition

$$\mathbf{C} = \mathbf{A} + \mathbf{B}. \quad (\text{G.9})$$

The magnitude of \mathbf{C} is given as

$$C = \sqrt{A^2 + B^2 + 2AB\hat{\mathbf{A}} \cdot \hat{\mathbf{B}}} \quad (\text{G.10})$$

with

$$\hat{\mathbf{A}} \cdot \hat{\mathbf{B}} = \cos \theta_A \cos \theta_B + \sin \theta_A \sin \theta_B \cos(\phi_A - \phi_B). \quad (\text{G.11})$$

The components of \mathbf{C} , which are projected on the axes of a Cartesian coordinate system, are given as

$$C_x = C \sin \theta_C \cos \phi_C = A \sin \theta_A \cos \phi_A + B \sin \theta_B \cos \phi_B$$

$$C_y = C \sin \theta_C \sin \phi_C = A \sin \theta_A \sin \phi_A + B \sin \theta_B \sin \phi_B$$

$$C_z = C \cos \theta_C = A \cos \theta_A + B \cos \theta_B.$$

Thus, one can find the angle θ_C as

$$\theta_C = \arccos \left(\frac{A \cos \theta_A + B \cos \theta_B}{C} \right). \quad (\text{G.12})$$

The azimuthal angle ϕ_C is determined uniquely by its sine and cosine together, which are given as

$$\begin{aligned}\cos \phi_C &= \frac{A \sin \theta_A \cos \phi_A + B \sin \theta_B \cos \phi_B}{C \sin \theta_C} \\ \sin \phi_C &= \frac{A \sin \theta_A \sin \phi_A + B \sin \theta_B \sin \phi_B}{C \sin \theta_C}.\end{aligned}$$

We get the unique value of ϕ_C in the following way

$$\phi_C = \begin{cases} \arccos \left(\frac{A \sin \theta_A \cos \phi_A + B \sin \theta_B \cos \phi_B}{C \sin \theta_C} \right) & \text{if } \sin \phi_C > 0 \\ 2\pi - \arccos \left(\frac{A \sin \theta_A \cos \phi_A + B \sin \theta_B \cos \phi_B}{C \sin \theta_C} \right) & \text{if } \sin \phi_C < 0 \\ (1 - \cos \phi_C) \frac{\pi}{2} & \text{if } \sin \phi_C = 0 \end{cases} \quad (\text{G.13})$$

G.2 Integration

We consider the Nd break-up process, where in the final state only one nucleon is detected. Therefore, to calculate the observables in the process we sum over all possible directions of the other two nucleons. This is realized by integrating over the direction of the Jacobi momentum \mathbf{p} of the undetected 2N subsystem, as shown in Eq. (6.24).

The $\hat{\mathbf{p}}$ -integration is two-fold, denoted as

$$I = \int_0^\pi d\theta_p \int_0^{2\pi} d\phi_p f(\theta_p, \phi_p). \quad (\text{G.14})$$

To calculate this integral we use the Gauss-Legendre quadrature and a linear mapping as mentioned in Section E.1. We vary the numbers of integration points to test the convergence of our integration, these are n_{θ_p} for the θ_p -integration and n_{ϕ_p} for the ϕ_p -integration. We found that with $n_{\theta_p} = 48$ and $n_{\phi_p} = 18$ the integration converges.

G.3 Interpolation

To calculate $U_0(\mathbf{p}, \mathbf{q})$ one needs the NN T-matrix elements. Let us for example take $T_{\Lambda\Lambda'}^{\pi S t}(p, \pi, \cos \theta'; E_p)$, which are needed to calculate $U_0^{(1)}(\mathbf{p}, \mathbf{q})$ given in Eq. (G.2). The NN T-matrix elements $T_{\Lambda\Lambda'}^{\pi S t}(p, \pi, \cos \theta'; E_p)$ are ideally obtained directly from the LSE's given in Eq. (3.73). Thus, one first solves the LSE's at various energies E_p and initial momenta π of the two nucleon subsystem. Then for each pair of E_p and π one knows the NN T-matrix elements on certain grids in final momenta p' and $\cos \theta''$. Among the p' -values is also the required on-shell value p . Next one uses the same LSE's again to calculate the NN T-matrix elements at the required angle $\cos \theta'$. This would be the ideal procedure and the same also to obtain the corresponding NN T-matrix elements for $U_0^{(2)}(\mathbf{p}, \mathbf{q})$ and

$U_0^{(3)}(\mathbf{p}, \mathbf{q})$. But it is not practical since very time consuming. Therefore, we think of a more economic way and choose to interpolate the NN T-matrix elements from the ones exactly obtained from the LSE's, which are prepared before the calculations. Though the NN T-matrix elements are determined by four arguments, for example p , π , $\cos \theta'$ and E_p in Eq. (G.2), the interpolation is three-dimensional, since p and E_p are related. In Eq. (6.48) the relation between p and E_p for the nonrelativistic case is given and in Eq. (6.127) for the relativistic case. Thus, we interpolate along $\cos \theta'$, π and E_p for $U_0^{(1)}(\mathbf{p}, \mathbf{q})$ in Eq. (G.2) and along the corresponding quantities for $U_0^{(2)}(\mathbf{p}, \mathbf{q})$ and $U_0^{(3)}(\mathbf{p}, \mathbf{q})$.

We use the same interpolation method as the one used in Chapter 4 for the AV18 potential, that is the modified cubic hermite splines [44]. This is a one-dimensional interpolation method, but can also be used for a multi-dimensional interpolation, described as follows: Using this method a one-dimensional interpolation is performed as

$$f(x_i) = \sum_{j=1}^4 S_{ij} f(y_{I_{ij}}), \quad (\text{G.15})$$

where $f(x_i)$ are the interpolated values at x_i and $f(y_{I_{ij}})$ the known values at $y_{I_{ij}}$ of the function f . The spline coefficients $S_{i,j}$ and the indices I_{ij} are determined beforehand by the sets $\{x\}$ and $\{y\}$. Now, as an example of a multi-dimensional interpolation, a 3D interpolation is performed as

$$f(x_i, y_j, z_k) = \sum_{r=1}^4 \sum_{s=1}^4 \sum_{t=1}^4 S_{ir} S_{js} S_{kt} f(u_{I_{ir}}, v_{I_{js}}, w_{I_{kt}}). \quad (\text{G.16})$$

Thus, in fact one performs three one-dimensional interpolations as shown in the following.

$$\begin{aligned} f(x_i, y_j, z_k) &= \sum_{r=1}^4 \sum_{s=1}^4 \sum_{t=1}^4 S_{ir} S_{js} S_{kt} f(u_{I_{ir}}, v_{I_{js}}, w_{I_{kt}}) \\ &= \sum_{r=1}^4 \sum_{s=1}^4 S_{ir} S_{js} f(u_{I_{ir}}, v_{I_{js}}, z_k) \\ &= \sum_{r=1}^4 S_{ir} f(u_{I_{ir}}, y_j, z_k) \\ &= f(x_i, y_j, z_k). \end{aligned} \quad (\text{G.17})$$

We prepare a 3D grid of the NN T-matrix elements, obtained from the LSE's given in Eq. (3.73). We found that the ranges of the grid axes in $U_0^{(1)}(\mathbf{p}, \mathbf{q})$, $U_0^{(2)}(\mathbf{p}, \mathbf{q})$ and $U_0^{(3)}(\mathbf{p}, \mathbf{q})$ are the same, as shown in the next section. Therefore, it is sufficient to show here only the ranges of $\cos \theta'$, π and E_p . The range of $\cos \theta'$ is set to be from -1 to 1:

$$-1 \leq \cos \theta' \leq 1. \quad (\text{G.18})$$

The ranges of E_p and π depend on the projectile's kinetic energy E_{lab} . For reasons of efficiency we prepare a grid such that it can be used for any value of E_{lab} within a certain

range, which we are interested in. The highest E_{lab} we are interested in is 500 MeV, where there are experimental data to compare with, and we choose the lowest E_{lab} to be 5 MeV. Thus, for

$$5 \text{ MeV} \leq E_{lab} \leq 500 \text{ MeV} \quad (\text{G.19})$$

we obtain the ranges of E_p and π as

$$2.5 \cdot 10^{-4} \text{ MeV} \leq E_p \leq 335 \text{ MeV} \quad (\text{G.20})$$

$$30.66 \text{ MeV} \leq \pi \leq 982 \text{ MeV}. \quad (\text{G.21})$$

See the next section for the connection between E_{lab} and E_p , π , and the determination of these ranges.

The $\cos\theta'$ -points within the range given in Eq. (G.18) are determined simply as the Gauss-Legendre quadrature points. We found that 80 points are sufficient for the interpolation to reach a certain accuracy given in the next paragraph. As the NN T-matrix elements change smoothly with the energy and are getting smoother as the energy raises we distribute the E_p -points within the range given in Eq. (G.20) exponentially as follows: Since in a lower energy region the NN T-matrix elements change stronger than in a higher one we divide the range in two regions as

$$E_{min} \leq E_p^{(1)} \leq E_{mid} \quad E_{mid} \leq E_p^{(2)} \leq E_{max}, \quad (\text{G.22})$$

where $E_{min} = 2.5 \cdot 10^{-4} \text{ MeV}$, $E_{max} = 335 \text{ MeV}$ and E_{mid} some energy between E_{min} and E_{max} . Next $E_p^{(1)}$ and $E_p^{(2)}$ are calculated as

$$E_{p,i}^{(1)} = e^{x_i^{(1)}} \quad E_{p,i}^{(2)} = e^{x_i^{(2)}}, \quad (\text{G.23})$$

with

$$x_i^{(1)} = \frac{i-1}{n_1-1} A^{(1)} + B^{(1)}, \quad A^{(1)} = \ln \frac{E_{mid}}{E_{min}}, \quad B^{(1)} = \ln E_{min}, \quad (i = 1, \dots, n_1) \quad (\text{G.24})$$

$$x_i^{(2)} = \frac{i}{n_2} A^{(2)} + B^{(2)}, \quad A^{(2)} = \ln \frac{E_{max}}{E_{mid}}, \quad B^{(2)} = \ln E_{mid}, \quad (i = 1, \dots, n_2). \quad (\text{G.25})$$

Here n_1 is the number of E_p -points in region 1 and n_2 in region 2. In this way the natural logarithm of the $E_p^{(i)}$ -point ($i = 1, 2$) varies linearly in $A^{(i)}$ and hence the $E_p^{(i)}$ -point varies exponentially in $A^{(i)}$. We use $n_1 = 16$ and $n_2 = 24$, with E_{mid} being fixed to 0.5 MeV. This value turned out to be our of suitable choices to keep the strong variations of the NN T-matrix at small energies and its interpolation under control. Thus, we put a higher density of points in the lower energy region. For the interpolation along π we determine the π -points within the range given in Eq. (G.21) by means of the Gauss-Legendre quadrature points and a tangential mapping given in Section E.1, with the parameter k being equal

to 5.068 fm^{-1} and the number n_π of π -points to 120. From the resulting list of π -points we discard π -points below 30.66 MeV and beyond 979.79 MeV, and then replace the special π -point 979.79 MeV with 982 MeV. There are left 50 points of π from 30.66 MeV to 982 MeV.

We test our 3D-interpolation by comparing with 600 data of the NN T-matrix elements, which are calculated exactly using the LSE's given in Eq. (3.73). Thus, we calculate the relative differences between the interpolated and the exact data. The 600 data are calculated for 30 different scattering angles from 0 to π , 10 NN c.m. kinetic energies from $3 \cdot 10^{-4}$ MeV to 330 MeV and 2 magnitudes of the initial momenta. The latter are chosen to be close to the corresponding on-shell nonrelativistic momenta of the chosen 10 energies. With the interpolation parameters given in the previous paragraph we obtain that for the singlet spin states all the relative differences are below 1% for the two NN potentials we use; these are the Bonn-B and the AV18. For the triplet spin states there are 60 cases for the NN potential Bonn-B and 34 for the AV18, where the relative differences are larger than 2%. All other relative differences are less than 2%. The 60 cases for the Bonn-B and 34 for the AV18 occur in two cases, i.e. near the points, where (1) the data change sign while their curves are crossing the zero line and (2) the NN T-matrix elements vary very sharply, for example, at the forward and backward directions. The test, hence, shows that the interpolation grid is acceptable.

Similar to the case of the NN T-matrix elements, it is also not practical to calculate the deuteron partial wave projected wave function $\psi_l(\pi')$ exactly at the value of π' . Therefore, we interpolate $\psi_l(\pi')$ from the exact ones, obtained from the deuteron equation. We prepare a grid of $\psi_l(\pi')$ along π' . The π' -range depends on E_{lab} and is the same as the ranges of the corresponding quantities for $U_0^{(2)}(\mathbf{p}, \mathbf{q})$ and $U_0^{(3)}(\mathbf{p}, \mathbf{q})$ as shown in the next section. For E_{lab} from 5 MeV to 500 MeV it is required to have the π' -range as

$$0.05 \text{ MeV} \leq \pi' \leq 982 \text{ MeV}. \quad (\text{G.26})$$

We determine the π' -points within this range using the Gauss-Legendre quadrature points and a hyperbolic-linear mapping given in Section E.1. Recall that this is the way by which we solved the deuteron wave function in Chapter 5. Here we use the parameters for the mapping as $q_1 = 0.1 \text{ fm}^{-1}$, $q_2 = 1.5 \text{ fm}^{-1}$, $q_3 = 5 \text{ fm}^{-1}$, 24 π' -points between 0 and q_2 , and 24 π' -points between q_2 and q_3 . We replace the first point $5.099 \cdot 10^{-2}$ MeV with $5 \cdot 10^{-2}$ MeV and the last point 984.98 MeV with 982 MeV. We test the interpolation by comparing with a more dense distribution of the deuteron partial wave projected wave function within the range given in Eq. (G.26), that is with 126 data. The test shows very small relative differences, which are below 0.1%. There are very few cases (less than 10

cases), where the relative differences are greater than 0.1% but below 2.5%. But these occur near the points, where the function changes sign while crossing the zero line. Thus, the test gives a good result.

G.4 Momenta and Energy Ranges for the Interpolation

To prepare the grid for the interpolations mentioned in the previous section one needs to know the lower and upper limits of the grid axes. For the grid axis $\cos \theta'$ and the corresponding axes in $U_0^{(2)}(\mathbf{p}, \mathbf{q})$ and $U_0^{(3)}(\mathbf{p}, \mathbf{q})$ the lower and upper limits are best set to be -1 and 1, thus all possible values of the cosines are covered. For the grid axes E_p , π and π' and the corresponding axes in $U_0^{(2)}(\mathbf{p}, \mathbf{q})$ and $U_0^{(3)}(\mathbf{p}, \mathbf{q})$ the lower and upper limits have to be found. We calculate these limits firstly for calculations of $U_0(\mathbf{p}, \mathbf{q})$ without relativistic kinematics. After that we test if the limits can also be used to calculate $U_0(\mathbf{p}, \mathbf{q})$ with relativistic kinematics. This is necessary, since energies and momenta in these two formulations have different ranges of values. Finally, we take a grid, which can be used for both calculations with and without relativistic kinematics.

Let us define the new notations $E_{NN}^{(i)}, Q_{\pi}^{(i)}, Q_{\pi'}^{(i)}$, where $i = 1, 2, 3$ refers to $U_0^{(1)}(\mathbf{p}, \mathbf{q})$, $U_0^{(2)}(\mathbf{p}, \mathbf{q})$ and $U_0^{(3)}(\mathbf{p}, \mathbf{q})$, such that

$$E_{NN}^{(1)} = E_p \quad Q_{\pi}^{(1)} = \pi \quad Q_{\pi'}^{(1)} = \pi'. \quad (\text{G.27})$$

Thus,

$$\text{for } U_0^{(1)}(\mathbf{p}, \mathbf{q}) : \begin{cases} E_{NN}^{(1)} = E_d + \frac{3}{4m} (q_0^2 - q^2) \\ Q_{\pi}^{(1)} = \left| \frac{1}{2}\mathbf{q} + \mathbf{q}_0 \right| \\ Q_{\pi'}^{(1)} = \left| -\mathbf{q} - \frac{1}{2}\mathbf{q}_0 \right| \end{cases} \quad (\text{G.28})$$

$$\text{for } U_0^{(2)}(\mathbf{p}, \mathbf{q}) : \begin{cases} E_{NN}^{(2)} = E_d + \frac{3}{4m} \left(q_0^2 - \left(\mathbf{p} - \frac{1}{2}\mathbf{q} \right)^2 \right) \\ Q_{\pi}^{(2)} = \left| \frac{1}{2} \left(\mathbf{p} - \frac{1}{2}\mathbf{q} \right) + \mathbf{q}_0 \right| \\ Q_{\pi'}^{(2)} = \left| - \left(\mathbf{p} - \frac{1}{2}\mathbf{q} \right) - \frac{1}{2}\mathbf{q}_0 \right| \end{cases} \quad (\text{G.29})$$

$$\text{for } U_0^{(3)}(\mathbf{p}, \mathbf{q}) : \begin{cases} E_{NN}^{(3)} = E_d + \frac{3}{4m} \left(q_0^2 - \left(\mathbf{p} + \frac{1}{2}\mathbf{q} \right)^2 \right) \\ Q_{\pi}^{(3)} = \left| -\frac{1}{2} \left(\mathbf{p} + \frac{1}{2}\mathbf{q} \right) + \mathbf{q}_0 \right| \\ Q_{\pi'}^{(3)} = \left| \mathbf{p} + \frac{1}{2}\mathbf{q} - \frac{1}{2}\mathbf{q}_0 \right| \end{cases}, \quad (\text{G.30})$$

where the magnitude q_0 of the relative momentum of the projectile to the deuteron is given as

$$q_0 = \frac{2}{3}k_{lab} = \sqrt{\frac{8}{9}mE_{lab}}. \quad (\text{G.31})$$

To calculate the lower and upper limits of $E_{NN}^{(i)}, Q_{\pi}^{(i)}, Q_{\pi'}^{(i)}$ we need to know the ranges of q as well as of $\left| \mathbf{p} \pm \frac{1}{2} \mathbf{q} \right|$. The q -range is known from the relation between q and p given in Eq. (6.10) to be

$$0 \leq q \leq \sqrt{q_0^2 + \frac{4}{3}mE_d} \equiv q_{max}. \quad (\text{G.32})$$

Thus, q is maximum if p is minimum and vice versa. The lower and upper limits of $\left| \mathbf{p} \pm \frac{1}{2} \mathbf{q} \right|$ are given as

$$\left| \mathbf{p} \pm \frac{1}{2} \mathbf{q} \right|_{min} = \left| p - \frac{1}{2}q \right|_{min} = 0 \quad (\text{G.33})$$

$$\left| \mathbf{p} \pm \frac{1}{2} \mathbf{q} \right|_{max} = \left(p + \frac{1}{2}q \right)_{max} = q_{max}. \quad (\text{G.34})$$

Equation (G.33) occurs at $q = \sqrt{\frac{3}{4}q_0^2 + mE_d}$ due to Eq. (6.10) and Eq. (G.34) is obtained using Eq. (6.10) in the following way:

$$\begin{aligned} y &= p + \frac{1}{2}q = \sqrt{\frac{3}{4}(q_0^2 - q^2) + mE_d} + \frac{1}{2}q \\ \frac{dy}{dq} \Big|_{y_{max}} &= \frac{-3q + 2\sqrt{\frac{3}{4}(q_0^2 - q^2) + mE_d}}{4\sqrt{\frac{3}{4}(q_0^2 - q^2) + mE_d}} \Big|_{y_{max}} = 0 \\ \implies q \Big|_{y_{max}} &= \frac{1}{2}\sqrt{q_0^2 + \frac{4}{3}mE_d} = \frac{1}{2}q_{max} \\ y_{max} &= \sqrt{q_0^2 + \frac{4}{3}mE_d} = q_{max}. \end{aligned}$$

In summarizing we have the ranges of q and $\left| \mathbf{p} \pm \frac{1}{2} \mathbf{q} \right|$ as

$$0 \leq \left\{ q, \left| \mathbf{p} \pm \frac{1}{2} \mathbf{q} \right| \right\} \leq \sqrt{q_0^2 + \frac{4}{3}mE_d}. \quad (\text{G.35})$$

Equation (G.35) together with Eqs. (G.28)-(G.30) tell us that the lower and upper limits of $E_{NN}^{(i)}, Q_{\pi}^{(i)}, Q_{\pi'}^{(i)}$ are the same for all $i = 1, 2, 3$. Let us take $E_{NN}^{(1)}, Q_{\pi}^{(1)}, Q_{\pi'}^{(1)}$ given in Eq. (G.28), since they have the simplest form, and then drop the superscript (1). The lower and upper limits of $E_{NN}, Q_{\pi}, Q_{\pi'}$ are obtained to be

$$E_{NN,min} = E_d + \frac{3}{4m}(q_0^2 - q_{max}^2) = 0 \quad (\text{G.36})$$

$$E_{NN,max} = E_d + \frac{3}{4m}(q_0^2 - q_{min}^2) = E_d + \frac{3}{4m}q_0^2 \quad (\text{G.37})$$

$$Q_{\pi,min} = -\frac{1}{2}q_{max} + q_0 = -\frac{1}{2}\sqrt{q_0^2 + \frac{4}{3}mE_d} + q_0 \quad (\text{G.38})$$

$$Q_{\pi,max} = \frac{1}{2}q_{max} + q_0 = \frac{1}{2}\sqrt{q_0^2 + \frac{4}{3}mE_d} + q_0 \quad (\text{G.39})$$

$$Q_{\pi',min} = -q|_{q=\frac{1}{2}q_0} + \frac{1}{2}q_0 = 0 \quad (\text{G.40})$$

$$Q_{\pi',max} = q_{max} + \frac{1}{2}q_0 = \sqrt{q_0^2 + \frac{4}{3}mE_d} + \frac{1}{2}q_0. \quad (\text{G.41})$$

To simplify we can neglect the deuteron binding energy E_d in Eqs. (G.36)-(G.41). Neglecting E_d does neither raise the minima nor lower the maxima of $E_{NN}, Q_\pi, Q_{\pi'}$. In fact it lowers the minima and raises the maxima of $E_{NN}, Q_\pi, Q_{\pi'}$. Therefore, it is justified to neglect E_d even for lower projectile's laboratory kinetic energy E_{lab} , and thus lower q_0 , since the interpolation grid can still be safely used. We obtain after neglecting E_d the ranges of $E_{NN}, Q_\pi, Q_{\pi'}$ to be

$$0 \leq E_{NN} \leq \frac{3}{4m}q_0^2 \quad (\text{G.42})$$

$$\frac{1}{2}q_0 \leq Q_\pi \leq \frac{3}{2}q_0 \quad (\text{G.43})$$

$$0 \leq Q_{\pi'} \leq \frac{3}{2}q_0. \quad (\text{G.44})$$

Now we check if the ranges of $E_{NN}, Q_\pi, Q_{\pi'}$ given in Eqs. (G.42)-(G.44) can also be used to calculate $U_0(\mathbf{p}, \mathbf{q})$ with relativistic kinematics. Finally we take a grid, which can be used to calculate $U_0(\mathbf{p}, \mathbf{q})$ with and without relativistic kinematics. It is sufficient to check only the maximum of E_{NN} , defined as $E_{NN,max}$, and q_0 , for which we define the corresponding relativistic quantities as $E_{NN,max}^{(r)}$ and $q_0^{(r)}$. If $E_{NN,max}$ in Eq. (G.42) is larger than or equal to the corresponding $E_{NN,max}^{(r)}$, then the E_{NN} -range given in Eq. (G.42) can be used to calculate $U_0(\mathbf{p}, \mathbf{q})$ with and without relativistic kinematics. If q_0 given in Eq. (G.31) is less than or equal to the corresponding $q_0^{(r)}$ we use $q_0^{(r)}$ to calculate the maxima of Q_π and $Q_{\pi'}$, and q_0 to calculate the minimum of Q_π . Here we keep E_{lab} as denoting the laboratory kinetic energy of the projectile, in contrast to what we did in Section 6.3, where we redefined E_{lab} as denoting the laboratory total energy of the projectile.

Referring to Eq. (6.127) the relativistic kinetic energy $E_{NN}^{(r)}$ in the 23-subsystem is given as

$$E_{NN}^{(r)} = 2\sqrt{m^2 + p^2} - 2m = M_{23} - 2m, \quad (\text{G.45})$$

where M_{23} is the invariant mass of the 23-subsystem. As can be checked in Eq. (6.104) M_{23} is connected to the invariant mass M_0 of the 3N system as

$$M_0 = \sqrt{m^2 + q^{(r)2}} + \sqrt{M_{23}^2 + q^{(r)2}} = \sqrt{9m^2 + 4mE_{lab}}, \quad (\text{G.46})$$

where the rightmost equality is taken from the definition of M_0 given in Eq. (6.96) by neglecting E_d . The maximal value of M_{23} is $M_0 - m$, where $q^{(r)} = 0$. Therefore, we obtain

$$E_{NN,max}^{(r)} = M_0 - 3m$$

$$= \sqrt{9m^2 + 4mE_{lab}} - 3m. \quad (\text{G.47})$$

Now we assume that $E_{NN,max}^{(r)}$ is less than $E_{NN,max}$ given in Eq. (G.42), with q_0 being given in Eq. (G.31). We check this assumption as follows:

$$\begin{aligned} E_{NN,max}^{(r)} &< E_{NN,max} \\ \sqrt{9m^2 + 4mE_{lab}} - 3m &< \frac{2}{3}E_{lab} \\ \sqrt{9m^2 + 4mE_{lab}} &< \frac{2}{3}E_{lab} + 3m \\ 9m^2 + 4mE_{lab} &< \frac{4}{9}E_{lab}^2 + 9m^2 + 4mE_{lab} \\ 0 &< \frac{4}{9}E_{lab}^2. \end{aligned} \quad (\text{G.48})$$

The assumption that $E_{NN,max}^{(r)} < E_{NN,max}$ is correct. Hence, the E_{NN} -range given in Eq. (G.42) can also be used to calculate $U_0(\mathbf{p}, \mathbf{q})$ with relativistic kinematics.

From Eq. (6.110) the relativistic initial Jacobi momentum $q_0^{(r)}$ is obtained by neglecting E_d as

$$\begin{aligned} q_0^{(r)} &= \frac{2m}{M_0} \mathbf{k}_{lab} \\ &= \frac{2m}{\sqrt{9m^2 + 4mE_{lab}}} \sqrt{E_{lab}^2 + 2mE_{lab}} \\ &= \sqrt{\frac{4m(E_{lab} + 2m)}{9m + 4E_{lab}}} E_{lab}. \end{aligned} \quad (\text{G.49})$$

Now we assume that $q_0^{(r)}$ is larger than q_0 given in Eq. (G.31). We check if the assumption is correct as follows:

$$\begin{aligned} q_0^{(r)} &> q_0 \\ \sqrt{\frac{4m(E_{lab} + 2m)}{9m + 4E_{lab}}} E_{lab} &> \sqrt{\frac{8}{9}mE_{lab}} \\ \frac{(E_{lab} + 2m)}{9m + 4E_{lab}} &> \frac{2}{9} \\ 9(E_{lab} + 2m) &> 2(9m + 4E_{lab}) \\ E_{lab} &> 0. \end{aligned} \quad (\text{G.50})$$

It is true that $q_0^{(r)} > q_0$. Hence, the ranges of Q_π and $Q_{\pi'}$ to be used for calculations of $U_0(\mathbf{p}, \mathbf{q})$ with and without relativistic kinematics are given as

$$\frac{1}{2}q_0 \leq Q_\pi \leq \frac{3}{2}q_0^{(r)} \quad (\text{G.51})$$

$$0 \leq Q_{\pi'} \leq \frac{3}{2}q_0^{(r)}. \quad (\text{G.52})$$

The ranges of E_{NN} given in Eq. (G.42) and of $Q_\pi, Q_{\pi'}$ given in Eqs. (G.51)-(G.52) are energy-dependent. They enlarge as E_{lab} increases. In addition the Q_π -range is also shifted as its minimum increases with E_{lab} . Now, for practical purposes we want to have an interpolation grid, which can be used for more than just one E_{lab} . Thus, we determined a certain range for E_{lab} we are interested in and then set the minimum of Q_π to correspond to the lowest E_{lab} , defined as $E_{lab,min}$, and the maxima of $E_{NN}, Q_\pi, Q_{\pi'}$ to the highest E_{lab} , defined as $E_{lab,max}$. Finally we obtain the ranges of $E_{NN}, Q_\pi, Q_{\pi'}$ as

$$0 \leq E_{NN} \leq \frac{2}{3}E_{lab,max} \quad (\text{G.53})$$

$$\sqrt{\frac{2}{9}mE_{lab,min}} \leq Q_\pi \leq \frac{3}{2}\sqrt{\frac{4m(E_{lab,max} + 2m)}{9m + 4E_{lab,max}}}E_{lab,max} \quad (\text{G.54})$$

$$0 \leq Q_{\pi'} \leq \frac{3}{2}\sqrt{\frac{4m(E_{lab,max} + 2m)}{9m + 4E_{lab,max}}}E_{lab,max}. \quad (\text{G.55})$$

Equations (G.53)-(G.55) must be taken as giving the narrowest and yet safe ranges of E_{NN}, Q_π and $Q_{\pi'}$ for the interpolations. Deviations are of course allowed as long as not lowering the range-maxima and / or raising the range-minima. But the zero-minima as in Eqs. (G.53) and (G.55) are exceptional. The NN T-matrix elements are known to drop drastically as the initial or the final momenta move away from the on-shell ones, corresponding to the NN kinetic energy. The NN kinetic energy corresponding to the minimum of Q_π in Eq. (G.54) is not zero unless $E_{lab,min}$ is equal to zero. Thus, one can replace the zero-minimum of E_{NN} in Eq. (G.53) with a small number, much less than the NN kinetic energy, which corresponds to the minimum of Q_π . The zero-minimum of $Q_{\pi'}$ in Eq. (G.55) can also be safely replaced by a small number, since near $Q_{\pi'} = 0$ the deuteron S-wave is almost flat and the D-wave is approaching zero. Moreover, numerical test shows that the minimum of $Q_{\pi'}$ is never really zero. We are interested to calculate the Nd break-up amplitude for E_{lab} up to 500 MeV, where data exist. Thus, we set $E_{lab,max}$ to be 500 MeV and choose 5 MeV as $E_{lab,min}$. The ranges of $E_{NN}, Q_\pi, Q_{\pi'}$ for this range of E_{lab} is

$$2.5 \cdot 10^{-4} \text{ MeV} \leq E_{NN} \leq 335 \text{ MeV} \quad (\text{G.56})$$

$$30.66 \text{ MeV} \leq Q_\pi \leq 982 \text{ MeV} \quad (\text{G.57})$$

$$0.05 \text{ MeV} \leq Q_{\pi'} \leq 982 \text{ MeV}. \quad (\text{G.58})$$

Bibliography

- [1] L. D. Faddeev, Sov. Phys. JETP **12**, 1014 (1961).
- [2] W. Glöckle, Nucl. Phys. **A141**, 620 (1970).
- [3] A. Aaron, R. D. Amado, Y. Y. Yam, Phys. Rev. **140**, B1291 (1965).
- [4] Y. Yamaguchi, Phys. Rev. **95**, 1628 (1954).
- [5] W. Glöckle, et. al., Phys. Rep. **274**, 107 (1996).
- [6] M. Lacombe, et. al., Phys. Rev. **C21**, 861 (1980).
- [7] M. M. Nagels, T. A. Rijken, J. J. de Swart, Phys. Rev. **D17**, 768 (1978).
- [8] K. Erkelenz, Phys. Rep. **13C**, 191 (1974).
- [9] R. B. Wiringa, R. A. Smith, T. L. Ainsworth, Phys. Rev. **C29**, 1207 (1984).
- [10] W. M. Kloet and J. A. Tjon, Nucl. Phys. **A210**, 380 (1973); Ann. Phys. **79**, 407 (1973); C. Stolk and J. A. Tjon, Phys. Rev. Lett. **35**, 985 (1975); Nucl. Phys. **A319**, 1 (1979).
- [11] A. Arriaga, V. R. Pandharipande, R. B. Wiringa, Phys. Rev. **C52**, 2362 (1995).
- [12] J. Carlson and R. Schiavilla, Rev. of Modern Physics **70**, 743 (1998).
- [13] Ch. Elster, et. al., Few-Body Systems **27**, 83 (1999).
- [14] W. Schadow, Ch. Elster, W. Glöckle, Few-Body Systems **28**, 15 (2000).
- [15] B. terHaar and R. Malfliet, Phys. Rep. **149**, 207 (1987).
- [16] J. Holz and W. Glöckle, Phys. Rev. **C37**, 1386 (1988); J. Comput. Phys. **76**, 131 (1988).
- [17] R. A. Rice and Y. E. Kim, Few-Body Systems **14**, 127 (1993).

- [18] D. L. Prout, et.al., Phys. Rev. **C65**, 034611 (2002).
- [19] T. Wakasa, et.al., Phys. Rev. **C59**, 3177 (1999).
- [20] R. B. Wiringa, V. G. J. Stoks, R. Schiavilla, Phys. Rev. **C51**, 38 (1995).
- [21] R. Machleidt, Adv. Nucl. Phys. **19**, 189 (1989).
- [22] R. G. Newton, *Scattering Theory of Waves and Particles* (McGraw Hill, New York 1966)
- [23] N. Hoshizaki, Suppl. Prog. Theor. Phys. **42**, 107 (1968).
- [24] J. Bystricky, F. Lehar, P. Winternitz, Le Journal de Physique **39**, 1 (1978).
- [25] W. Glöckle, *The Quantum Mechanical Few-Body Problem* (Springer Verlag, Berlin, 1983)
- [26] L. Wolfenstein and J. Ashkin, Phys. Rev. **85**, 947 (1952); L. Wolfenstein, Phys. Rev. **96**, 1654 (1954); Phys. Rev. **101**, 427 (1956).
- [27] I. Fachruddin, Ch. Elster, W. Glöckle, Nucl. Phys. **A689**, 507c (2001).
- [28] K. Erkelenz, R. Alzetta, K. Holinde, Nucl. Phys. **A176**, 413 (1971).
- [29] R. Alzetta, K. Erkelenz, K. Holinde, Nucl. Phys. **A185**, 459 (1972).
- [30] M. Jacob and G. C. Wick, Ann. Phys. **7**, 404 (1959).
- [31] M. E. Rose, *Elementary Theory of Angular Momentum* (Wiley, New York, 1957).
- [32] A. R. Edmonds, *Angular Momentum in Quantum Mechanics* (Princeton UP, New Jersey, 1996).
- [33] J. M. Blatt and L. C. Biedenharn, Phys. Rev. **86**, 399 (1952)
- [34] H. P. Stapp, T. J. Ypsilantis, N. Metropolis, Phys. Rev. **105**, 302 (1957)
- [35] R. Machleidt, K. Holinde, Ch. Elster, Phys. Rep. **149**, 1 (1987).
- [36] H. Yukawa, Proc. Phys. Math. Soc. Japan **17**, 48 (1935).
- [37] M. Taketani, S. Nakamura, M. Sasaki, Prog. Theor. Phys. **6**, 581 (1951).
- [38] V. G. J. Stoks, et. al., Phys. Rev. **C49** , 2950 (1994).
- [39] K. Hagiwara, et. al., Phys. Rev. **D66**, 010001 (2002).

- [40] R. Machleidt, F. Sammerruca, Y. Song, Phys. Rev. **C53**, R1483 (1996).
- [41] S. Okubo and R. E. Marshak, Ann. Phys. **4**, 166 (1958).
- [42] R. Machleidt, Proceedings of the XV11th European Conference on Few-Body Problem in Physics, Evora, 2000, edited by Stadler A., et. al.
- [43] B. Wiringa, private communication.
- [44] D. Hüber, et. al., Few-Body Systems **22**, 107 (1997).
- [45] J. L. Forest, et. al., Phys. Rev. **C54**, 646 (1996).
- [46] W. Rarita and J. Schwinger, Phys. Rev. **59**, 436 (1941).
- [47] T. Ericson and W. Weise, *Pions and Nuclei*, p. 49 (Claredon Press, Oxford, 1998)
- [48] R. A. Malfliet and J. A. Tjon, Nucl. Phys. **A127**, 161 (1969).
- [49] P. L. DeVries, *A First Course in Computational Physics* (Wiley, New York, 1994).
- [50] W. Glöckle, Nucl. Phys. **A381**, 343 (1982).
- [51] R. Fong and J. Sucher, J. Math. Phys. **5**, 456 (1964).
- [52] G. G. Ohlsen, Rep. Prog. Phys. **35**, 717 (1972).
- [53] M. Ichimura and K. Kawahigashi, Phys. Rev. **C45**, 1822 (1992).
- [54] H. Witała, private communication.
- [55] J. Golak, private communication.
- [56] W. N. Polyzou and W. Glöckle, Few-Body Systems **9**, 97 (1990).
- [57] X. Y. Chen, et.al., Phys. Rev. **C47**, 2159 (1993).
- [58] H. Kamada, et.al., Phys. Rev. **C66**, 044010 (2002).
- [59] B. D. Keister and W. N. Polyzou, Adv. Nucl. Phys. **20**, 225 (1991).
- [60] E. Epelbaum, PhD Thesis. Bochum 2000
- [61] T. Sasakawa and S. Ishikawa, Few-Body Systems **1**, 3 (1986).
- [62] C. R. Chen, et. al., Phys. Rev. **C33**, 1740 (1986).

- [63] A. Nogga, et. al., Phys. Lett. **B409**, 19 (1997).
- [64] A. Nogga, H. Kamada, W. Glöckle, Phys. Rev. Lett. **85**, 944 (2000).
- [65] A. Nogga, et. al., Phys. Rev. **C65**, 054003 (2002).
- [66] W. H. Press, et. al., *Numerical Recipes in Fortran* (Cambridge University Press, New York, 1992).
- [67] M. Abramowitz and I. A. Stegun, *Handbook of Mathematical Functions*, p. 890 (Dover Publications, Inc., New York, 1972).
- [68] M. I. Haftel and F. Tabakin, Nucl. Phys. **A158**, 1 (1970).

Acknowledgement

First of all I gratefully thank my supervisor, Prof. Dr. Walter Glöckle, for helping, stimulating, encouraging and supporting me to accomplish my PhD work in his group at Ruhr-Universität Bochum, not to mention for encouraging and supporting me to participate in some international physics conferences.

I gratefully thank Prof. Dr. Charlotte Elster from Ohio University, Athens for her help, suggestions and stimulations as well as for fruitful discussions.

I also thank the Deutscher Akademischer Austauschdienst (DAAD) for supporting me to come to and stay in Germany to pursue my PhD study.

I thank Prof. Dr. Witala and Dr. Jacek Golak from Uniwersytet Jagiellonski, Cracow for discussions and providing calculations for the pd break-up process to compare with. For the experimental data I thank Prof. Dr. J. Rapaport from Ohio University, Athens and Prof. Dr. H. Sakai from University of Tokyo, Tokyo.

I thank to Dr. Hiroyuki Kamada, who is now a professor at Kyushu Institut of Technology, Kyushu, for his help and for encouraging me in doing physics.

I thank Andreas Nogga, Andreas Krüger, Evgeny Epelbaum, Gernot Ziemer, Amel Hemandan and Htun Htun Oo for their help and for all nice things we have shared and experienced together.

Last but not least I thank Prof. Glöckle's secretary, Mrs. Elke Hannes, for all her kind help.

Lebenslauf

Persönliche Daten

Name : Imam Fachruddin
Geburtsort & -datum : Jakarta, 5. Dezember 1968
Adresse : Wittener Str. 141, 44803 Bochum
Familienstand : verheiratet, ein Kind

Ausbildung

Grundschule (1976-1981) : SD Muhammadiyah II, Jakarta
Erste Mittelschule (1981-1984) : SMP Negeri 5, Jakarta
Höhere Mittelschule (1984-1987) : SMA Negeri 1, Jakarta
Hochschulstudium (1987-1992) : Universitas Indonesia, Depok
Abschluß : Bachelor der Physik
Bachelorarbeit : $e^- - H$ Scattering
Magisterstudium (1993-1996) : Universitas Indonesia, Depok
Abschluß : Magister der Physik
Magisterarbeit : Muon's Energy Lost in Collision with Atom due to e^-e^+ Pair Production
Promotion (1998-2003) : Ruhr-Universität Bochum, Bochum
Abschluß : Doktor der Physik
Doktorarbeit : A Three-Dimensional Momentum Space Formulation for The NN System and The Nd Break-Up Process

Konferenz

1. *XVIth* National Symposium on Physics and Aseanip Regional Seminar on the Physics of Metal and Alloy, 12-14 December 1996, Bandung, Indonesia
2. Indonesian Students Scientific Meeting 1997, 2 August 1997, Wiesbaden, Germany
3. *2nd* Indonesian Students Scientific Meeting 1998, 4-5 September 1998, Paderborn, Germany
4. Symposium on Current Topics in The Field of Light Nuclei, 21-25 June 1999, Cracow, Poland
5. *1st* Asia-Pacific Conference on Few-Body Problems in Physics, 23-28 August 1999, Noda/Kashiwa, Japan
6. *XVII* European Conference on Few-Body Problems in Physics, 11-16 September 2000, Evora, Portugal
7. *2nd* Asia-Pacific Conference on Few-Body Problems in Physics, 27-30 August 2002, Shanghai, P. R. China

Publikation

1. I. Fachruddin and D. Kusno, Proceeding of *XVIth* National Symposium on Physics and Aseanip Regional Seminar on the Physics of Metal and Alloy, 12-14 December 1996, Bandung, Indonesia
2. I. Fachruddin and W. Glöckle, *Helicity Formalism for NN Scattering without Partial Wave Decomposition*, Few-Body Systems Suppl. **12**, 462 (2000)
3. I. Fachruddin, Ch. Elster and W. Glöckle, *Nucleon-Nucleon Scattering in a Three Dimensional Approach*, Phys. Rev. **C62**, 044002 (2000)
4. I. Fachruddin, Ch. Elster and W. Glöckle, *Nucleon-Nucleon Scattering in a Three-Dimensional Approach*, Nucl. Phys. **A689**, 507c (2001)
5. I. Fachruddin, Ch. Elster and W. Glöckle, *New Forms of Deuteron Equations and Wave Function Representations*, Phys. Rev. **C63**, 054003 (2001)
6. I. Fachruddin, Ch. Elster and W. Glöckle, *The Proton-Deuteron Break-Up process in a Three-Dimensional Approach*, Mod. Phys. Lett. **A18**, 452 (2003)

7. I. Fachruddin, Ch. Elster and W. Glöckle, *The Nd Break-Up Process in Leading Order in a Three-Dimensional Approach*, to be published in Phys. Rev. **C** (accepted in October 2003)